

ÉCOLE DOCTORALE Physique – Chimie physique
ICPEES-UMR7515

THÈSE présentée par :

Julien PEYRTON

soutenue le : **16 Décembre 2020**

pour obtenir le grade de : **Docteur de l'université de Strasbourg**

Discipline/ Spécialité : Chimie des polymères

**Développement de nouveaux matériaux polymères
biosourcés alvéolaires, à partir de synthons extraits de
microalgues**

THÈSE dirigée par :

Pr. AVÉROUS Luc

Professeur, Université de Strasbourg

RAPPORTEURS :

Dr. GUILLAUME Sophie
Dr. CAILLOL Sylvain

Directrice de Recherche CNRS, ISCR, Rennes
Directeur de Recherche CNRS, ICGM, Montpellier

AUTRE MEMBRES DU JURY :

Pr. DELAITE Christelle

Professeur, Université de Haute-Alsace

MEMBRE INVITE :

M. PERRIN Rémi

Directeur R&D, Soprema, Strasbourg

REMERCIEMENTS

Je souhaite remercier en premier lieu mon directeur de thèse, le Pr. Luc AVÉROUS, directeur de la BioTeam au sein de l'institut de chimie et procédés pour l'énergie l'environnement et la santé (ICPEES – CNRS - UMR7515) pour m'avoir accueilli au sein de son équipe. Cette thèse est le fruit d'une collaboration de trois années avec lui. Je lui suis également reconnaissant pour le temps qu'il m'a accordé, notamment pour la relecture des articles scientifiques. J'ai beaucoup appris à ses côtés et je lui adresse ma gratitude pour tout cela.

J'adresse tous mes remerciements à Madame Sophie GUILLAUME, Directrice de recherche au CNRS (UMR-6226), à ainsi qu'à Monsieur Sylvain CAILLOL, Directeur de recherche au CNRS (UMR-5253), de l'honneur qu'ils m'ont fait en acceptant d'être rapporteurs de cette thèse. J'exprime aussi ma gratitude à Madame Christelle DELAITE, Professeur à l'Université de Haute-Alsace qui a bien voulu être examinatrice.

Mes remerciements vont également à Monsieur Rémi PERRIN, directeur R&D de SOPREMA pour avoir suivi cette thèse pendant 3 ans et d'avoir accepté de participer à ce jury de thèse. Sa bonne humeur et ces idées ont égayés nos réunions d'avancements.

En mémoire de Jean-Pierre Pascault (1943-2020) un grand homme et chercheur qui a apporté ces conseils avisés tout au long du projet.

Je désire chaleureusement remercier tous mes collègues de travail au sein de la BioTeam pour leur sympathie et leur amitié. La bonne ambiance quotidienne qu'ils ont fait régner dans le laboratoire pendant ces trois ans a contribué au succès de cette thèse. Je remercie plus particulièrement Khantutta-Kim pour l'accueil chaleureux qu'elle m'a témoigné, ses conseils avisés, sa bienveillance et ses discussions scientifiques toujours très pointues. Je tiens également à remercier Pierre qui m'a initié à la formulation de mousse, au bureau « pøt » ainsi qu'au sorties du vendredi soir. Merci également à Alfred pour m'avoir supporté pendant deux ans dans le bureau et lors de nos innombrables Top 1. Un grand merci également à Sophie pour son soutien, sa sympathie, sa bonne humeur et ces discussions, sans oublier, tous les hauts ou les bas traversés ensemble pendant ces trois ans. Merci également à Audrey pour les moments partagés autour d'une mousse, d'un ordinateur, d'une mousse ou d'un petit bébé. Un grand merci à Sébastien de m'avoir montré que les colonnes ne sont pas si compliquées à réaliser. Et il est où le JACS ? Merci à Mohammad pour son apprentissage quotidien du libanais. Je souhaite également remercier Antoine pour l'exemple qu'il montre au laboratoire tous les jours. Bonne chance pour ta nouvelle vie de papa. Merci également à Cassandra ta gentillesse et ta douceur ont rayonné sur les journées au bureau. Merci également à Mathéo pour ton soutien constant. Merci à Alina pour m'avoir supporté pendant son séjour en France. Toutes les personnes que j'ai pu rencontrer, Clara, Connie, Gianni, Alexis, Marion, Agathe sans oublier toutes celles précédemment cités, ont contribué au bon déroulement de cette thèse et je les remercie pour cela.

Un énorme merci à Catherine. Nos discussions et moments partagés vont me manquer. Profites bien de la petite Jade ainsi que du nouveau petit qui arrive. Je souhaite également remercier Céline pour sa sympathie et bienveillance déployé tout au long de cette thèse. Son temps passé sur l'APC à changer de nombreuses pièces afin de la remettre sur pied a aussi été précieux. Je tiens également à remercier les inséparables Christophe S. et Christophe M. pour leurs compétences techniques respectives, mais aussi pour toutes nos discussions axées informatique, vie et sport.

REMERCIEMENTS

Je souhaite remercier les personnes que j'ai eues sous ma responsabilité, Clémence, Mélissandre, Marc, Camélia, Tanguy, Lucie et Amandine. Vos retours, votre patience et compréhension ont aussi forgé et permis ce travail. Un énorme merci plus particulier à Clémence pour tout ce que tu m'as apporté.

Bien sûr, atteindre ces objectifs n'aurait pas été possible sans l'aide des membres de SOPREMA qui ont participé au projet. Je souhaite notamment remercier Alexandru pour sa disponibilité et gentillesse. Nos discussions sur les mousses m'ont permis de mieux comprendre ces matériaux. Un grand merci à Isabelle pour sa patience, notamment lors de ma formation sur les mousses. Je désire en outre remercier tous les membres de SOPREMA (incluant ceux précédemment cités) pour leur sympathie et leur amitié. J'ai eu beaucoup de plaisir à partager du temps avec eux au travers des différents séminaires, réunions ou manipulations.

Je souhaite également remercier mes amis, les Muchos, Joris, Seb, JE, Romain et Nico. Comme le dirait un grand philosophe, « l'important ce sont les moments partagés ensemble ». Et en effet ces instants ont été une bouffée d'oxygène tout au long de cette thèse. Un grand merci donc pour toutes ces soirées, après-midi jeux, lendemain difficiles, city quest, rallye jeu, slow up, matchs de foot ou tout autres heures passer ensemble. Parmi eux, je tiens particulièrement à remercier Nico, pour avoir supporté mon caractère et mes expériences culinaires pendant trois ans durant notre colocation. Tout comme nos thèses, ramener la coupe d'Europe à la Bérichonne était un objectif élevé mais nous y sommes parvenus. N'oubliez pas à l'avenir de « mettre de la salade dans le fait-tout ».

Au terme de ce parcours, je remercie enfin celles et ceux qui me sont chers et que j'ai quelque peu délaissés ces derniers mois pour achever cette thèse. Je souhaite tout d'abord les remercier pour le travail de relecture effectué qui m'a été d'une aide précieuse. Un grand merci à ma sœur, Aurélie, son copain Cédric et leur petite fille Floriane qui m'ont redonné le sourire dans les périodes les plus compliquées. Merci aussi à mes parents qui ont toujours été là pour me soutenir et m'encourager. Ils ont toujours su trouver les mots justes pour me guider au travers de cette thèse, je les remercie de tout mon cœur.

Enfin, je remercie énormément, Audrey, pour ton amour et ton soutien inconditionnel dans les bons comme les mauvais moments. Tes mots, ta gentillesse m'ont permis de passer les obstacles au cours de cette thèse plus sereinement. Le meilleur est bien à venir dans notre future nouvelle vie. Avec tout mon amour, merci.

COMMUNICATIONS LIÉES AUX TRAVAUX DE THÈSE

Publications

Les résultats présentés dans cette thèse font l'objet de 4 articles d'une revue bibliographique.

Articles publiés :

- Peyrton J, Chambaretaud C, Avérous L. New Insight on the Study of the Kinetic of Biobased Polyurethanes Synthesis Based on Oleo-Chemistry. *Molecules* 2019;24:4332. <https://doi.org/10.3390/molecules24234332>.
- Peyrton J, Chambaretaud C, Sarbu A, Avérous L. Biobased Polyurethane Foams Based on New Polyol Architectures from Microalgae Oil. *ACS Sustainable Chem Eng* 2020;8:12187–96. <https://doi.org/10.1021/acssuschemeng.0c03758>.

Articles soumis :

- Peyrton J, Avérous L. Structure-properties relationships of cellular materials from biobased polyurethane foams. *Materials Science and Engineering - R: Reports*
- Peyrton J, Avérous L. Oxazolidone formation: myth or fact? The case of biobased polyurethane foams from different epoxidized triglycerides. *Polymer Chemistry*
- Peyrton J, Avérous L. Study of aza-Michael reactivity for biobased thermoset synthesis to substitute polyurethanes in a greener, safer and more sustainable way. *ACS Sustainable Chemistry & Engineering*

Conférence

Les résultats présentés dans cette thèse ont fait l'objet d'une communication orale dans une conférence internationale :

- Peyrton, J. Avérous, L. - “A specific kinetic study to understand better the ring-opening of epoxides from unsaturated fatty acid systems”, *poster*, 10th Workshop on Fats and Oils as Renewable Feedstock for the Chemical Industry, Karlsruhe (Allemagne, 17 au 19 mars 2019)

LISTE DES ABRÉVIATIONS

2-OHa	2-Hydroxyethyl acrylate
AA	Acetic acid
AlCl ₃	Aluminium trichloride
AO	Microalgae oil
ATR	Attenuated total reflection
BA	Blowing agent
BDE	Bis(2-dimethylaminoethyl)ether
BDMA	Benzyl dimethylamine
BEDA	N-(n-butyl)ethylenediamine
CDCl ₃	Deuterated chloroform
CFC	Chlorofluorocarbons
char	Carbonaceous
CNSL	Cashew nut shell liquid
CO ₂	Carbon dioxide
DAP	Diaminopropane
DBA	Dibutyl amine
DBN	1,5-Diazabicyclo(4.3.0)non-5-ene
DBU	1,8-Diazabicyclo(5.4.0)undec-7-ene
DCC	Dicyclohexylcarbodiimide
DEA	Diethylamine
DEG	Diethylene glycol
DETA	Diethylenetriamine
Deti	Diethyl itaconate
DGEBA	Diglycidyl ether of bisphenol A
DIFFA	Difurfuryl amine
DMCHA	N,N-dimethylcyclohexylamine
DMEDA	1,2-Dimethylethylenediamine
DMF	Dimethylformamide
DOPO	9,10-Dihydro-9-oxa-10-phosphaphenanthrene-10-oxide
DSC	Differential Scanning Calorimetry
DTG	Derivative of thermogravimetric
EAO	Epoxidized microalgae oil
EG	Ethylene glycol
EI	Epoxide index
EMAO	Epoxidized microalgae oil
EO	Ethylene oxide
EOO	Epoxidized olive oil
ERO	Epoxidized rapeseed oil
ESO	Epoxidized soybean oil
EtOH	Ethanol
EWG	Electron-withdrawing group
FAMEVHOSO	Fatty acid methyl ester of very high oleic sunflower oil
F-PUF	Flexible polyurethane foams
FTIR	Fourier transform infrared spectroscopy

LISTE DES ABRÉVIATIONS

GWP	Global warming potential
H ₁₂ MDI	4,4'-Methylenen bis cyclohexyl diisocyanate
HBr	Hydrobromic acid
HC	Hydrocarbons
HCFC	Hydrochlorofluorocarbons
HCFO	Hydrochlorofluoroolefin
HCl	Hydrochloric acid
HDI	Hexamethyleneisocyanate
HFC	Hydrofluorocarbon
HFP	Hydrofluoroolefin
I _A	Acidity index
Iet	Ethyl itaconate
Ietgl	4-Ethyl 1-(2-hydroxyethyl) 2-methylenesuccinate
I _{OH}	Hydroxyl density
IPDI	Isophorone diisocyanate
IV	Iodine value
KOAc	Potassium acetate
LOI	Limiting oxygen index
MAO	Microalgae oil
m-CPBA	m-Chloroperoxybenzoic acid
MDI	Methylene diphenyl 4,4'-diisocyanate
MEDA	Methylethylenediamine
MEK	Methyl ethyl ketone
Mund	Methyl undecylenate
Mundex	Epoxydized methyl undecylenate
mXDA	m-Xylenediamine
NCO	Isocyanate
NIPU	Non-isocyanate polyurethane
NMR	Nuclear magnetic resonance
OA	Octylamine
OH	Hydroxyl
OO	Olive oil
OPG	Oxypropylated glycerol
P2H-EG	Potassium 2-ethylhexanoate dissolved in ethylene glycol
PAO	Polyol obtained by ring-opening of epoxidized microalgae oil with methanol
pbw	Parts by weight
PEG	Polyethyleneglycol
PET	Polyethylene terephthalate
Pht	Phthalic anhydride
Pht-DEG	Phtalic anhydride esterified by diethylene glycol
PIR	Polyisocyanurate
pMDI	Polymeric methylene diphenyl 4,4'-diisocyanate
PO	Propylene oxide
PoSi	Polyether polysiloxane

PRO	Polyol obtained by ring-opening of epoxidized rapeseed oil with methanol
PTSa	p-Toluenesulfonic acid
PU	Polyurethane
PUF	Polyurethane foam
R	Anisotropic coefficient
RH	Relative humidity
RO	Ring-opening
R-PUF	Rigid polyurethane foams
SCO-H ₂ O	Sulfated castor oil dissolved in water
SEC	Size-exclusion chromatography
SEM	Scanning electron microscope
SI	Supporting information
TBAB	Tetra-n-butylammonium bromide
TCPP	Tris(1-chloro-2propyl) phosphate
TDH	1,3,5-Tris(3-dimethylaminopropyl)-s-hexahydrotriazine
TDH-BDE	Bis(2-dimethylaminoethyl)ether dissolved in dipropylene glycol
TDI	Toluene diisocyanate
TEG	Triethylene glycol
TEPA	Tetraethylenepentamine
T _g	Glass transition temperature
TGA	Thermogravimetric analysis
THF	Tetrahydrofuran
TMG	1,1,3,3-Tetramethylguanidine
UV	Ultra violet

SOMMAIRE

REMERCIEMENTS	I
COMMUNICATIONS LIÉES AUX TRAVAUX DE THÈSE	V
Publications	VI
Conférence	VI
LISTE DES ABRÉVIATIONS	VII
SOMMAIRE	XI
LISTE DES ILLUSTRATIONS.....	XVII
Figures	XVIII
Tableaux	XXIV
Schémas	XXVI
 INTRODUCTION GÉNÉRALE.....	1
Références	8
 CHAPITRE 1. RELATIONS STRUCTURES-PROPRIÉTÉS DANS LES MOUSSES POLYURÉTHANES BIOSOURCÉES.....	9
Introduction chapitre 1.....	10
Structure-properties relationships of cellular materials from biobased polyurethane foams.....	11
1. ABSTRACT	11
2. INTRODUCTION	12
3. PUF ENGINEERING AND FUNDAMENTALS	14
3.1. Isocyanate chemistry	14
3.2. PUF Formulation.....	16
4. FROM RENEWABLE SOURCES TO BIOBASED COMPONENTS FOR PUF.....	27
4.1. Lipids: Triglycerides and fatty acids	28
4.2. Carbohydrates	32
4.3. Polyphenols (Lignins and tannins)	35
4.4. Products from industrial wastes	39
4.5. Products from white biotechnology	41
5. STUDY OF “STRUCTURE-PROPERTIES” RELATIONSHIPS IN THE CASE OF BIOBASED R-PUF.....	43
5.1. Morphological and structural data.....	43
5.2. Mechanical properties	48
5.3. Thermal properties	52
5.4. Fire resistance	55
5.5. Some advanced properties.....	58
6. PERSPECTIVES ON BIOBASED PUF.....	59
6.1. Non-isocyanate polyurethane	60
6.2. Other potential approaches.....	62
7. REFERENCES	62
Conclusion Chapitre 1	79
 CHAPITRE 2. CINÉTIQUES DE FORMATION DE POLYOLS À PARTIR D’HUILE : UNE ÉTUDE MODÈLE	81
Introduction Chaptitre 2.....	82
New Insight on the Study of the Kinetic of Biobased Polyurethanes Synthesis Based on Oleo- Chemistry.....	83

1. ABSTRACT	83
2. INTRODUCTION	83
3. MATERIALS AND METHODS	84
3.1. Materials	84
3.2. Epoxidation of FAMEVHOSO	85
3.3. Ring-Opening of EVHOSO with Acetic Acid	85
3.4. Ring-Opening of EVHOSO with Ethanol	85
3.5. Ring-Opening of EVHOSO with Diethylamine	86
3.6. Ring-Opening of EVHOSO with Different Hydrogen Halides	86
3.7. Kinetic Study of Epoxide Ring-Opening with Ethanol	86
3.8. Kinetic Study of Urethane Formation	87
3.9. Kinetic Model of Ring-Opening	87
4. RESULTS.....	88
4.1. Synthesis of EVHOSO	88
4.2. Kinetics of Epoxide Ring-Opening by Ethanol.....	89
4.3. Kinetic Study of Urethane Formation from Fatty Acid.....	93
4.4. Study of the Reactivity with Different Isocyanates Structures.....	96
4.5. Synthesis of a Mono-Alcohol Model from Epoxidized Fatty Ester	97
4.6. Evaluation of the Potential from Alcohols Derived from Fatty Acid in Polyurethane Application	98
5. CONCLUSIONS	99
6. REFERENCES	99
7. SUPPORTING INFORMATION	101
7.1. FAMEVHOSO Characterization.....	101
7.2. Method Development: Kinetics of Epoxide Ring-Opening by Acetic Acid	103
7.3. Variation of k_{app_EtOH} with different temperature and catalyst quantity	107
7.4. Correlation between the mass of catalyst and the quantity of H^+	107
7.5. Determination of the Activation energy of ring-opening with ethanol	108
7.6. Method validation for the isocyanate titration.....	108
7.7. Determination of k_{app_U} with hydroxyl concentration variation	109
7.8. Comparison between urethane formation and ring-opening with ethanol.....	109
7.9. Reaction of VHOSO-DEA with aliphatic and aromatic isocyanate	110
Conclusion chapitre 2	111

CHAPITRE 3. MOUSSES POLYURÉTHANES BIOSOURCÉES À PARTIR DE NOUVEAUX POLYOLS DERIVÉS D'HUILE DE MICROALGUES

Introduction Chapitre 3.....	114
Biobased Polyurethane foams based on new polyols architectures from microalgae oil	115
1. ABSTRACT	115
2. INTRODUCTION	115
3. EXPERIMENTAL SECTION	117
3.1. Materials and chemicals	117
3.2. Triglyceride modifications to obtain polyols	118
3.3. Foam synthesis	118
3.4. Characterizations.....	118
4. RESULTS AND DISCUSSION	122
4.1. Polyol synthesis.....	122
4.2. Rate of foams synthesis.....	127
4.3. Analysis of the foam cell morphology	130
4.4. Biobased catalyst.....	133

4.5. Fire behavior, mechanical and thermal analysis of foams.....	134
5. CONCLUSION	138
6. REFERENCES	138
7. SUPPORTING INFORMATION	142
7.1. Characterization of MAO.....	142
7.2. EMAO synthesis	142
7.3. Polyol synthesis.....	144
7.4. ^{31}P I _{OH} measurements	145
7.5. Structural characterizations of polyols	146
7.6. Crystallization and viscosity behavior with temperature of the different polyols	147
7.7. Thermal stability of MAO, EMAO and polyols.....	151
7.8. Foams characteristic times and reactivity determined by Foamat measurements	154
7.9. Foam cells morphology.....	155
7.10. Foams core-temperature during foam process determined by Foamat measurements	156
7.11. The density of the foams	157
7.12. Synthesis and characterization of a catalytic polyol with ESO	157
7.13. Results of TGA and DTG of the foam	160
7.14. FTIR characterizations of foams	161
Conclusion chapitre 3	162

CHAPITRE 4. FORMATION D'OXAZOLIDONES À PARTIR D'HUILE ÉPOXYDÉE DANS LE CAS DES MOUSSES POLYURÉTHANES

Introduction Chapitre 4.....	164
Oxazolidone formation: myth or fact? The case of biobased polyurethane foams from different epoxidized triglycerides.....	165
1. ABSTRACT	165
2. INTRODUCTION.....	165
3. EXPERIMENTAL SECTION	167
3.1. Materials and chemicals	167
3.2. General procedure of PUF synthesis	167
3.3. PUF synthesized by gradual introduction of ESO.....	168
3.4. Recently synthetized PUF based on AO and EAO	169
3.5. Formerly synthesized PUF based on PAO, PRO, EAO and ERO.....	169
3.6. Liquid extraction from the foams	170
3.7. Synthesis of Methyl undecylenate (Mund)	171
3.8. Synthesis of epoxidized methyl undecylenate (Mundex).....	171
3.9. Synthesis of oxazolidone based on model systems	171
3.10. Characterizations.....	171
4. RESULTS AND DISCUSSION	172
4.1. Foams based on ESO	172
4.2. Study of freshly synthesized foams based on 25% of AO or EAO	173
4.3. Analysis of formerly synthesized foams based on PAO, PRO, EAO and ERO	177
4.4. Reactional models to study oxazolidone formation with different catalysts and epoxides-based systems	179
5. CONCLUSION	185
6. REFERENCES	186
7. SUPPORTING INFORMATION	189
7.1. Maximum height of the foam realized with gradual substitution of Pht-DEG by ESO	189
7.2. Identified soluble fractions in freshly synthesized foams	189
7.3. FTIR analysis of formerly synthesized foams	190

7.4. NMR Spectra of Mundex synthesis	191
7.5. Repartition of the extracted fraction in model study	191
7.6. ^1H NMR spectra of the DGEBA and major fraction of the DGEBA reactions	192
7.7. Mundex- AlCl_3 ^{13}C analysis	193
7.8. Complete NMR analysis of EVHOSO- $\text{Al}(\text{salen})_2$	193
Conclusion chapitre 4	196
CHAPITRE 5. ÉTUDE DE LA RÉACTIVITÉ DE LA RÉACTION D'AZA-MICHAEL POUR REPLACER LE POLYURÉTHANE DE FAÇON DURABLE.....	197
Introduction chapitre 5.....	198
Study of aza-Michael reactivity for biobased thermosets synthesis to substitute polyurethanes in a greener, safer and more sustainable way	199
1. ABSTRACT	199
2. INTRODUCTION.....	199
3. MATERIALS AND METHODS	201
3.1. Materials	201
3.2. Synthesis of ethyl itaconate (Iet)	202
3.3. Synthesis of 4-ethyl 1-(2-hydroxyethyl) 2-methylenesuccinate (Ietgl).....	202
3.4. Synthesis of diethyl itaconate (Deti)	202
3.5. Synthesis of epoxidized olive oil (EOO).....	203
3.6. Ring-opening of epoxidized oils with acrylic acid	203
3.7. Ring-opening of ESO with Iet (ESO_Iet)	203
3.8. Synthesis of Difurfurylamine (DIFFA).....	204
3.9. Characterizations.....	204
4. RESULTS AND DISCUSSION	206
4.1. Study of reactional models.....	206
4.2. Gel formations with Michael acceptors from epoxidized oils.....	213
4.3. Gelation behavior of thermosets via Michael addition.....	214
5. CONCLUSION	221
6. REFERENCES	222
7. SUPPORTING INFORMATION	225
7.1. Reactional model for kinetic studies with MEDA	225
7.2. Detailed proton spectra of Iet	227
7.3. Full NMR analysis of Ietgl.....	227
7.4. Full NMR analysis of Deti	230
7.5. ^{13}C APT NMR analysis of the reaction with OA.....	234
7.6. SEC of the Michael donors derived from triglycerides	237
7.7. Determination of the functionality of the Michael acceptors	238
7.8. DSC and TGA of the different Michael acceptors	241
7.9. Detailed ^1H spectra of DIFFA	242
7.10. Examples of gel time determination.....	242
7.11. TGA	243
Conclusion chapitre 5	244
CONCLUSION GÉNÉRALE	245
LISTE COMPLÈTE DES RÉFÉRENCES BIBLIOGRAPHIQUES	251

LISTE DES ILLUSTRATIONS

Figures

Introduction générale

Figure 0.1 - Les techniques majeures de mise en œuvre de matériaux expansés.	3
Figure 0.2 - Le projet thèse dans le cadre du consortium Trans'alg.	4
Figure 0.3 - Structure d'un triglycéride, composant majeur des huiles.	4
Figure 0.4 - Formation d'un polyuréthane.	5
Figure 0.5 - Schéma récapitulatif des différentes phases de la thèse.	6

Chapitre 1

Figure 1.1 - Examples of F-PUF (left) and R-PUF (right) applications.	13
Figure 1.2 - Main isocyanate reactions with H-labile groups.	15
Figure 1.3 - Effect of the NCO/OH index on the chemical architectures of PUF, PU-PIR and PIR foam networks.	17
Figure 1.4 - Detailed usual processes at lab scale for PUF elaboration: pour-in-place or molding process.	17
Figure 1.5 - Representation of silicone surfactant. Adapted from (Frey et al. 1996).	22
Figure 1.6 - Illustration of the significant perturbations in foam cell formation, with or without surfactant.	23
Figure 1.7 - Catalysts structures ranked according to their main activities in the foam formulation. Adapted from (Van Maris et al. 2005).	24
Figure 1.8 - Viscosity profile associated to the cell bubbles formation.	27
Figure 1.9 - Triglyceride structure and the most abundant fatty acids in vegetables, seeds and microalgae oil.	28
Figure 1.10 - Overview of the main oleochemistry pathways for the elaboration of different PUF components.	29
Figure 1.11 - Overview of the transformation of main carbohydrates into different PUF components.	33
Figure 1.12 - Composition of lignocellulosic resources and classification of main polyphenols: tannins and lignins. Adapted from (Isikgor and Becer 2015).	35
Figure 1.13 - Overview of the transformation of lignins and tannins into PUF components.	37
Figure 1.14 - Overview of the transformation of wastes from industrial processes into PUF components.	39
Figure 1.15 - Overview of the transformation of products from biotechnology into the PUF component.	41
Figure 1.16 - Viscosity of polyol vs. the cell size for PUF. Compilation of data from literature (Fang et al. 2019; Hejna et al. 2018; Huo et al. 2019; Jiang et al. 2018; Kahlerras et al. 2020; Kurańska et al. 2020b; Luo and Li 2014; Ng et al. 2017; Paruzel et al. 2017; Pawar et al. 2016b; Piszczyk et al. 2014; Ugarte et al. 2015; Veronese et al. 2011; Yang et al. 2012, 2019; Zieleniewska et al. 2015).	45
Figure 1.17 - Effect of the gelling/blowing balance vs. temperature, viscosity and foam cell morphology in three typical cases: (A) mainly blowing, (B) equilibrium and (C) mainly gelling.	46
Figure 1.18 - (A) Effect of the introduction of lignin-based polyol on the density and compressive strength of PUF. (B) Dependence of the compressive strength on density. Reproduced with permission from (Li et al. 2016a) and (Thirumal et al. 2008).	50
Figure 1.19 - Effect of lignin addition on the compressive strength of R-PUF. The ratio of lignin to polyol, the molar ratio of the OH groups from lignin. Hardwood ethanol organosolv lignin (HEL) and hardwood kraft lignin (HKL). Reproduced with permission from (Pan and Saddler 2013).	51
Figure 1.20 - (A) Dependence of the heat conductivity on porosity modeled with cell size of 300 µm and filled with air (B) Thermal conductivity evolution over 900 days of PUF and PUF modified with 1.5% of talc. Reproduced with permission from (Ferkl et al. 2017) and (Santiago-Calvo et al. 2019).	54
Figure 1.21 - Dependence of the char residue (A), weight loss at 5% (B), 10% (C) and 50% (D) on the I_{OH} of the polyol. The straight line represents the general trend of the data compiled from the literature. Compilation	

LISTE DES ILLUSTRATIONS

of data from literature (Contreras et al. 2020; Fang et al. 2019; Hejna et al. 2018; Huo et al. 2019; Jiang et al. 2018; Kahlerras et al. 2020; Kurańska et al. 2020b; Li et al. 2020b; Luo and Li 2014; Ng et al. 2017; Paruzel et al. 2017; Pawar et al. 2016a; Piszczk et al. 2014; Ugarte et al. 2015; Veronese et al. 2011; Yang et al. 2012, 2019; Zieleniewska et al. 2015).....	56
Figure 1.22 - Effect of the amount of insoluble bark residue on the flammability of PUF. Reproduced with permission from (Ge et al. 2000).....	58
Figure 1.23 - Overview of the different factors affecting several properties (cell morphology, mechanical, thermal and fire resistance behaviors).....	59
Figure 1.24 - Overview of the main synthetic routes to NIPU.....	60

Chapitre 2

Figure 2.1 - Determination of the epoxide partial order. Representation of $\ln([Ep]_0/[Ep])$ as a function of time at 30 °C, 50 °C, and 70 °C.....	89
Figure 2.2 - Determination of the catalyst partial order. Representation of $\ln(k_{app_EtOH})$ as a function of $\ln(H^+)$ at 30, 50, and 70 °C.....	90
Figure 2.3 - Determination of the sum of the ethanol and catalyst partial order. Representation of $\ln(k_{app_EtOH})$ as a function of $\ln(1/V_t)$ at 70 °C with 12 wt% catalyst loading.....	91
Figure 2.4 - Determination of the [NCO] partial order. Variation of $\ln([NCO]_0/[NCO])$ in function of time at 42 °C, 53 °C, 62 °C, and 74 °C.	94
Figure 2.5 - Determination of hydroxyl partial order. Linear regression of $\ln(k_{app_U})$ as a function of $\ln([OH])$..	94
Figure 2.6 - Reactivity comparison in urethane formation at 50 °C in dry toluene under inert atmosphere with EVHOSO-AA of different isocyanate structure: aromatic, aliphatic, and cyclo-aliphatic.	96
Figure 2.7 - Tautomer conformation of phenyl isocyanate.	96
Figure 2.8 - NMR Spectrum of the initial epoxidized fatty methyl ester (A) and after the RO with acetic acid (B), ethanol (C), hydrobromic acid (D), hydrochloric acid (E), and diethylamine (F).	97
Figure 2.9 - Reactivity comparison in urethane formation with phenyl isocyanate with different RO FAMEVHOSO: EVHOSO-HBr, EVHOSO-HCl, EVHOSO-AA, EVHOSO-EtOH, and EVHOSO-DEA.	98
Figure 2.10 - Electron releasing effect by mesomeric effect.....	98
Figure S2.11 - 1H NMR Spectra of the FAMEVHOSO unsaturated.....	102
Figure S2.12 - 1H NMR spectra of epoxidized FAMEVHOSO.....	102
Figure S2.13 - NMR analysis of epoxidized FAMEVHOSO (T_0) and the oil after 15, 35, 60, 120, 180, 240 and 300 min. of reaction at 90 °C with acetic acid.....	103
Figure S2.14 - Determination of the epoxide partial order. Representation of $\ln([Ep]_0/[Ep])$ as a function of time at 70 °C, 90 °C and 110 °C.....	104
Figure S2.15 - Determination of the k_{app_AA} with 8.6 mol/L, 12.8 mol/L and 16.6 mol/L of acetic acid.	105
Figure S2.16 - Determination of the acetic acid partial order. Representation of $\ln(k_{app_AA})$ as a function of $\ln([AA])$	106
Figure S2.17 - Determination of E_{A_AA} by plotting the $\ln(k_{AA})$ as a function of the inverse of the temperature.	106
Figure S2.18 - Correlation between the mass of Amberlyst® 15H and the proton quantity.....	107
Figure S2.19 - Arrhenius law for the RO of FAMEVHOSO with ethanol at 4, 12 and 20 wt% of catalyst loading.	108
Figure S2.20 - Representation of the gap between theoretical and experimental dosage of the NCO concentration.	108
Figure S2.21 - Determination of the k_{app_U} . Variation of $\ln([NCO]_0/[NCO])$ in function of time at 1.24, 1.51, 1.73, 1.98, 0.51 and 0.72 mol/L.	109
Figure S2.22 - Application of the Arrhenius equation to determine the temperature dependency of reaction rate for the urethane formation and the RO with ethanol.	109

Figure S2.23 - Conversion as a function of time for the reaction between phenyl isocyanate and VHOSO-AA, Hexyl isocyanate and VHOSO-AA and Hexyl isocyanate and VHOSO-DEA 110

Chapitre 3

Figure 3.1 - ^1H NMR spectrum of MAO.....	122
Figure 3.2 - Size exclusion chromatogram of EMAO-HCl, EMAO-DEA, EMAO-AA, EMAO-EtOH, EMAO and MAO.....	126
Figure 3.3 - Characteristic times of the different foams. The y-axis was broken since the gel time and tack-free time of ESO-DEAcat surpass 600 s and 1200 s, respectively.	129
Figure 3.4 - Expansion rates (mm/s) determined with Foamat device for DEA25, Ref, EtOH25, HCl25 and AA25.	130
Figure 3.5 - Feret diameters and aspect ratio in the longitudinal (A) and transversal (B) direction.	131
Figure 3.6 - SEM images of all formulations in the transverse direction (Scale = 500 microns).....	132
Figure 3.7 - Results of the flammability test for Ref, EtOH25, EtOH50, AA25 and HCl25 foams	135
Figure S3.8 - Infrared spectrum of MAO.....	142
Figure S3.9 - Proton NMR spectrum of EMAO.	143
Figure S3.10 - ^{31}P NMR analysis for hydroxyl titration of (A) EMAO-AA, (B) EMAO-EtOH, (C) EMAO-DEA and (D) EMAO-HCl.	145
Figure S3.11 - FTIR spectra of EMAO, EMAO-HCl, EMAO-AA, EMAO-EtOH and EMAO-DEA.	146
Figure S3.12 - Stacked proton NMR spectra of polyols from EMAO.	146
Figure S3.13 - Stacked proton NMR spectra of polyols from EMAO (zoom from 4.5 to 2.5 ppm).	147
Figure S3.14 - DSC thermogram of MAO.	147
Figure S3.15 - DSC thermogram of EMAO.....	148
Figure S3.16 - DSC thermogram of EMAO-AA.....	148
Figure S3.17 - DSC thermogram of EMAO-EtOH.	149
Figure S3.18 - DSC thermogram of EMAO-DEA.	149
Figure S3.19 - DSC thermogram of EMAO-HCl.	150
Figure S3.20 - Evolution of the viscosity with temperature of EMAO, EMAO-EtOH, EMAO-AA, EMAO-HCl, EMAO-DEA and ESO-DEA.	150
Figure S3.21 - TGA thermogram of MAO.....	151
Figure S3.22 - TGA thermogram of EMAO.	151
Figure S3.23 - TGA thermogram of EMAO-AA.	152
Figure S3.24 - TGA thermogram of EMAO-EtOH.....	152
Figure S3.25 - TGA thermogram of EMAO-DEA.	153
Figure S3.26 - TGA thermogram of EMAO-HCl.	153
Figure S3.27 - Expansion rate (mm/s) determined with the Foamat device for Ref, EtOH35, EtOH50, EtOH75, ESO-DEAcat.	154
Figure S3.28 - SEM images of all formulations in the longitudinal direction.....	155
Figure S3.29 - Representation of cell size modeled by a central binomial distribution.	155
Figure S3.30 - Temperature at the center of the foam recorded with the Foamat device of EtOH 35, EtOH50, EtOH75, Ref and ESO-DEAcat foams.	156
Figure S3.31 - Temperature at the centre of the foam recorded with the Foamat device of EtOH25, Ref, AA25, DEA25, HCl25 foams.....	156
Figure S3.32 - Proton NMR spectrum of ESO (A) and ESO-DEA (B).	158
Figure S3.33 - Size exclusion chromatography of ESO and ESO-DEA.	159
Figure S3.34 - TGA of Ref, AA25, HCl25, EtOH25 and EtOH50 foams under nitrogen.	160

LISTE DES ILLUSTRATIONS

Figure S3.35 - FTIR spectra in absorbance mode of Ref, AA25, HCl25, EtOH25, EtOH50 foams..... 161

Chapitre 4

Figure 4.1 - Chemical analysis of F1-Ref, F1-25AO, F1-EAO and P2H-EG by FTIR (A) and ^1H NMR (B)....	174
Figure 4.2 - Chemical analysis of F2-Ref, F2-25AO, F2-EAO and Pht-DEG by FTIR (A) and ^1H NMR (B)....	175
Figure 4.3 - Chemical analysis: (A) FTIR spectra of F3-Ref, F3-25AO, F3-EAO and (B) ^1H NMR spectra of F3-Ref, F3-25AO, F3-EAO and EAO-oil.....	177
Figure 4.4 - ^1H NMR spectra of (A) P2H-EG, F-OPG, F-PAO and F-PRO and (B) F-EAO, EAO-oil, F-PAO and PAO-oil	179
Figure 4.5 - FTIR spectra of DGEBA alone and the main fractions after DGEBA reaction with and without catalysts.....	182
Figure 4.6 - Chemical analysis: (A) FTIR spectra of Mundex alone and the main fractions of Mundex reaction with and without catalysts (B) ^1H NMR spectra of Mundex alone and the main fractions of Mundex reaction with and without catalysts.....	183
Figure 4.7 - (A) FTIR spectra of EVHOSO alone and the main fractions of Mundex reaction, with and without catalysts. (B) ^1H NMR spectra of EVHOSO alone and the main fractions of Mundex reaction, with and without catalysts.....	184
Figure S4.8 - Pictures of PUF realized with increasing content of ESO at then end of the rise. The pictures were adjusted to have an equivalent scale.....	189
Figure S4.9 - The identified fraction of soluble content of PIR ref, 25AO and 25 EAO foams.	189
Figure S4.10 - FTIR spectra of F-OPG, F-EAO, F-ERO, F-PAO and F-PRO.....	190
Figure S4.11 - FTIR spectra of OPG, EAO, ERO, PAO and PRO.....	190
Figure S4.12 - ^1H NMR spectra of undecylenic acid, Mund and Mundex.....	191
Figure S4.13 - ^1H NMR spectra of DGEBA and the main fraction of DGEBA reaction without catalyst and with BDMA, KOAc, TBAB, AlCl_3 or $\text{Al}(\text{salen})_2$	192
Figure S4.14 - ^{13}C NMR of Mundex- AlCl_3	193
Figure S4.15 - ^1H NMR spectrum of EVHOSO- $\text{Al}(\text{salen})_2$	193
Figure S4.16 - ^{13}C NMR Composite Programmed Decoupling (CPD) spectrum of EVHOSO- $\text{Al}(\text{salen})_2$	194
Figure S4.17 - ^{13}C Attached Proton test (APT) NMR spectrum of EVHOSO- $\text{Al}(\text{salen})_2$	194
Figure S4.18 - Heteronuclear Single Quantum Correlation (HSQC) NMR spectrum of EVHOSO- $\text{Al}(\text{salen})_2$..	195
Figure S4.19 - Heteronuclear Multiple Bond Correlation (HMBC) NMR spectrum of EVHOSO- $\text{Al}(\text{salen})_2$...	195

Chapitre 5

Figure 5.1 – Mutli-wave program presentation.....	205
Figure 5.2 - MEDA and BEDA conversions by reaction with 2-OHa at 25 °C and followed by ^1H NMR.	207
Figure 5.3 - (A) Reactional mechanisms: potential pathways for the chemical reaction between 2-OHa and MEDA (B) Assigned stacked ^{13}C NMR spectra of the reaction at different times in the 32-68 ppm region.	209
Figure 5.4 - ^1H NMR spectra of itaconic acid, anhydride itaconic, Iet, Ietgl and Deti. For clarity's sake, the x-axis was broken once (from 7.75 to 12 ppm) to show a potential carboxylic acid signal at around 12.5 ppm.	211
Figure 5.5 - Conversion of the double bond via the aza-Michael reaction between OA and 2OHa, Ietgl or Deti.	212
Figure 5.6 - Tan Δ , G' and G'' at 0.5, 1, 3 and 5 Hz resulting from the multi-waves method applied on EOOa and DMEDA polyaddition. Presentation of the different gel points.	215
Figure 5.7 - Gel times of aza-Michael thermosets. From left to right: ESOa_DMEDA, EOOa_DMEDA and ESO_Iet_DMEDA.....	216

Figure 5.8 - (A) Gel times of ESOa with DMEDA with 0.1 mol% of different catalysts. (B) Gel times linked to the reaction between ESOa and DAP, DETA, TEPA, DIFFA and mXDA, with the NH ₂ considered as monofunctional and difunctional.....	217
Figure 5.9 - T _g determined by DSC of the thermosets obtained by Michael addition of ESOa with different amines structures and stoichiometries.....	219
Figure 5.10 - TGA and DTG results of (A) ESOa_DMEDA, EOOa_DMEDA and ESO_Iet_DMEDA and (B) DAP2 and DAP4.....	220
Figure S5.11 - ¹³ C NMR kinetic study of the reaction between MEDA and 2-OHa. A: The reaction path with the assignation of the different carbon. B: Full ¹³ C spectra at different reaction times.....	225
Figure S5.12 - (A) The reaction path with the assignation of the different carbon. (B) Full-scale stacked ¹³ C NMR spectra of the reaction at different times. (C) Assigned stacked ¹³ C NMR spectra of the reaction at different times in the 22-48 ppm region.....	226
Figure S5.13 - ¹ H NMR spectrum of Iet.....	227
Figure S5.14 - ¹ H NMR spectrum of Ietgl.....	227
Figure S5.15 - ¹³ C NMR Composite Programmed Decoupling (CPD) spectrum of Ietgl.....	228
Figure S5.16 - ¹³ C Attached Proton test (APT) NMR spectrum of Ietgl.....	228
Figure S5.17 - Correlation spectroscopy (COSY) NMR spectrum of Ietgl.....	229
Figure S5.18 - Heteronuclear Single Quantum Correlation (HSQC) NMR spectrum of Ietgl.....	229
Figure S5.19 - Heteronuclear Multiple Bond Correlation (HMBC) NMR spectrum of Ietgl.....	230
Figure S5.20 - ¹ H NMR spectrum of Deti.....	230
Figure S5.21 - ¹³ C Composite Programmed Decoupling (CPD) NMR spectrum of Deti.....	231
Figure S5.22 - ¹³ C Attached Proton test (APT) NMR spectrum of Deti.....	231
Figure S5.23 - Correlation spectroscopy (COSY) NMR spectrum of Deti.....	232
Figure S5.24 - Heteronuclear Single Quantum Correlation (HSQC) NMR spectrum of Deti.....	232
Figure S5.25 - Heteronuclear Multiple Bond Correlation (HMBC) NMR spectrum of Deti.....	233
Figure S5.26 - ¹³ C NMR kinetic study of the reaction between OA and 2-OHa. (A) The reaction path with the assignation of the different carbon. (B) Full-scale stacked ¹³ C NMR spectra of the reaction at different times. (C) Assigned stacked ¹³ C NMR spectra of the reaction at different times in the 22-68 ppm region.....	234
Figure S5.27 - ¹³ C NMR kinetic study of the reaction between OA and Deti. (A) The reaction path with the assignation of the different carbon. (B) Full-scale stacked ¹³ C NMR spectra of the reaction at different times. (C) Assigned stacked ¹³ C NMR spectra of the reaction at different times in the 24-70 ppm region.....	235
Figure S5.28 - ¹³ C NMR kinetic study of the reaction between OA and Ietgl. (A) The reaction path with the assignation of the different carbon. (B) Full-scale stacked ¹³ C NMR spectra of the reaction at different times. (C) Assigned stacked ¹³ C NMR spectra of the reaction at different times in the 24-70 ppm region.....	236
Figure S5.29 - SEC analysis based on PS equivalent molar mass of ESO, ESOa and ESO_Iet with toluene as flow marker.....	237
Figure S5.30 - SEC analysis based on PS equivalent molar mass of Olive oil, EOO and EOOa with toluene as flow marker.....	237
Figure S5.31 - ESOa functionality determination by measurement of the storage and loss modulus with frequency sweep experiments for different stoichiometry.....	239
Figure S5.32 - EOOa functionality determination by measurement of the storage and loss modulus with frequency sweep experiments for different stoichiometry.....	240
Figure S5.33 - ESO_Iet functionality determination by measurement of the storage and loss modulus with frequency sweep experiments for different stoichiometry.....	240

LISTE DES ILLUSTRATIONS

Figure S5.34 - Crystallization and fusion temperatures of the Michael donor synthesized by ring-opening of epoxidized oil.	241
Figure S5.35 - TGA and DTG results of ESOa, EOOa and ESO_Iet.	241
Figure S5.36 – Detailed ¹ H NMR spectra of DIFFA.	242
Figure S5.37 - Examples of gel time determination of (A) ESOa-DMEDA, (B) EOOa-DMEDA and (C) ESO_Iet_DMEDA.	242

Tableaux

Chapitre 1

Table 1.1 - General foam formulation with quantities expressed in part by weight of the polyol.	16
Table 1.2 - Relative reactivity of isocyanates with alcohol groups for the 1 st and the 2 nd additions. Adapted from (Szycher 2013).....	18
Table 1.3 - Main requirements on polyols properties for F-PUF and R-PUF. Adapted from (Furtwengler and Avérous 2018; Ionescu 2005).....	19
Table 1.4 - Relative reactivity of hydrogen active compounds without catalyst. Adapted from (Ionescu 2005)..	20
Table 1.5 - BA structures, name physical properties and global warming potential (GWP). Data from literature (Bobbo et al. 2018; Gil and Kasperski 2018; Lai 2014; Mateu-Royo et al. 2019; Rapra 2014; Singh 2002; Yaws 2009, 1995).....	21

Chapitre 2

Table 2.1 - Thermodynamics data of the epoxidized Fatty Acid Methyl Ester of Very High Oleic Sunflower Oil (EVHOSO) ring-opening reaction with acetic acid and ethanol.....	92
Table 2.2 - Thermodynamics data of urethane formation by the reaction between phenyl isocyanate and EVHOSO with acetic acid (EVHOSO-AA).	95
Table S2.3 - Lipid profile. Fatty acids distribution in unsaturated FAMEVHOSO.	101
Table S2.4 - k_{app_EtOH} (min ⁻¹) with 30, 50 and 70 °C and 4, 12 and 20 wt% of amberlyst.....	107

Chapitre 3

Table 3.1 - Characteristics of the different polyols: fossil-based, MAO and their derivates.	124
Table 3.2 - Formulation in parts of the total polyol content of the different PUF studied systems.....	128
Table 3.3 - Formulation in parts of the total polyol content of the fossil-based reference (Ref) and the catalyst-free foam (ESO-DEAcat).	133
Table 3.4 - Thermal conductivity, closed-cell content and compression strength for Ref, AA25, HCl25, EtOH25 and EtOH50 foam.	136
Table 3.5 - Dimensional variation of Ref, AA25, HCl25, EtOH25 and EtOH50 foams in both environments (cold or warm & humid).	137
Table S3.6 - Fatty acid profile of MAO.	142
Table S3.7 - Repartition of the different chemical moieties in the EMAO.	143
Table S3.8 - Cream, gel and tack-free times and final height for the different foams.	154
Table S3.9 - Density of the different foams.	157
Table S3.10 - Calculation of the real I_{OH} index results and conversions.....	159
Table S3.11 - TGA and DTG data for Ref, AA25, HCl25, EtOH25 and EtOH50 foam.	160

Chapitre 4

Table 4.1 - PUF Formulations with increasing ESO content.	168
Table 4.2 - Formulations of recently synthesized PUF.	169
Table 4.3 - Formulations of formerly synthesized PUF. (Arbenz et al. 2017)	170
Table 4.4 - Major fractions identified with the different catalysts and epoxide systems.	185

LISTE DES ILLUSTRATIONS

Table S4.5 - Weight fraction of products separated by chromatography column of the DGEBA reactions.	191
Table S4.6 - Weight fraction of products separated by chromatography column of the Mundex reactions.	192
Table S4.7 - Weight fraction of products separated by chromatography column of the EVHOSO reactions....	192

Chapitre 5

Table 5.1 - Properties of Michael acceptors synthesized from epoxidized oils.	214
Table S5.2 - Temperature of first and second maximum degradation for the Michael donors and the materials realized with DMEDA.....	243
Table S5.3 - Temperature of first and second maximum degradation for materials realized with ESOa and different amines and stoichiometries.....	243

Schémas

Chapitre 1

Scheme 1.1 - The first synthesis of carbamate by Charles Adolf Wurtz. Adapted from (Wurtz 1846).	14
Scheme 1.2 - Metathesis and cyclization reactions.	30
Scheme 1.3 - Isosorbide production pathway from sorbitol.	34
Scheme 1.4 - Synthesis of diisocyanate from β -pinene. Adapted from (Kobilka et al. 2019).	43

Chapitre 2

Scheme 2.1 - General mechanism of an acidic catalyzed nucleophile ring-opening.	87
--	----

Chapitre 3

Scheme 3.1 - Side reactions occurring during polyol synthesis.	125
Scheme S3.2 - Possible reaction of epoxide ring-opening by phospholane reagent.	146

Chapitre 4

Scheme 4.1 - Oxazolidone group synthesis from epoxide and isocyanate.	166
Scheme 4.2 - Reaction between phenyl isocyanate and epoxide groups from different resources to form an oxazolidone group assisted by different catalysts, as a global model system.	180

Chapitre 5

Scheme 5.1 - Michael addition general scope and the particular case of the aza-Michael addition.	200
Scheme 5.2 - Aza-Michael reaction with secondary and primary amines.	206
Scheme 5.3 - Ring-opening of epoxidized oil with acrylic acid (A) or Iet (B).	207
Scheme 5.4 - Synthetic pathways from itaconic acid to Deti and Ietgl.	210

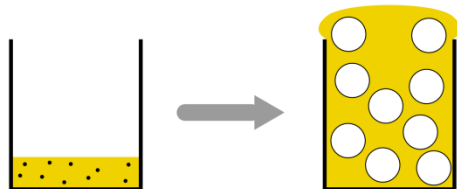
INTRODUCTION GÉNÉRALE

Les enjeux environnementaux actuels et la prise de conscience écologique collective combinés à l'accès de plus en plus limité à certaines fractions du pétrole poussent les entreprises à mettre sur le marché des produits ayant une empreinte écologique neutre, du choix des matières premières jusqu'à leurs fins de vie. Dans ce contexte, les domaines des matériaux et de la chimie évoluent afin de répondre aux nouvelles attentes sociétales et écologiques. Une chimie verte, en plein essor dans la dernière décennie est de plus en plus souvent développée. Elle se base sur 12 principes édités par les chimistes américains Paul Anastas et John C. Warner (Anastas and Warner 2000) en 1998 telles que l'utilisation de ressources renouvelables (7^{ème} principe), l'économie d'atomes (2^{ème} principe), la conception de produits chimiques plus sûr via des méthodes de synthèse moins dangereuses (3^{ème} et 4^{ème} principes) ou encore la réduction du nombre de dérivés (8^{ème} principe).

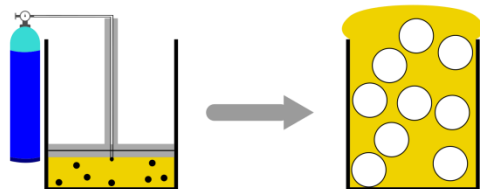
Les polymères, communément appelés plastiques, sont obtenus par multiple union de réactifs (monomères). Les macromolécules résultantes sont caractérisées par de hautes masses molaires et de multiples unités répétitives. Les propriétés finales des polymères peuvent être maîtrisées-contrôlées au travers de différents paramètres tels que de la structure des monomères, la séquence d'incorporation des monomères, le type de polymérisation, l'architecture macromoléculaire ainsi que la mise en œuvre et la formulation (Mülhaupt 2013). De nos jours, la production mondiale de matières plastiques avoisine les 360 millions de tonnes en 2019 (Plastics Europe 2019) mais elle est majoritairement issue de ressources fossiles. D'autre part, la fin de vie des plastiques apparaît comme étant problématique car mal maîtrisée, notamment avec l'exemple des microplastiques dans les océans (Cozar et al. 2014). Les polymères sont donc de moins en moins bien acceptés, comme en témoigne l'interdiction récente en France de certains produits plastiques à usage unique et une certaine tendance au dénigrement de ces matériaux, le « plastic-bashing ». Les matériaux polymères doivent être entièrement repensés afin de s'inscrire dans le cercle vertueux de l'économie circulaire avec une approche renouvelable. Ce chemin passe par une production à base de ressources renouvelables afin de produire des matériaux ayant des propriétés au moins équivalentes à leurs homologues d'origine fossile et une fin de vie et un coût maîtrisés.

Les matériaux alvéolaires ou moussettes sont formés d'une matrice polymère expansée à l'intérieur de laquelle sont situées des alvéoles (cellules) de gaz ouvertes ou fermées. Ces matériaux hautes performances sont mis en œuvre avec comme but d'alléger, amortir et/ou isoler et ceci avec des structures rigides à souples. Les différentes techniques de mise en œuvre de matériaux alvéolaires sont décrites sur la Figure 0.1. La première consiste à introduire dans une matrice polymère ou un mélange de monomère un liquide à faible température d'ébullition qui va changer d'état pendant la transformation. Selon un principe similaire, un composé peut par réaction ou décomposition dégager du gaz et expander un matériau formé ou en cours de polymérisation. Il s'agit dans ce cas d'expansion chimique. La seconde approche est basée sur l'expansion physique provoquée par la détente d'un gaz absorbé sous pression dans une matrice polymère. La troisième consiste à introduire de l'air par battage mécanique d'un latex ou d'une dispersion de polymère. La dernière technique repose sur la dissolution après mise en œuvre d'un ingrédient préalablement piégé dans la structure polymère (Biron 2003).

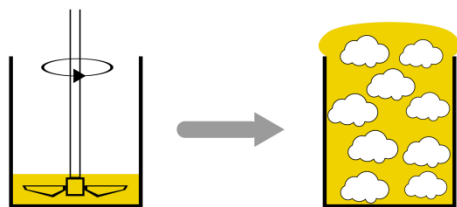
Expansion d'un ingrédient in-situ par réaction ou changement d'état



Dépressurisation d'un gaz absorbé à haute pression



Introduction d'air par battage mécanique



Dissolution d'un ingrédient après mise en œuvre

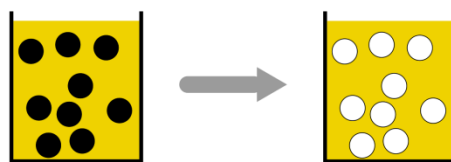


Figure 0.1 - Les techniques majeures de mise en œuvre de matériaux expansés.

Dans ce contexte, un projet de thèse intitulé « Développement de nouveaux matériaux polymères biosourcés alvéolaires à partir de synthons chimiques extrait de microalgues » a vu le jour au sein de l’Institut de Chimie et Procédés pour l’Energie, l’Environnement et la Santé (ICPEES – UMR CNRS 7515) dans l’équipe BioTeam dirigée par le Pr. Luc Avérous. Depuis deux décennies, cette équipe s’attache au développement de polymères biosourcés et/ou biodégradables pour l’environnement ou la santé.

Cette thèse s’inscrit dans le projet Trans’alg financé par la Banque Publique d’Investissement (BPI-France) dans le cadre du Programme d’investissements d’avenir (PIA). Ce projet a pour objectif de développer la production de microalgues afin de produire des molécules d’intérêts pour une chimie de commodité. Le consortium national « Trans’alg » impulsé par une PME spécialisée dans les biotechs et la culture de microalgues (Fermentalg), rassemble plusieurs partenaires industriels (Pierre Guérin, Seppic et SOPREMA) et académiques (CEA et CNRS). La Figure 0.2 permet de situer cette thèse par rapport aux différents acteurs du projet Trans’alg. Fermentalg produit l’huile de microalgues (triglycerides) et SOPREMA, leader mondial de solutions d’étanchéité et acteur majeur dans le secteur du bâtiment, valorise les matériaux alvéolaires développés. Cette thèse s’inscrit également dans le cadre de Mutaxio. Un laboratoire commun de recherche créé entre la BioTeam et SOPREMA en 2017 afin de développer de nouveaux matériaux biosourcés pour l’industrie du bâtiment. Il est à noter que SOPREMA n’a pas imposé de cahiers des charges pour ce travail.

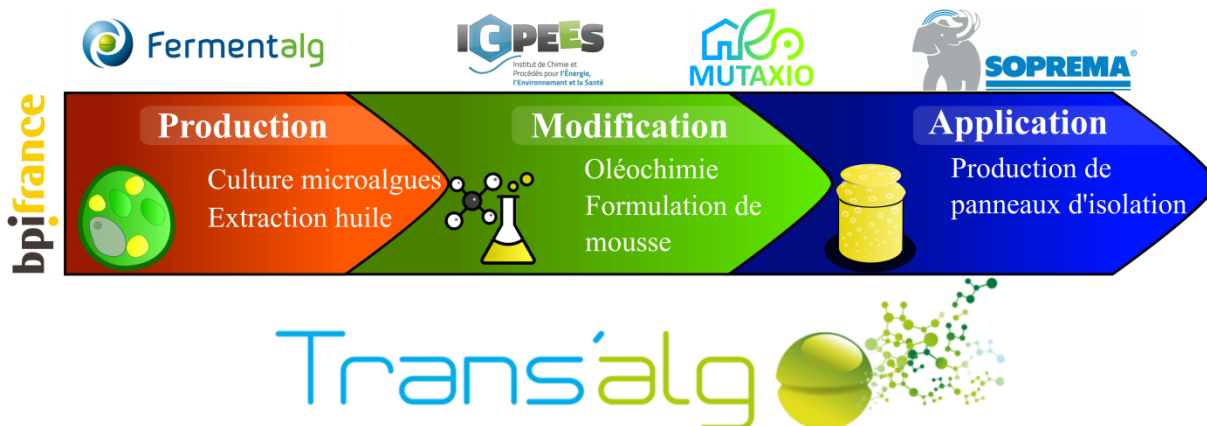


Figure 0.2 - Le projet thèse dans le cadre du consortium Trans'alg.

Au travers de différentes thèses, notamment, l'équipe BioTeam a développé de nombreux matériaux dans le domaine des polyuréthanes biosourcés issus de différentes biomasses (Furtwengler et al. 2017; Hablot et al. 2008; Laurichesse et al. 2014). Récemment l'expertise de la BioTeam dans le domaine des polyuréthanes s'est étendue aux matériaux alvéolaires au travers de différents projets. La synthèse de mousses à partir de tannins modifiés (Arbenz et al. 2016) est la genèse du développement de mousses polyuréthanes biosourcées au sein de l'équipe. Dans ce même projet, une preuve de concept a été établie concernant la formation de monomères adaptés à l'élaboration de mousses polyuréthanes à partir d'huile de microalgues (Arbenz et al. 2017). La présente thèse s'inscrit dans la continuité de ce projet.

Les huiles d'origines végétales ou animales sont depuis longtemps chimiquement transformées en produits du quotidien notamment dans un contexte d'oléochimie. La première transformation répertoriée est une saponification pour la création de savon dans les années 800 en Allemagne (List et al. 2017). La recherche sur les huiles a permis de caractériser leurs structures. Les huiles végétales sont principalement composées de triglycérides dont la structure est présentée en Figure 0.3. Ils sont composés d'une molécule de glycérol estérifiée par des acides gras qui peuvent être saturés, mono-insaturés ou poly-insaturés. Ces acides gras, possèdent également des longueurs de chaîne variables (jusqu'à 22 carbones) associés à la présence de groupes époxydes ou hydroxyles. La forme la plus couramment rencontré parmi les huiles végétales sont des acides gras de 16-18 carbones avec au maximum 3 insaturations.

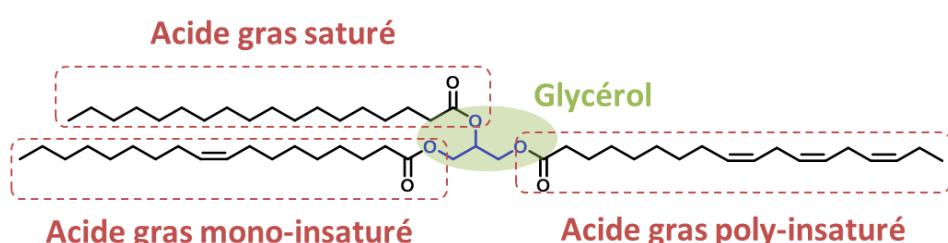


Figure 0.3 - Structure d'un triglycéride, composant majeur des huiles.

L'huile de microalgues étudiée au cours de cette thèse est aussi composée de triglycérides (Figure 0.3). Cependant, les acides gras qui les composent sont majoritairement plus longs (jusqu'à 22

INTRODUCTION GÉNÉRALE

carbones) et contiennent plus d'insaturations (jusqu'à 6). Les microalgues, outre la synthèse d'acides gras particuliers, présentent plusieurs avantages par rapport aux végétaux cultivés pour leur huile. Ces micro-organismes peuvent être cultivés dans les eaux douces, salées ou grises en consommant du CO₂. Par ailleurs, contrairement à certaines huiles végétales, l'utilisation de l'huile de microalgues comme synthons, ne génère pas de concurrence avec l'alimentation et ne mobilise pas des surfaces de terres arables. En outre, les microalgues présentent un faible coût de production et une haute productivité. Cette biomasse a également la particularité d'être entièrement valorisée, ce qui en fait une ressource renouvelable d'avenir. Les lipides, saccharides, protéines ou minéraux sont transformés en monomères, pigments, produits chimiques de bases ou à hautes valeurs ajoutées. La transformation chimique des lipides par oléochimie permet l'obtention de synthons importants pour l'industrie des matières plastiques et plus particulièrement des polyuréthanes.

Le groupement uréthane fut découvert en 1846 par Charles Adolf Wurtz. Ce fût ensuite Otto de Bayer qui en 1937 synthétisa les polyuréthanes par polyaddition entre un diisocyanate et un polyhydroxyl (Figure 0.4), autrement appelé polyol. Au fil des années, cette famille de polymères s'est installée dans notre quotidien. A tel point que, les polyuréthanes sont classés 6^{ème} famille de polymères la plus produite avec une production approchant les 22 millions de tonnes et un marché de 50 milliards de dollars en 2016. Les polyuréthanes peuvent s'adapter à de très nombreuses applications de par la richesse et la diversité des polyols et des polyisocyanates disponibles. Le marché des polyuréthanes représente cette diversité d'utilisation de ce matériau. Il est inégalement divisé en cinq parts : les mousses (65% du marché), les revêtements (13%), les élastomères (12%), les adhésifs (7%) ainsi que les autres applications incluant le domaine du biomédical (3%).

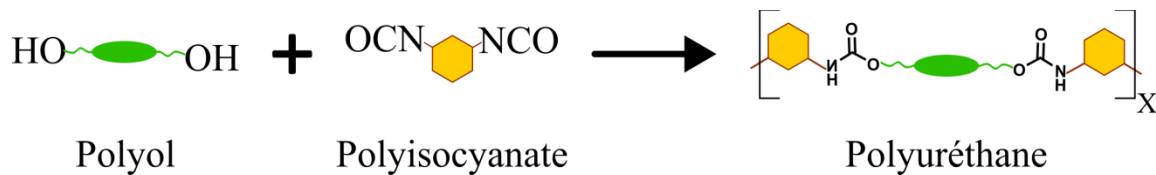


Figure 0.4 - Formation d'un polyuréthane.

Parmi les mousses, deux sous-catégories peuvent être identifiées : les mousses souples utilisées dans le domaine de la literie, de l'automobile ou du transport et les mousses rigides produites pour l'industrie du bâtiment, du transport climatisé ou des appareils électroménagers. Ces mousses se différencient au niveau de leurs propriétés, leurs morphologies et leurs architectures macromoléculaires. Les mousses rigides sont résistantes à la compression et isolantes d'un point de vue thermique. Ceci est dû à la présence de cellules fermées et d'un réseau polymère densément réticulé. Les mousses souples sont au contraire flexibles et élastiques. Les cellules ouvertes et l'élastomère qui les entoure permettent d'atteindre ces propriétés. Les mousses polyuréthanes sont généralement élaborées à partir de cinq composés indispensables, classés par ordre d'importance en masse : un polyisocyanate, un polyol, un agent gonflant, un catalyseur et un surfactant. Selon le type de mousses produites, la formulation peut être ajustée avec des additifs tels que des retardateurs de flamme, colorants ou des charges pour répondre à des cahiers des charges particuliers.

Les mousses polyuréthanes sont thermodurcissables et formées par une méthode appelée « one-shot ». Les composés excepté le polyisocyanate sont mélangés afin de former une émulsion. Le début de la mise en œuvre est marqué par l'introduction du dernier élément : le polyisocyanate.

L'expansion et la formation du réseau polymère doivent être coordonnées afin de former un matériau alvéolaire avec les propriétés souhaitées. Ainsi, chaque composé a un rôle précis, le polyisocyanate et le polyol forment le réseau polymère et donc la structure solide du matériau, l'agent gonflant permet l'expansion de la mousse. Dans le cas des matériaux polyuréthanes, il peut être chimique et réagir au contact d'un autre ingrédient de la formulation pour former du gaz ou physique et s'évaporer avec l'augmentation de la température dans le matériau généré par la polymérisation. L'équilibre entre l'expansion et la solidification du réseau, essentiel lors de la mise en œuvre des mousse, est contrôlé par des catalyseurs. Les surfactants ont deux rôles distincts : (i) ils permettent le mélange intime des différents composants au début de la mise en œuvre, et (ii) Ils assurent également un soutien des parois cellulaires les plus faibles lors de l'expansion du gaz.

L'objectif de cette thèse est d'élaborer des synthons pour la formation de matériaux alvéolaires. L'organisation des différents chapitres est présentée dans la Figure 0.5.

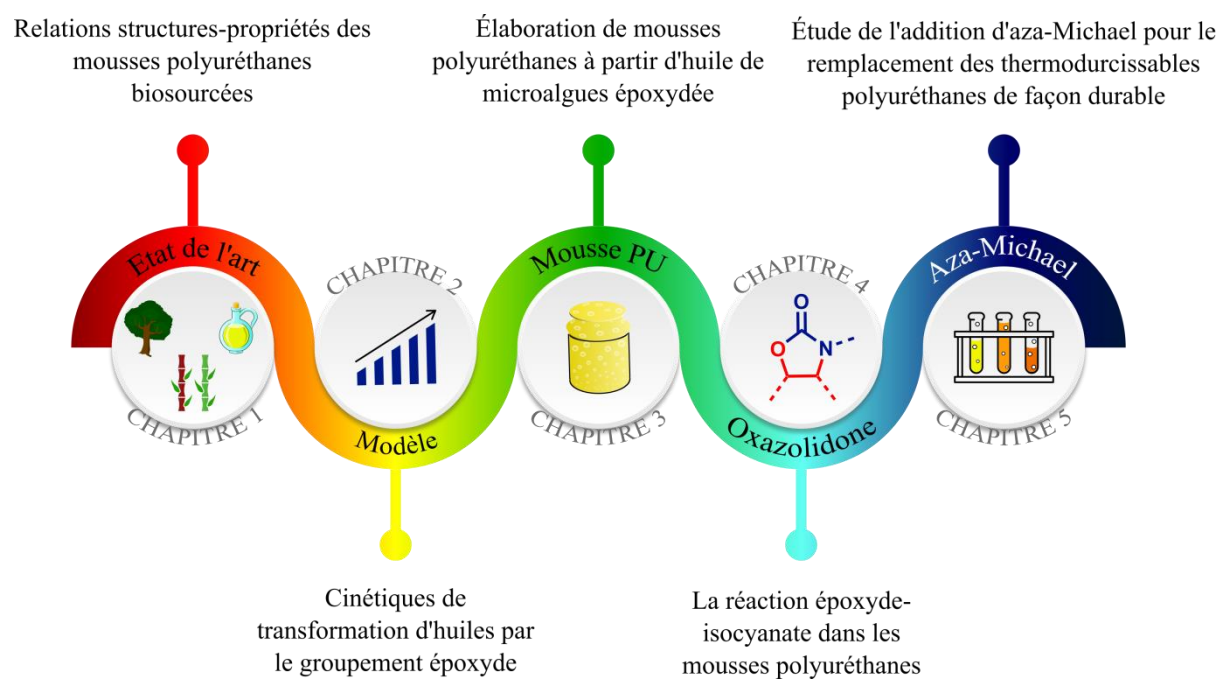


Figure 0.5 - Schéma récapitulatif des différentes phases de la thèse.

Le premier chapitre fait l'état de l'art concernant les relations « structures-propriétés » pour les mousse polyuréthanes biosourcées. Les bases en chimie et physique concernant l'élaboration des mousse polyuréthanes sont exposées. Un tour d'horizon des différentes voies de synthèse des composés essentiels à l'élaboration d'une mousse polyuréthane est effectué. Les relations entre les structures des monomères et les propriétés des matériaux polyuréthanes alvéolaires sont détaillées. Ce chapitre a permis d'engager les différents chapitres expérimentaux qui suivent.

Le deuxième chapitre présente une étude modèle de synthèse de polyols à partir de lipides. Les triglycérides sont souvent transformés en polyols via époxydation et ouverture de cycle. Cette étude vise à établir les équations et courbes cinétiques régissant l'ouverture des époxydes avec un nucléophile. L'impact des nucléophiles utilisés pour l'ouverture de cycle sur la vitesse de réaction des hydroxyles avec un isocyanate est aussi évalué.

INTRODUCTION GÉNÉRALE

Le troisième chapitre concerne la formation et la caractérisation de mousses polyuréthanes à partir de polyols dérivés d'huile de microalgues. Les protocoles de synthèse développés dans le deuxième chapitre sur une huile modèle sont appliqués ensuite à l'huile de microalgues. Après caractérisation, les polyols formés sont ajoutés jusqu'à 75% en remplacement d'un polyol conventionnel. La caractérisation des mousses résultantes permet l'évaluation de l'impact des polyols biosourcés sur les propriétés des matériaux alvéolaires.

Le quatrième chapitre étudie la formation de groupements oxazolidones par réaction d'huiles époxydées avec des isocyanates dans le cadre de la formation de mousses polyuréthanes. L'impact du remplacement du polyol par une huile époxydée sur l'élaboration d'une mousse polyuréthane est tout d'abord étudié. Les composés, non liés par liaisons covalentes au réseau polymère de mousses polyuréthanes formulées avec une portion d'huile époxydée, sont extraits et analysés. Finalement, l'huile époxydée et le polyisocyanate utilisés dans les mousses sont modélisés pour étudier en détail la formation d'oxazolidone avec différents catalyseurs.

Enfin le cinquième chapitre est une ouverture sur de potentiels futurs travaux qui pourraient mener à l'élaboration de mousses biosourcées plus sûres pour la santé et plus respectueuses de l'environnement dans une approche de développement durable. Le remplacement du polyuréthane par des polymères issus d'une chimie d'aza-Michael est évalué au niveau de la vitesse de réaction. Sur un système modèle, la réactivité de différents monomères est étudiée afin de classer les différents groupements réactifs. Puis le temps de gel d'un réseau polymère est mesuré par une méthode rhéologique multi-ondes. La variation des donneurs et accepteurs de Michael, les catalyseurs ainsi que de la stoechiométrie sont autant de paramètres qui permettent de contrôler, moduler la formation de gels des systèmes étudiés.

Références

Anastas, P.T., Warner, J.C., 2000. Green chemistry: theory and practice, 1. paperback. ed. Oxford Univ. Press, Oxford.

Arbenz, A., Frache, A., Cuttica, F., Avérous, L., 2016. Advanced biobased and rigid foams, based on urethane-modified isocyanurate from oxypropylated gambier tannin polyol. *Polym. Degrad. Stab.* **132**, 62–68. <https://doi.org/10.1016/j.polymdegradstab.2016.03.035>

Arbenz, A., Perrin, R., Avérous, L., 2018. Elaboration and Properties of Innovative Biobased PUIR Foams from Microalgae. *J. Polym. Environ.* **26**, 254–262. <https://doi.org/10.1007/s10924-017-0948-y>

Biron, M., 2003a. Polymères alvéolaires Présentation et propriétés. *Tech. Ing. Appl. Plast.*

Biron, M., 2003b. Polymères alvéolaires Monographies et transformation. *Tech. Ing. Appl. Plast.*

Cozar, A., Echevarria, F., Gonzalez-Gordillo, J.I., Irigoien, X., Ubeda, B., Hernandez-Leon, S., Palma, A.T., Navarro, S., Garcia-de-Lomas, J., Ruiz, A., Fernandez-de-Puelles, M.L., Duarte, C.M., 2014. Plastic debris in the open ocean. *Proc. Natl. Acad. Sci.* **111**, 10239–10244. <https://doi.org/10.1073/pnas.1314705111>

Furtwengler, P., Perrin, R., Redl, A., Avérous, L., 2017. Synthesis and characterization of polyurethane foams derived of fully renewable polyester polyols from sorbitol. *Eur. Polym. J.* **97**, 319–327. <https://doi.org/10.1016/j.eurpolymj.2017.10.020>

Hablot, E., Zheng, D., Bouquey, M., Avérous, L., 2008. Polyurethanes Based on Castor Oil: Kinetics, Chemical, Mechanical and Thermal Properties. *Macromol. Mater. Eng.* **293**, 922–929. <https://doi.org/10.1002/mame.200800185>

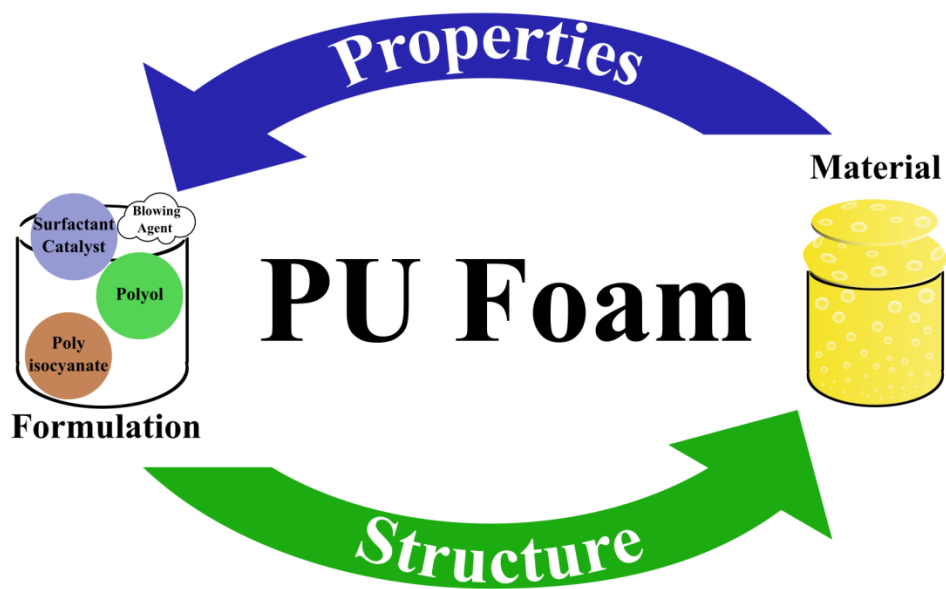
Laurichesse, S., Huillet, C., Avérous, L., 2014. Original polyols based on organosolv lignin and fatty acids: new bio-based building blocks for segmented polyurethane synthesis. *Green Chem.* **16**, 3958–3970. <https://doi.org/10.1039/C4GC00596A>

List, G.R., Kenar, J.A., Moser, B.R., 2017. History of Fatty Acids Chemistry. In 'Fatty Acids Chemistry, Synthesis, and Applications'. Elsevier, pp. 1–22. <https://doi.org/10.1016/B978-0-12-809521-8.00001-5>

Mülhaupt, R., 2013. Green Polymer Chemistry and Bio-based Plastics: Dreams and Reality. *Macromol. Chem. Phys.* **214**, 159–174. <https://doi.org/10.1002/macp.201200439>

Plastics Europe, 2019. Plastics-the Facts 2019.

CHAPITRE 1. RELATIONS STRUCTURES-PROPRIÉTÉS DANS LES MOUSSES POLYURÉTHANES BIOSOURCÉES



Introduction chapitre 1

La synthèse bibliographique présentée dans ce chapitre est consacrée aux relations « structures-propriétés » dans le domaine des mousses polyuréthanes biosourcées. Elle se présente sous la forme d'une revue intitulée « Structure-properties relationships of cellular materials from biobased polyurethane foams » soumise dans *Materials Science and Engineering - R: Reports*.

La première partie pose les bases dans la synthèse de mousses polyuréthanes et l'impact des différents constituants de la formulation sur la phase d'expansion. Les différentes ressources renouvelables et leurs modifications chimiques afin de produire des composés pour la synthèse des mousses polyuréthanes, sont ensuite décrites. Les relations entre les architectures macromoléculaires formées par l'utilisation de monomères biosourcés et les propriétés des mousses polyuréthanes sont analysées dans le cas spécifique des mousses rigides. Les structures des monomères sont mises en relation avec les propriétés morphologiques, mécaniques et thermiques des matériaux alvéolaires produits. Enfin, des perspectives dans le domaine mousses polyuréthanes sont abordées sous plusieurs angles : La synthèse de polyuréthanes sans isocyanate par aminolyse de carbonates cycliques afin de produire des mousses, et le développement de nouveaux matériaux avec la chimie de Michael et la formation de mousses à l'aide de micro-organismes.

Structure-properties relationships of cellular materials from biobased polyurethane foams

Julien Peyrton and Luc Avérous

Review submitted in *Materials Science and Engineering : R : Report*

1. ABSTRACT

The polyurethanes (PU) are a very versatile family of materials mainly obtained by combinations of polyols and polyisocyanates. Based on their annual worldwide production of around 20 million tons and a global market of \$50 billion (2016), PUs rank 6th among all polymers. Through their value chain, PUs involve different players: (i) the chemists producing most of PUs raw materials, (ii) the PUs producers from the raw materials, (iii) the compounders/assemblers who formulate PUs into their final products, and finally (iv) the end-users. Due to the multiplicity of their structures, PUs can be used in various forms and applications. Cellular materials are the largest part of this market (more than 60%) with segments including the furniture, automotive, bedding, insulation, building or construction markets. Two main types of foam can be fabricated: (i) flexible with open cells, stress and tensile properties, e.g., furniture or bedding, and (ii) rigid with closed cells, low thermal conductivity, low density and high dimensional stability mainly for thermal insulation, e.g., building industries. The formulation step significantly influences the microstructure or morphology of these cellular materials and impacts the final foam properties. Even if some partially biobased compounds (polyols) can be used, commercial PU cellular materials are till now mainly based on fossil resources. However, future materials will combine high performance with low environmental impact in order to fulfill societal expectations. In this way, new biobased compounds combining different fields such as biotech, chemistry, science and materials engineering are more and more used in complex formulations for renewable foams, leading to specific renewable macromolecular architectures.

This review aims to highlight the main biobased components (polyols, polyisocyanates and additives) used in formulations for PU foams, in relation to the corresponding fabrications, morphologies and properties. The main renewable sources come from (mono and poly)sugars, oleo-chemistry, polyphenols (lignins, tannins ...), or different compounds from white biotech processes from agro-wastes ... The impact of these different components on material performances is discussed more particularly for rigid polyurethane foams. The structure-property relationships are analyzed with a scope on cellular morphology, mechanical, thermal properties, fire resistance, and insulation behavior. Finally, an analysis focus on future perspectives on biobased PU foams is conducted.

2. INTRODUCTION

The depletion of some resources from fossil-based refineries, the degradation of the environment and its connection with the climate is at the core of every recent international forums. In 2015, the United Nations developed an agenda of action for people, planet, and prosperity regrouped in 17 establish goals. The “goal 12” entitled “Ensure sustainable consumption and production patterns” sets the sustainable management and efficient use of natural resources by 2030 (UN 2015). In this hot context, the development of new and/or greener polymer materials with higher performances and lower environmental impacts from cradle to cradle than the traditional fossil-based equivalent is a priority (Manzardo et al. 2019). This recent trend is also driven by the development of innovative molecular architectures with new properties, which can be extracted or bioproduced from various types of biomass combining different disciplines such as biotech, chemistry, science and materials engineering.

The global production of plastics reached around 360 million tons in 2018 (Plastics Europe 2019). The bioplastics, defined as biobased or biodegradable polymers, represent less than 1% of this worldwide plastics production ('Bioplastic materials' 2019; Garside 2020). Biobased polymers are defined as polymers obtained more or less directly from biomass, i.e., from all the living organisms, with a positive level of C¹⁴. The interest in biobased polymers knows an exponential growth in the last decades due to the desire to reduce the fossil-based products dependency (Babu et al. 2013) and the environmental impact. The production of biobased monomers for sustainable plastics was extensively developed to design common-like polymers such as polyamides (Winnacker and Rieger 2016), polyesters (Jiang and Loos 2016; de Jong et al. 2012), polyethylenes (Aeschelmann and Carus 2015) or polyurethanes (PUs) (Furtwengler and Avérous 2018). On the other hand, biodegradable plastics are defined as materials degraded into CO₂ or/and CH₄ and water mainly by the action of microorganisms (Iwata 2015) in normalized conditions (time, temperature, media). However, biodegradable polymers can also be produced from fossil-resource such as polycaprolactone. The development of biodegradable polymers is also linked to the vast and increasing problem of dispersion and accumulation of plastics in the environment. With the actual growth of microplastics accumulation in the ocean (Cozar et al. 2014) and global warming, the urge is to design sustainable polymeric materials.

Although PUs can be obtained without isocyanates (Non-Isocyanate Polyurethanes or NIPU) by, e.g., the reaction between polycyclocarbonates and polyamines (Carré et al. 2019), they are till now mostly obtained by polyaddition between polyisocyanates and polyols to obtain linear or crosslinked architectures. PU is the most versatile polymer family in terms of applications. This diversity originates from the myriad of chemical structures of the polyols and polyisocyanates and the particular property of the carbamate group. PUs rank 6th among all polymers with a production of around 22 million tons (Hicks and Austin 2017) and a global market of \$50 billion (2016). The PU market is usually segmented in 5 uneven parts with the foams (65% of the market), the coatings (13%), the elastomers (12%), the adhesives (7%) and the others, including the biomedical field (3%) (Akindoyo et al. 2016; Wendels and Avérous 2021). Two main types of PU foams (PUFs) can be identified: the flexible foam (F-PUF) with an open cell structure and the rigid (R-PUF) one with a closed-cell structure. Of course, intermediate systems can also be developed, e.g., the spray foams are rigid with open-cell structures. PUFs structures and properties can be tailored by (i) the structure and quantity of the monomers, (ii) the catalysts, (iii) the surfactants and (iv) the blowing agents (BA). To

this basic list, different other ingredients are also used, such as fillers, flame retardants (FR), pigments, or dyes.

F-PUFs representing the main part of the foams market (60%) are synthesized by molding or slabstock process (Randall and Lee 2002). As presented in Figure 1.1, PUFs are classified into several categories depending on their properties. The high resilience foams provide resilience and buoyancy compared to viscoelastic foams, which respond slower to stress. Integral skin foams are composed of a high-density skin and low-density core foam sandwich structure (Ashida 2007) obtained, e.g., by reaction injection molding (RIM). The foams formulation and processing are key points to obtain the required properties. The walls are melted after the cellular material synthesis to obtain very high consistency and controlled porosity for filter applications (Randall and Lee 2002). F-PUFs are used in various everyday life applications, such as filters, automotive and furniture/bedding cushioning (Figure 1.1).

The R-PUFs are classified into three categories (Figure 1.1) such as (i) the sprayed foams which are produced on-site with a high-pressure gun, (ii) the boardstocks are flat sheet products made with flexible facings and (iii) the sandwich panels encased by rigid facings (Randall and Lee 2002). The major R-PUFs are designed to be used as thermal insulation in appliances, construction, transport or pipe insulation. Despite the emergence of new materials with low thermal conductivity (Lang et al. 2016; Véjelis et al. 2010; Zhan et al. 2019), the R-PUF remains a major material used as thermal insulation due to their low thermal conductivity and density, compared to mineral wool, polystyrene or lignocellulose product (Abu-Jdayil et al. 2019). Thermal insulation is nowadays a major strategic field, e.g. in 2018, one third of the worldwide energy consumption was used for the heating or cooling of buildings (IEA 2020). In this context, the development of new sustainable materials with better properties than their fossil-based counterparts is an actual fascinating challenge. The most significant variables to get the best environmental performances of PUF were linked to the low thermal conductivity and density of the biobased PUFs (Manzardo et al. 2019).

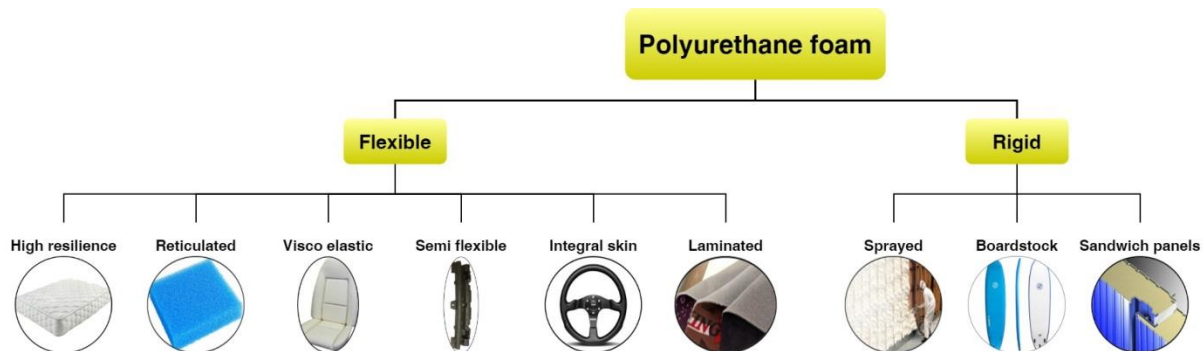


Figure 1.1 - Examples of F-PUF (left) and R-PUF (right) applications.

In the field of biobased PUs, different partial overviews can be found. Sustainable PUs were partially reviewed for adhesive applications (Tenorio-Alfonso et al. 2020) or foams (Agrawal et al. 2017; Furtwengler and Avérous 2018; Hayati et al. 2018). The goal of this review is to complement, update and expand these previous states of the art. This work is also expected to provide a deep insight into the biobased PUFs field, especially in the study and analysis of the “structure-properties” relationships. The second section of this review gives an overview of basic information to know about PUFs, such as the isocyanate chemistry, the process of foam and the role of each component in the

foam formation. The third section is focused on the renewable PUFs from biomass such as triglycerides, carbohydrates, polyphenols (lignins and tannins), wastes, and different molecules obtained by bioproduction as biobased building blocks for PUFs elaboration. The fourth section carefully reviews the relationships between these new biobased PU architectures, the cell morphology and the related properties such as the mechanical, thermal, fire resistance and acoustic behaviors. In the last section, very recent perspectives on the elaboration of foams from, e.g., NIPU, are analyzed and discussed.

3. PUF ENGINEERING AND FUNDAMENTALS

3.1. Isocyanate chemistry

The synthesis of urethane groups was first investigated in 1846 by Charles Adolf Wurtz (1817-1884) with the study of the reaction between the cyanogen chloride and ethanol described in Scheme 1.1 (Wurtz 1846). Otto Bayer was a scientist in charge of finding a substitute for the Nylon 6.6 recently developed by Dupont when he discovered the PU by polyaddition between a diisocyanate and a polyester diol in 1937. The first thermoplastic PU (TPU) had elastic properties and was industrially developed during the Second World War as a rubber substitute from hevea in the USA. The development of isocyanate production and their fast reaction with hydrogen-labile groups helped the tremendous development of the urethane market (Szycher 2013).



Scheme 1.1 - The first synthesis of carbamate by Charles Adolf Wurtz. Adapted from (Wurtz 1846).

Nowadays, the PU synthesis is still and mainly based on the polyaddition between polyisocyanates and polyols due to the high reactivity of the isocyanate groups with hydrogen-labile compounds, explained by the carbon electron deficiency. The isocyanate addition is a reversible reaction, exploited, for instance, to produce vitrimers called vinylous urethane (Denissen et al. 2015). However, the cyclization of the product or the generation of gas inhibits the reversibility. Figure 1.2 shows that the products of the isocyanate reactions can be classed according to the number of isocyanate additions (first, second and third) to yield it. The main PU synthesis results from the addition of isocyanate with an alcohol (A) yielding urethane group. This reaction is exothermic and releases 100 kJ/mol of heat (Ionescu 2005). Water has a similar reactivity as alcohol and, by reaction with isocyanate (B), produces unstable carbamic acid, which is instantaneously decomposed into CO₂ and amine (C). The water-isocyanate reaction releases almost two times more heat (197 kJ/mol) than the alcohol-isocyanate system. The gases released through the isocyanate additions are exploited to rapidly expand the polymer matrix for PUFs elaboration, mainly for soft foams with open cells. Analogously to the amine formation, the formation of amide by isocyanate and carboxylic acid addition (D) is accompanied by gaseous CO₂ formation. For instance, when formic acid is used as carboxylic acid, the reaction produces an amine, CO₂ and CO (E). Compared to the water-isocyanate addition, this particular reaction releases two moles of gas per mole of isocyanate. Furthermore, the

amine formed by water or formic acid addition also reacts with isocyanate to form a disubstituted urea group (F). The isocyanate can also react with compounds without labile-hydrogen, such as epoxides (G). In this case, the oxygen atom from the epoxide ring attacks the carbon of the isocyanate; therefore, the reaction is less favored and requires high temperatures and specific catalysts to yield oxazolidone.

The high reactivity of isocyanate enables the 2nd addition of isocyanate on the product resulting from a first addition. Both urethane and urea groups present labile hydrogens and can further react with isocyanate to synthesize allophanate (H) and biuret groups (I), respectively. Furthermore, isocyanate molecules can intermolecularly react and dimerize depending on the reaction conditions and catalysts into carbodiimide (J) or uretdione (K) (Fink 2018). Furthermore, the uretonimine group is irreversibly obtained after the third addition of isocyanate on carbodiimide (L). The combination of three isocyanate groups also leads to a stable and six-membered ring isocyanurate group. It was demonstrated that allophanate (M), biuret (N), oxazolidone (O) and uretdione (P) are intermediates in the synthetic pathway to isocyanurate (Al Nabulsi et al. 2018; Caille et al. 1990a; Gibb and Goodman 2013; Hoffman 1984). The polymerization of isocyanates with an appropriate catalyst was used to produce rigid foam exclusively composed of polyisocyanurate (PIR) network.

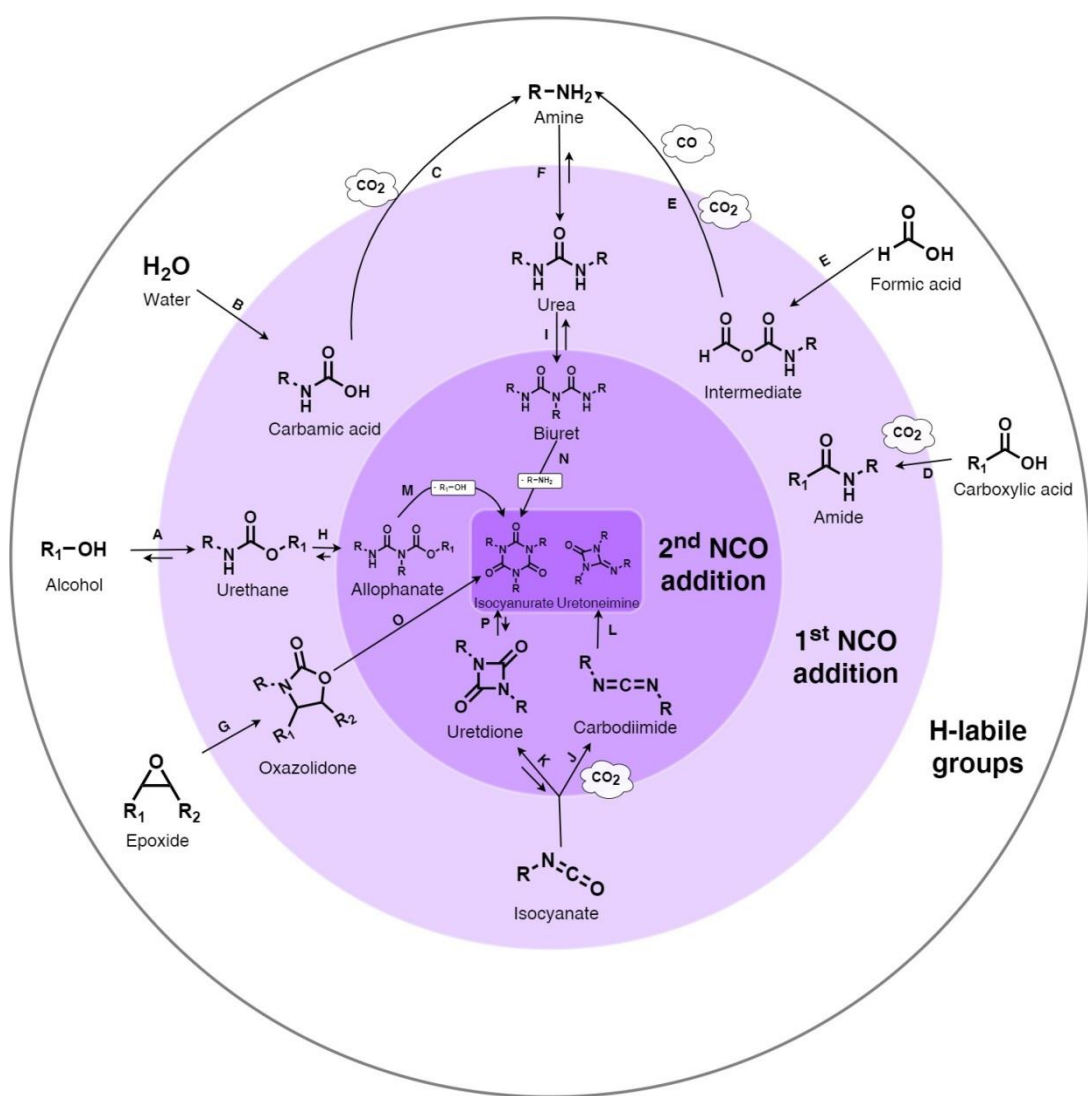


Figure 1.2 - Main isocyanate reactions with H-labile groups.

The diversity of the isocyanate reactions and the numerous different structures of polyols and polyisocyanates available make the PU a very versatile polymer family. PUs diversity of properties and the efficiency of the processing endorsed a growing market, which is mainly based on PUFs, from the soft to the rigid foams based on open or closed cells, respectively.

3.2. PUF Formulation

PUFs elaboration is a complex association of polyols, polyisocyanates, BAs, catalysts, surfactants and additives such as fillers or FRs. The general formulation quantities for PUFs in Table 1.1 are expressed in part by weight of polyol (pbw). The quantities of all components are calculated on a basis of 100 g of polyols to simplify the scale up or down. The BA quantity ranges from 3 to 30 pbw and depends on the targeted density and the BA structure. The dominant components in a PUF formulation are the polyisocyanate and polyol. Their contents, linked to the type of foam (R-PUF, F-PUF or PIR foam) and the targeted applications, are controlled by the NCO/OH index determined as the ratio between the isocyanate and the hydroxyl groups multiply by 100.

Table 1.1 - General foam formulation with quantities expressed in part by weight of the polyol.

Foam component	Polyisocyanate	Polyol	BA	Surfactant	Catalyst	Additives
Quantity (pbw ¹)	100-300 ²	100	3-30 ³	1-3	1-3	1-10

¹ part by weight of polyol ² Quantity depending on the ratio NCO/OH ³ Molar mass-dependent

Figure 1.3 presents the effect of the NCO/OH molar ratio on the chemical architectures of PUFs, hybrid PU-PIR foams and PIR foams. The PUFs are produced with a NCO/OH index between 80-120 to promote the urethane group formation. As presented in Figure 1.3, the PIR foam elaborated mainly from isocyanate is highly crosslinked and, consequently, highly brittle or friable (Baumann and Dietrich 1981). However, the PIR foam has excellent thermal stability properties due to the isocyanurate group. In order to take advantage of the thermal stability of the isocyanurate and avoid the formation of a highly crosslinked network, hybrid PU-PIR foams were developed. They are formulated with NCO/OH index higher than 120 to form an isocyanurate group and lower than 600 to avoid high friability (Reymore et al. 1975).

The PU-PIR foams combined the thermal stability of the PIR network with the flexibility of the PUF (Nawata et al. 1975). They are classed among R-PUFs due to their similar mechanical properties and morphologies and consequently they are mainly used in thermal insulation. The PU-PIR foams are explicitly used when the fire hazard is high due to their higher thermal stability compared to R-PUFs.

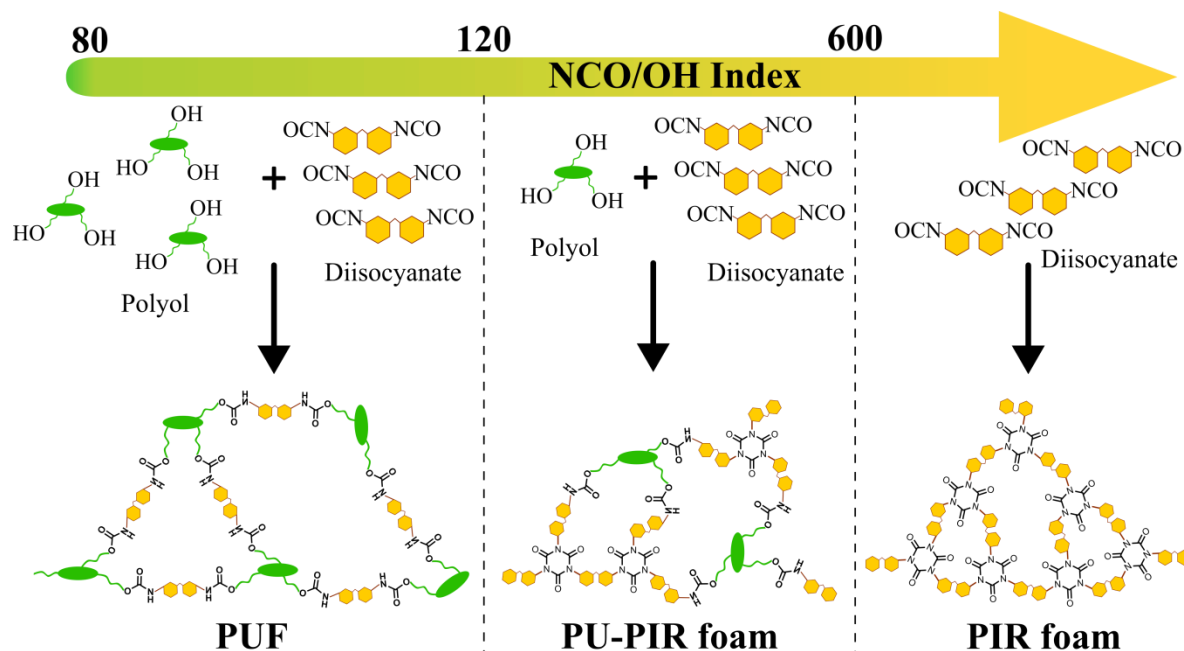


Figure 1.3 - Effect of the NCO/OH index on the chemical architectures of PUF, PU-PIR and PIR foam networks.

Several processes were developed industrially to produce PUFs, such as molding, slabstock, spaying, pour-in-place or frothing-in-place. In academic research, the two primary processes for the PUFs elaboration are the pour-in-place or molding method, described in Figure 1.4. The foaming process is based on the one-shot method, where the polyol and polyisocyanate are intimately mixed. The components are usually separated into two parts with (i) the A-part containing the polyol, the BA, the surfactant, the catalyst and the additives stirred vigorously to integrate air bubbles in the mixture and to obtain an emulsion (step 1 in Figure 1.4) and (ii) the B-part composed of the polyisocyanate. Both parts are then mixed under stirring (steps 2 and 3 in Figure 1.4). The reactive mixture is then poured into an open-cup for the pour-in-place process or in a closed mold with, depending on the targeted application, an optional control of the temperature for the molding process (step 4 in Figure 1.4) where the polyaddition releases heat and forms the polymer network. The BA vaporizes and expands through the heat generated by the reaction, and the foam rises (step 5 in Figure 1.4). In the end, a cellular material composed of gas-entrapping polymer cells is obtained (step 6 in Figure 1.4).

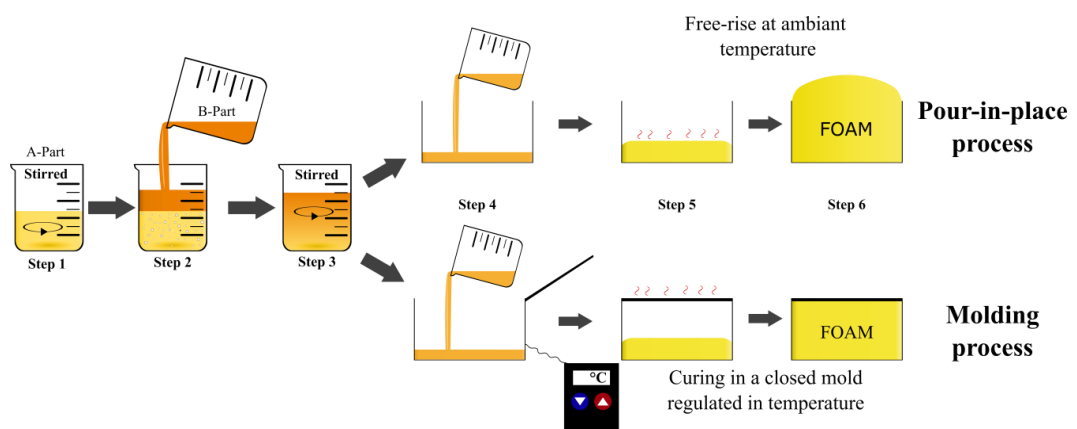


Figure 1.4 - Detailed usual processes at lab scale for PUF elaboration: pour-in-place or molding process.

3.2.1. Polyisocyanate

Several pathways can be used to synthesize isocyanate groups such as the Curtius, Hofmann or Lossen rearrangements but also the phosgenation of primary amine (Szycher 2013). At the industrial scale, although toxic for human health, the phosgene is the preferred pathway for the production of isocyanate due to the difficulty of handling the unstable azide groups in the rearrangement reactions (Cotarca and Eckert 2003; Knölker et al. 1995). The main used isocyanates are the toluene diisocyanate (TDI), the methylene diphenyl 4,4'-diisocyanate (MDI) and its polymeric form (pMDI) (Szycher 2013), which is mostly used since it presents lower volatility and reduced toxicity compared to the monomer form. The pMDI superior functionality compared to the other polyisocyanates is also a key point for R-PUF elaboration, which require highly crosslink network. On the contrary to the aromatic monomer polyisocyanates, the pMDI is liquid at ambient temperature, facilitating the implementation at industrial scale. In addition to the aromatic polyisocyanates, some aliphatic polyisocyanates are used, such as the hexamethyleneisocyanate (HDI), the isophorone diisocyanate (IPDI), or the 4,4'-methylene bis cyclohexyl diisocyanate (H₁₂ MDI). Their reactivities and structures are described in Table 1.2.

The stabilization of the mesomeric structures by the surroundings of the isocyanate group enhances the carbon electrophilic character and its reactivity. As shown in Table 1.2, the aromatic isocyanates are more reactive than the aliphatic or cycloaliphatic counterparts due to the delocalization of the negative charge on the aromatic ring. The reactivity of the aromatic TDI and MDI is two orders of magnitude higher than the aliphatic HDI, H₁₂ MDI and IPDI.

Table 1.2 shows that the first addition of alcohol on a diisocyanate decreases the reactivity of the second addition. The foam elaboration requires high reactivity; therefore, aromatic polyisocyanates are used. Besides, the aromaticity brings several properties to the final products, such as, e.g., higher flame resistance and mechanical properties. In general, the MDI and TDI are used for F-PUFs and pMDI for R-PUFs. They are the primary polyisocyanates used in PUFs formulation.

Table 1.2 - Relative reactivity of isocyanates with alcohol groups for the 1st and the 2nd additions. Adapted from (Szycher 2013).

Isocyanate	Structure	1 st addition	2 nd addition
TDI		702	58
MDI		561	193
HDI		1.8	0.9
IPDI		1.1	0.4
H ₁₂ MDI		1	0.7

3.2.2. Polyol

Since PUF are mainly crosslinked networks and since polyisocyanates are mainly bifunctional, polyols must present, on average, a functionality (f) higher than 2. Polyol mixes are often used to obtain the suitable requirements. Polyols are usually viscous liquids containing at least two or more hydroxyl (OH) groups per molecule. They are characterized by their OHs density (I_{OH}) expressed in mg KOH/g. Both main types of polyols are oligomers of polyether and polyester with OH ending chains. First, polyethers are produced from the alkoxylation with ethylene (EO) or propylene oxide (PO) from a simple starter molecule containing several OH or amine groups, primary and secondary. The polyol-starters can be pentaerythritol ($f=5$), sorbitol ($f=6$) or glycerol ($f=3$) and the polyamine starters can be ethylenediamine ($f=4$) or diethylenetriamine ($f=5$). From the starter to the corresponding oligomer, the I_{OH} is decreased. Similarly, the polyester polyols are produced from controlled polycondensation or polyaddition between a dicarboxylic acid or an anhydride with a polyol-starter molecule. In general, polyether polyols generally present a lower viscosity and higher dispersity than polyester polyols, due to the flexible ether links. They also provide higher softness, hydrolytic and aging stabilities compared to polyester polyols (Furtwengler and Avérous 2018).

Table 1.3 - Main requirements on polyols properties for F-PUF and R-PUF. Adapted from (Furtwengler and Avérous 2018; Ionescu 2005).

PUF type	I_{OH} (mg KOH/g)	Functionality (f)	Molar mass (g/mol)	Viscosity (Pa.s)
Rigid	300-800	3-8	300-1000	2-50
Flexible	15-100	2-3	3000-6500	0.2-20

Polyols properties have a profound impact on the behaviors and structures of the final cellular materials. Polyols for R-PUF have I_{OH} ranging between 350 and 800 mg KOH/g, with between 3 and 8 OH groups per molecule (Table 1.3). On the contrary, the polyols used for F-PUFs have lower I_{OH} and functionality. The higher the functionality of the polyols is, the higher the crosslinking density and rigidity of the foam should be. As depicted in Table 1.4, the reactivity toward isocyanate is mainly related to the nature of the H-labile group. The primary and secondary aliphatic amines, generally toxic for human health (Greim et al. 1998), are 1000 times more reactive than their OH aliphatic counterparts. Water and primary aliphatic OHs have similar reactivities. Then, the reaction of water with isocyanate formed a primary amine, which reacts immediately due to its high reactivity compared to OH. The urea formed by the addition of the amine and isocyanate is half as reactive as a secondary aliphatic hydroxyl. Therefore, the formation of biuret is generally considered as a source of crosslinking in foams. The aromatic OH, usually found in phenolic resources (e.g., lignin), is around 300 and 1000 times less reactive than secondary and primary aliphatic OHs, respectively. This explains the need to chemically modified polyphenol molecules before their introduction in PUF as shown in a next section.

Table 1.4 - Relative reactivity of hydrogen active compounds without catalyst. Adapted from (Ionescu 2005).

Hydrogen active compound	Structure	Uncatalyzed relative reactivity at 25 °C
Primary aliphatic amine	$\text{R}-\text{NH}_2$	3300
Secondary aliphatic amine	$\text{R}_1-\text{NH}-\text{R}$	650-1650
Primary aromatic amine		6.5-10
Primary aliphatic OH	$\text{R}-\text{OH}$	3.3
Water	$\text{H}-\text{O}-\text{H}$	3.3
Carboxylic acid	$\text{R}-\text{C}(=\text{O})-\text{OH}$	1.3
Secondary aliphatic OH	$\text{R}-\text{C}(\text{OH})-\text{R}_1$	1
Urea	$\text{R}-\text{NH}-\text{C}(=\text{O})-\text{NH}-\text{R}$	0.5
Tertiary aliphatic OH	$\text{R}_1-\text{C}(\text{OH})-\text{R}_2$	0.0017
Phenolic OH		0.003-0.017
Urethane	$\text{R}-\text{NH}-\text{C}(=\text{O})-\text{O}-\text{R}_1$	0.0033

3.2.3. Blowing agent

The choice of the BA is crucial to determine essential properties and morphologies which are related to the applications. Two main types of BA are used: (i) Chemical, where BA reacts with a system component during the polymerization to generate the gas. As presented in Figure 1.2, several H-labile compounds release gas by an exothermic reaction with isocyanates and, e.g., water or formic acid. (ii) Physical BA presents a phase change from liquid to gas during the polymerization using the energy released by the exothermic polyol-polyisocyanate reaction, with a strong and fast volume increase of the mix.

The key parameters of physical BAs are the molar mass, the boiling point, the heat of vaporization and conductivity in the gas phase. They are detailed in Table 1.5. Firstly, the molar mass of BA is essential for economic reasons. The quantity of gas and, by extension, the foam produced is inversely proportional to the molar mass. Therefore, in a formulation with a fixed mass of BA, the BA with a lower molar mass will generate a higher gas volume (Singh 2002). To obtain foams with similar densities starting from the same formulation, a higher amount of, e.g., trichlorofluoromethane (137.4 g/mol) than n-pentane (72.2 g/mol) would be used. Secondly, the boiling point of BAs determines the temperature and then the time when the foam starts to rise. It is the main parameter for the fine-tuning of the foam expansion kinetic. In the case of one component-foam, the BA agent has a propellant role. It is common to use a BA with an ebullition temperature under 0 °C. Thirdly, the heat of vaporization represents the energy needed to phase change a liquid into gas. The quantity of heat released by the PU formation must be controlled to avoid attaining the critical degradation temperature of the PU. The endothermic vaporization of the BA consumes the heat released and decreases the temperature during

the polymer formation, preventing degradation. Finally, some BA properties are related to particular applications such as R-PUF for thermal insulation, where the thermal conductivity must be the lowest. The total thermal conductivity is related to the conduction through the polymer matrix, through the gas phase and the radiation. In this case, the gas contribution accounts for 65% of the total thermal conductivity (Ferkel et al. 2017; Jarfelt and Ramnäs 2006). The lower the conductivity in the BA gas phase, the lower the overall conductivity of the foam should be. However, with the foam aging, the BA diffuses out of the cells and it is substituted by air.

Table 1.5 - BA structures, name physical properties and global warming potential (GWP). Data from literature (Bobbo et al. 2018; Gil and Kasperski 2018; Lai 2014; Mateu-Royo et al. 2019; Rapra 2014; Singh 2002; Yaws 2009, 1995).

Category	IUPAC name	Commercial name	Structure	Molar mass (g/mol)	Boiling point (°C)	Heat of vaporization (kJ/mol)	Conductivity (at 25 °C) (mW.K ⁻¹ .m ⁻¹)	GWP
Chemical BA	Carbon dioxide	CO ₂		44.0	-78.3	6.8	16.4	1
CFC ¹	Trichlorofluoromethane	CFC-11		137.4	23.8	24.8	7.9	4600
HCFC ²	1,1-dichloro-1-fluoroethane	HCFC-141b		116.9	32.9	25.8	10.0	700
HFC ³	1,1,1,3,3-pentafluoropropane	HFC-245fa		134.1	15.3	26.0	12.5	990
	1,1,1,3,3-pentafluorobutane	HFC-365mfc		148.1	40.2	26.2	11.6	910
HC ⁴	cyclopentane			70.1	49.3	27.3	12.8	11
	n-pentane			72.2	36.2	25.7	15.0	11
	iso-pentane			72.2	27.8	24.6	14.3	11
HFO ⁵	(Z)-1,1,1,4,4,4-hexafluorobut-2-ene	HFO-1336mzz (Z)		164.1	33.5	24.8	10.7	2
HCFO ⁶	(Z)-1-chloro-2,3,3,3-tetrafluoroprop-1-ene	HCFO-1224yd		148.5	14.6	21.6	9.1	1
	(E)-1-chloro-3,3,3-trifluoroprop-1-ene	HCFO-1233zd		130.5	18.3	22.3	10.2	7
	Air						26.0	

¹Chlorofluorocarbon, ²Hydrochlorofluorocarbon, ³Hydrofluorocarbon, ⁴Hydrocarbon,

⁵Hydrofluoroolefin, ⁶Hydrochlorofluoroolefin.

Historically, water was the only BA used until the 1950s and remains the primary chemical BA used today in F-PUFs. Foams developed only with water as BA faced several challenges: (i) high exothermic reaction causing scorching or fire, (ii) reduced flowability in mold due to higher viscosity, (iii) higher cost because water-blown foams consume more isocyanates. The water-blown R-PUF has high surface friability, high thermal conductivity, and poor dimensional stability. Furthermore, the higher amount of heat released by the urea induces a faster expansion of the foam. In consequence, some cell walls can be broken.

The development of the physical BA from 1970 to nowadays was conditioned by environmental concerns. The Montreal in 1987 and Kyoto in 1992 protocols banned chlorofluorocarbons, hydrofluorocarbons, and hydrochlorofluorocarbons due to their high ozone

depletion activities (Rowland and Molina 1975; Shine 2009). Indicators to measure the impact of a molecule on the environment, such as the ozone depletion potential, were implemented, i.e., the Global warming potential (GWP). Despite the ongoing utilization of forbidden substances by international protocols, the research turns toward new BAs more environmentally friendly such as hydrocarbons, hydrofluoroolefins or hydrochlorofluoroolefins (Table 1.5) (Mateu-Royo et al. 2019; Rigby et al. 2019).

3.2.4. Surfactant

Fine and homogeneous cell structure cannot be obtained without surfactants. Figure 1.5 details the principal surfactant structures used in PUFs formulation. The block and graft amphiphilic copolymers are based on hydrophobic siloxane groups and hydrophilic polyether grafted chains. The polyether/siloxane ratio, the EO unit content, the capping group (CAP in Figure 1.5), the molar mass and the molecular architecture of the surfactant can be finely tuned to fit with the different polyols-BAs systems (Hill 2019).

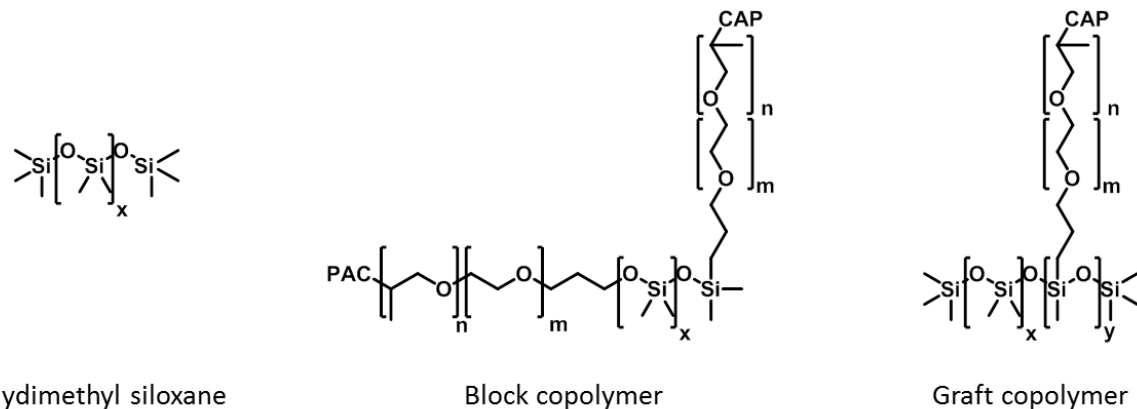


Figure 1.5 - Representation of silicone surfactant. Adapted from (Frey et al. 1996).

The surfactant has two main roles in the cell formation process: (i) the emulsification of the reagents and (ii) the stabilization of the formation of the bubbles (Schmidt et al. 1984). Firstly, before the polyaddition starts, surfactants participate in the emulsification of the BA and the air in the monomers mixture, by reduction of the surface tension (Hill 2019). Placed at the BA-polyol interfaces, the surfactant increases their miscibility and reduces the emulsion particle size. It was demonstrated that lower surface tension leads to higher bubble density in the A-part and, consequently, finer cell structure in the final foam (Zhang et al. 1999).

The second role of the surfactant is the stabilization of the growing cells, along with the polymerization and foaming process. The cell growth is disrupted by two phenomena described in the left part of Figure 1.6: (i) the Ostwald ripening and (ii) the cell drainage. The Ostwald ripening is controlled by the pressure difference between large and small bubbles. To equilibrate the pressure, the gas in small bubbles transfer into the larger ones (Figure 1.6), and the exchange rate depends on the permeability of the cell walls (Voorhees 1985). As shown in Figure 1.6, this phenomenon tends to decrease the bubble density and to form coarser cells if not controlled. Surfactant molecules aggregated at the surface between air and foaming liquid limit the Ostwald ripening (Figure 1.6). The

surfactant packing increases the permeability of the cell walls. Therefore, by limiting the gas transfer between two cells, a homogeneous cell structure is formed (Hill 2019).

On the other side, cell drainage is governed by the pressure difference and the viscosity of the liquid phase (Owen et al. 1967). Spherical bubbles collide when the gas volume fraction exceeds 70-75%, and distort into a multisided polyhedral (Zhang et al. 1999). The interface between two bubbles is described in the left bottom of Figure 1.6. The liquid between two expanding bubbles is forced, due to capillary pressures, to flow toward the exterior forming the Plateau border and a thin film between bubbles. Once the polymerization is completed, the thin film between two cells is called cell wall, and the Plateau border is named cell strut (Figure 1.6). Without surfactant, as shown in Figure 1.6, the bubbles are open. The foam collapses if the cells are open too early in the foaming process.

The bubble expansion causes a gradient of surfactant concentration at the surface, as shown in Figure 1.6. However, this surface tension gradient produces an antagonist effect on the film drainage, called the Marangoni effect. As shown in Figure 1.6, surfactant molecules flow from the high to the low surfactant concentration to equally distribute the surfactant molecules at the interface. In this motion, surfactant drags along foaming liquid and delays the cell opening (Obi 2018a). The transport rate from the bulk phase to the interphase and the absorption-desorption kinetics of the surfactant affects the efficiency against drainage (Beneventi et al. 2001; Malhotra and Wasan 1987). The cell drainage is fast without control, causing film ruptures, bubble coalescences, and very dense foams. In F-PUF formulations, cell rupture is wanted, and the surfactant controls the stage of cell opening. On the contrary, in R-PUF, the surfactant controls the film drainage to obtain closed cells.

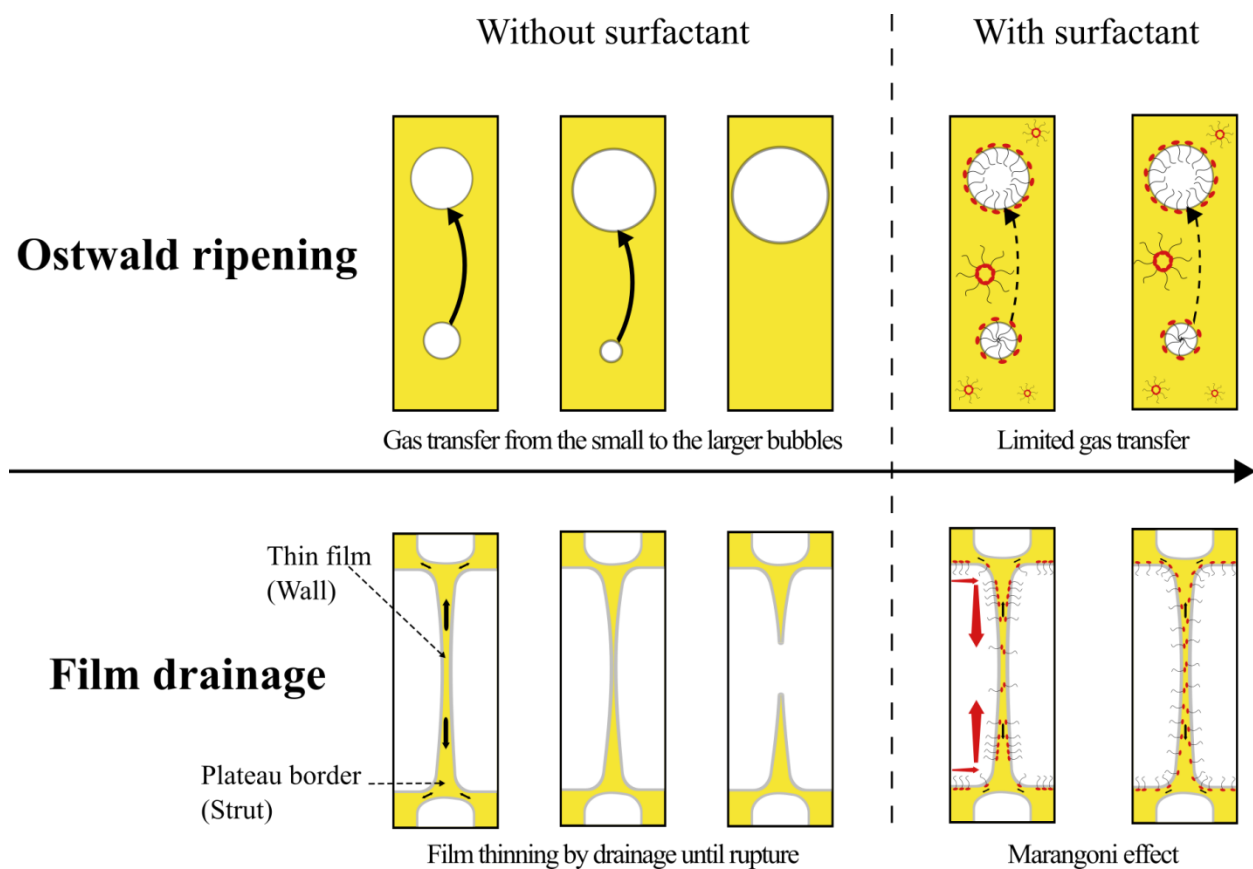


Figure 1.6 - Illustration of the significant perturbations in foam cell formation, with or without surfactant.

The surfactant has critical roles in the formation and expansion of bubbles and, by extension, the properties of the material. The surfactant quantity is optimized to obtain a good performance-price compromise. There were extensive researches to find the optimized quantity of surfactants to obtain the higher mechanical, thermal and morphological properties (Choe et al. 2019; Kang et al. 2010; Lim et al. 2008). Between 1 and 1.5 pbw of the polyol are used in F-PUFs to control cell expansion and promote the cell opening. However, too low quantity promotes collapsing, densification and splits of the foams (Kaushiva 1999). On the contrary, higher quantities are used in R-PUFs to obtain closed-cell structures. The average amount of surfactant used is between 1 and 3 pbw of the polyol (Table 1.1).

3.2.5. Catalyst

The main catalytic mechanisms for the PU formation described in the literature follow mainly two potential pathways: (i) The increase of the carbon electrophile character of the isocyanate group or (ii) the increase of the nucleophile character of the H-labile compound (Silva and Bordado 2004). In order to control the reaction kinetics, different catalysts presented in Figure 1.7 can be used. Catalysts activities can favor the urethane network formation (gelling) or the generation of gas generally via the water-isocyanate reaction (blowing) (Van Maris et al. 2005). The tin salts, i.e., stannous octoate and dibutyltin dilaurate, have higher gelling activity compared to hindered amine such as 1,4-diazabicyclo [2.2.2]octane (DABCO). The dibenzylamine, tetramethylethylenediamine and N,N-dimethylcyclohexanamine (Figure 1.7), which are less hindered tertiary amines than DABCO, are classified as balanced catalyst because they promote both gelling and blowing reactions. Catalysts containing ether bonds close to the tertiary amine group such as 2,2' dimorpholinodiethylether or 2,2'-oxybis (N,N-dimethylethan-1-amine) promote the blowing reactions. The carboxylate-potassium salts for PIR foams favor the trimerization that actively participates in the molecular crosslinking. Therefore, they are ranked in the gelling activities of Figure 1.7.

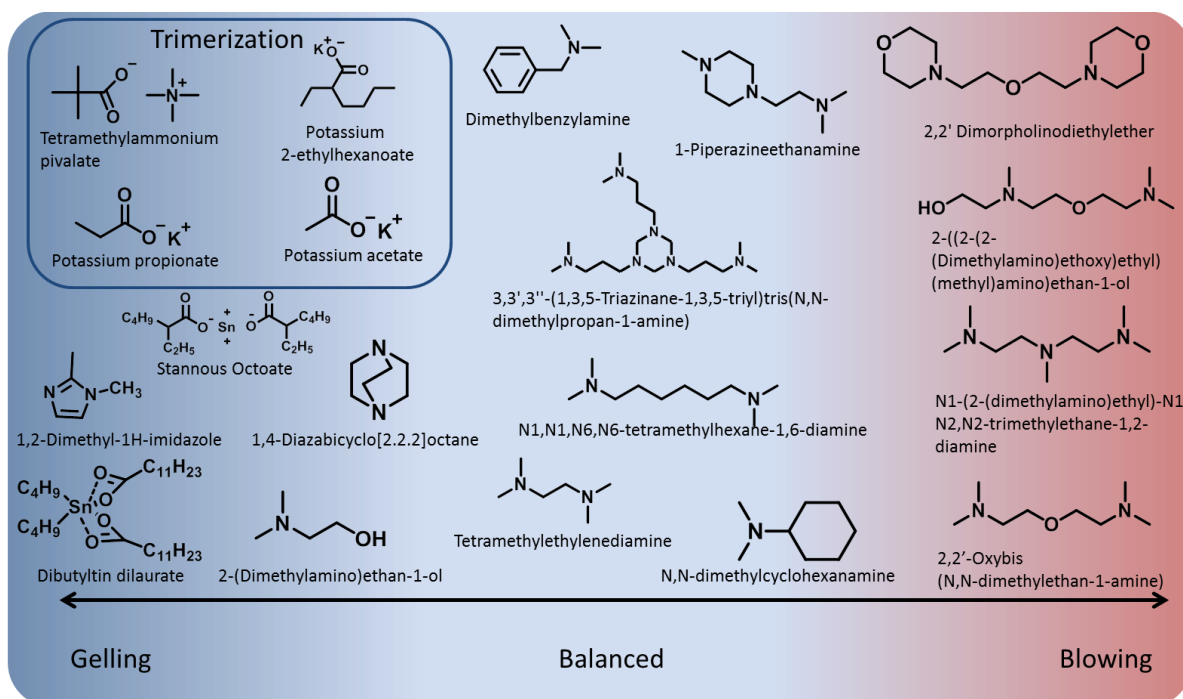


Figure 1.7 - Catalysts structures ranked according to their main activities in the foam formulation. Adapted from (Van Maris et al. 2005).

The PUF catalysts are trapped inside the polymer matrix and released over time. Therefore, a new generation of catalysts is designed with an H-labile group in their chemical structures to react with isocyanate and be part of the polymer network, to avoid a catalyst release. However, to obtain similar foaming kinetics, the catalyst loading tends to be higher due to the decreased catalytic activity linked to the loss of mobility.

In any case, the catalyst role is to equilibrate the blowing and gelling reaction to get the optimal foam. In the case of a fast gelling compared to the blowing reactions, the polymer gels faster and thus, the cells would not expand to the optimum volume (Banik and Sain 2008). Therefore, the density increase and all the properties related will be affected. On the contrary, a slow gelling produces a lower viscosity when the cells expand. In this case, the emulsion is destabilized. The gas blows the cell and the polymer gels later around big open cells (Kim et al. 1997).

3.2.6. Other additives

A large range of additives is used on PUF formulations. Additives such as FRs, dyes, pigments, or fillers can be, for instance, added. As inert additive or reactive systems, FRs are used in PUFs. Inert additives are directly added during the formulation. They are mainly composed of halogen or phosphorous compounds, although melamine, aluminum trihydrate and magnesium hydroxide may also be used (Wilkie and Morgan 2010). Reactive systems are based on active groups that are chemically linked to the PUF network (Wilkie and Morgan 2010), which are based on bromine or phosphorous atoms. Besides, more thermally stable groups can be introduced in the polymer network, such as isocyanurate, uretdione or carbodiimide (Saiki et al. 1994).

PU can also be formulated with macro or nano-fillers to improve the mechanical properties, the fire resistance or the nucleation during the foaming steps. This specific domain was recently reviewed (Agrawal et al. 2017; Kausar 2018) and will not be further detailed in this review.

3.2.7. Evolution of the cells morphology during the PUF processing

Foam expansions are monitored by three characteristic times taken along the foam elaboration process. First of all, the cream time is defined as the moment where the foam changes color and starts rising. Secondly, the gel time related to the formation of the polymer network (gelation of the polymer) is usually determined when the formation of a continuous film or a fine string between the foam and a wooden stick occurs. The foam will continue to cure and reach the tack-free time when the surface of the foam will no longer have tacking properties. For a standard PUF formulation, the characteristic times are, for instance, 2-20 sec, 10-100 sec and 15-300 sec for the cream, gel and tack-free time, respectively.

The foam development was followed by instrumented setups, which record the foam height, the temperature, the pressure inside the mold and the dielectric polarization constant over time. Equivalent characteristic times are determined from the corresponding-measured parameters. The cream time is characterized as when the foam reaches 15% of the maximum expansion rate. Furthermore, 15% of the pressure derivative is defined as the gel time. Additional characteristic times are designated, such as the rise time when the 95-98% of the height is reached or the curing time when the dielectric polarization value is under 10% of the peak maximum. This curing time indicates the

surface curing; the total curing time is proportional to the foam size. Generally, between 2 and 7 days at ambient temperature are sufficient.

Figure 1.8 shows the different phases of the cell morphology evolution correlated with the temperature and viscosity evolution over time. Phase 1 is the mixing of the A-part before the start of the polymerization. Phase 2 is the cell nucleation where two theories are in competition, or can also be concomitant. First, the classical theory of nucleation is based on the generation of cells from BA droplets after dispersion. A microphases dispersion of BA in polyols is obtained due to the BA low miscibility into polyol. The high-speed stirring splits the dispersed bubbles until an equilibrium is reached. These small bubbles are expanded to form the final cells when the polyaddition can start (Obi 2018b). A more recent theory is based on the effect of air pockets entrapped during the mixing stage (phase 1 in Figure 1.8) (Reignier et al. 2019). In this case, the BA migrates through the matrix into the air bubbles during the expansion.

The phase 2 in Figure 1.8 (expansion of the bubble) is controlled by the temperature and the viscosity of the mix. These two parameters are related to the kinetics of gelling and blowing steps and can be controlled by the catalyst. The temperature increase shown in Figure 1.8 comes from the exothermic polyaddition of isocyanate with water and polyol. The temperature increase is caused by a small portion of water that rapidly reacts and releases twice more heat than the reaction with an hydroxyl. After the cream time, a slight increase in temperature is enough to make the gas bubbles to expand. The bubble expansion is followed by a viscosity increase shown in Figure 1.8 since the bubbles act as thickener (Mcclusky et al. 1994).

The immediate drop in viscosity after the expansion of the cell around 60 seconds in Figure 1.8 is related to the thermal thinning of the reacting polymer. This drop in viscosity is beneficial for the cell expansion that starts to come into contact, forming the film, as shown in phase 4 of Figure 1.8. The temperature stabilizes after 70-80 seconds inside the foam because of the increased viscosity and thermal insulating material property of the foam (Figure 1.8). The increased concentration of urea groups formed by the reaction between isocyanate and water is responsible for a second viscosity rise. Urea groups strongly H-bond together and form hard domains in the polymer matrix, acting as reticulation points (Mcclusky et al. 1994). The next drop in viscosity shown in Figure 1.8 around 100 seconds is explained by the delay between hard segments formation and gelation of the urethane network. As explained in a previous Section, the cell wall drained by pressure difference is held by the surfactant until the network gelation occurs (phase 5 in Figure 1.8). The drop in viscosity is beneficial for the film breakage if the gelation of the network is too slow. Finally, the polyol reaction conversion with polyisocyanate reaches the gelation point, and the viscosity becomes infinite. The network gelation fixes the cell morphology of the foam.

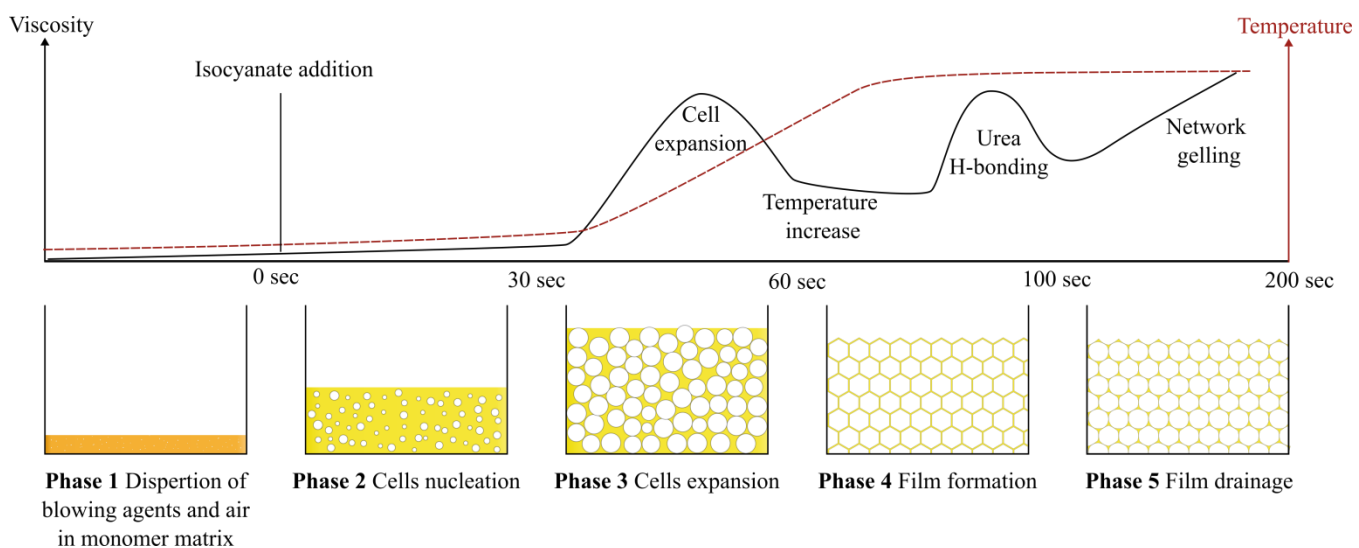


Figure 1.8 - Viscosity profile associated to the cell bubbles formation.

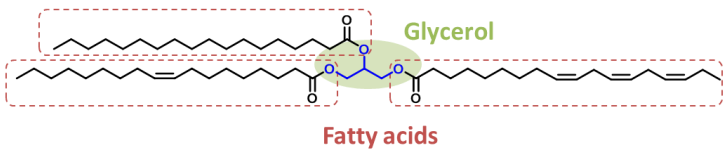
The profiles of temperature and viscosity in Figure 1.8 present a general case. Nevertheless, it can differ. For example, in PIR foams, catalysts for the trimerization are thermally activated (Okuzono et al. 2001). Therefore, the viscosity profile changes due to the additional reticulation points formed by the trimerization. Furthermore, in F-PUF, the drainage of the cell walls is controlled until the film rupture to produce open-cell.

4. FROM RENEWABLE SOURCES TO BIOBASED COMPONENTS FOR PUF

This chapter describes the different strategies recently developed to obtain the different renewable components to produce biobased PUFs from a large range of biomass, mainly from lipids, carbohydrates, polyphenols (lignins and tannins), and different others molecules from biorefinery obtained by biochemistry process, for instance. To a lesser extent than the polyols, the amines are used as raw materials in PU chemistry, either in the synthesis of polyureas or, in the case of low molar mass polyamines, as polyether polyol starters. As the production of biobased amines was recently reviewed (Froidevaux et al. 2016; Pelckmans et al. 2017), the amines will not be incorporated in this review.

The biorefinery converts the biomass into different outputs such as fuels, energy, food, feed and/or chemicals through jointly applied conversion technology (Cherubini 2010). Biorefineries are classified according to different and successive generations depending on their feedstocks. The first generation consumes edible crops such as starch, for instance. The second generation uses industrial residues and non-edible crops such as lignocellulosic compounds from wood, without food competition. Finally, the third one is based on algae and microalgae without arable land uses (Moncada et al. 2014). The utilization of different biological systems, i.e., enzymes, cell extracts or whole microorganisms (biotechnology), is increasingly integrated into the biorefinery conversion processes. The development of white biotechnology, defined as the industrial production of chemicals, increases the availability of biobased building blocks, e.g., for PUFs synthesis (Debuissy et al. 2018). The association between chemistry and biochemistry, also known as the chem-biotech approach, drives the evolution in the production of these renewable building blocks.

4.1. Lipids: Triglycerides and fatty acids



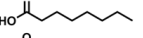
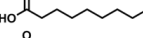
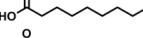
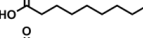
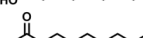
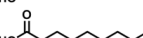
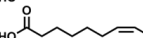
Name	Structure	Abbreviation
Caprylic		C8:0
Capric		C10:0
Lauric		C12:0
Myristic		C14:0
Palmitic		C16:0
Palmitoleic		C16:1
Stearic		C18:0
Oleic		C18:1
Linoleic		C18:2
Linolenic		C18:3
Ricinoleic		12-OH C18:1
Vernolic		12-epoxy C18:1
Docosapentaenoic		C22:5
Docosahexanoic		C22:6

Figure 1.9 - Triglyceride structure and the most abundant fatty acids in vegetables, seeds and microalgae oil.

Lipids are extracted from natural resources such as vegetables, seeds or micro-algae. They are composed of triglycerides, which can be decomposed in glycerol and three fatty acids per molecule, as shown in Figure 1.9. On the contrary to plants oil, microalgae do not compete with food nor need arable land to grow (Fabris et al. 2020; Zappi et al. 2019). They are an interesting source of lipids due to a higher average length and a higher number of double bonds per fatty acid.

The diversity in fatty acids presented in Figure 1.9 relies on the chain length (mainly till 24 carbons), position, configuration and types of unsaturation and additional substituents such as epoxide or hydroxyl groups along the aliphatic chain (Gunstone et al. 2007). The diversity of fatty acids distribution of lipids, which are species and growing conditions dependent, was used to develop various PU macromolecular architectures.

Taking into account the literature and the different previous reviews on this field (Desroches et al. 2012; Ghasemlou et al. 2019a; Maisonneuve et al. 2016; Petrovic 2008; Pfister et al. 2011; Singh et al. 2020), the main highlights of this state of the art are mainly based on recent publications on the transformation of lipids into polyols, isocyanate or additives used in foam formulations. Esters and double bonds are the starting point of the oleochemistry described in Figure 1.10 to access to different PUF components. Figure 1.10 shows the diversity of the oleochemistry with different pathways to obtain polyols. The particular case of castor oil, which contains an OH group, is described in the synthesis of an additive. The epoxidation and further ring-opening are the main transformations and were used to produce both polyols and additives.

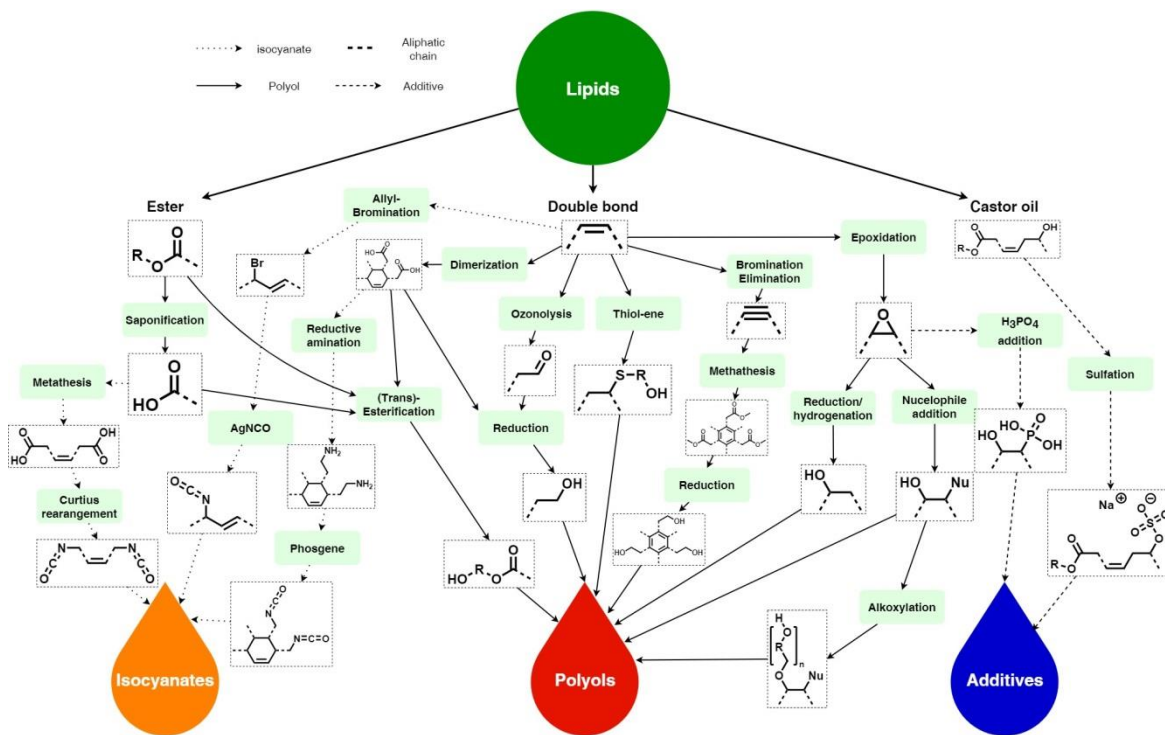


Figure 1.10 - Overview of the main oleochemistry pathways for the elaboration of different PUF components.

4.1.1. Polyols

Polyols are the main PUF components elaborated from fatty acid, even at an industrial scale. In this way, different approaches have been recently developed.

4.1.1.1. Epoxidation and ring-opening

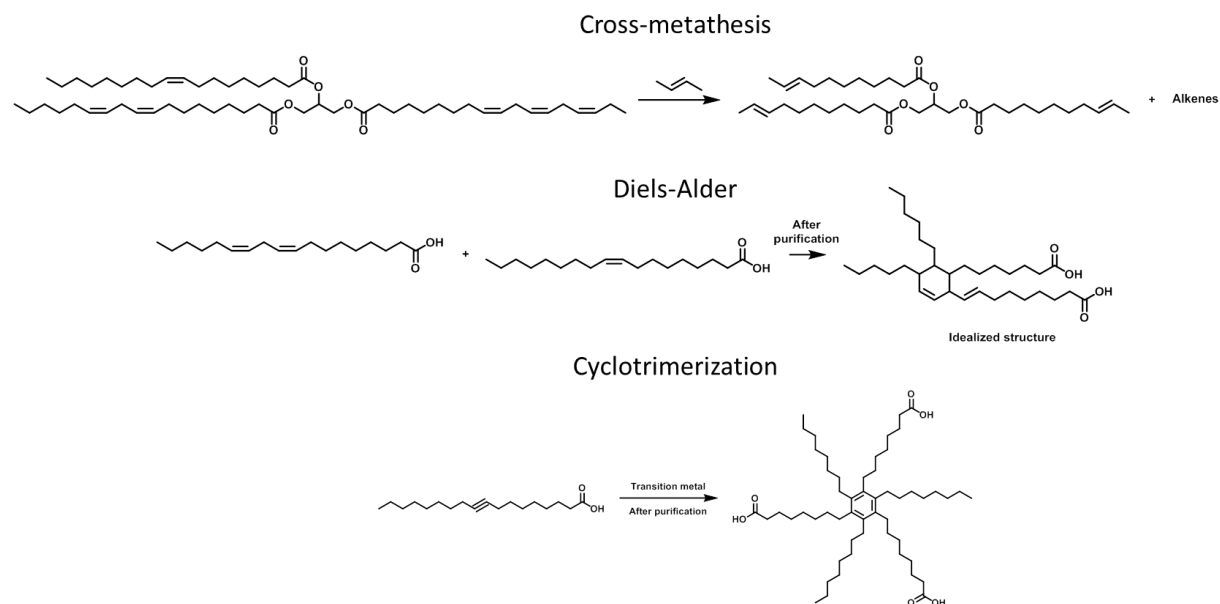
The formation of epoxide is one of the most investigated ways to obtain polyols via double bonds modification. OH groups can be obtained in two steps from the double bonds with the epoxidation and the subsequent ring-opening synthesis. The electrophilic nature of the strained three-membered ring epoxide facilitates the nucleophilic attack to afford a beta-substituted OH group (Fallah-Mehrjardi et al. 2018). Among the large variety of nucleophile used for ring-opening reaction, mono-alcohols (Arbenz et al. 2017; Campanella et al. 2009; Kahlerras et al. 2020; Petrović et al. 2013; Peyrton et al. 2020), diols (Borowicz et al. 2019; Fan et al. 2013; Kurańska et al. 2020b, 2019; Pawar et al. 2016b, 2016a; Zieleniewska et al. 2015), and carboxylic acids (Contreras et al. 2020; Fang et al. 2019; Herrán et al. 2019; Pawar et al. 2016b, 2016a; Peyrton et al. 2020) were the most investigated. Weaker nucleophiles such as amines (Biswas et al. 2005; Harry-O'kuru et al. 2015; Yang et al. 2012), water (Campanella et al. 2009; Testud et al. 2017) or thiols (Sharma et al. 2006a) were also studied, but the ring-opening reaction was found to be slower. Nevertheless, polyols produced by ring-opening with secondary amines were demonstrated to have catalytic activity (Peyrton et al. 2020, 2019). Efficient ring-opening nucleophiles rarely investigated are the hydrogen halides (Guo et al. 2000; Peyrton et al. 2020), even if they are used to quantitate epoxide groups on lipids since 1956 (Durbetaki 1956).

The secondary OH group was also formed by the reduction of the epoxide group with H₂ and Nickel of Raney (Guo et al. 2000; Petrović 2008; Pillai et al. 2018). Unfortunately, the method developed used an alkaline medium, which broke the ester, thus the triglyceride structure.

4.1.1.2. Miscellaneous double bond transformations

A recent trend in the modification of unsaturated triglyceride is the use of the “click” thiol-ene reaction where the double bond is transformed into thioether by radical addition of thiol under UV radiation. The mercaptoethanol was used to produced polyols for PUFs with castor, soybean or corn oil with high selectivity (Alagi et al. 2016; Ionescu et al. 2016; Ramanujam et al. 2019).

The cross-metathesis described in Scheme 1.2 is a reaction between the triglyceride double bond and an olefin yielding shorter monounsaturated fatty acid chains. The alkenes side products are hydrogenated to be suitable for diesel or jet propellant (Lutz 1986; Yelchuri et al. 2019). The previously developed double bond modification methods can be used to obtain polyols (Pillai et al. 2016). Another way to modify fatty acids is the 2+2 cycloaddition of oleic acid, and linoleic acid yields various six-membered cyclic diacids with long dangling chains, such as the theoretical structure shown in Scheme 1.2. OH groups can be introduced on this molecule by reduction or esterification of the carboxylic acid groups (Ghosh and Karak 2018). Oleon and Croda developed diols based on the dimerization of fatty acids. As shown in Scheme 1.2, the cyclotrimerization of oleic acid was used to transform the flexible fatty acid chains into an aromatic core with dangling chains bearing carboxylic acids (Lligadas et al. 2007).



Scheme 1.2 - Metathesis and cyclization reactions.

The ozonolysis of the double bonds of triglycerides was investigated on several substrates such as canola oil, soybean or trioline (Narine et al. 2007; Petrović et al. 2005). This reaction reduces the chain length of the fatty acid, sets the functionality at three and forms primary OH group.

4.1.1.3. Ester modifications

To obtain polyols, ester modification chemistry is largely less developed than the double bonds modification. There are only two possible pathways, such as (i) the transesterification of oil and (ii) the saponification of the ester, followed by esterification with a small polyol. The first method was extensively applied to castor oil due to the high content in ricinoleic fatty acid. The transesterification of castor oil was investigated with glycerol (Bresolin et al. 2018; Kaur and Kumar 2020; Li et al. 2016b; Veronese et al. 2011), ethylene glycol (EG) (Sahoo et al. 2016) or triethanolamine (Sahoo et al. 2016; Veronese et al. 2011). An acceleration was noted in the urethane formation kinetic with the hydroxy ketone group due to the activation of the OH group via hydrogen bonding assistance (Briou et al. 2020). The transesterification method was also applied to rapeseed (Prociak et al. 2018), soybean (Campanella et al. 2009), coconut (Paruzel et al. 2017) or andiroba oil (da Silva et al. 2018).

The second method comprises one more step, but the polyols produced have higher molar masses compared to the transesterification method. As an example, the glycerol monostearate was oligomerized with glutaric acid and yield a polyol with an average molar mass superior to 3000 g/mol and thus a low I_{OH} (Ng et al. 2017). The esterification consumes OH groups, which could be used in PU networks formation, to form ester bond; therefore, the ester formation reduces the I_{OH} . To avoid the reduction of I_{OH} , a polyol was produced by esterification of polymerized glycerol with castor oil fatty acid that contains a OH. In this particular case, the obtained polyols had an I_{OH} depending on the esterification time, around 550 mg KOH/g, suitable for PUFs synthesis (Hejna et al. 2018, 2017).

4.1.2. Polyisocyanate

The most known diisocyanate produced from oleochemistry is the 2-Heptyl-3,4-bis(9-isocyanatononyl)-1-pentylcyclohexane, commercialized by Cognis-BASF under the name DDI1410. This biobased isocyanate was used in thermoplastic (Charlon et al. 2014) or thermoset PU materials (Calvo-Correas et al. 2016; Li et al. 2014; Zhang et al. 2019a).

Other polyisocyanates were produced at a lower scale. Firstly, a dimer of oleic acid obtains by self-metathesis was transformed into diisocyanate by Curtius rearrangement (Hojabri et al. 2010). Secondly, sebacic acid and undecylenic acid derived from castor oil by alkali fusion and pyrolysis, respectively, were also transformed in diisocyanate via Curtius rearrangement (More et al. 2013). Thirdly, soybean oil was transformed by allylic bromination with N-bromosuccinimide, followed by substitution with silver isocyanate salt (Çaylı and Küsefoğlu 2008). This is the only report of polyisocyanates ($f > 2$) derived from lipids resources.

4.1.3. Some additives

4.1.3.1. Surfactant

Similarly to surfactant, lipids are constituted of long aliphatic and hydrophobic chains and a polar core with the ester groups. Linseed oil has been recently used as a renewable modifier in PUFs. Mechanical and thermal properties improvement has been reported in PUFs containing linseed oil as a unique surfactant (Czlonka et al. 2018). The sodium sulforicinate obtained by sulfation of castor oil dispersed in water was used in foam formulations, both as BA and surfactant (Arbenz et al. 2016).

4.1.3.2. FR

The modification of the lipids double bonds to enhance the thermal stability was achieved through the epoxidation and ring-opening process with phosphoric acid. The phosphorous compounds are known for their fire-retardant properties, especially in PUFs (Chang et al. 2019). Another strategy based on fatty acid as a modifier for a well-known FR: the 9,10-dihydro-9-oxa-10-phosphaphhenanthrene-10-oxide (DOPO) can be applied. The synthesis procedure introduced the terminal fatty reactive epoxide group on the DOPO molecule (Lligadas et al. 2006b). With this modification, the labile FR molecule is then attached to the polymer network.

4.2. Carbohydrates

Initially, carbohydrates were defined as molecules exclusively composed of carbon, oxygen and hydrogen atoms following the formula $C_n(H_2O)_n$ (Grunwald 2016). However, the definition was enlarged to encounter the reduced, oxidized and heteroatoms (sulfur or nitrogen) containing molecules (Stick 2001). Carbohydrates are divided into two categories: (i) the monosaccharides composed of C5 or C6 molecules and numerous OH groups such as the sorbitol, sucrose and lactitol (Figure 1.11). (ii) The polysaccharides obtained by condensation of monosaccharide building blocks, i.e., starch and chitosan (Figure 1.11) (Yarema 2005). The polysaccharides with a high molar mass such as starch, neat chitin or de-acetylated chitin (chitosan) are largely used for polymers synthesis (Gandini et al. 2016; Halley and Avérous 2014; Rinaudo 2006).

The different pathways from carbohydrates (mono, di and long polysaccharides) to PUF components are described in Figure 1.11. The esterification and the alkoxylation are the two main pathways for transforming mono, di and polysaccharides into polyols. The chitosan was slightly modified to be introduced as additives in PUFs. The isosorbide obtained from sorbitol was a platform for the biobased diisocyanates synthesis.

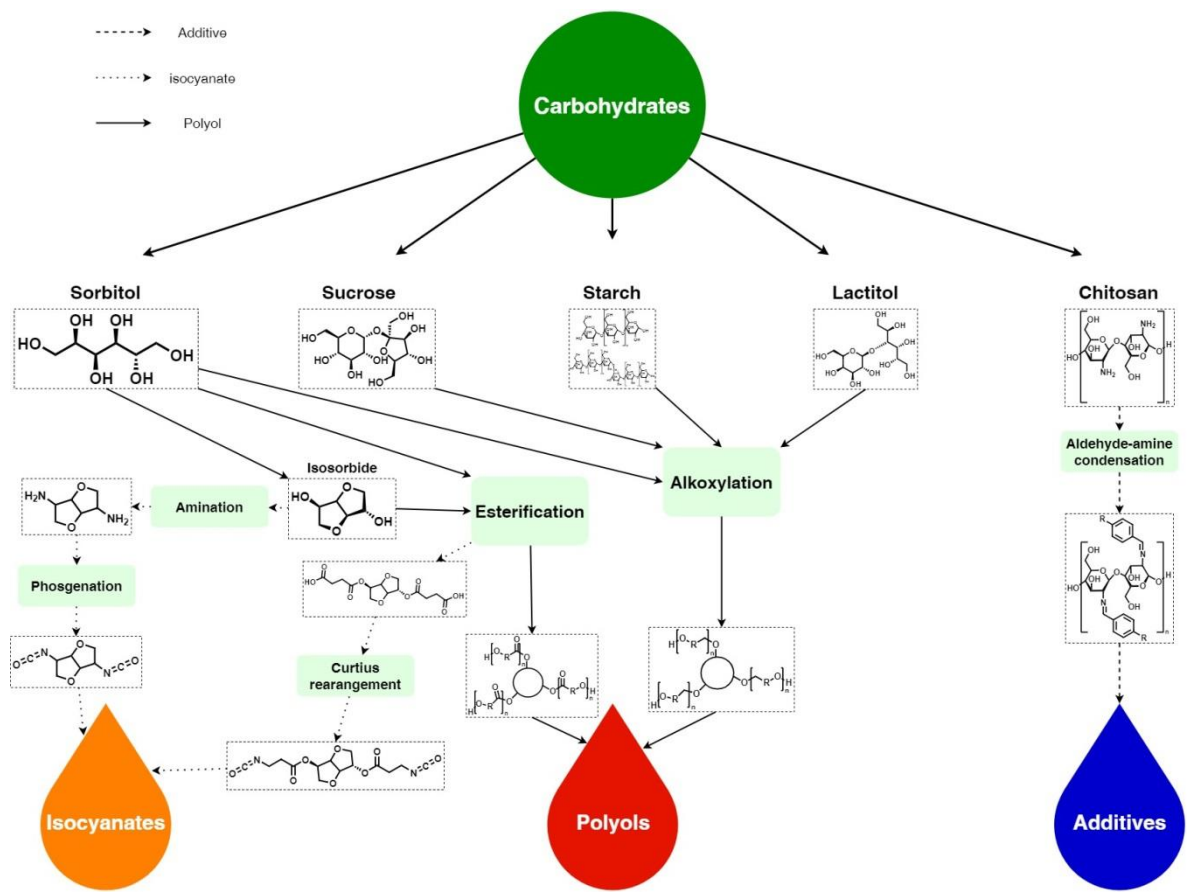


Figure 1.11 - Overview of the transformation of main carbohydrates into different PUF components.

4.2.1. Polyols

The carbohydrates are multi-OH compounds that are of great interest to produce polyols for PUFs formulation. Unfortunately, most of the carbohydrates are solids at ambient temperature, so impossible to use without modification. Several strategies were developed to modify the carbohydrates to produce adequate polyols for PUFs.

4.2.1.1. Alkoxylation

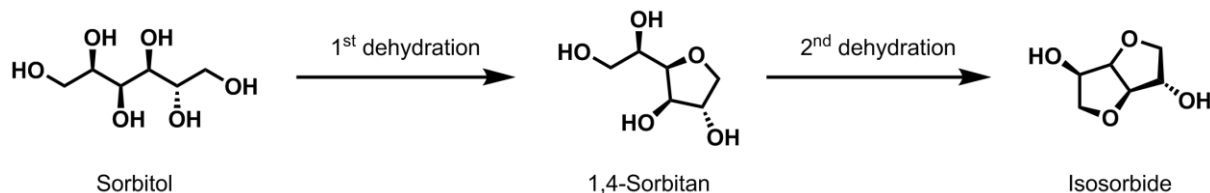
The first strategy, commonly called alkoxylation, is based on the anionic ring-opening polymerization (ROP) of epoxides. This reaction initiated by small polyols (starters) forms polyether chains ended by OHs. The reaction product has a higher molar mass and the same functionality in OH as the starter. It was early shown that the alkoxylation of monosaccharides produced polyols with suitable properties for PUFs. BASF was the first company to patent PUFs based on alkoxylated carbohydrates (Austin et al. 1978a, 1978b). The alkoxylation was successfully applied to sucrose (Ionescu and Petrović 2010), lactitol (Wilson et al. 1996), starch (Lubczak et al. 2020), sorbitol (Jiang et al. 2018; Ugarte et al. 2015) and reduced lactose (Hu et al. 1997) to produce PUFs.

The major drawback of this reaction is the production of the epoxide reagents. 33 million tons of small epoxides such as EO, PO or, to a lesser extend, butylene oxide used for the alkoxylation are mainly fossil-based (Herzberger et al. 2016). However, epoxides could be bio-derived from ethanol, butanol or glucose, in a greener way (Arbenz and Avérous 2014; Gandini and Lacerda 2015; Lee et al. 2019).

4.2.1.2. Esterification

Similarly to alkoxylation, the oligo-esterification increases the molar mass of monosaccharides with a reduction of the melting point and I_{OH} . For example, sorbitol esterification was realized in one step with adipic acid and dioctanol mediated by enzymatic catalysis (Gustini et al. 2015). Polyester polyols from sorbitol, adipic acid and diols with various chain lengths produced in two steps were also reported (Furtwengler et al. 2017). The resulting polyols based on two primary and four secondary OH groups were added in PUF and PU-PIR foams formulations (Furtwengler et al. 2018a, 2018b).

The sorbitol was also transformed through dehydration, as described in Scheme 1.3, to form isosorbide. This product, commercialized by, e.g., Roquette (France), raised much interest due to the bicyclic rigid structure (Dusenne et al. 2017). Suitable polyols for the PUFs industry were also obtained by esterification with fatty acid dimers (Khanday and Gite 2019). The combinations between the rigidity of the isosorbide and the flexibility of fatty acids are an exciting way to obtain new properties. Neat Isosorbide was also directly added in PUFs with reduced thermal reversibility of the urethane bond (Shin et al. 2019b). This reversibility at low temperatures was exploited to weaken the modulus of polymer located in the fragile thin wall. A decreased modulus combined with the heat increased the open-cell content.



Scheme 1.3 - Isosorbide production pathway from sorbitol.

4.2.1.3. Miscellaneous transformations

Neat carbohydrates were used in the PU system in a pre-polymerization step with a default of diisocyanates (Konieczny and Loos 2019; Marín et al. 2011) or as crosslinkers (Javaid et al. 2020; Ugarte et al. 2014). Furthermore, the integration of chitosans of different molar masses into a PUF formulation was tested with a higher reaction yield of chitosans with low molar masses (Qin and Wang 2019).

4.2.2. Polyisocyanate

The too numerous OH groups of the carbohydrates limit the transformation into isocyanates. Therefore, the isosorbide was a molecule of choice due to its two OHs and their transformation into isocyanate groups was achieved through a traditional amination-phosgenation route (Bachmann et al. 2001). Another strategy was applied with succinic anhydride to form acid pending groups on isosorbide. The isocyanate groups were then formed by Curtius rearrangement (Zenner et al. 2013).

4.2.3. Additives

Chitosan was introduced in PU formulations with phosphate derivatives to improve the char layer formation and the FR properties (Liu et al. 2017; Zhang et al. 2018b). Furthermore, with the

same goal, carbohydrates were modified with an alkyl chain to improve the mixing with the PUF components (Malwitz 1987). The synthesis of phosphorous-containing polyols with FR properties was achieved by the esterification of sorbitol and sucrose derivatives with dialkyl phosphonopropionate (Quinn 1970) or the treatment of propoxylated starch with polyphosphoric acid (Molotsky and Gramera 1976).

4.3. Polyphenols (Lignins and tannins)

Lignocellulosic resources presented in Figure 1.12 are primarily composed of cellulose (40-60%), hemicellulose (25-35%) and lignins (15-30%). Terpenes, alkaloids, or tannins are also accumulated by plants. Polyphenols such as lignins and tannins are then abundant. They are the first and second most abundant sources of aromatic biomolecules on earth, with an estimated worldwide production of 50 and 0.16 million tons per year, respectively (Laurichesse and Avérous 2014; Xu and Ferdosian 2017).

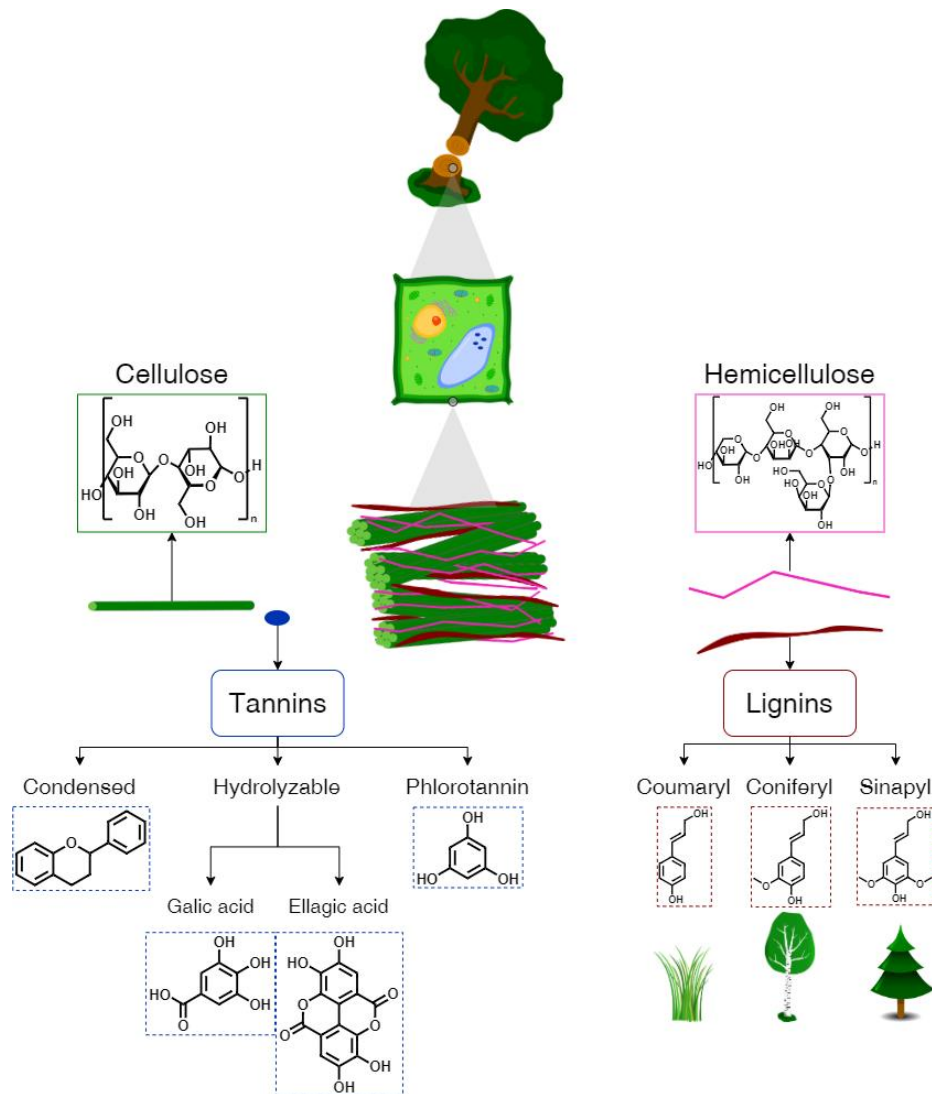


Figure 1.12 - Composition of lignocellulosic resources and classification of main polyphenols: tannins and lignins. Adapted from (Isikgor and Becer 2015).

Lignins can be defined as amorphous polyphenolic materials arising from an enzyme-mediated dehydrogenative polymerization of three monolignols: coumaryl, coniferyl and sinapyl alcohols (Figure 1.12) (Dence and Lin 1992). In softwood such as spruce, the lignin is primarily composed of coniferyl alcohol, while in hardwood (e.g., birch), the coniferyl and sinapyl monolignols are dominant. The coumaryl alcohol is mostly found in compression woods or grasses. It is mainly extracted from lignocellulosic resources through various processes (e.g., kraft, sulfite, solvent or soda pulping). Until recently, the lignin was considered as a waste by-product of the paper and ethanol/fuel industries and burned for power and heat generation (black liquor) (Xu and Ferdosian 2017).

Tannins are polyphenols defined as soluble compounds with a molar mass between 500 and 3000 g/mol or by their ability to precipitate protein. They present particular chemical and biological activities (HAGERMAN 2002). On the contrary to lignin, tannins are found in soft tissues and play a vital role, such as the defense against mushrooms or insects (Roux and Paulus 1962). The main categories of tannins presented in Figure 1.12 are the condensed tannins based on flavonoids structure, the hydrolyzable tannins composed of gallic esters derivatives and the phlorotannins (Singh and Kumar 2020).

Lignins and tannins chemical structures depend mainly on the extraction methods, botanical sources, locations, and seasons. Nevertheless, for both resources, phenol, aliphatic OH and carboxylic acid are the primary chemical groups available for transformation. The chemical transformation of lignins and tannins has been extensively reviewed (Arbenz and Avérous 2015; García et al. 2016; Karunarathna and Smith 2020; Laurichesse and Avérous 2014; Pizzi 2019). Main modifications are summarized in Figure 1.13 with a focus on the modifications for PUFs fabrication. The polyphenols sources were mainly divided into lignin and tannin structures. The liquefaction is one of the main pathways to obtain polyols from lignins, tannins or natural polyphenols sources. As shown in Figure 1.13, the aromatic structure of tannin was investigated to produce additives.

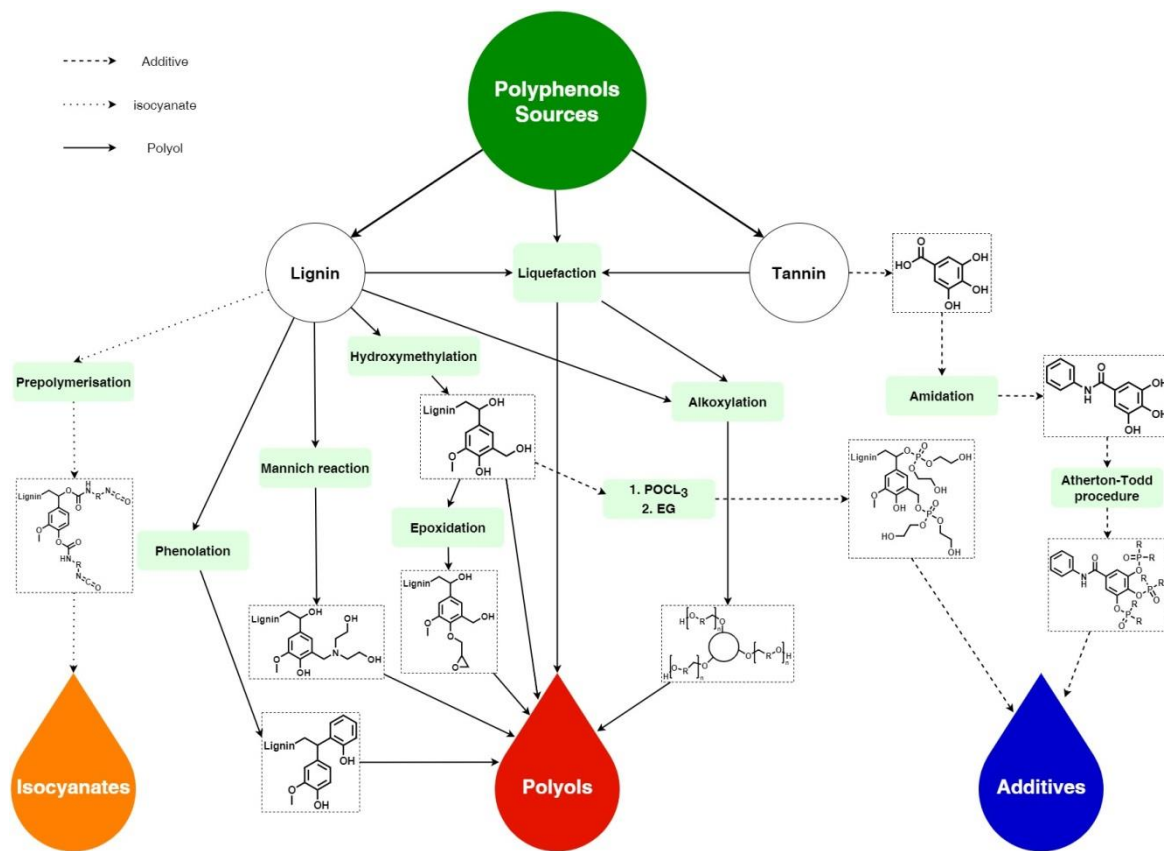


Figure 1.13 - Overview of the transformation of lignins and tannins into PUF components.

4.3.1. Development of aromatic polyols

4.3.1.1. Liquefaction

As described in Figure 1.12, the plant cell walls are primarily composed of cellulose, hemicellulose and lignin. The solvolysis of this biomass in harsh conditions is called the liquefaction process and was recently reviewed (D'Souza et al. 2017; Hu et al. 2014; Shao et al. 2019). This process was applied to produce polyols with lignins (Gao et al. 2015; Li et al. 2016a; Mahmood et al. 2016; Mohammadpour and Mir Mohamad Sadeghi 2020; Xu et al. 2014; Xue et al. 2015), woods (Maldas and Shiraishi 1996; Rastegarfar et al. 2018; Yue et al. 2017), barks (D'Souza et al. 2014; Ge et al. 2000), celluloses (Kosmela et al. 2018) or wattle tannins (Ge et al. 2003). Furthermore, the direct hydrolysis of lignin with water under strong alkali conditions was investigated and afforded suitable polyols for PUFs formulation (Mahmood et al. 2013; Pérez and Tuck 2018; Xue et al. 2017). The liquefaction process is a fast and efficient way to obtain a mixture of aliphatic and aromatic polyols for PUFs.

4.3.1.2. Alkoxylation

Similarly to carbohydrates, the different and more or less accessible OH groups can be transformed into more active OH groups at the end of polyether grafted chains via alkoxylation reactions. Organosolv (Arshanitsa et al. 2014; Cateto et al. 2014, 2009; Kurańska et al. 2020a; Li et al. 2020a; Li and Ragauskas 2012a; Nadji et al. 2005), pyrolytic (Saffar et al. 2020), Kraft (Cateto et al.

2014, 2009; Li and Ragauskas 2012b; Mahmood et al. 2015; Nadji et al. 2005; Wu and Glasser 1984), Soda (Cateto et al. 2014, 2009) lignins and tannins (Arbenz et al. 2016; Arbenz and Avérous 2014) were transformed into suitable polyols by this way. Epoxide rings for the alkoxylation can be synthesized from double bonds presents in biomass products. Nevertheless, the propylene carbonate, a well-known and non-toxic O-alkylating agent of phenol was used to graft polyether chains originated from phenol groups. Similarly to the alkoxylation reaction, the average number of polyether units per chain increase with the excess of propylene carbonates (Duval and Avérous 2016). The investigation with several carbonates demonstrated the potential of this solvent-free, fast and quantitative reaction to transform non-reactive phenol into reactive primary or secondary OHs toward isocyanate groups (Duval and Avérous 2017). The utilization of a kraft lignin polyol derived by this technique for PUFs production was realized using polyethylene glycerol (PEG) as a solvent (Zhang et al. 2019f).

4.3.1.3. Neat Polyphenols

Contrary to polysaccharides, lignins with adapted extraction technics and also tannins can be used directly without modification, neat, in PUFs formulation. Nevertheless, the solid and powdery aspect of the extracted lignin is the major drawback for this utilization. The dissolution in different polyols such as di- (DEG), tri-ethylene glycol (TEG), PEG, alkoxylated sucrose or molasses circumvented this problem, and the mixture can be introduced in the formulations (Hatakeyama et al. 2013, 2004; Hatakeyama and Hatakeyama 2005; Hayati et al. 2018; Liu et al. 2009). The properties of the corresponding PUFs can be adjusted depending on the lignin content. The utilization of biobased fatty acid and glycerol to disperse lignins was also investigated (Carriço et al. 2016). On the contrary to some works where the lignin is used as fillers (Thakur et al. 2014), the utilization of neat organosolv and kraft lignins as a polyol in PUFs formulations resulted in the integration of the lignin into the network architecture with covalent bonds (Pan and Saddler 2013). The dispersion of tannin in polyols was also applied with alkoxylated fatty amine to act as a reticulation agent (Basso et al. 2014b). Otherwise, the mildly-sulfided quebracho wood tannin was mixed with furfuryl alcohol to form aromatic PUFs (Basso et al. 2014a).

4.3.1.4. Miscellaneous transformations

The production of fully biobased polyol was achieved through the esterification of lignin with oleyl chloride and further epoxidation-ring opening of the oil double bonds (Laurichesse et al. 2014). Another strategy was the utilization of the Mannich reaction with lignin, diethanolamine and formaldehyde. The lignin-aminated was dissolved into PEG before the foaming process (Huo et al. 2012). Otherwise, alkali lignins were modified by hydroxymethylation, epoxidation and phenolation and then introduced in polyols. Despite the low portion of added lignin (1 wt%), the effect on the foam properties was notable (Yang et al. 2014).

4.3.2. Polyisocyanates

The pre-polymerization of lignin with a diisocyanate excess is the only strategy used to form polyisocyanate from neat phenolic biomass. The functionalization of lignin with pMDI was, for instance, realized (Zhang et al. 2018c). This surface-functionalized lignin was further introduced into PUFs (Zhang et al. 2019e, 2018c).

4.3.3. Additives

Lignins and tannins were widely investigated to form polyol thanks to the well-known increase of mechanical properties brought by the aromatic structure. However, aromatic structures are also known to be used as FR systems. The modified lignin contains primary OH groups to covalently linked to the PUFs network and phosphorous and aromatic compound for the FR properties (Xing et al. 2013). Another strategy was the transformation of a tannin monomer, the gallic acid (Howell et al. 2018).

4.4. Products from industrial wastes

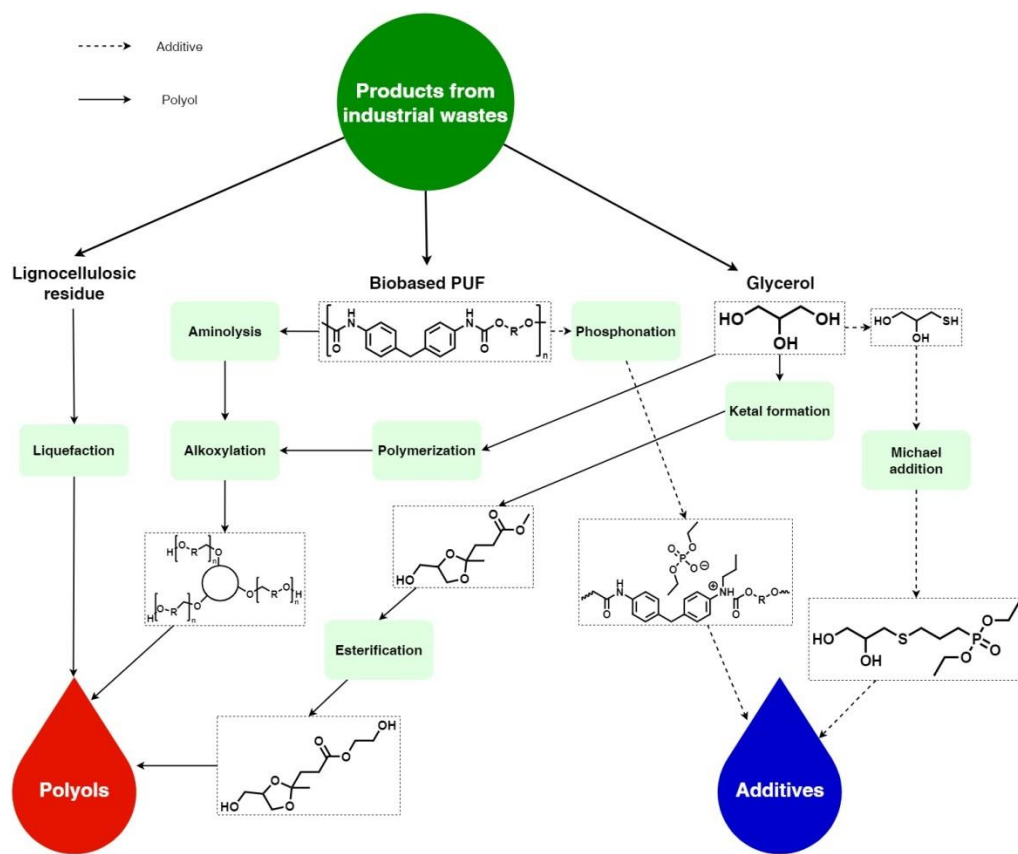


Figure 1.14 - Overview of the transformation of wastes from industrial processes into PUF components.

The production of industrial consumer goods inevitably generates wastes either from the production of non-compliant products or after the life of the product. This part is focused on the production of PUFs components based on three abundant wastes from industrial processes: biobased PUs, crude glycerol, and lignocellulosic residues presented in Figure 1.14. Alkoxylation and liquefaction are the main pathways to develop polyols from lignocellulosic residues, biobased PUs or glycerol, as shown with polyphenol resources. Actually, there are no developed routes from industrial wastes toward isocyanates.

4.4.1. Polyols

4.4.1.1. Biobased PUF

One way to obtain biobased components for PUFs, such as polyols, is to use compounds obtained from recycling biobased PUs, such as chemical or biological recycling. Despite the recent and fast developments on the enzymatic degradation of PUs, there is still work to understand mechanisms and develop higher scale productions (Magnin et al. 2020). The chemical degradation of PUs is achieved through various processes such as hydrolysis, aminolysis, phosphatation or alcoholysis. The two first methods yield amine, which can be further used in the epoxy resin formulation (Dai et al. 2002; Xue et al. 1995), and the third, based on phosphate reaction, will be detailed later. Aminolysis has been used on F-PUFs, followed by an alkoxylation reaction to produce polyols (Van Der Wal 1994). However, the first process to obtain polyols from PUs wastes is the alcoholysis. The process was applied to numerous wastes such as RIM (Modesti and Simioni 1996), foams (Nikje et al. 2006; Ulrich et al. 1978) or scrapped PUs (Sendijarevic 2007; Shin et al. 2019a). Green chemistry can be obtained, for instance, using transesterified coconut oil for the alcoholysis of PUs (Paruzel et al. 2017). The major drawback of this strategy is the high-energy consumption, which is balanced by the valorization of “plastic” wastes.

4.4.1.2. Glycerol

The biodiesel produced from the transesterification of triglycerides generates a considerable amount of glycerol as side products. This crude glycerol contains sodium generally used as the catalyst for the transesterification, residue of oils and water, which can be removed to obtain high purity glycerol (J. C. Thompson and B. B. He 2006). This triol with a high I_{OH} is introduced neat in a small portion as crosslinker with low I_{OH} co-polyol in PUFs formulations (Furtwengler et al. 2017; Narine et al. 2007; Ng et al. 2017). Glycerol can be polymerized to reduce the I_{OH} value and obtain long polyol chains (Ionescu and Petrović 2010; Piszczyk et al. 2014). Recently developed, the formation of a ketal between glycerol and the methyl levulinate derived from wheat straw was reported. The methyl ester was further transesterified with EG to form a diol introduced up to 100% in PUFs (Li et al. 2020b).

4.4.1.3. Liquefaction of waste from industrial process

Industrial processes such as sugar extraction from sugar cane generates biobased solid wastes composed mainly of the solid part of plant cell walls (Figure 1.12). It can be valorized into polyols for PUFs by the liquefaction process as detailed in the lignins and tannins section. This reaction was used with food industry wastes (Abdel Hakim et al. 2011, 2011; Amran et al. 2019; Lee et al. 2000; Pavier and Gandini 2000a; Sendijarevic et al. 2020; Zhang et al. 2019b, 2020, 2019c), straws (Hu et al. 2012; Jasiūnas et al. 2020), digested sewage sludges (Jasiūnas et al. 2020) or microalgae biomass (Hejna et al. 2018).

4.4.2. Additives

As previously presented, the PU can be degraded by phosphate. This strategy was employed to produce urethane oligomers with high phosphorous content (Troev 2000). Otherwise, a glycerol derivative was transformed in FR via a Michael addition. The thioglycerol was added to diethyl allyl phosphonate to produce a polyol with low viscosity and intrinsic FR properties due to the phosphorous compound (Bhoyate et al. 2018).

4.5. Products from white biotechnology

This part is linked to Figure 1.15. From different biobased molecules extracted from biomass mainly by biotechnology in biorefineries such as limonene, β -pinene, eugenol, malic and citric acid, furan, vanillic and syringic acid, oil cashew nut shell liquid (CNSL) or derived from amino acids, different PUFs components can be elaborated. One of the most common building blocks obtained by biotechnology for PU is the 1,4-butanediol. This diol is obtained industrially through hydrogenation of succinic acid obtained by biotechnology (Debuissy et al. 2018). Genomatica developed another strategy by bioengineering an *Escherichia coli* strain to directly produce 1,4-butanediol from renewable carbohydrate feedstocks (Yim et al. 2011). The 1,3-propanediol is another important diol bioproduced either from glycerol or glucose (Debuissy et al. 2018). In PUFs, these biobased diols are used as chain extenders (Li et al. 2020a; Rashmi et al. 2013) or through the synthesis of polyols (Furtwengler et al. 2017).

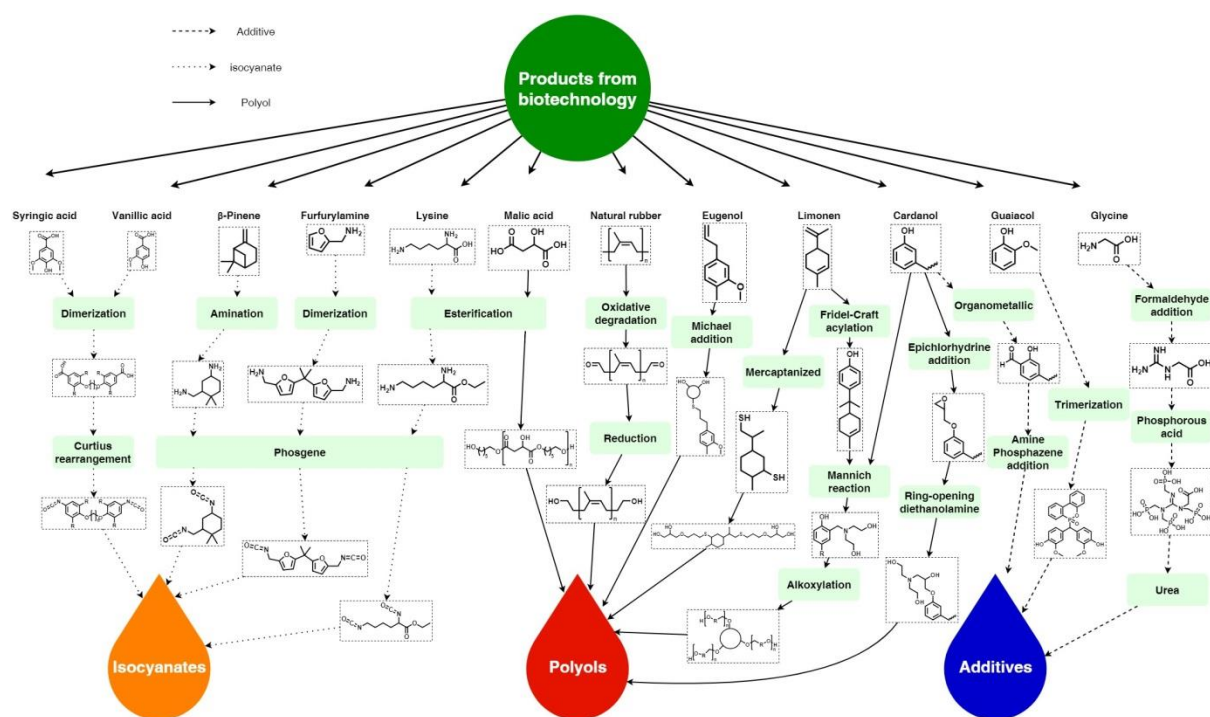


Figure 1.15 - Overview of the transformation of products from biotechnology into the PUF component.

4.5.1. Polyols

Different compounds can be more or less directly extracted from biomass to produce polyols. The processes are often integrated into biorefineries based on biotechnology and chemical steps.

For example, it is the case of the limonene, which is obtained, e.g., from orange peels or produced by microorganisms (Jongedijk et al. 2016). Based on a cyclic structure with two double bonds suitable for chemical transformation, it can be transformed into a Mannich polyol with 1,3-N-hydroxyethyl oxazolidine (Gupta et al. 2015). Otherwise, limonene was mercaptanized with hydrogen sulfide and then reacted with glycerol-1-allyl ether via Michael addition to form a polyol for PUFs

(Zhang et al. 2018a). In another study, the malic acid, a dicarboxylic acid potentially obtained by microbial fermentation (Kövilein et al. 2020), was oligomerized with 1,6 hexanediol to produce a polyol which is used in PUFs formulation. The presence of one OH group on malic acid increases the I_{OH} of the produced polyol (Yang et al. 2019).

As previously seen, carbohydrates are an important source for the elaboration of biobased molecules. The β -methyl- δ -valerolactone, a six-membered ester ring, was, for instance, synthesized from glucose with mevalonate as an intermediate (Xiong et al. 2014). It was transformed into a polyol via acid-catalyzed ring-opening transesterification with trimethylolpropane ethoxylate (Schneiderman et al. 2016).

Otherwise, alkoxylated (Shrestha and Ionescu 2018) or not (Hu et al. 2020) eugenol extracted from cloves was transformed through thiol-ene chemistry to produce polyols. In another study, the natural rubber was transformed through controlled oxidative degradation, followed by a reduction to obtain a OH-terminated natural rubber (Jaratrotkamjorn and Tanrattanakul 2020).

Another source of recent innovation in terms of new molecules is the CNSL, which is composed at 90% of anacardic acid, a particular lipid formed by a phenol with a carboxylic acid in the ortho position and an unsaturated carbon chain in the para position. The decarboxylation of anacardic acid by heating yields cardanol (Quirino et al. 2014). It was transformed into polyols via alkoxylation (Reese et al. 2010) or Mannich (Gandhi et al. 2015; Ionescu et al. 2012; Zhang et al. 2014) reaction. A hybrid polyol has recently been developed based on cardanol, composed of catalytic tertiary amine and polysiloxane chains similar to surfactants (Huo et al. 2019).

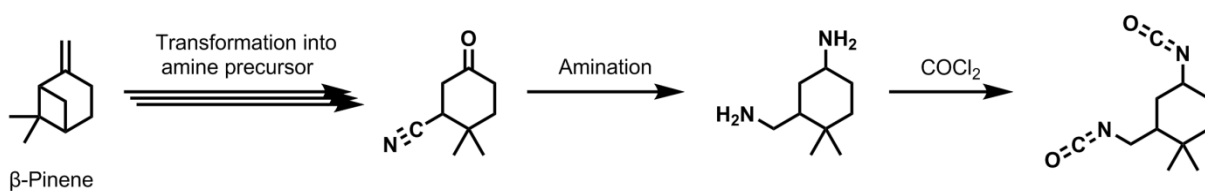
4.5.2. Additives

Cardanol was modified to obtain a FR molecule composed of 66% of cardanol and 3.4% of phosphorous (Amarnath et al. 2018). The trimerization of vanillic acid, guaiacol and DOPO to form a FR containing phosphorous was developed for the epoxy resin, but it could be adapted to be used in PUFs formulation (Liu et al. 2020). Another example, the guanidine acetic acid (glycocyamine), which is derived from the hydrolysis of proteins (i.e., glycine), was modified to form a FR compound (Wan et al. 2020).

4.5.3. Polyisocyanates

With lignin and tannins derivatives, aromatic isocyanates can be synthesized. Syringic and vanillic acid can be dimerized and further converted into isocyanate via Curtius rearrangement (Kuhire et al. 2017). This method has the particularity to produced diisocyanate with a control chain length between the two aromatic moieties.

The amino acid lysine was transformed into diisocyanate by esterification with ethanol and phosgenation of the amines. The ethyl ester (L) Lysine diisocyanate obtained is well known, especially in biomedical or coating applications (Acik et al. 2019; Calvo-Correas et al. 2015; Gustini et al. 2016; Li et al. 2015). Another synthetic route toward diisocyanate from β -pinene is described in Scheme 1.4. The β -pinene distilled from pine was transformed through several steps into a diamine and further in diisocyanate by phosgenation (Kobilka et al. 2019).



Scheme 1.4 - Synthesis of diisocyanate from β -pinene. Adapted from (Kobilka et al. 2019).

The furan derivatives obtained by dehydration of monosaccharides could be good candidates for the replacement of aromatic structures. Extensive researches are conducted on the furan and a major component to produce PEF (equivalent to PET) the polyethylene 2,5-furan dicarboxylic acid (de Jong et al. 2012). The furfuryl amine obtained from the biotransformation of furfural (Zhang et al. 2019d) was dimerized with acetone under mild conditions; the obtained difurfurylamine was transformed via phosgenation into diisocyanate (Cawse et al. 1984). The reactivity of furan isocyanates was found to be similar to aromatic analogs (TDI) (Belgacem et al. 1993; Boufi et al. 1995, 1993). A novel strategy to develop foams from furan derivatives was based on the modification of two carboxylic groups of the bis(5-carboxyfurfuryl)ether into carboxylic-azide. This precursor was introduced with polyols and heated to induce the Curtius rearrangement to form isocyanate from azide. The nitrogen released by this reaction served as a BA for the foam network composed of the newly formed diisocyanate and the polyol (Neumann et al. 2011).

5. STUDY OF “STRUCTURE-PROPERTIES” RELATIONSHIPS IN THE CASE OF BIOBASED R-PUF

The goal of this chapter is to study the relationship between the structure or morphology of the foams and some specific properties. This chapter is mainly focused on biobased R-PUFs, which are mainly used as insulation materials. The characterizations of these foams are then targeted and focussed on the application and largely less diverse than the F-PUFs. Besides, the processing and the additives differ from R-PUF to F-PUF, increasing the complexity to draw a general conclusion on the effect of the biobased components on all PUFs properties.

R-PUFs are at least mainly based on six components, such as the polyisocyanate, polyol, BA, surfactant, catalyst and additives (Table 1.1). The conventional polyisocyanates and surfactants are usually pMDI and polyether siloxane, respectively. The BAs and catalysts structures evolve in the formulation to reach the optimum properties in accordance with the targeted application. The comparison between the data of the literature is often difficult due to the multiplicity of foam formulations with different NCO/OH indexes, catalysts/surfactant loadings and structures, foaming environments or BAs.

5.1. Morphological and structural data

In R-PUFs, the cells are generally defined by a polyhedron shape close to an honeycomb structure. The faces of the polyhedron are called the walls, and the thicker edges the struts. In a partially open system such as a cup often use as a mold, the cells are elongated in the vertical

direction. This phenomenon was explained by the constraint expansion by the cup walls inducing a faster growth in the vertical direction than the horizontal direction (Hawkins et al. 2005). The cell morphology is defined by the density of the foam, the cells size and shape, and the closed-cell content. The related properties are affected by the foaming process and linked parameters (viscosity, surface tension, kinetics) and materials properties (phase separation).

5.1.1. Viscosity

Generally, the viscosity of polyols for R-PUFs is between 2 and 50 Pa.s (Table 1.3). Figure 1.16 represents the dependence between cell size and viscosity. The data were compiled from the literature of foams made with a biobased sole polyol. As shown in Figure 1.16, when the viscosity of the polyol is under 5 Pa.s, the produced foam presents dispersed cell sizes. On the contrary, the cells obtained with a moderately viscous polyol (5-25 Pa.s) are homogeneous and smalls, around 200 μm . Finally, few examples of cell size from foams realized with highly viscous (> 25 Pa.s) polyols are presented in Figure 1.16. The size varies from 250 to 490 μm .

The high viscosity of biobased polyols can originate from triglycerides crystallization (Ng et al. 2017), branched structure of phenolic compounds (Arbenz et al. 2016; Carriço et al. 2016; Hayati et al. 2018; Xu et al. 2014 p. 201), solid residues in the polyol (Abdel Hakim et al. 2011) or high molar masses (Furtwengler et al. 2018a; Ghaderian et al. 2015; Shin et al. 2019a). Moderate viscosity is requested to reduce the cell-size due to the limitation of bubble coalescence and expansion (Arbenz et al. 2016; Kurańska et al. 2020b). For example, the cell diameters of foam obtained from alkoxylated glycerol (0.2 Pa.s) and tannin (6.9 Pa.s) were 440 and 290 μm in the rise direction, respectively (Arbenz et al. 2016). The authors attributed this decrease in cell size to the high viscosity and functionality of the alkoxylated tannin. Furthermore, the nucleation of cells is heavily affected by the viscosity of the foaming liquid. In more viscous polyols, the concentration of air bubbles is higher due to the limited diffusion and coalescence. The nucleation was enhanced by the branched and pendant chains of triglycerides polyols (Fan et al. 2013) or solid lignins dispersion in the polyol (Hayati et al. 2018; Mohammadpour and Mir Mohamad Sadeghi 2020). The incorporation of 10 wt% of the unmodified lignin particles in the polyol improved the nucleation and can decrease the average cell size from 510 to 430 μm (Hayati et al. 2018). The introduction of long aliphatic segments enhanced the flexibility and decreased the viscosity; therefore, coarser and more irregular cells were obtained (Gaidukova et al. 2017). However, too high polyol viscosity was also observed to cause coarser and less uniform cells. The polyols prepared with 40 wt% of lignin were highly viscous (16.7 Pa.s) and caused less uniform and coarser cells (Pan and Saddler 2013). A similar trend was observed with soybean oil-based polyol. An increase in viscosity from 7 to 23 Pa.s of the soybean-polyols clearly produced PUFs with coarser cells affecting the nucleation process (Fang et al. 2019). The high viscosity of polyols induces mixing drawbacks and therefore a higher dispersity in cell sizes, as shown in Figure 1.16.

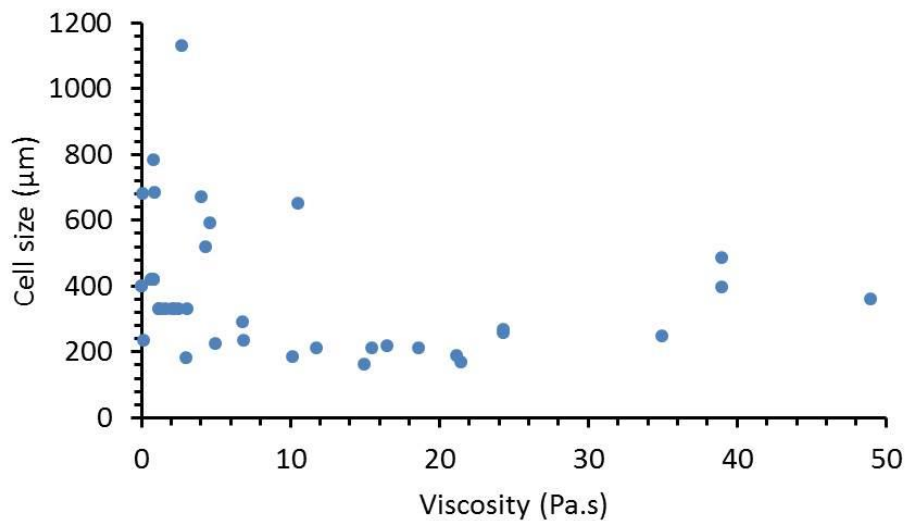


Figure 1.16 - Viscosity of polyol vs. the cell size for PUF. Compilation of data from literature (Fang et al. 2019; Hejna et al. 2018; Huo et al. 2019; Jiang et al. 2018; Kahlerras et al. 2020; Kurańska et al. 2020b; Luo and Li 2014; Ng et al. 2017; Paruzel et al. 2017; Pawar et al. 2016b; Piszczek et al. 2014; Ugarte et al. 2015; Veronese et al. 2011; Yang et al. 2012, 2019; Zieleniewska et al. 2015).

5.1.2. Surface tension

The surface tension was shown to play a crucial role in the formation of small cells. The growth of bubbles is closely related to the surface tension of the foaming mixture by the Laplace equation (Furtwengler et al. 2018b). The increase in surface tension induced by the sorbitol polyester polyol slows down the growth of the cell. Cell size can be partially controlled by formulation, cells were reduced from 410 to 270 μm in the longitudinal direction by the addition of polyester polyol from 10 to 35 wt% (Furtwengler et al. 2018b).

5.1.3. Reaction kinetics

In the same study (Furtwengler et al. 2018b), the faster gelling of the polymer network was shown to help the generation of small cells. As previously explained, the expansion of bubbles is closely related to the equilibrium between blowing and gelling reaction. Significant modification in the formulation, such as the substitution of the polyol, alters the gelling/blowing balance. Figure 1.17 represents the evolution of the temperature, viscosity and cell morphology over time in different cases: the balance is in favor of the blowing (Figure 1.17A), equilibrium of the blowing/gelling balance (Figure 1.17B) and the balance in favor of the gelling (Figure 1.17C).

In the case of high blowing efficiency, the foam size increases rapidly due to a sudden temperature increase (Figure 1.17A). Therefore, the cell size and elongation increase and the density decrease as represented in Figure 1.17A in comparison with Figure 1.17B. Moreover, fast cell expansion often induces breaks in the thin walls to form open cells (Figure 1.17A). A decrease of density from 102 to 66 kg/m^3 attributed to the increased blowing efficiency was observed when the polytrimethylene ether glycol content was increased in the foam formulation (Ugarte et al. 2015). The hydrophilic character of the polyol and thus, its water content could explain this increased blowing activity, as it was observed with linseed oil used as a surfactant (Czlonka et al. 2018). Higher water

content promotes the rapid and sudden release of CO_2 producing larger cells with thinner walls (John et al. 2002). Furthermore, the closed-cell content decreased under 10% with higher foaming rate polyols (Furtwengler et al. 2018a).

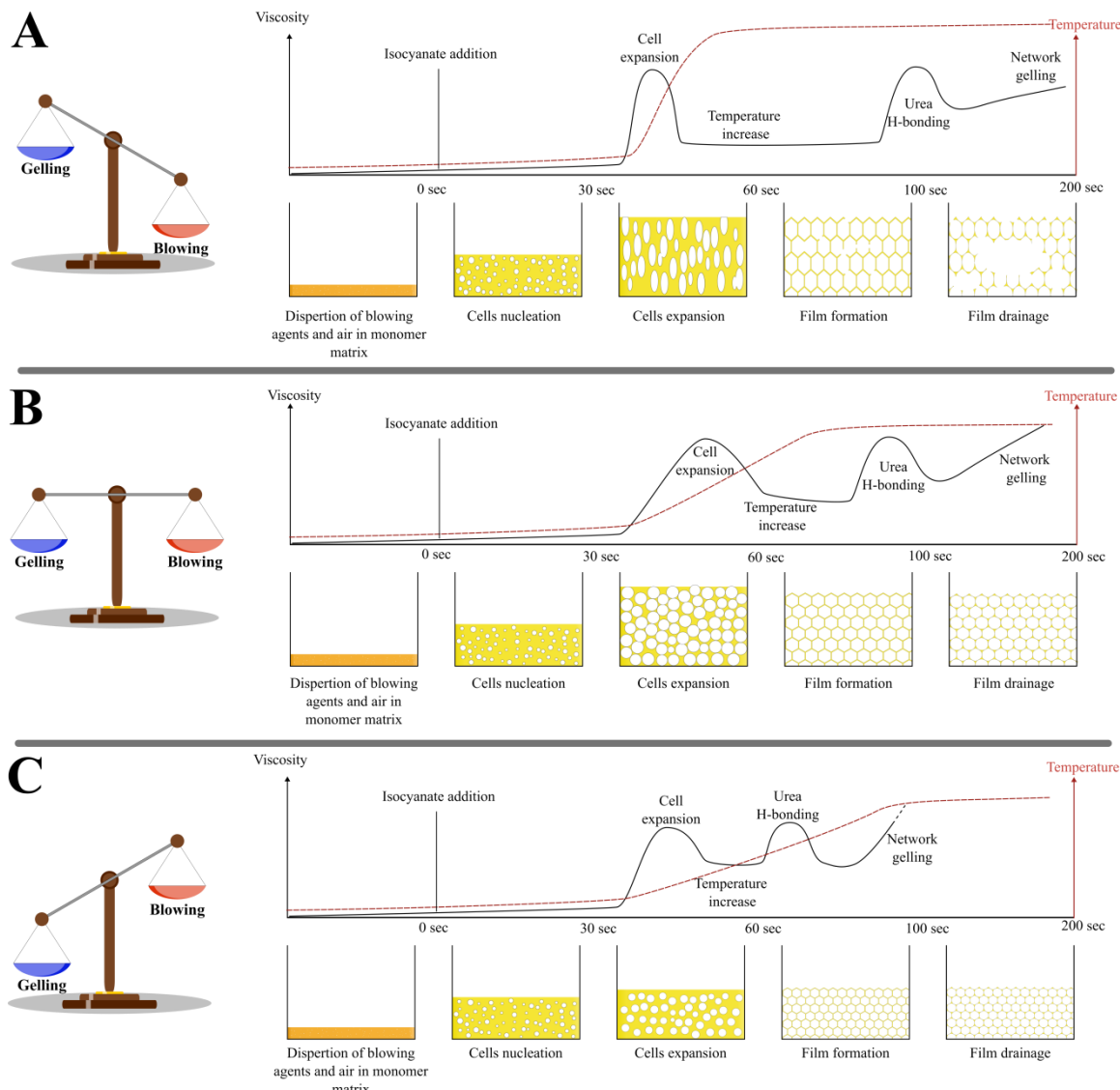


Figure 1.17 - Effect of the gelling/blowing balance vs. temperature, viscosity and foam cell morphology in three typical cases: (A) mainly blowing, (B) equilibrium and (C) mainly gelling.

Nevertheless, the primary effect observed, coupled with a higher blowing activity, is related to the decrease of the gelling activity. Figure 1.17A represents the evolution of the viscosity over time when the gelling is lower than the blowing activity. In this case, the longer gel time is characteristic of a slow network formation around the growing bubbles; thus, cell drainage and Ostwald ripening get a longer time to deteriorate the closed-cell morphology (Figure 1.17A). Therefore, the cells are coarser, and the closed-cell content decrease (Amran et al. 2019; D'Souza et al. 2014; Furtwengler et al. 2018a; Li et al. 2016a; Mahmood et al. 2016). For example, the introduction of less reactive liquefied lignin compared to conventional polyols was observed to produce a broader cell distribution (Li et al. 2016a). In another study, the introduction of liquefied biomass formed large and widely distributed cells. The coalescence of cells by Ostwald ripening explained the difference of the mean diameter between the

reference foam made with PEG-glycerol (660 μm) and the biobased system (780 μm). The authors pointed out the low reactivity of phenols from the biobased aromatic polyols (Amran et al. 2019).

The lower reactivity of the polymer network formation was also explained by lower I_{OH} (Maldas and Shiraishi 1996; Ugarte et al. 2015). The OH density is related to the functionality of the polyol, and it is well known that the higher the functionality is, and the lower the conversion to reach the gel point will be (Flory 1941; Stockmayer 1944). Furthermore, with similar I_{OH} , the decrease in gelling rates can be explained by the lower reactivity of the secondary (Fan et al. 2013; Peyrton et al. 2020) or even phenolic OH groups (Amran et al. 2019), compared to primary OHs. Furthermore, a high acidity of the polyols resulting from the biomass transformation can reduce the amine catalysis activity and forms coarser cells (Arshanitsa et al. 2014; Peyrton et al. 2020). The gel time was proved to increase from 200 to 510 s with the substitution of 50 wt% of the polyol by lignin. The authors explained that lignin contained free acetic/formic acid, which, once bonded with an amine catalyst, reduced its activity. This hypothesis was further supported by the decrease in density explained by the free carboxylic acid reaction with isocyanates forming amide and CO_2 (Arshanitsa et al. 2014). If the gelling is very low compared to the blowing, the cells burst, and the foam falls back before the polymer solidifies (Campanella et al. 2009; Fan et al. 2013; Hejna et al. 2017).

On the contrary, when the gelling reaction is favored, the polymer solidifies faster than the gas expands. This is represented in Figure 1.17C by a rapid increase in viscosity compared to Figure 1.17B. Therefore, smaller cell size, higher closed cell content and an increase in density are generally observed (Figure 1.17C). Polyols with high I_{OH} makes the polymer network gel faster because less conversion is required to form a crosslinked structure. For example, the transesterification of castor oil with crude glycerol produces polyols with lower I_{OH} (350 mg KOH/g) than neat glycerol (540 mg KOH/g). The crude glycerol polyol formed lighter foams (95 vs 245 kg/m^3) with bigger cells (600 vs 400 μm) (Bresolin et al. 2018). Similar results were observed on biobased polyols with high I_{OH} produced with oils (Riyapan et al. 2019), carbohydrates (Furtwengler et al. 2018b) or liquefied lignins (Li et al. 2020a). Furthermore, the shrinkage reduced from 4 to 0.4% and the collapsing from 2.3 to 0.1% within foam elaborated from 250 mg KOH/g polyol instead of 100 mg KOH/g (Riyapan et al. 2019). This is due to the thicker cell walls presented in Figure 1.17C compared to Figure 1.17B.

The higher content of more reactive primary OHs increased the gelling rate of foam (Piszczek et al. 2014; Sendijarevic et al. 2020). As shown in Figure 1.17C, a faster gelling form low cell size compared to Figure 1.17B. A decrease in cell size of 150 μm was observed with the introduction of more reactive polyols obtained from liquefied spent coffee grounds. This phenomenon was explained by the reduction of the coalescence due to the faster polymerization (Sendijarevic et al. 2020). Another way to increase the gelling activity of the polyol is the incorporation of catalytic sites inside the polyols structure. The introduction of a tertiary amine in model fatty ester alcohol was proved to increases the reaction rate between the OH group and isocyanate (Peyrton et al. 2019). In PUFs, it was achieved with Mannich reaction on limonene based polyols (Gupta et al. 2015), triglycerides epoxidation and ring-opening with amine (Peyrton et al. 2020) and modified cardanol (Huo et al. 2019). However, this kind of polyol cannot substitute the standard polyol without a complete disequilibrium between the gelling and blowing balance. For example, the substitution of 25 wt% of conventional polyol by epoxidized microalgae oil ring-opened with diethylamine was proved to increase the kinetics of the foam and deteriorate the cell morphology (Peyrton et al. 2020). However, in the same study, the epoxidized soybean oil ring-opened by diethylamine was successfully used as a

unique catalyst to form low-density foams (36 kg/m^3). Another strategy can balance blowing and gelling with a cardanol based “autocatalytic” polyol (Huo et al. 2019).

In some rare cases, the substitution of biobased polyols did not affect the foaming process (Figure 1.17B). For example, the introduction of alkoxylated lignin produces foam with similar reactivity compared to fossil-based polyol. It was assumed that a similar structure composed of PO units plays a key role in similar kinetics (Mahmood et al. 2016). Despite the lower reactivity observed with an oil-based polyol, the foaming process and the cell morphology were not affected (Borowicz et al. 2019; Herrán et al. 2019).

5.1.4. Microphase segregation

A particularity of the PU networks is the capacity to segregate into (i) strongly H-bonded hard segments and (ii) long flexible chains called soft segments. The microphase separation in PUFs generally explains a defect in the foam, such as irregular pores (Arbenz et al. 2017; Ng et al. 2017) or wrinkles (Jiang et al. 2018). The activity of the soft segments formed by the long and flexible chain on the microphase separation is not yet fully understood. Some theories claimed that the higher flexibility of this soft segment allows a better migration of the surfactant with the formation of coarser cells and lower densities (Borowicz et al. 2019; Contreras et al. 2020). It was also noticed that the small molar mass molecules in liquefied bark polyols had a plasticizing effect increasing the drainage and open-cell content. Otherwise, the decline in the free volume of polymer with the gradual substitution of glycerol by lignin extended the density from 60 kg/m^3 to 115 kg/m^3 with 10 wt% and 40 wt% of lignin, respectively (Carriço et al. 2016). Nevertheless, these effects need to be further investigated with more in-depth analysis.

To summarize, the cell morphology is highly influenced by the structure of the biobased component via its reactivity, viscosity, nucleation capacity, surface tension or resulting microphase separation. In most cases, the foams are formulated by substitution of a weight portion of the fossil-based polyol by the biobased one, with every other parameters being constant. The advantage of this method is to show the influence of the biobased compound on the foaming process by the characterization of the density, cell size and closed-cell content. Formulation optimization should always complete this approach because the biobased polyol, by its structure difference, have certainly different interaction compared to the fossil-based. Furthermore, the morphology of the cell profoundly affects other properties such as mechanical, thermal or fire resistance. Consequently, the biobased compound impact on these properties is never really isolated and then determined.

5.2. Mechanical properties

Cellular materials are a combination of excellent mechanical properties on lightweight materials (Erjavec 2011). In PUFs, the compression strength is the most common measurement to evaluate the mechanical properties of the material. The compression behavior of foams can be decomposed into several stages: First, the linear region is governed by the compression and bending of the cells struts, then the stretching of the cell walls and finally, the compression of the trapped gases

(Weißenborn et al. 2016). The effects of the cell morphology, the crosslink density and the structure of the biobased component on the compression strength properties of PUFs are given below.

5.2.1. Morphological structure of cells

The compression strength highly depends on the density of the material. The lower the density is, the lower the compression strength will be (Ghaderian et al. 2015; Yang et al. 2012). Figure 1.18A shows the evolution of the density and the compressive strength of foams with a gradual introduction of lignin-based polyol (Li et al. 2016a). Figure 1.18A shows that the increase in compressive strength follows directly the increase in density. Furthermore, the compression strength (σ) was correlated with the foam density (ρ) with a power-law model expressed in Equation 1.1.

$$\log(\sigma) = \log A + B * \log(\rho) \quad (1.1)$$

Figure 1.18B represents the compressive strength evolution over the density in logarithmic scales, modeled by Equation 1.1. The linear regression slope value was 1.5 in Figure 1.18B for a series of water-blown foams realized with varying amounts of water. This value was in agreement with the literature value ranging between 1 and 2 (Thirumal et al. 2008). The compressive strength can be normalized according to Gibson-Ashby (Gibson and Ashby 1997) equation, expressed in Equation 1.2 to compare foams with different densities.

$$\sigma_n = \sigma_m * \left(\frac{X}{\rho_f} \right)^2 \left(\frac{1 + \sqrt{\frac{X}{\rho_s}}}{1 + \sqrt{\frac{\rho_f}{\rho_s}}} \right)^2 \quad (1.2)$$

Where σ_n is the normalized compressive strength, σ_m the measured, ρ_f the measured density of the PUF, ρ_s the density of solid PU (1200 kg/m^3) and X the density of normalization (Shin et al. 2019a). The compressive strength of the flexible cell foams relies on bending and cell wall axial deformation. On the contrary, in closed-cell foams, the air inside the cell and the walls contribute to the compressive strength (Arbenz et al. 2016; D'Souza et al. 2014; Gibson and Ashby 1997). It is worth mentioning that open-cell foams have higher compressive strength than closed-cell material with cell walls ruptured. The broken walls are unable to contribute to stress reinforcement and will initiate rupture when the cells are under load (Narine et al. 2007). The homogeneity and cell size also affect the mechanical properties such as compression. R-PUFs with small and organized cells have higher compression strength due to homogeneous repartition of the load (Amran et al. 2019; Cateto et al. 2014; D'Souza et al. 2014; Fang et al. 2019; Li et al. 2016b; Ng et al. 2017; Pan and Saddler 2013; Zhang et al. 2019f).

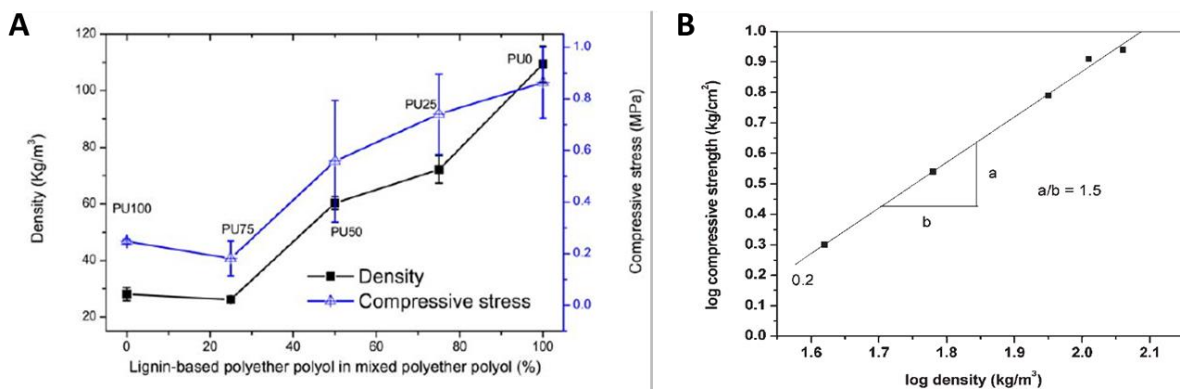


Figure 1.18 - (A) Effect of the introduction of lignin-based polyol on the density and compressive strength of PUF. (B) Dependence of the compressive strength on density. Reproduced with permission from (Li et al. 2016a) and (Thirumal et al. 2008).

5.2.2. Crosslink density

I_{OH} represents the OH groups density of a given system. In the final material, OHs are transformed into urethane groups; therefore, the higher the I_{OH} of the polyol is, the higher the density of urethane and crosslinking will be. This property indicates the strength of the polymer network and profoundly affects the mechanical properties. A high I_{OH} gives high compressive strength (Abdel Hakim et al. 2011; Arbenz et al. 2016; Hayati et al. 2018; Hejna et al. 2018; Kosmela et al. 2019; Kurańska et al. 2020a; Mahmood et al. 2016; Maldas and Shiraishi 1996; Ng et al. 2017; Riyapan et al. 2019) and vice-versa (Amran et al. 2019; Jiang et al. 2018; Pan and Saddler 2013; Ramanujam et al. 2019; Ugarte et al. 2015). For example, an increase in compressive strength from 26 to 81 kPa has been obtained with an increase of I_{OH} from 100 to 250 mg KOH/g (Riyapan et al. 2019). Furthermore, the gradual substitution from 0 to 70 wt% of fossil-based by crude glycerol-based polyol demonstrated a constant increase in compressive strength in parallel and perpendicular directions (Hejna et al. 2018). Finally, the compressive strength of foams realized with an increasing portion of liquefied biomass was shown to increase due to the larger crosslink density of the sample. The authors confirmed this hypothesis with the decrease of the soluble fraction in the foam elaborated with the highest I_{OH} (Kosmela et al. 2018). However, the introduction of biobased polyol with lower I_{OH} can be detrimental to the mechanical properties as Eceiza and coworkers showed with the introduction of 30 wt% of polytrimethylene ether glycol. The specific compressive properties decreased from 9.9 to 6.0 kPa·kg⁻¹·m³ with the substitution of the fossil-based (444 mg KOH/g) by the biobased (80 mg KOH/g) polyol.

5.2.3. Molecular structure

The different biomass sources, previously described, present a large range of chemical structures. This variety of biobased components induces a multitude of new macromolecular architectures. The compression strength of the PUFs depends on the molecular level interactions in the studied system. The next part aims to detail the impact of the different biobased structures on the mechanical properties.

The triglycerides are composed of different long aliphatic chains. The corresponding increase of flexibility in the polyols gives higher elastic properties to the polymer network and then impacts the

compression strength. The foam realized with 50 wt% of polyol synthesized from mercaptoethanol thiol-ene addition with corn oil had a compressive strength of 120 kPa (Ramanujam et al. 2019). This value was lower than foam with similar density realized by epoxidation and ring-opening with ethanol of microalgae oil (270 kPa) (Peyrton et al. 2020). This difference can be explained by the higher I_{OH} due to the higher double bonds quantity of the microalgae compared to corn oil, for instance. Furthermore, the concentration of unfunctionalized long fatty chains called dangling chains higher in corn oil caused higher flexibility.

The increasing portion of dangling chains is said to plasticize the network, reducing the compression strength (Narine et al. 2007 p. 20; Ng et al. 2017; Pillai et al. 2016; Zieleniewska et al. 2015). Narine and coworkers studied the effect of the dangling ends in PUFs. They used different polyols with similar I_{OH} synthesized by various methods. The authors found that the compressive strength of soybean polyol realized by epoxidation and ring-opening was the lowest with the plasticizing effect of the dangling ends (Narine et al. 2007). The PUF realized with rapeseed oil-based polyol had compression strength 15% lower than the fossil-based reference due to the plasticizing effect of dangling chains-ends (Zieleniewska et al. 2015).

As previously explained, the epoxidation followed by ring-opening is one of the most popular ways to obtain polyols from vegetable oil. The ring-opening reaction is often accompanied by side reactions such as epoxide polymerization, which can modify the final properties. Then, an unexpected increase of compressive strength was obtained for foams with 30 to 50 wt% of epoxidized soybean oil ring-opened by EG. The authors hypothesized that the polyether network formed by this polymerization supported the network (Fan et al. 2013).

Lignins produced with different extraction methods are often a powder. Unfortunately, the foam processing is not adapted for the integration of solid polyols at high content. This is shown in Figure 1.19, by the compressive strength evolution over the lignin/polyol ratio. The introduction of a small portion (25 wt%) of raw lignin instead of the polyol made the compressive strength drop from 500 to 250 kPa without significant change in density (Pan and Saddler 2013). In Figure 1.19, the gradual introduction of lignins into PUFs showed a plateau in compressive strength from 25 to 60 wt%. However, after 60%, the poor dispersion of lignin into the matrix results in a ruin of mechanical properties (Figure 1.19).

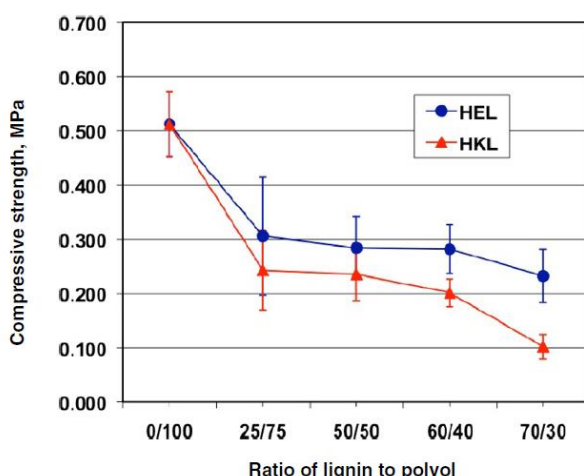


Figure 1.19 - Effect of lignin addition on the compressive strength of R-PUF. The ratio of lignin to polyol, the molar ratio of the OH groups from lignin. Hardwood ethanol organosolv lignin (HEL) and hardwood kraft lignin (HKL). Reproduced with permission from (Pan and Saddler 2013).

As previously detailed, the liquefaction or alkoxylation of lignin was explored to introduce a higher lignin content into PUF. The liquefaction and alkoxylation products are a mixture of lignin with flexible chains bearing OH groups with unreacted low molar mass glycols. It is well-known that the alkoxylation generates free homopolymer chains of polyethers as by-products. This homopolymer can be removed by solvent extraction. However, to avoid extra steps, this by-product is often left in the mix (Pavier and Gandini 2000b). These small polyols increase the flexibility of the polymer network and thus decrease the compression strength (Cateto et al. 2014; Li et al. 2016a; Li and Ragauskas 2012b). The introduction of 25 wt% of liquefied lignin polyol in PUFs decreased the compressive strength despite similar I_{OH} and density. The authors explained this trend by the flexibility of PEG 400 used for the liquefaction of the lignin (Li et al. 2016a).

The addition of alkoxylated lignin as a unique polyol increased the compression strength of the network from 100 to 140 kPa due to the rigid aromatic and 3D structures of the lignocellulosic resources (Li and Ragauskas 2012b). Furthermore, polyols made from rapeseed oil or lignin with similar I_{OH} were gradually introduced up to 30 wt% in PUFs. The compressive strength of the lignin-based foams was always superior to the one realized with triglycerides. The authors explained this behavior by the presence of aromatic rings, which increase the rigidity (Kurańska et al. 2020a). Another example, the increase in mechanical properties in PUFs made with alkoxylated lignin could be related to the PPO chains, which enhance the miscibility of modified lignin in the network (Saffar et al. 2020).

Another possibility to produce biobased polyols with an aromatic structure is the alcoholysis of biobased PUs with small diols or triols. The capacity of the aromatic to stack added with a high crosslink density generates a highly rigid and brittle structure detrimental to the compressive strength. A polyol was obtained from liquefied aromatic waste by transesterified coconut oil. The long and flexible chain of coconut oil avoided the excessive rigidity and brittleness of the PUFs. Furthermore, the authors claimed that the combination of rigid aromatic and aliphatic flexible structure provided optimal block segregation (Paruzel et al. 2017). CNSL combined rigid aromatic structures like lignins and flexible aliphatic chains as triglycerides. The introduction of a higher portion into PUFs was found to increase the compression strength thanks to the rigid aromatic structure (Ionescu et al. 2012).

5.3. Thermal properties

R-PUFs are widely used as thermal insulation material in the building industry or for transportation where the thermal conductivity is a primary property (Zhang et al. 2017b). The thermal insulation is related to the cell morphology, e.g., cell size, closed-cell content and density, the material properties, e.g., conductivity and complex index of refraction of the polymer and the conductivity of the gas entrapped in the cells (Ferkl et al. 2017). From a physical point of view, the thermal conductivity (λ) of the foams is related to the total heat transfer (q_t) passing through a thickness of foam (L) induced by a delta of temperature ΔT , as described by Equation 1.3.

$$\lambda = q_t * \frac{L}{\Delta T} \quad (1.3)$$

Where q_t is a sum of three components which are described in Equation 1.4 with the conduction through the polymer matrix (q_{PUR}), through the gas phase (q_{gas}) and the radiation (q_{rad}). The

convection transfer is negligible for closed-cell porous materials with a cell size inferior to 3 mm (Gibson and Ashby 1997).

$$q_t = q_{PUR} + q_{gas} + q_{rad} \quad (1.4)$$

The different contributions were physically examined and detailed in Equations 1.5, 1.6 and 1.7 (Hilyard et al. 2012).

$$q_g = -\delta \sum_{i=1}^N \frac{y_i * k g_i}{\sum_{j=1}^N y_j A_{ij}} \frac{dT}{dX} \quad (1.5)$$

$$\delta \approx 1 - \frac{\rho_f}{\rho_s}$$

With

Where δ is called the void fraction, ρ_f the foam density and ρ_s the solid polymer density, y_i is the mole fraction of the i^{th} gas in the foam, N the number of gases in the foam, $k g_i$ the thermal conductivity of the pur i^{th} gas and A_{ij} a complex coefficient depending on the viscosity, molar mass and temperature of gases.

$$q_s = -\frac{1-\delta}{3} * k_p \left[f_s \sqrt{a/b} + 2(1-f_s) * \left(\frac{a}{b} \right)^{0.25} \right] \frac{dT}{dX} \quad (1.6)$$

Where k_p is the conductivity of the polymer and a/b the cell aspect ratio.

$$q_r = -\frac{16\sigma T^3}{3K} \frac{dT}{dX}$$

$$K = \frac{4.10}{d} * \sqrt{\frac{f_s \rho_f}{\rho_s}} + \left[\frac{(1-f_s) \rho_f}{\rho_s} \right] K_w$$

With

Where d is the cell diameter, f_s the solid fraction, σ is the Boltzmann constant and K_w the extinction coefficient of the solid polymer. Equation 1.7 is known as the Rossland equation.

These equations show the multitude of factors that affect the total thermal conductivity. Figure 1.20A shows the evolution of the modeled thermal conductivity of R-PUFs over the closed-cell content. The conductivity through the gas phase accounts for 70% of the total thermal conductivity. The conduction through the polymer matrix is 20%, and the radiation is 10% (Ferkel et al. 2017). Figure 1.20A demonstrates that the reduction of the total thermal conductivity with the porosity depends on the reduction of the conduction through the solid part of the foam.

The major contribution depends on the gas mixture enclosed in cells, which tends to flow out and be substituted by air over time. The thermal conductivity was measured on PUFs samples over 900 days to study the diffusion of the BA gases out of cells, and the results are shown in Figure 1.20B. Within 100 days, the substitution of low conductivity BA gases ($16.4 \text{ mW.K}^{-1} \cdot \text{m}^{-1}$ for CO_2 and $12.8 \text{ mW.K}^{-1} \cdot \text{m}^{-1}$ for cyclopentane) by atmospheric air ($25.6 \text{ mW.K}^{-1} \cdot \text{m}^{-1}$) raise the initial $21 \text{ mW.K}^{-1} \cdot \text{m}^{-1}$ thermal conductivity to almost $27 \text{ mW.K}^{-1} \cdot \text{m}^{-1}$ (Santiago-Calvo et al. 2019). Figure 1.20B shows the thermal conductivity value plateau around $29 \text{ mW.K}^{-1} \cdot \text{m}^{-1}$ after one year of aging. Therefore, the thermal conductivity must be analyzed in the utilization conditions and not considered as a constant property (Berardi and Madzarevic 2020).

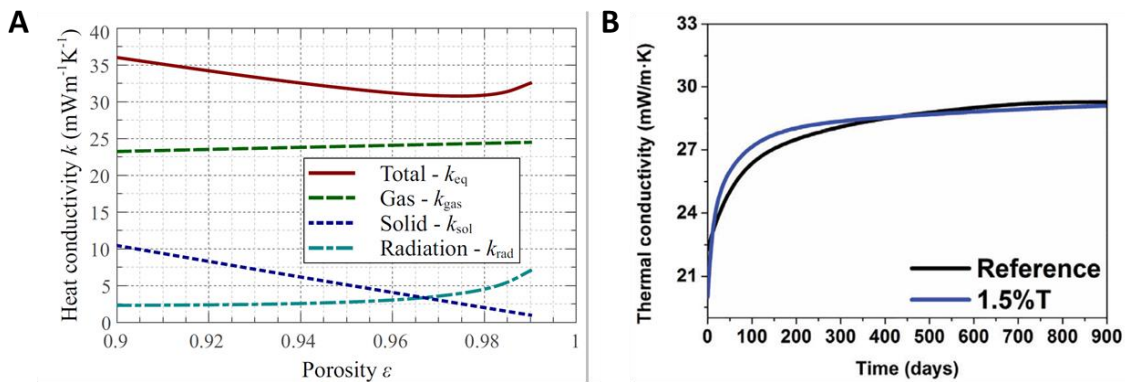


Figure 1.20 - (A) Dependance of the heat conductivity on porosity modeled with cell size of 300 μm and filled with air (B) Thermal conductivity evolution over 900 days of PUF and PUF modified with 1.5% of talc. Reproduced with permission from (Ferkl et al. 2017) and (Santiago-Calvo et al. 2019).

5.3.1. Effect of closed cell-content

Low closed cell content enhances the diffusion phenomenon and the substitution of BA gases by air; thus, decreasing the overall thermal conductivity of foams. As previously described, the utilization of biobased components directly impacts cell morphology. As a result, the decrease of the closed-cell content reduced the thermal conductivity (Arbenz et al. 2016; Borowicz et al. 2019; Hayati et al. 2018; Hejna et al. 2017; Piszczyk et al. 2014). For example, the decline of closed-cell content from 95 to 85% implied an increase in thermal conductivity of $5 \text{ mW.K}^{-1}.\text{m}^{-1}$ (Hejna et al. 2017). The thermal conductivity decreased linearly with the closed-cell content (Piszczyk et al. 2014).

Furthermore, it has been proved that the increase in average cell diameters from 250 to 600 μm caused an increase in the thermal conductivity coefficient by almost 50% (Randall and Lee 2002). This variation is explained by the Rossland equation (1.7), where the lower cell size (d) contributes to the reduction of the radiative transfers (Arbenz et al. 2016; Furtwengler et al. 2018b; Ugarte et al. 2015). Besides, in denser materials, the heat transport passed through more quantity of solid; therefore, the contribution to the foam overall conductivity of the conduction through the polymer matrix (q_{PUR}) is more important in denser materials (Hejna et al. 2017). The thermal conductivity increases with the density of the material due to the increased quantity of solid material by which the heat must be transported (Ugarte et al. 2015).

5.3.2. Effect of the chemical structure

To some extent, the thermal conductivity was directly correlated to the chemical structure of the biobased components. The addition of long dangling chain-end in the polymer network with triglycerides polyol seems to enhance the diffusion of heat in the material (Borowicz et al. 2019). An increase in thermal conductivity from 20 to $25 \text{ mW.K}^{-1}.\text{m}^{-1}$ with the increased substitution of fossil-based polyol by modified mustard oil was shown. Otherwise, the utilization of 2.5 to 5 wt% of kraft lignin as polyol was beneficial for the thermal conductivity, which was observed to decrease from 25.6 to $24.7 \text{ mW.K}^{-1}.\text{m}^{-1}$ due to the increased aromaticity, which reduces the gas transfer outward of the foam and therefore increases the thermal conductivity (Hayati et al. 2018).

5.4. Fire resistance

The test of the FR-based materials depends on the application and, thus, the corresponding fire risk scenario. In PUFs, the assessment of the enhancement or degradation of the FR properties by a biobased material is performed with thermogravimetric analysis (TGA) measurement, burning test or determining the limiting oxygen index (LOI).

TGA is a dynamic measurement of material degradation. The weight of a material is followed over a determined temperature cycle, generally a rise at 10 or 20 °C/min. The degradation of PUFs samples takes place in two steps: (i) the urethane and urea bonds dissociation in the hard domain (200-300 °C) and (ii) the decomposition of the fragments and the isocyanurate structures (400-500 °C) (Furtwengler et al. 2018b; Kurańska et al. 2020b). The burning test is the application of a flame, for 15 or 30 s depending on the test condition, on a foam specimen, and the flaming time is recorded (EN ISO 11925-2). The LOI is an international normalized test (ISO 4589-2). A candle-like flame is applied to the top of a specific PUFs specimen under a controlled atmosphere. The objective is to find the minimum oxygen concentration in nitrogen that will induce a combustion of at least 3 min (Wilkie and Morgan 2010).

Thermal decomposition and degradation must be dissociated. The first one is the degradation of material properties due to exposure to heat, and the latter is related to the free-radical bond cleavage and subsequent pyrolysis of smaller molar mass fragments of a polymer upon exposure to heat (Wilkie and Morgan 2010). The relations between the enhancement or degradation of the FR properties of PUFs and the structure of the biobased polyol defined by the I_{OH} , the rigidity, the molecular composition, the low molar mass compounds added through chemical transformation and the insoluble content are given below.

5.4.1. OH Index

In TGA analysis, characteristic temperatures are recorded at 5, 10 and 50% of weight loss to measure the FR of the related materials. Furthermore, the quantity of samples at the end of the measurement called char residue is also an indicator of the fire resistance of the foam. The evolution of the char residue, weight loss at 5, 10 and 50% over the average polyol I_{OH} is represented in Figure 1.21. The data were compiled from the literature of foams made without FR additive. The general trend observed in Figure 1.21 is an increase of the characteristic temperature with I_{OH} augmentation. The char residue presented in Figure 1.21A is close to 0% when the I_{OH} is inferior to 200 mg KOH/g. Such polyols are often used in F-PUFs (Table 1.3), producing open-cells morphology. As discussed previously, low closed cell content decreases the thermal insulation properties. Therefore, the heat transfer is facilitated, and the material burns completely. In the case of higher closed-cell content, the heat transfer toward the center is hindered by the numerous cells wall. Figure 1.21A shows an increase in char residue after 200 mg KOH/g. This is linked to the foam structure formed by a higher crosslink density, which limits heat transfers (Riyapan et al. 2019). Besides, a crosslinked network requires higher activation energy to initiate chain movement and decomposition compared to less branched polymers (Rastegarfar et al. 2018; Ugarte et al. 2015).

Figure 1.21B, Figure 1.21C and Figure 1.21D present a high distribution of value directly linked to the difference in foam formulations. However, the general trend observed is the increase in the temperature at 5, 10 or 50% weight loss with the average I_{OH} of polyol increase. The thermal

decomposition of PUFs starts with the urethane bond dissociation around 250 °C. The high density of OH groups will be transformed into urethane groups in the final materials. Therefore, a polyol with high I_{OH} will produce a material that will take an extended time to dissociate (Furtwengler et al. 2018b; Huo et al. 2019). Finally, the increase of FR properties with the I_{OH} presented in Figure 1.21 is low, and other factors such as the molecular energy, the molar mass and the structure of the polyol affect the fire resistance of the foam.

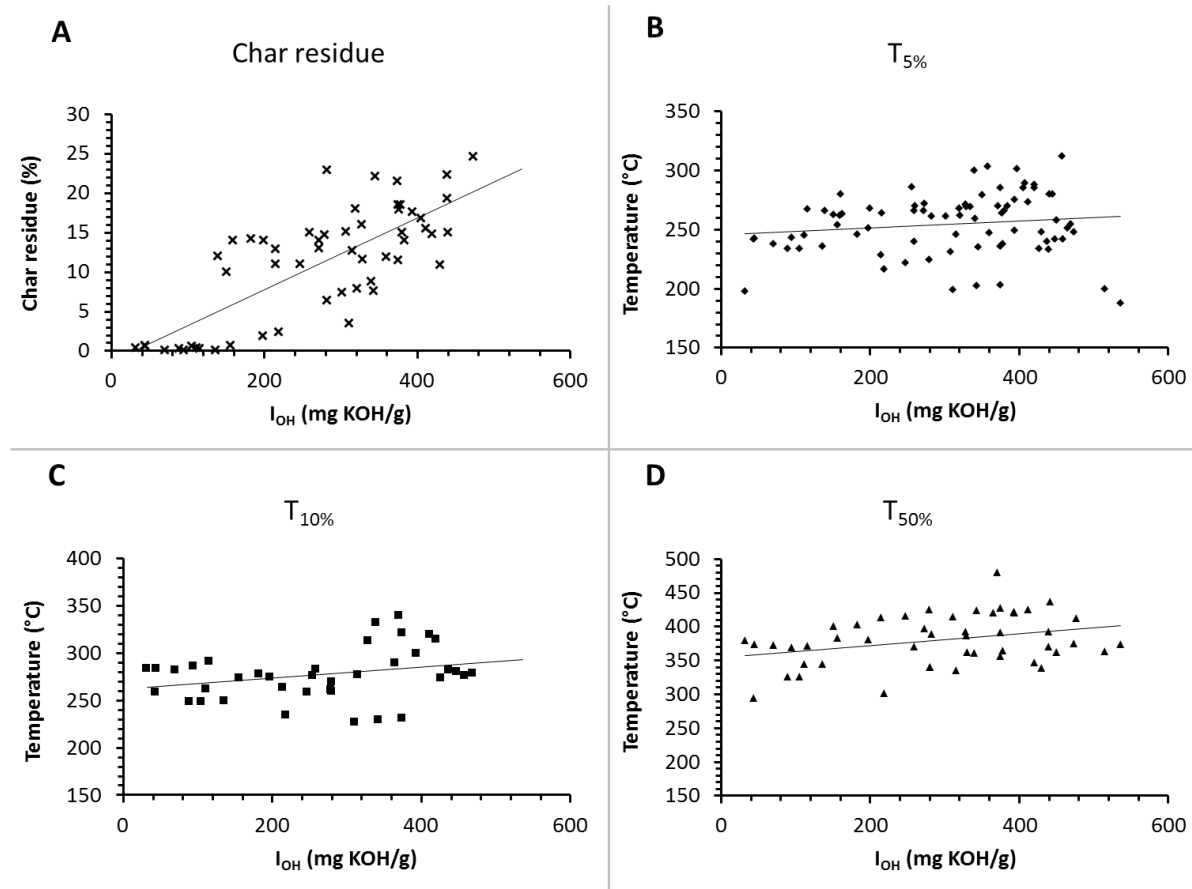


Figure 1.21 - Dependence of the char residue (A), weight loss at 5% (B), 10% (C) and 50% (D) on the I_{OH} of the polyol. The straight line represents the general trend of the data compiled from the literature. Compilation of data from literature (Contreras et al. 2020; Fang et al. 2019; Hejna et al. 2018; Huo et al. 2019; Jiang et al. 2018; Kahleras et al. 2020; Kurańska et al. 2020b; Li et al. 2020b; Luo and Li 2014; Ng et al. 2017; Paruzel et al. 2017; Pawar et al. 2016a; Piszczek et al. 2014; Ugarte et al. 2015; Veronese et al. 2011; Yang et al. 2012, 2019; Zieleniewska et al. 2015).

5.4.2. Activation energy

The activation energy of materials decomposition is directly related to the mobility of the chains. A very stable alkane structure forms the dangling chains in lipids-based polyols. Therefore, PUF realized with similar I_{OH} , but different dangling chain quantities had different thermal stability. The polyol prepared via ozonolysis, which reduced by 60%, the end chains had the fastest first loss at 335 °C compared to castor oil or epoxidized and ring-opened soybean oil-polyol (380 °C) (Narine et al. 2007). On the contrary, the rigid structure formed by isosorbide polyol needs higher energy to initiate decomposition (Jiang et al. 2018). The 3D structure of lignin, liquefied or alkoxylated, is stiffer than fossil-based polyol and degraded at higher temperatures (Li et al. 2016a; Saffar et al. 2020).

5.4.3. Low molar mass compounds

Low molar mass polyols such as PEG or glycerol are introduced into foams via biobased polyols synthesis (e.g., alcoholysis of wastes, lignin liquefaction or dispersion) or as an additional polyol. Their thermal stability was also investigated; for example, PEG is known to enhance the thermal stability of foams due to the thermally stable ether bonds and the increase in crosslink density (Li et al. 2016b; Ng et al. 2017; Rastegarfar et al. 2018). For example, the temperature of 50% weight loss shifted from 379 to 370 °C, with the integration of 0 to 100% of palm oil polyester polyol. The authors explained this trend by the decrease in PEG added as co-polyol (Ng et al. 2017). In another study, foam realized with 40 wt% of EG had a higher LOI value (25%), than without (20%) (Li et al. 2016b). Furthermore, the addition of crude glycerol increased the onset temperature in TGA measurements from 210 to 223 °C with 0 and 70 wt% of crude glycerol, respectively (Hejna et al. 2018).

5.4.4. Molecular architecture

As introduced in the last section, the polyol structure plays a key role in the degradation of cellular materials. For instance, the presence of sulfur in the chemical structure of the mustard oil polyol increases the LOI value from 23 to 26% and thus, the thermal stability of the PUFs. Sulfur has several oxidation levels and is transformed into SO_2 and SO_3 acids in the decomposition process. This oxygen consummation, combined with the catalytic activity of these acids for the decomposition of a fire intermediate (ionic peroxide), inhibited the chain reaction of oxidation (Borowicz et al. 2019).

The epoxidation and further ring-opening reactions produced numerous lipids based polyols was previously detailed. To reduce the synthesis steps, 25 wt% of epoxidized oil were directly introduced in PUFs formulations and compared to polyols formed one step further. The weight loss for the first degradation peak was improved from 45 to 40% with a polyol and with epoxidized oil, respectively. Some authors hypothesized the enhancement to originate from the formation of thermally stable oxazolidone groups (Arbenz et al. 2017). However, the oxazolidone formation was not evidenced in PUFs with epoxidized oils.

Otherwise, polyester polyol based on sorbitol had a low onset temperature (170 °C) compared to conventional PUFs (200-250 °C). The authors explained that the ester scissions happen at lower temperatures than ether groups. Therefore, the decomposition of the soft segment is detected at a lower temperature in TGA (Furtwengler et al. 2018a).

Aromatic structures are well known to improve the thermal degradation with smoke production, which expands the char layer. This expanded layer is denoted as intumescent and protects the material from flame exposition and limits the transfer of oxygen toward the flame (Duquesne et al. 2001). The improvement of thermal stability by an increased aromatic content was observed with tannins (Arbenz et al. 2016), lignins (D’Souza et al. 2014; Li et al. 2020a), PUFs wastes (Paruzel et al. 2017; Shin et al. 2019a) and CNSL (Ionescu et al. 2012), for instance. Foam realized with oxypropylated tannin had a lower peak of heat released and propagation of the flame rates than oxypropylated glycerol. The authors explained that the aromatic structure of the tannin is coke forming. This hypothesis was supported by the measurement of the total smoke release, which was higher with tannin than glycerol-based polyol (Arbenz et al. 2016). With 15 and 30 wt% of fractionated and alkoxylated lignin, the maximum loss rate was lower than without. Furthermore, the

temperature at half mass loss and the residual mass at 800 °C was also higher than the reference foam. This degradation profile seems to be linked to the higher density of the aromatic structure.

It is well-known that the presence of thermally stable fillers increases the overall thermal stability of the foams by increasing the residue amounts (Delucis et al. 2018). The evolution of the foam flammability over the content of insoluble residue in the liquefaction mixture of the polyol is represented in Figure 1.22. The trend was clear; the flammability decreased with the increase of insoluble residue (Figure 1.22). The recalcitrant liquefaction residue of lignin improved the FR properties of the PUFs made thereof. This improvement is explained by the inorganic components present in liquefied bark polyol (Ge et al. 2000).

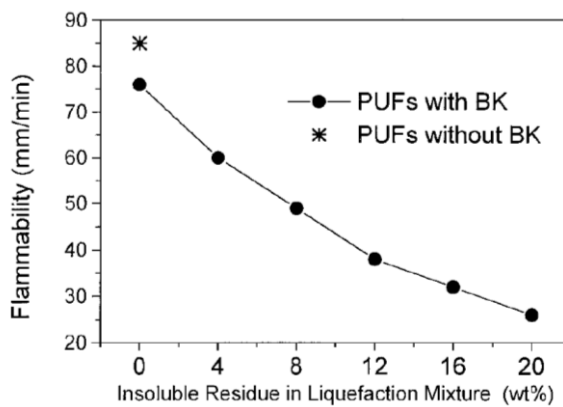


Figure 1.22 - Effect of the amount of insoluble bark residue on the flammability of PUF. Reproduced with permission from (Ge et al. 2000).

5.5. Some advanced properties

5.5.1. Glass transition temperature

The glass transition temperature (T_g) of a polymer is critical information to know the network better. In thermosets like PUFs, the α -transition temperature determined by temperature-dependent dynamic mechanical analysis in temperature is linked to the T_g determined by differential scanning calorimetry. Transition temperatures depend on the isocyanate index, cross-link density, aromaticity, plasticizer and PIR content in PUFs (Wu et al. 2008). When phase separation occurred, two T_g are identified, the first one for the soft segment around -50 °C and the second for the hard segment found between 50 and 80 °C in R-PUFs. The substitution of fossil-based polyol by a biobased one induces a change in the network structure, which can be seen by a T_g shift. The dangling chains and the long flexible structure of lipids based polyols are responsible for a plasticizing effect and a decrease in T_g (Kahlerras et al. 2020; Zieleniewska et al. 2015). The small reactants present for the polyglycerol formation are also plasticizers of the PUFs network (Piszczek et al. 2014). Furthermore, the T_g heavily depends on the PEG length used to plasticize lignins (Hatakeyama et al. 2004). The other effect observed with biobased polyols is the correlation between the T_g increase and the augmentation in crosslink density explained by the reduced chain motions (Hayati et al. 2018; Kosmela et al. 2019; Narine et al. 2007; Pawar et al. 2016a).

5.5.2. Acoustic property

R-PUFs are principally used in thermal insulation, and their acoustic properties are often overlooked because open cell structures are considered good sound absorbers. It was proved that lower closed cell content resulted in higher sound absorption (Zhang et al. 2012). However, foams based on palm oil with closed cell structure has been elaborated for such applications. High sound absorption coefficients (< 90%) defined as the ratio of the acoustic energy absorbed by the foam to the incident acoustic energy, were obtained. They explained that the damping effect from the increased urethane group content and network density dissipated sound energy into heat (Riyapan et al. 2019).

The R-PUFs properties can be affected by numerous factors represented in Figure 1.23, and the structure of the components and the cell morphology are the dominant effects.

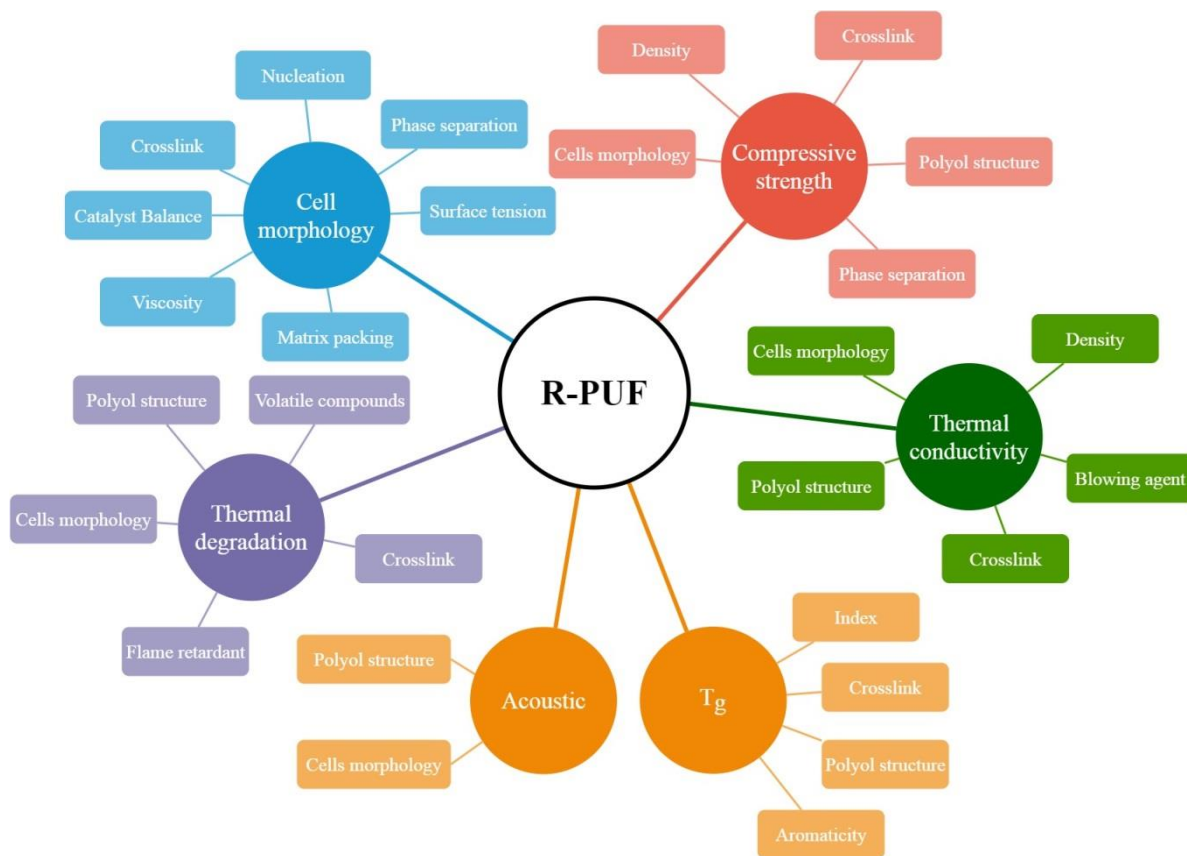


Figure 1.23 - Overview of the different factors affecting several properties (cell morphology, mechanical, thermal and fire resistance behaviors).

6. PERSPECTIVES ON BIOBASED PUF

Polyols are one of the main biobased compounds used in PUFs formulations. However, it represents often less than 50 wt% of the PUF (Table 1.1). Another major component are the polyisocyanates, which are more rarely biobased. Besides, the toxicity for human health (Brugsch and Elkins 1963; Peters 1970) of the isocyanate group is highly problematic. Moreover, their industrial synthesis is based on hazardous compounds (e.g., phosgene). The isocyanate reduction and elimination

in the foam elaboration join the sustainability approach discussed in this review. In the next part, NIPU and other chemistries are outlined to produce greener biobased foams without isocyanate for a more sustainable and safe future.

6.1. Non-isocyanate polyurethane

Urethane groups are usually formed by addition of isocyanate and hydroxyl groups. However, several alternative pathways presented in Figure 1.24 to form NIPU can be developed (Guan et al. 2011; Kreye et al. 2013; Maisonneuve et al. 2015; Rokicki et al. 2015; Suryawanshi et al. 2019). Carbamoyl chloride, ring-opening polymerization, chloroformate, aziridine and alkyl-carbonate routes presented in Figure 1.24 involve precursors synthesized via toxic phosgene derivatives, or the precursor itself (e.g., aziridine) is hazardous (Ghasemlou et al. 2019b). Furthermore, all these routes require elevated temperatures. The polyaddition between cyclocarbonates and amines forming polyhydroxyurethane (PHU) networks can be carried out at ambient temperature, and no toxic phosgene is involved. Moreover, PHU precursors have manageable toxicity and can be conveniently obtained from a wide range of renewable and sustainable resources (Carré et al. 2019; Ghasemlou et al. 2019b; Suryawanshi et al. 2019). In the green chemistry frame, the cyclic carbonate route is the most sustainable pathway to obtain NIPU.

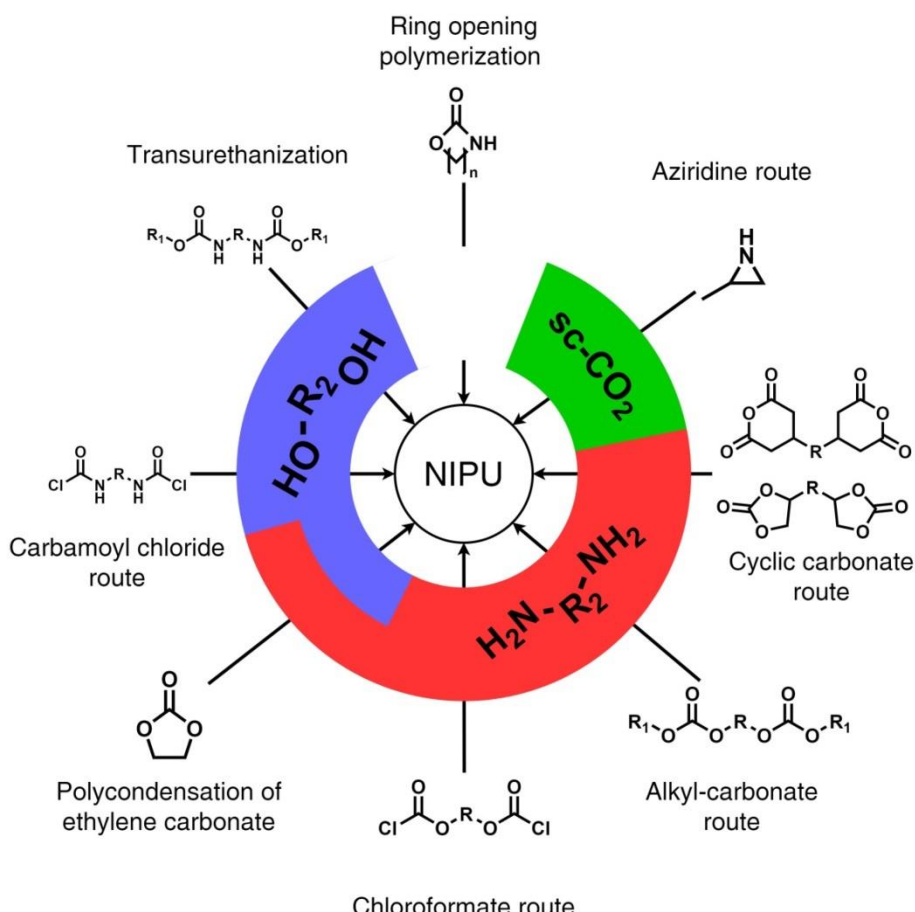


Figure 1.24 - Overview of the main synthetic routes to NIPU.

Figure 1.24 shows that polyamines and 5 or 6-membered cyclic carbonates are the main building blocks toward a biobased PHU network. Although very few natural amines are available (i.e., chitosan and lysine), sustainable amines can be produced through various chemical processes from carbohydrate, lignins or oleochemical sources (Froidevaux et al. 2016; Pelckmans et al. 2017). One promising route toward sustainable diamines was recently highlighted as dianiline was recovered from the enzymatic recycling of PUs (Magnin et al. 2019).

Cyclocarbonates were initially synthesized from the reaction between diol and phosgene (Nemirovsky 1883). However, the current and industrial common pathway transforms epoxide into cyclocarbonates with high pressure of sustainable and naturally occurring CO_2 (Carré et al. 2019), for instance from fermentation process. The production of fully biobased carbonates was achieved through the carboxylation of epoxidized oil (Mann et al. 2008; Pérez-Sena et al. 2018).

In PHU synthesis, no difference in reaction conditions, kinetics, products, nor side reactions was observed between structurally similar biobased and fossil-based monomers (Carré et al. 2019). Similarly to conventional PUs, the nature of the renewable source directly impacts the properties of the PHU. Therefore, the development of innovative molecular architectures extracted or bioproduced from various biomass types can bring new properties for the PHU networks. Very recently, the synthesis of the PHU network from carbonated biobased triglycerides and glycine was patented. The authors claimed similar mechanical properties as conventional PUs (Dong et al. 2020).

Figovsky patented the first NIPU solution to substitute conventional PUFs in 2004. In this study, acrylic NIPU was foamed by radical polymerization of acrylate with pentane as BA (Figovsky et al. 2004). The first foam realized with the reaction between cyclic carbonate and diamine to obtain PHU networks was recently developed by Caillol and coworkers. The reagents were mixed with polymethylhydrogenosiloxane, which H_2 release after reaction with diamine and heated at 80 °C (Cornille et al. 2015). The corresponding foams were dense (200-300 kg/m³) compared to conventional PUFs. The method was improved by adding thiourea as a catalyst; therefore, the curing temperature was reduced until ambient (Cornille et al. 2016). The resulting foams were still dense (270-300 kg/m³). Furthermore, the open cells of the NIPU foams were coarser (300-1300 μm) compared to conventional PUFs (350-850 μm). Due to the bigger open-cells, the thermal conductivity was higher (100 vs. 67 $\text{mW.K}^{-1}.\text{m}^{-1}$), and the thermal stability was slightly inferior compared to the conventional PUFs.

The synthesis of closed and small cells NIPU foams was achieved with supercritical CO_2 at high temperature or high pressure. The samples were foamed by fast depressurization of the cell leading to a density of 110 kg/m³ with small pores (10 μm) and high thermal conductivity (50 $\text{mW.K}^{-1}.\text{m}^{-1}$) (Grignard et al. 2016). Mulhaupt and coworkers used a liquid hydrofluorocarbon to produce NIPU foams at 80 °C (Blattmann et al. 2016). The authors produced dense foams (142 kg/m³) with cell size similar to R-PUFs (171 μm). Pizzi and coworkers recently developed self-blown NIPU foams. The reaction was performed between a synthesized glucose-NIPU with maleic acid and glutaraldehyde as a crosslinker. The soft foam was formed within 5h at ambient temperature (Xi et al. 2019). Recently, self-blown NIPU foams were elaborated by amine and thiol reaction with cyclocarbonates catalyzed by 1,8-diazabicyclo[5.4.0]undec-7-ene (Monie et al. 2020). As the reaction thiol-cyclocarbonate reaction forms hydroxythioether and carbon dioxide, thiol is used as chemical blowing agent. Unfortunately, as most of the other, these NIPU foams are slow to form, mainly open cells and flexible. In order to improve the mechanical properties of NIPU foams by aminolysis, rigid cyclocarbonate such as lignin could be used (Salanti et al. 2016). Another development axis toward

green foams, could be the adaptation of new chemical BAs, a subject recently reviewed (Coste et al. 2020), to new polymers or formulations. However, the route toward a large substitution of R-PUF and F-PUF by NIPU foams or equivalents is still long.

6.2. Other potential approaches

The question linked to the future of the foams could be not only related to PU macromolecular architectures. As previously described, the formation of reactive foams needs an exothermic and fast reaction associated with a BA. The development of the well-known epoxide chemistry with epoxidized oil was widely investigated to produce foams (Dworakowska et al. 2015; Huang et al. 2019; Khundamri et al. 2019; Negrell et al. 2017). Furthermore, some recent investigations raised some exciting new pathways toward biobased foams. The modification of soybean oil was achieved to introduce alkoxysilane groups. They were subsequently used in a Piers-Rubinsztajn reaction, which released methane to expand the polymer and produce foams. PDMS added as chain extender controls the density and Young's modulus of the produced foams (Gale et al. 2019). Carbon-Michael chemistry has been investigated as a new way of foam elaboration. First, they quickly transformed polyols used in PUFs into poly-acetoacetate, a Michael donor, via transesterification. These new molecules were added into a mix of polyacrylates (Michael acceptor), surfactants, catalysts and physical BAs. The foams had entirely raised in less than 5 minutes, with more than 80% of closed cells and a low density of around 35 kg/m³ comparable to conventional PUFs (Sonnenchein et al. 2016). Another approach has been recently developed. A fully biobased foam with closed-cell was developed by Pelletier and coworkers, based on fungal mycelium. It was found to be promising fully biobased alternatives for acoustic shielding to the traditional fossil-based polymer based on synthetic fibers (Pelletier et al. 2019).

7. REFERENCES

Abdel Hakim, A.A., Nassar, M., Emam, A., Sultan, M., 2011. Preparation and characterization of rigid polyurethane foam prepared from sugar-cane bagasse polyol. *Mater. Chem. Phys.* **129**, 301–307. <https://doi.org/10.1016/j.matchemphys.2011.04.008>

Abu-Jdayil, B., Mourad, A.-H., Hittini, W., Hassan, M., Hameedi, S., 2019. Traditional, state-of-the-art and renewable thermal building insulation materials: An overview. *Constr. Build. Mater.* **214**, 709–735. <https://doi.org/10.1016/j.conbuildmat.2019.04.102>

Acik, G., Karabulut, H.R.F., Altinkok, C., Karatavuk, A.O., 2019. Synthesis and characterization of biodegradable polyurethanes made from cholic acid and 1-lysine diisocyanate ethyl ester. *Polym. Degrad. Stab.* **165**, 43–48. <https://doi.org/10.1016/j.polymdegradstab.2019.04.015>

Aeschelmann, F., Carus, M., 2015. Biobased Building Blocks and Polymers in the World: Capacities, Production, and Applications—Status Quo and Trends Towards 2020. *Ind. Biotechnol.* **11**, 154–159. <https://doi.org/10.1089/ind.2015.28999.fae>

Agrawal, A., Kaur, R., Walia, R.S., 2017. PU foam derived from renewable sources: Perspective on properties enhancement: An overview. *Eur. Polym. J.* **95**, 255–274. <https://doi.org/10.1016/j.eurpolymj.2017.08.022>

Akindoyo, J.O., Beg, M.D.H., Ghazali, S., Islam, M.R., Jeyaratnam, N., Yuvaraj, A.R., 2016. Polyurethane types, synthesis and applications – a review. *RSC Adv.* **6**, 114453–114482. <https://doi.org/10.1039/C6RA14525F>

Al Nabulsi, A., Cozzula, D., Hagen, T., Leitner, W., Müller, T.E., 2018. Isocyanurate formation during rigid polyurethane foam assembly: a mechanistic study based on *in situ* IR and NMR spectroscopy. *Polym. Chem.* **9**, 4891–4899. <https://doi.org/10.1039/C8PY00637G>

Alagi, P., Choi, Y.J., Seog, J., Hong, S.C., 2016. Efficient and quantitative chemical transformation of vegetable oils to polyols through a thiol-ene reaction for thermoplastic polyurethanes. *Ind. Crops Prod.* **87**, 78–88. <https://doi.org/10.1016/j.indcrop.2016.04.027>

Amarnath, N., Appavoo, D., Lochab, B., 2018. Eco-Friendly Halogen-Free Flame Retardant Cardanol Polyphosphazene Polybenzoxazine Networks. *ACS Sustain. Chem. Eng.* **6**, 389–402. <https://doi.org/10.1021/acssuschemeng.7b02657>

Amran, U.A., Zakaria, S., Chia, C.H., Roslan, R., Jaafar, S.N.S., Salleh, K.M., 2019. Polyols and rigid polyurethane foams derived from liquefied lignocellulosic and cellulosic biomass. *Cellulose* **26**, 3231–3246. <https://doi.org/10.1007/s10570-019-02271-w>

Arbennz, A., Avérous, L., 2015. Chemical modification of tannins to elaborate aromatic biobased macromolecular architectures. *Green Chem.* **17**, 2626–2646. <https://doi.org/10.1039/C5GC00282F>

Arbennz, A., Avérous, L., 2014. Synthesis and characterization of fully biobased aromatic polyols – oxybutylation of condensed tannins towards new macromolecular architectures. *RSC Adv.* **4**, 61564–61572. <https://doi.org/10.1039/C4RA10691A>

Arbennz, A., Frache, A., Cuttica, F., Avérous, L., 2016. Advanced biobased and rigid foams, based on urethane-modified isocyanurate from oxypropylated gambier tannin polyol. *Polym. Degrad. Stab.* **132**, 62–68. <https://doi.org/10.1016/j.polymdegradstab.2016.03.035>

Arbennz, A., Perrin, R., Avérous, L., 2017. Elaboration and Properties of Innovative Biobased PUIR Foams from Microalgae. *J. Polym. Environ.* **26**, 254–262. <https://doi.org/10.1007/s10924-017-0948-y>

Arshanitsa, A., Paberza, A., Vevere, L., Cabulis, U., Telysheva, G., 2014. Two approaches for introduction of wheat straw lignin into rigid polyurethane foams. Presented at the Proceedings of PPS-29: The 29th International Conference of the Polymer Processing Society - Conference Papers, Nuremberg, Germany, pp. 388–391. <https://doi.org/10.1063/1.4873806>

Ashida, K., 2007. Polyurethane and related foams: chemistry and technology. CRC/Taylor & Francis, Boca Raton, FL.

Austin, A., Levis, W., Pizzini, L., Hartman, R., 1978a. Process for preparing a polyurethane foam from an oxyalkylated product. US4177335A.

Austin, A., Levis, W., Pizzini, L., Hartman, R., 1978b. Polyurethane foam from an oxyalkylated product. US4105597A.

Babu, R.P., O'Connor, K., Seeram, R., 2013. Current progress on bio-based polymers and their future trends. *Prog. Biomater.* **2**, 8. <https://doi.org/10.1186/2194-0517-2-8>

Bachmann, F., Reimer, J., Ruppenstein, M., Thiem, J., 2001. Synthesis of Novel Polyurethanes and Polyureas by Polyaddition Reactions of Dianhydrohexitol Configurated Diisocyanates. *Macromol. Chem. Phys.* **202**, 3410–3419. [https://doi.org/10.1002/1521-3935\(20011101\)202:17<3410::AID-MACP3410>3.0.CO;2-Q](https://doi.org/10.1002/1521-3935(20011101)202:17<3410::AID-MACP3410>3.0.CO;2-Q)

Banik, I., Sain, M.M., 2008. Water Blown Soy Polyol-Based Polyurethane Foams of Different Rigidities. *J. Reinf. Plast. Compos.* **27**, 357–373. <https://doi.org/10.1177/0731684407083955>

Basso, M., Pizzi, A., Lacoste, C., Delmotte, L., Al-Marzouki, F., Abdalla, S., Celzard, A., 2014a. MALDI-TOF and ¹³C NMR Analysis of Tannin–Furanic–Polyurethane Foams Adapted for Industrial Continuous Lines Application. *Polymers* **6**, 2985–3004. <https://doi.org/10.3390/polym6122985>

Basso, M.C., Giovando, S., Pizzi, A., Pasch, H., Pretorius, N., Delmotte, L., Celzard, A., 2014b. Flexible-elastic copolymerized polyurethane-tannin foams. *J. Appl. Polym. Sci.* **131**, 40499. <https://doi.org/10.1002/app.40499>

Baumann, G.F., Dietrich, W., 1981. Isocyanurate Rigid Foam: Relationship Between Structure and Properties. *J. Cell. Plast.* **17**, 144–147. <https://doi.org/10.1177/0021955X8101700302>

Belgacem, M.N., Quillerou, J., Gandini, A., 1993. Urethanes and polyurethanes bearing furan moieties—3. Synthesis, characterization and comparative kinetics of the formation of diurethanes. *Eur. Polym. J.* **29**, 1217–1224. [https://doi.org/10.1016/0014-3057\(93\)90151-5](https://doi.org/10.1016/0014-3057(93)90151-5)

Beneventi, D., Carre, B., Gandini, A., 2001. Role of surfactant structure on surface and foaming properties. *Colloids Surf. Physicochem. Eng. Asp.* **189**, 65–73. [https://doi.org/10.1016/S0927-7757\(01\)00602-1](https://doi.org/10.1016/S0927-7757(01)00602-1)

Berardi, U., Madzarevic, J., 2020. Microstructural analysis and blowing agent concentration in aged polyurethane and polyisocyanurate foams. *Appl. Therm. Eng.* **164**, 114440. <https://doi.org/10.1016/j.applthermaleng.2019.114440>

Bhoyate, S., Ionescu, M., Kahol, P.K., Gupta, R.K., 2018. Sustainable flame-retardant polyurethanes using renewable resources. *Ind. Crops Prod.* **123**, 480–488. <https://doi.org/10.1016/j.indcrop.2018.07.025>

Bioplastic materials [WWW Document], 2019. . *Eur. Bioplastics*. URL <https://www.european-bioplastics.org/bioplastics/materials/> (accessed 8.25.20).

Biswas, A., Adhvaryu, A., Gordon, S.H., Erhan, S.Z., Willett, J.L., 2005. Synthesis of Diethylamine-Functionalized Soybean Oil. *J. Agric. Food Chem.* **53**, 9485–9490. <https://doi.org/10.1021/jf050731o>

Blattmann, H., Lauth, M., Mülhaupt, R., 2016. Flexible and Bio-Based Nonisocyanate Polyurethane (NIPU) Foams. *Macromol. Mater. Eng.* **301**, 944–952. <https://doi.org/10.1002/mame.201600141>

Bobbo, S., Nicola, G.D., Zilio, C., Brown, J.S., Fedele, L., 2018. Low GWP halocarbon refrigerants: A review of thermophysical properties. *Int. J. Refrig.* **90**, 181–201. <https://doi.org/10.1016/j.ijrefrig.2018.03.027>

Borowicz, M., Paciorek-Sadowska, J., Lubczak, J., Czupryński, B., 2019. Biodegradable, Flame-Retardant, and Bio-Based Rigid Polyurethane/Polyisocyanurate Foams for Thermal Insulation Application. *Polymers* **11**, 1816. <https://doi.org/10.3390/polym11111816>

Boufi, S., Belgacem, M.N., Quillerou, J., Gandini, A., 1993. Urethanes and polyurethanes bearing furan moieties. 4. Synthesis, kinetics and characterization of linear polymers. *Macromolecules* **26**, 6706–6717. <https://doi.org/10.1021/ma00077a003>

Boufi, S., Gandini, A., Belgacem, M.N., 1995. Urethanes and polyurethanes bearing furan moieties: 5. Thermoplastic elastomers based on sequenced structures. *Polymer* **36**, 1689–1696. [https://doi.org/10.1016/0032-3861\(95\)99015-M](https://doi.org/10.1016/0032-3861(95)99015-M)

Bresolin, D., Valério, A., de Oliveira, D., Lenzi, M.K., Sayer, C., de Araújo, P.H.H., 2018. Polyurethane Foams Based on Biopolymers from Castor Oil and Glycerol. *J. Polym. Environ.* **26**, 2467–2475. <https://doi.org/10.1007/s10924-017-1138-7>

Briou, B., Vu, N.D., Caillol, S., Robin, J., Duguet, N., Lemaire, M., Etienne, P., Bonnet, L., Lapinte, V., 2020. Polyurethane Thermosets Using Lipidic Poly(α -Hydroxyketone). *J. Am. Oil Chem. Soc.* **97**, 81–91. <https://doi.org/10.1002/aocs.12289>

Brugsch, H.G., Elkins, H.B., 1963. Toluene Di-Isocyanate (TDI) Toxicity. *N. Engl. J. Med.* **268**, 353–357. <https://doi.org/10.1056/NEJM196302142680705>

Caille, D., Pascault, J.P., Tighzert, L., 1990a. Reaction of a diepoxide with a diisocyanate in bulk: I. Use of a tertiary amine catalyst. *Polym. Bull.* **24**, 23–30. <https://doi.org/10.1007/BF00298317>

Calvo-Correas, T., Martin, M.D., Retegi, A., Gabilondo, N., Corcuer, M.A., Eceiza, A., 2016. Synthesis and Characterization of Polyurethanes with High Renewable Carbon Content and Tailored Properties. *ACS Sustain. Chem. Eng.* **4**, 5684–5692. <https://doi.org/10.1021/acssuschemeng.6b01578>

Calvo-Correas, T., Santamaría-Echart, A., Saralegi, A., Martin, L., Valea, Á., Corcuer, M.A., Eceiza, A., 2015. Thermally-responsive biopolyurethanes from a biobased diisocyanate. *Eur. Polym. J.* **70**, 173–185. <https://doi.org/10.1016/j.eurpolymj.2015.07.022>

Campanella, A., Bonnaillie, L.M., Wool, R.P., 2009. Polyurethane foams from soyoil-based polyols. *J. Appl. Polym. Sci.* **112**, 2567–2578. <https://doi.org/10.1002/app.29898>

Carré, C., Ecochard, Y., Caillol, S., Avérous, L., 2019. From the Synthesis of Biobased Cyclic Carbonate to Polyhydroxyurethanes: A Promising Route towards Renewable Non-Isocyanate Polyurethanes. *ChemSusChem* **12**, 3410–3430. <https://doi.org/10.1002/cssc.201900737>

Carriço, C.S., Fraga, T., Pasa, V.M.D., 2016. Production and characterization of polyurethane foams from a simple mixture of castor oil, crude glycerol and untreated lignin as bio-based polyols. *Eur. Polym. J.* **85**, 53–61. <https://doi.org/10.1016/j.eurpolymj.2016.10.012>

Cateto, C.A., Barreiro, M.F., Ottati, C., Lopretti, M., Rodrigues, A.E., Belgacem, M.N., 2014. Lignin-based rigid polyurethane foams with improved biodegradation. *J. Cell. Plast.* **50**, 81–95. <https://doi.org/10.1177/0021955X13504774>

Cateto, C.A., Barreiro, M.F., Rodrigues, A.E., Belgacem, M.N., 2009. Optimization Study of Lignin Oxypropylation in View of the Preparation of Polyurethane Rigid Foams. *Ind. Eng. Chem. Res.* **48**, 2583–2589. <https://doi.org/10.1021/ie801251r>

Cawse, J.L., Stanford, J.L., Still, R.H., 1984. Polymers from renewable sources, 1. Diamines and diisocyanates containing difurylalakne moieties. *Makromol. Chem.* **185**, 697–707. <https://doi.org/10.1002/macp.1984.021850408>

Çaylı, G., Küsefoğlu, S., 2008. Biobased polyisocyanates from plant oil triglycerides: Synthesis, polymerization, and characterization. *J. Appl. Polym. Sci.* **109**, 2948–2955. <https://doi.org/10.1002/app.28401>

Chang, B.P., Thakur, S., Mohanty, A.K., Misra, M., 2019. Novel sustainable biobased flame retardant from functionalized vegetable oil for enhanced flame retardancy of engineering plastic. *Sci. Rep.* **9**, 15971. <https://doi.org/10.1038/s41598-019-52039-2>

Charlon, M., Heinrich, B., Matter, Y., Couzigné, E., Donnio, B., Avérous, L., 2014. Synthesis, structure and properties of fully biobased thermoplastic polyurethanes, obtained from a diisocyanate based on modified dimer fatty acids, and different renewable diols. *Eur. Polym. J.* **61**, 197–205. <https://doi.org/10.1016/j.eurpolymj.2014.10.012>

Cherubini, F., 2010. The biorefinery concept: Using biomass instead of oil for producing energy and chemicals. *Energy Convers. Manag.* **51**, 1412–1421. <https://doi.org/10.1016/j.enconman.2010.01.015>

Choe, H., Choi, Y., Kim, J.H., 2019. Threshold cell diameter for high thermal insulation of water-blown rigid polyurethane foams. *J. Ind. Eng. Chem.* **73**, 344–350. <https://doi.org/10.1016/j.jiec.2019.02.003>

Contreras, J., Valdés, O., Mirabal-Gallardo, Y., de la Torre, A.F., Navarrete, J., Lisperguer, J., Durán-Lara, E.F., Santos, L.S., Nachtigall, F.M., Cabrera-Barjas, G., Abril, D., 2020. Development of eco-friendly polyurethane foams based on Lesquerella fendleri (A. Grey) oil-based polyol. *Eur. Polym. J.* **128**, 109606. <https://doi.org/10.1016/j.eurpolymj.2020.109606>

Cornille, A., Dworakowska, S., Bogdal, D., Boutevin, B., Caillol, S., 2015. A new way of creating cellular polyurethane materials: NIPU foams. *Eur. Polym. J.* **66**, 129–138. <https://doi.org/10.1016/j.eurpolymj.2015.01.034>

Cornille, A., Guillet, C., Benyahya, S., Negrell, C., Boutevin, B., Caillol, S., 2016. Room temperature flexible isocyanate-free polyurethane foams. *Eur. Polym. J.* **84**, 873–888. <https://doi.org/10.1016/j.eurpolymj.2016.05.032>

Coste, G., Negrell, C., Caillol, S., 2020. From gas release to foam synthesis, the second breath of blowing agents. *Eur. Polym. J.* **140**, 110029.

Cotarca, L., Eckert, H., 2003. Phosgenations - A Handbook, 1st ed. Wiley. <https://doi.org/10.1002/3527602623>

Cozar, A., Echevarria, F., Gonzalez-Gordillo, J.I., Irigoien, X., Ubeda, B., Hernandez-Leon, S., Palma, A.T., Navarro, S., Garcia-de-Lomas, J., Ruiz, A., Fernandez-de-Puelles, M.L., Duarte, C.M., 2014. Plastic debris in the open ocean. *Proc. Natl. Acad. Sci.* **111**, 10239–10244. <https://doi.org/10.1073/pnas.1314705111>

Członka, S., Bertino, M.F., Kośny, J., Strąkowska, A., Maśłowski, M., Strzelec, K., 2018. Linseed oil as a natural modifier of rigid polyurethane foams. *Ind. Crops Prod.* **115**, 40–51. <https://doi.org/10.1016/j.indcrop.2018.02.019>

Dai, Z., Hatano, B., Kadokawa, J., Tagaya, H., 2002. Effect of diaminotoluene on the decomposition of polyurethane foam waste in superheated water. *Polym. Degrad. Stab.* **76**, 179–184. [https://doi.org/10.1016/S0141-3910\(02\)00010-1](https://doi.org/10.1016/S0141-3910(02)00010-1)

Debuissy, T., Pollet, E., Avérous, L., 2018. Biotic and Abiotic Synthesis of Renewable Aliphatic Polyesters from Short Building Blocks Obtained from Biotechnology. *ChemSusChem* **11**, 3836–3870. <https://doi.org/10.1002/cssc.201801700>

Delucis, R. de A., Magalhães, W.L.E., Petzhold, C.L., Amico, S.C., 2018. Thermal and combustion features of rigid polyurethane biofoams filled with four forest-based wastes. *Polym. Compos.* **39**, E1770–E1777. <https://doi.org/10.1002/pc.24784>

Dence, C.W., Lin, S.Y., 1992. Introduction. In 'Methods in Lignin Chemistry' 'Springer Series in Wood Science' (Eds. Lin, S.Y., Dence, C.W.). Springer Berlin Heidelberg, Berlin, Heidelberg, pp. 3–19. https://doi.org/10.1007/978-3-642-74065-7_1

Denissen, W., Rivero, G., Nicolay, R., Leibler, L., Winne, J.M., Du Prez, F.E., 2015. Vinylogous Urethane Vitrimers. *Adv. Funct. Mater.* **25**, 2451–2457. <https://doi.org/10.1002/adfm.201404553>

Desroches, M., Escouvois, M., Auvergne, R., Caillol, S., Boutevin, B., 2012. From Vegetable Oils to Polyurethanes: Synthetic Routes to Polyols and Main Industrial Products. *Polym. Rev.* **52**, 38–79. <https://doi.org/10.1080/15583724.2011.640443>

Dong, T., Laurens, L.M.L., Pienkos, P.T., Fabian Spinelli, P., 2020. Renewable Polymers and resins and methods of making the same. US2020/0017638.

D'Souza, J., Camargo, R., Yan, N., 2017. Biomass Liquefaction and Alkoxylation: A Review of Structural Characterization Methods for Bio-based Polyols. *Polym. Rev.* **57**, 668–694. <https://doi.org/10.1080/15583724.2017.1283328>

D'Souza, J., Camargo, R., Yan, N., 2014. Polyurethane foams made from liquefied bark-based polyols. *J. Appl. Polym. Sci.* **131**, 40599. <https://doi.org/10.1002/app.40599>

Duquesne, S., Le Bras, M., Bourbigot, S., Delobel, R., Camino, G., Eling, B., Lindsay, C., Roels, T., Vezin, H., 2001. Mechanism of fire retardancy of polyurethanes using ammonium polyphosphate. *J. Appl. Polym. Sci.* **82**, 3262–3274. <https://doi.org/10.1002/app.2185>

Durbetaki, A.J., 1956. Direct Titration of Oxirane Oxygen with Hydrogen Bromide in Acetic Acid. *Anal. Chem.* **28**, 2000–2001. <https://doi.org/10.1021/ac60120a055>

Dussenne, C., Delaunay, T., Wiatz, V., Wyart, H., Suisse, I., Sauthier, M., 2017. Synthesis of isosorbide: an overview of challenging reactions. *Green Chem.* **19**, 5332–5344. <https://doi.org/10.1039/C7GC01912B>

Duval, A., Avérous, L., 2017. Cyclic Carbonates as Safe and Versatile Etherifying Reagents for the Functionalization of Lignins and Tannins. *ACS Sustain. Chem. Eng.* **5**, 7334–7343. <https://doi.org/10.1021/acssuschemeng.7b01502>

Duval, A., Avérous, L., 2016. Oxyalkylation of Condensed Tannin with Propylene Carbonate as an Alternative to Propylene Oxide. *ACS Sustain. Chem. Eng.* **4**, 3103–3112. <https://doi.org/10.1021/acssuschemeng.6b00081>

Dworakowska, S., Cornille, A., Bogdał, D., Boutevin, B., Caillol, S., 2015. Formulation of bio-based epoxy foams from epoxidized cardanol and vegetable oil amine: Cardanol-based epoxy foams. *Eur. J. Lipid Sci. Technol.* **117**, 1893–1902. <https://doi.org/10.1002/ejlt.201500232>

Erjavec, M., 2011. Mechanical properties of cellular materials. *Fac. Math. Phys. Univ. Ljubl.* **15**.

Fabris, M., Abbriano, R.M., Pernice, M., Sutherland, D.L., Commault, A.S., Hall, C.C., Labeeuw, L., McCauley, J.I., Kuzhiuparambil, U., Ray, P., Kahlke, T., Ralph, P.J., 2020. Emerging Technologies in Algal Biotechnology: Toward the Establishment of a Sustainable, Algae-Based Bioeconomy. *Front. Plant Sci.* **11**, 279. <https://doi.org/10.3389/fpls.2020.00279>

Fallah-Mehrjardi, M., Kiasat, A.R., Niknam, K., 2018. Nucleophilic ring-opening of epoxides: trends in β -substituted alcohols synthesis. *J. Iran. Chem. Soc.* **15**, 2033–2081. <https://doi.org/10.1007/s13738-018-1400-5>

Fan, H., Tekeei, A., Suppes, G.J., Hsieh, F.-H., 2013. Rigid polyurethane foams made from high viscosity soy-polyols. *J. Appl. Polym. Sci.* **127**, 1623–1629. <https://doi.org/10.1002/app.37508>

Fang, Z., Qiu, C., Ji, D., Yang, Z., Zhu, N., Meng, J., Hu, X., Guo, K., 2019. Development of High-Performance Biodegradable Rigid Polyurethane Foams Using Full Modified Soy-Based Polyols. *J. Agric. Food Chem.* **67**, 2220–2226. <https://doi.org/10.1021/acs.jafc.8b05342>

Ferkl, P., Toulec, M., Laurini, E., Pricl, S., Fermeglia, M., Auffarth, S., Eling, B., Settels, V., Kosek, J., 2017. Multi-scale modelling of heat transfer in polyurethane foams. *Chem. Eng. Sci.* **172**, 323–334. <https://doi.org/10.1016/j.ces.2017.06.035>

Figovsky, O., Shapovalov, L., Potashnikov, R., Tzaid, Y., Bordado, J.C., Letnik, D., De Schijuer, A., 2004. Foamable photo-polymerized composition. US 2004/0176485 A1.

Fink, J.K., 2018. Poly(urethane)s. In 'Reactive Polymers: Fundamentals and Applications'. Elsevier, pp. 71–138. <https://doi.org/10.1016/B978-0-12-814509-8.00002-6>

Flory, P.J., 1941. Molecular Size Distribution in Three Dimensional Polymers. I. Gelation. *J. Am. Chem. Soc.* **63**, 3083–3090. <https://doi.org/10.1021/ja01856a061>

Frey, J.H., Grimminger, J., Stevens, R.E., 1996. New Silicone Surfactants for Rigid Polyurethane Foam. Presented at the UTECH, p. 24.

Froidevaux, V., Negrell, C., Caillol, S., Pascault, J.-P., Boutevin, B., 2016. Biobased Amines: From Synthesis to Polymers; Present and Future. *Chem. Rev.* **116**, 14181–14224. <https://doi.org/10.1021/acs.chemrev.6b00486>

Furtwengler, P., Avérous, L., 2018. Renewable polyols for advanced polyurethane foams from diverse biomass resources. *Polym. Chem.* **9**, 4258–4287. <https://doi.org/10.1039/C8PY00827B>

Furtwengler, P., Boumbimba, R.M., Avérous, L., 2018a. Elaboration and Characterization of Advanced Biobased Polyurethane Foams Presenting Anisotropic Behavior. *Macromol. Mater. Eng.* **303**, 1700501. <https://doi.org/10.1002/mame.201700501>

Furtwengler, P., Matadi Boumbimba, R., Sarbu, A., Avérous, L., 2018b. Novel Rigid Polyisocyanurate Foams from Synthesized Biobased Polyester Polyol with Enhanced Properties. *ACS Sustain. Chem. Eng.* **6**, 6577–6589. <https://doi.org/10.1021/acssuschemeng.8b00380>

Furtwengler, P., Perrin, R., Redl, A., Avérous, L., 2017. Synthesis and characterization of polyurethane foams derived of fully renewable polyester polyols from sorbitol. *Eur. Polym. J.* **97**, 319–327. <https://doi.org/10.1016/j.eurpolymj.2017.10.020>

Gaidukova, G., Ivdre, A., Fridrihsone, A., Verovkins, A., Cabulis, U., Gaidukovs, S., 2017. Polyurethane rigid foams obtained from polyols containing bio-based and recycled components and functional additives. *Ind. Crops Prod.* **102**, 133–143. <https://doi.org/10.1016/j.indcrop.2017.03.024>

Gale, C.B., Chin, B., Tambe, C., Graiver, D., Brook, M.A., 2019. Silicone Structurants for Soybean Oil: Foams, Elastomers, and Candles. *ACS Sustain. Chem. Eng.* **7**, 1347–1352. <https://doi.org/10.1021/acssuschemeng.8b05047>

Gandhi, T.S., Patel, M.R., Dholakiya, B.Z., 2015. Mechanical, thermal and fire properties of sustainable rigid polyurethane foam derived from cashew nut shell liquid. *Int. J. Plast. Technol.* **19**, 30–46. <https://doi.org/10.1007/s12588-015-9114-3>

Gandini, A., Lacerda, T.M., 2015. From monomers to polymers from renewable resources: Recent advances. *Prog. Polym. Sci.* **48**, 1–39. <https://doi.org/10.1016/j.progpolymsci.2014.11.002>

Gandini, A., Lacerda, T.M., Carvalho, A.J.F., Trovatti, E., 2016. Progress of Polymers from Renewable Resources: Furans, Vegetable Oils, and Polysaccharides. *Chem. Rev.* **116**, 1637–1669. <https://doi.org/10.1021/acs.chemrev.5b00264>

Gao, L., Zheng, G., Zhou, Y., Hu, L., Feng, G., 2015. Improved mechanical property, thermal performance, flame retardancy and fire behavior of lignin-based rigid polyurethane foam nanocomposite. *J. Therm. Anal. Calorim.* **120**, 1311–1325. <https://doi.org/10.1007/s10973-015-4434-2>

García, D.E., Glasser, W.G., Pizzi, A., Paczkowski, S.P., Laborie, M.-P., 2016. Modification of condensed tannins: from polyphenol chemistry to materials engineering. *New J. Chem.* **40**, 36–49. <https://doi.org/10.1039/C5NJ02131F>

Garside, M., 2020. Production capacity of bioplastics worldwide from 2017 to 2024, by type [WWW Document]. *Statista*. URL <https://www.statista.com/statistics/678684/global-production-capacity-of-bioplastics-by-type/#statisticContainer> (accessed 8.25.20).

Ge, J., Shi, X., Cai, M., Wu, R., Wang, M., 2003. A novel biodegradable antimicrobial PU foam from wattle tannin. *J. Appl. Polym. Sci.* **90**, 2756–2763. <https://doi.org/10.1002/app.12928>

Ge, J., Zhong, W., Guo, Z., Li, W., Sakai, K., 2000. Biodegradable polyurethane materials from bark and starch. I. Highly resilient foams. *J. Appl. Polym. Sci.* **77**, 2575–2580. [https://doi.org/10.1002/1097-4628\(20000919\)77:12<2575::AID-APP30>3.0.CO;2-L](https://doi.org/10.1002/1097-4628(20000919)77:12<2575::AID-APP30>3.0.CO;2-L)

Ghaderian, A., Haghghi, A.H., Taromi, F.A., Abdeen, Z., Boroomand, A., Taheri, S.M.-R., 2015. Characterization of Rigid Polyurethane Foam Prepared from Recycling of PET Waste. *Period. Polytech. Chem. Eng.* **59**, 296–305. <https://doi.org/10.3311/PPch.7801>

Ghasemlou, M., Daver, F., Ivanova, E.P., Adhikari, B., 2019a. Polyurethanes from seed oil-based polyols: A review of synthesis, mechanical and thermal properties. *Ind. Crops Prod.* **142**, 111841. <https://doi.org/10.1016/j.indcrop.2019.111841>

Ghasemlou, M., Daver, F., Ivanova, E.P., Adhikari, B., 2019b. Bio-based routes to synthesize cyclic carbonates and polyamines precursors of non-isocyanate polyurethanes: A review. *Eur. Polym. J.* **118**, 668–684. <https://doi.org/10.1016/j.eurpolymj.2019.06.032>

Ghosh, T., Karak, N., 2018. Biobased Multifunctional Macroglycol Containing Smart Thermoplastic Hyperbranched Polyurethane Elastomer with Intrinsic Self-Healing Attribute. *ACS Sustain. Chem. Eng.* **6**, 4370–4381. <https://doi.org/10.1021/acssuschemeng.8b00001>

Gibb, J.N., Goodman, J.M., 2013. The formation of high-purity isocyanurate through proazaphosphatrane-catalysed isocyanate cyclo-trimerisation: computational insights. *Org. Biomol. Chem.* **11**, 90–97. <https://doi.org/10.1039/C2OB26547H>

Gibson, L.J., Ashby, M.F., 1997. The mechanics of foams: Basic results. In 'Cellular Solids: Structure and Properties'. Cambridge University Press. <https://doi.org/10.1017/CBO9781139878326>

Gil, B., Kasperski, J., 2018. Efficiency Evaluation of the Ejector Cooling Cycle using a New Generation of HFO/HCFO Refrigerant as a R134a Replacement. *Energies* **11**, 2136. <https://doi.org/10.3390/en11082136>

Greim, H., Bury, D., Klimisch, H.-J., Oeben-Negele, M., Ziegler-Skylakakis, K., 1998. Toxicity of aliphatic amines: Structure-activity relationship. *Chemosphere* **36**, 271–295. [https://doi.org/10.1016/S0045-6535\(97\)00365-2](https://doi.org/10.1016/S0045-6535(97)00365-2)

Grignard, B., Thomassin, J.-M., Gennen, S., Poussard, L., Bonnaud, L., Raquez, J.-M., Dubois, P., Tran, M.-P., Park, C.B., Jerome, C., Detrembleur, C., 2016. CO₂-blown microcellular non-isocyanate polyurethane (NIPU) foams: from bio- and CO₂-sourced monomers to potentially thermal insulating materials. *Green Chem.* **18**, 2206–2215. <https://doi.org/10.1039/C5GC02723C>

Grunwald, P. (Ed.), 2016. Handbook of carbohydrate-modifying biocatalysts 'Pan Stanford series on biocatalysis'. Pan Stanford Publishing, Singapore.

Guan, J., Song, Y., Lin, Y., Yin, X., Zuo, M., Zhao, Y., Tao, X., Zheng, Q., 2011. Progress in Study of Non-Isocyanate Polyurethane. *Ind. Eng. Chem. Res.* **50**, 6517–6527. <https://doi.org/10.1021/ie101995j>

Gunstone, F.D., Harwood, J.L., Harwood, J.L., 2007. The Lipid Handbook with CD-ROM, 3rd ed. CRC Press. <https://doi.org/10.1201/9781420009675>

Guo, A., Cho, Y., Petrović, Z.S., 2000. Structure and properties of halogenated and nonhalogenated soy-based polyols. *J. Polym. Sci. Part Polym. Chem.* **38**, 3900–3910. [https://doi.org/10.1002/1099-0518\(20001101\)38:21<3900::AID-POLA70>3.0.CO;2-E](https://doi.org/10.1002/1099-0518(20001101)38:21<3900::AID-POLA70>3.0.CO;2-E)

Gupta, R.K., Ionescu, M., Wan, X., Radojcic, D., Petrović, Z.S., 2015. Synthesis of a Novel Limonene Based Mannich Polyol for Rigid Polyurethane Foams. *J. Polym. Environ.* **23**, 261–268. <https://doi.org/10.1007/s10924-015-0717-8>

Gustini, L., Lavilla, C., Finzel, L., Noordover, B.A.J., Hendrix, M.M.R.M., Koning, C.E., 2016. Sustainable coatings from bio-based, enzymatically synthesized polyesters with enhanced functionalities. *Polym. Chem.* **7**, 6586–6597. <https://doi.org/10.1039/C6PY01339B>

Gustini, L., Noordover, B.A.J., Gehrels, C., Dietz, C., Koning, C.E., 2015. Enzymatic synthesis and preliminary evaluation as coating of sorbitol-based, hydroxy-functional polyesters with controlled molecular weights. *Eur. Polym. J.* **67**, 459–475. <https://doi.org/10.1016/j.eurpolymj.2014.12.025>

HAGERMAN, A., 2002. Tannin handbook. <http://www.users.muohio.edu/hagermae/>.

Halley, P.J., Avérous, L., 2014. Starch polymers: from genetic engineering to green applications. Elsevier, Burlington, MA.

Harry-O'kuru, R.E., Tisserat, B., Gordon, S.H., Gravett, A., 2015. Osage Orange (*Maclura pomifera* L.) Seed Oil Poly(α -hydroxydibutylamine) Triglycerides: Synthesis and Characterization. *J. Agric. Food Chem.* **63**, 6588–6595. <https://doi.org/10.1021/acs.jafc.5b01625>

Hatakeyama, H., Hatakeyama, T., 2005. Environmentally Compatible Hybrid-Type Polyurethane Foams Containing Saccharide and Lignin Components. *Macromol. Symp.* **224**, 219–226. <https://doi.org/10.1002/masy.200550619>

Hatakeyama, H., Hirogaki, A., Matsumura, H., Hatakeyama, T., 2013. Glass transition temperature of polyurethane foams derived from lignin by controlled reaction rate. *J. Therm. Anal. Calorim.* **114**, 1075–1082. <https://doi.org/10.1007/s10973-013-3132-1>

Hatakeyama, T., Matsumoto, Y., Asano, Y., Hatakeyama, H., 2004. Glass transition of rigid polyurethane foams derived from sodium lignosulfonate mixed with diethylene, triethylene and polyethylene glycols. *Thermochim. Acta* **416**, 29–33. <https://doi.org/10.1016/j.tca.2002.12.002>

Hawkins, M.C., O'Toole, B., Jackovich, D., 2005. Cell Morphology and Mechanical Properties of Rigid Polyurethane Foam. *J. Cell. Plast.* **41**, 267–285. <https://doi.org/10.1177/0021955X05053525>

Hayati, A.N., Evans, D.A.C., Laycock, B., Martin, D.J., Annamalai, P.K., 2018. A simple methodology for improving the performance and sustainability of rigid polyurethane foam by incorporating industrial lignin. *Ind. Crops Prod.* **117**, 149–158. <https://doi.org/10.1016/j.indcrop.2018.03.006>

Hejna, A., Kirpluks, M., Kosmela, P., Cabulis, U., Haponiuk, J., Piszczyk, Ł., 2017. The influence of crude glycerol and castor oil-based polyol on the structure and performance of rigid polyurethane-polyisocyanurate foams. *Ind. Crops Prod.* **95**, 113–125. <https://doi.org/10.1016/j.indcrop.2016.10.023>

Hejna, A., Kosmela, P., Kirpluks, M., Cabulis, U., Klein, M., Haponiuk, J., Piszczyk, Ł., 2018. Structure, Mechanical, Thermal and Fire Behavior Assessments of Environmentally Friendly Crude Glycerol-Based Rigid Polyisocyanurate Foams. *J. Polym. Environ.* **26**, 1854–1868. <https://doi.org/10.1007/s10924-017-1086-2>

Herrán, R., Amalvy, J.I., Chiacchiarelli, L.M., 2019. Highly functional lactic acid ring-opened soybean polyols applied to rigid polyurethane foams. *J. Appl. Polym. Sci.* **136**, 47959. <https://doi.org/10.1002/app.47959>

Herzberger, J., Niederer, K., Pohlitz, H., Seiwert, J., Worm, M., Wurm, F.R., Frey, H., 2016. Polymerization of Ethylene Oxide, Propylene Oxide, and Other Alkylene Oxides: Synthesis, Novel Polymer Architectures, and Bioconjugation. *Chem. Rev.* **116**, 2170–2243. <https://doi.org/10.1021/acs.chemrev.5b00441>

Hicks, D., Austin, A., 2017. A review of the global PU industry 2016 and outlook for 2017. *PU Mag.* **14**, 4–16.

Hill, R.M., 2019. Siloxane Surfactants. In 'Silicone Surfactants' (Ed. Hill, R.M.). Routledge, pp. 1–48. <https://doi.org/10.1201/9780203739754-1>

Hilyard, N.C., Cunningham, A., Glicksman, L.R., 2012. Heat transfer in foams. In 'Low Density Cellular Plastics: Physical Basis of Behaviour'. Springer Netherlands, Dordrecht.

Hoffman, D.K., 1984. Model System for a Urethane-Modified Isocyanurate Foam. *J. Cell. Plast.* **20**, 129–137. <https://doi.org/10.1177/0021955X8402000205>

Hojabri, L., Kong, X., Narine, S.S., 2010. Novel long chain unsaturated diisocyanate from fatty acid: Synthesis, characterization, and application in bio-based polyurethane. *J. Polym. Sci. Part Polym. Chem.* **48**, 3302–3310. <https://doi.org/10.1002/pola.24114>

Howell, B.A., Oberdorfer, K.L., Ostrander, E.A., 2018. Phosphorus Flame Retardants for Polymeric Materials from Gallic Acid and Other Naturally Occurring Multihydroxybenzoic Acids. *Int. J. Polym. Sci.* **2018**, 1–12. <https://doi.org/10.1155/2018/7237236>

Hu, M., Hwang, J.-Y., Kurth, M.J., Hsieh, Y.-L., Shoemaker, C.F., Krochta, J.M., 1997. Polyurethane Rigid Foam Derived from Reduced Sweet Whey Permeate. *J. Agric. Food Chem.* **45**, 4156–4161. <https://doi.org/10.1021/jf9701650>

Hu, S., Luo, X., Li, Y., 2014. Polyols and Polyurethanes from the Liquefaction of Lignocellulosic Biomass. *ChemSusChem* **7**, 66–72. <https://doi.org/10.1002/cssc.201300760>

Hu, S., Wan, C., Li, Y., 2012. Production and characterization of biopolyols and polyurethane foams from crude glycerol based liquefaction of soybean straw. *Bioresour. Technol.* **103**, 227–233. <https://doi.org/10.1016/j.biortech.2011.09.125>

Hu, Y., Tian, Y., Cheng, J., Zhang, J., 2020. Synthesis of Eugenol-Based Polyols via Thiol–Ene Click Reaction and High-Performance Thermosetting Polyurethane Therefrom. *ACS Sustain. Chem. Eng.* **8**, 4158–4166. <https://doi.org/10.1021/acssuschemeng.9b06867>

Huang, X., Yang, X., Liu, H., Shang, S., Cai, Z., Wu, K., 2019. Bio-based thermosetting epoxy foams from epoxidized soybean oil and rosin with enhanced properties. *Ind. Crops Prod.* **139**, 111540. <https://doi.org/10.1016/j.indcrop.2019.111540>

Huo, S., Jin, C., Liu, G., Chen, J., Wu, G., Kong, Z., 2019. Preparation and properties of biobased autocatalytic polyols and their polyurethane foams. *Polym. Degrad. Stab.* **159**, 62–69. <https://doi.org/10.1016/j.polymdegradstab.2018.11.019>

Huo, S.-P., Nie, M.-C., Kong, Z.-W., Wu, G.-M., Chen, J., 2012. Crosslinking kinetics of the formation of lignin-aminated polyol-based polyurethane foam. *J. Appl. Polym. Sci.* **125**, 152–157. <https://doi.org/10.1002/app.35401>

IEA, 2020. World Energy Balances: Overview [WWW Document]. *iea.org*. URL <https://www.iea.org/reports/world-energy-balances-overview> (accessed 8.15.20).

Ionescu, M., 2005. Chemistry and technology of polyols for polyurethanes, 1st ed. Rapra Technology, Shawbury, Shrewsbury, Shropshire, U.K.

Ionescu, M., Petrović, Z.S., 2010. High Functionality Polyether Polyols Based on Polyglycerol. *J. Cell. Plast.* **46**, 223–237. <https://doi.org/10.1177/0021955X09355887>

Ionescu, M., Radojčić, D., Wan, X., Shrestha, M.L., Petrović, Z.S., Upshaw, T.A., 2016. Highly functional polyols from castor oil for rigid polyurethanes. *Eur. Polym. J.* **84**, 736–749. <https://doi.org/10.1016/j.eurpolymj.2016.06.006>

Ionescu, M., Wan, X., Bilić, N., Petrović, Z.S., 2012. Polyols and Rigid Polyurethane Foams from Cashew Nut Shell Liquid. *J. Polym. Environ.* **20**, 647–658. <https://doi.org/10.1007/s10924-012-0467-9>

Isikgor, F.H., Becer, C.R., 2015. Lignocellulosic biomass: a sustainable platform for the production of bio-based chemicals and polymers. *Polym. Chem.* **6**, 4497–4559. <https://doi.org/10.1039/C5PY00263J>

Iwata, T., 2015. Biodegradable and Bio-Based Polymers: Future Prospects of Eco-Friendly Plastics. *Angew. Chem. Int. Ed.* **54**, 3210–3215. <https://doi.org/10.1002/anie.201410770>

J. C. Thompson, B. B. He, 2006. Characterization of crude glycerol from biodiesel production from multiple feedstocks. *Appl. Eng. Agric.* **22**, 261–265. <https://doi.org/10.13031/2013.20272>

Jaratrotkamjorn, R., Tanrattanakul, V., 2020. Bio-based flexible polyurethane foam synthesized from palm oil and natural rubber. *J. Appl. Polym. Sci.* **137**, 49310. <https://doi.org/10.1002/app.49310>

Jarfelt, U., Ramnäs, O., 2006. Thermal conductivity of polyurethane foam Best performance. Presented at the 10th International Symposium on district heating and cooling, Chalmers University of Technology Goteborg, Sweden, pp. 3–5.

Jasiūnas, L., McKenna, S.T., Bridžiūviėnė, D., Miknius, L., 2020. Mechanical, Thermal Properties and Stability of Rigid Polyurethane Foams Produced with Crude-Glycerol Derived Biomass Biopolymers. *J. Polym. Environ.* **28**, 1378–1389. <https://doi.org/10.1007/s10924-020-01686-y>

Javaid, M.A., Zia, K.M., Iqbal, A., Ahmad, S., Akram, N., Liu, X., Nawaz, H., Khosa, M.K., Awais, M., 2020. Utilization of waxy corn starch as an efficient chain extender for the preparation of polyurethane elastomers. *Int. J. Biol. Macromol.* **148**, 415–423. <https://doi.org/10.1016/j.ijbiomac.2020.01.011>

Jiang, T., Wang, W., Yu, D., Huang, D., Wei, N., Hu, Y., Huang, H., 2018. Synthesis and characterization of polyurethane rigid foams from polyether polyols with isosorbide as the bio-based starting agent. *J. Polym. Res.* **25**, 140. <https://doi.org/10.1007/s10965-018-1538-y>

Jiang, Y., Loos, K., 2016. Enzymatic Synthesis of Biobased Polyesters and Polyamides. *Polymers* **8**, 243. <https://doi.org/10.3390/polym8070243>

John, J., Bhattacharya, M., Turner, R.B., 2002. Characterization of polyurethane foams from soybean oil. *J. Appl. Polym. Sci.* **86**, 3097–3107. <https://doi.org/10.1002/app.11322>

de Jong, E., Dam, M.A., Sipos, L., Gruter, G.-J.M., 2012. Furandicarboxylic Acid (FDCA), A Versatile Building Block for a Very Interesting Class of Polyesters. In 'Biobased Monomers, Polymers, and Materials' 'ACS Symposium Series' (Eds. Smith, P.B., Gross, R.A.). American Chemical Society, Washington, DC, pp. 1–13. <https://doi.org/10.1021/bk-2012-1105.ch001>

Jongedijk, E., Cankar, K., Buchhaupt, M., Schrader, J., Bouwmeester, H., Beekwilder, J., 2016. Biotechnological production of limonene in microorganisms. *Appl. Microbiol. Biotechnol.* **100**, 2927–2938. <https://doi.org/10.1007/s00253-016-7337-7>

Kahlerras, Z., Irinislimane, R., Bruzaud, S., Belhaneche-Bensemra, N., 2020. Elaboration and Characterization of Polyurethane Foams Based on Renewably Sourced Polyols. *J. Polym. Environ.* **28**, 3003–3018. <https://doi.org/10.1007/s10924-020-01833-5>

Kang, M.J., Kim, Y.H., Park, G.P., Han, M.S., Kim, W.N., Park, S.D., 2010. Liquid nucleating additives for improving thermal insulating properties and mechanical strength of polyisocyanurate foams. *J. Mater. Sci.* **45**, 5412–5419. <https://doi.org/10.1007/s10853-010-4594-1>

Karunaratna, M.S., Smith, R.C., 2020. Valorization of Lignin as a Sustainable Component of Structural Materials and Composites: Advances from 2011 to 2019. *Sustainability* **12**, 734. <https://doi.org/10.3390/su12020734>

Kaur, R., Kumar, M., 2020. Addition of anti-flaming agents in castor oil based rigid polyurethane foams: studies on mechanical and flammable behaviour. *Mater. Res. Express* **7**, 015333. <https://doi.org/10.1088/2053-1591/ab68a2>

Kausar, A., 2018. Polyurethane Composite Foams in High-Performance Applications: A Review. *Polym.-Plast. Technol. Eng.* **57**, 346–369. <https://doi.org/10.1080/03602559.2017.1329433>

Kaushiva, B.D., 1999. Structure-Property Relationships Of Flexible Polyurethane Foams (Dissertation). Virginia Polytechnic Institute and State University, Blacksburg, Virginia.

Khanderay, J.C., Gite, V.V., 2019. Fully biobased polyester polyols derived from renewable resources toward preparation of polyurethane and their application for coatings. *J. Appl. Polym. Sci.* **47558**. <https://doi.org/10.1002/app.47558>

Khundamri, N., Aouf, C., Fulcrand, H., Dubreucq, E., Tanrattanakul, V., 2019. Bio-based flexible epoxy foam synthesized from epoxidized soybean oil and epoxidized mangosteen tannin. *Ind. Crops Prod.* **128**, 556–565. <https://doi.org/10.1016/j.indcrop.2018.11.062>

Kim, Y.-H., Koczo, K., Wasan, D.T., 1997. Dynamic Film and Interfacial Tensions in Emulsion and Foam Systems. *J. Colloid Interface Sci.* **187**, 29–44. <https://doi.org/10.1006/jcis.1996.4507>

Knölker, H.-J., Braxmeier, T., Schlechtingen, G., 1995. A Novel Method for the Synthesis of Isocyanates Under Mild Conditions. *Angew. Chem. Int. Ed. Engl.* **34**, 2497–2500. <https://doi.org/10.1002/anie.199524971>

Kobilka, B., Kuczynski, J., Porter, J., Wertz, J., 2019. Pinene-Derived diisocyanates. US 2019/0106383A1.

Konieczny, J., Loos, K., 2019. Green Polyurethanes from Renewable Isocyanates and Biobased White Dextrins. *Polymers* **11**, 256. <https://doi.org/10.3390/polym11020256>

Kosmela, P., Gosz, K., Kazimierski, P., Hejna, A., Haponiuk, J.T., Piszczyk, Ł., 2019. Chemical structures, rheological and physical properties of biopolyols prepared via solvothermal liquefaction of Enteromorpha and Zostera marina biomass. *Cellulose* **26**, 5893–5912. <https://doi.org/10.1007/s10570-019-02540-8>

Kosmela, P., Hejna, A., Formela, K., Haponiuk, J., Piszczyk, Ł., 2018. The Study on Application of Biopolyols Obtained by Cellulose Biomass Liquefaction Performed with Crude Glycerol for the Synthesis of Rigid Polyurethane Foams. *J. Polym. Environ.* **26**, 2546–2554. <https://doi.org/10.1007/s10924-017-1145-8>

Kövilein, A., Kubisch, C., Cai, L., Ochsenreither, K., 2020. Malic acid production from renewables: a review. *J. Chem. Technol. Biotechnol.* **95**, 513–526. <https://doi.org/10.1002/jctb.6269>

Kreye, O., Mutlu, H., Meier, M.A.R., 2013. Sustainable routes to polyurethane precursors. *Green Chem.* **15**, 1431. <https://doi.org/10.1039/c3gc40440d>

Kuhire, S.S., Nagane, S.S., Wadgaonkar, P.P., 2017. Poly(ether urethane)s from aromatic diisocyanates based on lignin-derived phenolic acids: Poly(ether urethane)s from aromatic diisocyanates. *Polym. Int.* **66**, 892–899. <https://doi.org/10.1002/pi.5333>

Kurańska, M., Banaś, J., Polaczek, K., Banaś, M., Prociak, A., Kuc, J., Uram, K., Lubera, T., 2019. Evaluation of application potential of used cooking oils in the synthesis of polyol compounds. *J. Environ. Chem. Eng.* **7**, 103506. <https://doi.org/10.1016/j.jece.2019.103506>

Kurańska, M., Pinto, J.A., Salach, K., Barreiro, M.F., Prociak, A., 2020a. Synthesis of thermal insulating polyurethane foams from lignin and rapeseed based polyols: A comparative study. *Ind. Crops Prod.* **143**, 111882. <https://doi.org/10.1016/j.indcrop.2019.111882>

Kurańska, M., Polaczek, K., Auguściak-Królikowska, M., Prociak, A., Ryszkowska, J., 2020b. Open-cell rigid polyurethane bio-foams based on modified used cooking oil. *Polymer* **190**, 122164. <https://doi.org/10.1016/j.polymer.2020.122164>

Lai, N.A., 2014. Thermodynamic properties of HFO-1243zf and their application in study on a refrigeration cycle. *Appl. Therm. Eng.* **70**, 1–6. <https://doi.org/10.1016/j.applthermaleng.2014.04.042>

Lang, S., Gerschitzka, M., Bauer, D., Drück, H., 2016. Thermal Conductivity of Vacuum Insulation Materials for Thermal Energy Stores in Solar Thermal Systems. *Energy Procedia* **91**, 172–181. <https://doi.org/10.1016/j.egypro.2016.06.196>

Laurichesse, S., Avérous, L., 2014. Chemical modification of lignins: Towards biobased polymers. *Prog. Polym. Sci.* **39**, 1266–1290. <https://doi.org/10.1016/j.progpolymsci.2013.11.004>

Laurichesse, S., Huillet, C., Avérous, L., 2014. Original polyols based on organosolv lignin and fatty acids: new bio-based building blocks for segmented polyurethane synthesis. *Green Chem.* **16**, 3958–3970. <https://doi.org/10.1039/C4GC00596A>

Lee, S.-H., Yoshioka, M., Shiraishi, N., 2000. Liquefaction of corn bran (CB) in the presence of alcohols and preparation of polyurethane foam from its liquefied polyol. *J. Appl. Polym. Sci.* **78**, 319–325. [https://doi.org/10.1002/1097-4628\(20001010\)78:2<319::AID-APP120>3.0.CO;2-Z](https://doi.org/10.1002/1097-4628(20001010)78:2<319::AID-APP120>3.0.CO;2-Z)

Lee, S.Y., Kim, H.U., Chae, T.U., Cho, J.S., Kim, J.W., Shin, J.H., Kim, D.I., Ko, Y.-S., Jang, W.D., Jang, Y.-S., 2019. A comprehensive metabolic map for production of bio-based chemicals. *Nat. Catal.* **2**, 18–33. <https://doi.org/10.1038/s41929-018-0212-4>

Li, B., Zhou, M., Huo, W., Cai, D., Qin, P., Cao, H., Tan, T., 2020a. Fractionation and oxypropylation of corn-stover lignin for the production of biobased rigid polyurethane foam. *Ind. Crops Prod.* **143**, 111887. <https://doi.org/10.1016/j.indcrop.2019.111887>

Li, H.-Q., Shao, Q., Luo, H., Xu, J., 2016a. Polyurethane foams from alkaline lignin-based polyether polyol. *J. Appl. Polym. Sci.* **133**, 43261–43267. <https://doi.org/10.1002/app.43261>

Li, P., Xiao, Z., Chang, C., Zhao, S., Xu, G., 2020b. Efficient Synthesis of Biobased Glycerol Levulinate Ketal and Its Application for Rigid Polyurethane Foam Production. *Ind. Eng. Chem. Res.* **59**, 17520–17528. <https://doi.org/10.1021/acs.iecr.9b06038>

Li, Q.F., Feng, Y.L., Wang, J.W., Yin, N., Zhao, Y.H., Kang, M.Q., Wang, X.W., 2016b. Preparation and properties of rigid polyurethane foam based on modified castor oil. *Plast. Rubber Compos.* **45**, 16–21. <https://doi.org/10.1080/14658011.2015.1112538>

Li, Y., Noordover, B.A.J., van Benthem, R.A.T.M., Koning, C.E., 2015. Bio-based poly(urethane urea) dispersions with low internal stabilizing agent contents and tunable thermal properties. *Prog. Org. Coat.* **86**, 134–142. <https://doi.org/10.1016/j.porgcoat.2015.04.018>

Li, Y., Noordover, B.A.J., van Benthem, R.A.T.M., Koning, C.E., 2014. Property profile of poly(urethane urea) dispersions containing dimer fatty acid-, sugar- and amino acid-based building blocks. *Eur. Polym. J.* **59**, 8–18. <https://doi.org/10.1016/j.eurpolymj.2014.06.016>

Li, Y., Ragauskas, A.J., 2012a. Ethanol organosolv lignin-based rigid polyurethane foam reinforced with cellulose nanowhiskers. *RSC Adv.* **2**, 3347. <https://doi.org/10.1039/c2ra00646d>

Li, Y., Ragauskas, A.J., 2012b. Kraft Lignin-Based Rigid Polyurethane Foam. *J. Wood Chem. Technol.* **32**, 210–224. <https://doi.org/10.1080/02773813.2011.652795>

Lim, H., Kim, S.H., Kim, B.K., 2008. Effects of silicon surfactant in rigid polyurethane foams. *Express Polym. Lett.* **2**, 194–200. <https://doi.org/10.3144/expresspolymlett.2008.24>

Liu, J., Dai, J., Wang, S., Peng, Y., Cao, L., Liu, X., 2020. Facile synthesis of bio-based reactive flame retardant from vanillin and guaiacol for epoxy resin. *Compos. Part B Eng.* **190**, 107926. <https://doi.org/10.1016/j.compositesb.2020.107926>

Liu, X., Gu, X., Sun, J., Zhang, S., 2017. Preparation and characterization of chitosan derivatives and their application as flame retardants in thermoplastic polyurethane. *Carbohydr. Polym.* **167**, 356–363. <https://doi.org/10.1016/j.carbpol.2017.03.011>

Liu, Z., Yu, F., Fang, G., Yang, H., 2009. Performance characterization of rigid polyurethane foam with refined alkali lignin and modified alkali lignin. *J. For. Res.* **20**, 161–164. <https://doi.org/10.1007/s11676-009-0028-9>

Lligadas, G., Ronda, J.C., Galià, M., Cádiz, V., 2007. Polyurethane Networks from Fatty-Acid-Based Aromatic Triols: Synthesis and Characterization. *Biomacromolecules* **8**, 1858–1864. <https://doi.org/10.1021/bm070157k>

Lligadas, G., Ronda, J.C., Galià, M., Cádiz, V., 2006b. Synthesis and properties of thermosetting polymers from a phosphorous-containing fatty acid derivative. *J. Polym. Sci. Part Polym. Chem.* **44**, 5630–5644. <https://doi.org/10.1002/pola.21691>

Lubczak, R., Szczech, D., Lubczak, J., 2020. From starch to oligoetherols and polyurethane foams. *Polym. Bull.* **77**, 5725–5751. <https://doi.org/10.1007/s00289-019-03052-y>

Luo, X., Li, Y., 2014. Synthesis and Characterization of Polyols and Polyurethane Foams from PET Waste and Crude Glycerol. *J. Polym. Environ.* **22**, 318–328. <https://doi.org/10.1007/s10924-014-0649-8>

Lutz, E.F., 1986. Shell higher olefins process. *J. Chem. Educ.* **63**, 202. <https://doi.org/10.1021/ed063p202>

Magnin, A., Pollet, E., Perrin, R., Ullmann, C., Persillon, C., Phalip, V., Avérous, L., 2019. Enzymatic recycling of thermoplastic polyurethanes: Synergistic effect of an esterase and an amidase and recovery of building blocks. *Waste Manag.* **85**, 141–150. <https://doi.org/10.1016/j.wasman.2018.12.024>

Magnin, A., Pollet, E., Phalip, V., Avérous, L., 2020. Evaluation of biological degradation of polyurethanes. *Biotechnol. Adv.* **39**, 107457. <https://doi.org/10.1016/j.biotechadv.2019.107457>

Mahmood, N., Yuan, Z., Schmidt, J., Charles Xu, C., 2013. Production of polyols via direct hydrolysis of kraft lignin: Effect of process parameters. *Bioresour. Technol.* **139**, 13–20. <https://doi.org/10.1016/j.biortech.2013.03.199>

Mahmood, N., Yuan, Z., Schmidt, J., Tymchyshyn, M., Xu, C.C., 2016. Hydrolytic liquefaction of hydrolysis lignin for the preparation of bio-based rigid polyurethane foam. *Green Chem.* **18**, 2385–2398. <https://doi.org/10.1039/C5GC02876K>

Mahmood, N., Yuan, Z., Schmidt, J., Xu, C.C., 2015. Preparation of bio-based rigid polyurethane foam using hydrolytically depolymerized Kraft lignin via direct replacement or oxypropylation. *Eur. Polym. J.* **68**, 1–9. <https://doi.org/10.1016/j.eurpolymj.2015.04.030>

Maisonneuve, L., Chollet, G., Grau, E., Cramail, H., 2016. Vegetable oils: a source of polyols for polyurethane materials. *OLC* **23**, D508. <https://doi.org/10.1051/ocl/2016031>

Maisonneuve, L., Lamarzelle, O., Rix, E., Grau, E., Cramail, H., 2015. Isocyanate-Free Routes to Polyurethanes and Poly(hydroxy Urethane)s. *Chem. Rev.* **115**, 12407–12439. <https://doi.org/10.1021/acs.chemrev.5b00355>

Maldas, D., Shiraishi, N., 1996. Liquefaction of Wood in the Presence of Polyol Using NaOH as a Catalyst and its Application to Polyurethane Foams. *Int. J. Polym. Mater.* **33**, 61–71. <https://doi.org/10.1080/00914039608028608>

Malhotra, A.K., Wasan, D.T., 1987. Effects of surfactant adsorption-desorption kinetics and interfacial rheological properties on the rate of drainage of foam and emulsion films. *Chem. Eng. Commun.* **55**, 95–128. <https://doi.org/10.1080/00986448708911921>

Malwitz, N., 1987. Fire-retardant Polyurethane Foam and Method and Resin for Preparing the Same. US4654375A.

Mann, N., Mendon, S.K., Rawlins, J.W., Thames, S.F., 2008. Synthesis of Carbonated Vernonia Oil. *J. Am. Oil Chem. Soc.* **85**, 791–796. <https://doi.org/10.1007/s11746-008-1249-3>

Manzardo, A., Marson, A., Roso, M., Boaretti, C., Modesti, M., Scipioni, A., Lorenzetti, A., 2019. Life Cycle Assessment Framework To Support the Design of Biobased Rigid Polyurethane Foams. *ACS Omega* **4**, 14114–14123. <https://doi.org/10.1021/acsomega.9b02025>

Marín, R., Alla, A., Ilarduya, A.M., Muñoz- Guerra, S., 2011. Carbohydrate-based polyurethanes: A comparative study of polymers made from isosorbide and 1,4-butanediol. *E-Polym.* **11**. <https://doi.org/10.1515/epoly.2011.11.1.700>

Mateu-Royo, C., Navarro-Esbrí, J., Mota-Babiloni, A., Amat-Albuixech, M., Molés, F., 2019. Thermodynamic analysis of low GWP alternatives to HFC-245fa in high-temperature heat pumps: HCFO-1224yd(Z), HCFO-1233zd(E) and HFO-1336mzz(Z). *Appl. Therm. Eng.* **152**, 762–777. <https://doi.org/10.1016/j.applthermaleng.2019.02.047>

Mcclusky, J.V., O'Neill, R.E., Priester, R.D., Ramsey, W.A., 1994. Vibrating Rod Viscometer: A Valuable Probe into Polyurethane Chemistry. *J. Cell. Plast.* **30**, 224–241. <https://doi.org/10.1177/0021955X9403000302>

Modesti, M., Simioni, F., 1996. Chemical recycling of reinforced polyurethane from the automotive industry. *Polym. Eng. Sci.* **36**, 2173–2178. <https://doi.org/10.1002/pen.10614>

Mohammadpour, R., Mir Mohamad Sadeghi, G., 2020. Effect of Liquefied Lignin Content on Synthesis of Bio-based Polyurethane Foam for Oil Adsorption Application. *J. Polym. Environ.* **28**, 892–905. <https://doi.org/10.1007/s10924-019-01650-5>

Molotsky, H., Gramera, R., 1976. Flame retardant polyurethane foams. US3957702Z.

Moncada, J., Tamayo, J.A., Cardona, C.A., 2014. Integrating first, second, and third generation biorefineries: Incorporating microalgae into the sugarcane biorefinery. *Chem. Eng. Sci.* **118**, 126–140. <https://doi.org/10.1016/j.ces.2014.07.035>

Monie, F., Grignard, B., Thomassin, J.-M., Mereau, R., Tassaing, T., Jerome, C., Detrembleur, C., 2020. Chemo- and Regioselective Additions of Nucleophiles to Cyclic Carbonates for the Preparation of Self-Blowing Non-Isocyanate Polyurethane Foams. *Angew. Chem. Int. Ed.* **59**, 17033–17041. <https://doi.org/10.1002/anie.202006267>

More, A.S., Lebarbé, T., Maisonneuve, L., Gadenne, B., Alfos, C., Cramail, H., 2013. Novel fatty acid based di-isocyanates towards the synthesis of thermoplastic polyurethanes. *Eur. Polym. J.* **49**, 823–833. <https://doi.org/10.1016/j.eurpolymj.2012.12.013>

Nadji, H., Bruzzèse, C., Belgacem, M.N., Benaboura, A., Gandini, A., 2005. Oxypropylation of Lignins and Preparation of Rigid Polyurethane Foams from the Ensuing Polyols. *Macromol. Mater. Eng.* **290**, 1009–1016. <https://doi.org/10.1002/mame.200500200>

Narine, S.S., Kong, X., Bouzidi, L., Sporns, P., 2007. Physical Properties of Polyurethanes Produced from Polyols from Seed Oils: II. Foams. *J. Am. Oil Chem. Soc.* **84**, 65–72. <https://doi.org/10.1007/s11746-006-1008-2>

Nawata, T., Kresta, J.E., Frisch, K.C., 1975. Comparative Studies of Isocyanurate and Isocyanurate-Urethane Foams. *J. Cell. Plast.* **11**, 267–278. <https://doi.org/10.1177/0021955X7501100506>

Negrell, C., Cornille, A., de Andrade Nascimento, P., Robin, J.-J., Caillol, S., 2017. New bio-based epoxy materials and foams from microalgal oil: Agal oil epoxy materials and foams. *Eur. J. Lipid Sci. Technol.* **119**, 1600214. <https://doi.org/10.1002/ejlt.201600214>

Nemirovsky, J., 1883. Ueber die Einwirkung von Chlorkohlenoxyd auf Aethylenglycol; vorläufige Mittheilung. *J. Für Prakt. Chem.* **28**, 439–440. <https://doi.org/10.1002/prac.18830280136>

Neumann, C.N.D., Bulach, W.D., Rehahn, M., Klein, R., 2011. Water-Free Synthesis of Polyurethane Foams Using Highly Reactive Diisocyanates Derived from 5-Hydroxymethylfurfural. *Macromol. Rapid Commun.* **32**, 1373–1378. <https://doi.org/10.1002/marc.201100205>

Ng, W.S., Lee, C.S., Chuah, C.H., Cheng, S.-F., 2017. Preparation and modification of water-blown porous biodegradable polyurethane foams with palm oil-based polyester polyol. *Ind. Crops Prod.* **97**, 65–78. <https://doi.org/10.1016/j.indcrop.2016.11.066>

Nikje, M.M.A., Haghshenas, M., Garmarudi, A.B., 2006. Glycolysis of Waste Polyurethane Integral Skin Foams from Steering Wheel. *Polym.-Plast. Technol. Eng.* **45**, 569–573. <https://doi.org/10.1080/03602550600554174>

Obi, B.E., 2018a. Foaming Processes. In 'Polymeric Foams Structure-Property-Performance'. Elsevier, pp. 131–188. <https://doi.org/10.1016/B978-1-4557-7755-6.00006-9>

Obi, B.E., 2018b. Fundamentals of Polymeric Foams and Classification of Foam Types. In 'Polymeric Foams Structure-Property-Performance'. Elsevier, pp. 93–129. <https://doi.org/10.1016/B978-1-4557-7755-6.00005-7>

Okuzono, S., Tokumoto, K., Tamano, Y., Lowe, D.W., 2001. New Polyisocyanurate Catalysts Which Exhibit High Activity at Low Temperature. *J. Cell. Plast.* **37**, 72–89. <https://doi.org/10.1106/DWGD-PX79-WR0G-9GBW>

Owen, M.J., Kendrick, T.C., Kingston, B.M., Lloyd, N.C., 1967. The surface chemistry of polyurethane foam formation. *J. Colloid Interface Sci.* **24**, 141–150. [https://doi.org/10.1016/0021-9797\(67\)90211-1](https://doi.org/10.1016/0021-9797(67)90211-1)

Pan, X., Saddler, J.N., 2013. Effect of replacing polyol by organosolv and kraft lignin on the property and structure of rigid polyurethane foam. *Biotechnol. Biofuels* **6**, 12. <https://doi.org/10.1186/1754-6834-6-12>

Paruzel, A., Michałowski, S., Hodan, J., Horák, P., Prociak, A., Beneš, H., 2017. Rigid Polyurethane Foam Fabrication Using Medium Chain Glycerides of Coconut Oil and Plastics from End-of-Life Vehicles. *ACS Sustain. Chem. Eng.* **5**, 6237–6246. <https://doi.org/10.1021/acssuschemeng.7b01197>

Pavier, C., Gandini, A., 2000a. Oxypropylation of sugar beet pulp. 1. Optimisation of the reaction. *Ind. Crops Prod.* **12**, 1–8. [https://doi.org/10.1016/S0926-6690\(99\)00039-4](https://doi.org/10.1016/S0926-6690(99)00039-4)

Pavier, C., Gandini, A., 2000b. Oxypropylation of sugar beet pulp. 2. Separation of the grafted pulp from the propylene oxide homopolymer. *Carbohydr. Polym.* **42**, 13–17. [https://doi.org/10.1016/S0144-8617\(99\)00124-1](https://doi.org/10.1016/S0144-8617(99)00124-1)

Pawar, M.S., Kadam, A.S., Dawane, B.S., Yemul, O.S., 2016a. Synthesis and characterization of rigid polyurethane foams from algae oil using biobased chain extenders. *Polym. Bull.* **73**, 727–741. <https://doi.org/10.1007/s00289-015-1514-1>

Pawar, M.S., Kadam, A.S., Singh, P.C., Kusumkar, V.V., Yemul, O.S., 2016b. Rigid polyurethane foams from cottonseed oil using bio-based chain extenders: a renewable approach. *Iran. Polym. J.* **25**, 59–68. <https://doi.org/10.1007/s13726-015-0401-9>

Pelckmans, M., Renders, T., Van de Vyver, S., Sels, B.F., 2017. Bio-based amines through sustainable heterogeneous catalysis. *Green Chem.* **19**, 5303–5331. <https://doi.org/10.1039/C7GC02299A>

Pelletier, M.G., Holt, G.A., Wanjura, J.D., Greetham, L., McIntyre, G., Bayer, E., Kaplan-Bie, J., 2019. Acoustic evaluation of mycological biopolymer, an all-natural closed cell foam alternative. *Ind. Crops Prod.* **139**, 111533. <https://doi.org/10.1016/j.indcrop.2019.111533>

Pérez, E., Tuck, C.O., 2018. Quantitative analysis of products from lignin depolymerisation in high-temperature water. *Eur. Polym. J.* **99**, 38–48. <https://doi.org/10.1016/j.eurpolymj.2017.11.053>

Pérez-Sena, W.Y., Cai, X., Kebir, N., Vernières-Hassimi, L., Serra, C., Salmi, T., Leveneur, S., 2018. Aminolysis of cyclic-carbonate vegetable oils as a non-isocyanate route for the synthesis of polyurethane: A kinetic and thermal study. *Chem. Eng. J.* **346**, 271–280. <https://doi.org/10.1016/j.cej.2018.04.028>

Peters, J.M., 1970. Studies of isocyanate toxicity. *Proc. R. Soc. Med.* **63**, 372–375.

Petrovic, Z., 2008. Polyurethanes from Vegetable Oils. *Polym. Rev.* **48**, 109–155. <https://doi.org/10.1080/15583720701834224>

Petrović, Z.S., Wan, X., Bilić, O., Zlatanić, A., Hong, J., Javni, I., Ionescu, M., Milić, J., Degruson, D., 2013. Polyols and Polyurethanes from Crude Algal Oil. *J. Am. Oil Chem. Soc.* **90**, 1073–1078. <https://doi.org/10.1007/s11746-013-2245-9>

Petrović, Z.S., Zhang, W., Javni, I., 2005. Structure and Properties of Polyurethanes Prepared from Triglyceride Polyols by Ozonolysis. *Biomacromolecules* **6**, 713–719. <https://doi.org/10.1021/bm049451s>

Peyrton, J., Chambaretaud, C., Avérous, L., 2019. New Insight on the Study of the Kinetic of Biobased Polyurethanes Synthesis Based on Oleo-Chemistry. *Molecules* **24**, 4332. <https://doi.org/10.3390/molecules24234332>

Peyrton, J., Chambaretaud, C., Sarbu, A., Avérous, L., 2020. Biobased Polyurethane Foams Based on New Polyol Architectures from Microalgae Oil. *ACS Sustain. Chem. Eng.* **8**, 12187–12196. <https://doi.org/10.1021/acssuschemeng.0c03758>

Pfister, D.P., Xia, Y., Larock, R.C., 2011. Recent Advances in Vegetable Oil-Based Polyurethanes. *ChemSusChem* **4**, 703–717. <https://doi.org/10.1002/cssc.201000378>

Pillai, P.K.S., Li, S., Bouzidi, L., Narine, S.S., 2018. Polyurethane foams from chlorinated and non-chlorinated metathesis modified canola oil polyols: Research Article. *J. Appl. Polym. Sci.* **135**, 46616. <https://doi.org/10.1002/app.46616>

Pillai, P.K.S., Li, S., Bouzidi, L., Narine, S.S., 2016. Solvent-free synthesis of polyols from 1-butene metathesized palm oil for use in polyurethane foams. *J. Appl. Polym. Sci.* **133**, 43509. <https://doi.org/10.1002/app.43509>

Piszczek, Ł., Strankowski, M., Danowska, M., Hejna, A., Haponiuk, J.T., 2014. Rigid polyurethane foams from a polyglycerol-based polyol. *Eur. Polym. J.* **57**, 143–150. <https://doi.org/10.1016/j.eurpolymj.2014.05.012>

Pizzi, 2019. Tannins: Prospectives and Actual Industrial Applications. *Biomolecules* **9**, 344. <https://doi.org/10.3390/biom9080344>

Plastics Europe, 2019. Plastics-the Facts 2019.

Prociak, A., Kurańska, M., Cabulis, U., Ryszkowska, J., Leszczyńska, M., Uram, K., Kirpluks, M., 2018. Effect of bio-polyols with different chemical structures on foaming of polyurethane systems and foam properties. *Ind. Crops Prod.* **120**, 262–270. <https://doi.org/10.1016/j.indcrop.2018.04.046>

Qin, H., Wang, K., 2019. Study on preparation and performance of PEG-based polyurethane foams modified by the chitosan with different molecular weight. *Int. J. Biol. Macromol.* **140**, 877–885. <https://doi.org/10.1016/j.ijbiomac.2019.08.189>

Quinn, E.J., 1970. Properties and Stability of Fire-Retardant Rigid Polyurethane Foams from Phosphonopropionate Polyols. *Ind. Eng. Chem. Prod. Res. Dev.* **9**, 48–53. <https://doi.org/10.1021/i360033a009>

Quirino, R.L., Garrison, T.F., Kessler, M.R., 2014. Matrices from vegetable oils, cashew nut shell liquid, and other relevant systems for biocomposite applications. *Green Chem.* **16**, 1700–1715. <https://doi.org/10.1039/C3GC41811A>

Ramanujam, S., Zequine, C., Bhoyate, S., Neria, B., Kahol, P., Gupta, R., 2019. Novel Biobased Polyol Using Corn Oil for Highly Flame-Retardant Polyurethane Foams. *C* **5**, 13. <https://doi.org/10.3390/c5010013>

Randall, D., Lee, S. (Eds.), 2002. The polyurethanes book. John Wiley & Sons, Inc., Everberg, Belgium.

Rapra, S., 2014. Blowing agents & foaming processes 'conference proceedings. Presented at the Blowing Agents & Foaming Processes Conference, Smithers Rapra, Imperial Riding School Renaissance.

Rashmi, B.J., Rusu, D., Prashantha, K., Lacrampe, M.F., Krawczak, P., 2013. Development of water-blown bio-based thermoplastic polyurethane foams using bio-derived chain extender. *J. Appl. Polym. Sci.* **128**, 292–303. <https://doi.org/10.1002/app.38183>

Rastegarfar, N., Behrooz, R., Barikani, M., 2018. Characterization of polyurethane foams prepared from liquefied sawdust by crude glycerol and polyethylene glycol. *J. Polym. Res.* **25**, 154. <https://doi.org/10.1007/s10965-018-1516-4>

Reese, J., Moore, M., Wardius, D., Hager, S., 2010. Polyether polyols based on cashew nutshell liquid and flexible foams. US 7,828,991 B2.

Reignier, J., Alcouffe, P., Méchin, F., Fenouillot, F., 2019. The morphology of rigid polyurethane foam matrix and its evolution with time during foaming – New insight by cryogenic scanning electron microscopy. *J. Colloid Interface Sci.* **552**, 153–165. <https://doi.org/10.1016/j.jcis.2019.05.032>

Reymore, H.E., Carleton, P.S., Kolakowski, R.A., Sayigh, A.A.R., 1975. Isocyanurate Foams: Chemistry, Properties and Processing. *J. Cell. Plast.* **11**, 328–344. <https://doi.org/10.1177/0021955X7501100608>

Rigby, M., Park, S., Saito, T., Western, L.M., Redington, A.L., Fang, X., Henne, S., Manning, A.J., Prinn, R.G., Dutton, G.S., Fraser, P.J., Ganesan, A.L., Hall, B.D., Harth, C.M., Kim, J., Kim, K.-R., Krummel, P.B., Lee, T., Li, S., Liang, Q., Lunt, M.F., Montzka, S.A., Mühle, J., O'Doherty, S., Park, M.-K., Reimann, S., Salameh, P.K., Simmonds, P., Tunnicliffe, R.L., Weiss, R.F., Yokouchi, Y., Young, D., 2019. Increase in CFC-11 emissions from eastern China based on atmospheric observations. *Nature* **569**, 546–550. <https://doi.org/10.1038/s41586-019-1193-4>

Rinaudo, M., 2006. Chitin and chitosan: Properties and applications. *Prog. Polym. Sci.* **31**, 603–632. <https://doi.org/10.1016/j.progpolymsci.2006.06.001>

Riyapan, D., Saetung, A., Saetung, N., 2019. A Novel Rigid PU Foam Based on Modified Used Palm Oil as Sound Absorbing Material. *J. Polym. Environ.* **27**, 1693–1708. <https://doi.org/10.1007/s10924-019-01460-9>

Rokicki, G., Parzuchowski, P.G., Mazurek, M., 2015. Non-isocyanate polyurethanes: synthesis, properties, and applications: Non-Isocyanate Polyurethanes: Synthesis, Properties, and Applications. *Polym. Adv. Technol.* **26**, 707–761. <https://doi.org/10.1002/pat.3522>

Roux, D., Paulus, E., 1962. Condensed tannins. 13. Interrelationships of flavonoid components from the heartwood of Robinia pseudacacia. *Biochem. J.* **82**, 324–330. <https://doi.org/10.1042/bj0820324>

Rowland, F.S., Molina, M.J., 1975. Chlorofluoromethanes in the environment. *Rev. Geophys.* **13**, 1. <https://doi.org/10.1029/RG013i001p00001>

Saffar, T., Bouafif, H., Braghieri, F.L., Magdouli, S., Langlois, A., Koubaa, A., 2020. Production of Bio-based Polyol from Oxypropylated Pyrolytic Lignin for Rigid Polyurethane Foam Application. *Waste Biomass Valorization* **11**, 6411–6427. <https://doi.org/10.1007/s12649-019-00876-7>

Sahoo, S., Kalita, H., Mohanty, S., Nayak, S.K., 2016. Synthesis of Vegetable Oil-Based Polyurethane: A Study on Curing Kinetics Behavior. *Int. J. Chem. Kinet.* **48**, 622–634. <https://doi.org/10.1002/kin.21020>

Saiki, K., Sasaki, K., Ashida, K., 1994. Carbodiimide-Modified Polyisocyanurate Foams: Preparation and Flame Resistance. *J. Cell. Plast.* **30**, 470–484. <https://doi.org/10.1177/0021955X9403000504>

Salanti, A., Zoia, L., Orlandi, M., 2016. Chemical modifications of lignin for the preparation of macromers containing cyclic carbonates. *Green Chem.* **18**, 4063–4072. <https://doi.org/10.1039/C6GC01028H>

Santiago-Calvo, M., Tirado-Mediavilla, J., Ruiz-Herrero, J.L., Villaña, F., Rodríguez-Pérez, M.Á., 2019. Long-term thermal conductivity of cyclopentane–water blown rigid polyurethane foams reinforced with different types of fillers. *Polym. Int.* **68**, 1826–1835. <https://doi.org/10.1002/pi.5893>

Schmidt, D.L., Clarke, D.H., Urchick, D., 1984. The Effect of Surfactant Properties on a Rigid Foam System. *J. Cell. Plast.* **20**, 220–226. <https://doi.org/10.1177/0021955X8402000306>

Schneiderman, D.K., Vanderlaan, M.E., Mannion, A.M., Panthani, T.R., Batiste, D.C., Wang, J.Z., Bates, F.S., Macosko, C.W., Hillmyer, M.A., 2016. Chemically Recyclable Biobased Polyurethanes. *ACS Macro Lett.* **5**, 515–518. <https://doi.org/10.1021/acsmacrolett.6b00193>

Sendijarevic, I., Pietrzik, K.W., Schiffman, C.M., Sendijarevic, V., Kiziltas, A., Mielewski, D., 2020. Polyol from spent coffee grounds: Performance in a model pour-in-place rigid polyurethane foam system. *J. Cell. Plast.* **0021955X2091220**. <https://doi.org/10.1177/0021955X20912204>

Sendijarevic, V., 2007. Chemical Recycling of Mixed Polyurethane Foam Stream Recovered from Shredder Residue into Polyurethane Polyols. *J. Cell. Plast.* **43**, 31–46. <https://doi.org/10.1177/0021955X07066107>

Shao, H., Zhao, H., Xie, J., Qi, J., Shupe, T.F., 2019. Agricultural and Forest Residues towards Renewable Chemicals and Materials Using Microwave Liquefaction. *Int. J. Polym. Sci.* **2019**, 1–16. <https://doi.org/10.1155/2019/7231263>

Sharma, B.K., Adhvaryu, A., Erhan, S.Z., 2006a. Synthesis of Hydroxy Thio-ether Derivatives of Vegetable Oil. *J. Agric. Food Chem.* **54**, 9866–9872. <https://doi.org/10.1021/jf061896f>

Shin, S., Kim, H., Liang, J., Lee, S., Lee, D., 2019a. Sustainable rigid polyurethane foams based on recycled polyols from chemical recycling of waste polyurethane foams. *J. Appl. Polym. Sci.* **136**, 47916. <https://doi.org/10.1002/app.47916>

Shin, S.-R., Liang, J.-Y., Ryu, H., Song, G.-S., Lee, D.-S., 2019b. Effects of Isosorbide Incorporation into Flexible Polyurethane Foams: Reversible Urethane Linkages and Antioxidant Activity. *Molecules* **24**, 1347. <https://doi.org/10.3390/molecules24071347>

Shine, K.P., 2009. The global warming potential—the need for an interdisciplinary retrial: An editorial comment. *Clim. Change* **96**, 467–472. <https://doi.org/10.1007/s10584-009-9647-6>

Shrestha, M.L., Ionescu, M., 2018. Aliphatic–Aromatic Polyols by Thiol–Ene Reactions. *J. Polym. Environ.* **26**, 2257–2267. <https://doi.org/10.1007/s10924-017-1123-1>

Silva, A.L., Bordado, J.C., 2004. Recent Developments in Polyurethane Catalysis: Catalytic Mechanisms Review. *Catal. Rev.* **46**, 31–51. <https://doi.org/10.1081/CR-120027049>

da Silva, J.A.P., Cardozo, N.S.M., Petzhold, C.L., 2018. Enzymatic synthesis of andiroba oil based polyol for the production of flexible polyurethane foams. *Ind. Crops Prod.* **113**, 55–63. <https://doi.org/10.1016/j.indcrop.2018.01.020>

Singh, A.P., Kumar, S., 2020. Applications of Tannins in Industry. In 'Tannins- Structural Properties, Biological Properties and Current Knowledge' (Ed. Aires, A.). IntechOpen, Rijeka. <https://doi.org/10.5772/intechopen.85984>

Singh, I., Samal, S.K., Mohanty, S., Nayak, S.K., 2020. Recent Advancement in Plant Oil Derived Polyol-Based Polyurethane Foam for Future Perspective: A Review. *Eur. J. Lipid Sci. Technol.* **122**, 1900225. <https://doi.org/10.1002/ejlt.201900225>

Singh, S.N., 2002. Blowing agents for polyurethane foams. ISmithers Rapra Publishing, Shawbury, U.K.

Sonnenschein, M.F., Werness, J.B., Patankar, K.A., Jin, X., Larive, M.Z., 2016. From rigid and flexible foams to elastomers via Michael addition chemistry. *Polymer* **106**, 128–139. <https://doi.org/10.1016/j.polymer.2016.10.054>

Stick, R.V., 2001. Grandfather Glucose. In 'Carbohydrates'. Elsevier, pp. 9–18. <https://doi.org/10.1016/B978-012670960-5/50004-2>

Stockmayer, W.H., 1944. Theory of Molecular Size Distribution and Gel Formation in Branched Polymers II. General Cross Linking. *J. Chem. Phys.* **12**, 125–131. <https://doi.org/10.1063/1.1723922>

Suryawanshi, Y., Sanap, P., Wani, V., 2019. Advances in the synthesis of non-isocyanate polyurethanes. *Polym. Bull.* **76**, 3233–3246. <https://doi.org/10.1007/s00289-018-2531-7>

Szycher, M., 2013. Szycher's handbook of polyurethanes, 2nd ed. Taylor & Francis, Boca Raton, FL.

Tenorio-Alfonso, A., Sánchez, M.C., Franco, J.M., 2020. A Review of the Sustainable Approaches in the Production of Bio-based Polyurethanes and Their Applications in the Adhesive Field. *J. Polym. Environ.* **28**, 749–774. <https://doi.org/10.1007/s10924-020-01659-1>

Testud, B., Pintori, D., Grau, E., Taton, D., Cramail, H., 2017. Hyperbranched polyesters by polycondensation of fatty acid-based AB_n-type monomers. *Green Chem.* **19**, 259–269. <https://doi.org/10.1039/C6GC02294D>

Thakur, V.K., Thakur, M.K., Raghavan, P., Kessler, M.R., 2014. Progress in Green Polymer Composites from Lignin for Multifunctional Applications: A Review. *ACS Sustain. Chem. Eng.* **2**, 1072–1092. <https://doi.org/10.1021/sc500087z>

Thirumal, M., Khastgir, D., Singha, N.K., Manjunath, B.S., Naik, Y.P., 2008. Effect of foam density on the properties of water blown rigid polyurethane foam. *J. Appl. Polym. Sci.* **108**, 1810–1817. <https://doi.org/10.1002/app.27712>

Troev, K., 2000. A novel approach to recycling of polyurethanes: chemical degradation of flexible polyurethane foams by triethyl phosphate. *Polymer* **41**, 7017–7022. [https://doi.org/10.1016/S0032-3861\(00\)00054-9](https://doi.org/10.1016/S0032-3861(00)00054-9)

Ugarte, L., Fernández-d’Arlas, B., Valea, A., González, M.L., Corcuera, M.A., Eceiza, A., 2014. Morphology-properties relationship in high-renewable content polyurethanes. *Polym. Eng. Sci.* **54**, 2282–2291. <https://doi.org/10.1002/pen.23777>

Ugarte, L., Gómez-Fernández, S., Peña-Rodríguez, C., Prociak, A., Corcuera, M.A., Eceiza, A., 2015. Tailoring Mechanical Properties of Rigid Polyurethane Foams by Sorbitol and Corn Derived Biopolyol Mixtures. *ACS Sustain. Chem. Eng.* **3**, 3382–3387. <https://doi.org/10.1021/acssuschemeng.5b01094>

Ulrich, H., Odinak, A., Tucker, B., Sayigh, A.A.R., 1978. Recycling of polyurethane and polyisocyanurate foam. *Polym. Eng. Sci.* **18**, 844–848. <https://doi.org/10.1002/pen.760181103>

UN, 2015. Transforming our world: the 2030 Agenda for Sustainable Development. United Nation.

Van Der Wal, H.R., 1994. New Chemical Recycling Process for Polyurethanes. *J. Reinf. Plast. Compos.* **13**, 87–96. <https://doi.org/10.1177/073168449401300106>

Van Maris, R., Tamano, Y., Yoshimura, H., Gay, K.M., 2005. Polyurethane Catalysis by Tertiary Amines. *J. Cell. Plast.* **41**, 305–322. <https://doi.org/10.1177/0021955X05055113>

Vējelis, S., Gailius, A., Vējelienē, J., Vaitkus, S., 2010. Research on thermal conductivity of vacuum insulating materials. *10th Int. Conf. Mod. Build. Mater. Struct. Tech.*

Veronese, V.B., Menger, R.K., Forte, M.M. de C., Petzhold, C.L., 2011. Rigid polyurethane foam based on modified vegetable oil. *J. Appl. Polym. Sci.* **120**, 530–537. <https://doi.org/10.1002/app.33185>

Voorhees, P.W., 1985. The theory of Ostwald ripening. *J. Stat. Phys.* **38**, 231–252. <https://doi.org/10.1007/BF01017860>

Wan, C., Zhang, G., Zhang, F., 2020. A novel guanidine ammonium phosphate for preparation of a reactive durable flame retardant for cotton fabric. *Cellulose* **27**, 3469–3483. <https://doi.org/10.1007/s10570-020-03003-1>

Weißenborn, O., Ebert, C., Gude, M., 2016. Modelling of the strain rate dependent deformation behaviour of rigid polyurethane foams. *Polym. Test.* **54**, 145–149. <https://doi.org/10.1016/j.polymertesting.2016.07.007>

Wendels, S., Avérous, L., 2021. Biobased polyurethanes for biomedical applications. *Bioact. Mater.* **6**, 1083–1106. <https://doi.org/10.1016/j.bioactmat.2020.10.002>

Wilkie, C.A., Morgan, A.B. (Eds.), 2010. Fire retardancy of polymeric materials, 2nd ed. CRC Press, Boca Raton.

Wilson, M.E., Hu, M., Kurth, M.J., Hsieh, Y.-L., Krochta, J.M., 1996. Preparation and characterization of lactitol-based poly(ether polyol)s for rigid polyurethane foam. *J. Appl. Polym. Sci.* **59**, 1759–1768. [https://doi.org/10.1002/\(SICI\)1097-4628\(19960314\)59:11<1759::AID-APP12>3.0.CO;2-P](https://doi.org/10.1002/(SICI)1097-4628(19960314)59:11<1759::AID-APP12>3.0.CO;2-P)

Winnacker, M., Rieger, B., 2016. Biobased Polyamides: Recent Advances in Basic and Applied Research. *Macromol. Rapid Commun.* **37**, 1391–1413. <https://doi.org/10.1002/marc.201600181>

Wu, L., Gemert, J.V., Camargo, R.E., 2008. Rheology Study in Polyurethane Rigid Foams 12.

Wu, L.C.-F., Glasser, W.G., 1984. Engineering plastics from lignin. I. Synthesis of hydroxypropyl lignin. *J. Appl. Polym. Sci.* **29**, 1111–1123. <https://doi.org/10.1002/app.1984.070290408>

Wurtz, A., 1846. Note sur la Formation de l’Urethane par l’Action du Chlorure de Cyanogène. *Compte Rendus Séances Académie Sci.* **22**, 503–505.

Xi, X., Pizzi, A., Gerardin, C., Lei, H., Chen, X., Amirou, S., 2019. Preparation and Evaluation of Glucose Based Non-Isocyanate Polyurethane Self-Blowing Rigid Foams. *Polymers* **11**, 1802. <https://doi.org/10.3390/polym11111802>

Xing, W., Yuan, H., zhang, P., Yang, H., Song, L., Hu, Y., 2013. Functionalized lignin for halogen-free flame retardant rigid polyurethane foam: preparation, thermal stability, fire performance and mechanical properties. *J. Polym. Res.* **20**, 234. <https://doi.org/10.1007/s10965-013-0234-1>

Xiong, M., Schneiderman, D.K., Bates, F.S., Hillmyer, M.A., Zhang, K., 2014. Scalable production of mechanically tunable block polymers from sugar. *Proc. Natl. Acad. Sci.* **111**, 8357–8362. <https://doi.org/10.1073/pnas.1404596111>

Xu, C., Ferdosian, F., 2017. Conversion of lignin into bio-based chemicals and materials 'Green chemistry and sustainable technology. Springer Berlin Heidelberg, Berlin, Heidelberg. <https://doi.org/10.1007/978-3-662-54959-9>

Xu, J., Jiang, J., Hse, C.-Y., Shupe, T.F., 2014. Preparation of polyurethane foams using fractionated products in liquefied wood. *J. Appl. Polym. Sci.* **131**, 40096. <https://doi.org/10.1002/app.40096>

Xue, B.-L., Huang, P.-L., Sun, Y.-C., Li, X.-P., Sun, R.-C., 2017. Hydrolytic depolymerization of corncob lignin in the view of a bio-based rigid polyurethane foam synthesis. *RSC Adv.* **7**, 6123–6130. <https://doi.org/10.1039/C6RA26318F>

Xue, B.-L., Wen, J.-L., Sun, R.-C., 2015. Producing Lignin-Based Polyols through Microwave-Assisted Liquefaction for Rigid Polyurethane Foam Production. *Materials* **8**, 586–599. <https://doi.org/10.3390/ma8020586>

Xue, S., Omoto, M., Hidai, T., Imai, Y., 1995. Preparation of epoxy hardeners from waste rigid polyurethane foam and their application. *J. Appl. Polym. Sci.* **56**, 127–134. <https://doi.org/10.1002/app.1995.070560202>

Yang, L., Wang, X., Cui, Y., Tian, Y., Chen, H., Wang, Z., 2014. Modification of renewable resources-lignin-by three chemical methods and its applications to polyurethane foams. *Polym. Adv. Technol.* **25**, 1089–1098. <https://doi.org/10.1002/pat.3356>

Yang, L.-T., Zhao, C.-S., Dai, C.-L., Fu, L.-Y., Lin, S.-Q., 2012. Thermal and Mechanical Properties of Polyurethane Rigid Foam Based on Epoxidized Soybean Oil. *J. Polym. Environ.* **20**, 230–236. <https://doi.org/10.1007/s10924-011-0381-6>

Yang, R., Wang, B., Li, M., Zhang, X., Li, J., 2019. Preparation, characterization and thermal degradation behavior of rigid polyurethane foam using a malic acid based polyols. *Ind. Crops Prod.* **136**, 121–128. <https://doi.org/10.1016/j.indcrop.2019.04.073>

Yarema, K.J. (Ed.), 2005. *Handbook of Carbohydrate Engineering*, 1st ed. CRC Press. <https://doi.org/10.1201/9781420027631>

Yaws, C.L., 2009. *Thermophysical properties of chemicals and hydrocarbons*. William Andrew, Norwich, NY.

Yaws, C.L., 1995. *Handbook of Thermal Conductivity: Organic Compounds C1 to C4*. Elsevier, Burlington.

Yelchuri, V., Srikanth, K., Prasad, R.B.N., Karuna, M.S.L., 2019. Olefin metathesis of fatty acids and vegetable oils. *J. Chem. Sci.* **131**, 39. <https://doi.org/10.1007/s12039-019-1615-8>

Yim, H., Haselbeck, R., Niu, W., Pujol-Baxley, C., Burgard, A., Boldt, J., Khandurina, J., Trawick, J.D., Osterhout, R.E., Stephen, R., Estadilla, J., Teisan, S., Schreyer, H.B., Andrae, S., Yang, T.H., Lee, S.Y., Burk, M.J., Van Dien, S., 2011. Metabolic engineering of *Escherichia coli* for direct production of 1,4-butanediol. *Nat. Chem. Biol.* **7**, 445–452. <https://doi.org/10.1038/nchembio.580>

Yue, D., Oribayo, O., Rempel, G.L., Pan, Q., 2017. Liquefaction of waste pine wood and its application in the synthesis of a flame retardant polyurethane foam. *RSC Adv.* **7**, 30334–30344. <https://doi.org/10.1039/C7RA03546B>

Zappi, M.E., Bajpai, R., Hernandez, R., Mikolajczyk, A., Lord Fortela, D., Sharp, W., Chirdon, W., Zappi, K., Gang, D., Nigam, K.D.P., Revellame, E.D., 2019. Microalgae Culturing To Produce Biobased Diesel Fuels: An Overview of the Basics, Challenges, and a Look toward a True Biorefinery Future. *Ind. Eng. Chem. Res.* **58**, 15724–15746. <https://doi.org/10.1021/acs.iecr.9b01555>

Zenner, M.D., Xia, Y., Chen, J.S., Kessler, M.R., 2013. Polyurethanes from Isosorbide-Based Diisocyanates. *ChemSusChem* **6**, 1182–1185. <https://doi.org/10.1002/cssc.201300126>

Zhan, H.-J., Wu, K.-J., Hu, Y.-L., Liu, J.-W., Li, H., Guo, X., Xu, J., Yang, Y., Yu, Z.-L., Gao, H.-L., Luo, X.-S., Chen, J.-F., Ni, Y., Yu, S.-H., 2019. Biomimetic Carbon Tube Aerogel Enables Super-Elasticity and Thermal Insulation. *Chem* **5**, 1871–1882. <https://doi.org/10.1016/j.chempr.2019.04.025>

Zhang, C., Bhoyate, S., Ionescu, M., Kahol, P.K., Gupta, R.K., 2018a. Highly flame retardant and bio-based rigid polyurethane foams derived from orange peel oil. *Polym. Eng. Sci.* **58**, 2078–2087. <https://doi.org/10.1002/pen.24819>

Zhang, C., Li, J., Hu, Z., Zhu, F., Huang, Y., 2012. Correlation between the acoustic and porous cell morphology of polyurethane foam: Effect of interconnected porosity. *Mater. Des.* **41**, 319–325. <https://doi.org/10.1016/j.matdes.2012.04.031>

Zhang, C., Wang, H., Zeng, W., Zhou, Q., 2019a. High Biobased Carbon Content Polyurethane Dispersions Synthesized from Fatty Acid-Based Isocyanate. *Ind. Eng. Chem. Res.* **58**, 5195–5201. <https://doi.org/10.1021/acs.iecr.8b05936>

Zhang, G., Wu, Y., Chen, W., Han, D., Lin, X., Xu, G., Zhang, Q., 2019b. Open-Cell Rigid Polyurethane Foams from Peanut Shell-Derived Polyols Prepared under Different Post-Processing Conditions. *Polymers* **11**, 1392. <https://doi.org/10.3390/polym11091392>

Zhang, H., Fang, W.-Z., Li, Y.-M., Tao, W.-Q., 2017b. Experimental study of the thermal conductivity of polyurethane foams. *Appl. Therm. Eng.* **115**, 528–538. <https://doi.org/10.1016/j.applthermaleng.2016.12.057>

Zhang, J., Hori, N., Takemura, A., 2020. Influence of NCO/OH ratio on preparation of four agricultural wastes liquefied polyols based polyurethane foams. *Polym. Degrad. Stab.* **179**, 109256. <https://doi.org/10.1016/j.polymdegradstab.2020.109256>

Zhang, J., Hori, N., Takemura, A., 2019c. Optimization of preparation process to produce polyurethane foam made by oilseed rape straw based polyol. *Polym. Degrad. Stab.* **166**, 31–39. <https://doi.org/10.1016/j.polymdegradstab.2019.05.022>

Zhang, M., Zhang, J., Chen, S., Zhou, Y., 2014. Synthesis and fire properties of rigid polyurethane foams made from a polyol derived from melamine and cardanol. *Polym. Degrad. Stab.* **110**, 27–34. <https://doi.org/10.1016/j.polymdegradstab.2014.08.009>

Zhang, P., Liao, X., Ma, C., Li, Q., Li, A., He, Y., 2019d. Chemoenzymatic Conversion of Corncob to Furfurylamine via Tandem Catalysis with Tin-Based Solid Acid and Transaminase Biocatalyst. *ACS Sustain. Chem. Eng.* **7**, 17636–17642. <https://doi.org/10.1021/acssuschemeng.9b03510>

Zhang, S., Liu, X., Jin, X., Li, H., Sun, J., Gu, X., 2018b. The novel application of chitosan: Effects of cross-linked chitosan on the fire performance of thermoplastic polyurethane. *Carbohydr. Polym.* **189**, 313–321. <https://doi.org/10.1016/j.carbpol.2018.02.034>

Zhang, X., Jeremic, D., Kim, Y., Street, J., Shmulsky, R., 2018c. Effects of Surface Functionalization of Lignin on Synthesis and Properties of Rigid Bio-Based Polyurethanes Foams. *Polymers* **10**, 706. <https://doi.org/10.3390/polym10070706>

Zhang, X., Kim, Y., Eberhardt, T.L., Shmulsky, R., 2019e. Lab-scale structural insulated panels with lignin-incorporated rigid polyurethane foams as core. *Ind. Crops Prod.* **132**, 292–300. <https://doi.org/10.1016/j.indcrop.2019.02.035>

Zhang, X., Kim, Y., Elsayed, I., Taylor, M., Eberhardt, T.L., Hassan, E.B., Shmulsky, R., 2019f. Rigid polyurethane foams containing lignin oxyalkylated with ethylene carbonate and polyethylene glycol. *Ind. Crops Prod.* **141**, 111797. <https://doi.org/10.1016/j.indcrop.2019.111797>

Zhang, X.D., Macosko, C.W., Davis, H.T., Nikolov, A.D., Wasan, D.T., 1999. Role of Silicone Surfactant in Flexible Polyurethane Foam. *J. Colloid Interface Sci.* **215**, 270–279. <https://doi.org/10.1006/jcis.1999.6233>

Zieleniewska, M., Leszczyński, M.K., Kurańska, M., Prociak, A., Szczepekowski, L., Krzyżowska, M., Ryszkowska, J., 2015. Preparation and characterisation of rigid polyurethane foams using a rapeseed oil-based polyol. *Ind. Crops Prod.* **74**, 887–897. <https://doi.org/10.1016/j.indcrop.2015.05.081>

Conclusion Chapitre 1

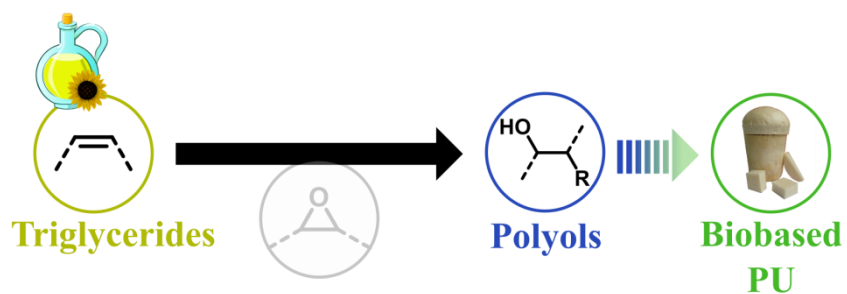
Cette synthèse bibliographique a présenté les mousses polyuréthanes biosourcées de la synthèse à la caractérisation en passant par leur mise en œuvre. Les phénomènes physiques décrits dans la première partie permettent de comprendre la complexité des phénomènes chimiques, physique et physico-chimique rencontrées lors de l'élaboration d'une mousse polyuréthane.

Les voies de synthèse pour la production de polyols, polyisocyanates ou additifs adaptés aux mousses polyuréthanes à partir de différentes biomasses sont ensuite développées. L'étude de la transformation des lipides permet de sélectionner les modifications les plus prometteuses pour l'intégration de l'huile de microalgues dans les mousses polyuréthanes. L'époxydation des doubles liaisons suivi de l'ouverture par divers nucléophiles apparaît comme une voie pertinente dans la synthèse de polyols et d'additifs.

Le cœur de cette synthèse bibliographie est consacré aux relations « structures-propriétés » dans les mousses polyuréthanes rigides, lesquelles étant au cœur de ce travail de doctorat. Dans le volet synthèse, les polyols ont été identifiés comme étant le composé biosourcé présentant les structures les plus diverses et les plus souvent biosourcés. L'impact prépondérant de la structure et paramètres des polyols est détaillé autour des différentes propriétés clés des mousses polyuréthanes rigides : la morphologie (taille de cellule, densité, pourcentage de cellules fermées), la résistance à la compression ainsi que la conductivité et stabilité thermique. La réactivité est un point essentiel pour obtenir des cellules fermées formant des mousses polyuréthanes rigides.

L'avenir des mousses polyuréthanes est discuté, dans le cadre de la synthèse de polyuréthanes sans isocyanate. Seule l'addition des carbonates cycliques et des amines est en adéquation avec les principes d'une chimie verte. Les premières mousses rapportés dans la littérature par cette voie de synthèse sont généralement flexibles et très denses aussi sur ce thème qui ne sera pas abordé dans ce travail de doctorat, laisse la porte ouverte à de futurs grands développements. A l'avenir, la synthèse des mousses peut aussi se tourner vers d'autres chimies réactives plus durables, comme les époxydes ou les additions de Michael ceci fera l'objet du dernier volet complet de ce travail de doctorat.

CHAPITRE 2. CINÉTIQUES DE FORMATION DE POLYOLS À PARTIR D'HUILE : UNE ÉTUDE MODÈLE



Model and Kinetics Study

Introduction Chaptitre 2

Ce chapitre se présente sous la forme d'un article intitulée « New Insight on the Study of the Kinetic of Biobased Polyurethanes Synthesis Based on Oleo-Chemistry » publié dans *Molecules*.

L'état de l'art du chapitre précédent a exposé les transformations existantes pour synthétiser à partir de biomasses des polyols adaptés à la formulation de mousse polyuréthanes. La stratégie de synthèse la plus employée pour les lipides est la formation d'époxyde à partir des doubles liaisons présentes sur les acides gras puis son ouverture par un nucléophile. Cette voie de synthèse maintes fois utilisée pour la formation de polyols, a cependant rarement été étudiée en détail notamment d'un point de vue cinétique. Or la connaissance des paramètres cinétiques est crucial notamment pour le passage à l'échelle industrielle.

Le chapitre précédent a aussi rappelé l'impact des cinétiques de formation des mousse polyuréthanes sur les propriétés finales des matériaux alvéolaires. Le remplacement d'un polyol d'origine fossile par un équivalent biosourcé peut altérer l'équilibre entre la formation du réseau polymère et l'expansion du système. Cette balance est critique pour obtenir une mousse polyuréthane aux propriétés équivalentes aux standards visés. Comme démontré dans le chapitre précédent, les voies de synthèses choisies modifient les propriétés du polyol. L'étude approfondie de la réactivité des polyols permet de valider leurs propriétés, en amont de l'introduction dans la formulation de la mousse polyuréthane.

L'objectif de ce chapitre est donc d'étudier et de caractériser la formation de polyols à partir de triglycérides pour la formulation de mousse polyuréthanes. La voie de synthèse du polyol à étudier est l'époxydation des doubles liaisons présentes sur l'huile suivie d'une ouverture de cycle par divers nucléophiles. Pour les besoins de l'étude, l'huile de microalgues composée de multiples doubles liaisons est modélisée par un ester méthylique d'acide gras comportant une double liaison.

New Insight on the Study of the Kinetic of Biobased Polyurethanes Synthesis Based on Oleo-Chemistry

Julien Peyrton, Clémence Chambaretaud and Luc Avérous

Article published in *Molecules* in 2019, Vol. 24, page 4332

1. ABSTRACT

Nowadays, polyols are basic chemicals for the synthesis of a broad range of polymers, such as polyurethane foams (PUF), which are produced with several other compounds, such as polyisocyanates. During the last decades, the oleo-chemistry has developed several routes from glycerides to polyols for the polyurethanes (PU) industry to replace mainly conventional fossil-based polyols. An extensive range of biobased polyols can now be obtained by epoxidation of the double bonds and ring-opening (RO) of the subsequent epoxides with different chemical moieties. In preliminary studies, the RO kinetics of an epoxidized model molecule (methyl oleate) with ethanol and acetic acid were investigated. Subsequently, polyols that were derived from unsaturated triglycerides were explored in the frame of, e.g., PUF formulations. Different associations were studied with different mono-alcohols derived from epoxidized and ring-opened methyl oleate while using several ring-openers to model such systems and for comparison purposes. Kinetic studies were realized with the pseudo-first-order principle, meaning that hydroxyls are in large excess when compared to the isocyanate groups. The rate of isocyanate consumption was found to be dependent on the moiety located in β -position of the reactive hydroxyl, following this specific order: tertiary amine \gg ether $>$ ester. The tertiary amine in β -position of the hydroxyl tremendously increases the reactivity toward isocyanate. Consequently, a biobased reactive polyurethane catalyst was synthesized from unsaturated glycerides. These approaches offer new insights regarding the replacement of current catalysts often harmful, pungent, and volatile used in PU and PUF industry, in order to revisit this chemistry.

2. INTRODUCTION

The polyurethane (PU) is a very versatile family of polymer that is mainly obtained by polyaddition between polyols and polyisocyanates (Bayer 1947). PUs can be used in various forms to fulfill different applications for a worldwide market of \$50 Billion in 2016 due to the multiplicity of

their structures. With more than 60%, foams are the most significant part of this market, with segments including the furniture, bedding, insulation, building, or construction materials. Foams are elaborated through a complex formulation that is based on polyols, polyisocyanates, blowing agents, and several other additives (Furtwengler et al. 2018a; Obi 2018c). Commercial foams are mainly formulated with fossil-based components. However, increasing foams are obtained from renewable resources nowadays.

The abundance and versatility of vegetable oils are the key points for replacing petrochemical products in polymer synthesis and developing very promising renewable compounds while using a well-established oleo-chemistry. During the last decades, starting from unsaturated triglycerides, extensive research (Maisonneuve et al. 2016; Petrovic 2008; Zhang et al. 2017a) has been performed to obtain new macromolecular architectures. Multiple strategies were developed to obtain polyols from unsaturated glycerides for the PU industry (Pfister et al. 2011) (i) the hydroformylation and ozonolysis, followed by a catalytic reduction are developed at an industrial scale, (ii) the transesterification, (iii) the introduction of hydroxyl groups via double-bonds with microorganisms is promising (Takeuchi et al. 2013), and (iv) the epoxidation of the double bonds and subsequent the ring-opening (RO) of the epoxides. The last way keeps the initial glyceride structure and the opportunity to synthesized different polyols structures, even at an industrial level.

In the case of vegetable oils and fats, the epoxide is mainly disubstituted and, consequently, less reactive than a terminal one. Nevertheless, several different types of reagents can be considered for the RO, such as amines (Biswas et al. 2005; Durán Pachón et al. 2003; Yang et al. 2012), alcohols (Chen et al. 2015; Dai et al. 2009; Turco et al. 2017), carboxylic acids (Schuster et al. 2008; Shuo et al. 2015), or hydrogen halides (Durbetaki 1956; Guo et al. 2000). The epoxidation procedure is carried out while using a short carboxylic acid (Petrović et al. 2002). Although it is not entirely new, for instance, few publications are focused on the study of the RO kinetics of epoxide by acetic or formic acid (Gan et al. 1992; Zaher et al. 1989).

The presently studied way to obtain PUs from polyunsaturated triglycerides contains three steps: 1. Epoxidation of double bonds, 2. RO reaction, and 3. Polymerization with polyisocyanate. In our study, the polyunsaturated triglycerides were modeled by a fatty ester only containing one double-bond: methyl oleate. The double bond was chemically converted into epoxide by a peracetic acid that was formed in situ. The objective of this preliminary study was to understand the acid-catalyzed RO of a disubstituted epoxide. To do so, a new kinetic method that was based on Nuclear magnetic resonance (NMR) was developed to monitor the epoxide RO reaction. Subsequently, it was applied to the kinetic study of acid-catalyzed RO reactions of epoxidized methyl oleate. In the second part of this paper, the reactivity of different alcohols (models) that were obtained from the RO of epoxidized fatty esters with various conditions was compared in the frame of PU synthesis. The model-alcohols were synthesized by the RO of the epoxide, with acetic acid, ethanol, hydrogen halide, or diethylamine.

3. MATERIALS AND METHODS

3.1. Materials

Fatty Acid Methyl Ester of Very High Oleic Sunflower Oil (FAMEVHOSO) with 3.32 mmol double bond/g was kindly supplied by the ITERG group (Canéjan, France). The FAMEVHOSO is

composed of 83% of oleic acid. Table S2.3 presents the distribution of fatty methyl esters of unsaturated FAMEVHOSO. Glacial acetic acid (AA), toluene (99%), H_2O_2 30%, ethyl acetate (99%), and ethanol (99.9%) were obtained from Fisher Scientific (Illkirch-Graffenstaden, France). Amberlyst® 15H (strongly acidic cation exchanger dry), Amberlite® IR120H (strongly acidic hydrogen form), $CDCl_3$, phenyl isocyanate (98%), dibutyl amine (DBA) (99.5%), HBr (48% in water), HCl (37% in water), and diethylamine (99%) (DEA) were provided by Sigma-Aldrich (Saint-Quentin-Fallavier, France). Ethanol absolute (EtOH) was purchased from VWR (Briare, France). All of the chemicals were used without any purification.

3.2. Epoxidation of FAMEVHOSO

According to a previously described protocol (Arbenz et al. 2017), 200 g of FAMEVHOSO (0.66 mol, 1 eq.), 50 g of Amberlite® IR 120H (25 wt% of FAMEVHOSO) were introduced in a 1 L three-neck flask that was equipped with a reflux condenser, a magnetic stirrer, and a dropping funnel. 20 mL of acetic acid (0.35 mol, 0.5 eq.) and 200 mL of toluene were added. The mixture was heated to 70 °C under vigorous magnetic stirring. Afterward, 90 mL of H_2O_2 30% (1.15 mmol, 1.7 eq.) was added dropwise by the dropping funnel for 30 min. to prevent overheating and epoxide RO. The mixture was heated at 70 °C for 7 h additional hours. At the end, the mixture was recovered in 500 mL of ethyl acetate. The Amberlite® IR 120H was filtered off. The organic phase was washed with saturated $NaHCO_3$ solution until neutral pH. Afterward, it was washed with a brine solution, dried with anhydrous sodium sulfate, and then filtered. The solvent was evaporated under reduced pressure. The epoxidized FAMEVHSOSO (EVHOSO) was dried overnight in a vacuum oven at 40 °C. The yield was 90 mol%.

3.3. Ring-Opening of EVHOSO with Acetic Acid

The reaction was carried out in a round bottom flask that was equipped with a reflux condenser and a magnetic stirrer. The flask was filled with 50 g of EVHOSO 3.05 mmol epoxide/g, (0.24 mol, 1 eq.) and 100 mL of acetic acid (2.8 mol, 11.5 eq.). The mixture was stirred at 90 °C for 7 h. At the end, the mixture was recovered in 300 mL of ethyl acetate. The organic phase was washed with saturated $NaHCO_3$ solution until neutral pH. Subsequently, it was washed with brine solution, dried with anhydrous sodium sulfate, and then filtered. The solvent was evaporated under reduced pressure. The ring-opened EVHOSO with acetic acid (EVHOSO-AA) was dried overnight in a vacuum oven at 40 °C. The yield was 82 mol%.

3.4. Ring-Opening of EVHOSO with Ethanol

The protocol was adapted from a previously published work (Palaskar et al. 2012). The reaction was carried out in a round bottom flask that was equipped with a reflux condenser and a magnetic stirrer. The flask was filled with 50 g of EVHOSO 3.05 mmol epoxide/g, (0.15 mol, 1 eq.) and 2 g of Amberlyst® 15 H. 100 mL of ethanol (1.7 mol, 11.5 eq.). The mixture was stirred at 70 °C

for 9 h. At the end, the mixture was recovered in 300 mL of ethyl acetate. The organic phase was washed with saturated NaHCO_3 solution until neutral pH. Subsequently, it was washed with brine solution, dried with anhydrous sodium sulfate, and then filtered. The solvent was evaporated under reduced pressure. The ring-opened EVHOSO with ethanol (EVHOSO-EtOH) was dried overnight in a vacuum oven at 40 °C. The yield was 92 mol%.

3.5. Ring-Opening of EVHOSO with Diethylamine

The protocol was adapted from a previously published work (Harry-O’kuru et al. 2015). The reaction was carried out in a round bottom flask that was equipped with a reflux condenser and a magnetic stirrer. The flask was filled with 5 g of anhydrous ZnCl_2 (0.5 eq.). 25 g of EVHOSO 3.05 mmol epoxide/g (76 mmol, 1 eq.) was dissolved in 20 mL of diethylamine (193 mmol, 2.5 eq.). The solution was added into the flask. The mixture was stirred at reflux for 15 h. At the end, the mixture was recovered in 300 mL of ethyl acetate and deionized water. The organic phase was washed with saturated NaHCO_3 solution until neutral pH. Afterward, it was washed with a brine solution, dried with anhydrous sodium sulfate, and then filtered. The solvent was evaporated under reduced pressure. The ring-opened EVHOSO with diethylamine (EVHOSO-DEA) was dried overnight in a vacuum oven at 40 °C. The yield was 90 mol%.

3.6. Ring-Opening of EVHOSO with Different Hydrogen Halides

The reaction was carried out in a round bottom flask that was equipped with a reflux condenser and a magnetic stirrer. The flask was filled with 25 g of EVHOSO 3.05 mmol epoxide/g (76 mmol, 1 eq.) dissolved in 15 mL of acetone. The halogen halide (1.5 eq.) was added dropwise for 15 min. to avoid overheating. The mixture was stirred at room temperature for 30 min. At the end, the mixture was recovered in 300 mL of ethyl acetate and deionized water. The organic phase was washed with saturated NaHCO_3 solution until neutral pH. Subsequently, it was washed with brine solution, dried over anhydrous sodium sulfate, and then filtered. The solvent was evaporated under reduced pressure. The ring-opened EVHOSO with hydrochloric acid (EVHOSO-HCl) or hydrobromic acid (EVHOSO-HBr) was dried overnight in a vacuum oven at 40 °C. The yield was 99 mol%.

3.7. Kinetic Study of Epoxide Ring-Opening with Ethanol

In a typical procedure, 0.5 g of EVHOSO (1.7 mmol, 1 eq.) and between 4 to 20 wt% (depending on the experiment) of Amberlyst® 15H in a 50 mL round bottom flask was heated to the desired temperature while using a hot plate that was equipped with magnetic stirring. When the temperature was attained, 3.8 mL of absolute ethanol was added (65 mmol, 38 eq.). A few drops of the reaction mixture were taken at different reaction times and recovered in ethyl acetate and washed two times with water to remove any trace of acid. The solvent was evaporated on a rotary evaporator. The drops of oil were recovered with CDCl_3 and analyzed by NMR.

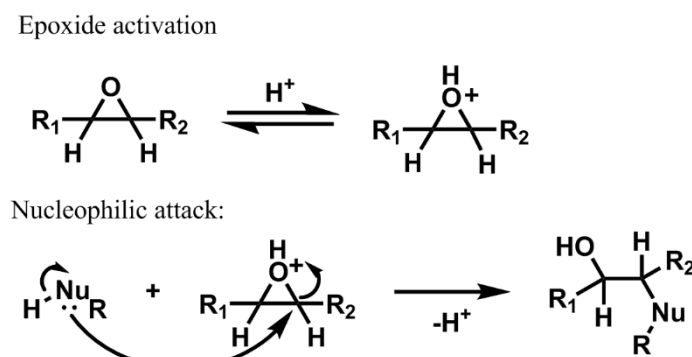
3.8. Kinetic Study of Urethane Formation

In a typical procedure, 3 g of VHOSO-AA (7.2 mmol, 11.5 eq.) was introduced in a round bottom flask that was equipped with a magnetic stirrer. The flask was heated to the desired temperature. The flask was put under vacuum for 15 min. and then flushed with argon. 1 mL of a 0.62 mol/L solution of phenyl isocyanate in toluene was introduced. The conditions were set to avoid any contact with humidity or another nucleophile. The isocyanate content ([NCO]) over time was determined by taking aliquots of 0.4 mL quenched by a DBA solution. [NCO] was determined by potential titration of the excess of DBA by an acid.

3.9. Kinetic Model of Ring-Opening

3.9.1. Mechanism of Ring-Opening

The RO of the epoxide is catalyzed by acid (Parker and Isaacs 1959), as shown in Scheme 2.1. The nucleophilic attack is favored by the enhancement of the electrophilic character of epoxide group carbons. The nucleophilic species can be alcohol, carboxylic acid, water, hydrogen halide, etc.



Scheme 2.1 - General mechanism of an acidic catalyzed nucleophile ring-opening.

The reaction forms a secondary hydroxyl and another group, depending on the nature of the nucleophile. Reactions with acid groups, such as carboxylic acid or halogen halide, are self-catalyzed.

3.9.2. Kinetic Equations

The activation step that is presented in Scheme 2.1 is considered to be fast. Subsequently, the nucleophilic attack is the rate-determining step. The acid-catalyzed RO rate is described by Equation 2.1:

$$r = k * [Ep]^\alpha * [B]^\beta * [Cat]^\delta \quad (2.1)$$

where k is the reaction rate constant, $[Ep]$ is the epoxide concentration, $[B]$ the RO reagent concentration, $[Cat]$ the catalyst concentration, and α , β and δ are the respective partial orders. The consummation of epoxide over time, depending on the reaction rate, is written as Equation 2.2:

$$-\frac{d[Ep]}{dt} = k * [Ep]^\alpha * [B]^\beta * [Cat]^\delta \quad (2.2)$$

The kinetic parameters were determined while using a pseudo-first-order assumption (Espenson 1995). The nucleophile (B) was in large excess as compared to the epoxide groups (Ep). Subsequently, the concentration of the nucleophile ($[B]$) was considered to be constant during the reaction. Furthermore, the catalyst is regenerated along the reaction, $[Cat]$ is a constant over time. When considering these hypotheses, the rate of reaction that is expressed in Equation 2.2 is transformed in Equation 2.3:

$$-d \frac{[Ep]}{dt} = k_{app} * [Ep]^\alpha \quad (2.3)$$

where k_{app} is a constant, as expressed in Equation 2.4:

$$k_{app} = k * [B]^\beta * [Cat]^\delta \quad (2.4)$$

3.9.3. NMR

The NMR analyses were realized on a 400 MHz Bruker spectrometer. The ^1H number of scans was set to 32. Each spectrum was calibrated with the CDCl_3 signals, being set at $\delta=7.26$ ppm.

3.9.4. NCO Concentration Measurement

The isocyanate content $[NCO]$ was determined by the adaptation of ISO 14896:2009. Aliquots were dissolved in a 20 mL solution of 5×10^{-3} mol/L dibutyl amine in toluene. The resulting mixture was stirred for 20 min. Afterward, 20 mL of acetone was added to avoid a dephasing of the solution, and the excess of dibutyl amine was titrated with an automatic titrator by a 4.6×10^{-3} mol/L molar solution of HCl. The equivalence was determined by a potential leap. $[NCO]$ was calculated with Equation 2.5:

$$[NCO] = \frac{((V_{Bl} - V_{eq}) * [HCl])}{V_{Aliquot}} \quad (2.5)$$

with V_{Bl} the equivalence volume of 20 mL of dibutyl amine solution, V_{eq} the equivalence volume of the aliquot, $[HCl]$ the chlorhydric acid concentration, and $V_{aliquot}$ the volume of solution taken from the solution for each kinetic measurement.

4. RESULTS

4.1. Synthesis of EVHOSO

Table S2.3 presents FAMEVHOSO data. The average double bond per molecule is 1 by calculation. It is well known that unsaturated fatty acids are sensitive to UV oxidation (Kenaston et al. 1955). An NMR measurement was undertaken to control the double bond quantity before the epoxidation. 0.93 double bonds per molecule were calculated by the integration of the proton of the double bond on the NMR spectrum (Figure S2.11). The FAMEVHOSO was in-situ epoxidized with peracid in a biphasic system. The reaction converts 90% of the double bonds in epoxides (Figure S2.12). Side reactions, such as RO by acetic acid, limit the reaction yield. The number of epoxides per molecule is only 0.83.

4.2. Kinetics of Epoxide Ring-Opening by Ethanol

The NMR method that is described in Section 7.2 on the RO with acetic acid was applied to the RO with ethanol.

4.2.1. Determination of the Epoxide Partial Order

The epoxide partial order was determined at three temperatures, with all other parameters remaining equal. The pseudo-first-order was applied by introducing a large excess (11 eq.) of ethanol and constant catalyst content. Integrating Equation 2.3 with $\alpha = 1$ gives Equation 2.6:

$$\ln\left(\frac{[Ep]_0}{[Ep]}\right) = \ln\left(\frac{1}{1-\chi}\right) = k_{app_EtOH} * t \quad (2.6)$$

where χ is the yield of the reaction, t the time in minute, and k_{app_EtOH} the pseudo-reaction rate constant. $\ln([Ep]_0/[Ep])$ was presented as a function of time in Figure 2.1.

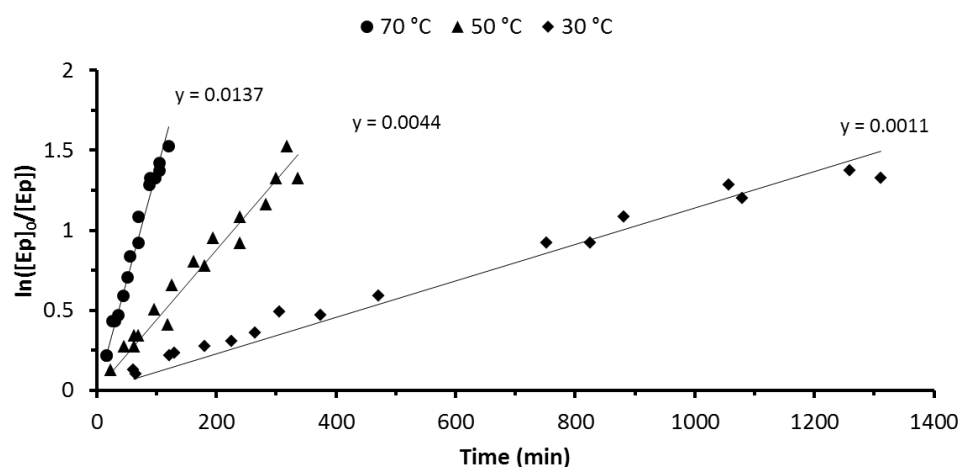


Figure 2.1 - Determination of the epoxide partial order. Representation of $\ln([Ep]_0/[Ep])$ as a function of time at 30 °C, 50 °C, and 70 °C.

The model of a partial order of 1 for the epoxide is well confirmed by experiments at 30, 50, and 70 °C, respectively. The range of validity of the method is between 20–95% of conversion due to the exponential character of the conversion against time, as demonstrated with the acetic acid kinetic experiment (Figure S2.13-S2.17).

4.2.2. Determination of the Catalyst Partial Order

Experiments with catalyst content variations from 4 to 20 wt% were performed at 30, 50, and 70 °C to determine the partial order of $[Cat]$. k_{app_EtOH} were determined by the linear regression of $\ln([Ep]_0/[Ep])$ as a function of time, and Table S2.4 presents the results. The catalyst is an acidic resin of divinylbenzene and styrene sulfonated (Rios 2003). The correlation between $[H^+]$ and the mass of catalyst was determined by the pH measurement of 49 mg to 1 g of resin in 20 mL of water (Figure S2.18). Equation 2.7 expresses the application of Equation 2.4 in the ethanol RO:

$$k_{app_EtOH} = k_{EtOH} * [EtOH]^\beta * [H^+]^\delta \quad (2.7)$$

where $[EtOH]$ and $[H^+]$ are the concentration of ethanol and acid, respectively. The partial order of catalyst was determined by the slope of the linear regression of $\ln(k_{app_EtOH})$ as a function of $\ln([Cat])$, as presented in Figure 2.2.

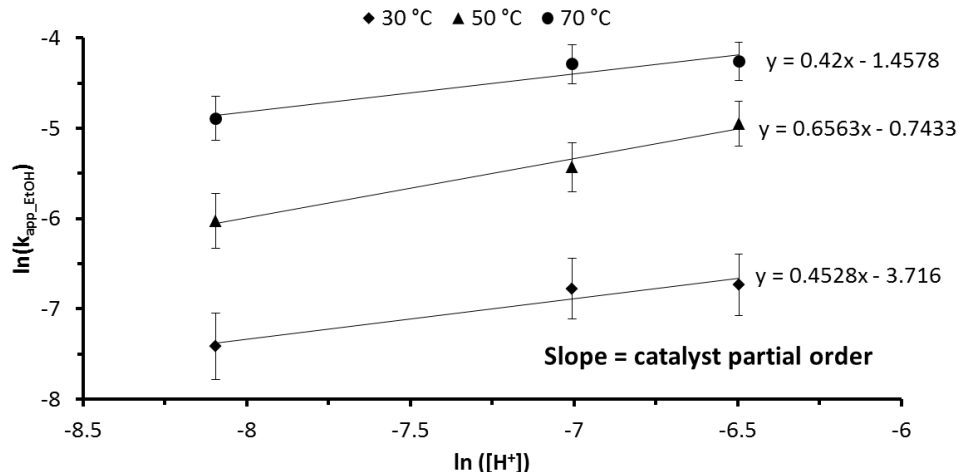


Figure 2.2 - Determination of the catalyst partial order. Representation of $\ln(k_{app_EtOH})$ as a function of $\ln(H^+)$ at 30, 50, and 70 °C.

The coefficients of determination are between 0.93 and 0.98, and the three slopes are tending toward 0.5, which represents the catalyst partial order. It was expected that the catalyst would have a more substantial influence on the reaction rate. The catalyst is decreasing the activation energy in the thermodynamic side of the reaction, but it has less influence on the kinetics. The right amount of catalyst can be selected, depending on the thermal sensibility of the epoxidized studied molecule.

4.2.3. Determination of the Ethanol Partial Order

Experiments with $[EtOH]$ variations from 15 to 4.5 mol/L were performed at 70 °C to determine the partial order of $[EtOH]$. The catalyst loading was kept constant then, with the volume variation, $[H^+]$ was varying along experiments. k_{app_EtOH} , as expressed in Equation 2.7, can be expressed as a function of the total volume of solution, giving Equation 2.8:

$$k_{app_EtOH} = k_{EtOH} * \left(\frac{V_{EtOH} * d_{EtOH}}{V_t} \right)^\beta * \left(\frac{m_{cat} * IA_{eq}}{V_t} \right)^\delta \quad (2.8)$$

where V_{EtOH} is the volume of ethanol introduced in the solution, m_{cat} , the mass of catalyst, and IA_{eq} is the acid equivalent of the resin determined by Figure S2.18. By logarithmic transformation and rearrangement, $\ln(k_{app_EtOH})$ is expressed in Equation 2.9 as a linear function of $\ln(1/V_t)$, with the sum of partial order as the slope.

$$\ln(k_{app_EtOH}) = K + (\beta + \delta) * \ln\left(\frac{1}{V_t}\right) \quad (2.9)$$

where K is a constant, including V_{EtOH} , d_{EtOH} , m_{cat} , IA_{eq} , and k_{EtOH} . Figure 2.3 represents the experimental results.

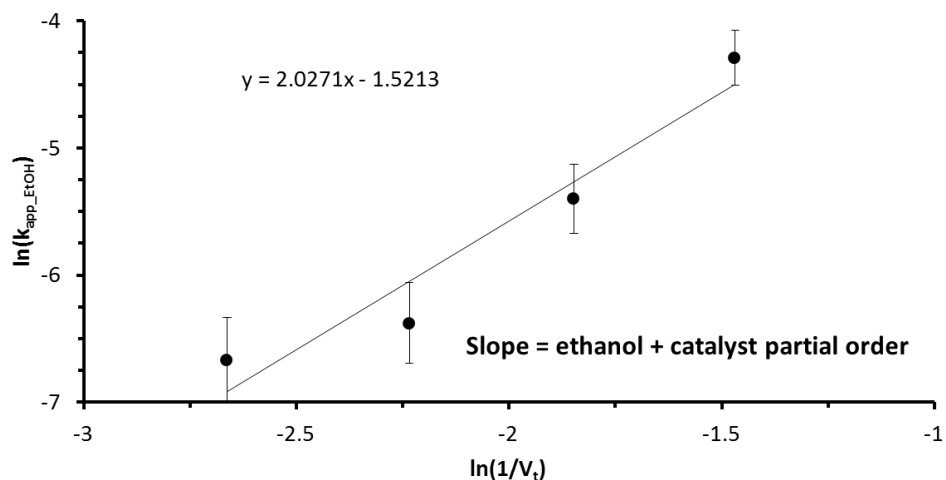


Figure 2.3 - Determination of the sum of the ethanol and catalyst partial order. Representation of $\ln(k_{app\text{-}EtOH})$ as a function of $\ln(1/V_t)$ at 70 °C with 12 wt% catalyst loading.

The sum of the partial order of $[H^+]$ and $[EtOH]$ is 2, as the partial order of $[H^+]$ was determined to be 0.5, the partial order with respect to $[EtOH]$ is 1.5. These results were confirmed by an experiment design to compensate for the dilution of catalyst that was induced by the change of concentration. Equation 2.10 describes the final equation rate:

$$r = k_{EtOH} * [Ep]^1 * [EtOH]^{1.5} [H^+]^{0.5} \quad (2.10)$$

The major factor impacting the reaction rate is the $[EtOH]$, followed by the $[Ep]$ and then the $[H^+]$. This order is only accurate if the catalyst is present; otherwise, the reaction is slower. In this case, there is no activation step when compared to the mechanism presented in Scheme 2.1.

4.2.4. Thermodynamics Data

Once the reaction rate determined, the thermodynamic constants were calculated and are summarized in Table 2.1. The sum of the catalyst partial order and the ethanol is the same as the partial order of $[AA]$. It can also confirm hypotheses that are given in the literature (Gan et al. 1992; Zaher et al. 1989) regarding the autocatalysis of the acetic acid due to its acidic properties. The separation between the catalysis and the reagent action in the acetic acid case would be possible by the isolation of the reaction intermediate. Overall, the order of the reaction is the same for both reactions: third order.

Table 2.1 - Thermodynamics data of the epoxidized Fatty Acid Methyl Ester of Very High Oleic Sunflower Oil (EVHOSO) ring-opening reaction with acetic acid and ethanol.

Thermodynamics Data	Acetic Acid ¹	Acetic Acid	Ethanol
Equation rate	$r = k_{AA} * [Ep]^1 * [AA]^2$	$r = k_{EtOH} * [Ep]^1 * [EtOH]^{1.5} * [H^+]^{0.5}$	
k (70 °C) ($L^2 \cdot mol^{-2} \cdot min^{-1}$)	3.3×10^{-5}	$(2 \pm 0.2) \times 10^{-5}$	$(7.8 \pm 0.4) \times 10^{-3}$
Frequency factor (min)	2.31×10^7	$(8.8 \pm 0.8) \times 10^4$	$(1.28 \pm 0.06) \times 10^6$
E_a (kJ/mol)	66	63 ± 6	54 ± 3
ΔH^\ddagger (70 °C) (kJ/mol)	63	60 ± 5	51 ± 3
ΔS^\ddagger (70 °C) (J/mol/K)	-182	-160 ± 10	-138 ± 7
ΔG^\ddagger (70 °C) (kJ/mol)	126	120 ± 10	98 ± 5

¹ RO kinetic study made on epoxidized soybean oil by measuring the epoxide function concentration from (Petrović et al. 2002).

The rate constant at 70 °C, k (70 °C), is an indication of the rate of a chemical reaction at this specified temperature (Menzinger and Wolfgang 1969). The corresponding unit depends on the reaction order. From a kinetic point of view, the ethanol RO is faster when compared to the case with acetic acid due to the two decades difference in terms of k (70 °C). The reaction constant is a function of the temperature following an Arrhenius law, as described by Equation 2.11:

$$k(T) = A * \exp\left(\frac{E_a}{R * T}\right) \quad (2.11)$$

where A is the frequency factor, E_a the activation energy of the reaction, R the gas constant, and T the temperature in Kelvin. E_a is determined by the slope of the linear regression of $\ln(k)$ as a function of the inverse of the temperature (Figure S2.19). It represents the energy barrier to overcome to form the intermediate state. E_a can be decreased while using a catalyst, but the catalyst loading does not affect it (Figure S2.19). The EVHOSO-EtOH intermediate state requires less energy to be formed than EVHOSO-AA. The enthalpy of activation (ΔH^\ddagger) is the energy difference between the reagents and the intermediate state (Avery 1974). It was calculated according to Equation 2.12:

$$\Delta H^\ddagger = E_a - RT \quad (2.12)$$

An exothermic reaction has a negative ΔH^\ddagger and both intermediate RO reactions are endothermic. They absorb energy from the environment to reach an intermediate state. The entropy of activation variation (ΔS^\ddagger) is a measurement of the disorders of the reaction. Negative ΔS^\ddagger represents the loss of freedom or an order increase (Avery 1974). Kinetics data ΔS^\ddagger is calculated via Equation 2.13:

$$\Delta S^\ddagger = R * \left[\ln\left(\frac{h * k_b}{k * T}\right) + \frac{\Delta H^\ddagger}{RT} \right] \quad (2.13)$$

where h is the Planck constant, k the Boltzman constant, k_b the rate constant, T the temperature, and R the gas constant. In RO, by acetic acid or ethanol, the intermediate states have fewer degrees of freedom than the reactants. The entropy variation is more important in a previous publication (Zaher et al. 1989) because the model molecule studied is based on epoxidized soybean oil

with more than one epoxide. The loss of freedom degree is then higher and can explain the gaps in ΔS^\ddagger and E_a .

The sign of the free enthalpy of activation ΔG^\ddagger is the combination of the entropic and enthalpic contribution, representing the spontaneity of the reaction (Equation 2.14).

$$\Delta G^\ddagger = \Delta H^\ddagger - T\Delta S^\ddagger \quad (2.14)$$

A negative ΔG^\ddagger indicates a spontaneous reaction (Avery 1974). From the thermodynamic point of view, both RO intermediates are not spontaneously formed. Thermodynamics is then not favorable to reach the intermediate of the RO of epoxide with acetic acid or ethanol, but the temperature and the kinetic are making the reaction possible in less than 10 h.

4.3. Kinetic Study of Urethane Formation from Fatty Acid

The kinetics of the reaction between an isocyanate and alcohol derived from a fatty acid was investigated. The phenyl isocyanate was chosen to model the methylene diphenyl diisocyanate (MDI) that was used in foaming processes. EVHOSO-AA was the alcohol used for this study. The measurements were made while using the pseudo-first-order principle (Avery 1974) by putting the hydroxyl moieties in large excess and measuring the concentration of isocyanate $[NCO]$ over time. The same model as for the RO kinetic can be applied. The reaction proceeds without catalyst and Equations 2.15 and 2.16 are then expressed.

$$-d \frac{[NCO]}{dt} = k_{app_U} * [NCO]^\alpha \quad (2.15)$$

where α is the partial order of the isocyanate concentration ($[NCO]$), and k_{app_U} is:

$$k_{app_U} = k * [OH]^\beta \quad (2.16)$$

The determination of the isocyanate content method was tested with known phenyl isocyanate contents before starting the kinetics measurement (Figure S2.20). The precision of the method was around 96%, and the studied concentration range was from 7×10^{-3} to 0.6 mol/L.

4.3.1. Determination of the Isocyanate Partial Order

The isocyanate partial order was determined by the variation of the temperature, with all other parameters being equal. The pseudo-first-order was applied by introducing a large excess (11 eq.) of VHOSO-AA. While considering Equation 2.15, the logarithm of $[NCO]_0/[NCO]$ was represented as a function of time in Figure 2.4.

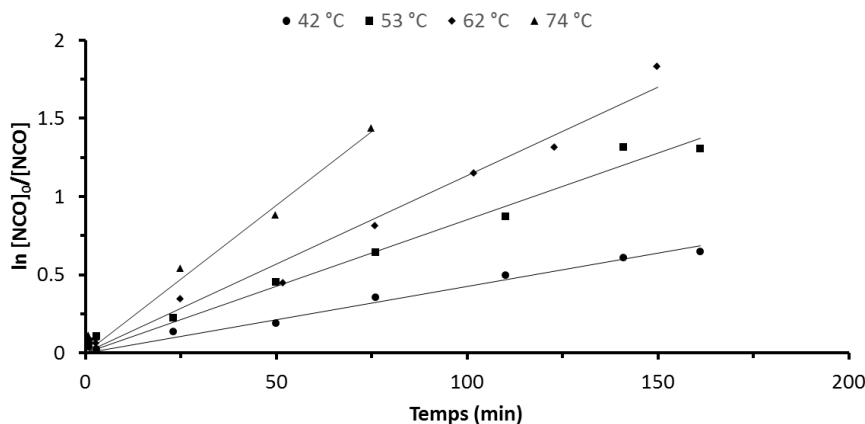


Figure 2.4 - Determination of the [NCO] partial order. Variation of $\ln([NCO]_0/[NCO])$ in function of time at 42 °C, 53 °C, 62 °C, and 74 °C.

The partial order of 1 for the isocyanate is well confirmed by experiments at different temperatures, which are 42, 53, 62, and 74 °C. For the conversion above 99%, the limit of the titration techniques was attained. The back titration of the [NCO] is determined by Equation 2.5, and a 1% difference between V_{eq} and V_{bl} is the limit of detection of the titration method.

4.3.2. Determination of the Hydroxyl Partial Order

The determination of the hydroxyl partial order is made by varying the concentration of hydroxyl while maintaining the significant excess as compared to the isocyanate group. The variation of concentration was made by diluting the solution with toluene. The determination of $k_{app,U}$ with 0.51, 0.72, 1.24, 1.51, 1.73, and 1.98 mol/L of hydroxyl are, respectively, presented in Figure S2.21. The slope of the linear regression of $\ln(k_{app,U})$ in the function of $\ln([OH])$ that is represented in Figure 2.5 can establish the partial order of hydroxyl.

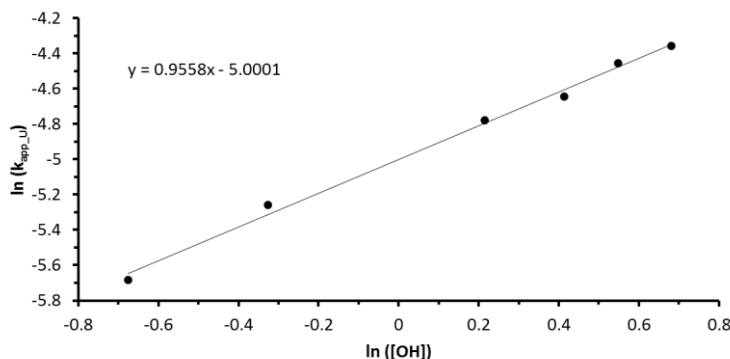


Figure 2.5 - Determination of hydroxyl partial order. Linear regression of $\ln(k_{app,U})$ as a function of $\ln([OH])$.

The coefficient of determination is 0.995. The partial order of [OH] can be round up to 1. Table 2.2 presents the final rate equation with the thermodynamic data of the intermediate state. The partial order of hydroxyl and isocyanate were both equal to 1. This result is in perfect agreement with the results that were found in the literature (Burkus and Eckert 1958; Dyer et al. 1949).

The energy of activation (44 kJ/mol) is in good agreement with the results from the literature. The energy of activation reported for a reaction between phenyl isocyanate and 2-butanol is 41 kJ/mol (Dyer et al. 1949) and 52 kJ/mol (Lovering and Laidler 1962) for a reaction with or without xylene as a solvent, respectively. The reaction rate constant that is presented in Table 2.2 (1.0×10^{-3} L.mol $^{-1} \cdot \text{min}^{-1}$) is six times smaller than data from the literature (Dyer et al. 1949) for the reaction between secondary alcohol and phenyl isocyanate. The 2-butanol is less sterically hindered than the mono-alcohols that were derived from methyl oleate. For instance, the reaction rate constant ratio between 2-hexanol and 3-hexanol was recently proved to be 1.5 for a reaction with an isocyanate (Nagy et al. 2017).

From the value of the activation energy and the reaction constant of 6.0×10^{-3} L.mol $^{-1} \cdot \text{min}^{-1}$, enthalpy, entropy, and free energy were calculated with Equations 2.12 to 2.14, respectively. The significant negative entropy of activation is an indication of the dissociation of the charged centers in the activation complex (Lovering and Laidler 1962). The difference of free energy of activation can be explained by better stabilization of the intermediate complex by toluene when compared to xylene (Sato 1962).

Table 2.2 - Thermodynamics data of urethane formation by the reaction between phenyl isocyanate and EVHOSO with acetic acid (EVHOSO-AA).

Thermodynamics Data	Ref ¹	PIC ² /EVHOSO-AA
Equation rate		$r = k_{AA} * [OH]^l * [NCO]^l$
k (25 °C) (L.mol $^{-1} \cdot \text{min}^{-1}$)	6.0×10^{-3}	$(1.0 \pm 0.05) \times 10^{-3}$
Frequency factor (min)		$(5.3 \pm 0.3) \times 10^4$
E _a (kJ/mol)	41	44 ± 2
ΔH [‡] (50 °C) (kJ/mol)	39	41 ± 2
ΔS [‡] (50 °C) (J/mol/K)	-198	-160 ± 8
ΔG [‡] (50 °C) (kJ/mol)	103	92 ± 5

¹ Reaction between 2-propanol and phenyl isocyanate in xylene from (Dyer et al. 1949),

² Phenylisocyanate.

The rate constant is similar to the one that was found for EVHOSO-EtOH with 20 °C of difference. By applying the Arrhenius Equation 2.11, the reaction rate at 70 °C for urethane formation is 1×10^{-2} L.mol $^{-1} \cdot \text{min}^{-1}$. The reaction between hydroxyl and aromatic isocyanate is faster than the RO by ethanol of a disubstituted epoxide. The urethane formation is not catalyzed. Catalysts, such as tertiary amine or tin salt, substantially reduce the E_a, which increases the reaction rate by several orders of magnitude. The frequency factor makes the rate of the RO with ethanol faster with temperature, despite the difference of activation energies (Figure S2.22). The ΔS[‡] of the urethane formation is higher than the one of RO with ethanol. The transition state has fewer degrees of freedom in urethane formation.

The kinetics and thermodynamics parameters of the reaction between fatty ester alcohol and an aromatic isocyanate were determined. These parameters are specific to the studied reaction, and they cannot be generalized to all isocyanates and hydroxyl substrates.

4.4. Study of the Reactivity with Different Isocyanates Structures

This section aims to compare the reactivity of different isocyanate and fatty ester alcohol since different chemical architectures are available for polyols or polyisocyanates to produce a broad range of materials for the polyurethane industry. The reactivity of the system is an essential factor, especially for foam, where the polyaddition must be fast.

Different isocyanate structures were compared in terms of reactivity with our model EVHOSO-AA: aromatic, aliphatic, and cycloaliphatic. The results are presented in Figure 2.6, once again demonstrated the higher reactivity of the aromatic isocyanate on agreement with previous results (Baker and Holdsworth 1947; Sato 1960).

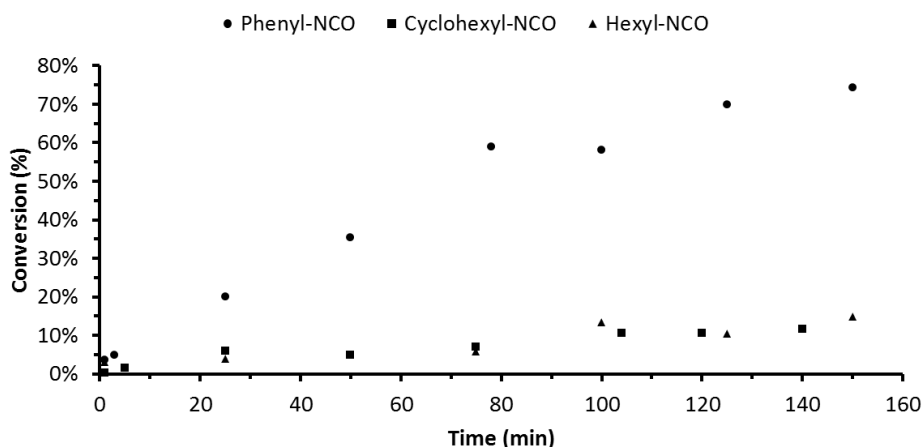


Figure 2.6 - Reactivity comparison in urethane formation at 50 °C in dry toluene under inert atmosphere with EVHOSO-AA of different isocyanate structure: aromatic, aliphatic, and cyclo-aliphatic.

The reactions from Figure 2.6 were performed in the same conditions with an excess of hydroxyl moiety. Both aliphatic isocyanates have the same reactivity toward hydroxyl. The steric hindrance due to the cycle (cyclo-aliphatic chemical) does not influence the beginning of the reaction (less than 15% of conversion) with secondary alcohol. The higher reactivity of aromatic isocyanate is due to the tautomer conformation that is presented in Figure 2.7.

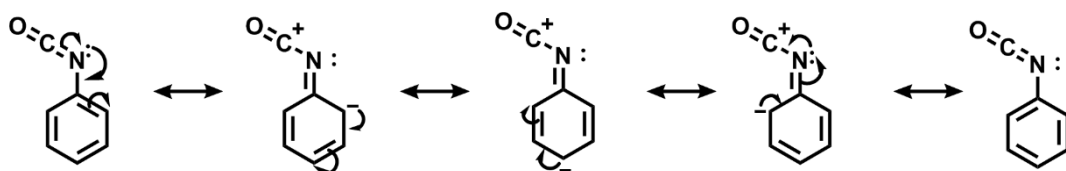


Figure 2.7 - Tautomer conformation of phenyl isocyanate.

The delocalization of the lone pair of electrons of the nitrogen atom on the aromatic cycle is increasing the electrophile character of the carbon (Baker and Holdsworth 1947; Sato 1960). It can be easily attacked by nucleophiles like hydroxyl moieties. Our model based on fatty ester hydroxyl confirms this trend. For foams, the necessary fast polyaddition can be reached by the use of p-MDI, due to its aromatic character, which also leads to higher mechanical properties. Our model reaction confirms that, despite the steric hindrance of the aromatic moieties and the secondary character of the

corresponding hydroxyl, aromatic isocyanates are the most suitable chemical for foam formulation with hydroxyl that is derived from fatty esters.

4.5. Synthesis of a Mono-Alcohol Model from Epoxidized Fatty Ester

RO can be conducted with alcohol, carboxylic acid, hydrogen halide, and secondary amine leading, respectively, to ether, ester, halide, and tertiary amine groups plus a secondary hydroxyl group. A series of different alcohols derived from fatty ester were synthesized by epoxide RO, with ethanol, acetic acid, HCl, HBr, and DEA (Figure 2.8).

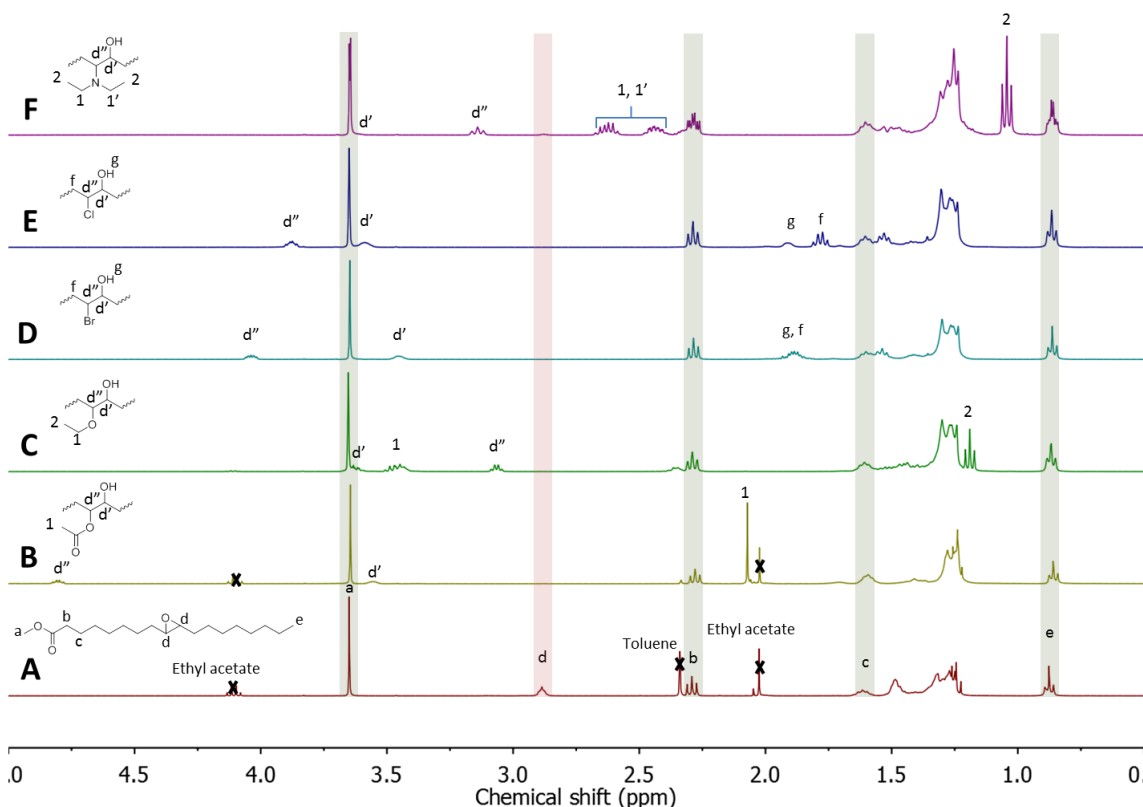


Figure 2.8 - NMR Spectrum of the initial epoxidized fatty methyl ester (A) and after the RO with acetic acid (B), ethanol (C), hydrobromic acid (D), hydrochloric acid (E), and diethylamine (F).

There is clear disappearance of the epoxide signal (d) located at $\delta=2.8$ ppm on the NMR spectrum for all the RO reagents. Signals that are characteristic of the proton located in alpha position to the newly created hydroxyl (d') are located in the $\delta=3.2-3.7$ ppm zone. The signal located at $\delta=3.7$ ppm, which is characteristic of the methyl close to the fatty ester bond (a), is constant in all products indicating non-significant ester breaking by transesterification, hydrolysis, or amidation. The RO protocols that were developed with the EVHOSO model molecule are efficient, and they cause no significant ester bond breaking. These characteristics are essential for the RO of more complex oils, such as triglycerides bearing several epoxide groups.

4.6. Evaluation of the Potential from Alcohols Derived from Fatty Acid in Polyurethane Application

The reactivity toward isocyanate of different models based on hydroxyl groups was investigated. The potential of the previously synthesized model alcohol in a urethane material was investigated through the scope of the reactivity. The reactions were carried out with a constant concentration of hydroxyl and isocyanate. The phenyl isocyanate concentration was followed over time by taking aliquots of the reaction. The results presented in Figure 2.9 show a clear tendency of reactivity with this evolution from the lowest to the highest, EVHOSO-HCl/HBr < EVHOSO-AA < EVHOSO-EtOH << EVHOSO-DEA.

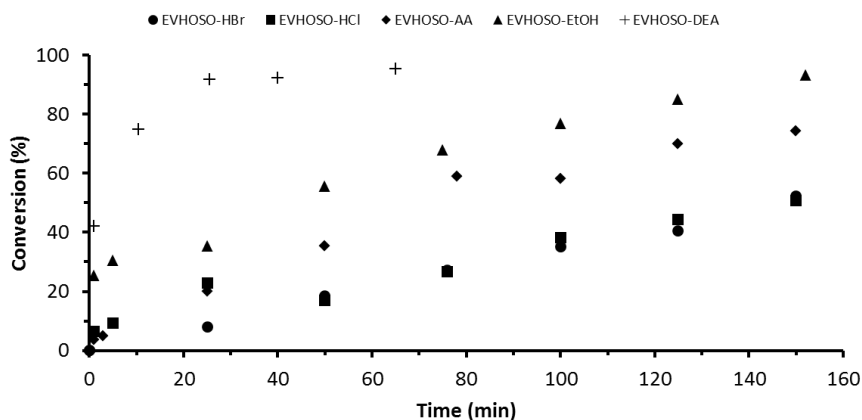


Figure 2.9 - Reactivity comparison in urethane formation with phenyl isocyanate with different RO FAMEVHOSO: EVHOSO-HBr, EVHOSO-HCl, EVHOSO-AA, EVHOSO-EtOH, and EVHOSO-DEA.

As demonstrated, the aromatic isocyanates are very reactive toward nucleophilic attack. The surrounding of the active hydrogen group impacts the reactivity. The electron releasing groups increase the electron density of the hydroxyl by the mesomeric or inductive effect. The studied groups have an inductive withdrawing effect. Except for tertiary amine, they are all electron releasing groups by mesomeric effect (Taft et al. 1959). In general, the mesomeric effect is predominant.

Furthermore, the inductive effect is decreasing with distance (Stock 1972). In our case, the two carbons distance between the inductive electron-withdrawing group and the hydroxyl decreased the effect. The reactivity is then explained by the difference in the strength of electron releasing groups according to the evolution that is presented in Figure 2.10. The EVHOSO-EtOH has a richer electron density around the hydroxyl group when compared to EVHOSO-AA and EVHOSO-Cl/Br.



Figure 2.10 - Electron releasing effect by mesomeric effect.

When considering the tertiary amine, the inductive effect reduced by the two carbons distance is counterbalanced by a catalytic effect. In the polyurethane industry, the catalytic activity of the amine by complexation with the isocyanate or by alcohol deprotonation is well established (Ionescu 2005; Silva and Bordado 2004; Van Maris et al. 2005). Afterward, the experiments confirmed the catalytic activity of the EVHOSO-DEA with aromatic or aliphatic isocyanate (Figure S2.23). The proximity of the reactive hydroxyl and tertiary amine must increase the corresponding catalytic activity.

5. CONCLUSIONS

This paper leads to different main and new results while considering the literature. An innovative NMR method was developed and successfully applied to determine the complete kinetic parameters of the EVHOSO RO reaction with ethanol. The calculated activation energy was determined, with 54 and 63 kJ/mol for the RO reaction with ethanol and acetic acid, respectively. This study led to a better understanding of the acid-catalyzed RO reaction of epoxides.

Model-alcohols were successfully synthesized by epoxide RO reaction with acetic acid, ethanol, hydrogen halide, and diethylamine. The reactivity comparison with the phenyl isocyanate shows a clear tendency, with a clear evolution from the lowest to the highest, EVHOSO-HCl/HBr < EVHOSO-AA < EVHOSO-EtOH << EVHOSO-DEA.

This work can be considered as a model to better understand the oleo-chemistry approaches leading to biobased polyols. In this frame, the RO of multi-epoxidized oil with hydrogen halide, ethanol and acetic acid, or diethylamine is leading to biobased reactive additives, polyols or catalysts, respectively. The transition from model to practical application is often complicated due to the limitations of the model. However, these approaches offer new insights on the replacement of current catalysts, additives, and polyols often fossil-based, used in the PUF industry, in order to revisit this chemistry. In the future, the accuracy of the kinetic model for the RO reaction needs to be tested on more complex oils. The reactivity of future triglyceride based polyols could be adjusted, depending on the RO reagent used. The potential of each RO reaction to provide a biobased substitute for the actual additives or polyols in the PUF industry could be investigated.

6. REFERENCES

Arbenz, A., Perrin, R., Avérus, L., 2017. Elaboration and Properties of Innovative Biobased PUIR Foams from Microalgae. *J Polym Environ* **26**, 254–262. <https://doi.org/10.1007/s10924-017-0948-y>

Avery, H.E., 1974. Basic reaction kinetics and mechanisms. Macmillan, London.

Baker, J.W., Holdsworth, J.B., 1947. 135. The mechanism of aromatic side-chain reactions with special reference to the polar effects of substituents. Part XIII. Kinetic examination of the reaction of aryl isocyanates with methyl alcohol. *J. Chem. Soc.* 713–726. <https://doi.org/10.1039/jr9470000713>

Bayer, O., 1947. Das Di-Isocyanat-Polyadditionsverfahren (Polyurethane). *Angew. Chem.* **59**, 257–272. <https://doi.org/10.1002/ange.19470590901>

Biswas, A., Adhvaryu, A., Gordon, S.H., Erhan, S.Z., Willett, J.L., 2005. Synthesis of Diethylamine-Functionalized Soybean Oil. *J. Agric. Food Chem.* **53**, 9485–9490. <https://doi.org/10.1021/jf050731o>

Burkus, J., Eckert, C.F., 1958. The Kinetics of the Triethylamine-catalyzed Reaction of Diisocyanates with 1-Butanol in Toluene. *J. Am. Chem. Soc.* **80**, 5948–5950. <https://doi.org/10.1021/ja01555a015>

Chen, R., Zhang, C., Kessler, M.R., 2015. Polyols and polyurethanes prepared from epoxidized soybean oil ring-opened by polyhydroxy fatty acids with varying OH numbers. *J. Appl. Polym. Sci.* **132**. <https://doi.org/10.1002/app.41213>

Dai, H., Yang, L., Lin, B., Wang, C., Shi, G., 2009. Synthesis and Characterization of the Different Soy-Based Polyols by Ring Opening of Epoxidized Soybean Oil with Methanol, 1,2-Ethanediol and 1,2-Propanediol. *J Am Oil Chem Soc* **86**, 261–267. <https://doi.org/10.1007/s11746-008-1342-7>

Durán Pachón, L., Gamez, P., van Brussel, J.J.M., Reedijk, J., 2003. Zinc-catalyzed aminolysis of epoxides. *Tetrahedron Letters* **44**, 6025–6027. [https://doi.org/10.1016/S0040-4039\(03\)01480-1](https://doi.org/10.1016/S0040-4039(03)01480-1)

Durbetaki, A.J., 1956. Direct Titration of Oxirane Oxygen with Hydrogen Bromide in Acetic Acid. *Anal. Chem.* **28**, 2000–2001. <https://doi.org/10.1021/ac60120a055>

Dyer, Elizabeth., Taylor, H.A., Mason, S.J., Samson, Jan., 1949. The Rates of Reaction of Isocyanates with Alcohols. I. Phenyl Isocyanate with 1- and 2-Butanol. *J. Am. Chem. Soc.* **71**, 4106–4109. <https://doi.org/10.1021/ja01180a064>

Espenson, J.H., 1995. Chemical kinetics and reaction mechanisms, 2. ed. ed 'McGraw Hill series in advanced chemistry. McGraw Hill, New York.

Furtwengler, P., Boumbimba, R.M., Avérous, L., 2018a. Elaboration and Characterization of Advanced Biobased Polyurethane Foams Presenting Anisotropic Behavior. *Macromol. Mater. Eng.* **303**, 1700501. <https://doi.org/10.1002/mame.201700501>

Gan, L.H., Goh, S.H., Ooi, K.S., 1992. Kinetic studies of epoxidation and oxirane cleavage of palm olein methyl esters. *J Am Oil Chem Soc* **69**, 347–351. <https://doi.org/10.1007/BF02636065>

Guo, A., Cho, Y., Petrović, Z.S., 2000. Structure and properties of halogenated and nonhalogenated soy-based polyols. *Journal of Polymer Science Part A: Polymer Chemistry* **38**, 3900–3910. [https://doi.org/10.1002/1099-0518\(20001101\)38:21<3900::AID-POLA70>3.0.CO;2-E](https://doi.org/10.1002/1099-0518(20001101)38:21<3900::AID-POLA70>3.0.CO;2-E)

Harry-O'kuru, R.E., Tisserat, B., Gordon, S.H., Gravett, A., 2015. Osage Orange (*Maclura pomifera* L.) Seed Oil Poly(α-hydroxydibutylamine) Triglycerides: Synthesis and Characterization. *J. Agric. Food Chem.* **63**, 6588–6595. <https://doi.org/10.1021/acs.jafc.5b01625>

Ionescu, M., 2005. Chemistry and technology of polyols for polyurethanes, 1st ed. Rapra Technology, Shawbury, Shrewsbury, Shropshire, U.K.

Kenaston, C.B., Wilbur, K.M., Ottolenghi, A., Bernheim, F., 1955. Comparison of methods for determining fatty acid oxidation produced by ultraviolet irradiation. *J Am Oil Chem Soc* **32**, 33–35. <https://doi.org/10.1007/BF02636476>

Lovering, E.G., Laidler, K.J., 1962. KINETIC STUDIES OF SOME ALCOHOL-ISOCYANATE REACTIONS. *Can. J. Chem.* **40**, 31–36. <https://doi.org/10.1139/v62-006>

Maisonneuve, L., Chollet, G., Grau, E., Cramail, H., 2016. Vegetable oils: a source of polyols for polyurethane materials. *OCL* **23**, D508. <https://doi.org/10.1051/ocl/2016031>

Menzinger, M., Wolfgang, R., 1969. The Meaning and Use of the Arrhenius Activation Energy. *Angew. Chem. Int. Ed. Engl.* **8**, 438–444. <https://doi.org/10.1002/anie.196904381>

Nagy, L., Nagy, T., Kuki, Á., Purgel, M., Zsuga, M., Kéki, S., 2017. Kinetics of Uncatalyzed Reactions of 2,4'- and 4,4'-Diphenylmethane-Diisocyanate with Primary and Secondary Alcohols: KINETICS OF UNCATALYZED REACTIONS OF 2,4'-MDI AND 4,4'-MDI WITH ALCOHOLS. *Int. J. Chem. Kinet.* **49**, 643–655. <https://doi.org/10.1002/kin.21104>

Obi, B.E., 2018c. Polymeric foams structure-property-performance: a design guide 'PDL handbook series. William Andrew is an imprint of Elsevier, Oxford, United Kingdom.

Palaskar, D.V., Boyer, A., Cloutet, E., Le Meins, J.-F., Gadenne, B., Alfos, C., Farcet, C., Cramail, H., 2012. Original diols from sunflower and ricin oils: Synthesis, characterization, and use as polyurethane building blocks. *J. Polym. Sci. A Polym. Chem.* **50**, 1766–1782. <https://doi.org/10.1002/pola.25944>

Parker, R.E., Isaacs, N.S., 1959. Mechanisms Of Epoxide Reactions. *Chem. Rev.* **59**, 737–799. <https://doi.org/10.1021/cr50028a006>

Petrovic, Z., 2008. Polyurethanes from Vegetable Oils. *Polymer Revs.* **48**, 109–155. <https://doi.org/10.1080/15583720701834224>

Petrović, Z.S., Zlatanić, A., Lava, C.C., Sinadinović-Fišer, S., 2002. Epoxidation of soybean oil in toluene with peroxyacetic and peroxyformic acids — kinetics and side reactions. *European Journal of Lipid Science and Technology* **104**, 293–299. [https://doi.org/10.1002/1438-9312\(200205\)104:5<293::AID-EJLT293>3.0.CO;2-W](https://doi.org/10.1002/1438-9312(200205)104:5<293::AID-EJLT293>3.0.CO;2-W)

Pfister, D.P., Xia, Y., Larock, R.C., 2011. Recent Advances in Vegetable Oil-Based Polyurethanes. *ChemSusChem* **4**, 703–717. <https://doi.org/10.1002/cssc.201000378>

Rios, L. alberto, 2003. Heterogeneously Catalyzed Reactions with Vegetable Oils: Epoxidation and Nucleophilic Epoxide Ring-Opening with Alcohols. RWTH Aachen University, Germany.

Sato, M., 1962. The Rate of the Reaction of Isocyanates with Alcohols. II. *J. Org. Chem.* **27**, 819–825. <https://doi.org/10.1021/jo01050a031>

Sato, M., 1960. The Rates of Reaction of 1-Alkenyl Isocyanates with Methanol. *J. Am. Chem. Soc.* **82**, 3893–3897. <https://doi.org/10.1021/ja01500a027>

Schuster, H., Rios, L.A., Weckes, P.P., Hoelderich, W.F., 2008. Heterogeneous catalysts for the production of new lubricants with unique properties. *Applied Catalysis A: General* **348**, 266–270. <https://doi.org/10.1016/j.apcata.2008.07.004>

Shuo, X., Ligong, C., Lan, X., Liang, L., Xin, Y., Liye, Z., 2015. Diester Derivatives from Chemically Modified Waste Cooking Oil as Substitute for Petroleum Based Lubricating Oils 8.

Silva, A.L., Bordado, J.C., 2004. Recent Developments in Polyurethane Catalysis: Catalytic Mechanisms Review. *Catalysis Reviews* **46**, 31–51. <https://doi.org/10.1081/CR-120027049>

Stock, L.M., 1972. The origin of the inductive effect. *J. Chem. Educ.* **49**, 400. <https://doi.org/10.1021/ed049p400>

Taft, R.W., Ehrenson, S., Lewis, I.C., Glick, R.E., 1959. Evaluation of Resonance Effects on Reactivity by Application of the Linear Inductive Energy Relationship. ^{1,2} VI. Concerning the Effects of Polarization and Conjugation on the Mesomeric Order. *J. Am. Chem. Soc.* **81**, 5352–5361. <https://doi.org/10.1021/ja01529a026>

Takeuchi, M., Kishino, S., Tanabe, K., Hirata, A., Park, S.-B., Shimizu, S., Ogawa, J., 2013. Hydroxy fatty acid production by *Pediococcus* sp. *Eur. J. Lipid Sci. Technol.* **115**, 386–393. <https://doi.org/10.1002/ejlt.201200414>

Turco, R., Tesser, R., Vitiello, R., Russo, V., Andini, S., Serio, M.D., 2017. Synthesis of Biolubricant Basestocks from Epoxidized Soybean Oil. *Catalysts* **7**, 309. <https://doi.org/10.3390/catal7100309>

Van Maris, R., Tamano, Y., Yoshimura, H., Gay, K.M., 2005. Polyurethane Catalysis by Tertiary Amines. *Journal of Cellular Plastics* **41**, 305–322. <https://doi.org/10.1177/0021955X05055113>

Yang, L.-T., Zhao, C.-S., Dai, C.-L., Fu, L.-Y., Lin, S.-Q., 2012. Thermal and Mechanical Properties of Polyurethane Rigid Foam Based on Epoxidized Soybean Oil. *J Polym Environ* **20**, 230–236. <https://doi.org/10.1007/s10924-011-0381-6>

Zaher, F.A., El-Mallah, M.H., El-Hefnawy, M.M., 1989. Kinetics of oxirane cleavage in epoxidized soybean oil. *J Am Oil Chem Soc* **66**, 698–700. <https://doi.org/10.1007/BF02669955>

Zhang, C., Garrison, T.F., Madbouly, S.A., Kessler, M.R., 2017a. Recent advances in vegetable oil-based polymers and their composites. *Progress in Polymer Science* **71**, 91–143. <https://doi.org/10.1016/j.progpolymsci.2016.12.009>

7. SUPPORTING INFORMATION

7.1. FAMEVHOSO Characterization

The repartition in fatty acid was determined according by the ISO 12966-2 method comprising a methylation followed by a gas chromatography analysis.

Table S2.3 - Lipid profile. Fatty acids distribution in unsaturated FAMEVHOSO.

Fatty acids	Palmitic acid (C16:0)	Palmitoleic acid (C16:1)	Stearic acid (C18:1)	Oleic acid (C18:1)	Linoleic acid (C18:2)	Linolenic acid (C18:3)	Arachidic acid (C20:0)	Eicosenoic acid (C20:1)	Behenic acid (C22:0)	Erucic acid (C22:1)	Other
Repartition (%)	3.6	0.1	2.7	82.8	9.1	0.1	0.3	0.2	0.8	0.3	0.1

The average double bond per molecule is determined from the number of double bond per fatty acid.

The NMR spectra of the FAMEVHOSO and EVHOSO are presented on Figure S2.11 and Figure S2.12, respectively.

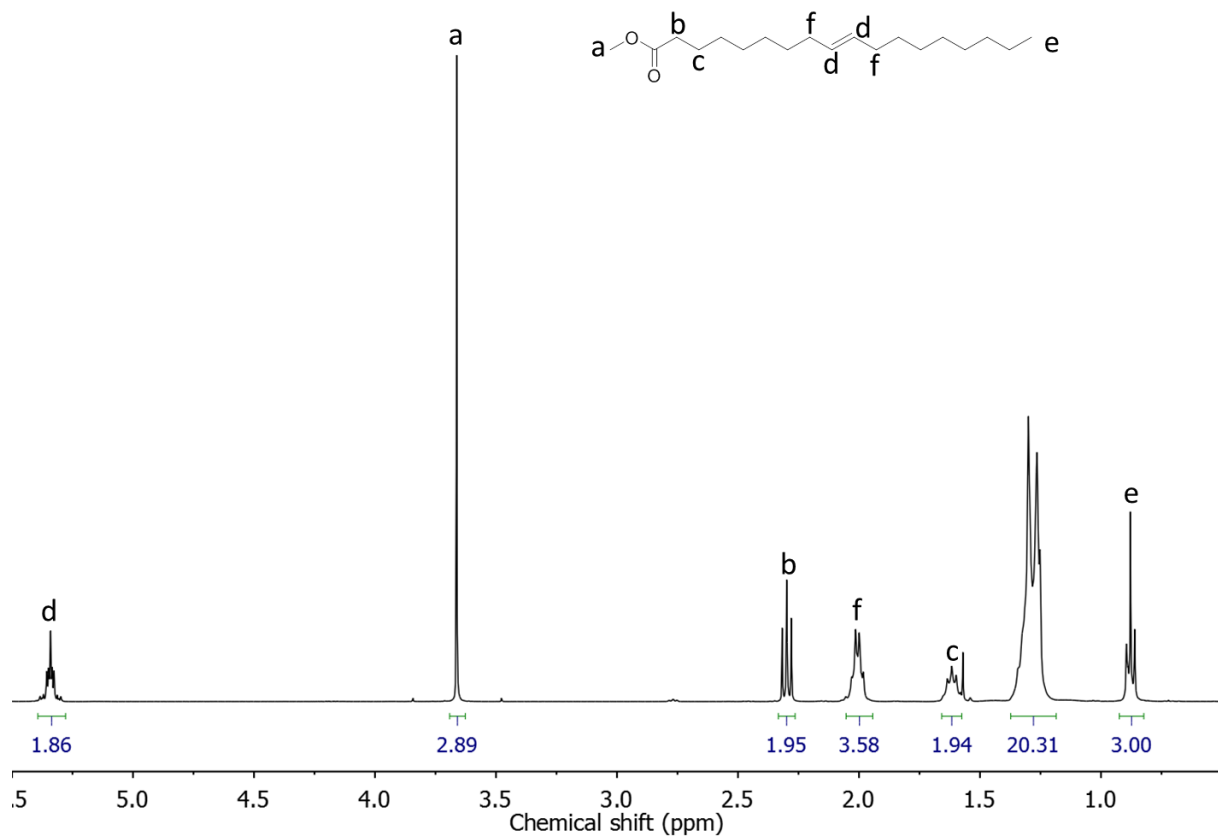


Figure S2.11 – ^1H NMR Spectra of the FAMEVHOSO unsaturated.

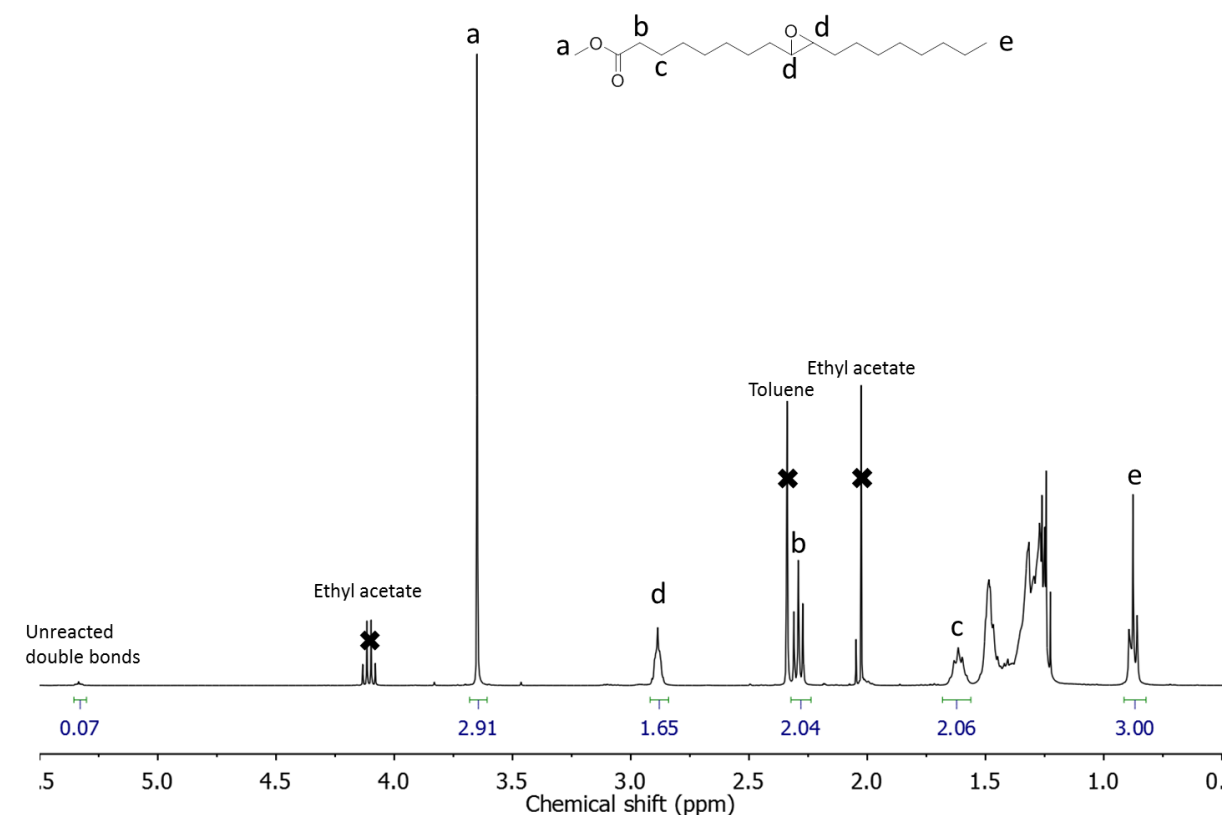


Figure S2.12 - ^1H NMR spectra of epoxidized FAMEVHOSO.

7.2. Method Development: Kinetics of Epoxide Ring-Opening by Acetic Acid

7.2.1. NMR Method for the Yield Determination

In the literature, the acetic acid rate law was determined by chemical dosage (Gan et al. 1992; Zaher et al. 1989), and never by NMR. A new NMR method was developed to determine the kinetic of RO reactions. The reaction between EVHOSO and an excess of acetic acid was carried out in bulk. Aliquots were washed to remove the excess of acetic acid and then analyzed by NMR spectroscopy. The chemical shifts between the EVHOSO and the ring-opened are defined and detectable (Figure S2.13).

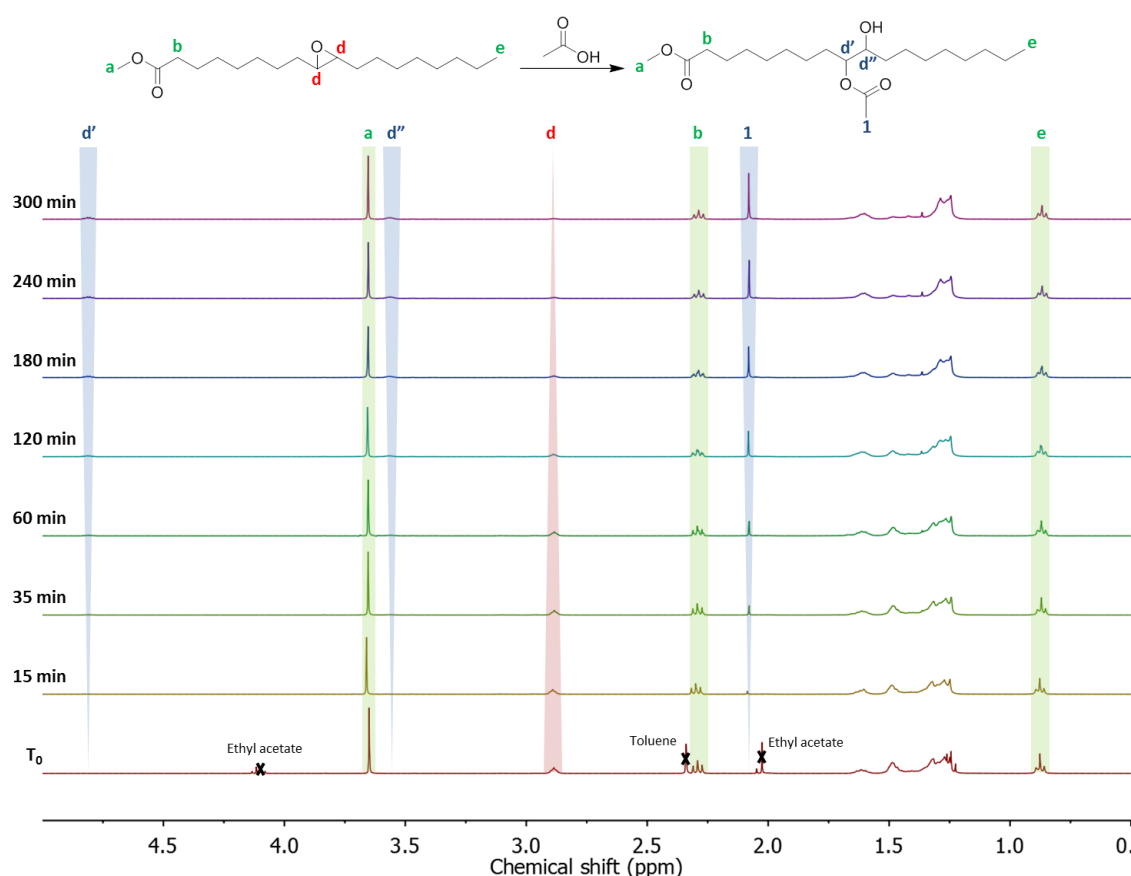


Figure S2.13 - NMR analysis of epoxidized FAMEVHOSO (T_0) and the oil after 15, 35, 60, 120, 180, 240 and 300 min. of reaction at 90 °C with acetic acid.

The absence of singlet at $\delta=2.10$ ppm indicates the efficiency of the aliquots washing. The signals of the backbone's protons of the methyl fatty ester were constant while the integration of the protons d adjacent to the epoxide was decreased over time. Signals of protons characteristic of the VHOSO-AA d', d'' and 1 were increased over time, indicating a progression of the reaction until completion. Among the three signals indicating the progress of the reaction, the signal 1 is not specific to the RO reaction because it can be the result of transesterification. The signals of free acetic and ethyl acetate are close. The signal d'' is too close to the signal of the methyl ester to be quantitative.

The signal d' was chosen to calculate the yield by comparison with the d signal, according to Equation S2.1:

$$Yield (\%) = \chi = \frac{I_{d'}}{1.66/2} \quad (S2.1)$$

where $I_{d'}$ is the integration of the d' signal, 1.66 is the integration of the d signal on the EVHOSO. Based on this calculation, the determination of the different partial orders and the activation energy were accomplished and compared to the literature for a validation method.

7.2.2. Determination of the Epoxide Partial Order

The reaction is done without catalyst, the Equations 2.3 and 2.4 applied to the acetic acid become Equation S2.2:

$$-d \frac{[Ep]}{dt} = k_{app_AA} * [Ep]^{\alpha} \quad (S2.2)$$

where $[Ep]$ is the concentration of epoxide over time, α the partial order of $[Ep]$. k_{app_AA} is detailed by Equation S2.3:

$$k_{app_AA} = k_{AA} * [AA]^{\beta} \quad (S2.3)$$

where k_{AA} is the rate constant of the reaction, $[AA]$ the concentration of acetic acid and β the partial order of $[AA]$.

The epoxide partial order was determined by the variation of the temperature with an excess of acetic acid. The pseudo-first-order was applied by introducing a large excess (11 eq.) of acetic acid.

The integration of the Equation S2.2 with $\alpha = 1$ gives Equation S2.4:

$$\ln\left(\frac{[Ep]_0}{[Ep]}\right) = \ln\left(\frac{1}{1-\chi}\right) = k_{app_AA} * t \quad (S2.4)$$

where χ is the yield of the reaction and t the time in minute. The logarithm of $[Ep]_0/[Ep]$ was represented as a function of time in Figure S2.14. The linear regression fit the experimental data with a correlation coefficient of 0.85 for 110 °C, 0.99 for 90 and 70 °C, respectively. The lack of correlation at high temperature is the result of the fast rates of reaction and so an increased error and the side reactions.

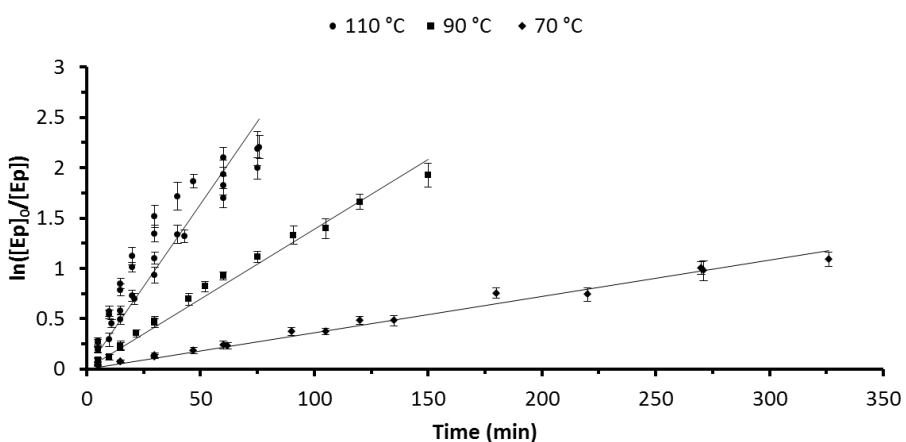


Figure S2.14 - Determination of the epoxide partial order. Representation of $\ln([Ep]_0/[Ep])$ as a function of time at 70 °C, 90 °C and 110 °C.

The model of a partial order of 1 for the epoxide is well confirmed by experiments at different temperatures. The precision diminishes when the conversion is less than 20% due to the noise on the NMR spectra. The average NMR precision on the conversion is around 5% on the 20–95% interval. The precision is similar to the one obtained in previous studies (Gan et al. 1992; Zaher et al. 1989).

7.2.3. Determination of the Acetic Acid Partial Order

The determination of the acetic acid partial order is performed by varying the concentration of acetic acid while maintaining a significant excess compared to epoxide. The acetic acid concentration was set at 8.6, 12.8 or 16.6 mol/L by diluting with ethyl acetate. To determine k_{app_AA} , the linear regression of $\ln([Ep_0]/[Ep])$ in the function of time was plotted (Figure S2.15).

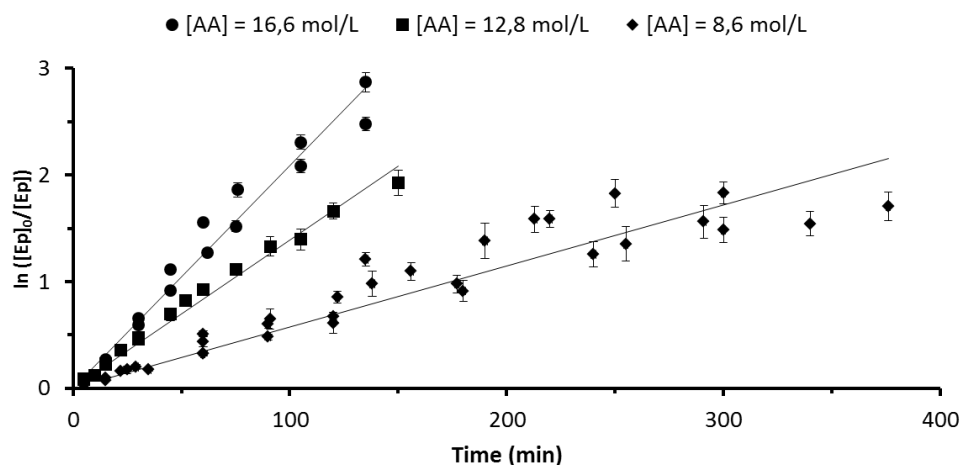


Figure S2.15 - Determination of the k_{app_AA} with 8.6 mol/L, 12.8 mol/L and 16.6 mol/L of acetic acid.

For the highest concentration, the coefficient of correlation is superior to 0.97. For the smallest concentration, the data points are sparser, due to the logarithm character of the model. The rate of reaction decreases at the end and reaches a plateau. In Equation S2.2, k_{app_AA} depends only on $[AA]$; the other factors are constant. The logarithm of Equation S2.2 gives the Equation S2.5.

$$\ln(k_{app_AA}) = \ln(k_{AA}) + \beta * \ln([AA]), \quad (S2.5)$$

The combination of Equation S2.5 and the k_{app_AA} obtained at different $[AA]$, linear regression of the logarithm of k_{app_AA} as a function of the $[AA]$, was presented in Figure S2.16, in order to determine β .

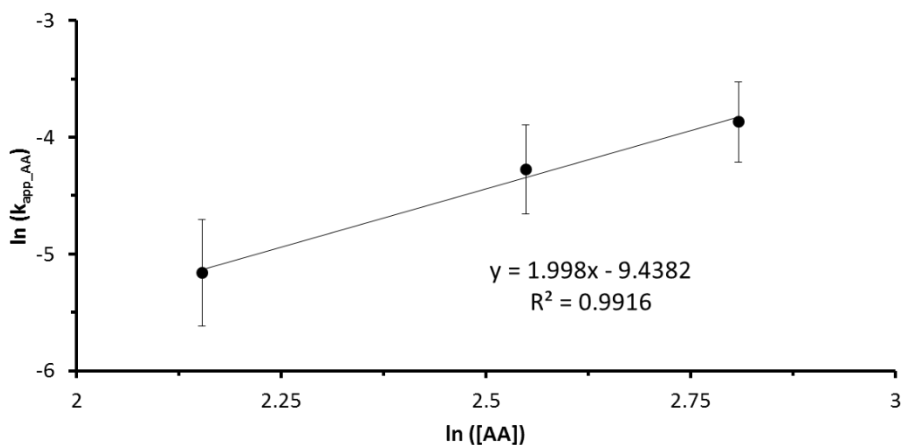


Figure S2.16 - Determination of the acetic acid partial order. Representation of $\ln(k_{\text{app,AA}})$ as a function of $\ln([\text{AA}])$.

The partial order for $[\text{AA}]$ was determined to be 2. The overall kinetic rate is expressed as Equation S2.6:

$$r = k * [E_p] * [\text{AA}]^2, \quad (\text{S2.6})$$

which is in agreement with the previous results found in the literature (Gan et al. 1992; Zaher et al. 1989). The rate constant k can be calculated from all the $k_{\text{app,AA}}$ by dividing them by $[\text{AA}]^2$. The average k was calculated at 70, 90 and 110 °C. The temperature dependence of k was modeled with an Arrhenius law described by Equation 2.11. The linear regression of $\ln(k_{\text{AA}})$ in the function of $1/T$ (Figure S2.17) was used to determine $E_{\text{A,AA}}$.

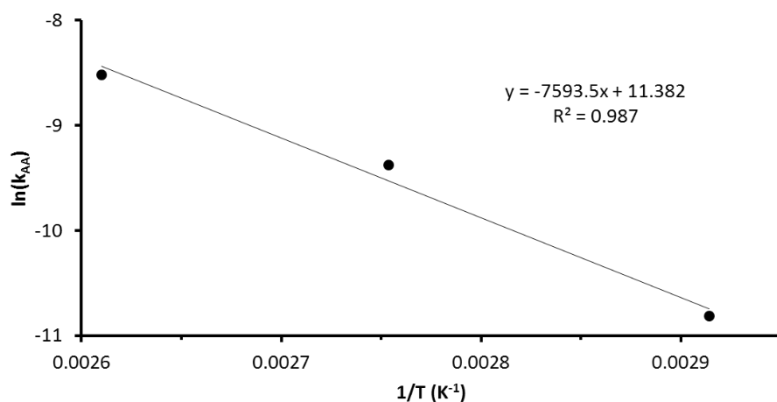


Figure S2.17 - Determination of $E_{\text{A,AA}}$ by plotting the $\ln(k_{\text{AA}})$ as a function of the inverse of the temperature.

The energy of activation (63 kJ/mol) is in good agreement with the results from the literature. The energies of activation reported are 66 kJ/mol (Zaher et al. 1989) and 73 kJ/mol (Gan et al. 1992) for the RO with acetic acid of epoxidized soybean oil or epoxidized methyl ester of palm oil, respectively. The RO of disubstituted epoxide by acetic acid was studied. Despite the difference in systems and methods, the kinetic rate was found to be the same as the one in the literature, and the calculated activation energy is close to the one matching our system. This is validating our NMR method for the determination of the reaction rate. Thus, it can be applied to the study of the RO of ethanol with acid catalysis.

7.3. Variation of $k_{app\text{-}EtOH}$ with different temperature and catalyst quantity

By combining the linear regression slope of experiment performed at 30, 50 and 70 °C with 4, 12 and 20 wt% of amberlyst, respectively, Table S2.4 is obtained.

Table S2.4 - $k_{app\text{-}EtOH}$ (min⁻¹) with 30, 50 and 70 °C and 4, 12 and 20 wt% of amberlyst.

Amberlyst wt% eq.	$k' (30)$	$k' (50)$	$k' (70)$
4	0.000601	0.00241	0.0075
12	0.00114	0.00439	0.0137
20	0.00119	0.0071	0.0141

7.4. Correlation between the mass of catalyst and the quantity of H^+

In order to know the relation between the mass of catalyst and the proton quantity, an experiment was designed: Different mass of Amberlyst® 15H was put in a beaker with 40 mL of water, then the pH was measured. Experimental results are shown in Figure S2.18.

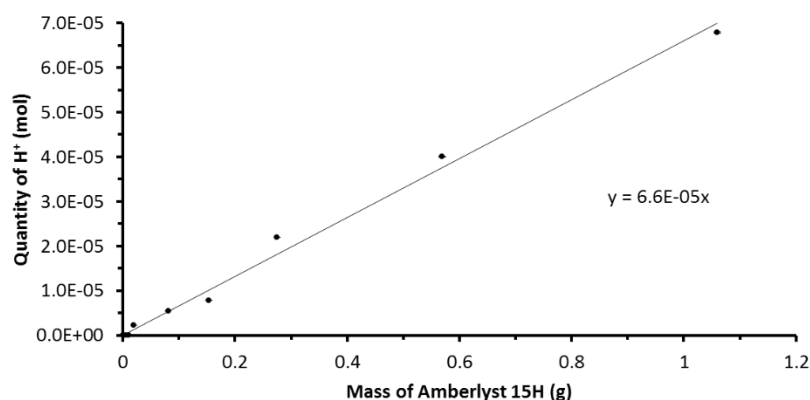


Figure S2.18 - Correlation between the mass of Amberlyst® 15H and the proton quantity.

7.5. Determination of the Activation energy of ring-opening with ethanol

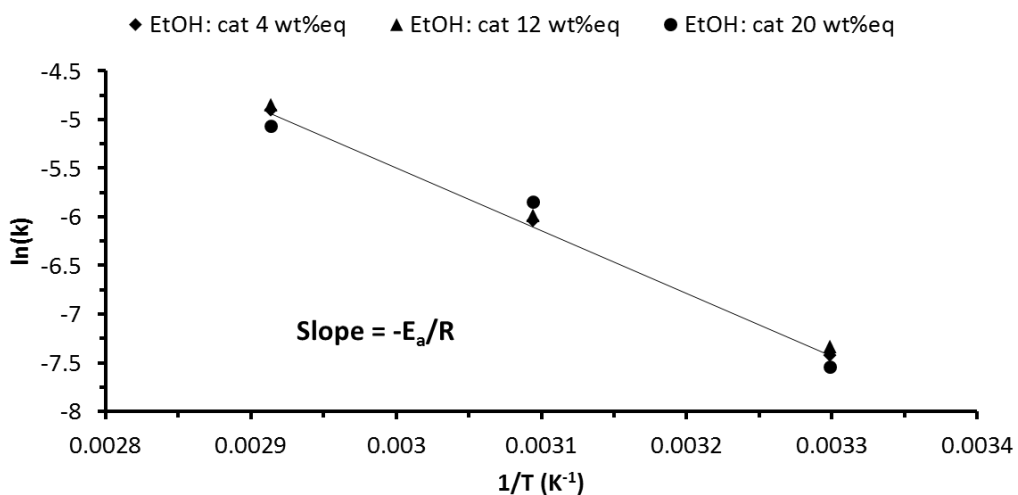


Figure S2.19 - Arrhenius law for the RO of FAMEVHOSO with ethanol at 4, 12 and 20 wt% of catalyst loading.

7.6. Method validation for the isocyanate titration

A known concentration of phenyl isocyanate was titrated by the protocol. The value obtained was then compared with the theoretical one in Figure S2.20.

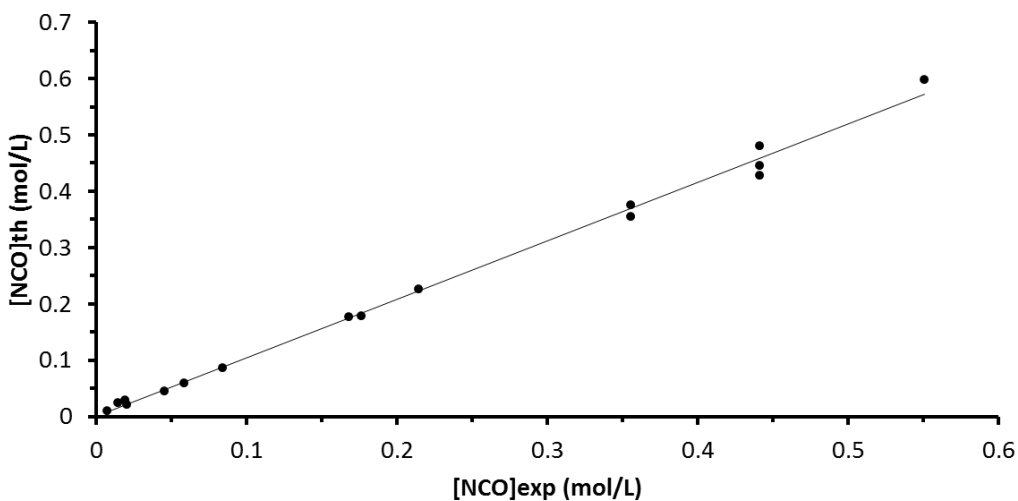


Figure S2.20 - Representation of the gap between theoretical and experimental dosage of the NCO concentration.

The linear regression slope is 1.04. The error made on the dosage is 4% between 7×10^{-3} and 0.6 mol/L of isocyanate groups.

7.7. Determination of k_{aap_U} with hydroxyl concentration variation

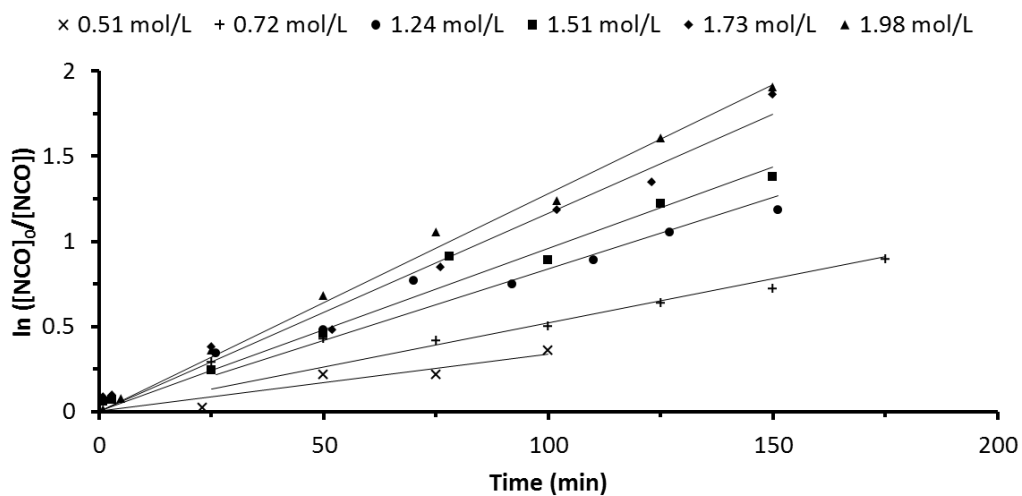


Figure S2.21 - Determination of the k_{aap_U} . Variation of $\ln([NCO]_0/[NCO])$ in function of time at 1.24, 1.51, 1.73, 1.98, 0.51 and 0.72 mol/L.

7.8. Comparison between urethane formation and ring-opening with ethanol

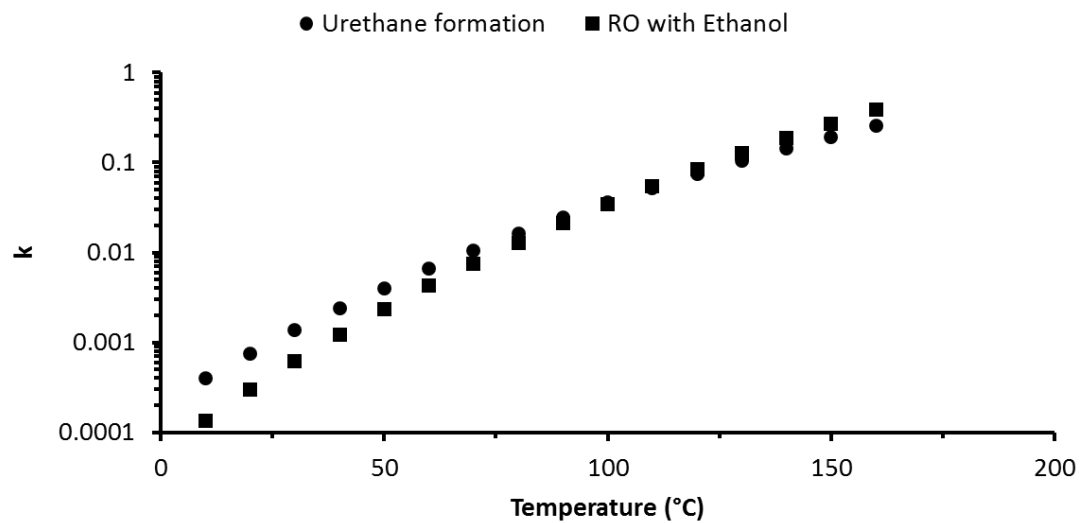


Figure S2.22 - Application of the Arrhenius equation to determine the temperature dependency of reaction rate for the urethane formation and the RO with ethanol.

7.9. Reaction of VHOSO-DEA with aliphatic and aromatic isocyanate

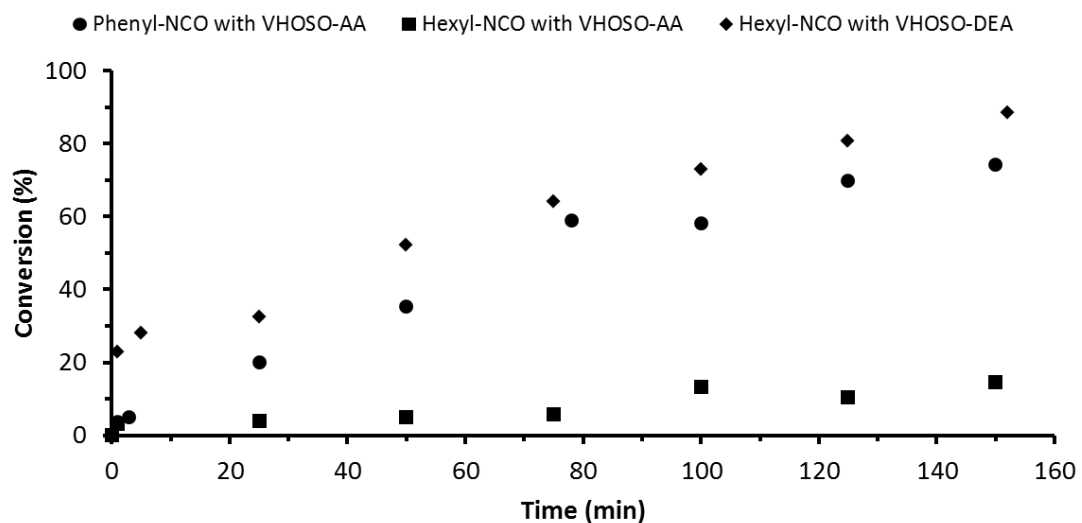


Figure S2.23 - Conversion as a function of time for the reaction between phenyl isocyanate and VHOSO-AA, Hexyl isocyanate and VHOSO-AA and Hexyl isocyanate and VHOSO-DEA.

Conclusion chapitre 2

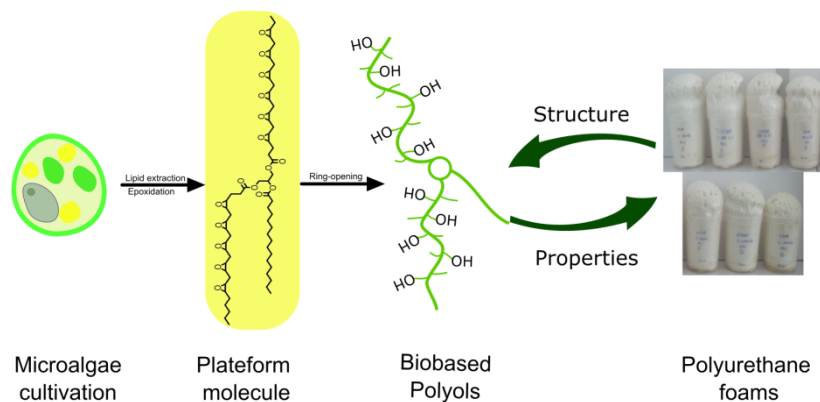
Le but de ce chapitre était d'étudier la formation d'un polyol à partir de ressources lipidiques pour l'élaboration de mousses polyuréthanes. La double liaison d'une huile modèle a été époxydée. La réaction d'ouverture de cycles génère un groupement hydroxyle. Ceci a été suivi cinétiquement. Enfin, l'impact des nucléophiles utilisés pour l'ouverture des époxydes a été étudié. La réactivité du groupement hydroxyle formé a été évaluée par dosage de la teneur en isocyanates au cours du temps.

Les équations cinétiques des réactions d'ouverture des époxydes ont été obtenues par suivi de la quantité d'époxydes sur des systèmes modèles. Une nouvelle méthode de suivi de l'avancement par spectroscopie RMN simple et efficace a été validée. Les dosages des fonctions isocyanates permettent de déterminer que la réactivité des groupements hydroxyles est influencée par ses proches substituants. L'ouverture des époxydes avec la diéthylamine forme un groupement hydroxyle extrêmement réactif par rapport aux autres ouvertures étudiées. Ce résultat est expliqué par la présence d'une amine tertiaire à proximité du groupement hydroxyle. Cette structure est fréquemment utilisée dans la catalyse des polyuréthanes. Tous les polyols modèles étudiés possèdent une réactivité adaptée pour la formulation de mousses polyuréthanes.

Ces travaux démontrent clairement le potentiel des ressources lipidiques pour la fabrication de mousses polyuréthanes. La formation de polyols et de catalyseur par réaction d'époxydation et ouverture de cycle a été validée.

Les différents protocoles développés dans ce chapitre sur une huile modèle, seront ensuite appliqués à des huiles polyfonctionnelles. L'huile de microalgues sera particulièrement étudiée. Les polyols produits seront testés en formulation de mousses polyuréthanes afin de valider les résultats obtenus sur le modèle développé dans ce chapitre.

CHAPITRE 3. MOUSSES POLYURÉTHANES BIOSOURCÉES À PARTIR DE NOUVEAUX POLYOLS DÉRIVÉS D'HUILE DE MICROALGUES



Introduction Chapitre 3

Les travaux présentés dans ce chapitre sont sous la forme d'un article intitulée « Biobased Polyurethane foams based on new polyols architectures from microalgae oil » publié dans *ACS Sustainable Chemistry & Engineering*.

Le chapitre précédent a évalué la synthèse de polyol via l'époxydation et l'ouverture des cycles correspondants sur une huile modèle. Les protocoles d'ouverture des époxydes par différents nucléophiles ont été développés dans le but d'obtenir les groupements hydroxyles avec une grande sélectivité. L'étude a aussi permis de déterminer l'impact des différents nucléophiles sur la réactivité des groupements hydroxyles formés. Les résultats ont mis en avant le potentiel des produits obtenus par ouverture avec la diéthylamine à la fois comme polyol et comme catalyseur.

Les polyols issus de ressources lipidiques précédemment synthétisés dans la littérature sont principalement issus d'oléagineux. Ces polyols ont des propriétés adaptées pour les mousses polyuréthanes. Cependant, cette utilisation des huiles végétales engendre une concurrence avec l'alimentation humaine, au contraire de l'huile de microalgues utilisée dans cette étude. En outre, la culture de microalgues ne mobilise pas de terre arable et consomme du CO₂. Cette biomasse a également la particularité d'être entièrement valorisée, ce qui en fait une ressource adaptée pour une chimie plus respectueuse de l'environnement et durable.

Outre les aspects environnementaux, le développement récent des biotechnologies pour la production des microalgues fourni l'accès à des nouveaux synthons biosourcés. Les triglycérides notamment, sont généralement plus longs (jusqu'à 22 carbones) et contiennent plus d'insaturations (jusqu'à 6) par rapport aux huiles végétales. La formation de polyols à partir d'huiles de microalgues a été précédemment étudiée par époxydation suivi par l'ouverture de cycle (Arbenz et al. 2017; Petrović et al. 2013) ou par hydroformylation (Pawar et al. 2016a). Ces études préliminaires ont démontré tout le potentiel de l'huile de microalgues pour constituer des polyols biosourcés performants pour l'élaboration de mousses polyuréthanes.

L'objectif de ce chapitre est d'étudier en profondeur l'impact des polyols biosourcés issus d'huile de microalgues sur les propriétés finales des mousses polyuréthanes. Les polyols sont synthétisés à partir de l'huile de microalgues par époxydation puis ouverture avec divers nucléophiles. Ces polyols sont entièrement caractérisés. Ils se substituent ensuite à un polyol fossile conventionnel jusqu'à 75%, dans une formulation de mousse polyuréthane. Après mise en œuvre, la morphologie, les propriétés mécaniques et thermiques des nouvelles mousses sont mesurées, analysées, commentées et comparées à une mousse de référence composée uniquement de polyol conventionnel fossile.

Biobased Polyurethane foams based on new polyols architectures from microalgae oil

Julien Peyrton, Clémence Chambaretaud, Alexandru Sarbu and Luc Avérous

Article published in *ACS Sustainable Chemistry & Engineering* in 2020, Vol. 8, page 12187

1. ABSTRACT

Environmental concerns continuously drive research to find alternatives to fossil-based constituents in a greener way. Industrial polyurethane foams are usually obtained from the polyaddition reaction between fossil-based polyols and polymeric 4,4'-methylene bis(phenyl isocyanate). The very recent development at the industrial scale of microalgae production provides accessibility to original building blocks and new macromolecular architectures. In this study, the green chemistry principles were highly prioritized to synthesize different polyols from microalgae oil. The resulting microalgae derived polyols were structurally, chemically and physically characterized, and then compared. Polyurethane foams were synthesized using a conventional fossil-based polyol substituted incrementally by microalgae derived polyols. The corresponding cellular materials were extensively characterized in terms of reactivity, morphology and performances, and then compared to conventional foams. A new biobased foam formulation containing 25 wt% biobased polyols matched the compliance levels of a fossil-based reference foam. For the first time, a catalyst-free foam with a similar density as the reference was achieved with a biobased triglyceride catalytic polyol.

2. INTRODUCTION

Nowadays, our society is facing severe and urgent challenges. Among them, there is climate change, the depletion of some fossil resources and environmental degradation. To address these challenges, industries and academics of the material science community focus their research on the use of renewable sources. This recent trend is also driven by the development of new molecular architectures that can be extracted from various types of biomass. Nevertheless, these developments must be done without competition with food resources. In this way, the growth of engineered microalgae technology seems to fulfill this requirement.

Microalgae are unicellular photosynthetic organisms cultivated without the mobilization of arable land. The cultivation can be conducted in fresh, sea and waste-water using CO₂ as raw materials (Fabris et al. 2020). Microalgae are a diverse family with an estimated 20-800 000 different species (Oncel 2013), which can be engineered to biosynthesize particular unsaturated lipids and fatty acids

compared to the conventional ones obtained from plants (Zhu et al. 2016). Lipids are mainly composed of triglycerides with fatty acid chemical structures that vary in terms of length (number of carbons), number of double bonds and with or without the presence of reactive groups such as epoxides or hydroxyl groups. The tremendous potential of lipids accumulation (Syrpas and Venskutonis 2020) of this resource captivates the interest of the biodiesel industry (Becker 2008; Olivieri et al. 2014; Ugwu et al. 2008) to supplant the 2nd generation biodiesel, based on residues and non-edible crops. The advantages of the microalgae are the low production cost, sustainability, (Gordon and Polle 2007; Rawat et al. 2013) no competition with food and high productivity (Brennan and Owende 2010). The microalgae market is not limited to the production of lipids for biodiesel production; all biomass components can be valorized (Wijffels et al. 2010). Lipids, carbohydrates, proteins and minerals are transformed into monomers (e.g. lactic acid, diols) (Roesle et al. 2014), basic chemicals (e.g. ethanol, butanol, acetic acid) (Abdel-Rahman et al. 2013), added-value products (e.g. iodine, omega fatty acid) (Chew et al. 2017) or pigments (e.g. beta-carotene) (Borowitzka 2013).

As is the case of conventional vegetable oils, the fatty acid composition of microalgae is species and growing conditions dependent (Banerjee et al. 2018, 2016; Negrell et al. 2017). In comparison to vegetable oils derived from agricultural resources, microalgae oil (MAO) fatty acids can contain longer unsaturated chains, up to 24 carbons long. The triglyceride structure offers high functionality, which is often required in thermoset polymer synthesis (Galià et al. 2010). Then, a large variety of macromolecular architectures can be obtained.

The Oleochemistry produces biobased polyols mainly from vegetable oil, e.g., for polyurethanes (PU). This production based on several steps is now worldwide developed (Maisonneuve et al. 2016; Petrovic 2008; Pfister et al. 2011). For such a synthesis, epoxidation of the double bond is efficient and industrially accessible. The epoxide group can undergo a ring-opening reaction by several nucleophiles, leading to a myriad of biobased polyols (Biswas et al. 2005; Guo et al. 2000; Palaskar et al. 2012). Different PU morphologies can be tailored according to the used polyols. For example, PU foams (PUF) are obtained from a blowing agent expansion during the polyaddition between a polyisocyanate and a polyol. The substitution of fossil-based polyols in PUF has received significant attention due to environmental and economic concerns (Furtwengler and Avérous 2018). The synthesis of polyols for PUF derived from MAO has been only scarcely explored via two main pathways: i) epoxidation and ring-opening by methanol (Arbenz et al. 2017; Petrović et al. 2013), ethylene glycol (Pawar et al. 2016a) and lactic acid (Pawar et al. 2016a), and ii) hydroformylation (Petrović et al. 2013). The high potential of this bioresource for PUF has mainly been demonstrated through these preliminary studies. Complete and transversal studies from the elaboration to the full evaluation of the morphology and behavior of PUF were marginal in the literature.

The objective of this work is to present a complete and transversal study from the synthesis to an extensive characterization of biobased PUF with closed-cells using MAO derivatives in connection with potential applications. MAO chemical transformations were realized following, to the best extent, the main principles of green chemistry. In this approach, the numerous carbon-carbon double bonds in this oil were converted into epoxides to yield epoxidized microalgae oil (EMAO). This step was followed by the ring-opening reaction by the respective use of acetic acid (AA), diethylamine (DEA), ethanol (EtOH) or hydrochloric acid (HCl) to yield the corresponding biobased polyols. The biobased polyols synthesized were extensively characterized, most notably in terms of viscosity, molar mass, functionality, hydroxyl, epoxide and acid content. The biobased polyols were used in combination

with a fossil-based polyether polyol for the elaboration of PUF. In the first set of experiments, 25 wt% of the fossil-based polyol was replaced by the respective newly synthesized biobased polyols for foam elaboration. In a second set 25, 35, 50 and 75 wt% of fossil-based polyol were exclusively substituted by one biobased derived polyol. A catalyst-free foam was achieved by the replacement of the conventional catalyst by a catalytic polyol synthesized by the ring-opening reaction of epoxidized soybean oil (ESO) by diethylamine. The PUF results were compared to an industrial fossil-based PUF reference in terms of foaming reactivity, cell size and density. In order also to evaluate this global and transversal process based on several green principles, the best performing biobased foams from microalgae were also characterized mainly in terms of performance by mechanical, thermal conductivity and flammability tests and indicated several perspectives for several potential applications.

3. EXPERIMENTAL SECTION

3.1. Materials and chemicals

MAO was kindly supplied by Fermentalg (France) and was extracted from microalgae (*Schizochytrium sp.*). The microalgae were cultivated in a 180 m³ reactor in the dark with an external carbon source for energy (heterotrophic system). After cultivation, the unicellular biomass was lysed to liberate the lipids, which were then isolated by centrifugation. The process was carried out under a nitrogen (N₂) atmosphere to prevent the oxidation of the oil. The double bond content of MAO was 336 g I₂/100 g (13.2 mmol double bond/g). The fatty acid composition of the unsaturated MAO was presented in Table S3.6 in supporting information (SI). Glacial acetic acid, toluene (99%), ethyl acetate (99%), methyl ethyl ketone (MEK), diethyl ether, cyclohexane, sodium thiosulfate, potassium iodide and Wijs solution were obtained from Fisher Scientific (France). Amberlyst® 15H (strongly acidic cation exchanger dry), CDCl₃, HCl (37% in water), diethylamine (99%) and 2-chloro-4,4,5,5-tetramethyl-1,3,2-dioxaphospholane were provided by Sigma-Aldrich (France). Absolute ethanol was purchased from VWR (France). Commercially available ESO Weepox01 was provided by Brenntag (Germany).

The polyisocyanate used is the polymeric 4,4'-methylene bis(phenyl isocyanate) identified as pMDI (NCO index = 31%), Desmodur 44V70L from Covestro (Germany). N,N-dimethylcyclohexylamine (DMCHA) provided by Sigma-Aldrich (France) was used as a balanced catalyst between blowing and gelling reactions. Tegostab B84501 from Evonik (Germany), a polyether polysiloxane copolymer, was used as a surfactant. Tris(1-chloro-2propyl) phosphate (TCPP, Shekoy-China) was used as a flame retardant. Isopentane (boiling point 28 °C) (Inventec-Dehon-France) and demineralized water were used as a physical and chemical blowing agent, respectively. Daltolac R570 (Huntsman-Germany) was used as the reference fossil-based polyether polyol. It is mainly composed of alkoxylated glycerol.

All chemicals were used without any purification.

3.2. Triglyceride modifications to obtain polyols

The epoxidation of MAO (1 eq.) was performed by ITERG (France) via an in-situ peracid formation using formic acid (0.33 eq.), toluene (0.5 L/kg of MAO) and H₂O₂ (2.5 eq.) according to a previously described protocol (Arbenz et al. 2017; Petrović et al. 2013). The resulting EMAO was obtained with a 74 wt% yield. Polyols were obtained by ring-opening of EMAO by AA, HCl, DEA or EtOH to yield the corresponding respective polyols: EMAO-AA, EMAO-HCl, EMAO-DEA or EMAO-EtOH. The detailed synthesis procedures of the polyols are given in SI.

3.3. Foam synthesis

The isocyanate/hydroxyl molar ratio (NCO/OH) was set at 1.15 in all formulations. Every reactive hydroxyl in the formulation was accounted for, i.e., water and polyols, to determine the isocyanate quantity. The isocyanate group is very reactive with water present in the air. The polyisocyanate was introduced in excess to counter the side reaction with air humidity and maximize the conversion of hydroxyl into urethane. The fossil-based polyol was progressively replaced in weight by biobased polyols. Foams were prepared via an A-B composition. In a plastic cup, the A-part consists of the polyol mixture, the catalyst (DMCHA), the surfactant (polyether polysiloxane copolymer), the flame retardant (TCPP), the physical (isopentane) and chemical (water) blowing agents. They were weighed and mixed using a mechanical stirrer. The water, TCPP and surfactant were kept constant at 1.6, 10 and 2.5 parts by weight (pbw), respectively. The isopentane content was determined to obtain foams with similar densities. The B-part containing the polyisocyanate is quickly added. The final mixture is vigorously stirred with a mechanical stirrer for 5 seconds, and the foam is let to rise freely in a plastic cup for the reactivity study or poured into a mold for other characterizations. The foams were kept for one week at room temperature and 50% Relative humidity (RH) to allow the system to cure before analysis and to be stabilized.

3.4. Characterizations

3.4.1. Polyol analysis

The ¹H NMR analyses were realized on a 400 MHz Bruker spectrometer. Deuterated chloroform (CDCl₃) was used as solvent to prepare the samples. The ¹H NMR number of scans was set to 32. Each spectrum was calibrated with the CDCl₃ signal, being set at δ =7.26 ppm.

Iodine value (IV) is the measure of the double bond content expressed in grams of iodine (I₂) per hundred grams of sample. It was determined using the Wijs method. Approximately 200 mg of precisely weighed sample was diluted in 10 mL of cyclohexane:acetic acid (1:1) solution. Then, 20 mL of Wijs solution composed of 1.0 M of iodine chloride in acetic acid was added. The solution was left in a dark place for one hour. 20 mL of potassium iodide solution in water and 100 mL of water were added to quench the excess of potassium iodide. The solution was then rapidly titrated with a 0.1 mol/L solution of sodium thiosulfate (Na₂S₂O₃). Starch was used as an indicator. IV is determined according to Equation 3.1.

$$IV = \frac{(V_{Bl} - V_{eq}) * C_{TS} * 126.9}{W_s} * 100 \quad (3.1)$$

Where V_{Bl} is the blank equivalence volume, V_{eq} the equivalence volume, C_{TS} the concentration of the thiosulfate solution, 126.9 half of the molar mass of iodine molecule and W_s the sample weight.

Epoxide index (EI) is expressed in wt% of oxygen in the form of epoxides in the fatty compound. In an Erlenmeyer flask, between 150 and 200 mg of sample was precisely weighed and dissolved in 5 mL of MEK. Exactly 10 mL of 0.4 mol/L HCl solution in MEK was added. The flask was closed and left to react at ambient temperature under magnetic stirring for 30 min. Then 3 mL of water was added. The excess of HCl is titrated with 0.1 mol/L KOH solution. Phenolphthalein was used as the equivalence indicator. The epoxide index is determined according to Equation 3.2.

$$EI = \frac{(V_{Bl} - V_{eq} + V_{Ac}) * C_{KOH} * 16}{W_s * 10} \quad (3.2)$$

Where V_{Bl} is the blank equivalence volume, V_{eq} the equivalence volume, V_{Ac} the volume of acid titration (without adding HCl solution), C_{KOH} the concentration of the KOH solution, 16 is the molar mass of oxygen and W_s the sample weight.

Acidity index (I_A) is expressed in milligrams of KOH required to neutralize all acid moieties in one gram of oil. Between 1 and 3 grams of sample was weighed in a beaker and dissolved with a 1:1 solution of ethanol:diethyl ether. The solution is directly titrated with a 0.1 mol/L KOH solution. Phenolphthalein is used as the equivalence indicator. The I_A is calculated according to Equation 3.3.

$$I_A = \frac{V_{eq} * C_{KOH} * 56.1}{W_s} \quad (3.3)$$

Where V_{eq} the equivalence volume, C_{KOH} the concentration of the KOH solution, 56.1 the molar mass of KOH and W_s the sample weight.

Hydroxyl index (I_{OH}) is a key parameter in polyol characterization. It is expressed in milligrams of KOH equivalent to OH content in one gram of polyol. I_{OH} can be determined by ^{31}P NMR-assisted titration method (Argyropoulos et al. 1993). According to a previously described protocol (Korntner et al. 2015), approximately 20 mg of precisely weighed sample precisely weighted was diluted in 500 μ L of 1:1.6 $CDCl_3$ /pyridine mixture, 100 μ L of 0.01 mol/L cholesterol solution (internal standard) and 100 μ L of chromium acetylacetonate [$Cr(acac)_3$; 5 mg/mL] (relaxation agent) was added. After thorough mixing, 100 μ L of 2-chloro-4,4,5,5-tetramethyl-1,3,2-dioxaphospholane (phospholane reagent) was added to the solution. The sample was stirred at room temperature for one hour and then transferred into an NMR-tube. ^{31}P NMR analyses were performed with the use of a Bruker 400 MHz spectrophotometer, and the number of scans was set to 128 at 25 °C. Peak analysis and quantitative analysis were performed according to previous reports (Dais and Spyros 2007).

Rheological measurements were carried out on a TA instrument discovery HR-3 using parallel plate geometry. The viscosity was measured with a shear rate varying from 10^{-5} to 100 s^{-1} in 5 min, and after 10 min of rest, the shear rate varied from 100 to 10^{-5} s^{-1} in 5 min. The viscosity values were taken at the plateau region for different temperatures.

The polyols functionality was determined based on the Flory-Stockmayer (Flory 1941; Stockmayer 1944) equation applied to a reaction between a polyisocyanate and a polyol, described in Equation 3.4.

$$r^* p_{NCO} = \frac{1}{(f_{OH} - 1)(f_{NCO} - 1)} \quad (3.4)$$

This equation mathematically explains the relation at the gel point between the molar ratio of OH over NCO (r), the isocyanate conversion at the gel point (p_{NCO}) and the average functionality of the monomers (f_{OH} and f_{NCO}). The equation relies on three hypotheses (i) all functions are equally reactive, (ii) there is no intramolecular reaction and (iii) the network is only formed by the reaction between the polyol and the isocyanate. The hydroxyl is in excess so that the conversion of isocyanate is complete. Moreover, the use of a diisocyanate transformed Equation 3.4 to Equation 3.5.

$$r = \frac{1}{(f_{OH} - 1)} \quad (3.5)$$

A series of materials with different r ratios were produced. The full conversion of isocyanate was controlled by FTIR and the disappearance of the band associate to isocyanate at $\tilde{\nu}=2260-2240 \text{ cm}^{-1}$. The rheological behavior at the gel point was described by Winter & Chambon (Chambon and Winter 1987; Winter and Chambon 1986). The rheological experiments were performed on a TA Instrument Discovery HR-3 using parallel 20 mm geometry. The samples were analyzed in oscillatory conditions, applying a strain of 0.1% between 0.01 and 80 Hz. The linear viscoelastic domain conditions were determined before the functionality determination by applying a strain from 0.001% to 5% at a frequency of 80 Hz on a sample with equimolar component ($r = 1$). For $r = 1$, one should obtain the most cross-linked material, which translates into the most brittle sample.

The size exclusion chromatography (SEC) experiments were performed with an Acquity-APC (Waters) in tetrahydrofuran (THF) equipped with three columns (Acquity APC XT 450 Å 2.5 μm 4.6 x 150 mm, 200 and 45) heated at 40 °C. Before the injection, samples were dissolved in THF and filtered with a 0.2 μm PTFE membrane. Polystyrene standard samples were used for the molar mass calibration.

3.4.2. Foam analysis

The main foam characteristic times are the cream time (the beginning of the foam rising initiated by the water-isocyanate reaction), the gel time (linked to the formation of the thermoset network) and the tack-free time (time to cure the surface), which were recorded for each foam. Core temperature, foam height and expansion rate were recorded using a Foamat FPM 150 (Messtechnik GmbH, Germany). The apparatus was equipped with a cylindrical container (180 mm in height and 75 mm in radius), an ultrasonic probe (recording with ultrasound waves the foam height), a Pt sensor (for the temperature). The data were recorded and analyzed using dedicated software.

Closed-cell content was determined using an Ultrapyc 1200e from Quantachrome instruments based on the technique of gas expansion (Boyle's law). Cubic foam samples (roughly 2.5 cm x 2.5 cm x 2.5 cm) were cut for the first measurement, then the sample was sectioned once more into eight pieces, and measurement was re-run to correct the closed-cell content based on closed cells which were cut open during slicing. Measurements were performed according to EN ISO4590 and ASTM 6226 techniques.

Parallelepipedic foam samples were measured with a caliper and weighed to determine the apparent foam density.

Attenuated total reflection (ATR) Fourier transform infrared spectroscopy (FTIR) spectra were recorded on Thermo Scientific Nicolet iS210 instrument using a Smart Orbit Diamond. An atmospheric background was collected before each sample analysis (32 scans, resolution 4 cm⁻¹).

Foam cell morphology was observed with a Vega-3 (Tescan) emission scanning electron microscope. Cubic foam samples were cut with a microtome blade and were analyzed in two characteristic orientations: parallel and perpendicular to the foam rise direction denoted as longitudinal and transversal direction, respectively. Before the examination, samples were coated with a thin layer of gold using a sputter coater (Quorum Q 150 RS, Quo-rum Technologies). Using ImageJ software (Open source program), the cell average size was measured as well as the cell anisotropy coefficient defined by Equation 3.6 (Andersons et al. 2016).

$$R = \frac{1}{n} \sum_{i=1}^n \frac{D_{iF}^{\max}}{D_{iF}^{\min}} \quad (3.6)$$

Where D_F^{max} and D_F^{min} are the maximum and minimum cell Feret diameters and n is the number of measured cells for a given sample. The number of measured cells is ranging from 200 to 1500 in both directions.

Thermogravimetric analysis (TGA) was performed using a TA Instrument Hi-Res TGA Q5000 under N₂ (flow rate 25 mL/min). Samples of 1–3 mg were heated from room temperature to 700 °C at 10 °C/min. The main characteristic degradation temperatures were determined at the maximum of the derivative of thermogravimetric (DTG) curve.

Foam fire behavior was evaluated according to the EN ISO 11925-2 standard method. This flammability test consists of exposing a plane foam sample for 15 seconds to a small direct flame (20 mm high). This flammability test is evaluated by measuring the maximum flame propagation on the plane surface of the foam. The persistence of flame on samples after exposure to the direct flame was timed.

The quasi-static compression tests were carried out with an Instron 3367 compression testing machine, equipped with a 30 kN load sensor, at room temperature and constant strain rate of 6 mm/min. The sample size for the compression test was 100 mm x 100 mm x 60 mm. Samples were compressed in the longitudinal direction (corresponding to the foam rise) until 10% of deformation is reached. The test was realized according to the EN 826 standard method, and the data were recorded and analyzed using the Bluehill 3 software.

Thermal conductivity measurements were carried out with a Heat flowmeter HFM 436 from Netzsch. The measurements were performed according to the EN 12667 standard procedure. Typically, the setup consists of a hot and a cold plate equipped with two thermocouples to determine their temperatures. The device is also equipped with sensors dedicated to the measurement of the heating time and the cycle time. The heat and cycle times were used to correct the maximum conduction heat flux, which is necessary for the determination of the thermal conductivity coefficient, through the Fourier law, assuming steady-state thermal condition. Specimens of different foams, with dimensions of 175 mm x 175 mm x 60 mm, have been used for the determination of the thermal conductivity coefficient. The data were recorded and analyzed using QLab software.

4. RESULTS AND DISCUSSION

4.1. Polyol synthesis

The oil extract from microalgae is an orange liquid with a marine smell. The highly unsaturated triglycerides structure explains the color. The MAO fatty acid composition was determined by gas chromatography and presented in Table S3.6 in SI. The predominant fatty acids in MAO were docosahexaenoic (C22:6) (60%), palmitic (C16:0) (22%) and docosapentaenoic (C22:5) (10%) acids. The ^1H NMR of MAO is shown in Figure 3.1, with the corresponding peak assignments of an ideal structure composed of the three primary fatty acids. The triglyceride structure is identified by glyceral protons (i) and (h) at δ =5.3 ppm and 4.1-4.4 ppm, respectively. The signal at δ =0.88 ppm (a) is characteristic of the terminal methyl groups of fatty acids. When a double bond is located at the third carbon from the terminal methyl group (omega-3 acid), this group signal appeared downfield at δ =0.97 ppm (a'). The methylene protons (b) were located between δ =1.2 and 1.4 ppm. Signals of protons in the vicinity of the carbonyl groups (c) and (e) were observed at δ =1.6 and 2.3 ppm, respectively. In the case of C22:6 or C22:5 the vicinity of the double bond shifts those signals downfield at δ = 2.4 ppm (f). Allyls protons positioned between two double bonds (g) were located at δ =2.8 ppm. The vinyl protons, (j) were located at δ =5.4 ppm. According to NMR calculation, the average double bond functionality of MAO is 12. FTIR spectrum of MAO presented in Figure S3.8 in SI shows C=O stretching characteristic band of the ester group at $\tilde{\nu}$ =1742 cm^{-1} . The C=C and C=C-H vibration bands were located at $\tilde{\nu}$ =3012 and 1652 cm^{-1} , respectively.

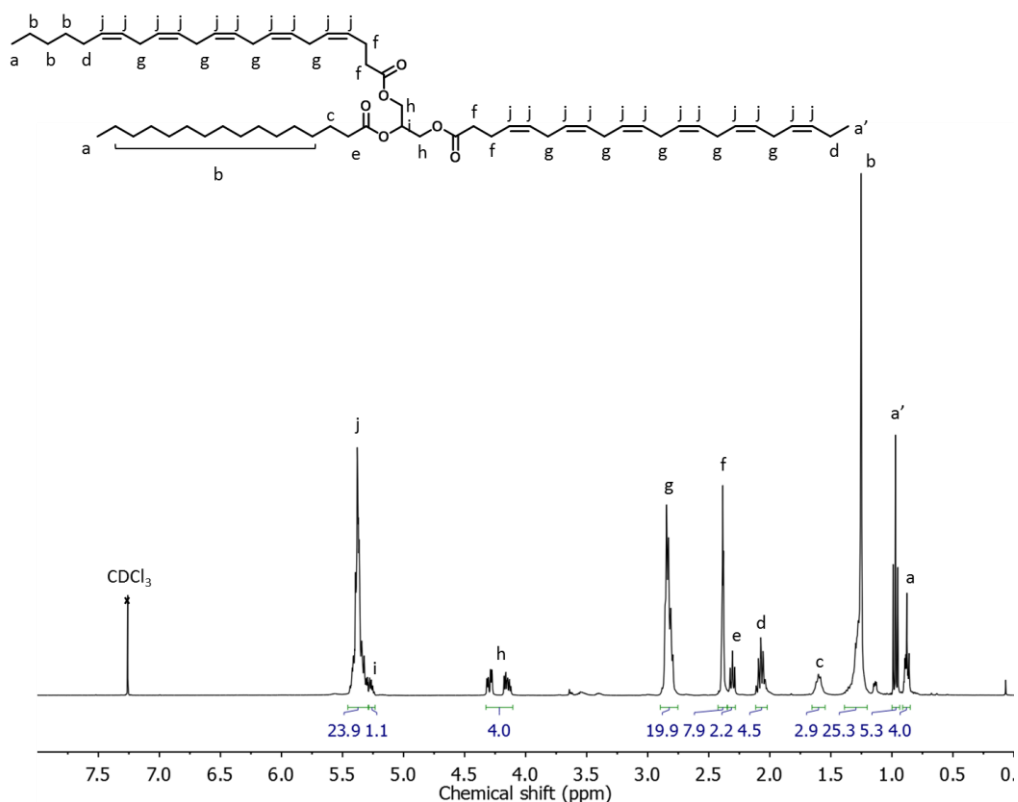


Figure 3.1 - ^1H NMR spectrum of MAO.

At first, MAO obtained from microalgae was epoxidized via the in-situ formation of performic acid to obtain an odorless, yellowish waxy product (EMAO). The NMR analysis of the EMAO structure is detailed in Figure S3.9 in SI. The successful epoxidation of the double bonds is indicative of the substantial decrease of vinyl protons at $\delta=5.4$ ppm and the appearance of the epoxide signal at $\delta=2.8-3.2$ ppm. According to NMR calculations, 80% of double bonds were transformed into epoxide groups, 6% were epoxidized and underwent ring-opening by the water in the medium and 14% were unconverted (Table S3.7 in SI). The transformation of the double bonds into epoxides is performed at the oil-water interphase. The incomplete reaction can be explained by the difficulty for the performic acid to access all the double bonds linked to the polyunsaturated MAO structure. The reaction can be further hindered by the increasing viscosity of the oil phase during the reaction. The reaction temperature was set at 70 °C to favor the epoxide formation, all the while minimizing further ring-opening with water (Arbenz et al. 2017).

EMAO was used as a starting material to build a chemical platform of several polyols via ring-opening reactions using of different nucleophiles including: ethanol (EMAO-EtOH), acetic acid (EMAO-AA), hydrochloric acid (EMAO-HCl) or diethylamine (EMAO-DEA). The detailed synthesis procedures of the polyols are given in SI. The ring-opening reactions were carried out to adhere to the best possible extent to the principles of green chemistry. In addition to the MAO, several ring-opening reagents can be biobased (EtOH and AA). The principle of atom economy was applied in all syntheses to achieve polyols. Reactions were carried in reactive solvents, except for EMAO-HCl, where the minimum amount of acetone (1.2 mL/g) was used. For the synthesis of EMAO-EtOH and EMAO-DEA, heterogeneous catalysts were used and can be recovered and re-used. The resulting polyols were then used without further purification from any side-products in order to minimize the generation of additional waste, in agreement with some principles of green chemistry. Green chemistry is an essential tool for the design of sustainable molecular architectures (Anastas and Eghbali 2010). The application to the best possible extent of the green chemistry principles was achieved, most notably by atom economy, catalysis, use of renewable feedstock and minimized use of solvents.

The synthesized polyols were characterized by the following characterizations: I_{OH} , EI and I_A , functionality, viscosity, melting temperature and TGA, and these results are summarized in Table 3.1. The I_{OH} was determined by ^{31}P NMR titration using 2-chloro-4,4,5,5-tetramethyl-1,3,2-dioxaphospholane as phospholane reagent. Detailed ^{31}P NMR spectra of the polyols are available in Figure S3.10 in SI. The phospholane reagent is also reacting with epoxides, and the suggested mechanism is described in Scheme S3.2 in SI. The ^{31}P NMR titration quantifies the sum of the epoxide and hydroxyl groups.

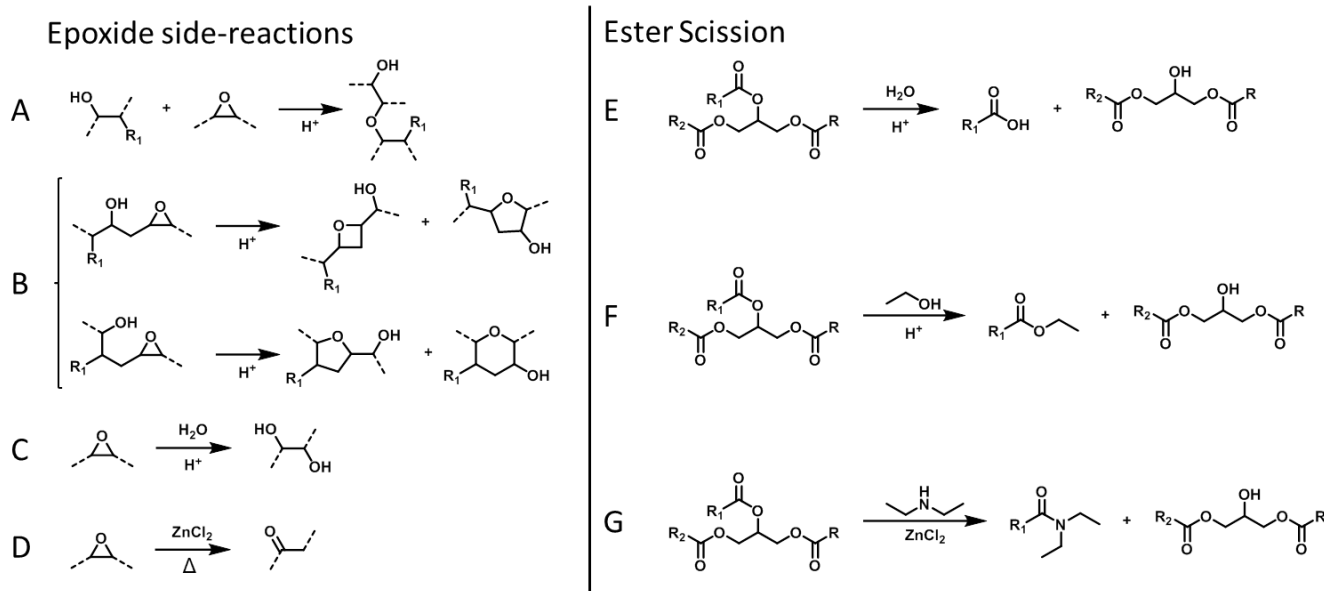
Table 3.1 - Characteristics of the different polyols: fossil-based, MAO and their derivates.

Polyol	I _{OH} exp (mg KOH/g)	I _{OH} th (mg KOH/g)	OH molar yield (%)	EI %	Functionality	I _A (mg KOH/g)	Viscosity at 25 °C (Pa.s)	Melting temperature (°C)	DTG peak ¹ (°C)
Daltolac									
R570	570 ± 10				3.0		0.70 ± 0.07		
(fossil-based)									
MAO					12 ²		0.10 ± 0.01	0 ± 10	412 ± 10
EMAO				10 ± 0.2	10 ²		900 ± 90	10 ± 10	298 ± 10
EMAO-EtOH	260 ± 10	410	63	0.03 ± 0.002	7.6 ± 0.6	1.8 ± 0.1	3400 ± 300	30 ± 20	315 ± 10
EMAO-AA	70 ± 10	370	19	0.30 ± 0.02	2.4 ± 0.1	21.8 ± 0.1	300 ± 30	24 ± 10	332 ± 10
EMAO-HCl	180 ± 10	440	41	0.60 ± 0.03	5.0 ± 0.5	9.4 ± 0.1	(5.3 ± 0.5)*10 ⁴	40 ± 10	365 ± 10
EMAO-DEA	130 ± 10	340	38	0.30 ± 0.02	4.7 ± 0.3	NA ³	(3.8 ± 0.4)*10 ⁶	45 ± 15	311 ± 10

¹ Determined by the higher value of DTG ² Determined by NMR ³ The basicity of the amine is superior to the acidity index

The EMAO has an EI of 10%. The polyol synthesis was monitored by epoxide titration. The reactions were stopped when more than 90% of epoxide groups were consumed. The nearly complete reaction of the epoxide groups was confirmed by the low final EI values depicted in Table 3.1. As previously discussed, the I_{OH} determined by ³¹P NMR does not differentiate between epoxide and hydroxyl groups. The epoxide contribution to the ³¹P NMR determined I_{OH} of polyols is then negligible. The ³¹P NMR measured I_{OH} is then predominantly accounting only for hydroxyl groups for the synthesized polyols. The disappearance of the epoxide stretching band located at $\tilde{\nu} = 826 \text{ cm}^{-1}$ on the FTIR spectra of polyols, depicted in Figure S3.11, is indicative of the total epoxide consumption. Furthermore, the appearance of the OH stretching band at $\tilde{\nu} = 3400 \text{ cm}^{-1}$ is indicative of the formation of hydroxyl groups.

For all the polyols synthesized, the conversion of epoxide to hydroxyl groups should be expected to be higher. However, during ring-opening reactions, side reactions can occur, as presented in Scheme 3.1. First of all, under acidic conditions (Lligadas et al. 2006a) or with a coordination agent (Del Rio et al. 2010), hydroxyl groups already formed can protonate and attack an epoxide on another molecule, leading to homopolymerization (Scheme 3.1-A). Under milder acidic conditions, only oligomers were formed. Wang *et al.* demonstrated ether oligomers formation by ring-opening of a fatty epoxide by carboxylic acid (Miao et al. 2008). Furthermore, the proximity of the epoxide on the EMAO molecules could lead to an intramolecular attack (Scheme 3.1-B). Depending on the ring-opening position and attack of the hydroxyl, 4, 5 or 6 membered cyclic ethers could be formed. The low-intensity peaks detected between $\delta = 3.2$ and 4.0 ppm in the ¹H NMR spectra, presented in Figure S3.12 and Figure S3.13 in SI, are in the typical range of ether signals. These NMR peaks could be indicative of the epoxide polymerization side reactions and thus accounts as to why such low I_{OH} were observed.



Scheme 3.1 - Side reactions occurring during polyol synthesis.

Another side reaction that can occur under acidic conditions is linked to the epoxide ring-opening by the remaining moisture in the medium (Scheme 3.1-**C**) (Sharma et al. 2006b). However, the hydrophobic character of triglycerides reduces this side reaction (Caillol et al. 2012). Moreover, such a side reaction would increase polyols I_{OH} . On the contrary, the epoxide ring-opening using a secondary amine and catalyzed by $ZnCl_2$ can induce epoxide isomerization (Scheme 3.1-**D**). This side reaction was observed for temperatures superior to 100 °C and $ZnCl_2$ was used as a catalyst (Weissberger 1964). The presence of acid is promoting this side reaction. The side reactions on the epoxide group can explain the average conversion of epoxide to hydroxyl.

The occurrence of side reactions during polyol synthesis can be further observed by SEC characterization. The calibration method for the SEC is defined using the molar mass of a polystyrene standard. The interactions between the columns and the studied samples do not coincide with polystyrene, therefore the exact molar mass was not determined. However, the samples can be studied and compared in terms of retention time. As a reminder, the smaller the molecules are, the higher their retention time will be. As shown in Figure 3.2, MAO and EMAO present a narrow distribution, which corresponds to the unsaturated and epoxidized triglycerides, respectively. Polyols present a broader distribution in molar mass. During epoxide ring-opening, chains with lower molar mass were formed, and this can be due to the ester scission side reactions, as presented in Scheme 3.1. Transesterification (Scheme 3.1-**E** & **F**) (Caillol et al. 2012) and transamination (**G**) (Harry-O'kuru et al. 2015) divide the triglycerides into diglycerides and fatty acids. Only EMAO-EtOH presents a significant portion of high molar masses with retention time close to the one of the EMAO distribution. For a portion of the EMAO-EtOH polyol, the triglyceride structure is conserved. As depicted in Table 3.1, this is confirmed by the average functionality of EMAO-EtOH, which is the highest. Significant portions of low molar masses were formed for EMAO-HCl, EMAO-DEA and EMAO-AA.

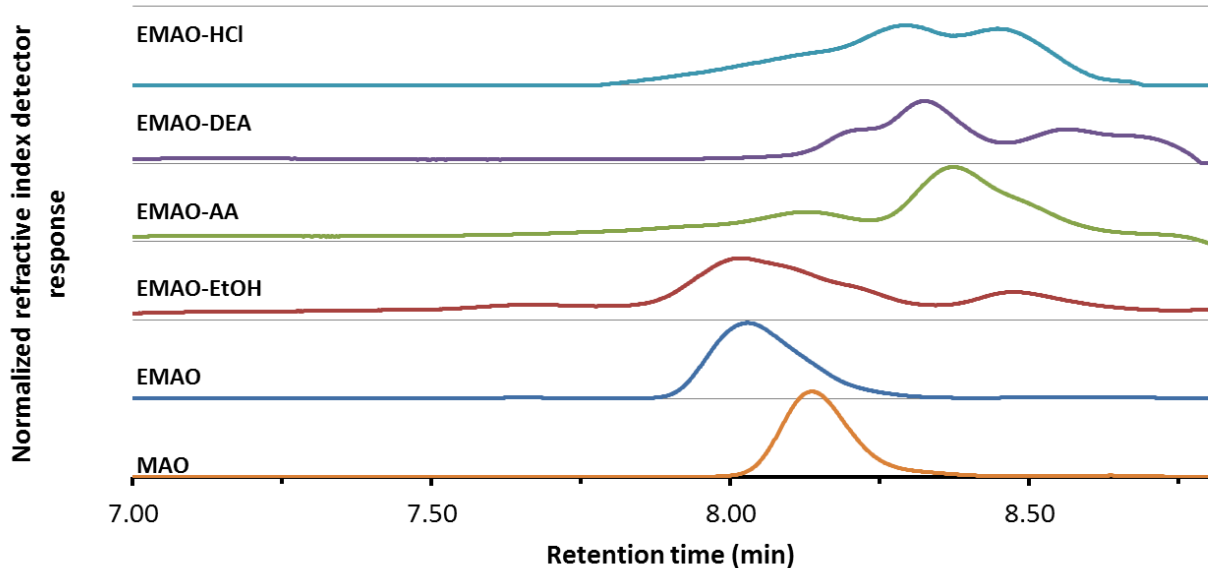


Figure 3.2 - Size exclusion chromatogram of EMAO-HCl, EMAO-DEA, EMAO-AA, EMAO-EtOH, EMAO and MAO.

In the PU industry, polyols are notably characterized by their acidity index. The acids can slow the PU network formation by coordination and thus induce deactivation of catalysts. The the I_A of crude polyols was between 60 and 100 mg KOH/g. Basic washings were performed on the crude polyols using sodium bicarbonate (NaHCO_3) and should have removed most of the residual acid reagents. EMAO-AA and EMAO-HCl acidity index were 21.8 and 9.4 mg KOH/g, respectively. One reason for this high acidity can be related to the presence of fatty acid formed and residual acid reagents used for the polyols syntheses. The fatty acid formation during polyol synthesis via side reactions was also identified by high retention times in SEC characterization. In the case of EMAO-DEA, the tertiary amine present on the polyol structure shielded the acidity. Thus the acidity index could not be performed.

For the PUF synthesis, the viscosity of the polyol plays a crucial role. The quantity of air bubbles trapped in the liquid foam mixture and the diffusion of isocyanate molecules toward polyol is controlled by the viscosity. In the PUF industry, the polyol used are required to have a viscosity preferentially under 50 Pa.s (Ionescu 2005). As stated in Table 3.1, the measured viscosity of the fossil-based polyol is 0.7 Pa.s, and the biobased polyols range from 10^2 to 10^6 Pa.s. The viscosity of all bio-based polyols is high compared to fossil-based polyol. One reason for this high viscosity can be related to the crystalline structure of oils. The crystallization of triglycerides is a complex phenomenon (Gunstone et al. 2007) depending on numerous factors such as the symmetry of the chain, the number of carbon atoms, the interactions between the chains (H-bonding) (Knothe and Steidley 2005) and the fatty acid/diglyceride content (Jacobsberg and Oh Chuan Ho 1976). Differential scanning calorimetry (DSC) experiments realized on MAO, EMAO and the polyols, presented in Table 3.1 and Figure S3.14-19 in SI, show the primary crystallization and melting temperature. Among the EMAO derived polyols, EMAO-AA has the lowest viscosity. According to DSC, it also has the lowest melting temperature, lower than 20 °C. This melting temperature can be explained by the low I_{OH} content in the polyol. On the contrary, the EMAO-DEA has an extremely high viscosity, exhibiting an almost solid behavior at room temperature. This high melting point can be explained by the presence of H-

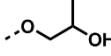
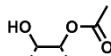
bonding atom, such as nitrogen in the polyol enhancing the crystal stability. The DSC results show a high melting point, superior to 40 °C, which explains the soaring viscosity. The significant thinning effect with the temperature is presented in Figure S3.20 in SI.

The thermal stability of the polyols was evaluated with thermogravimetric analysis. The main degradation temperature, determined at the maximum of the DTG curve of MAO, EMAO and the polyols are presented in Table 3.1. The detailed TGA and DTG results are presented in Figure S3.21-S3.26 in SI. The epoxidation reaction shifted the main degradation from 412 °C for MAO to 298 °C for EMAO. The introduction of a three-membered ring with oxygen increased chain scission and thus induces degradation. EMAO-AA, EMAO-EtOH and EMAO-DEA exhibit similar main degradation temperatures around 320 °C. The main degradation in EMAO-HCl polyols is around 365 °C. This 45 °C difference can be explained by the chlorine introduced in the polyols structure, which could trap radicals in the gas phase, thus limiting initial thermal degradation (Wilkie and Morgan 2010).

4.2. Rate of foams synthesis

The foams were prepared via an A-B composition procedure. The detailed formulations of the studied PUF were presented in Table 3.2. The foams are denoted according to the ring-opening nucleophile used for the polyol synthesis and the weight percentage of fossil-based substituted by the biobased polyol. For example, the foam made with 25 wt% of the fossil-based polyol substituted by EMAO-AA is denoted AA25. The A-part was composed of polyols, a catalyst, a surfactant, a flame retardant and two blowing agents. The catalyst was miscible in the polyol phase, and the surfactant reduced the surface tension between the polyol and the blowing agent phase. The low viscosity of this complex blend was driven by the primary component: the polyol mixture. As previously discussed, the biobased polyols were more viscous than the fossil-based polyol. Furthermore, the biobased polyols were not miscible into the fossil-based polyols at room temperature. To address this issue, each biobased polyol was mixed with a fossil-based polyol in the proportion described in Table 3.2, at 60 °C. The polyol mixture was cooled down to room temperature and then introduced into the A-part as a sole polyol. The B-part composed of the polymeric 4,4'-methylene bis(phenyl isocyanate) (pMDI) was then added to the A-part under vigorous stirring for 5 seconds. The foams were let to rise freely in a plastic cup.

Table 3.2 - Formulation in parts of the total polyol content of the different PUF studied systems.

Foam formulation	Ref	AA 25	DEA 25	EtOH 25	HCl 25	EtOH 35	EtOH 50	EtOH 75
<i>A-Part</i>								
Polyols	Daltolac	100	75	75	75	65	50	25
								
	R570 (fossil-based)							
		EMAO-AA		25				
		EMAO-DEA		25				
		EMAO-EtOH			25		35	50
		EMAO-HCl			25			75
Catalyst ¹	DMCHA ²	2.0	1.76	1.79	1.85	1.81	1.79	1.7
Surfactant	Tegostab B84501	2.5	2.5	2.5	2.5	2.5	2.5	2.5
Flame retardant	TCPP ³	10	10	10	10	10	10	10
Blowing agent	Water	1.6	1.6	1.6	1.6	1.6	1.6	1.6
	Isopentane	15.0	12.4	12.7	13.4	13.0	12.7	11.8
<i>B-Part</i>								
Isocyanate	pMDI	168	155	158	168	162	159	145
								122

¹ Catalyst was set at 1.5 wt% in all formulations ² N,N-dimethylcyclohexylamine ³ Tris(1-chloro-2propyl) phosphate

The expansion behavior of PUF was first evaluated by two methods. The first method is the determination of characteristic times during PUF formation such as the cream, gel and tack-free times. The second method is based on temperature and expansion rates recorded with a Foamat device. As a reminder, the results of PUF foams containing biobased polyols were compared to a reference containing solely a fossil-based polyol formulation, identified as Ref. Figure 3.3 and Table S3.8 in SI present the PUF formation characteristic times. Characteristic times of Ref were 12, 47 and 62 seconds for cream, gel and tack-free time, respectively. The cream, gel and tack-free times were higher with the biobased polyols except in the case of EMAO-DEA polyol. The slow reactivities of HCl25 and AA25 were further confirmed by the corresponding increased expansion rates (Figure 3.4 and Figure S3.27 in SI). The lower reactivity of the biobased polyols can be explained by the hydroxyl group

position, which was in the middle of a hindered chain. Moreover, the hydroxyl groups of the biobased polyols are secondary hydroxyls, whereas the fossil-based polyol contains primary hydroxyls and have an increased reactivity to isocyanate groups. The gel time of EMAO-DEA was 12 seconds faster than the Ref. The epoxide ring-opening with secondary amine forms tertiary amine in beta position of the hydroxyl. This tertiary amine included on the polyol catalyzes the reaction between isocyanate and hydroxyl groups (Peyrton et al. 2019). The expansion rate of DEA25 detailed in Figure 3.4, confirms the acceleration of the blowing reaction.

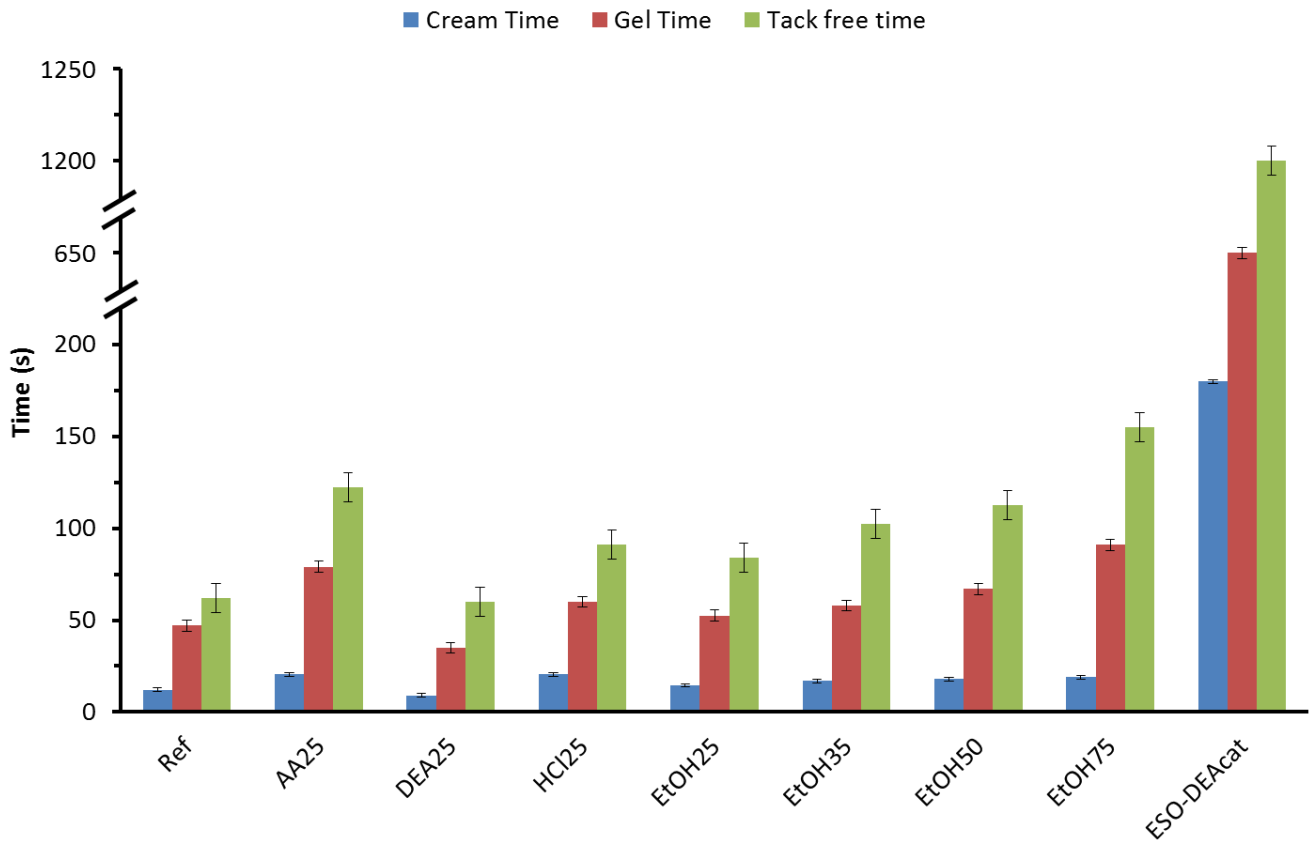


Figure 3.3 - Characteristic times of the different foams. The y-axis was broken since the gel time and tack-free time of ESO-DEAcat surpass 600 s and 1200 s, respectively.

The substitution of 25 wt% of fossil-based polyol by EMAO-EtOH in a PUF formulation has little influence on the foam reactivity. The corresponding lower I_{OH} value seems to be balanced out by the higher functionality of this biobased polyol. The transition between 25 to 75 wt% of EMAO-EtOH in PUF results in an increased gel time from 53 to 91 seconds. PUF made with increasing amounts of EMAO-EtOH were less reactive than the reference. This is confirmed by the expansion profiles of these PUF (Figure S3.27 in SI), where the peak of the expansion rate was delayed in time. Moreover, the maximum rate and acceleration were lower than the Ref PUF. With increase weight substitution of EMAO-EtOH, the lower I_{OH} became critical for the reactivity of the PUF.

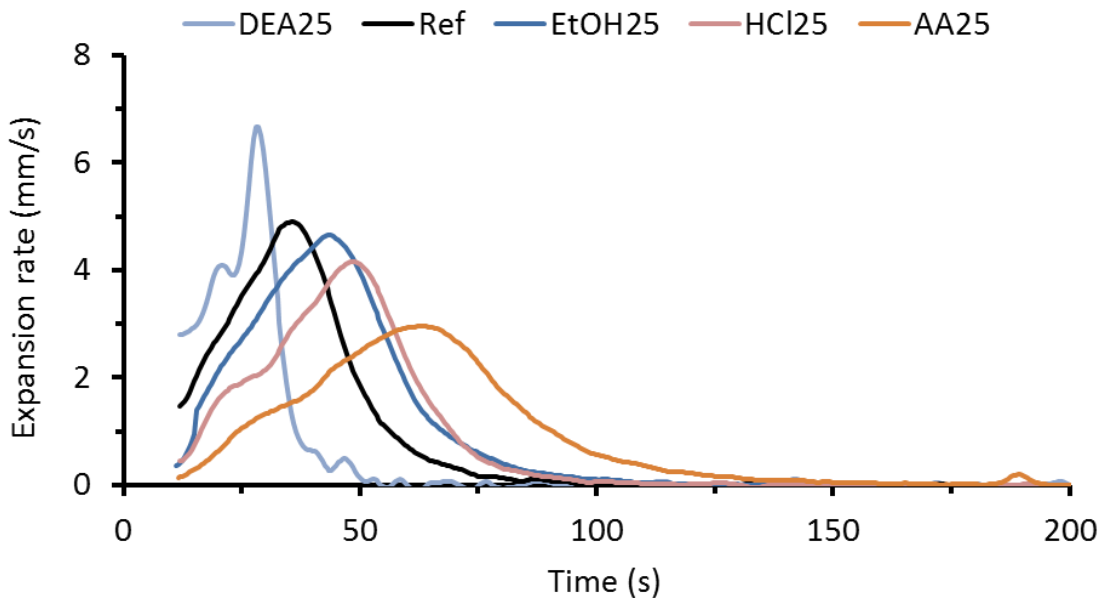


Figure 3.4 - Expansion rates (mm/s) determined with Foamat device for DEA25, Ref, EtOH25, HCl25 and AA25.

4.3. Analysis of the foam cell morphology

The cell morphology of PUF foams impacts their mechanical and thermal properties directly. The anisotropic coefficient (R) presented in Figure 3.5 is a parameter of the cells shape of the foams observed by microscopy. The R coefficients range between 1 (spherical cell) and 2 (ellipsoidal cell) (Furtwengler et al. 2018b). The cells were elongated in the longitudinal (parallel to the foam rise direction, Figure 3.5A) direction, as shown by a higher anisotropy coefficient of 1.6. Cells stretched in the longitudinal direction were characteristic of a partially free foaming process performed in an open cylindrical mold (Hawkins et al. 2005). For the reference PUF, in the transverse direction (perpendicular to the foam rise direction, Figure 3.5B), R was between 1.2 and 1.3, relatively close to a spherical cell. The emission scanning electron microscope (SEM) images of Figure 3.6 and Figure S3.28 in SI exemplify the spherical and ellipsoidal cell shapes in the transverse and longitudinal direction, respectively. The substitution of the fossil-based polyol by synthesized polyols in the formulation did not influence R in the transverse direction. However, in the longitudinal direction, the introduction of 25 wt% of EMAO-HCl, EMAO-DEA and EMAO-EtOH decreases significantly R. The polyols structure was composed of long non-polar carbon chains and chains with polar groups such as hydroxyls and esters. This combination of polar and non-polar groups is generally specific to surfactants (Beneventi et al. 2001). The lower R coefficient could be explained by reduced surface tension between the polymers mixture and the blowing agent. Furthermore, the substitution of the fossil-based polyol by biobased polyols increased the viscosity of the premix. In the case of AA25 and EtOH35, the anisotropy coefficient was 1.8 and 1.9, respectively. Higher R compared to Ref can be an indication of low compatibility between these polyols and the reference polyols. The introduction of 35 wt% of EMAO-EtOH could be a critical value for the polyols' compatibility. The decrease of R with the increasing portion of EMAO-EtOH after 35 wt% of substitution supports this theory.

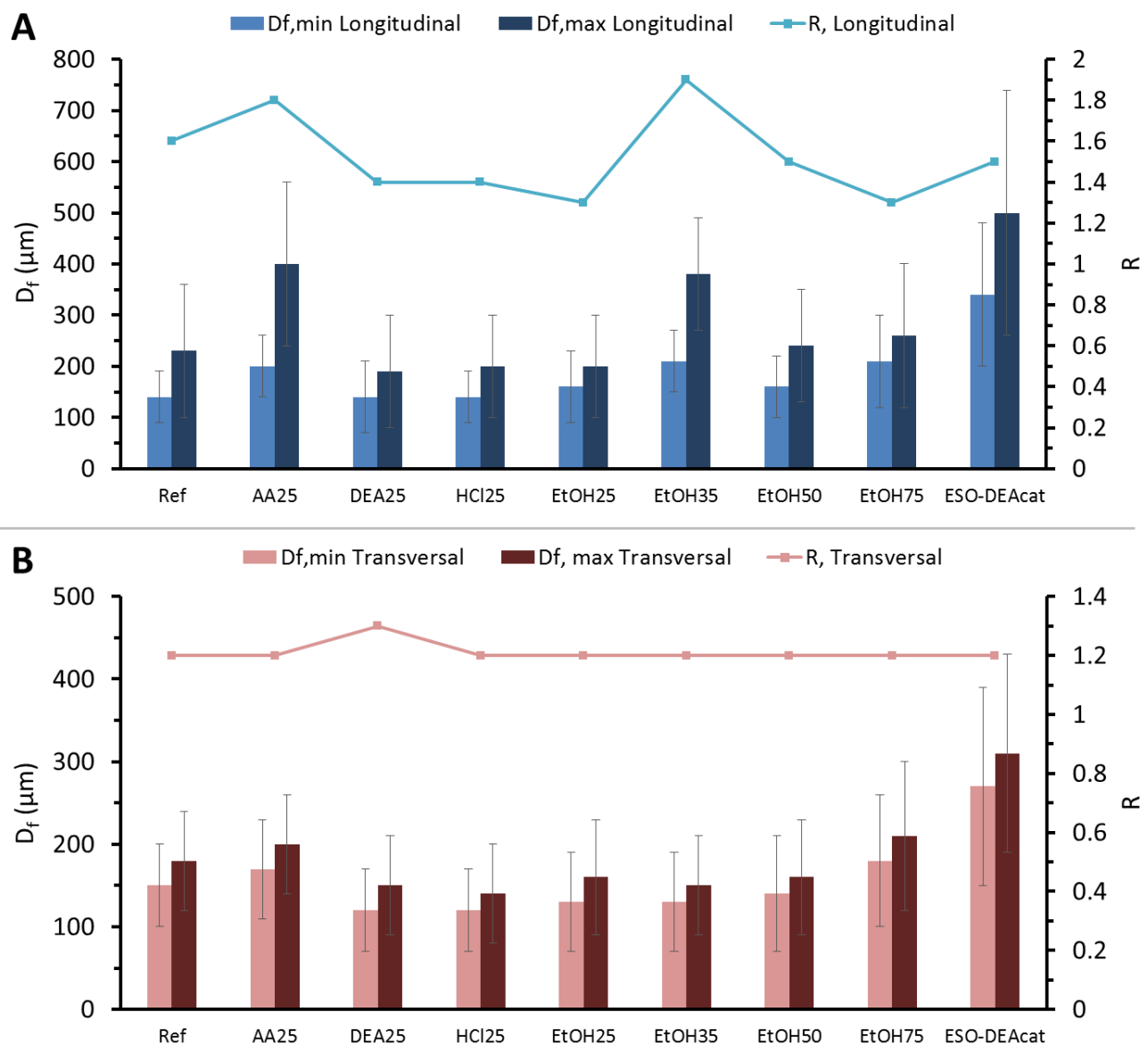


Figure 3.5 - Feret diameters and aspect ratio in the longitudinal (A) and transversal (B) direction.

The cell sizes of PUF foams were measured on SEM images in the transverse and longitudinal direction, represented in Figure 3.6 and Figure S3.28 in SI, respectively. The wide distribution of cell sizes observed on SEM photos results in a high standard deviation for the cell size measurement. A portion of DEA25 cells in the transverse direction seem damaged (Figure 3.6). This unusual cell morphology was due to the fast expansion of the DEA 25 foam (Figure 3.4). In this case, the cream and gel times were 25% shorter than the Ref, which generates a more sudden foaming behavior of the reaction mixture. This faster reactivity allows less time for the organization of the cells in the medium before gelation. The corresponding distribution, modeled by a central binomial distribution, was represented in Figure S3.29 in SI. The EtOH75 cell sizes were larger than the reference ones. The EtOH75 formulation was the slowest to cross-link, with a gel time two-fold longer than the reference. The cell size was controlled by the polymerization of the solid PU struts and walls around air bubbles. The classical theory of nucleation is based on the generation of cells from the isopentane droplet (Pardo-Alonso et al. 2012). This theory is partially discussed and contested for the benefit of the

pockets of air entrapped during the mixing stage (Reignier et al. 2019). The blowing agent droplets migrate into the air bubbles. In the case of a slow network formation, air bubbles and thus cells grow bigger through a coalescence phenomenon combined with Ostwald ripening (Voorhees 1985). Furthermore, the EtOH75 formulation has the lowest temperature throughout the foaming process, as depicted in Figure S3.30 and Figure S3.31 in SI. Thus, a long gel time combined with low exothermic behavior results in coarser cell morphology.

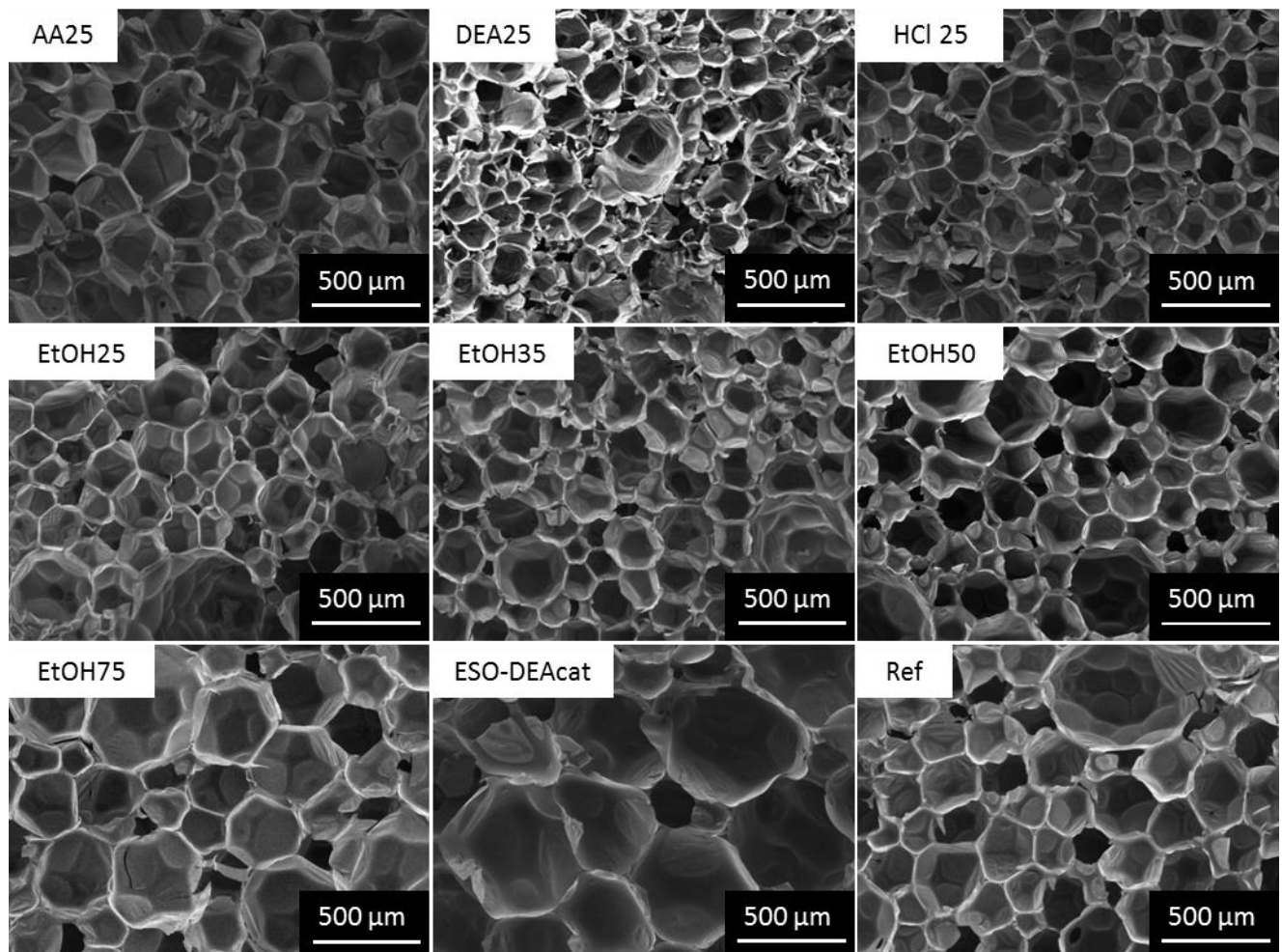


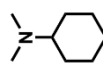
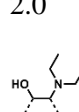
Figure 3.6 - SEM images of all formulations in the transverse direction (Scale = 500 microns).

Despite the various reaction times, expansion rates and cell sizes, the final synthesized PUF densities ranged between 28 and 32 kg/m³, and are detailed in Table S3.9 in SI. The foams were produced at 20 °C, and isopentane has a boiling point of 28 °C. Thus, a small increase in the core temperature of the material is sufficient enough to vaporize the physical blowing agent. The volume change from liquid to gas (expansion ratio) is around five times for the isopentane (Garg et al. 2013). According to the perfect gas law, in order for its volume to double, a mole of gas needs to increase its temperature of 300 °C. The principal volume change is done by the state change between liquid and gas. The reaction between isocyanate and water occurs first and liberates enough energy to vaporize the isopentane. Moreover, the reaction generates gaseous CO₂, accounting for a third of the total gas amount in the foam, thus contributing to the expansion.

4.4. Biobased catalyst

As previously described, the substitution of 25 wt% of fossil-based polyol by EMAO-DEA in a PUF increases the reactivity of the foam. The EMAO-DEA was described as a catalytic polyol because the structure contained tertiary amines that increased the isocyanate and hydroxyl groups reactivity. As previously discussed, EMAO-DEA exhibits an almost solid behavior at room temperature. This high viscosity caused mixing issues that made it difficult to be used solely as a catalyst. Thus, to achieve a biobased PUF catalytic polyol with lower viscosity, epoxidized soybean oil (ESO) underwent a ring-opening reaction by DEA to yield ESO-DEA. The detailed synthesis procedure of ESO-DEA is detailed in SI. The viscosity of ESO-DEA was 33 Pa.s at ambient temperature and six orders of magnitude lower than EMAO-DEA (Figure S3.20 in SI). The epoxide signal located at $\delta=2.8\text{--}3.2$ ppm in ^1H NMR of ESO-DEA presented in Figure S3.32 in SI demonstrated an incomplete epoxide conversion. As previously discussed, the ^{31}P NMR I_{OH} measurement is not selective toward hydroxyl groups. The detailed estimation of the epoxide and hydroxyl groups content in ESO-DEA is depicted in Equations S3.1 to S3.4 in SI. The epoxide conversion was estimated at 59% by ^1H NMR analysis, 66% by OH titration and 68% by epoxide titration (Table S3.10 in SI). ESO-DEA was a polyol with two different catalytic sites: tertiary amine for the urethane, urea and isocyanurate formation and epoxide for the isocyanurate formation (Williams et al. 1992). The retention time of ESO and ESO-DEA, determined by SEC analysis (Figure S3.33 in SI), were similar. In contrast to EMAO-DEA, the structure of the triglycerides of ESO-DEA is mainly conserved after the ring-opening reaction.

Table 3.3 - Formulation in parts of the total polyol content of the fossil-based reference (Ref) and the catalyst-free foam (ESO-DEAcat).

Foam formulation		Ref	ESO- DEAcat
<i>A-Part</i>			
Polyols	Daltolac R570 (fossil-based)	100	100
Catalyst ¹	DMCHA	2.0	
	ESO-DEA		4.57 ¹
Surfactant	B84501	2.5	2.5
Flame retardant	TCPP	10	10
Blowing agent	Water	1.6	1.6
	Isopentane	15.0	15.4
<i>B-Part</i>			
Isocyanate	pMDI	168	193

¹ the OH groups were taken into account for the index calculation.

A trial foam was carried out by a complete substitution of the fossil-based catalyst, as depicted in formulation ESO-DEAcat in Table 3.3. The other parameters were kept constant with respect to Ref formulation. The hydroxyl content of the ESO-DEA was taken into account to calculate the index and

the isocyanate quantity. The ESO-DEAcat PUF rise time was 15 times longer than the Ref with fossil-based catalyst. The reactivity was sluggish (Figure S3.27 in SI), and the core temperature was close to room temperature (Figure S3.30 in SI). The slow reactivity can be possibly explained by the presence of hydroxyl groups near the tertiary amine. The electron-withdrawing effect of the hydroxyl groups decreased the catalytic activity of the tertiary amine (Van Maris et al. 2005). The slow rise of the foam led to cells almost twice as large as Ref cells (Figure 3.6 and Figure S3.28 in SI). ESO-DEAcat has a density of 36 kg/m^3 . The density is almost not impacted by the slow reactivity of the foam. As previously explained, the main volume change was due to the transition between liquid to gas state (Garg et al. 2013). The physical blowing agent, isopentane, vaporizes at 28°C to form the foam. The foam produced with a biobased catalyst has an acceptable density but rather low reactivity and large cells.

4.5. Fire behavior, mechanical and thermal analysis of foams

The characteristic times and cell size investigation empowers the selection of foams with comparable reactivity and cell morphology compared to Ref for further characterization. EMAO-EtOH was the most suitable polyol and EtOH25 formulation was the closest to Ref in terms of reactivity. PUF EtOH25, EtOH50, AA25 and HCl25 were further thoroughly investigated by compression tests, flammability tests and thermal conductivity measurements. These properties are specifically linked to requirements for applications, such as, thermal insulations (foams for buildings, transportation and housing).

In order to reduce the flammability of the PUF (Duquesne et al. 2001), flame retardants Tris(1-chloro-2propyl) phosphate (TCPP) was used in the formulations (Table 3.2). TCPP is a phosphorous-based compound used in the PU formulation and, in the presence of fire, creates a carbonaceous (char) barrier. The system is denoted as intumescent if the char layer is foamed by the gas released by the thermal degradation of the material (Duquesne et al. 2000). This barrier protects the material from flame exposition and limits the transfer of oxygen toward the flame (Duquesne et al. 2000). The intumescent behavior is heightened by the aromatic structure of the isocyanate (Duquesne et al. 2001). It acts as a radical scavenger, limiting the oxidation propagation and then forms a char layer by condensation of partially oxidized aromatic species (Duquesne et al. 2001). Figure 3.7 displays 18 cm long cross-section of the previously mentioned foams once exposed to a 2 cm long flame at the bottom of the foam. Two reference samples were performed for this test to determine the consistency of the flame persistence time. Prior to the test, the HCl25 was brown due to the dark color of the biobased polyol. Once the test performed, all samples present a carbonaceous black layer (Figure 3.7).

	Ref1	Ref2	EtOH25	EtOH50	AA25	HCl25
Foam before flammability test						
Foam after flammability test						
Flame Height cm		> 18 cm				
Persistance s		26 s	21 s	22 s	38 s	30 s
						24 s

Figure 3.7 - Results of the flammability test for Ref, EtOH25, EtOH50, AA25 and HCl25 foams.

The flame height and the carbon layer on the samples indicated flame propagation throughout the entire surface of the sample. All samples burned so fast that the flame retardant only limits the flame propagation. The char layer formed did not stop the propagation of the fire and it spread along the foam. The persistence of the flame was more significant in EtOH50. Furthermore, the foam had a cracked surface after the test. The substitution of 50% of fossil-based polyol by a biobased one decreases the intumescence character. The polyols synthesized at the lab scale could contain residual solvent, favoring fire propagation. As displayed in TGA thermogram of EMAO-EtOH Figure S3.24 in SI, some weight loss occurs at temperatures below 100 °C. This could correspond to some traces of ethanol or ethyl acetate. Moreover, MAO contains C16:0 fatty acids, long alkane carbonated chains that can quickly burn. As previously discussed, EMAO-HCl had higher thermal stability due to the presence of chlorine, so improved fire behavior of HCl25 was expected (Weil and Levchik 2004; Wilkie and Morgan 2010). Nevertheless, HCl25 has the same flammability results as reference materials. The result of this flammability test for HCl25 was insufficient to assess further the flame retardant activity of EMAO-HCl25.

The TGA results depicted in Figure S3.34 and Table S3.11 in SI showed a similar weight loss profile for all foams. The temperature at 5% ($T_{5\%}$) and 50% ($T_{50\%}$) weight loss were around 220 °C and 360 °C, respectively. The PU polymer matrix was characterized by three significant steps of degradation. The first degradation was characteristic of the hard segments, the second degradation stage was related to the rigid part of the PU network, and the last step was the degradation of the more thermally stable isocyanurate formed partially as a secondary product (Williams et al. 1992) during the foaming process and partially during the dissociation of the urethane bond (Chattopadhyay and

Webster 2009). The foam system is complex and composed of several different chemical groups (urethane, urea, ester, etc.) whose degradation can coincide.

The thermal conductivity (λ) of the foams is related to the total heat transfer (q_t) passing through the foam, as described by Equation 3.7.

$$\lambda = q_t * \frac{L}{\Delta T} \quad (3.7)$$

Where q_t has three components described in Equation 3.8: the conduction through the polymer matrix (q_{PUR}), through the gas phase (q_{gas}) and the radiation (q_{rad}). The convection transfer is negligible for closed-cell porous materials with a cell size inferior to 3 mm (Kuhn et al. 1992).

$$q_t = q_{PUR} + q_{gas} + q_{rad} + q_{conv} \quad (8)$$

The EN 12667 standard procedure requires the measurement to be performed at an average temperature of 10 °C. Nevertheless, at this temperature, water condensation could happen at the surface of the sample and thus distort the results. Thus, PUF were also measured at an average temperature of 20 °C to confirm the observed trend. As depicted in Table 3.4, the thermal conductivity of the reference foam was 23.9 mW/(K.m). The foams with biobased polyols have a similar thermal conductivity. The q_{gas} represents 65% of q_t (Jarfelt and Ramnäs 2006). Isopentane was used as a physical blowing agent for all foams; thus, the thermal conductivity was similar. The variation of thermal conductivity can be explained by the conduction through the matrix and the radiation. It was demonstrated that smaller cell size decreases lambda values via the expression of q_{rad} by the Rossland equation (Furtwengler et al. 2018b; Hilyard and Cunningham 1994). The larger cells of EtOH50 and AA25 and the smaller closed-cell content could explain the higher thermal conductivity. The substitution of 25 wt% of the fossil-based polyol by EMAO-HCl or EMAO-EtOH did not influence λ .

Table 3.4 - Thermal conductivity, closed-cell content and compression strength for Ref, AA25, HCl25, EtOH25 and EtOH50 foam.

	Ref	AA25	HCl25	EtOH25	EtOH50
Thermal conductivity 10 °C initial value	$mW/(K.m)$	23.9 ± 0.5	24.6 ± 0.5	24.3 ± 0.5	24.0 ± 0.5
Thermal conductivity 20 °C initial value	$mW/(K.m)$	25.4 ± 0.5	26.1 ± 0.5	25.7 ± 0.5	25.2 ± 0.5
Closed-cell content	%	93 ± 1	91 ± 1	93 ± 1	93 ± 1
Compression strength	kPa	330 ± 20	260 ± 20	300 ± 20	290 ± 20

The foam mechanical properties depend on numerous factors such as the macromolecular architecture of polyol and polyisocyanate, density, cell sizes and morphology. As previously discussed, the foam densities were comparable. As depicted by the values in Table 3.4, compression strength measured in the longitudinal direction ranges from 261 to 334 kPa. The identification of the primary moieties present in the foams was performed by FTIR, presented in Figure S3.35 in SI. All foams present similar FTIR spectra and characteristic PUF peaks (de Haseth et al. 1993), such as the N-H stretching band between $\tilde{\nu}=3400-3200 \text{ cm}^{-1}$ for the urethane group. The signal at $\tilde{\nu}=1715 \text{ cm}^{-1}$ was due to the different C=O stretching of ester and urethane groups. The Ph-H stretching in the phenyl group from the polymeric isocyanate was located at $\tilde{\nu}=1595 \text{ cm}^{-1}$. Surprisingly, band at $\tilde{\nu}=1410 \text{ cm}^{-1}$ attributed to the isocyanurate ring appears. Isocyanurates were isocyanate trimers formed by the

isocyanate excess in the presence of an amine catalyst at high temperature during the foaming process (Al Nabulsi et al. 2018; Williams et al. 1992). The I_{OH} value is a representation of the density of hydroxyl groups in the polyol. The microalgae derived polyols present a lower I_{OH} than the fossil-based polyol. As the ratio NCO/OH was kept constant, a slightly higher cross-linking density was obtained with the reference foam. The mechanical properties of HCl25 and EtOH25 were similar to the reference. Compared to EMAO-AA, the value of I_{OH} of EMAO-EtOH and EMAO-HCl is higher. The lower cross-link density could explain the lower mechanical properties of AA25.

The dimensional stability was performed by dimension measurement of foam specimen before and after being placed for 48 hours in a cold (-20 °C) or warm and humid (70 °C and 90% RH) environment. The dimensional stability at 70 °C under 90% RH demonstrates the soaking properties of the foam. As presented in Table 3.5, the dimension of all foams increased by a maximum of 1.4% in the warm environment. The humidity present in the chamber soaks the foam. Foams obtained with MAO derived polyols tend to absorb less water. The hydrophobic character of the polyol must be reducing the water absorption. This point was confirmed by the EtOH50 dimension evolutions, which were the lowest.

The cold environment reduces the pressure applied by the gaseous blowing agents on the closed-cell walls. The glass transition temperature of the PUF system is around - 50 °C, so the decrease in temperature decreases the chain mobility. The shrinkage of the foam in a cold environment was minimal (inferior to 0.5%). Nevertheless, EtOH50 and AA25 have a slight tendency to contract more than the reference foam. The cells sizes impact the dimensional variation. A higher gas volume causes a more significant pressure drop. As a confirmation, AA25 and EtOH50 both have coarser cells and higher shrinkage than the reference.

Table 3.5 - Dimensional variation of Ref, AA25, HCl25, EtOH25 and EtOH50 foams in both environments (cold or warm & humid).

	Ref	AA25	HCl25	EtOH25	EtOH50
48h at 70 °C, 90% RH					
Length	%	1.4	1.3	1.2	0.9
Width	%	1.4	1.3	1.2	0.9
Thickness	%	0.2	0.1	0.3	0.1
48h at -20 °C					
Length	%	-0.2	-0.3	-0.2	-0.3
Width	%	-0.1	-0.3	-0.2	-0.3
Thickness	%	0.1	0.1	0.1	0.1

The substitution of a fossil-based by biobased polyols was performed, and the impact on the main foam properties was minimal. The introduction of MAO derived polyols slightly improves the dimensional foam stability in a warm and moist environment.

5. CONCLUSION

This study shows the great interest in developing closed-cell PUF from microalgae resources, more particularly polyunsaturated triglycerides from extracted oil, without competition with food applications. Several biobased PUF systems have been successfully elaborated using different green chemistry approaches. Compared to fossil-based systems, they present high performances in connection with, e.g., insulation applications.

The modification of unsaturated MAO into efficient polyols through epoxidation and ring-opening was successfully accomplished. The biobased polyols reported lower overall hydroxyl functionality than expected due to the inherent side reactions of the ring-opening of epoxides via ethanol, diethylamine, acetic acid and hydrochloric acid. Nevertheless, the I_{OH} of the newly synthesized biobased polyols were controlled and suitable for PUF synthesis. The substitution of a conventional fossil-based polyol by microalgae derived polyol was examined up to 75 wt% and well-performing rigid PUF were obtained. The substitution of 25 wt% of the fossil-based polyol by EMAO-EtOH produces foams with low thermal conductivity of 24.0 mW/(K.m), which is comparable to commercial systems. The cells are slightly smaller than the fully fossil-based foam and the corresponding compression strength is 290 kPa. The other properties were similar in every aspect to the reference. In this study, for the first time, a catalyst-free rigid PUF was synthesized with a triglyceride-based catalytic polyol. Despite a slow expansion rate, ESO-DEAcat PUF has a density of 36 kg/m³. The regulation on volatile compounds in the building industry makes the catalytic polyol a viable solution. Nevertheless, the actual slow reactivity is a problem for the adaptation to an industrial process.

The perspectives of this work are vast. The optimization of the ring-opening reaction of epoxidized microalgae oil with ethanol could lead to biobased polyols which present high performance in connection with the targeted materials. The reduction of side reactions could be achieved by decreasing the temperature or the use of a solvent. This optimization should increase the I_{OH} and functionality of the polyol and lead to higher reactivity, cross-link density and, thus, mechanical properties of the foam. The ring-opening of biobased oils with secondary amine paves the way to a new generation of biobased catalytic polyol. Future works should focus on the development of more efficient catalysts by the introduction of more sterically hindered secondary amine on oils. To further assess the intumescence properties of chlorine-containing polyols such as EMAO-HCl, limiting oxygen index or calorimetric cone experiments could be further investigated.

The ring-opening reaction on MAO could be used to produce surfactants by the introduction of a long alkyl chain or, similarly, a flame retardant component by the introduction of phosphorous moieties. With some additional studies, polyols, catalysts, surfactants and fire retardants could be synthesized by ring-opening of the platform molecule MAO. And finally, the utilization of biobased dimethyl diisocyanate could lead to a fully biobased PUF.

6. REFERENCES

Abdel-Rahman, M.A., Tashiro, Y., Sonomoto, K., 2013. Recent advances in lactic acid production by microbial fermentation processes. *Biotechnol. Adv.* **31**, 877–902. <https://doi.org/10.1016/j.biotechadv.2013.04.002>

Al Nabulsi, A., Cozzula, D., Hagen, T., Leitner, W., Müller, T.E., 2018. Isocyanurate formation during rigid polyurethane foam assembly: a mechanistic study based on *in situ* IR and NMR spectroscopy. *Polym. Chem.* **9**, 4891–4899. <https://doi.org/10.1039/C8PY00637G>

Anastas, P., Eghbali, N., 2010. Green Chemistry: Principles and Practice. *Chem Soc Rev* **39**, 301–312. <https://doi.org/10.1039/B918763B>

Andersons, J., Kirpluks, M., Stiebra, L., Cabulis, U., 2016. Anisotropy of the stiffness and strength of rigid low-density closed-cell polyisocyanurate foams. *Mater. Des.* **92**, 836–845. <https://doi.org/10.1016/j.matdes.2015.12.122>

Arbennz, A., Perrin, R., Avérous, L., 2017. Elaboration and Properties of Innovative Biobased PUIR Foams from Microalgae. *J. Polym. Environ.* **26**, 254–262. <https://doi.org/10.1007/s10924-017-0948-y>

Argyropoulos, D.S., Bolker, H.I., Heitner, C., Archipov, Y., 1993. ^{31}P NMR Spectroscopy in Wood Chemistry. Part IV. Lignin Models: Spin Lattice Relaxation Times and Solvent Effects in ^{31}P NMR. *Holzforschung* **47**, 50–56. <https://doi.org/10.1515/hfsg.1993.47.1.50>

Banerjee, A., Banerjee, C., Negi, S., Chang, J.-S., Shukla, P., 2018. Improvements in algal lipid production: a systems biology and gene editing approach. *Crit. Rev. Biotechnol.* **38**, 369–385. <https://doi.org/10.1080/07388551.2017.1356803>

Banerjee, C., Singh, P.K., Shukla, P., 2016. Microalgal bioengineering for sustainable energy development: Recent transgenesis and metabolic engineering strategies. *Biotechnol. J.* **11**, 303–314. <https://doi.org/10.1002/biot.201500284>

Becker, E.W., 2008. Microalgae: biotechnology and microbiology 'Cambridge studies in biotechnology. Cambridge Univ. Press, Cambridge.

Beneventi, D., Carre, B., Gandini, A., 2001. Role of surfactant structure on surface and foaming properties. *Colloids Surf. Physicochem. Eng. Asp.* **189**, 65–73. [https://doi.org/10.1016/S0927-7757\(01\)00602-1](https://doi.org/10.1016/S0927-7757(01)00602-1)

Biswas, A., Adhvaryu, A., Gordon, S.H., Erhan, S.Z., Willett, J.L., 2005. Synthesis of Diethylamine-Functionalized Soybean Oil. *J. Agric. Food Chem.* **53**, 9485–9490. <https://doi.org/10.1021/jf050731o>

Borowitzka, M.A., 2013. High-value products from microalgae—their development and commercialisation. *J. Appl. Phycol.* **25**, 743–756. <https://doi.org/10.1007/s10811-013-9983-9>

Brennan, L., Owende, P., 2010. Biofuels from microalgae—A review of technologies for production, processing, and extractions of biofuels and co-products. *Renew. Sustain. Energy Rev.* **14**, 557–577. <https://doi.org/10.1016/j.rser.2009.10.009>

Caillol, S., Desroches, M., Boutevin, G., Loubat, C., Auvergne, R., Boutevin, B., 2012. Synthesis of new polyester polyols from epoxidized vegetable oils and biobased acids. *Eur. J. Lipid Sci. Technol.* **114**, 1447–1459. <https://doi.org/10.1002/ejlt.201200199>

Chambon, F., Winter, H.H., 1987. Linear Viscoelasticity at the Gel Point of a Crosslinking PDMS with Imbalanced Stoichiometry. *J. Rheol.* **31**, 683–697. <https://doi.org/10.1122/1.549955>

Chattopadhyay, D.K., Webster, D.C., 2009. Thermal stability and flame retardancy of polyurethanes. *Prog. Polym. Sci.* **34**, 1068–1133. <https://doi.org/10.1016/j.progpolymsci.2009.06.002>

Chew, K.W., Yap, J.Y., Show, P.L., Suan, N.H., Juan, J.C., Ling, T.C., Lee, D.-J., Chang, J.-S., 2017. Microalgae biorefinery: High value products perspectives. *Bioresour. Technol.* **229**, 53–62. <https://doi.org/10.1016/j.biortech.2017.01.006>

Dais, P., Spyros, A., 2007. ^{31}P NMR spectroscopy in the quality control and authentication of extra-virgin olive oil: A review of recent progress. *Magn. Reson. Chem.* **45**, 367–377. <https://doi.org/10.1002/mrc.1985>

Del Rio, E., Galià, M., Cádiz, V., Lligadas, G., Ronda, J.C., 2010. Polymerization of epoxidized vegetable oil derivatives: Ionic-coordinative polymerization of methylepoxyoleate. *J. Polym. Sci. Part Polym. Chem.* **48**, 4995–5008. <https://doi.org/10.1002/pola.24297>

Duquesne, S., Le Bras, M., Bourbigot, S., Delobel, R., Camino, G., Eling, B., Lindsay, C., Roels, T., Vezin, H., 2001. Mechanism of fire retardancy of polyurethanes using ammonium polyphosphate. *J. Appl. Polym. Sci.* **82**, 3262–3274. <https://doi.org/10.1002/app.2185>

Duquesne, S., Le Bras, M., Bourbigot, S., Delobel, R., Poutch, F., Camino, G., Eling, B., Lindsay, C., Roels, T., 2000. Analysis of Fire Gases Released from Polyurethane and Fire-Retarded Polyurethane Coatings. *J. Fire Sci.* **18**, 456–482. <https://doi.org/10.1106/6CRG-Q8VD-PV3G-ELDD>

Fabris, M., Abbriano, R.M., Pernice, M., Sutherland, D.L., Commault, A.S., Hall, C.C., Labeeuw, L., McCauley, J.I., Kuzhiuparambil, U., Ray, P., Kahlke, T., Ralph, P.J., 2020. Emerging Technologies in Algal Biotechnology: Toward the Establishment of a Sustainable, Algae-Based Bioeconomy. *Front. Plant Sci.* **11**, 279. <https://doi.org/10.3389/fpls.2020.00279>

Flory, P.J., 1941. Molecular Size Distribution in Three Dimensional Polymers. I. Gelation. *J. Am. Chem. Soc.* **63**, 3083–3090. <https://doi.org/10.1021/ja01856a061>

Furtwengler, P., Avérous, L., 2018. Renewable polyols for advanced polyurethane foams from diverse biomass resources. *Polym. Chem.* **9**, 4258–4287. <https://doi.org/10.1039/C8PY00827B>

Furtwengler, P., Matadi Boumbimba, R., Sarbu, A., Avérous, L., 2018b. Novel Rigid Polyisocyanurate Foams from Synthesized Biobased Polyester Polyol with Enhanced Properties. *ACS Sustain. Chem. Eng.* **6**, 6577–6589. <https://doi.org/10.1021/acssuschemeng.8b00380>

Galià, M., de Espinosa, L.M., Ronda, J.C., Lligadas, G., Cádiz, V., 2010. Vegetable oil-based thermosetting polymers. *Eur. J. Lipid Sci. Technol.* **112**, 87–96. <https://doi.org/10.1002/ejlt.200900096>

Garg, P., Kumar, P., Srinivasan, K., Dutta, P., 2013. Evaluation of isopentane, R-245fa and their mixtures as working fluids for organic Rankine cycles. *Appl. Therm. Eng.* **51**, 292–300. <https://doi.org/10.1016/j.applthermaleng.2012.08.056>

Gordon, J.M., Polle, J.E.W., 2007. Ultrahigh bioproductivity from algae. *Appl. Microbiol. Biotechnol.* **76**, 969–975. <https://doi.org/10.1007/s00253-007-1102-x>

Gunstone, F.D., Harwood, J.L., Harwood, J.L., 2007. The Lipid Handbook with CD-ROM, 3rd ed. CRC Press. <https://doi.org/10.1201/9781420009675>

Guo, A., Cho, Y., Petrović, Z.S., 2000. Structure and properties of halogenated and nonhalogenated soy-based polyols. *J. Polym. Sci. Part Polym. Chem.* **38**, 3900–3910. [https://doi.org/10.1002/1099-0518\(20001101\)38:21<3900::AID-POLA70>3.0.CO;2-E](https://doi.org/10.1002/1099-0518(20001101)38:21<3900::AID-POLA70>3.0.CO;2-E)

Harry-O'kuru, R.E., Tisserat, B., Gordon, S.H., Gravett, A., 2015. Osage Orange (*Maclura pomifera* L.) Seed Oil Poly(α-hydroxydibutylamine) Triglycerides: Synthesis and Characterization. *J. Agric. Food Chem.* **63**, 6588–6595. <https://doi.org/10.1021/acs.jafc.5b01625>

de Haseth, J.A., Andrews, J.E., McClusky, J.V., Priester, R.D., Harthcock, M.A., Davis, B.L., 1993. Characterization of Polyurethane Foams by Mid-Infrared Fiber/FT-IR Spectrometry. *Appl. Spectrosc.* **47**, 173–179. <https://doi.org/10.1366/0003702934048334>

Hawkins, M.C., O'Toole, B., Jackovich, D., 2005. Cell Morphology and Mechanical Properties of Rigid Polyurethane Foam. *J. Cell. Plast.* **41**, 267–285. <https://doi.org/10.1177/0021955X05053525>

Hilyard, N.C., Cunningham, A. (Eds.), 1994. Low density cellular plastics: Physical basis of behaviour. Springer Netherlands, Dordrecht. <https://doi.org/10.1007/978-94-011-1256-7>

Ionescu, M., 2005. Chemistry and technology of polyols for polyurethanes, 1st ed. Rapra Technology, Shawbury, Shrewsbury, Shropshire, U.K.

Jacobsberg, B., Oh Chuan Ho, 1976. Studies in palm oil crystallization. *J. Am. Oil Chem. Soc.* **53**, 609–617. <https://doi.org/10.1007/BF02586272>

Jarfelt, U., Ramnäs, O., 2006. Thermal conductivity of polyurethane foam Best performance. Presented at the 10th International Symposium on district heating and cooling, Chalmers University of Technology Goteborg, Sweden, pp. 3–5.

Knothe, G., Steidley, K.R., 2005. Kinematic viscosity of biodiesel fuel components and related compounds. Influence of compound structure and comparison to petrodiesel fuel components. *Fuel* **84**, 1059–1065. <https://doi.org/10.1016/j.fuel.2005.01.016>

Korntner, P., Sumerskii, I., Bacher, M., Rosenau, T., Potthast, A., 2015. Characterization of technical lignins by NMR spectroscopy: optimization of functional group analysis by ³¹P NMR spectroscopy. *Holzforschung* **69**, 807–814. <https://doi.org/10.1515/hf-2014-0281>

Kuhn, J., Ebert, H.-P., Arduini-Schuster, M.C., Büttner, D., Fricke, J., 1992. Thermal transport in polystyrene and polyurethane foam insulations. *Int. J. Heat Mass Transf.* **35**, 1795–1801. [https://doi.org/10.1016/0017-9310\(92\)90150-Q](https://doi.org/10.1016/0017-9310(92)90150-Q)

Lligadas, G., Ronda, J.C., Galià, M., Biermann, U., Metzger, J.O., 2006a. Synthesis and characterization of polyurethanes from epoxidized methyl oleate based polyether polyols as renewable resources. *J. Polym. Sci. Part Polym. Chem.* **44**, 634–645. <https://doi.org/10.1002/pola.21201>

Maisonneuve, L., Chollet, G., Grau, E., Cramail, H., 2016. Vegetable oils: a source of polyols for polyurethane materials. *OLC* **23**, D508. <https://doi.org/10.1051/ocl/2016031>

Miao, S., Zhang, S., Su, Z., Wang, P., 2008. Chemoenzymatic synthesis of oleic acid-based polyesters for use as highly stable biomaterials. *J. Polym. Sci. Part Polym. Chem.* **46**, 4243–4248. <https://doi.org/10.1002/pola.22721>

Negrell, C., Cornille, A., de Andrade Nascimento, P., Robin, J.-J., Caillol, S., 2017. New bio-based epoxy materials and foams from microalgal oil: Agal oil epoxy materials and foams. *Eur. J. Lipid Sci. Technol.* **119**, 1600214. <https://doi.org/10.1002/ejlt.201600214>

Olivieri, G., Salatino, P., Marzocchella, A., 2014. Advances in photobioreactors for intensive microalgal production: configurations, operating strategies and applications: Advances in photobioreactors for intensive microalgal production. *J. Chem. Technol. Biotechnol.* **89**, 178–195. <https://doi.org/10.1002/jctb.4218>

Oncel, S.S., 2013. Microalgae for a macroenergy world. *Renew. Sustain. Energy Rev.* **26**, 241–264. <https://doi.org/10.1016/j.rser.2013.05.059>

Palaskar, D.V., Boyer, A., Cloutet, E., Le Meins, J.-F., Gadenne, B., Alfos, C., Farcet, C., Cramail, H., 2012. Original diols from sunflower and ricin oils: Synthesis, characterization, and use as polyurethane building blocks. *J. Polym. Sci. Part Polym. Chem.* **50**, 1766–1782. <https://doi.org/10.1002/pola.25944>

Pardo-Alonso, S., Solórzano, E., Estravís, S., Rodríguez-Perez, M.A., de Saja, J.A., 2012. In situ evidence of the nanoparticle nucleating effect in polyurethane–nanoclay foamed systems. *Soft Matter* **8**, 11262. <https://doi.org/10.1039/c2sm25983d>

Pawar, M.S., Kadam, A.S., Dawane, B.S., Yemul, O.S., 2016a. Synthesis and characterization of rigid polyurethane foams from algae oil using biobased chain extenders. *Polym. Bull.* **73**, 727–741. <https://doi.org/10.1007/s00289-015-1514-1>

Petrovic, Z., 2008. Polyurethanes from Vegetable Oils. *Polym. Rev.* **48**, 109–155. <https://doi.org/10.1080/15583720701834224>

Petrović, Z.S., Wan, X., Bilić, O., Zlatanić, A., Hong, J., Javni, I., Ionescu, M., Milić, J., Degruson, D., 2013. Polyols and Polyurethanes from Crude Algal Oil. *J. Am. Oil Chem. Soc.* **90**, 1073–1078. <https://doi.org/10.1007/s11746-013-2245-9>

Peyrton, J., Chambaretaud, C., Avérous, L., 2019. New Insight on the Study of the Kinetic of Biobased Polyurethanes Synthesis Based on Oleo-Chemistry. *Molecules* **24**, 4332. <https://doi.org/10.3390/molecules24234332>

Pfister, D.P., Xia, Y., Larock, R.C., 2011. Recent Advances in Vegetable Oil-Based Polyurethanes. *ChemSusChem* **4**, 703–717. <https://doi.org/10.1002/cssc.201000378>

Rawat, I., Ranjith Kumar, R., Mutanda, T., Bux, F., 2013. Biodiesel from microalgae: A critical evaluation from laboratory to large scale production. *Appl. Energy* **103**, 444–467. <https://doi.org/10.1016/j.apenergy.2012.10.004>

Reignier, J., Alcouffe, P., Méchin, F., Fenouillot, F., 2019. The morphology of rigid polyurethane foam matrix and its evolution with time during foaming – New insight by cryogenic scanning electron microscopy. *J. Colloid Interface Sci.* **552**, 153–165. <https://doi.org/10.1016/j.jcis.2019.05.032>

Roesle, P., Stempfle, F., Hess, S.K., Zimmerer, J., Rfo Bártulos, C., Lepetit, B., Eckert, A., Kroth, P.G., Mecking, S., 2014. Synthetic Polyester from Algae Oil. *Angew. Chem. Int. Ed.* **53**, 6800–6804. <https://doi.org/10.1002/anie.201403991>

Sharma, B.K., Adhvaryu, A., Liu, Z., Erhan, S.Z., 2006b. Chemical modification of vegetable oils for lubricant applications. *J. Am. Oil Chem. Soc.* **83**, 129–136. <https://doi.org/10.1007/s11746-006-1185-z>

Stockmayer, W.H., 1944. Theory of Molecular Size Distribution and Gel Formation in Branched Polymers II. General Cross Linking. *J. Chem. Phys.* **12**, 125–131. <https://doi.org/10.1063/1.1723922>

Syrpas, M., Venskutonis, P.R., 2020. Algae for the production of bio-based products. In 'Biobased Products and Industries'. Elsevier, pp. 203–243. <https://doi.org/10.1016/B978-0-12-818493-6.00006-3>

Ugwu, C.U., Aoyagi, H., Uchiyama, H., 2008. Photobioreactors for mass cultivation of algae. *Bioresour. Technol.* **99**, 4021–4028. <https://doi.org/10.1016/j.biortech.2007.01.046>

Van Maris, R., Tamano, Y., Yoshimura, H., Gay, K.M., 2005. Polyurethane Catalysis by Tertiary Amines. *J. Cell. Plast.* **41**, 305–322. <https://doi.org/10.1177/0021955X05055113>

Voorhees, P.W., 1985. The theory of Ostwald ripening. *J. Stat. Phys.* **38**, 231–252. <https://doi.org/10.1007/BF01017860>

Weil, E.D., Levchik, S.V., 2004. Commercial Flame Retardancy of Polyurethanes. *J. Fire Sci.* **22**, 183–210. <https://doi.org/10.1177/0734904104040259>

Weissberger, A. (Ed.), 1964. Chemistry of Heterocyclic Compounds: Heterocyclic Compounds with Three- and Four-Membered Rings 'Chemistry of Heterocyclic Compounds: A Series Of Monographs. John Wiley & Sons, Inc., Hoboken, NJ, USA. <https://doi.org/10.1002/9780470239704>

Wijffels, R.H., Barbosa, M.J., Eppink, M.H.M., 2010. Microalgae for the production of bulk chemicals and biofuels. *Biofuels Bioprod. Biorefining* **4**, 287–295. <https://doi.org/10.1002/bbb.215>

Wilkie, C.A., Morgan, A.B. (Eds.), 2010. Fire retardancy of polymeric materials, 2nd ed. CRC Press, Boca Raton.

Williams, R.J.J., Vázquez, A., Pascault, J.P., 1992. Gelation in the cyclotrimerization of dicyanates considering substitution effects. *Polym. Bull.* **28**, 219–225. <https://doi.org/10.1007/BF00299659>

Winter, H.H., Chambon, F., 1986. Analysis of Linear Viscoelasticity of a Crosslinking Polymer at the Gel Point. *J. Rheol.* **30**, 367–382. <https://doi.org/10.1122/1.549853>

Zhu, Y., Romain, C., Williams, C.K., 2016. Sustainable polymers from renewable resources. *Nature* **540**, 354–362. <https://doi.org/10.1038/nature21001>

7. SUPPORTING INFORMATION

7.1. Characterization of MAO

Table S3.6 - Fatty acid profile of MAO.

Fatty acids	C14:0	C16:0	C16:1	C18:0	C18:1	C18:3	C18:4	C20:3	C20:5	C22:0	C22:5	C22:6	Other
Distribution (%)	1.5	21.8	0.2	0.9	0.3	0.3	0.1	1.0	0.5	0.6	9.9	60.2	2.7

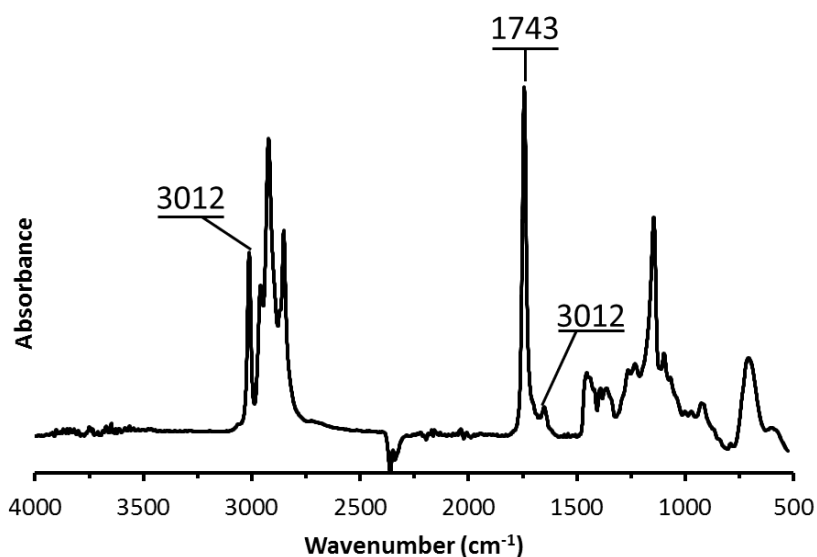


Figure S3.8 - Infrared spectrum of MAO.

IR: $\tilde{\nu} = 3012$ (C=C vibration), 1743 (ester, C=O stretching), 1652 cm^{-1} (C=C-H vibration)

7.2. EMAO synthesis

According to a previously described protocol (Arbenz et al. 2017), 11.1 kg of MAO (145 mol, 1eq), 6 L toluene and 2.2 kg of formic acid (48 mol, 0.33 eq.) were introduced in a 100 L reactor equipped with a reflux condenser, a mechanical stirrer and a dropping funnel. The mixture was heated at 40 °C under an inert atmosphere with a 250 rpm agitation for one hour. Then, 31.2 kg of H₂O₂ (35%) (360 mol, 2.45 eq.) was added slowly over 5h not to raise the temperature above 75 °C under the agitation of 500 rpm. The mixture turned white and thickened along with the reaction. Once the addition finished, the temperature is stabilized between 70 °C and 75 °C and the mixture is stirred for 3 hours. The viscosity of the mixture was decreased by 5 L of toluene. The organic phase was washed with 20 L of water at 65 °C until neutral pH. The solvent was evaporated under reduced pressure. 9.89 kg of epoxidized MAO (EMAO) was obtained with 74 wt% and 80 mol% yield.

¹H NMR (400 MHz, CDCl₃): $\delta = 5.63\text{--}5.45$ (m, 1H; C=C), 5.25 (tt, 1H; CH-Glycerine), 4.30 (d, 2H; CH₂-Glycerine), 4.15 (d, 2H; CH₂-Glycerine), 3.2–2.8 (m, 2H; epoxide), 1.35–1.13 (m, 30H; aliphatic CH₂), 1.03 (t, 3H; CH₃-CH₂-Epoxide), 0.88 ppm (t, 3H; CH₃).

IR: $\tilde{\nu} = 3500$ (OH vibration), 1738 (Ester, C=O Stretching), 826 cm⁻¹ (epoxide vibration)

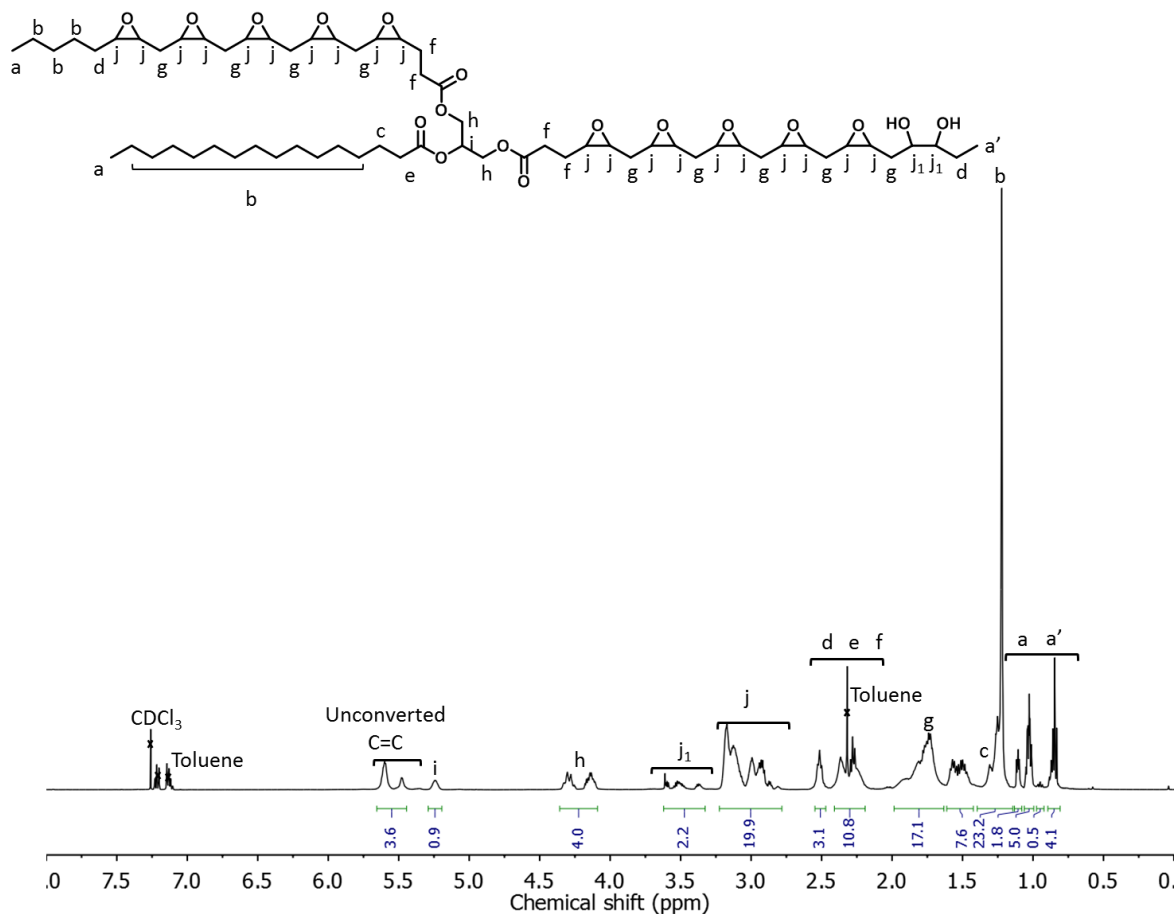


Figure S3.9 - Proton NMR spectrum of EMAO.

Table S3.7 - Repartition of the different chemical moieties in the EMAO.

Name	Structure	Molar quantity (%)
Double bond		16%
Epoxide		80%
Hydroxyl		4%

7.3. Polyol synthesis

7.3.1. Ring-opening of EMAO with acetic acid (EMAO-AA)

The protocol was adapted from a previously published work (Peyrton et al. 2019). The reaction was carried out in a round bottom flask equipped with a reflux condenser and a mechanical stirrer. The flask was filled with 500 g of MAO 11 mmol epoxide/g (5.5 mol, 1 eq.) and 1.6 L of acetic acid (28 mol, 5 eq). The mixture was stirred at 90 °C for 24 hours. 500 mL of ethyl acetate were added to decrease the viscosity of the mixture. The organic phase was washed with saturated NaHCO_3 solution until neutral pH. Then it was washed with brine solution, dried with anhydrous sodium sulfate and then filtered. The solvent was evaporated under reduced pressure. The ring-opened EMAO with acetic acid (EMAO-AA) was dried overnight in a vacuum oven at 40 °C. The yield was 73 wt%.

^1H NMR (400 MHz, CDCl_3): δ =5.63-5.45 (m, 1H; C=C)), 5.25 (tt, 1H; CH-Glycerine), 1.35–1.13 (m, 30H; aliphatic CH_2), 0.88 ppm (t, 3H; CH_3).

FTIR: $\tilde{\nu}$ = 3500 (OH vibration), 1734 cm^{-1} (Ester, C=O Stretching)

7.3.2. Ring-opening of EMAO with Ethanol (EMAO-EtOH)

The protocol was adapted from a previously published work (Palaskar et al. 2012; Peyrton et al. 2019). The reaction was carried out in a round bottom flask equipped with a reflux condenser and a mechanical stirrer. The flask was filled with 500 g of MAO 11 mmol epoxide/g, (5.5 mol, 1 eq.), 50 g of Amberlyst® 15H and 1.5 L of ethanol (25.7 mol, 4.7 eq.). The mixture was stirred at 90 °C for 24 hours. The catalyst was removed by filtration. 500 mL of ethyl acetate were added to decrease the viscosity of the mixture. Then the organic phase was treated with NaHCO_3 and water until the pH was neutral. Then it was washed with brine solution, dried with anhydrous sodium sulfate and then filtered. The solvent was evaporated under reduced pressure. The ring-opened EMAO with ethanol (EMAO-EtOH) was dried overnight in a vacuum oven at 40 °C. The yield was 76 wt%.

^1H NMR (400 MHz, CDCl_3): δ =5.63-5.45 (m, 1H; C=C)), 5.25 (tt, 1H; CH-Glycerine), 1.35–1.13 (m, 30H; aliphatic CH_2), 0.88 ppm (t, 3H; CH_3).

FTIR: $\tilde{\nu}$ = 3500 (OH vibration), 1733 cm^{-1} (Ester, C=O Stretching)

7.3.3. Ring-opening of EMAO with diethylamine (EMAO-DEA)

The protocol was adapted from a previously published work (Harry-O'kuru et al. 2015; Peyrton et al. 2019). The reaction was carried out in a round bottom flask equipped with a reflux condenser and a mechanical stirrer. The flask was filled with 500 g of MAO 11 mmol epoxide/g (5.5 mol, 1 eq.), 180 g of ZnCl_2 (1.3 mol, 0.24 eq.) and 0.9 L of diethylamine (8.7 mol, 1.6 eq.). The mixture was stirred at 110 °C for 24 hours. The catalyst was removed by filtration. 500 mL of ethyl acetate were added to decrease the viscosity of the mixture. Then the organic phase was treated with NaHCO_3 and water until the pH was neutral. Then it was washed with brine solution, dried with anhydrous sodium sulfate and then filtered. The solvent was evaporated under reduced pressure. The ring-opened EMAO with diethylamine (EMAO-DEA) was dried overnight in a vacuum oven at 40 °C. The yield was 78 wt%.

¹H NMR (400 MHz, CDCl₃): δ=5.63-5.45 (m, 1H; C=C)), 5.25 (tt, 1H; CH-Glycerine), 1.35–1.13 (m, 30H; aliphatic CH₂), 0.88 ppm (t, 3H; CH₃).

FTIR: $\tilde{\nu}$ = 3500 (OH vibration), 1732 cm⁻¹ (Ester, C=O Stretching)

7.3.4. Ring-opening of EMAO with hydrochloric acid (EMAO-HCl)

The protocol was adapted from a previously published work (Guo et al. 2000; Peyrton et al. 2019). The reaction was carried out in a round bottom flask equipped with a reflux condenser and a mechanical stirrer. The flask was filled with 500 g of MAO 11 mmol epoxide/g (5.5 mol, 1 eq.), 500 mL of HCl (6 mol, 1.1 eq.) and 0.6 L of acetone. To avoid overheating, the hydrochloric acid (1.5 eq.) was added dropwise in a water-ice bath. The mixture was stirred at room temperature for 2 hours. At the end, the mixture was recovered in 300 mL of ethyl acetate and deionized water. The organic phase was treated with NaHCO₃ until neutral pH. Then it was washed with brine solution, dried over anhydrous sodium sulfate and then filtered. The solvent was evaporated under reduced pressure. The ring-opened EMAO with hydrochloric acid (EMAO-HCl) was dried overnight in a vacuum oven at 40 °C. The yield was 86 wt%.

¹H NMR (400 MHz, CDCl₃): δ=5.63-5.45 (m, 1H; C=C)), 5.25 (tt, 1H; CH-Glycerine), 1.35–1.13 (m, 30H; aliphatic CH₂), 0.88 ppm (t, 3H; CH₃).

FTIR: $\tilde{\nu}$ = 3500 (OH vibration), 1732 cm⁻¹ (Ester, C=O Stretching)

7.4. ³¹P I_{OH} measurements

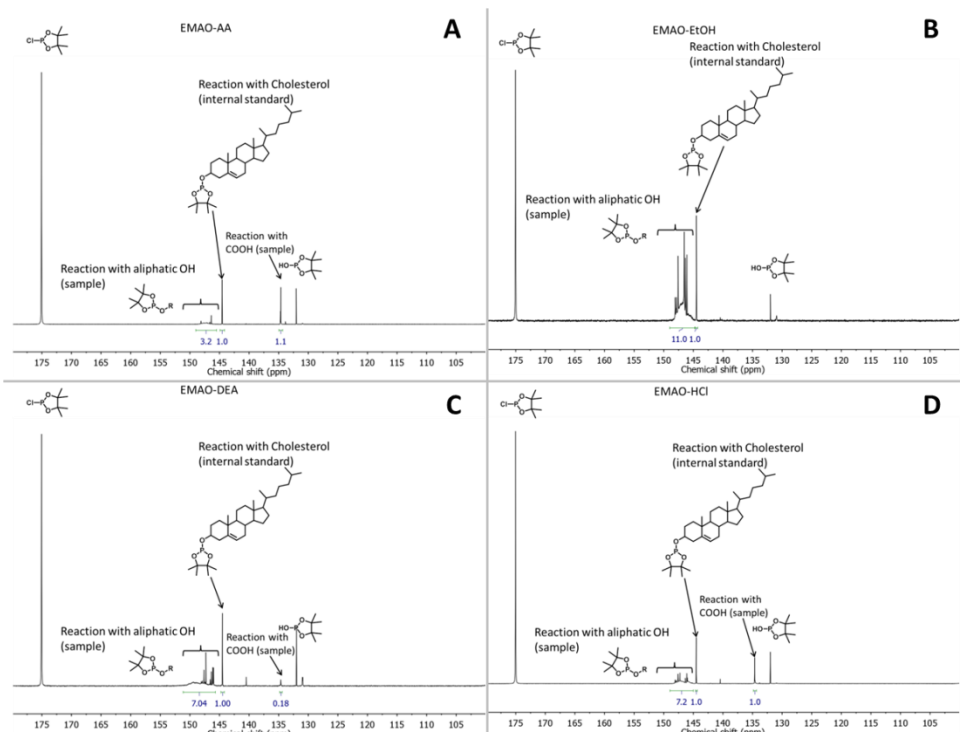
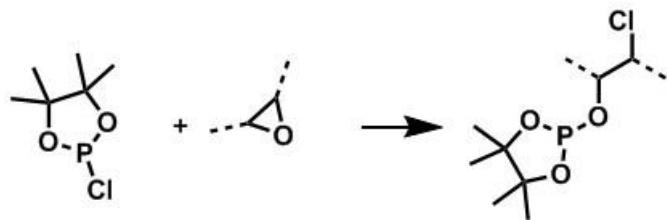


Figure S3.10 - ³¹P NMR analysis for hydroxyl titration of (A) EMAO-AA, (B) EMAO-EtOH, (C) EMAO-DEA and (D) EMAO-HCl.



Scheme S3.2 - Possible reaction of epoxide ring-opening by phospholane reagent.

7.5. Structural characterizations of polyols

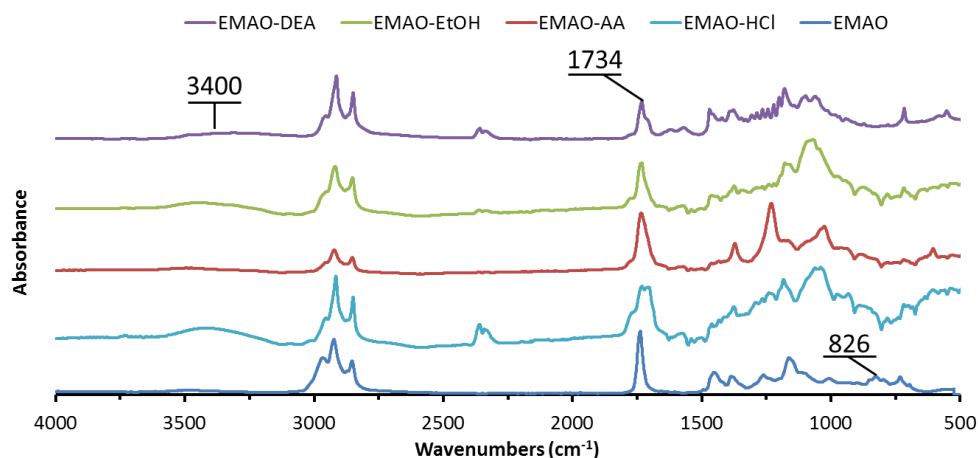


Figure S3.11 - FTIR spectra of EMAO, EMAO-HCl, EMAO-AA, EMAO-EtOH and EMAO-DEA.

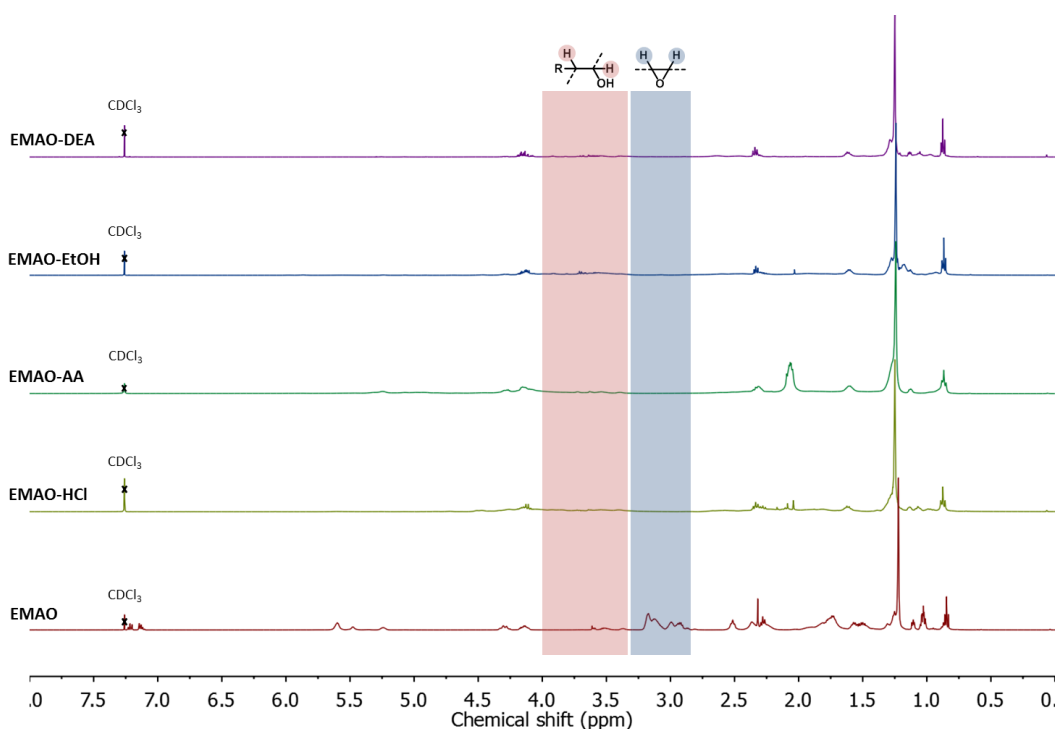


Figure S3.12 - Stacked proton NMR spectra of polyols from EMAO.

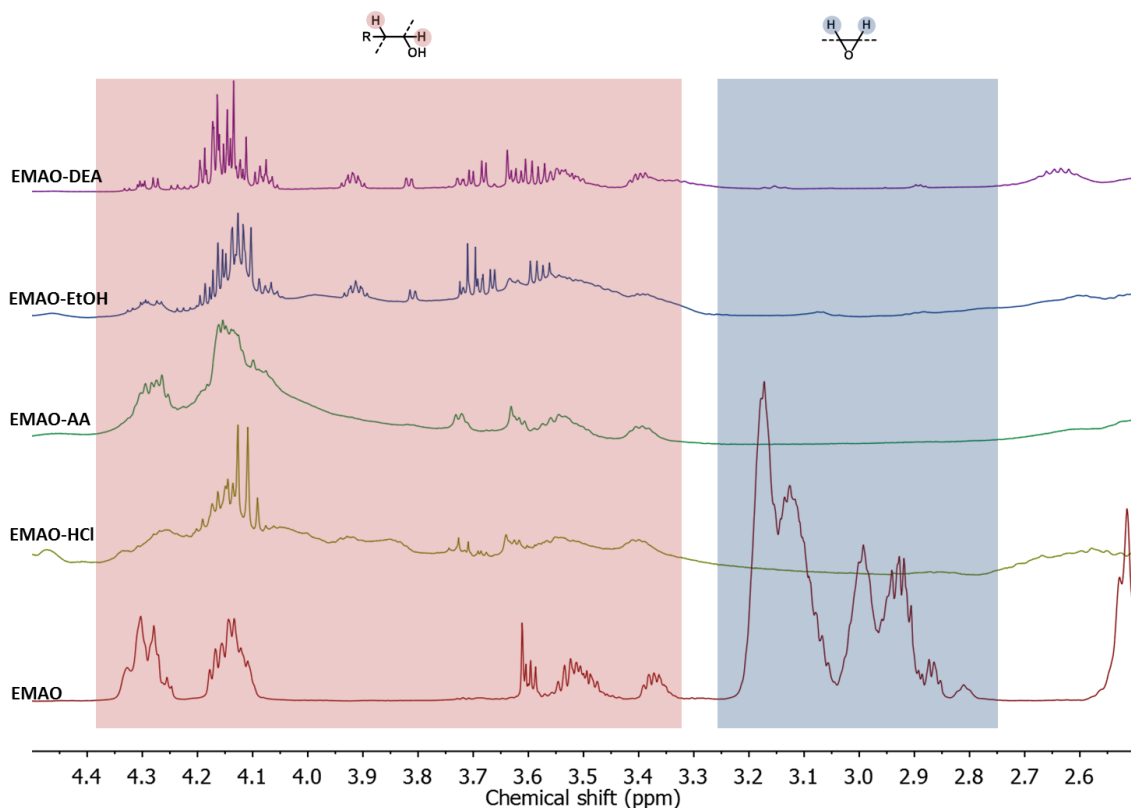


Figure S3.13 - Stacked proton NMR spectra of polyols from EMAO (zoom from 4.5 to 2.5 ppm).

7.6. Crystallization and viscosity behavior with temperature of the different polyols

All the analyses were performed in non-hermetic capsule and the thermograms present the first cooling and second heating ramp.

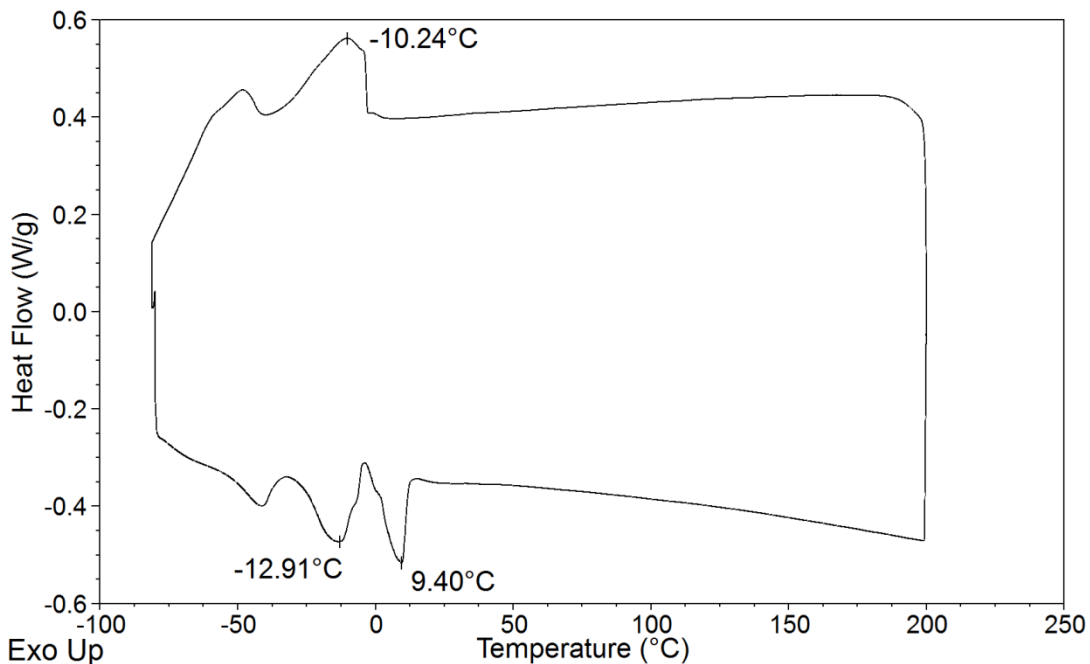


Figure S3.14 - DSC thermogram of MAO.

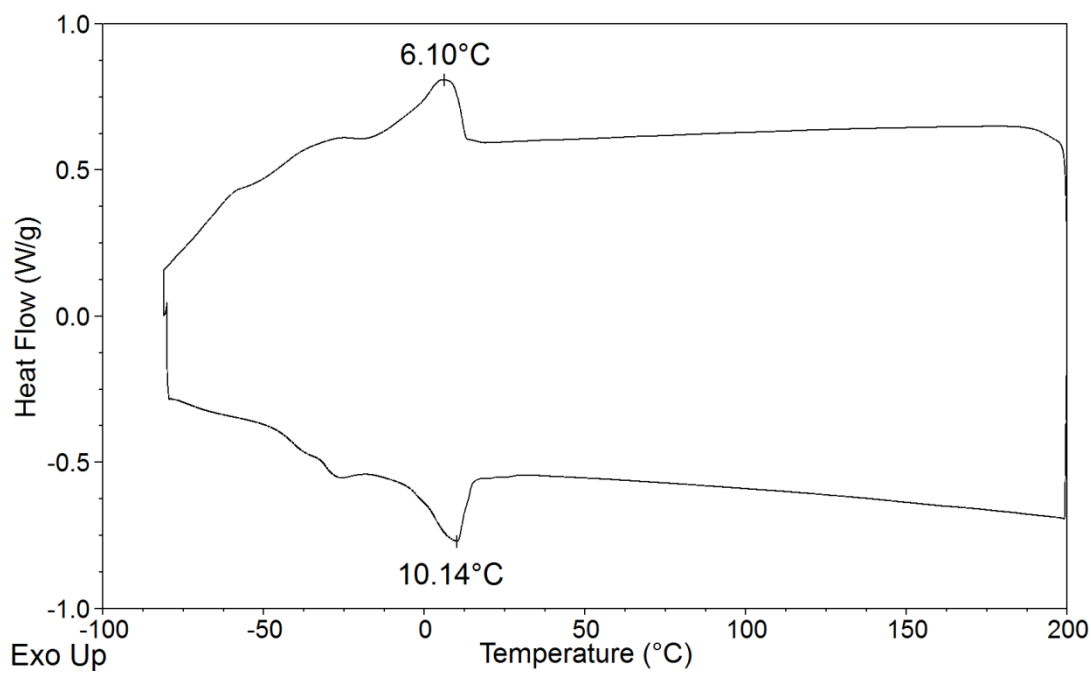


Figure S3.15 - DSC thermogram of EMAO.

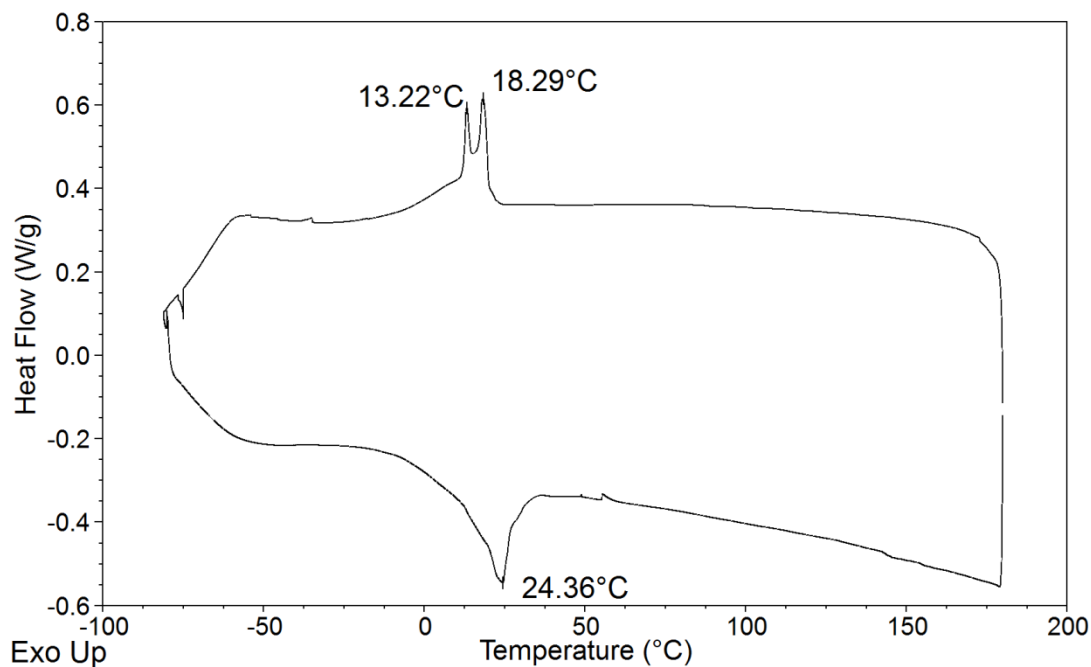


Figure S3.16 - DSC thermogram of EMAO-AA.

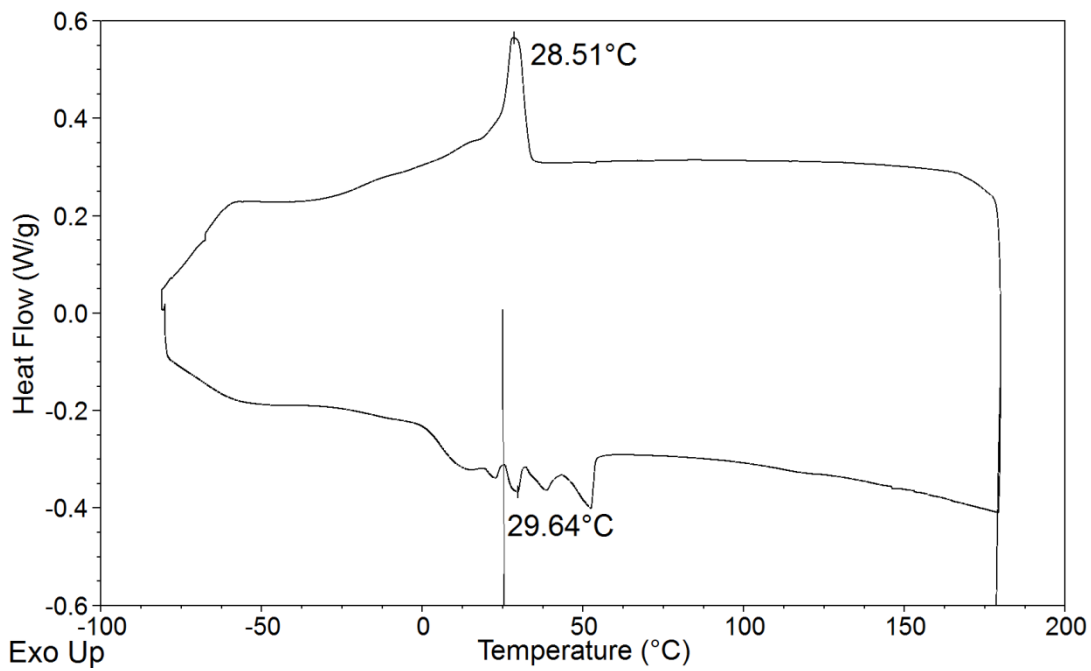


Figure S3.17 - DSC thermogram of EMAO-EtOH.

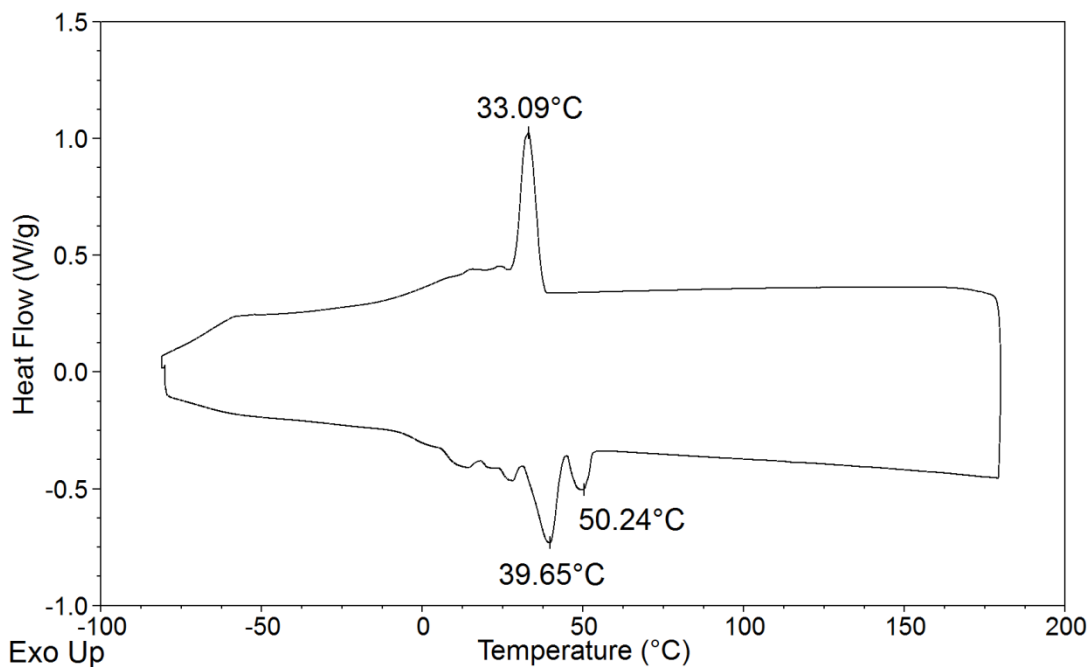


Figure S3.18 - DSC thermogram of EMAO-DEA.

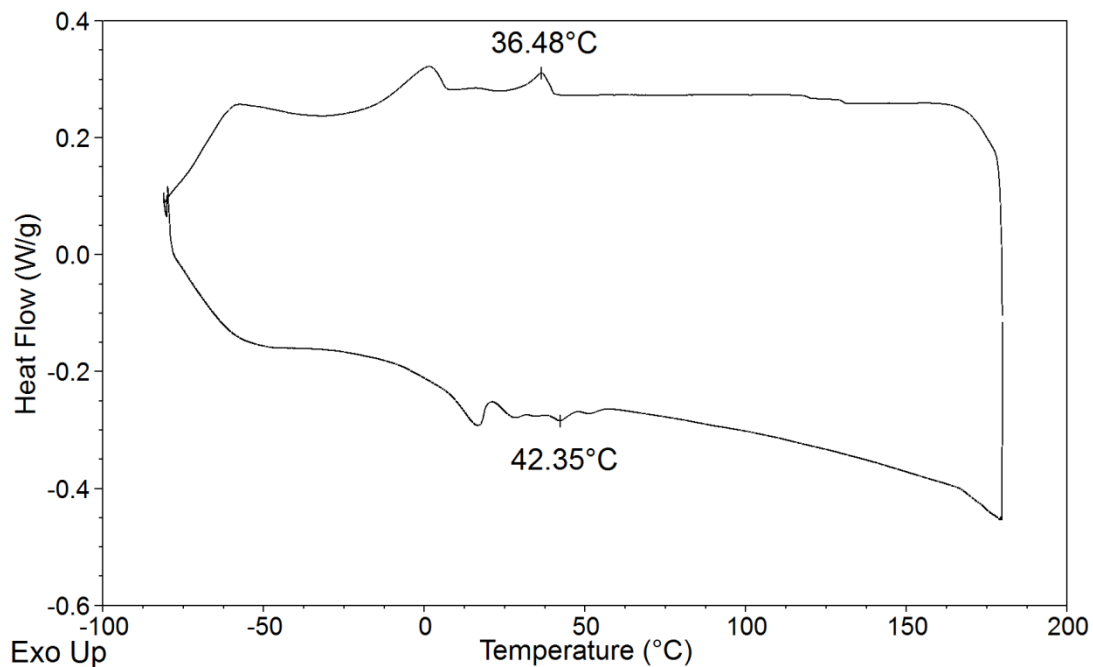


Figure S3.19 - DSC thermogram of EMAO-HCl.

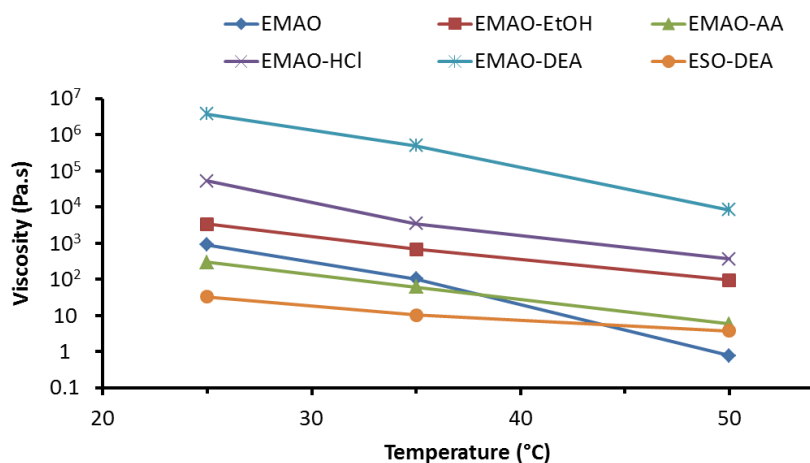


Figure S3.20 - Evolution of the viscosity with temperature of EMAO, EMAO-EtOH, EMAO-AA, EMAO-HCl, EMAO-DEA and ESO-DEA.

7.7. Thermal stability of MAO, EMAO and polyols

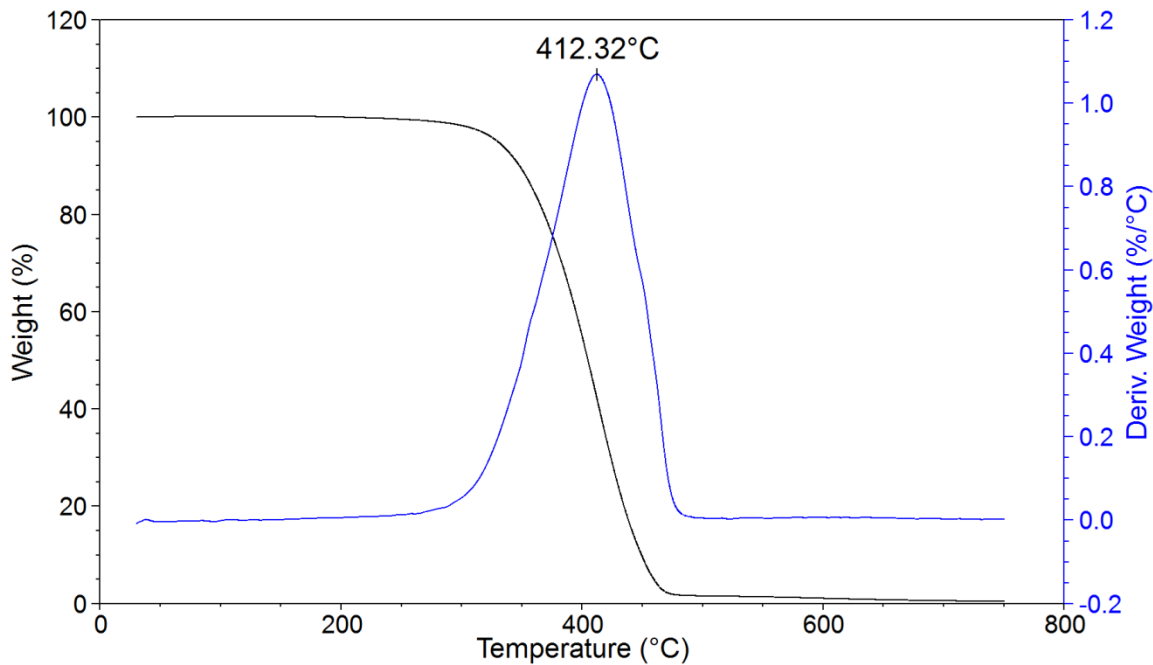


Figure S3.21 - TGA thermogram of MAO.

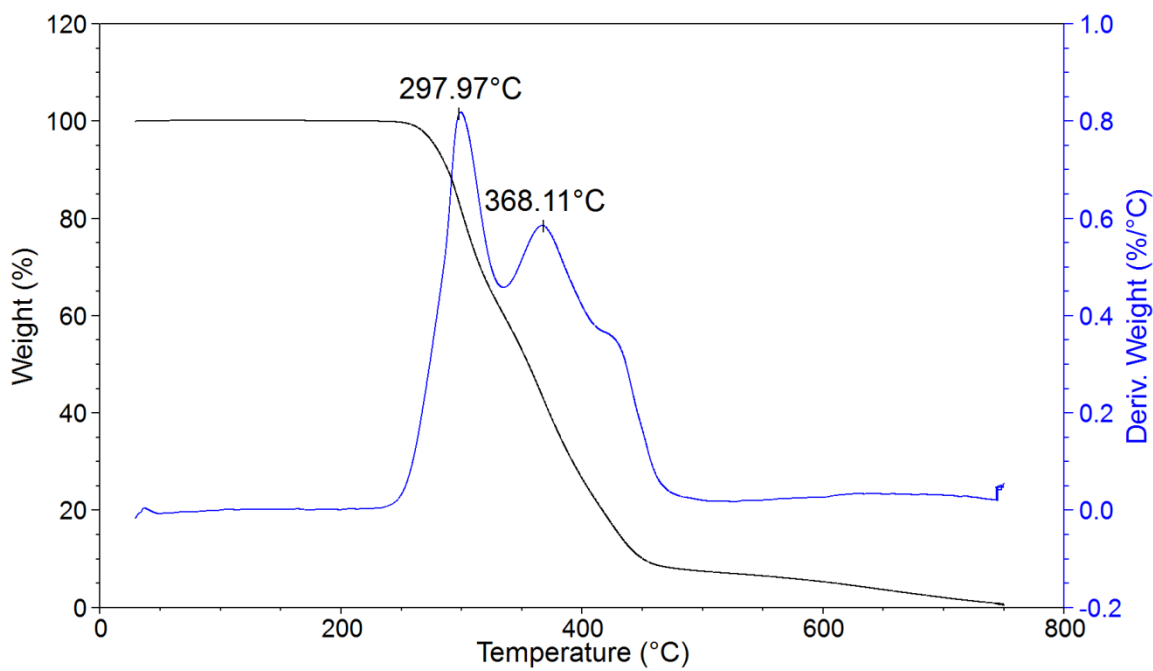


Figure S3.22 - TGA thermogram of EMAO.

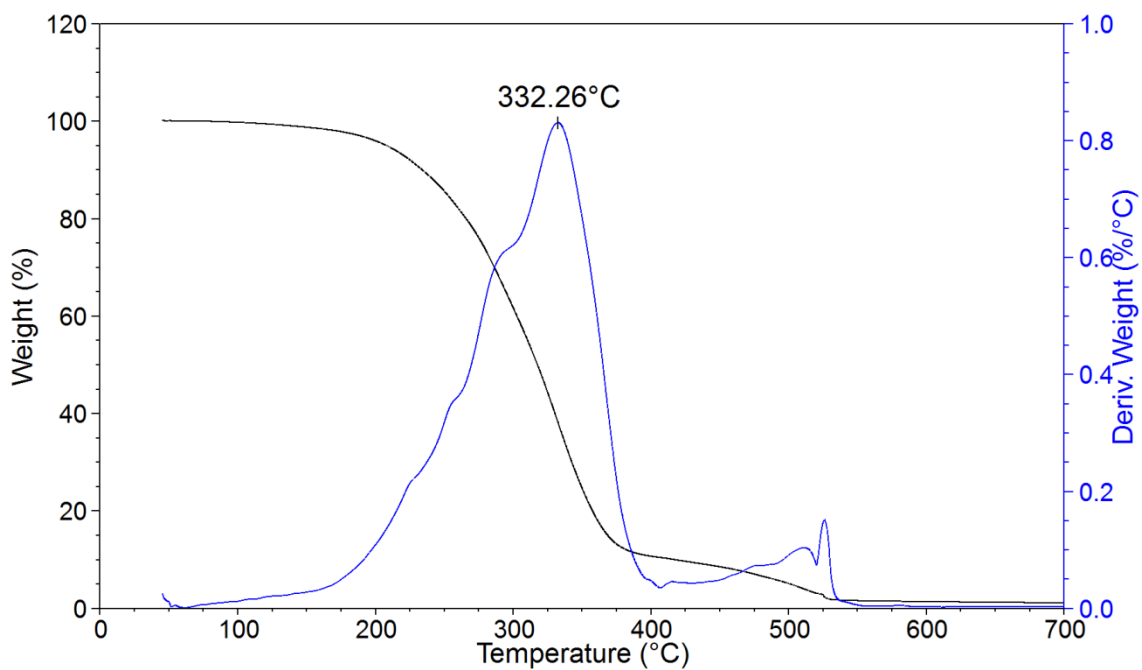


Figure S3.23 - TGA thermogram of EMAO-AA.

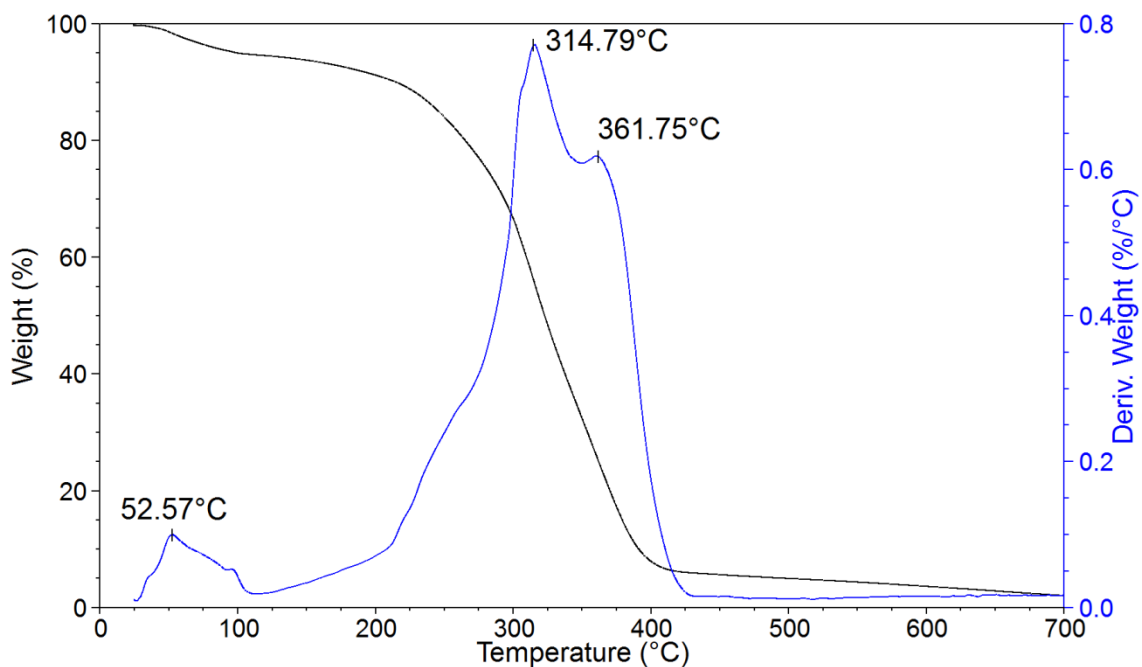


Figure S3.24 - TGA thermogram of EMAO-EtOH.

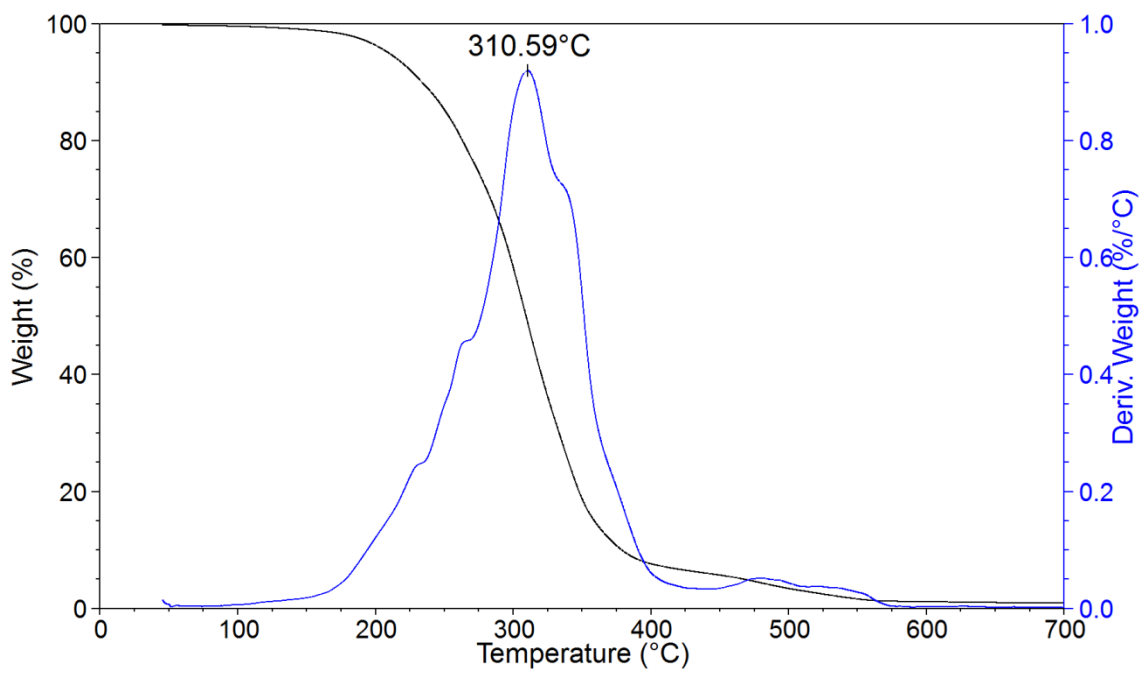


Figure S3.25 - TGA thermogram of EMAO-DEA.

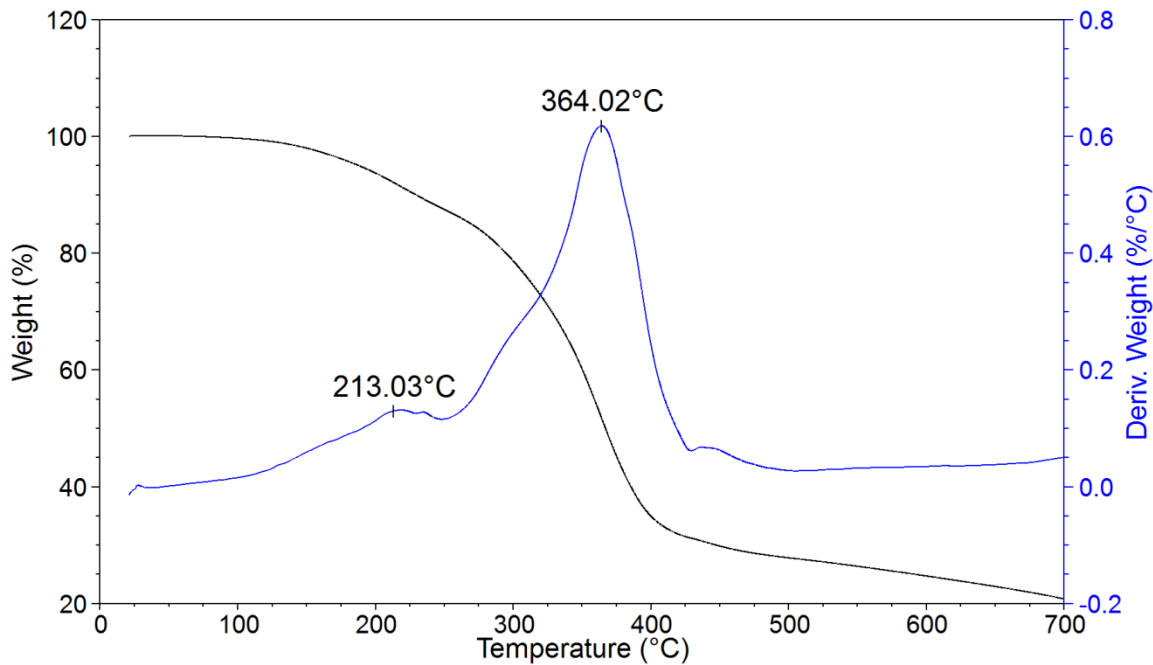


Figure S3.26 - TGA thermogram of EMAO-HCl.

7.8. Foams characteristic times and reactivity determined by Foamat measurements

Table S3.8 - Cream, gel and tack-free times and final height for the different foams.

	Ref	AA 25	DEA 25	HCl 25	EtOH 25	EtOH 35	EtOH 50	EtOH 75	ESO- DEAcat	
<i>Characteristic time (s)</i>										
Cream Time		12 ± 1	21 ± 1	9 ± 1	21 ± 1	15 ± 1	17 ± 1	18 ± 1	19 ± 1	180 ± 1
Gel Time		47 ± 3	79 ± 3	35 ± 3	60 ± 3	53 ± 3	58 ± 3	67 ± 3	91 ± 3	650 ± 3
Tack-free time		62 ± 8	123 ± 8	60 ± 8	91 ± 8	84 ± 8	103 ± 8	113 ± 8	155 ± 8	8
		18.9 ±	18.9 ±	17.4 ±	18 ±	19.1 ±	18.8 ±	18.1 ±	15.8 ±	14.5 ±
Final height (cm)		0.2	0.2	0.2	0.2	0.2	0.2	0.2	0.2	0.2

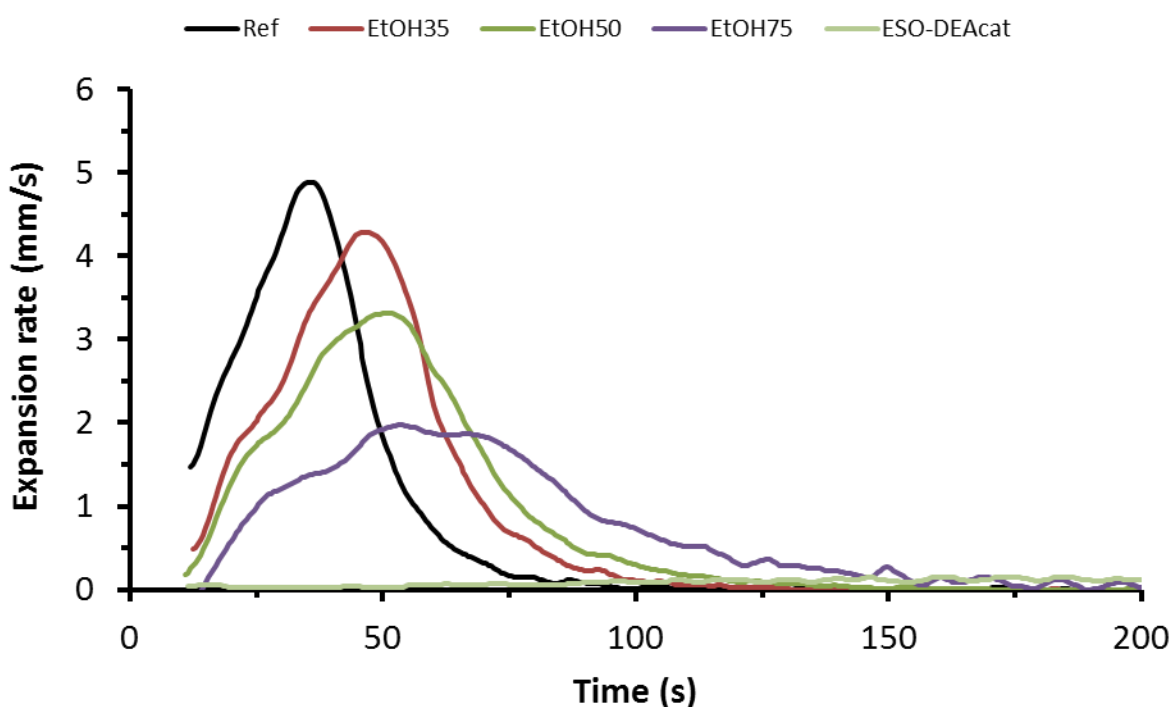


Figure S3.27 - Expansion rate (mm/s) determined with the Foamat device for Ref, EtOH35, EtOH50, EtOH75, ESO-DEAcat.

7.9. Foam cells morphology

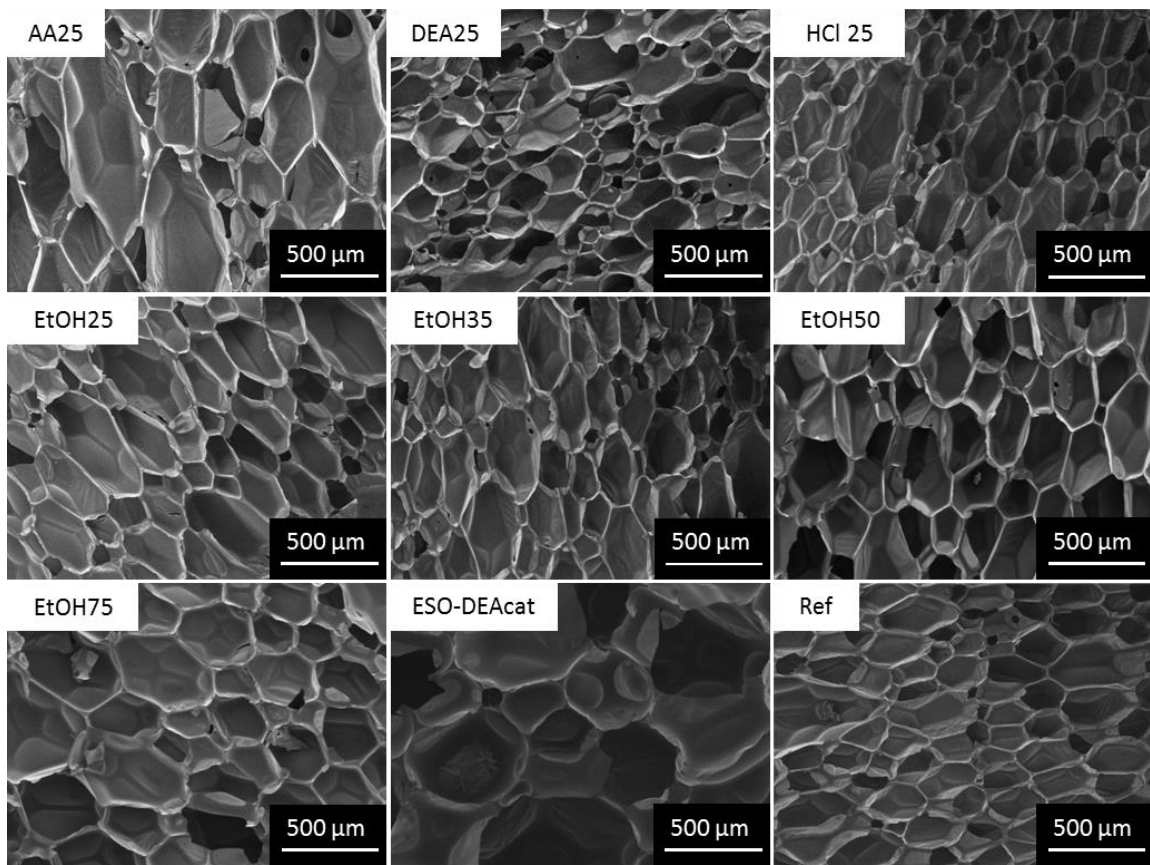


Figure S3.28 - SEM images of all formulations in the longitudinal direction.

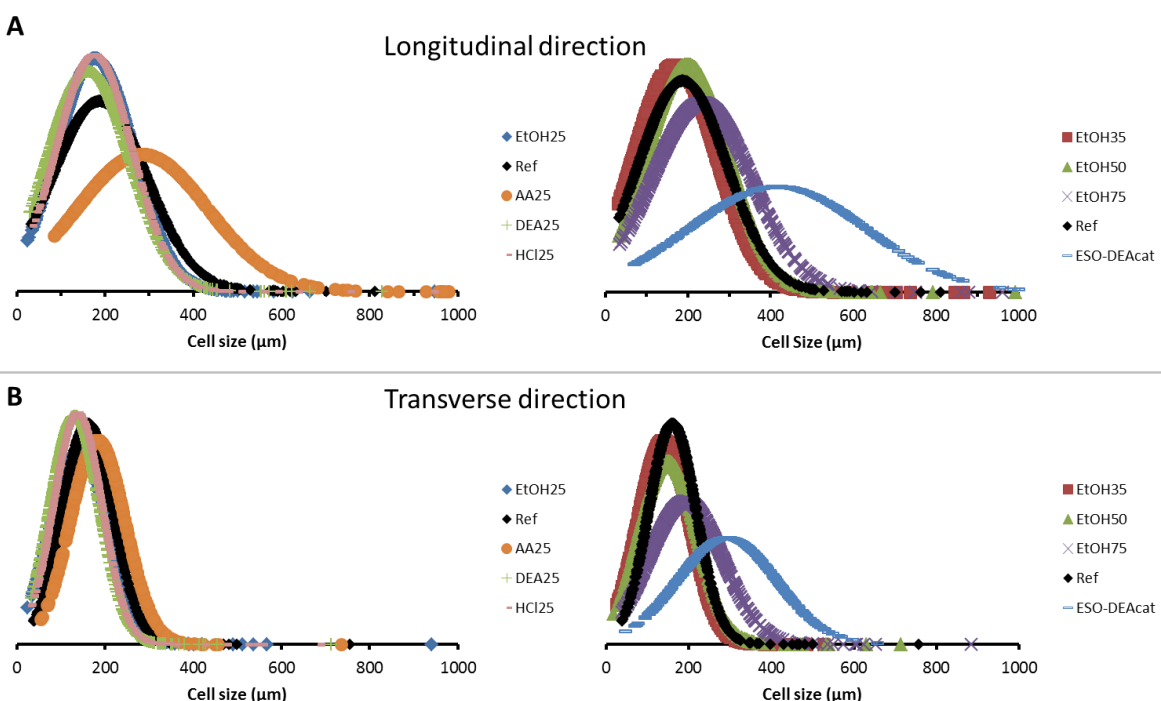


Figure S3.29 - Representation of cell size modeled by a central binomial distribution.

7.10. Foams core-temperature during foam process determined by Foamat measurements

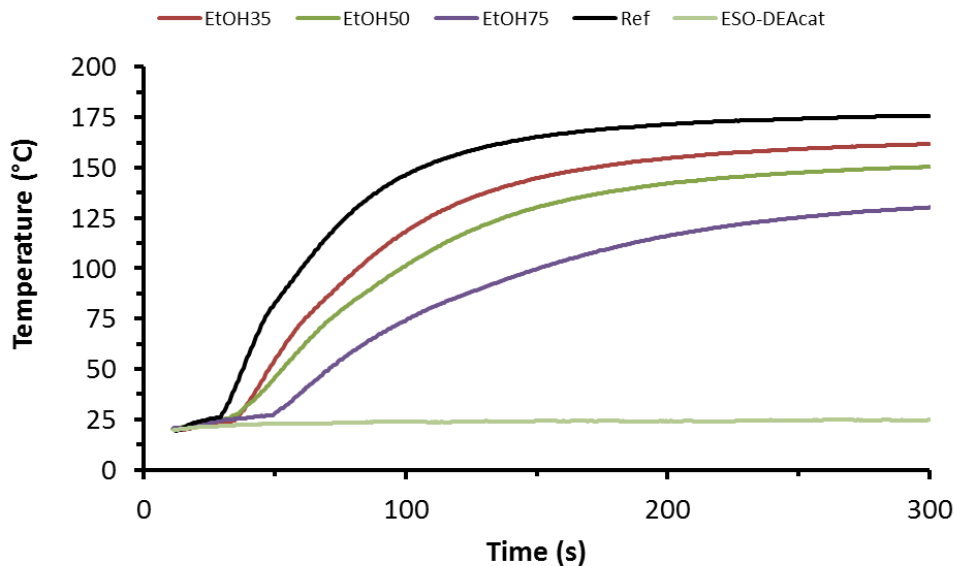


Figure S3.30 - Temperature at the center of the foam recorded with the Foamat device of EtOH 35, EtOH50, EtOH75, Ref and ESO-DEAcat foams.

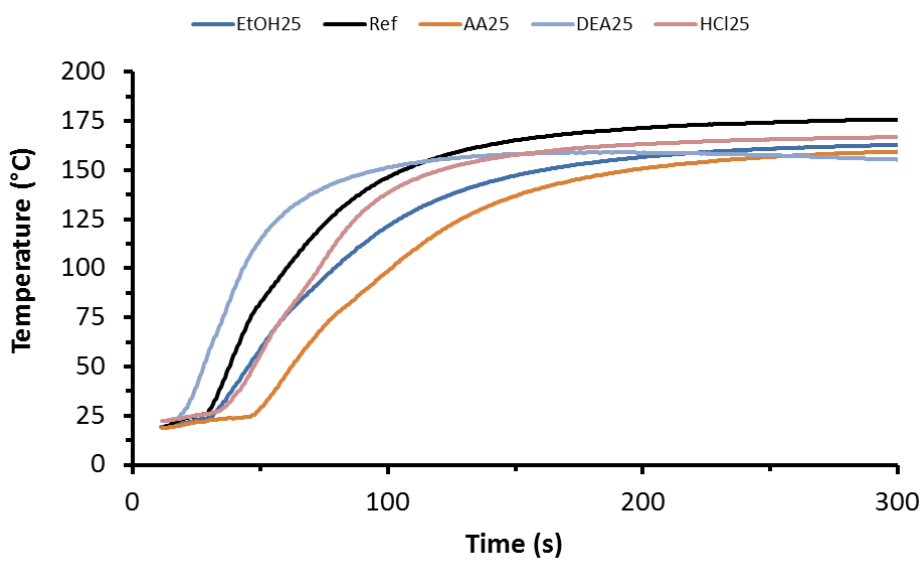


Figure S3.31 - Temperature at the centre of the foam recorded with the Foamat device of EtOH25, Ref, AA25, DEA25, HCl25 foams.

7.11. The density of the foams

Table S3.9 - Density of the different foams.

Ref	AA 25	DEA 25	HCl 25	EtOH 25	EtOH 35	EtOH 50	EtOH 75	ESO- DEAcat	
Density (kg/m ³)	31 ± 2	29 ± 1	30 ± 1	31 ± 1	28 ± 1	28 ± 1	30 ± 1	32 ± 1	36 ± 1

7.12. Synthesis and characterization of a catalytic polyol with ESO

7.12.1. Ring-opening of ESO with diethylamine

The protocol was adapted from a previously published work (Harry-O'kuru et al. 2015; Peyrton et al. 2019). The reaction was carried out in a round bottom flask equipped with a reflux condenser and a mechanical stirrer. The flask was filled with 100 g of ESO 4.1 mmol epoxide/g, (0.41 mol, 1 eq.), 10 g of ZnCl₂ (0.07 mol, 0.18 eq.) and 50 mL of diethylamine (0.48 mol, 1.2 eq.). The mixture was stirred at 90 °C for 24 hours. The catalyst was removed by filtration. 100 mL of ethyl acetate were added to decrease the viscosity of the mixture. Then the organic phase was treated with NaHCO₃ and water until the pH was neutral. Then it was washed with brine solution, dried with anhydrous sodium sulfate and then filtered. The solvent was evaporated under reduced pressure. The ring-opened ESO with diethylamine (ESO-DEA) was dried overnight in a vacuum oven at 40 °C. The yield determined by NMR was 59 mol%.

¹H NMR (400 MHz, CDCl₃): δ= 5.25 (tt, 1H; CH-Glycerine), 4.30 (d, 2H; CH₂-Glycerine), 4.15 (d, 2H; CH₂-Glycerine), 3.2-2.8 (m, 2H; epoxide) 1.35–1.13 (m, 30H; aliphatic CH₂), 0.88 ppm (t, 3H; CH₃)

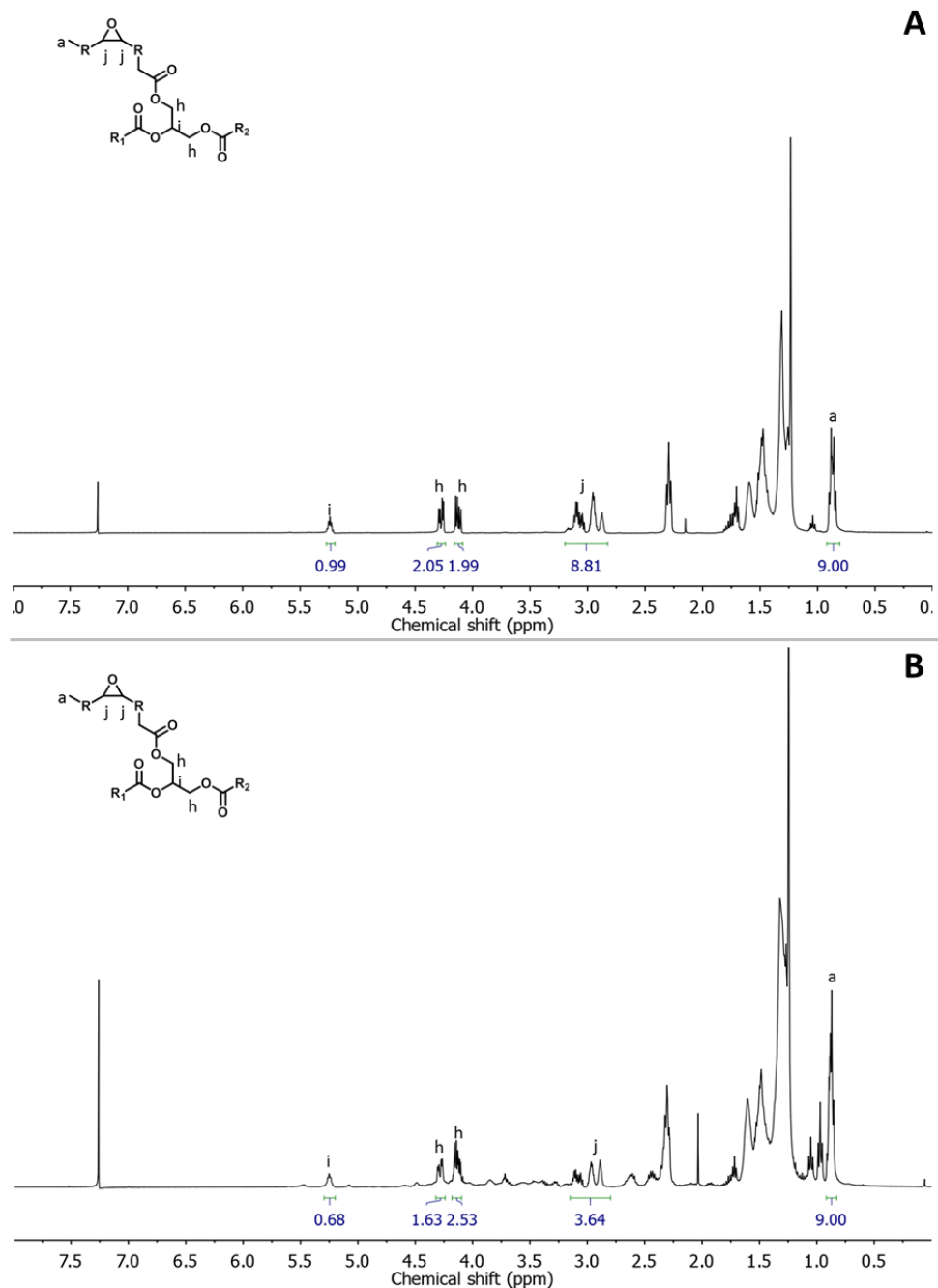


Figure S3.32 - Proton NMR spectrum of ESO (A) and ESO-DEA (B).

7.12.2. Calculation of the real I_{OH} from ^{31}P I_{OH} and epoxide index

The epoxide index unit is changed from the percentage of oxygen to mol epoxide/g by Equation S3.1:

$$EO(\text{mol}_\text{epoxide}/\text{g}) = \frac{EO(\%O)}{1600} \quad (\text{S3.1})$$

Assuming full conversion of epoxide in hydroxyl without side-reactions, the quantity in moles of epoxide is the same as the quantity of hydroxyl, but the molar mass is changing with the addition of the ring-opening reagent. In this case, the diethylamine (73.14 g/mol) was taken as the ring-opening

reagent. From the EO (mol_epoxide/g), the theoretical I_{OH} in mol OH/g can be calculated by Equation S3.2.

$$I_{OH_{Th}} = \frac{EO(\text{mol_epoxide} / \text{g})}{(1 + 73.14 * EO(\text{mol_epoxide} / \text{g}))} \quad (\text{S3.2})$$

The transformation of the I_{OH} (mol OH/g) in mg KOH/g is done with Equation S3.3.

$$I_{OH}(\text{mgKOH} / \text{g}) = I_{OH}(\text{mol_OH} / \text{g}) * 56100 \quad (\text{S3.3})$$

The real I_{OH} is calculated from the I_{OH} results from ^{31}P measurement and the epoxide index with Equation S3.4.

$$\text{Real_}I_{OH}(\text{mgKOH} / \text{g}) = I_{OH}(\text{mol_OH} / \text{g}) - EO(\text{mol_epoxide} / \text{g}) \quad (\text{S3.4})$$

Calculations were done on the partially ring-opened ESO by diethylamine and synthesized in Table S3.10.

Table S3.10 - Calculation of the real I_{OH} index results and conversions.

Characterization	Unit	Result	Conversion (function)
Initial epoxide index	% OE	6.6	
	mmol epoxide/g	4.13 ± 0.06	
Epoxide index	% OE	2.1 ± 0.1	68% (epoxide)
	mmol epoxide/g	1.31 ± 0.06	
I_{OH} exp	(mg KOH/g)	190 ± 10	
	mmol OH/g	3.39 ± 0.2	
I_{OH} th	(mg KOH/g)	180	
Real IOH	(mg KOH/g)	120 ± 10	
	mmol OH/g	2.1 ± 0.1	66% (OH)

The NMR conversion based on Figure S3.32 is 59%.

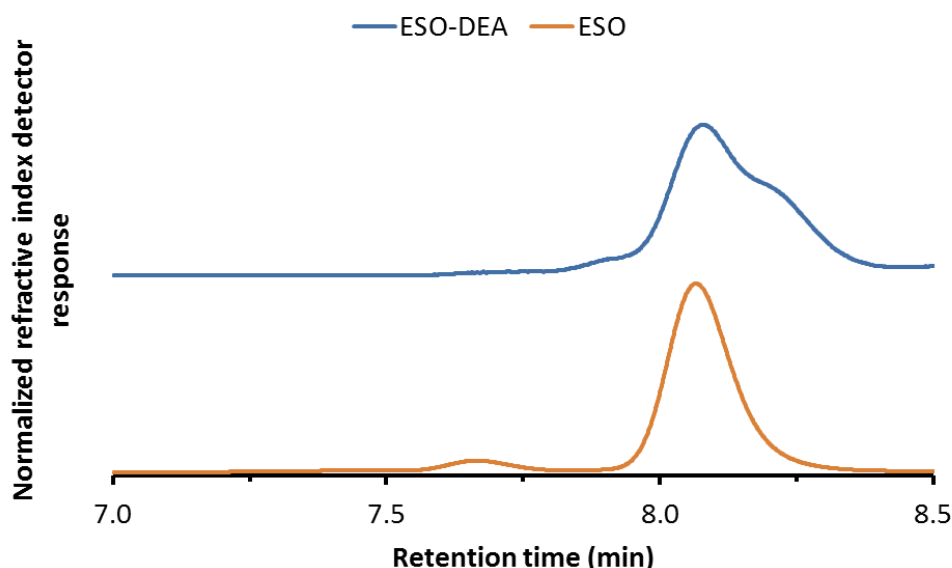


Figure S3.33 - Size exclusion chromatography of ESO and ESO-DEA.

7.13. Results of TGA and DTG of the foam

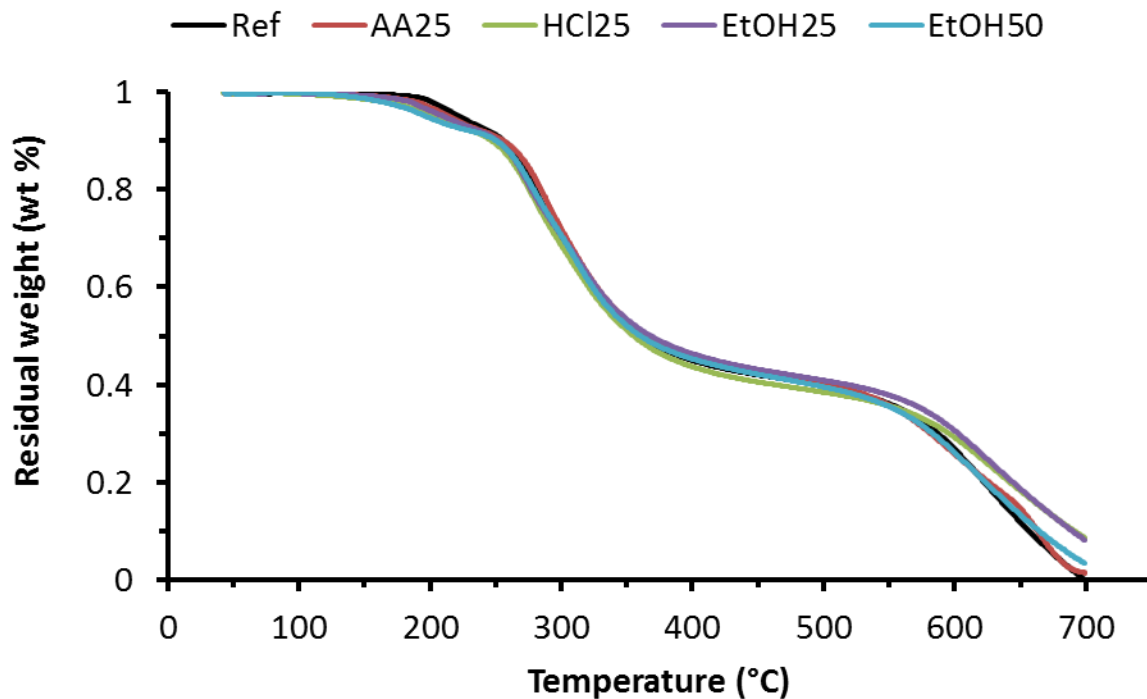


Figure S3.34 - TGA of Ref, AA25, HCl25, EtOH25 and EtOH50 foams under nitrogen.

Table S3.11 - TGA and DTG data for Ref, AA25, HCl25, EtOH25 and EtOH50 foam.

		Ref	AA25	HCl25	EtOH25	EtOH50
TGA	$T_{5\%}$	223	206	219	218	204
	$T_{50\%}$	359	358	367	361	356
DTG	$T_{deg\ max\ 1}$	280	279	288	273	277
	$T_{deg\ max\ 2}$	331	315	312	318	311
	$T_{deg\ max\ 3}$	615	615	660	615	620

7.14. FTIR characterizations of foams

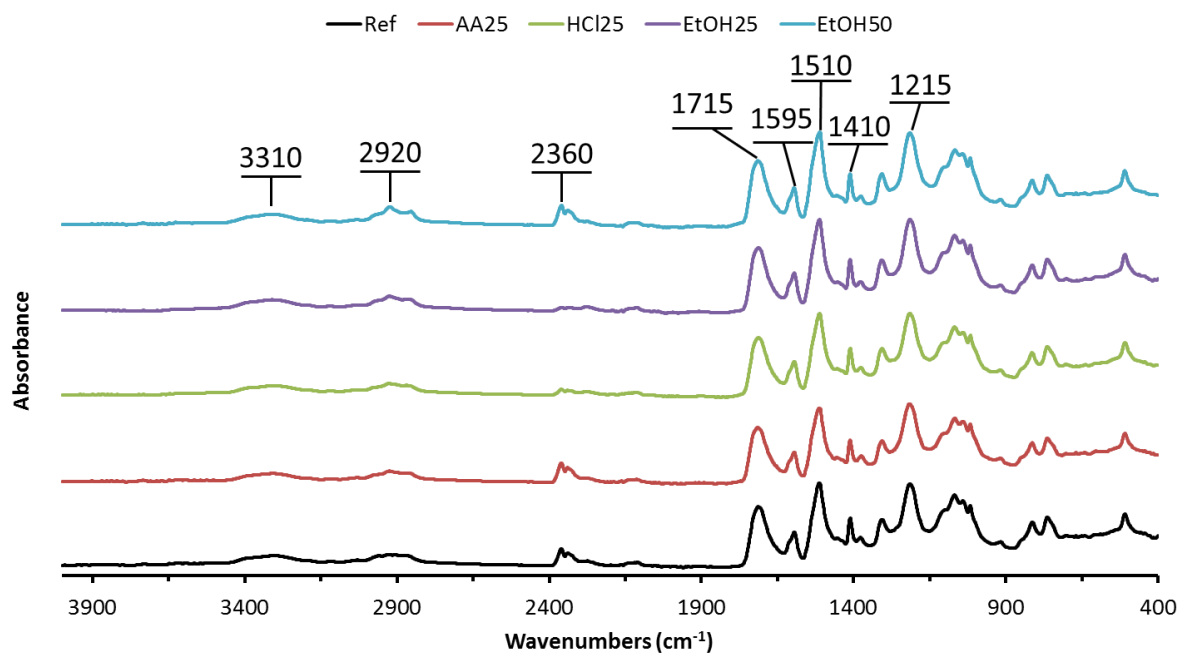


Figure S3.35 - FTIR spectra in absorbance mode of Ref, AA25, HCl25, EtOH25, EtOH50 foams.

Conclusion chapitre 3

Le but de ce chapitre était d'étudier l'impact des polyols dérivés d'huile de microalgues sur les mousses polyuréthanes. Cet objectif a été atteint avec une caractérisation complète des monomères, de la mise en œuvre des mousses et des propriétés finales des matériaux.

Les protocoles développés dans le chapitre précédent ont été appliqués à l'huile de microalgues pour synthétiser des polyols. Après caractérisation en terme de viscosité, fonctionnalité, masse molaire, stabilité thermique, teneur en hydroxyle, époxyde et acide, le polyol obtenu par ouverture avec l'éthanol présente des caractéristiques très proches de polyols conventionnels classiquement utilisés pour les mousses polyuréthanes. La stabilité thermique légèrement supérieure du polyol obtenu par ouverture de cycle avec l'acide chlorhydrique, est attribuée à la présence d'atomes de chlore.

Les nouveaux polyols biosourcés synthétisés ont tout d'abord été introduits dans les formulation des mousses à hauteur de 25% en masse par remplacement du polyol conventionnel. Leur impact sur la formation de la mousse est mesuré en suivant la vitesse d'expansion, la température au cœur de la mousse et les différents temps caractéristiques. La mousse produite avec le polyol obtenu par ouverture de cycle avec l'éthanol présente des propriétés de mise en œuvre très proches de la mousse de référence. Afin d'étudier en profondeur l'impact de ce polyol, trois mousses supplémentaires avec des taux de substitution plus élevés ont ensuite été réalisées. Les propriétés de mise en œuvre de ces mousses se sont éloignées de la mousse de référence. Ces caractérisations mettent aussi en avant la réactivité élevée du polyol obtenu par ouverture de cycle avec la diéthylamine. La réactivité élevée des polyols obtenus par ouverture d'huile epoxydée avec la diéthylamine a été mise à profit pour former une mousse sans catalyseur. Dans ce cas, l'huile de soja a été utilisé du fait de sa plus faible viscosité par rapport à l'huile de microalgues. La vitesse d'expansion de cette mousse est très lente comparée à la référence. La densité de la mousse réalisée avec le catalyseur biosourcé est cependant similaire aux autres mousses réalisées dans cette étude. Ce résultat est une avancée significative pour le domaine des catalyseurs biosourcés pour les mousses polyuréthanes.

Les mousses proches de la référence en termes de paramètres de mise en œuvre ont été plus amplement analysées. Leur morphologie, résistance à la compression et tenue au feu ont été mesurées et comparées à la mousse de référence fossile. La conductivité thermique a également été mesurée en pour évaluer un paramètre majeur pour des mousses rigides à cellules fermées : l'isolation thermique. Toutes ces caractérisations démontrent que le polyol d'origine fossile peut être partiellement remplacé par un polyol obtenu à partir d'huile de microalgues sans perte de propriétés.

CHAPITRE 4. FORMATION D'OXAZOLIDONES À PARTIR D'HUILE ÉPOXYDÉE DANS LE CAS DES MOUSSES POLYURÉTHANES



Introduction Chapitre 4

Ce chapitre se présente sous la forme d'un article intitulé « Oxazolidone formation: myth or fact? The case of biobased polyurethane foams from different epoxidized triglycerides » soumis dans *Polymer Chemistry*.

Le chapitre précédent a mis en avant la possibilité de former des polyols adéquats par époxydation et ouverture de cycle pour la formulation de mousses polyuréthanes. Elles ont été obtenues par polyaddition entre un polyol et un polyisocyanate. En théorie, les époxydes régissent aussi avec les fonctions isocyanates pour former des hétérocycles à 5 membres : les oxazolidones. Ces groupements ont une stabilité thermique plus élevée que les groupements uréthanes. La formation d'oxazolidones par réaction directe entre les huiles époxydées et les isocyanates dans les mousses polyuréthanes pourrait permettre de renforcer leur résistance à la dégradation thermique et de s'affranchir d'une étape de synthèse.

La formation d'oxazolidone par réaction avec des isocyanates a été étudiée avec des époxydes terminaux, peu encombrés et réactifs. Parmi eux, le diglycidyl éther de bisphénol A (DGEBA) et ses dérivés ont été très explorés. Les époxydes provenant de triglycérides sont disubstitués et sont donc moins réactifs. Néanmoins, l'introduction d'huile époxydée en remplacement du polyol dans les polyuréthanes a été étudiée auparavant notamment dans le cadre d'une thèse au sein de l'institut. Selon ces études, la dégradation thermique est ralentie par la présence d'oxazolidones. Cependant, ce groupement n'a cependant jamais été clairement identifié lors de la production de mousses.

L'objectif de ce chapitre est d'étudier la formation de groupements oxazolidones à partir d'huile époxydée dans les mousses polyuréthanes. L'impact sur la mise en œuvre des mousses du remplacement du polyol par l'huile de soja époxydée est étudié. Des mousses sont synthétisées avec du polyol issus d'huile de microalgues en partie. Les composés non liés par liaisons covalentes au réseau polymère sont ensuite extraits dans des matériaux alvéolaires élaborés, issus de différentes origines. Les analyses permettent de déterminer les structures de ces composés. Enfin, les huiles époxydées et les polyisocyanates utilisés dans les mousses sont modélisés (modèles réactionnels) pour mieux comprendre la formation des oxazolidones afin de tenter de répondre à diverses questions scientifiques encore ouvertes.

Oxazolidone formation: myth or fact? The case of biobased polyurethane foams from different epoxidized triglycerides

Julien Peyrton and Luc Avérous

Article submitted in *Polymer Chemistry*

1. ABSTRACT

Polyurethane foams (PUF) are generally obtained by polyaddition between polyisocyanate and polyols. In this context, biobased polyols can be obtained by oleochemistry, modifying triglycerides by epoxidation and epoxide ring-opening with a nucleophile. In the frame of green chemistry principles, which claims, e.g., the reduction of the derivatives and the synthesis steps, we explore the direct use of epoxidized oil for PUF fabrication to avoid the specific intermediate step of polyols synthesis. The reaction between epoxides and isocyanates is known to yield the thermally stable oxazolidone groups. In PUF system, the incomplete reaction between epoxidized oil and isocyanate was proved by the presence of unreacted epoxidized oil identified by ^1H NMR and FTIR in compounds unbonded to the polymer network. To understand this incomplete reaction, oxazolidone formation was largely investigated through different reactional models using various catalysts and epoxides. The steric hindrance of the epoxide group was found to limit the formation of oxazolidone.

2. INTRODUCTION

Polyurethanes (PUs) are major polymers since they rank 6th among all polymers with a production of around 22 million tons (Hicks and Austin 2017) and a global market of \$50 billion in 2016. The PU market is usually segmented into five uneven parts such as the soft and rigid foams (65% of the market), the coatings (13%), the elastomers (12%), the adhesives (7%) and the others, including biomedical field (3%) (Akindoyo et al. 2016).

PU can be obtained without isocyanate (Carré et al. 2019), but the very rich and conventional PU chemistry is till now mainly linked to the high reactivity of isocyanates toward the H-labile groups, e.g., alcohols, water or amines. Furthermore, the intermolecular reactions between two isocyanates form uretdiones or carbodiimides (Fink 2018). The trimerization of polyisocyanate yields a polyisocyanurate network (PIR), which presents high thermal stability compared to PU systems. The

thermal stability of the oxazolidone group obtained by reaction between epoxide and isocyanate (Scheme 4.1) was found to be an intermediate between urethane and isocyanurate group (Kordomenos et al. 1987). The first synthesis of oxazolidone was reported in 1958 by the reaction between ethylene oxide and phenyl isocyanate with quaternary ammonium halide catalyst (Speranza and Peppel 1958). This epoxide-isocyanate reaction was further investigated and proved to be catalyzed by ammonium salts (Javni et al. 2003; Speranza and Peppel 1958), lanthanide salts (Barros and Phillips 2010; Qian and Zhu 1994; Wu et al. 2003), halides (Aroua and Baklouti 2007; Herweh et al. 1968; Herweh 1968; Siegel and Wittmann 1982), tertiary amines (Caille et al. 1990a), imidazoles (Caille et al. 1990b) or Lewis acids (Baronsky et al. 2013). The studies to synthesize thermally stable polymers were primarily developed with a monosubstituted epoxide, particularly the diglycidyl ether of bisphenol A (DGEBA) and its derivatives (Bakry et al. 2016; Flores et al. 2012; Pilawka et al. 2014; Robert et al. 2018).



Scheme 4.1 - Oxazolidone group synthesis from epoxide and isocyanate.

To reduce the environmental impact of the polymers, they are more and more often biobased, i.e., obtained from biomass. It is, for instance, particularly the case of the PUs, which are largely produced from oleochemistry in a sustainable approach. The building blocks, obtained more or less directly from biomass, can present particular chemical structures. Then, new PUs with innovative macromolecular architectures are more and more often produced (Furtwengler and Avérous 2018). From the biomass extraction to the material elaboration, the biomolecules are transformed through various chemical or biological processes to introduce reactive groups. The reduction of these synthesis steps fulfills at least one of the principles for green chemistry with also several economic advantages (Anastas and Eghbali 2010). The triglycerides are often epoxidized and further ring-opened with a nucleophile to form polyols for PU synthesis (Desroches et al. 2012; Maisonneuve et al. 2016). However, in vegetable oils and fats, the double bonds are not generally terminal, and the epoxides are then mainly disubstituted and, consequently, less reactive than terminal ones. Several studies investigated the introduction of epoxidized oils into various PU (Arbenz et al. 2017; Fourati et al. 2017; Lee et al. 2007). In the case of PUF, the substitution of 25wt% of the polyol by epoxidized microalgae oil was, for instance, claimed to improve the thermal stability of the foam (Arbenz et al. 2017). However, the oxazolidone formation was never clearly identified due to the numerous groups formed in the foam system.

This work aims to clarify the potential formation of oxazolidone with epoxidized oils in PUF systems. Foams with gradual substitution from 0 to 100 wt% of the polyol by epoxidized soybean oil (ESO) were studied to evaluate the impact of the ESO on the maximum foam height. Different PUF from microalgae oil (AO), epoxidized AO (EAO) and epoxidized rapeseed oil (ERO) were Soxhlet extracted in order to identify potential unreacted reagents. The identification of the molecules present

in the soluble fraction was realized by FTIR and ^1H NMR after purification with column chromatography. To further understand the reaction occurring in PUF between epoxide and isocyanate, a model system was designed with different epoxides: (i) a monosubstituted epoxide (DGEBA), (ii) an epoxidized methyl undecylenate (Mundex) and (iii) an epoxidized methyl oleate (EVHOSO). The reaction between epoxide and phenyl isocyanate was catalyzed by different catalysts, i.e., used in PUF formulation or specific to the oxazolidone formation. Each corresponding products were separated and carefully identified to endorse the oxazolidone formation in PUF.

3. EXPERIMENTAL SECTION

3.1. Materials and chemicals

AO was kindly supplied by Fermentalg (France) and was extracted from microalgae (*Schizochytrium sp.*). The epoxidation of AO (1 eq.) was performed by ITERG (France) via an in-situ peracid formation using formic acid (0.33 eq.), toluene (0.5 L/kg of AO) and H_2O_2 (2.5 eq.) according to a previously described protocol (Arbenz et al. 2017; Petrović et al. 2013). The resulting EAO was obtained with a 74 wt% yield. The EVHOSO was obtained from a previous protocol (Peyrton et al. 2019).

Meta-Chloroperoxybenzoic (m-CPBA), anhydrous aluminium trichloride (AlCl_3) (98.5%), tetra-n-butylammonium bromide (TBAB) (98%), ethyl acetate (99%), methanol and cyclohexane were obtained from Fisher Scientific (France). Deuterated chloroform (CDCl_3), phenyl isocyanate (98%), benzyl dimethylamine (BDMA) (99%), potassium acetate (KOAc) (99%) and aluminum complexed by salen ligand ($\text{Al}(\text{salen})_2$) were provided by Sigma-Aldrich (France). Acetone was purchased from VWR (France). Commercial ESO (Weepox01 from Brenntag in German) and low molar mass epoxy resin, DGEBA, (epoxy value = 175 g/mol, supplied by Dow chemicals) were also supplied by their corresponding providers.

The polyisocyanate used is a polymeric 4,4'-methylene bis(phenyl isocyanate) identified as pMDI (NCO index = 31%, Desmodur® 44V70L from Covestro in Germany). N,N-Dimethylcyclohexylamine (DMCHA) provided by Sigma-Aldrich (France) was used as a catalyst for both blowing and gelling reactions. Potassium 2-ethyl hexanoate dissolved in ethylene glycol (P2H-EG) and a mixture of 1,3,5tris(3-dimethylaminopropyl)-s-hexahydrotriazine and Bis(2-dimethylaminoethyl)ether dissolved in dipropylene glycol (52%) (TDH-BDE) catalyzed the trimerization reaction (Kzero 3000 and PM 20+ from Momentive in Germany). A polyether polysiloxane (PoSi) copolymer (Tegostab® B84501 from Evonik in Germany) was used as a surfactant. Pentane, diethyl ether or demineralized water were used as a blowing agent. A reference fossil-based aromatic polyester polyol synthesized by esterification of phthalic anhydride by diethylene glycol (Pht-DEG) (Stepanpol® PS1912 from Stepan in the Netherlands) was used. This polyol is usually designed for rigid PUF with closed cells.

3.2. General procedure of PUF synthesis

Foams were prepared via an A-B composition. In a plastic cup, the A-part consists of the polyols mixture, catalysts, the surfactant (PoSi), the physical (diethyl ether or pentane) and chemical (water) blowing agents. They were weighed and mixed using a mechanical stirrer. The physical blowing agent content was determined to obtain foams with similar densities. The B-part containing the polyisocyanate is quickly added. The final mixture is vigorously stirred with a mechanical stirrer for 5 seconds, and the foam is let to rise freely in a plastic cup.

3.3. PUF synthesized by gradual introduction of ESO

Different foams were recently synthesized to investigate the impact of fossil-based polyol (Pht-DEG) substitution by a renewable epoxidized oil (ESO), to skip the conventional intermediate step based on the polyol synthesis. The PUFs presented in Table 4.1 were elaborated with a gradual substitution of Pht-DEG by ESO from 0 to 100 wt%. The formulations were named according to the substitution degree. For example, the foam named 35ESO corresponds to a substitution of 35 wt% of Pht-DEG by ESO.

The isocyanate/hydroxyl (NCO/OH) molar ratio was kept constant at 3.2, in all formulations. Every reactive group toward isocyanate in the formulation was accounted for, i.e., water, Pht-DEG and ESO, to determine the isocyanate quantity. Isocyanate groups are in large excess for PIR foams fabrication. The catalyst (P2H-EG and TDH-BDE), surfactant (PoSi) and chemical blowing agent (water) contents were fixed at 1.2, 3, 2.5 and 0.9 parts by weight of polyol, respectively. The physical blowing agent (diethyl ether) content was adapted to produce foams with an equivalent density.

Table 4.1 - PUF Formulations with increasing ESO content.

Foam formulation		0ESO	15ESO	35ESO	50ESO	75ESO	100ESO
<i>A-Part</i>							
Polyols	Pht-DEG (fossil-based)	100	85	65	50	25	0
	ESO		15	35	50	75	100
Catalyst	TDH-BDE	1.2	1.2	1.2	1.2	1.2	1.2
	P2H-EG	3	3	3	3	3	3
Surfactant	PoSi	2.5	2.5	2.5	2.5	2.5	2.5
Blowing agent	Water	0.9	0.9	0.9	0.9	0.9	0.9
	Diethyl ether	18.2	18.7	19.3	19.8	20.6	21.4
<i>B-Part</i>							
Isocyanate	pMDI	194	201	209	216	226	237

The PUFs were elaborated according to the previously described procedure. The foaming process was camera recorded to study the impact of the ESO on the foaming process.

3.4. Recently synthesized PUF based on AO and EAO

Different foams were recently synthesized to determine the molecular structures in the soluble fraction. The foams presented in Table 4.2 were realized with 25wt% of Pht-DEG substitute by AO (25AO) or EAO (25EAO). The results were compared with a 100% Pht-DEG foam (Ref). The AO has no reactive group to bond with the urethane network. Therefore, the 25AO foam was used as a positive control to confirm the potential of the extraction to recover molecules unbonded to the polymer network.

The NCO/OH index was kept constant at 3 for all formulations. The epoxide groups were taken into accounts for the index calculation. However, the 25AO foams formulation was prepared with the substitution of EAO by AO. The DMCHA, P2H-EG, PoSi and water were kept constant at 0.5, 2.76, 3.14 and 1.12 parts by weight of polyol, respectively.

Table 4.2 - Formulations of recently synthesized PUF.

Foam formulation		Ref	25AO	25EAO
<i>A-Part</i>				
Polyols	Pht-DEG (fossil-based)	100	75	75
	AO		25	
	EAO			25
Catalyst	DMCHA	0.5	0.5	0.5
	Pht-DEG	2.76	2.76	2.76
Surfactant	PoSi	3.14	3.14	3.14
Blowing agent	Water	1.12	1.12	1.12
	Pentane	16.7	17.5	17.5
<i>B-Part</i>				
Isocyanate	pMDI	192	203	203
Theoretical soluble fraction		2.0%	2.0%	2.0%

The PUFs were elaborated according to the previously described procedure. The foams were kept for one week at room temperature and 50 of relative humidity (%RH) to allow the system to cure and stabilized before analysis.

3.5. Formerly synthesized PUF based on PAO, PRO, EAO and ERO

Different foams were synthesized to demonstrate the potential of the AO derivatives in PUF in a previous study (Arbenz et al. 2017), which used rapeseed oil (RO) as a reference for comparison purposes. The proof of concept that AO derivatives can be used as sustainable building blocks for PUF

was demonstrated by the transformation of AO into a polyol. AO and RO were epoxidized (EAO and ERO) and converted into polyols by ring-opening with methanol (PAO and PRO). The corresponding modified triglycerides were used to partially replace a very conventional polyether polyol based on oxypropylated glycerol (OPG).

The foams presented in Table 4.3 were realized with DMCHA and P2H-EG (catalyst), PoSi (surfactant) and isopentane (physical blowing agent). Sulfated castor oil dissolved in water (SCO-H₂O) was used as a chemical blowing agent. The quantity of DMCHA, P2H-EG, PoSi, SCO-H₂O and isopentane were fixed at 0.1, 0.7, 0.8, 0.6 and 5.5 wt% of the formulation, respectively. The NCO/OH index was kept constant at 3 for all formulations.

Table 4.3 - Formulations of formerly synthesized PUF. (Arbenz et al. 2017)

Foam formulation	F-OPG	F-EAO	F-ERO	F-PAO	F-PRO
<i>A-Part</i>					
Polyols					
	OPG	100	75	75	75
	EAO		25		
	ERO			25	
	PAO				25
	PRO				
Catalyst ¹	DMCHA	0.4	0.5	0.5	0.61
	P2H-EG	2.2	2.76	2.76	3.36
Surfactant	PoSi	2.5	3.14	3.14	3.82
Blowing agent					
	SCO-H ₂ O ¹	1.78	2.24	2.24	2.72
	Isopentane	16.9	21.2	21.2	25.8
					24.6
<i>B-Part</i>					
Isocyanate	pMDI	182	254	254	330
	Theoretical soluble fraction	1.7%	1.7%	1.7%	1.7%

¹ SCO-H₂O: Sulfated castor oil dissolved in water.

The PUFs were elaborated according to the previously described procedure. The PUFs were kept in the dark for three years at room temperature and 50 %RH, before specific analysis.

3.6. Liquid extraction from the foams

After total curing, the extractable fraction comprises every compounds not covalently bonded to the polymer matrix. In PUF formulation, additives and unreacted monomers trapped by the macromolecular matrix compose the soluble fraction. The Soxhlet extraction is commonly used to extract soluble compounds trapped inside an unsoluble solid matrix. In a typical procedure, the foam

was shredded and sieved through a 5 mm grid for a better extraction. Foam powder was precisely weighted to be introduced into a Soxhlet cartridge. The Soxhlet extraction was realized with a 1:1 in volume solution of acetone:cyclohexane as the solvent. The combination of highly polar acetone and highly apolar cyclohexane maximizes the potential of the extraction. They were mixed in an equal portion to obtain an average polarity. Furthermore, the PUF additives and the epoxidized oils are very soluble in both solvents. The extraction was realized over 24 hours, and each cycle was around 20 min, which is classical in Soxhlet extraction. The solvent was removed under reduced pressure.

3.7. Synthesis of Methyl undecylenate (Mund)

The reaction was carried out in a round bottom flask equipped with a reflux condenser and a magnetic stirrer. The flask was filled with 50 g of undecylenic acid (0.25 mol, 1 eq.) and 7 g of strongly acidic polysulfone ion exchange resin. A large excess of methanol (500 mL) was introduced. The mixture was stirred under reflux for 15 hours. The solution was filtered to remove the catalyst. Then the solvent was evaporated under reduced pressure.

3.8. Synthesis of epoxidized methyl undecylenate (Mundex)

The reaction was carried out in a round bottom flask equipped with a reflux condenser and a magnetic stirrer. The flask was filled with 50 g of Mund (0.25 mol, 1 eq.). 85 g of m-CPBA (0.38 mol, 1.5 eq.) was dissolved in 600 mL dichloromethane. The m-CPBA solution was added dropwise in the flask cooled at 0 °C. The mixture was stirred at ambient temperature for 4 hours. The solution was filtered. The organic phase was washed with sodium sulfite to quench the excess of m-CPBA, then washed with a saturated NaHCO_3 solution. Then it was washed with brine solution, dried over anhydrous sodium sulfate and then filtered. The solvent was evaporated under reduced pressure. The slightly yellow oil was dried overnight in a vacuum oven at 40 °C.

3.9. Synthesis of oxazolidone based on model systems

In a typical procedure, 1 eq. of epoxide (DGEBA, Mundex or EVHOSO) was introduced in a two-necked glass equipped with a reflux condenser. The flask was dry under vacuum then put under argon flux. 2 mL of dry- dimethylformamide (DMF) was introduced into the system. The reaction mixture was heated under DMF reflux (153 °C) and vigorously stirred. 1 eq. of phenyl isocyanate was added slowly to the reaction mixture. The mixture was heated under magnetic stirring for 4 hours. The products were separated by column chromatography, and only the major fractions were analyzed.

3.10. Characterizations

The ^1H NMR analyses were realized on a 400 MHz Bruker spectrometer. CDCl_3 was used as a solvent to prepare the samples. The ^1H NMR number of scans was set to 32. Each spectrum was calibrated with the CDCl_3 signal, being set at $\delta=7.26$ ppm.

ATR FTIR spectra were recorded on Thermo Scientific Nicolet iS210 instrument using a Smart Orbit Diamond. An atmospheric background was collected before each sample analysis (32 scans, resolution 4 cm^{-1}).

4. RESULTS AND DISCUSSION

4.1. Foams based on ESO

The reaction between reactive isocyanate groups and epoxides is known to yield the cyclic oxazolidone groups (Scheme 4.1) (Sendijarević et al. 1987; Speranza and Peppel 1958). The double bonds of vegetable and microalgae oil were transformed into epoxide groups to be further ring-opened to obtain suitable polyols for PUF (Arbenz et al. 2017; Desroches et al. 2012; Maisonneuve et al. 2016; Pawar et al. 2016a; Petrović et al. 2013; Peyrton et al. 2020). Therefore, the idea of a direct synthesis by introducing epoxidized oil in PUF production was investigated. The formation of foam is based on the equilibrium between the network formation by polyaddition of polyols with polyisocyanates, and the gas expansion. Changes in formulation directly impact the resulting PUF, especially the foam height. Therefore, the effect of ESO on PUF was investigated by gradual substitution in the weight of the fossil-based polyol (Pht-DEG) by ESO from 0 to 100 wt% (Table 4.1).

The free-rise foam process started just after the fast introduction and stirring of pMDI into the polyol, catalyst, blowing agent and surfactant mixture. The foam growth was recorded, and a picture was taken after 3min20 when the foams were fully raised (Figure S4.8 in Supporting information (SI)). The addition of 15wt% of ESO did not significantly modify the foaming process since the 15ESO foam had a similar height than 0ESO. However, the introduction of ESO limits the expansion of the other foams. A gradual decrease of the final height of the foam was observed in Figure S4.8 in SI with increasing substitution of Pht-DEG by ESO. The expansion of 100ESO was low compared to the other foams.

This global trend was expected and is explained by the lower reactivity of the oxirane group compared to the hydroxyl one. With the gradual substitution of the polyol, the energy provided by the reaction at low temperature between hydroxyl and isocyanate group decreased. As the oxazolidone group was reported to be formed at high temperatures (Lee et al. 2007), the lack of energy probably prevents the oxazolidone formation and the foam expansion. The urethane formation was observed by DSC in the range 40-90 °C compared to 140-260 °C for the oxazolidone (Kadurina et al. 1992). In the same study (Kadurina et al. 1992), the DSC thermogram up to 300 °C of (3,4-Epoxy cyclohexyl methylene)-3,4-epoxy cyclohexyl bearing disubstituted epoxide did not show an exothermic peak on the contrary to the monosubstituted epoxide tested.

However, it was not expected that the 100ESO expanded to form a foam. The low reactivity of epoxide combined with the absence of energy provided by the urethane formation should prevent the poly-oxazolidone network formation. The 100ESO foam is potentially due to a small portion of water, which formed a polyurea network, and the formation of the PIR network. This study emphasizes the challenge of the low epoxide reactivity to overcome when an epoxidized vegetable oil substitutes the polyol in a PUF.

4.2. Study of freshly synthesized foams based on 25% of AO or EAO

To further investigate the reaction between isocyanate and epoxide in the PUF, a series of foams were elaborated (Table 4.2) with 25 wt% of the polyol substitute by AO (25AO) and EAO (25EAO) and compared with a reference foam based on 100% polyol. According to the previous experiment, substitution between 15 and 35 wt% gives foams with a similar density than the reference. The higher functionality in epoxide groups of EAO compared to ESO is expected to increase the potential of reaction between epoxidized oil and isocyanate. Furthermore, 25 wt% of EAO was already used to produce PIR foams in the literature (Arbenz et al. 2017). However, in this study, the oxazolidone formation was never well confirmed in the foam system.

After two days of curing at ambient temperature, the PUFs were shredded and sieved. The soluble fraction was extracted using a Soxhlet with an equal content of polar acetone and apolar cyclohexane. The average polarity combined with the solubility of the additives in both solvents maximizes the extraction potential. As this solvent forms a low boiling azeotrope, the energy consumed for the Soxhlet extraction is lower. The soluble fraction calculated from Table 4.2 represents 2 wt% of the formulations. After Soxhlet extraction during 24 hours, the soluble fractions extracted were 7.6, 9.3 and 8.7 wt% for Ref, 25AO and 25 EAO, respectively. They were higher than expected. An incomplete foam curing could explain these higher values.

Although the raw fractions were analyzed, no constituent was clearly identified. Therefore, the fraction constituents were separated according to their polarities by chromatography column to identify their structures. F1-Ref, F2-Ref means, e.g., the first and the second fraction for the Ref foam, respectively. Each fraction was weighed, and the mass distribution was presented in Figure S4.9 in SI for Ref, 25AO and 25EAO foams. The F1-Ref, F1-AO and F1-EAO represent an approximately similar portion with 16-26 wt%. The portion of F3-25EAO (33 wt%) is higher than F3-Ref (22 wt%) and F3-25AO (6 wt%). The residue composed of the molecules interacting strongly with the silica of the chromatography column was between 11 and 29 wt%. The higher residue content in 25AO (29 wt%) and a small portion of F3-25AO (6 wt%) could be related to the presence of highly polar compounds in this foam. These fractions were analyzed by FTIR and ¹H NMR spectra to determined their chemical structures.

4.2.1. Analysis of F1

The FTIR spectrum of F1-Ref, F1-25AO and F1-25EAO shown in Figure 4.1A were quasi similar. It was then assumed that the less polar compound was the same for all foams. The F1-Ref, F1-25AO and F1-25EAO extracts also presented carbonyl stretching band at $\tilde{\nu}=1740\text{ cm}^{-1}$, the vibration of C-CH₃ at $\tilde{\nu}=1460\text{ cm}^{-1}$ and alkane antisymmetric and symmetric CH₂ stretching at $\tilde{\nu}=2852$ and 2921 cm^{-1} , respectively (Pretsch et al. 2009; Wertz et al. 2018) typical of P2H-EG (Figure 4.1A). However, the band related to the ethylene glycol at $\tilde{\nu}=3350$ (OH stretching) and 1400 cm^{-1} (COH vibration) shielded the 2-ethyl hexanoate signals. On the contrary to the EG, the potassium 2-ethyl hexanoate should not be integrated into the PU network during the foam elaboration. The potassium carboxylate identified by the band at $\tilde{\nu}=1555\text{ cm}^{-1}$ corresponding to the COO-K vibration was potentially transformed in a carboxylic acid ($\tilde{\nu}=1740\text{ cm}^{-1}$) during the foam processing.

¹H NMR analyses were conducted and presented in Figure 4.1B to confirm the structure hypothesized in FTIR. In ¹H NMR, the alkane protons at δ =1.25 ppm and the end of chain CH_3 at δ =0.88 ppm are identified in the F1 fractions and P2H-EG spectra. The ethylene glycol identified at δ =2.62 ppm in the ¹H NMR spectra of P2H-EG (Figure 4.1B) reacted with isocyanate and was integrated into the polymer network. The combined FTIR and ¹H NMR spectroscopy confirmed the presence of potassium 2-ethyl hexanoate originating from P2H-EG in every F1 fraction.

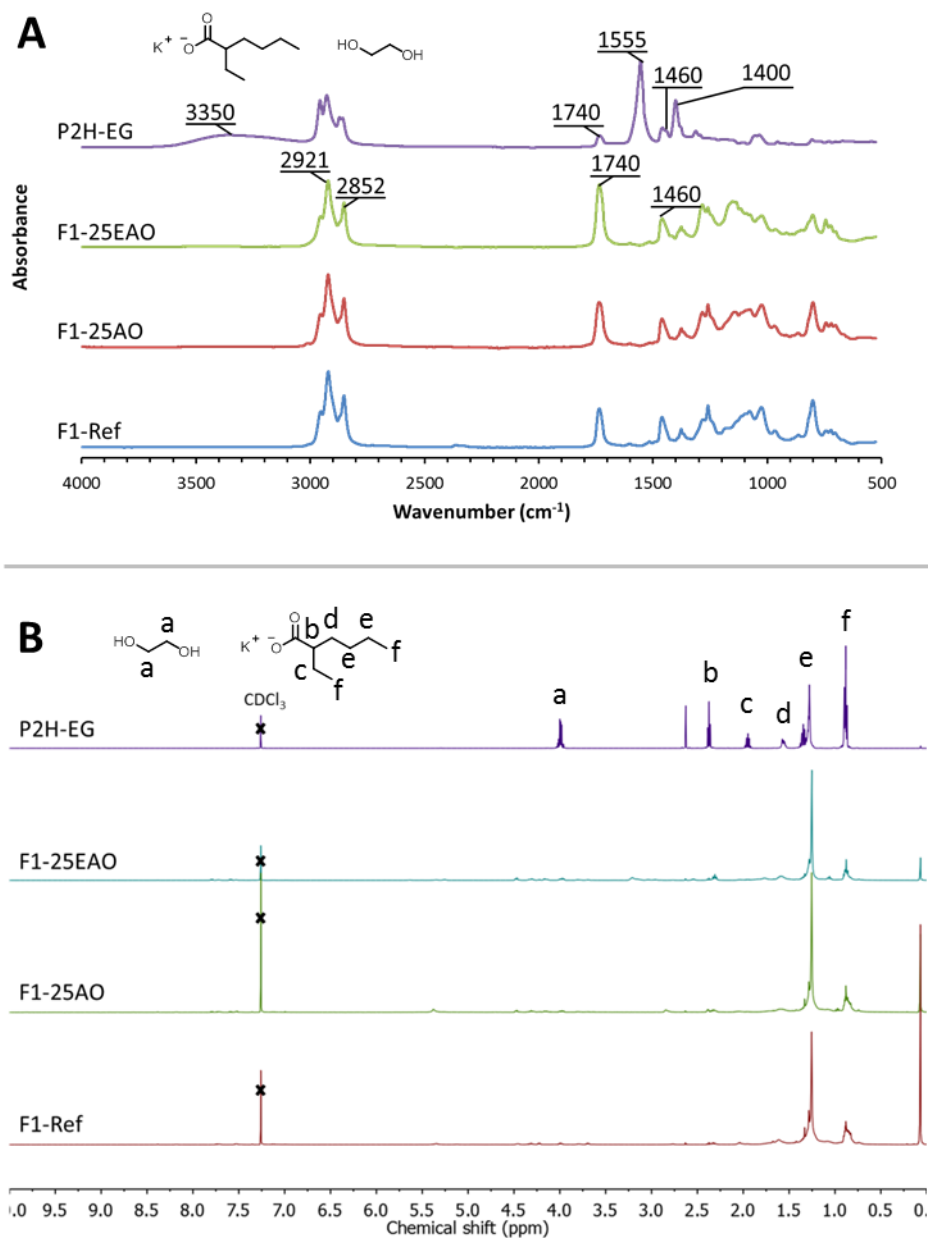


Figure 4.1 - Chemical analysis of F1-Ref, F1-25AO, F1-EAO and P2H-EG by FTIR (A) and ¹H NMR (B).

4.2.2. Analysis of F2

The FTIR spectra of F2-Ref, F2-25AO and F2-25EA0 were similar (Figure 4.2A). Surprisingly, the carbonyl stretching at $\tilde{\nu}$ =1720 cm^{-1} , ether C-O-C stretching at $\tilde{\nu}$ =1290 cm^{-1} and terminal $\text{CH}_2\text{-CH}_2\text{-O}$ at $\tilde{\nu}$ =990 cm^{-1} (Matsuura and Miyazawa 1967) were identified. These bands were

also present in the Pht-DEG spectra (Figure 4.2A). Therefore, the second fractions could be attributed to unreacted polyol. However, the absence of the characteristic hydroxyl band at $\tilde{\nu}=3450\text{ cm}^{-1}$ contradicted this hypothesis. The esterification of phthalic acid with diethylene glycol industrially produces Pht-DEG. One of the side-reaction is the formation of cyclic ester, which could explain the similar FTIR spectra of Pht-DEG and the second fractions.

For the second fraction, the ^1H NMR (Figure 4.2B) confirmed the glimpse gave by the FTIR. An aromatic chemical shift matching with the Pht-DEG spectrum appeared at $\delta=7.80$ and 7.58 ppm . It was expected that 100% of the polyol reacted by polyaddition with the polyisocyanate. Therefore, only the side-products without OH groups should be extracted from the foams. The cyclic ester side product of the polyol synthesis was identified in F2-Ref, F2-25AO and F2-25EA0 spectra (Figure 4.2B) by peaks at $\delta=4.71$ (c') and 3.95 (d') ppm. The other peaks observed in the ^1H NMR spectra of the second fractions could be explained by some additives such as surfactants, present in the industrially produced Pht-DEG.

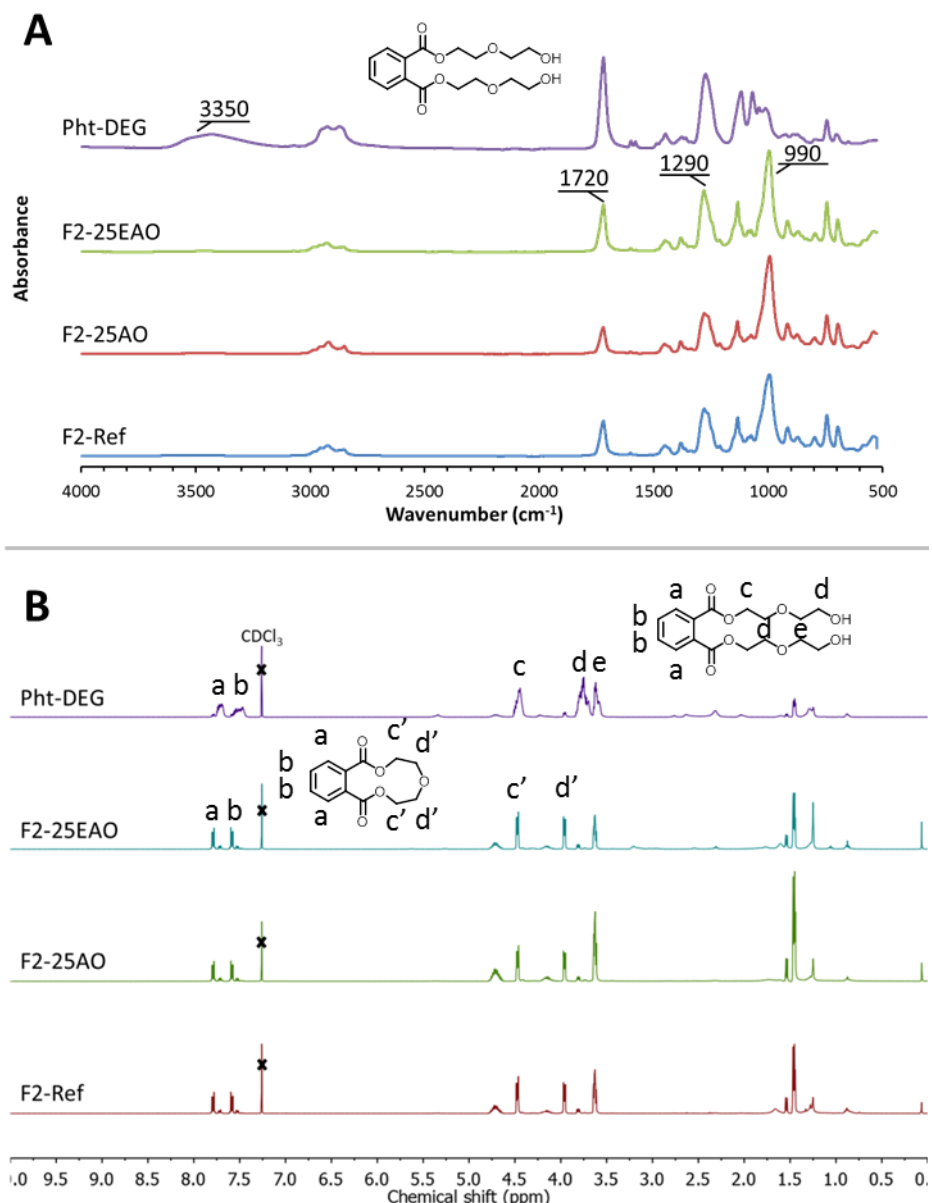


Figure 4.2 - Chemical analysis of F2-Ref, F2-25AO, F2-EAO and Pht-DEG by FTIR (A) and ^1H NMR (B).

4.2.3. Analysis of F3

The FTIR spectra of F3-Ref, F3-25AO and F3-25EAO presented in Figure 4.3A, did not present significant difference compared to F2 fractions spectra. The Pht-DEG bands of carbonyl stretching at $\tilde{\nu}=1720\text{ cm}^{-1}$, ether C-O-C at $\tilde{\nu}=1290$ and 990 cm^{-1} were identified.

Further investigations by ^1H NMR were conducted to identify the structure of the third fractions (Figure 4.3B). Surprisingly, no trace of AO was found in the analyzed fractions of F3-25AO. The elevated temperature during the foaming process could have initiated a radical polymerization of the double bonds. The AO polymer network would be insoluble. This explained why there is no trace of AO in the soluble fractions. Despite the use of strong polar solvents, neither DMCHA nor PoSi signals were detected. The tertiary amine catalyst and the surfactant strongly interact with the silica column and explain the high residue values.

In F3-Ref, the aromatic signals located in the region $\delta=7.80\text{-}7.58\text{ ppm}$ and signals at $\delta=4.70$ and 3.62 ppm in the ^1H NMR spectrum, as already stated, indicated the presence of Pht-DEG cyclic ester side-products. Despite the absence of aromatic signals, the Pht-DEG cyclic ester was also identified in F3-AO and F3-EAO (Figure 4.3B) at $\delta=4.70$ and 3.62 ppm .

In the F3-25EAO, EAO was identified by the chemical shift of the glycerin protons at $\delta=5.25$, 4.31 and 4.15 ppm , the epoxide signal at $\delta=2.8\text{-}3.2\text{ ppm}$ and the methylene protons in between two epoxide groups at $\delta=1.75\text{ ppm}$ (Figure 4.3B). The presence of EAO in the F3-EAO indicates that at least one portion of the EAO did not react and was not integrated into the polymer network in freshly synthesized PUF.

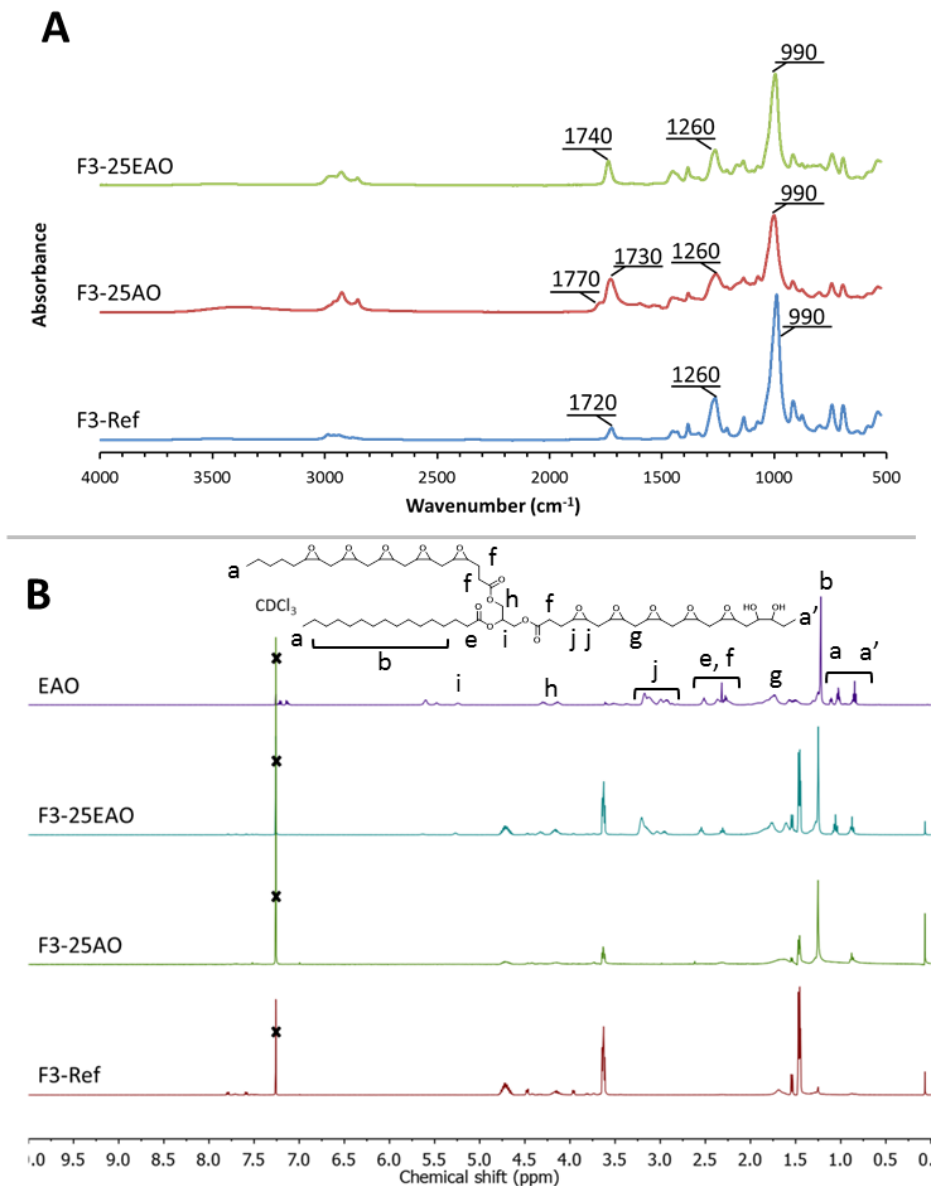


Figure 4.3 - Chemical analysis: (A) FTIR spectra of F3-Ref, F3-25AO, F3-EAO and (B) ¹H NMR spectra of F3-Ref, F3-25AO, F3-EAO and EAO-oil.

4.3. Analysis of formerly synthesized foams based on PAO, PRO, EAO and ERO

The previous section has demonstrated the incomplete reaction of EAO in recently synthesized PUF. As previously stated, at ambient temperature, the foam continues to cure since EAO could be slow to react with isocyanate. In order to test this hypothesis, foams synthesized three years ago (Arbenz et al. 2017) with 25 wt% of OPG substitute by two epoxidized oil (EAO and ERO) and polyols obtained by the ring-opening of the two epoxidized oil (PAR and PRO). The foams were named according to the new derivatives introduced. For example, F-PAO is obtained by the substitution of 25 wt% of polyol by PAO. This series of foams formerly produced and compared with a reference foam based on 100% OPG (F-OPG) (Table 4.3) were analyzed using the previously

described procedure. The aging should decrease the content of unreacted polyols and epoxidized oils unbonded to the polymer network. Furthermore, the additives could migrate outside of the foam due to aging. Therefore, the quantity of foams to extract was increased compared to the previous study on recent foams, to anticipate the decrease of the soluble fractions. 0.7, 1.5, 3.6, 0.7 and 0.4% were extracted from F-OPG, F-EAO, F-ERO F-PAO and F-PRO, respectively. These values were close to the theoretical soluble fraction value of 1.7% calculated from the formulation described in Table 4.3 and lower than the recent foams as expected. Furthermore, only one product was obtained by column chromatography purification. It was noticed that the foam realized with epoxidized oil, i.e., EAO and ERO had a higher soluble fraction than the 100% polyol foams.

4.3.1. FTIR analysis

The FTIR confirmed the structure difference between compounds extracted from the foams realized with epoxidized oil (F-EAO or F-ERO) and the others (Figure S4.10 in SI). The stretching and vibration of CH_2 and CH_3 ($\tilde{\nu}=2921, 2852, 1460$ and 1260 cm^{-1}) and the carbonyl stretching ($\tilde{\nu}=1740 \text{ cm}^{-1}$) corresponding to triglycerides long chains were present on every spectrum shown in Figure S4.10 in SI. However, typical epoxidized oil bands, such as the C-O-C asymmetric stretching at $\tilde{\nu}=1160 \text{ cm}^{-1}$, the epoxide ring symmetric stretching at $\tilde{\nu}=845 \text{ cm}^{-1}$ and epoxide ring vibration at $\tilde{\nu}=825 \text{ cm}^{-1}$ were identified on the F-ERO and F-EAO spectra (Figure S4.10 in SI). Furthermore, the FTIR spectra of F-EAO and F-ERO are very similar to the EAO or ERO presented in Figure S4.11 in SI. F-OPG, F-PAO and F-PRO presented spectra similarities with F1 fractions of the recent foams previously identified as potassium 2-ethyl hexanoate from P2H-EG.

4.3.2. NMR analysis

^1H NMR analysis was performed to characterize the purified fractions of the foams. In accordance with the FTIR, the foams were separated into the two same groups. Peaks at $\delta=4.0, 2.63, 2.37, 1.28$ and 0.88 ppm were common to F-OPG, F-PAO, F-PRO and P2H-EG ^1H spectra presented in Figure 4.4A. This confirmed the hypothesis formulated after the FTIR analysis: the fraction of F-OPG, F-PAO and F-PRO of foam is composed of potassium 2-ethyl hexanoate.

For the other group composed of F-PAO and F-EAO, similar ^1H NMR chemical shifts were observed in the spectra of PAO, F-PAO, EAO and F-EAO, shown in Figure 4.4B. The characteristic glycerin protons of oil were identified by the chemical shift at $\delta=5.20 \text{ ppm}$ and $\delta=4.35-4.11 \text{ ppm}$. The proton in the alpha position of the ester group by the triplet at $\delta=2.30 \text{ ppm}$ and the epoxide at $\delta=2.80-3.20 \text{ ppm}$. The very similar NMR spectra between the oil introduced and extracted of the foams confirmed the hypothesis previously formulated: the epoxidized oil did not wholly react with a polyisocyanate in PUF. This result consolidated the main results previously obtain on freshly synthesized foams. However, the aging reduced the soluble fraction and the number of extracted molecules. Epoxidized oil was still recovered from the foams after three years of storage at ambient temperature. However, we can notice that the extraction method is not quantitative enough to fully confirm that 100% of the epoxide did not directly react with the isocyanate. Furthermore, the epoxide group was proved to react with isocyanate to form oxazolidone but also ketone, urethane and carbonate groups depending on the catalyst (Javni et al. 2003). This point has been studied.

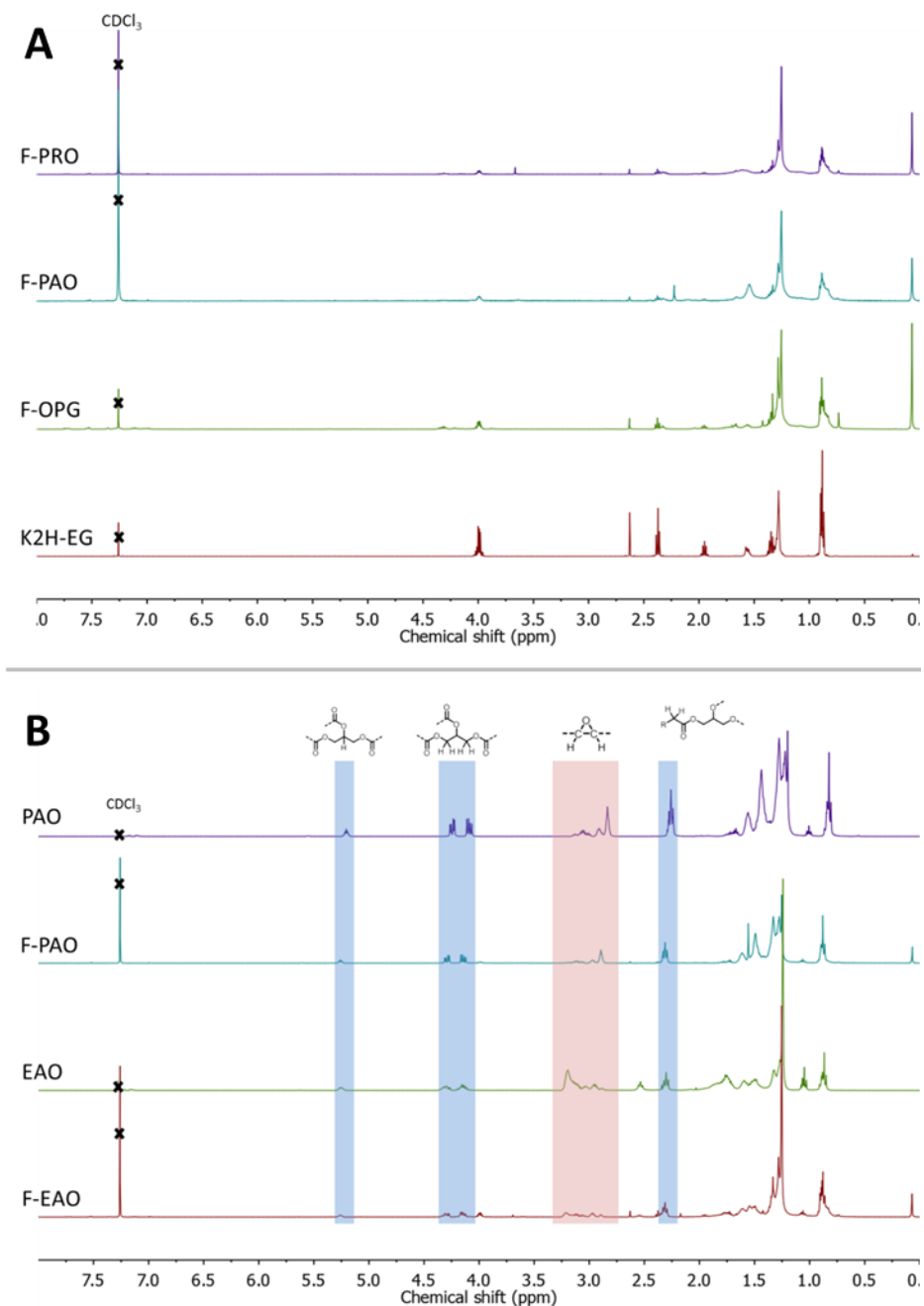
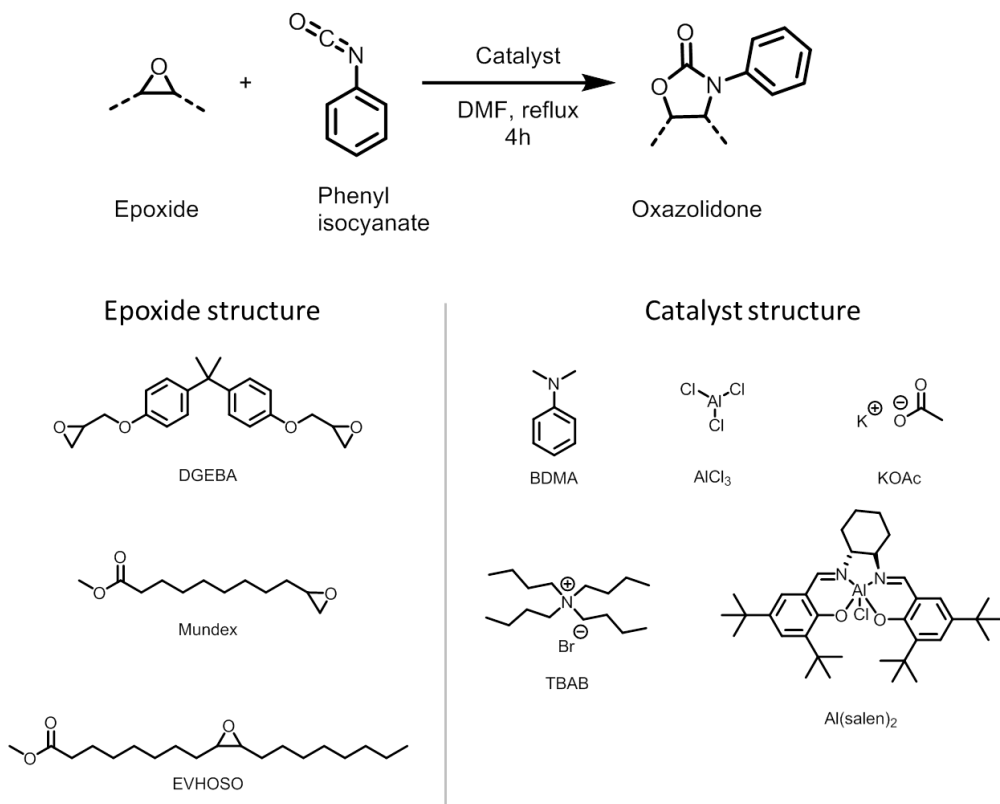


Figure 4.4 - ^1H NMR spectra of (A) P2H-EG, F-OPG, F-PAO and F-PRO and (B) F-EAO, EAO-oil, F-PAO and PAO-oil.

4.4. Reactional models to study oxazolidone formation with different catalysts and epoxides-based systems

The last section has shown that even with very long aging, the epoxidized oil did not fully react in the PIR foam systems. A question is still open concerning the formation of oxazolidone groups. To answer this point and better understand the formation of oxazolidone in PUF, a model system was designed. The reaction conditions are described in Scheme 4.2, in connection with a previous publication that investigated the reaction between phenyl isocyanate and 9,10

epoxyoctadecane (Javni et al. 2003). Low temperatures favored the formation of isocyanurates, and the highest favored the oxazolidone formation (Chen et al. 2016). In agreement with the literature, this reaction to form oxazolidone was carried at high temperature in refluxing DMF (156 °C) for 4h. The literature shows that the formation of oxazolidone can be catalyzed by DMF (Dileone 1970), tertiary amines (Caille et al. 1990a; Chen et al. 2018, 2016; Chian and Yi 2001; Flores et al. 2012 p. 20; Galante and Williams 1995; Lee et al. 2007), quaternary ammoniums (Dyen and Swern 1968; Pelzer et al. 2018; Sandler 1967; Speranza and Peppel 1958; Uribe and Hodd 1984), Lewis acids (Ansari and Ahmad 1987; Baronsky et al. 2013; Javni et al. 2003; Kordomenos et al. 1987), imidazoles (Caille et al. 1990b; Kinjo et al. 1983; Pilawka et al. 2014; Uribe and Hodd 1984), lithium bases (Azechi and Endo 2014; Dileone 1970; Yeganeh et al. 2006) or carboxylic salts (Ashida et al. 1978). In this study, the oxazolidone formation was particularly investigated with BDMA, KOAc, TBAB, AlCl_3 or $\text{Al}(\text{salen})_2$ presented in Scheme 4.2 and without a catalyst. The choice of the studied catalysts was established according to different criteria. The BDMA and KOAc were selected due to their high boiling points and their uses in PUF/PIR foam formulations. Since quaternary ammonium halides were an efficient catalyst for the oxazolidone formation (Speranza and Peppel 1958), TBAB was also tested in the model study. Otherwise, AlCl_3 and $\text{Al}(\text{salen})_2$ were used to produce oxazolidone from disubstituted epoxide (Ansari and Ahmad 1987; Baronsky et al. 2013; Javni et al. 2003; Lee et al. 2007). The excess of epoxide was proved to form a mixture of isocyanurate, urethane and oxazolidone groups (Galante and Williams 1995). On the contrary, the excess of isocyanate favors the trimerization reaction (Caille et al. 1990a). Therefore, epoxide and isocyanate groups were added in stoichiometric quantity.



Scheme 4.2 - Reaction between phenyl isocyanate and epoxide groups from different resources to form an oxazolidone group assisted by different catalysts, as a global model system.

The model system was designed with phenyl isocyanate and three different and representative epoxides: DGEBA, Mundex and EVHOSO. The different chemical structures are shown in Scheme 4.2. The monoisocyanate was chosen because of its high reactivity and structural similarity with the pMDI, largely used in foams fabrication.

The oxazolidone formation between isocyanate and DGEBA was already proved even in PUF (Chen et al. 2018). Therefore, DGEBA was used as a positive control to confirm the potential of oxazolidone formation with each tested catalyst. Mundex is a fatty ester with a terminal epoxide synthesized by esterification of undecylenic acid with methanol (Mund) followed by an epoxidation with a stable peracid, i.e., m-CPBA. The ^1H NMR spectra of undecylenic acid, Mund and Mundex were detailed in Figure S4.12, in SI. The Mundex was compared to EVHOSO to study the effect of the epoxide substitution and steric hindrance in methyl fatty ester. Furthermore, The EVHOSO modeled the epoxidized oil used in PUF formulations. Besides, only a few studies treated the oxazolidone formation with a disubstituted epoxide (Ansari and Ahmad 1987; Baronsky et al. 2013; Boufi et al. 1993; Javni et al. 2003; Kadurina et al. 1992; Lee et al. 2007).

The reaction products obtained with the different catalysts were separated by chromatography column. The eluants were carefully chosen to optimize the separation of the products. The number and percentage of the fractions collected on each sample were detailed in Table S4.5-S4.7 in SI. ^1H NMR and FTIR structural investigations were performed only on the principal fractions, representing between 47 and 76 wt% of the total product.

4.4.1. DGEBA

The FTIR spectrum of DGEBA, presented in Figure 4.5, was characterized by the aromatic ring bending and stretching at $\tilde{\nu}=1600$ and 1500 cm^{-1} , respectively and the epoxide ring symmetric stretching and vibration at $\tilde{\nu}=913$ and 826 cm^{-1} , respectively. The isolated major fraction of the reaction products with different catalysts presented similar FTIR spectra (Figure 4.5). The well-documented carbonyl stretching of oxazolidone was identified at $\tilde{\nu}=1751\text{ cm}^{-1}$ (Lee et al. 2007; Merline et al. 2007). Furthermore, the oxazolidone formation was identified with a high-intensity band at $\tilde{\nu}=756\text{ cm}^{-1}$ and $\tilde{\nu}=694\text{ cm}^{-1}$, which correspond to the C-O-N bond vibration out of the plan and the deformation of the ring, respectively (Figure 4.5) (Michalska et al. 2017). Supplementary aromatic bands were identified at $\tilde{\nu}=1632\text{ cm}^{-1}$ and 1587 cm^{-1} , probably from the addition of phenyl group connected via the nitrogen of the oxazolidone group. The band at $\tilde{\nu}=826\text{ cm}^{-1}$ in Figure 4.5 could indicate the incomplete conversion of the epoxide group.

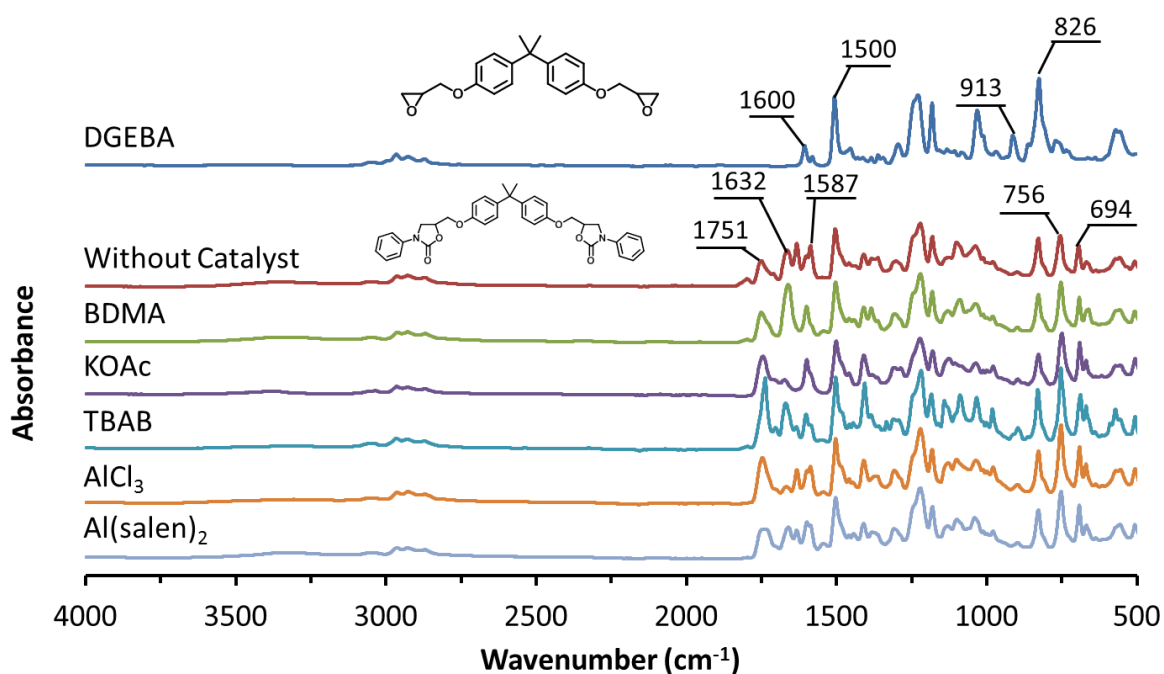


Figure 4.5 - FTIR spectra of DGEBA alone and the main fractions after DGEBA reaction with and without catalysts.

The formation of oxazolidone was confirmed by ^1H NMR spectra (Figure S4.13 in SI) with the appearance of a typical chemical shift of oxazolidone at $\delta=5.0$ ppm and extra aromatic chemical shift at $\delta=7.6-7.4$ ppm. However, the signals for the epoxide protons, at $\delta=2.75$, 2.90 and 3.34, completely disappeared on the product spectra regardless of the used catalyst. Therefore, the conversion into oxazolidone groups was significant. The series of reactions confirmed the possibility of forming oxazolidone in these conditions regardless of the catalyst.

4.4.2. Mundex

The characteristic FTIR band of fatty esters, such as carbonyl ester stretching at $\tilde{\nu}=1740\text{ cm}^{-1}$, the vibration of $\text{C}-\text{CH}_3$ at $\tilde{\nu}=1460\text{ cm}^{-1}$ and alkane antisymmetric and symmetric CH_2 stretchings at $\tilde{\nu}=2852$ and 2921 cm^{-1} , respectively, were observed in the FTIR spectrum of Mundex (Figure 4.6A). Similarly to the DGEBA, the epoxide ring symmetric stretching and the ring vibration at $\tilde{\nu}=913$ and 826 cm^{-1} , respectively, were identified in Mundex. In the FTIR spectra of the major fractions with the different catalysts (Figure 4.6A), the characteristic bands of the aromatic group of the phenyl were observed at $\tilde{\nu}=1600$ and 1500 cm^{-1} . Furthermore, the oxazolidone band was observed at $\tilde{\nu}=750$ and $\tilde{\nu}=692\text{ cm}^{-1}$. However, the oxazolidone carbonyl stretching was coincident with the carbonyl ester stretching and formed a shoulder at $\tilde{\nu}=1740\text{ cm}^{-1}$, except for the reaction conducted without catalyst where the band at $\tilde{\nu}=1672\text{ cm}^{-1}$ could be attributed to the carbonyl stretching of oxazolidone. Finally, the band located at $\tilde{\nu}=1217\text{ cm}^{-1}$ in Figure 4.6A could be attributed to the $\text{C}-\text{N}$ and $\text{C}-\text{H}$ stretching in the oxazolidone ring (Michalska et al. 2017). The FTIR spectra showed multiple bands that can be linked to the formation of oxazolidone from Mundex epoxide.

The ^1H NMR analysis (Figure 4.6B) confirmed the formation of oxazolidone with the peak at $\delta=4.1$ (a') and 4.6 (b') ppm associated with the protons of the oxazolidone ring. The characteristic aromatic chemical shifts also appeared at $\delta=7.6-7.2$ ppm in Figure 4.6B. The ^{13}C analysis of the

Mundex reaction realized with AlCl_3 (Figure S4.14 in SI) showed a peak at $\delta=73.3$ and 50.5 ppm corresponding to b' and a' carbons, respectively. Furthermore, the chemical shift at $\delta=155.2$ ppm was correlated with the carbonyl carbon of the oxazolidone group. However, in Figure 4.6B, the chemical shift at $\delta=2.89$, 2.74 and 2.45 ppm indicated an incomplete transformation of the epoxide into oxazolidone with BDMA, KOAc and TBAB catalyst. In conclusion, the formation of oxazolidone was also identified with monosubstituted epoxide derived from fatty acid.

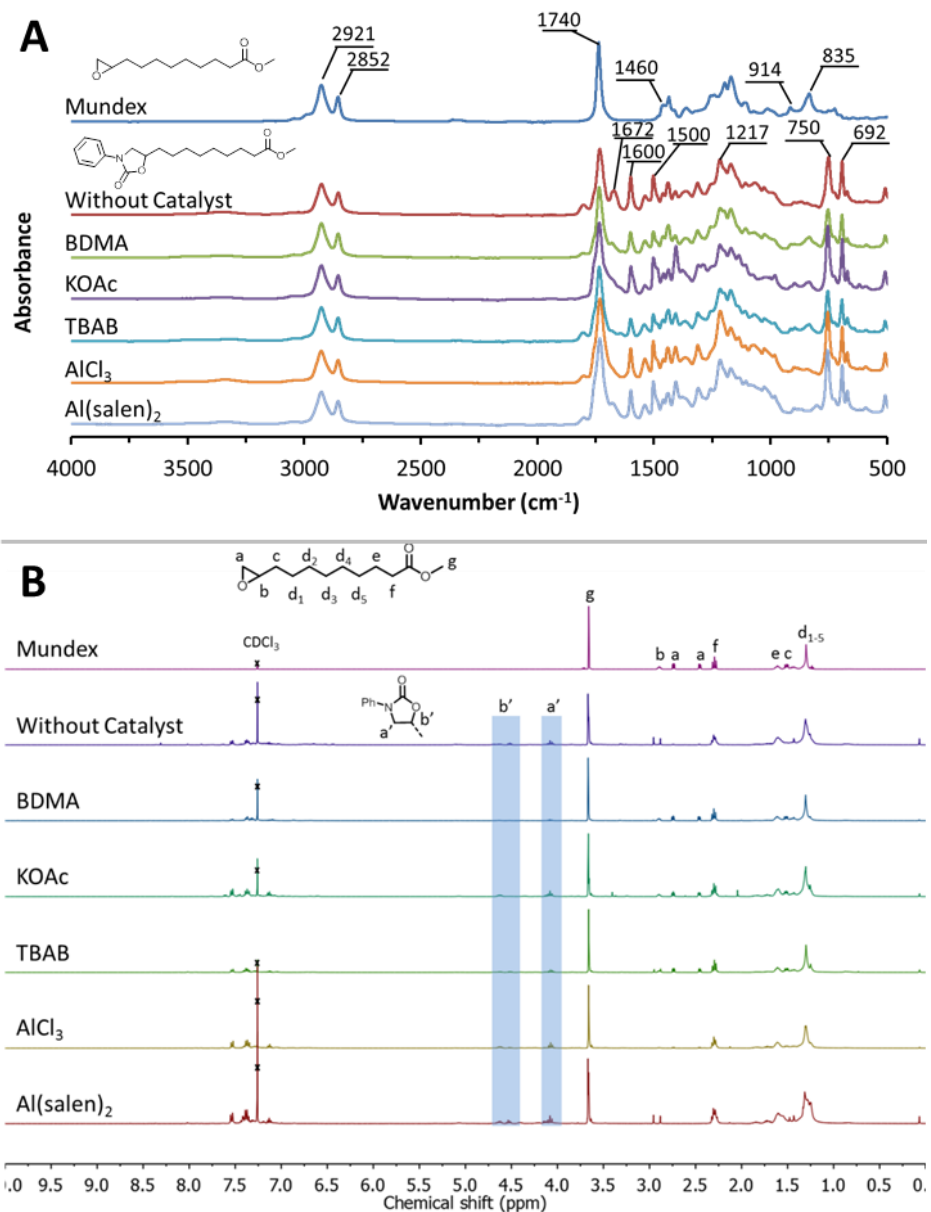


Figure 4.6 - Chemical analysis: (A) FTIR spectra of Mundex alone and the main fractions of Mundex reaction with and without catalysts (B) ^1H NMR spectra of Mundex alone and the main fractions of Mundex reaction with and without catalysts.

4.4.3. EVHOSO

The EVHOSO FTIR spectra (Figure 4.7A) showed characteristic fatty ester band with the vibration of C-CH₃, alkane antisymmetric and symmetric CH₂ stretchings at $\tilde{\nu}$ =1460, 2852 and 2921 cm⁻¹, respectively. The carbonyl stretching and the epoxide ring vibration were identified in Figure 4.7A at $\tilde{\nu}$ =1740 and 827 cm⁻¹, respectively. For the reaction products, the spectra were separated into two groups: The first group comprising the reaction products without catalyst or with BDMA, KOAc, and TBAB still had an epoxide band at $\tilde{\nu}$ =827 cm⁻¹. The other group without an epoxide band was formed by the products of the Lewis acid catalysts (AlCl₃ and Al(salen)₂). For the latter group, a shoulder at $\tilde{\nu}$ =1718 cm⁻¹ is identified and could correspond to the ketone carbonyl stretching because the epoxide is known to isomerize with temperatures above 100 °C and Lewis acid catalysts (Katritzky and Lagowski 1967). Small oxazolidone ($\tilde{\nu}$ =750 and 693 cm⁻¹) and aromatic ($\tilde{\nu}$ =1600 cm⁻¹) bands were identified with TBAB and Lewis acid catalysts. These bands indicated a small formation of the oxazolidone group with a disubstituted epoxide compared to the monosubstituted epoxide.

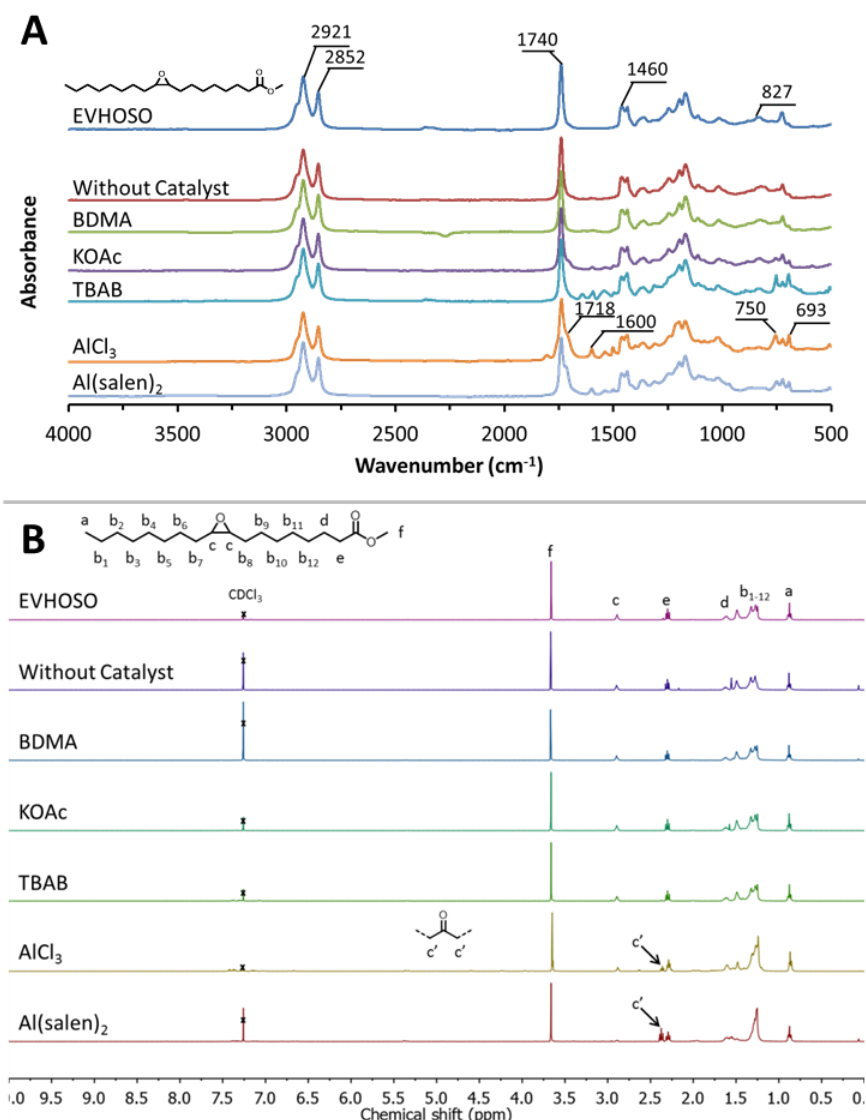


Figure 4.7 - (A) FTIR spectra of EVHOSO alone and the main fractions of Mundex reaction, with and without catalysts. (B) ¹H NMR spectra of EVHOSO alone and the main fractions of Mundex reaction, with and without catalysts.

The ^1H NMR spectra shown in Figure 4.7B confirmed the hypothesis formulated with the FTIR analysis. The major fraction of each reaction conditions was composed of the EVHOSO characteristic chemical shifts: methyl ester proton at $\delta=3.67$ ppm (f), the methylene proton in alpha position of the ester at $\delta=2.3$ ppm (e), the methylene protons at $\delta=1.55-1.20$ ppm (b_{1-12}) and the terminal methyl group at $\delta=0.88$ ppm (a). The methine (CH) epoxide protons are also identified at $\delta=2.9$ ppm in Figure 4.7B. A new peak appeared at $\delta=2.38$ ppm with the Lewis acid catalysts, i.e., AlCl_3 and $\text{Al}(\text{salen})_2$, associated with the alpha proton of the ketone group produced by oxidation of the epoxide group. This was proved by ^{13}C and 2D NMR analysis presented in Figure S4.15-S3.19 in SI.

No signals corresponded to the oxazolidone nor aromatic group in the reaction with the disubstituted epoxide. The main fraction of the epoxidized oil did not react with the isocyanate to largely form oxazolidone groups.

Table 4.4 overviewed the main identified chemical structures in the final reactional systems based on various catalysts. The other fractions represented a small portion of the final product and should be composed of ketone, urethane and carbonate as previously identified in the study of the reaction between 9,10-epoxyoctadecane and phenylisocyanate (Javni et al. 2003).

The difference of reactivity between monosubstituted (i.e., Mundex) and disubstituted (i.e., EVHOSO) epoxides was clearly evidenced in the frame of the oxazolidone formation with finally and in perspective, a lower impact of the catalyst systems.

Table 4.4 - Major fractions identified with the different catalysts and epoxide systems.

Catalyst	DGEBA	Mundex	EVHOSO
-	Oxazolidone	Oxazolidone	Epoxide
BDMA	Oxazolidone	Oxazolidone	Epoxide
$\text{Al}(\text{salen})_2$	Oxazolidone	Oxazolidone	Ketone
TBAB	Oxazolidone	Oxazolidone	Epoxide
AlCl_3	Oxazolidone	Oxazolidone	Epoxide/Ketone
KOAc	Oxazolidone	Oxazolidone	Epoxide

5. CONCLUSION

The frame of this study is dedicated to the elaboration of biobased PUF from different epoxidized triglycerides following several principles for a green chemistry. In this way, the reduction of the number of synthesis steps to transform biobased triglycerides into PUF was particularly investigated, skipping the conventional intermediate step of polyols synthesis. To do it, a deep study on the reactivity between epoxide and isocyanate has been developed.

The characterization of the soluble fractions of fresh and aged PUF formulated with epoxidized oil demonstrated the incomplete reactions between fatty epoxide and isocyanate. To understand the presence of unreacted epoxidized oil in these PUF soluble fractions, the formation of

oxazolidone by reaction between polyisocyanate and epoxidized oil was investigated using different reactional models.

Oxazolidone group was clearly obtained with monosubstituted epoxides. However, these results clearly demonstrated the difficulty to obtain a significant content of oxazolidone group from polysubstituted epoxides, usually found from epoxidized oils. Despite the favorable conditions of the studied reactional models (i.e., prolonged reaction time, solvents, high temperature), the model epoxidized oil did not react with isocyanate using conventional catalysts for PUF.

The myth around oxazolidone formation from epoxidized oil in PUF was broken through. The conditions for the oxazolidone formation in a significant content are not fulfilled in PUF. The steric hindrance due to the substitution of the epoxide group from epoxidized oil prevented the oxazolidone formation.

Future investigations must be focused on the quantification and comparison of oxazolidone formation and side reactions (epoxides homopolymerization and isocyanates trimerization) in PUF. Besides, the condition of the reaction between epoxidized oil and polyisocyanate to quantitatively obtain oxazolidone should also be studied.

6. REFERENCES

Akindoyo, J.O., Beg, M.D.H., Ghazali, S., Islam, M.R., Jeyaratnam, N., Yuvaraj, A.R., 2016. Polyurethane types, synthesis and applications – a review. *RSC Adv.* **6**, 114453–114482. <https://doi.org/10.1039/C6RA14525F>

Anastas, P., Eghbali, N., 2010. Green Chemistry: Principles and Practice. *Chem Soc Rev* **39**, 301–312. <https://doi.org/10.1039/B918763B>

Ansari, M.H., Ahmad, M., 1987. Reaction of methyl *trans* -2,3-epoxyoctadecanoate with phenyl isocyanate: Synthesis of fatty 3-phenyl-2-oxazolidones. *J. Am. Oil Chem. Soc.* **64**, 1544–1547. <https://doi.org/10.1007/BF02609363>

Arbennz, A., Perrin, R., Avérous, L., 2017. Elaboration and Properties of Innovative Biobased PUIR Foams from Microalgae. *J. Polym. Environ.* **26**, 254–262. <https://doi.org/10.1007/s10924-017-0948-y>

Aroua, L., Baklouti, A., 2007. Synthesis of α,ω -Bis(oxazolidinone)polyoxyethylene via a Lithium Bromide–Catalyzed Reaction of Oligoethylene Glycol Diglycidyl Ethers with Isocyanates. *Synth. Commun.* **37**, 1935–1942. <https://doi.org/10.1080/00397910701316920>

Ashida, K., Frisch, K.C., Kordomenos, P., 1978. Oxazolidone catalyst. US4066628A.

Azechi, M., Endo, T., 2014. Synthesis and property of polyoxazolidone having fluorene moiety by polyaddition of diisocyanate and diepoxide. *J. Polym. Sci. Part Polym. Chem.* **52**, 1755–1760. <https://doi.org/10.1002/pola.27181>

Bakry, A., Aversano, R., D’Ilario, L., Di Lisio, V., Francolini, I., Piozzi, A., Martinelli, A., 2016. Flexible aliphatic poly(isocyanurate-oxazolidone) resins based on poly(ethylene glycol) diglycidyl ether and 4,4'-methylene dicyclohexyl diisocyanate. *J. Appl. Polym. Sci.* **133**, 43404. <https://doi.org/10.1002/app.43404>

Baronsky, T., Beattie, C., Harrington, R.W., Irfan, R., North, M., Osende, J.G., Young, C., 2013. Bimetallic Aluminum(salen) Catalyzed Synthesis of Oxazolidinones from Epoxides and Isocyanates. *ACS Catal.* **3**, 790–797. <https://doi.org/10.1021/cs4001046>

Barros, M.T., Phillips, A.M.F., 2010. The first enantioselective [3+2] cycloaddition of epoxides to arylisocyanates: asymmetric synthesis of chiral oxazolidinone phosphonates. *Tetrahedron Asymmetry* **21**, 2746–2752. <https://doi.org/10.1016/j.tetasy.2010.10.028>

Boufi, S., Belgacem, M.N., Quillerou, J., Gandini, A., 1993. Urethanes and polyurethanes bearing furan moieties. 4. Synthesis, kinetics and characterization of linear polymers. *Macromolecules* **26**, 6706–6717. <https://doi.org/10.1021/ma00077a003>

Caille, D., Pascault, J.P., Tighzert, L., 1990a. Reaction of a diepoxide with a diisocyanate in bulk: I. Use of a tertiary amine catalyst. *Polym. Bull.* **24**, 23–30. <https://doi.org/10.1007/BF00298317>

Caille, D., Pascault, J.-P., Tighzert, L., 1990b. Reaction of a diepoxide with a diisocyanate in bulk. II. Use of an imidazole or a blocked isocyanate catalysts. *Polym. Bull.* **24**, 30–31.

Carré, C., Ecochard, Y., Caillol, S., Avérous, L., 2019. From the Synthesis of Biobased Cyclic Carbonate to Polyhydroxyurethanes: A Promising Route towards Renewable Non-Isocyanate Polyurethanes. *ChemSusChem* **12**, 3410–3430. <https://doi.org/10.1002/cssc.201900737>

Chen, K., Tian, C., Cao, F., Liang, S., Jia, X., Wang, J., 2016. Preparation and characterization of highly thermostable polyisocyanurate foams modified with epoxy resin. *J. Appl. Polym. Sci.* **133**, 43085. <https://doi.org/10.1002/app.43085>

Chen, K., Tian, C., Liang, S., Zhao, X., Wang, X., 2018. Effect of stoichiometry on the thermal stability and flame retardation of polyisocyanurate foams modified with epoxy resin. *Polym. Degrad. Stab.* **150**, 105–113. <https://doi.org/10.1016/j.polymdegradstab.2018.02.015>

Chian, K.S., Yi, S., 2001. Synthesis and characterization of an isocyanurate-oxazolidone polymer: Effect of stoichiometry. *J. Appl. Polym. Sci.* **82**, 879–888. <https://doi.org/10.1002/app.1919>

Desroches, M., Escouvois, M., Auvergne, R., Caillol, S., Boutevin, B., 2012. From Vegetable Oils to Polyurethanes: Synthetic Routes to Polyols and Main Industrial Products. *Polym. Rev.* **52**, 38–79. <https://doi.org/10.1080/15583724.2011.640443>

Dileone, R.R., 1970. Synthesis of poly-2-oxazolidones from diisocyanates and diepoxides. *J. Polym. Sci. [A1]* **8**, 609–615. <https://doi.org/10.1002/pol.1970.150080304>

Dyen, M.E., Swern, D., 1968. Chemistry of epoxy compounds. xxii. preparation of some long-cham 2-oxazolidones. *J. Am. Oil Chem. Soc.* **45**, 325–330. <https://doi.org/10.1007/BF02667102>

Fink, J.K., 2018. Poly(urethane)s. In 'Reactive Polymers: Fundamentals and Applications'. Elsevier, pp. 71–138. <https://doi.org/10.1016/B978-0-12-814509-8.00002-6>

Flores, M., Fernández-Francos, X., Moráncho, J.M., Serra, À., Ramis, X., 2012. Ytterbium triflate as a new catalyst on the curing of epoxy-isocyanate based thermosets. *Thermochim. Acta* **543**, 188–196. <https://doi.org/10.1016/j.tca.2012.05.012>

Fourati, Y., Hassen, R.B., Bayramoğlu, G., Boufi, S., 2017. A one step route synthesis of polyurethane network from epoxidized rapeseed oil. *Prog. Org. Coat.* **105**, 48–55. <https://doi.org/10.1016/j.porgcoat.2016.12.021>

Furtwengler, P., Avérous, L., 2018. Renewable polyols for advanced polyurethane foams from diverse biomass resources. *Polym. Chem.* **9**, 4258–4287. <https://doi.org/10.1039/C8PY00827B>

Galante, M.J., Williams, R.J.J., 1995. Polymer networks based on the diepoxide–diisocyanate reaction catalyzed by tertiary amines. *J. Appl. Polym. Sci.* **55**, 89–98. <https://doi.org/10.1002/app.1995.070550109>

Herweh, J.E., Foglia, T.A., Swern, D., 1968. Synthesis and nuclear magnetic resonance spectra of 2-oxazolidones. *J. Org. Chem.* **33**, 4029–4033. <https://doi.org/10.1021/jo01275a007>

Herweh, J.K., 1968. Bis-2-oxazolidones-preparation and characterization. *J. Heterocycl. Chem.* **5**, 687–690.

Hicks, D., Austin, A., 2017. A review of the global PU industry 2016 and outlook for 2017. *PU Mag.* **14**, 4–16.

Javni, I., Guo, A., Petrovic, Z.S., 2003. The study of oxazolidone formation from 9,10-epoxyoctadecane and phenylisocyanate. *J. Am. Oil Chem. Soc.* **80**, 595–600. <https://doi.org/10.1007/s11746-003-0744-7>

Kadurina, T.I., Prokopenko, V.A., Omelchenko, S.I., 1992. Curing of epoxy oligomers by isocyanates. *Polymer* **33**, 3858–3864. [https://doi.org/10.1016/0032-3861\(92\)90373-5](https://doi.org/10.1016/0032-3861(92)90373-5)

Katritzky, A.R., Lagowski, J.M., 1967. Heterocyclic Compounds with Three- and Four-Membered Rings. In 'The Principles of Heterocyclic Chemistry'. Elsevier, pp. 159–164. <https://doi.org/10.1016/B978-1-4832-3304-8.50009-9>

Kinjo, N., Numata, S.-I., Koyama, T., Narahara, T., 1983. Synthesis and viscoelastic properties of new thermosetting resins having isocyanurate and oxazolidone rings in their molecular structures. *J. Appl. Polym. Sci.* **28**, 1729–1741. <https://doi.org/10.1002/app.1983.070280516>

Kordomenos, P.I., Kresta, J.E., Frisch, K.C., 1987. Thermal stability of isocyanate-based polymers. 2. Kinetics of the thermal dissociation of model urethane, oxazolidone, and isocyanurate block copolymers. *Macromolecules* **20**, 2077–2083. <https://doi.org/10.1021/ma00175a006>

Lee, C.S., Ooi, T.L., Chuah, C.H., Ahmad, S., 2007. Rigid Polyurethane Foam Production from Palm Oil-Based Epoxidized Diethanolamides. *J. Am. Oil Chem. Soc.* **84**, 1161–1167. <https://doi.org/10.1007/s11746-007-1150-5>

Maisonneuve, L., Chollet, G., Grau, E., Cramail, H., 2016. Vegetable oils: a source of polyols for polyurethane materials. *OLC* **23**, D508. <https://doi.org/10.1051/ocl/2016031>

Matsuura, H., Miyazawa, T., 1967. Infra-red spectra of polyethylene glycols and O-deuterated derivatives. *Spectrochim. Acta Part Mol. Spectrosc.* **23**, 2433–2447. [https://doi.org/10.1016/0584-8539\(67\)80135-1](https://doi.org/10.1016/0584-8539(67)80135-1)

Merline, J.D., Reghunadhan Nair, C.P., Gouri, C., Sadhana, R., Ninan, K.N., 2007. Poly(urethane–oxazolidone): Synthesis, characterisation and shape memory properties. *Eur. Polym. J.* **43**, 3629–3637. <https://doi.org/10.1016/j.eurpolymj.2007.05.032>

Michalska, K., Bednarek, E., Gruba, E., Lewandowska, K., Mizera, M., Cielecka-Piontek, J., 2017. Comprehensive spectral identification of key intermediates to the final product of the chiral pool synthesis of radezolid. *Chem. Cent. J.* **11**, 82. <https://doi.org/10.1186/s13065-017-0309-x>

Pawar, M.S., Kadam, A.S., Dawane, B.S., Yemul, O.S., 2016a. Synthesis and characterization of rigid polyurethane foams from algae oil using biobased chain extenders. *Polym. Bull.* **73**, 727–741. <https://doi.org/10.1007/s00289-015-1514-1>

Pelzer, T., Eling, B., Thomas, H.-J., Luinstra, G.A., 2018. Toward polymers with oxazolidin-2-one building blocks through tetra-n-butyl-ammonium halides (Cl, Br, I) catalyzed coupling of epoxides with isocyanates. *Eur. Polym. J.* **107**, 1–8. <https://doi.org/10.1016/j.eurpolymj.2018.07.039>

Petrović, Z.S., Wan, X., Bilić, O., Zlatanić, A., Hong, J., Javni, I., Ionescu, M., Milić, J., Degruson, D., 2013. Polyols and Polyurethanes from Crude Algal Oil. *J. Am. Oil Chem. Soc.* **90**, 1073–1078. <https://doi.org/10.1007/s11746-013-2245-9>

Peyrton, J., Chambaretaud, C., Avérous, L., 2019. New Insight on the Study of the Kinetic of Biobased Polyurethanes Synthesis Based on Oleo-Chemistry. *Molecules* **24**, 4332. <https://doi.org/10.3390/molecules24234332>

Peyrton, J., Chambaretaud, C., Sarbu, A., Avérous, L., 2020. Biobased Polyurethane Foams Based on New Polyol Architectures from Microalgae Oil. *ACS Sustain. Chem. Eng.* **8**, 12187–12196. <https://doi.org/10.1021/acssuschemeng.0c03758>

Pilawka, R., Goracy, K., Wilpiszewska, K., 2014. High-performance isocyanate-epoxy materials. *Pigment Resin Technol.* **43**, 332–340. <https://doi.org/10.1108/PRT-11-2013-0110>

Pretsch, E., Bühlmann, P., Badertscher, M., 2009. Structure determination of organic compounds: tables of spectral data, 4th, rev.enl. ed ed. Springer, Berlin.

Qian, C., Zhu, D., 1994. A facile synthesis of oxazolidinones via lanthanide-catalyzed cycloaddition of epoxides with isocyanates. *Synlett* 129–130.

Robert, T.M., Nair, S., Mathew, D., Reghunadhan Nair, C.P., 2018. Room temperature processable heat-resistant epoxy-oxazolidone-based syntactic foams. *Polym. Adv. Technol.* **29**, 121–129. <https://doi.org/10.1002/pat.4094>

Sandler, S.R., 1967. Preparation of mono and poly-2-oxazolidones from 1,2-epoxides and isocyanates. *J. Polym. Sci. [A1]* **5**, 1481–1485. <https://doi.org/10.1002/pol.1967.150050628>

Sendijarević, A., Sendijarević, V., Frisch, K.C., 1987. Studies in the formation of poly(oxazolidones) I. Kinetics and mechanism of the model oxazolidone formation from phenyl isocyanate and phenylglycidyl ether. Selectivity of catalysts. *J. Polym. Sci. Part Polym. Chem.* **25**, 151–170. <https://doi.org/10.1002/pola.1987.080250113>

Siegel, H., Wittmann, H., 1982. Substitutions-und Additionsreaktionen an Spiro-oxiranen. *Monatshefte Für Chemie/Chemical Mon.* **113**, 1005–1017.

Speranza, G.P., Peppel, W.J., 1958. Preparation of Substituted 2-Oxazolidones from 1,2-Epoxides and Isocyanates. *J. Org. Chem.* **23**, 1922–1924. <https://doi.org/10.1021/jo01106a027>

Uribe, M., Hodd, K.A., 1984. The catalysed reaction of isocyanate and epoxide groups: A study using differential scanning calorimetry. *Thermochim. Acta* **77**, 367–373. [https://doi.org/10.1016/0040-6031\(84\)87075-6](https://doi.org/10.1016/0040-6031(84)87075-6)

Wertz, J.H., Tang, P.L., Quye, A., France, D.J., 2018. Characterisation of oil and aluminium complex on replica and historical 19th c. Turkey red textiles by non-destructive diffuse reflectance FTIR spectroscopy. *Spectrochim. Acta. A. Mol. Biomol. Spectrosc.* **204**, 267–275. <https://doi.org/10.1016/j.saa.2018.05.109>

Wu, H., Ding, J., Liu, Y., 2003. Samarium Triiodide Catalyzed Cycloaddition of Epoxides with Isocyanates: A Facile Synthesis of Oxazolidinones. *ChemInform* **34**, no-no.

Yeganeh, H., Jamshidi, S., Talemi, P.H., 2006. Synthesis, characterization and properties of novel thermally stable poly(urethane-oxazolidone) elastomers. *Eur. Polym. J.* **42**, 1743–1754. <https://doi.org/10.1016/j.eurpolymj.2006.02.011>

7. SUPPORTING INFORMATION

7.1. Maximum height of the foam realized with gradual substitution of Pht-DEG by ESO

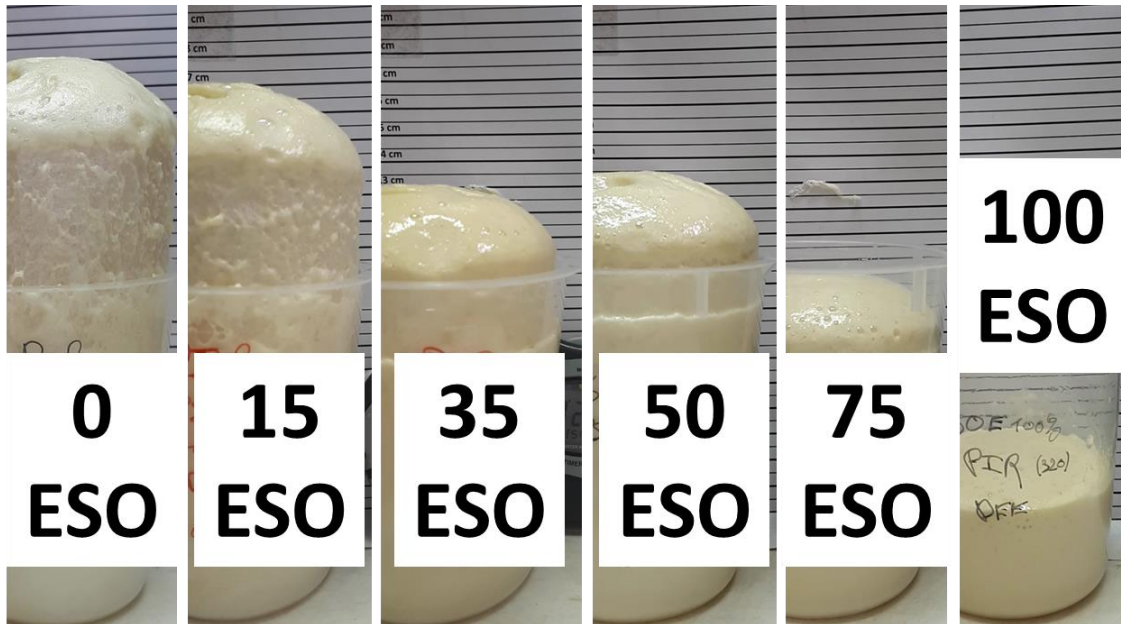


Figure S4.8 - Pictures of PUF realized with increasing content of ESO at then end of the rise. The pictures were adjusted to have an equivalent scale.

7.2. Identified soluble fractions in freshly synthesized foams

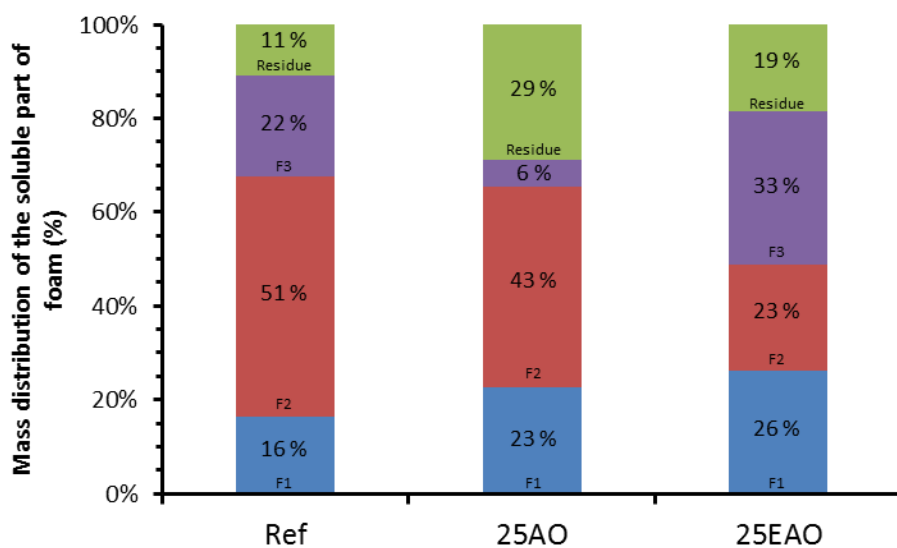


Figure S4.9 - The identified fraction of soluble content of PIR ref, 25AO and 25 EAO foams.

7.3. FTIR analysis of formerly synthesized foams

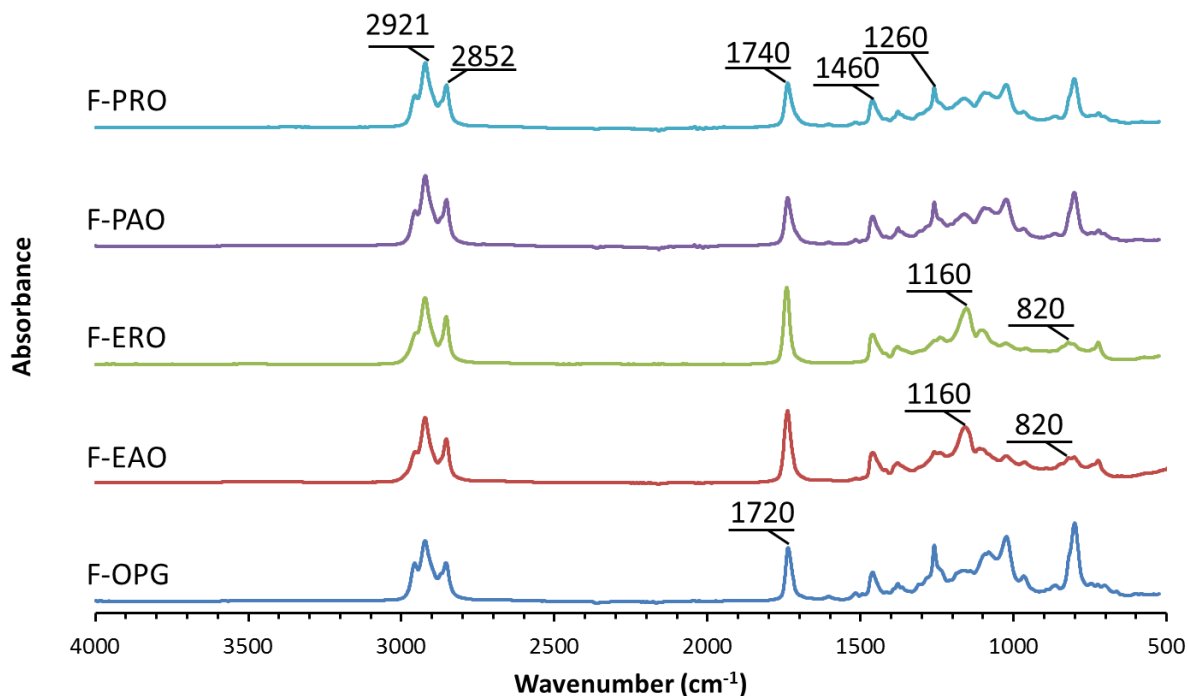


Figure S4.10 - FTIR spectra of F-OPG, F-EAO, F-ERO, F-PAO and F-PRO.

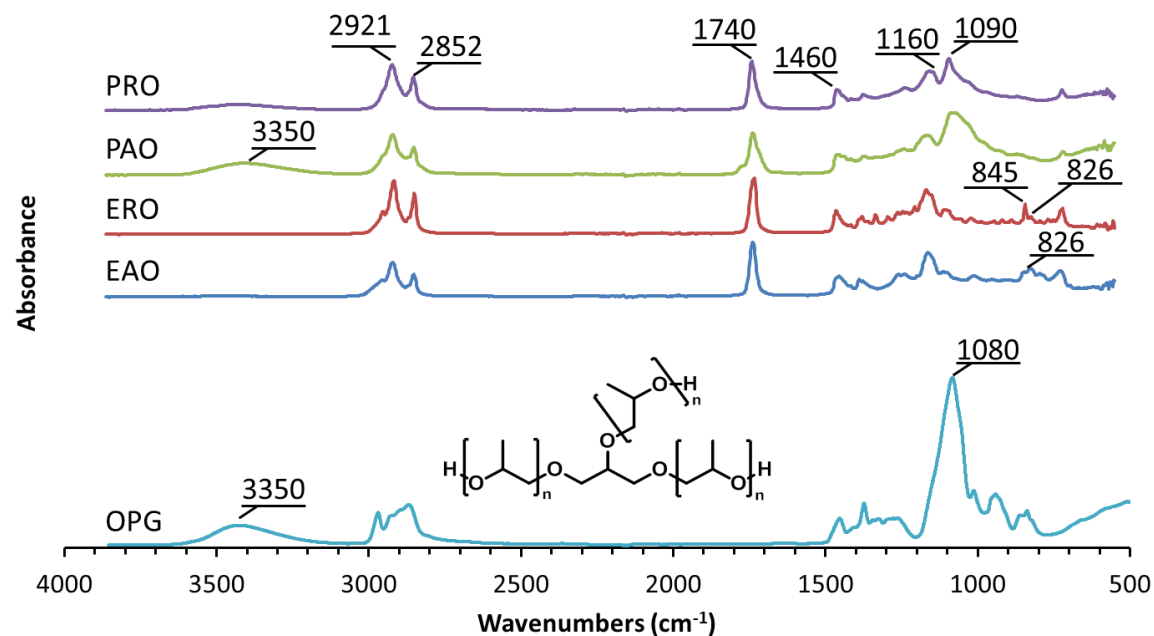


Figure S4.11 - FTIR spectra of OPG, EAO, ERO, PAO and PRO.

7.4. NMR Spectra of Mundex synthesis

Undecylenic acid produced in large quantities as intermediate in the synthesis of PA-11 is derived from the pyrolysis of ricinoleic fatty acid. The fatty acid structure is identified by the ester methylene protons at $\delta=2.33$ ppm (f in Figure S4.12). The terminal double bond protons are located at $\delta=5.80$ and 4.90 ppm (a and b in Figure S4.12). Mund was obtained in quantitative yield (98 wt%) by esterification of undecylenic acid with an excess of methanol. The formation of Mund was identified by the methyl ester peak at $\delta=3.66$ ppm in the ^1H NMR spectra (g in Figure S4.12). Mund was further epoxidized with the meta-chloroperoxybenzoic acid, a stable peroxycarboxylic acid, to yield Mundex at 80 wt%. The formation of Mundex was shown by the complete disappearance of the vinyl proton at $\delta=5.80$ and 4.90 ppm, and the presence of the epoxides protons signals at $\delta=2.89$, 2.74 and 2.45 ppm (Figure S4.12).

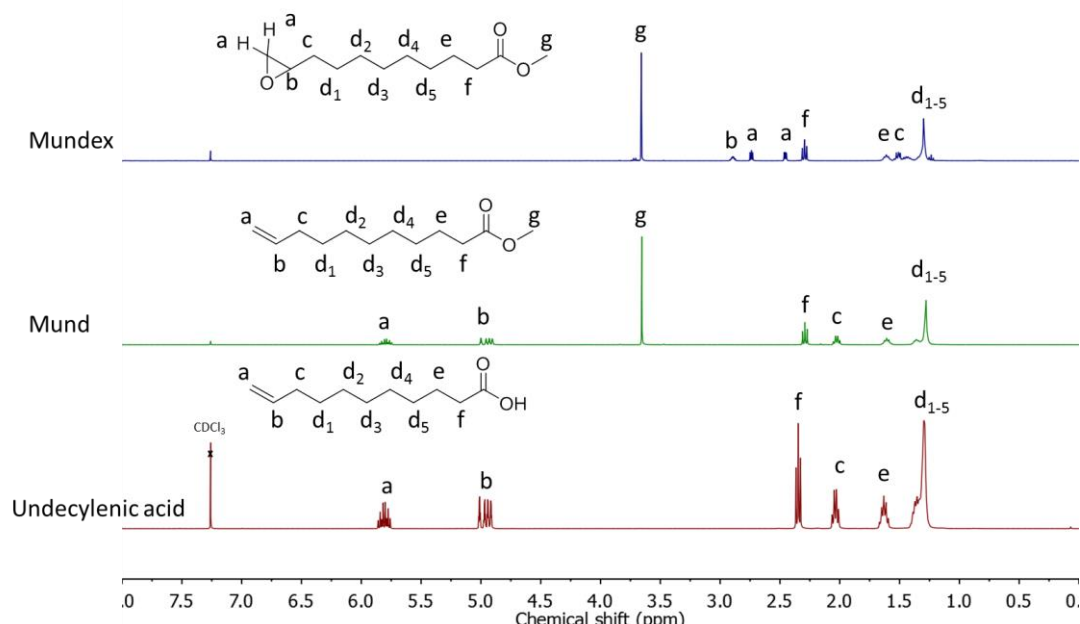


Figure S4.12 - ^1H NMR spectra of undecylenic acid, Mund and Mundex.

7.5. Repartition of the extracted fraction in model study

Table S4.5 - Weight fraction of products separated by chromatography column of the DGEBA reactions.

DGEBA	F1	F2	F3	Residue	Total
Without cat	73%	25%		2%	100%
BDMA	9%	76%	5%	16%	105%
KOAc	71%			29%	100%
TBAB	26%	47%	15%	12%	100%
ALC3	5%	57%	24%	14%	100%
Al(salen)2	18%	66%		36%	121%

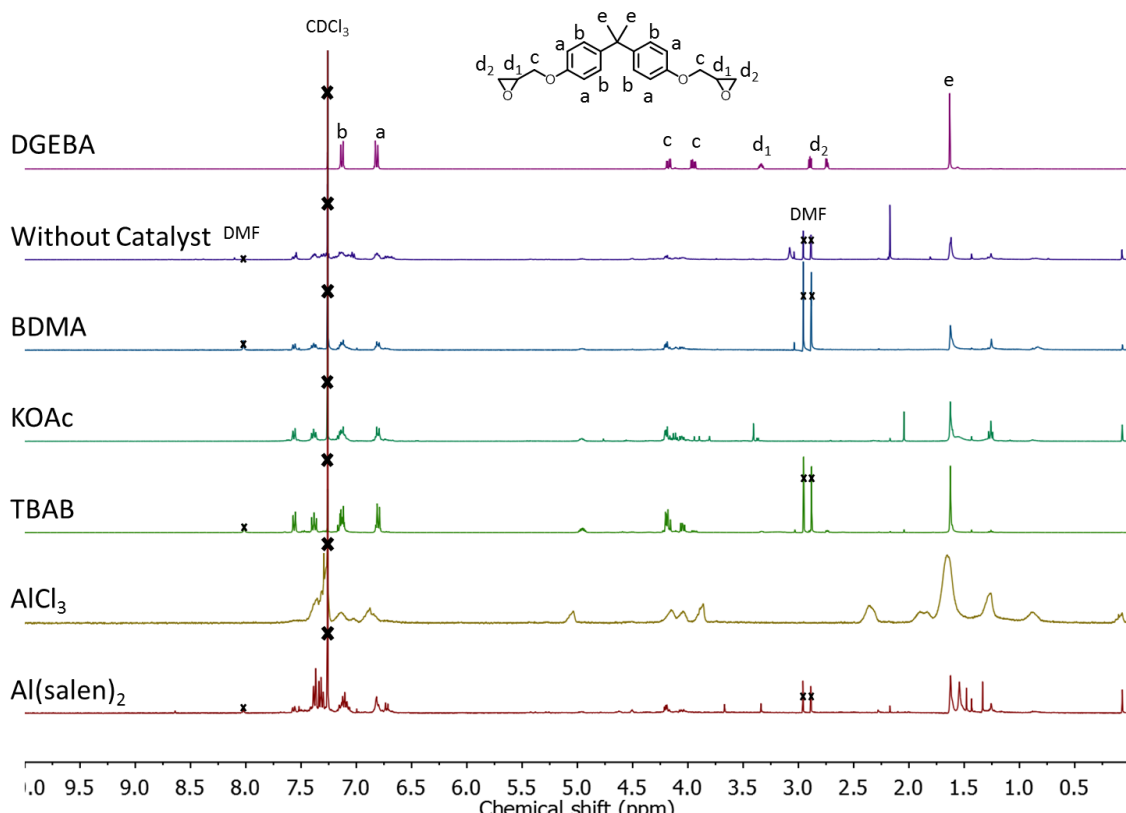
Table S4.6 - Weight fraction of products separated by chromatography column of the Mundex reactions.

Mundex	F1	F2	F3	F4	Residue	Total
Without cat	54%	6%			39%	100%
BDMA	72%	0.1%	1%	6%	26%	106%
KOAc	73%	1%	3%	2%	24%	102%
TBAB	60%	11%			29%	100%
ALC ₃	69%	7%	4%		24%	104%
Al(salen) ₂	54%	11%	3%		35%	103%

Table S4.7 - Weight fraction of products separated by chromatography column of the EVHOSO reactions.

EVHOSO	F1	F2	F3	F4	Residue	Total
Without cat	58%	10%	11%	17%	4%	100%
BDMA	57%	27%	3%		13%	100%
KOAc	62%	9%	11%	14%	4%	100%
TBAB	69%	4%	3%		25%	100%
ALC ₃	58%	11%	4%		27%	100%
Al(salen) ₂	59%	20%	7%	5%	9%	100%

7.6. ¹H NMR spectra of the DGEBA and major fraction of the DGEBA reactions

**Figure S4.13 - ¹H NMR spectra of DGEBA and the main fraction of DGEBA reaction without catalyst and with BDMA, KOAc, TBAB, AlCl₃ or Al(salen)₂.**

7.7. Mundex- AlCl_3 ^{13}C analysis

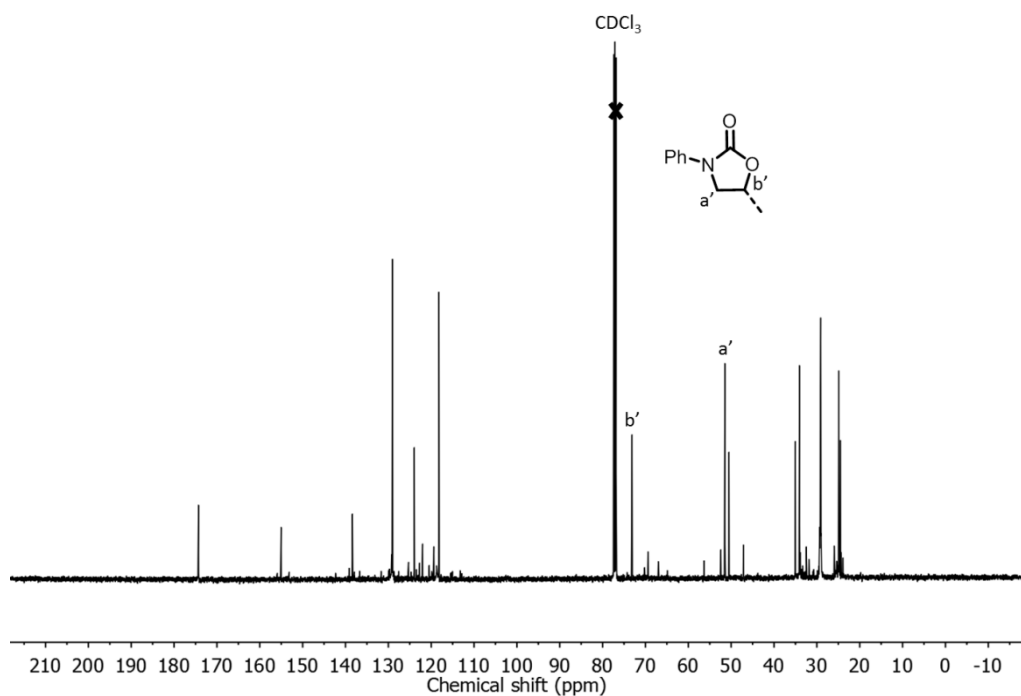


Figure S4.14 - ^{13}C NMR of Mundex- AlCl_3 .

7.8. Complete NMR analysis of EVHOSO-Al(salen) $_2$

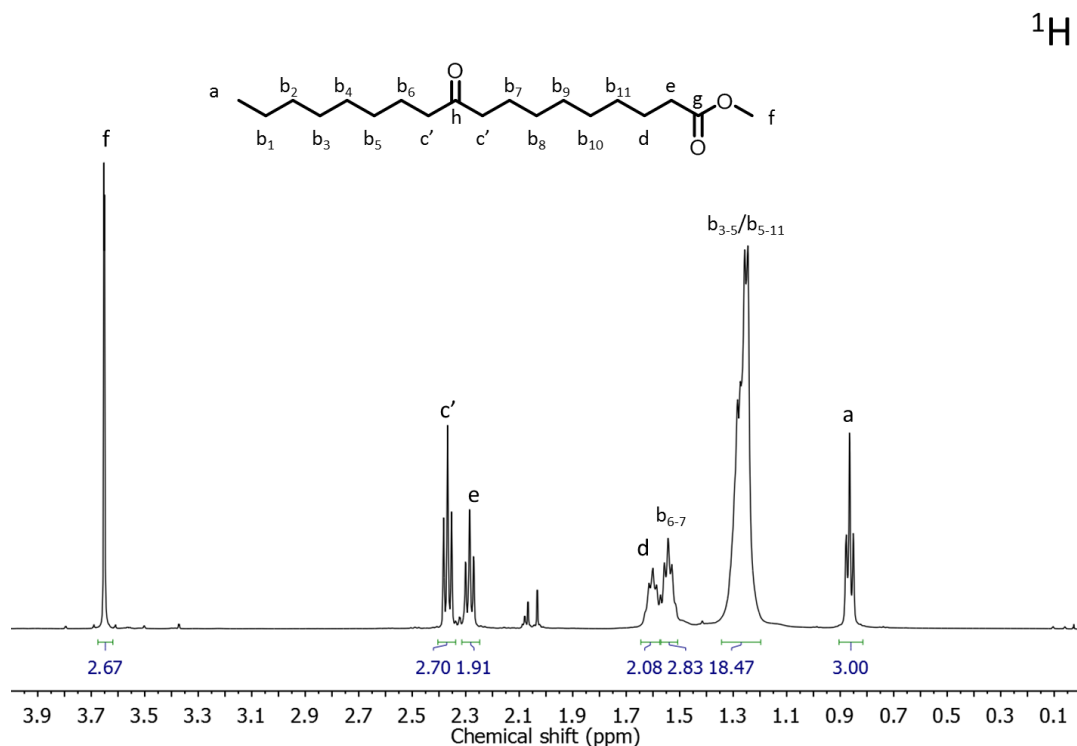


Figure S4.15 - ^1H NMR spectrum of EVHOSO-Al(salen) $_2$.

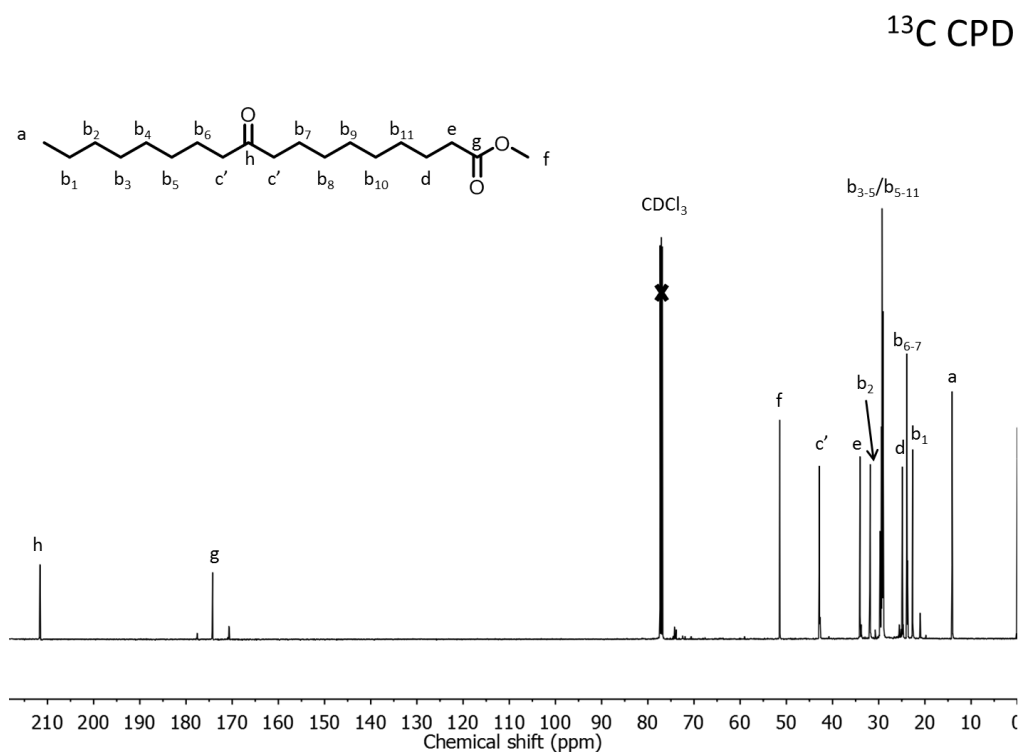


Figure S4.16 - ¹³C NMR Composite Programmed Decoupling (CPD) spectrum of EVHOSO-Al(salen)₂.

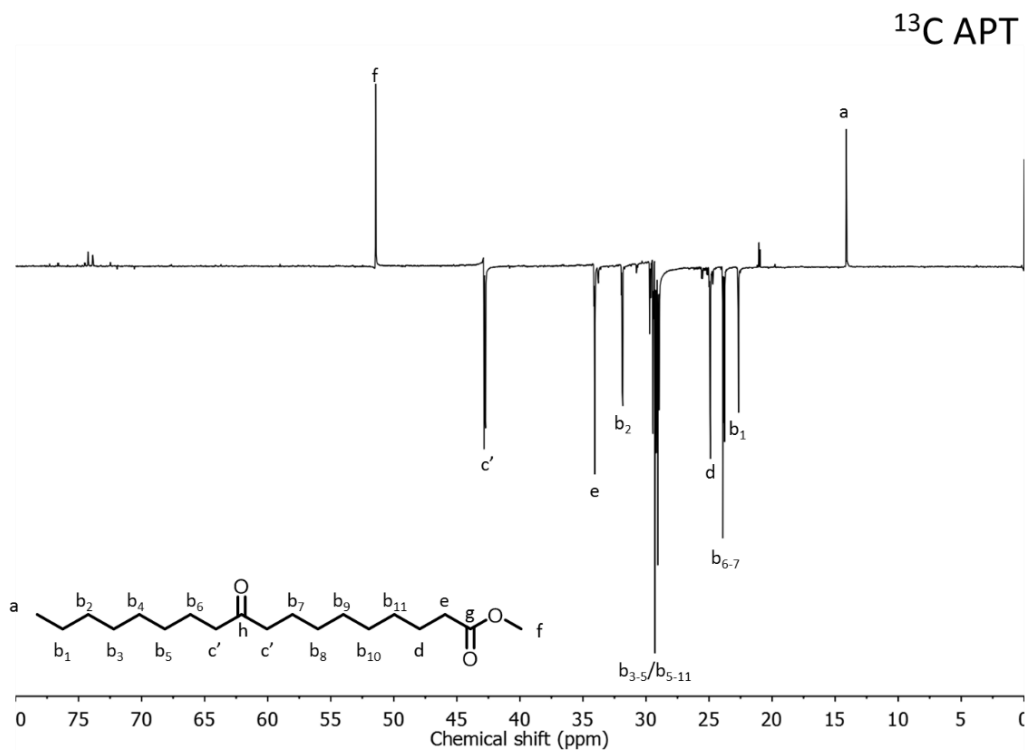


Figure S4.17 - ¹³C Attached Proton test (APT) NMR spectrum of EVHOSO-Al(salen)₂.

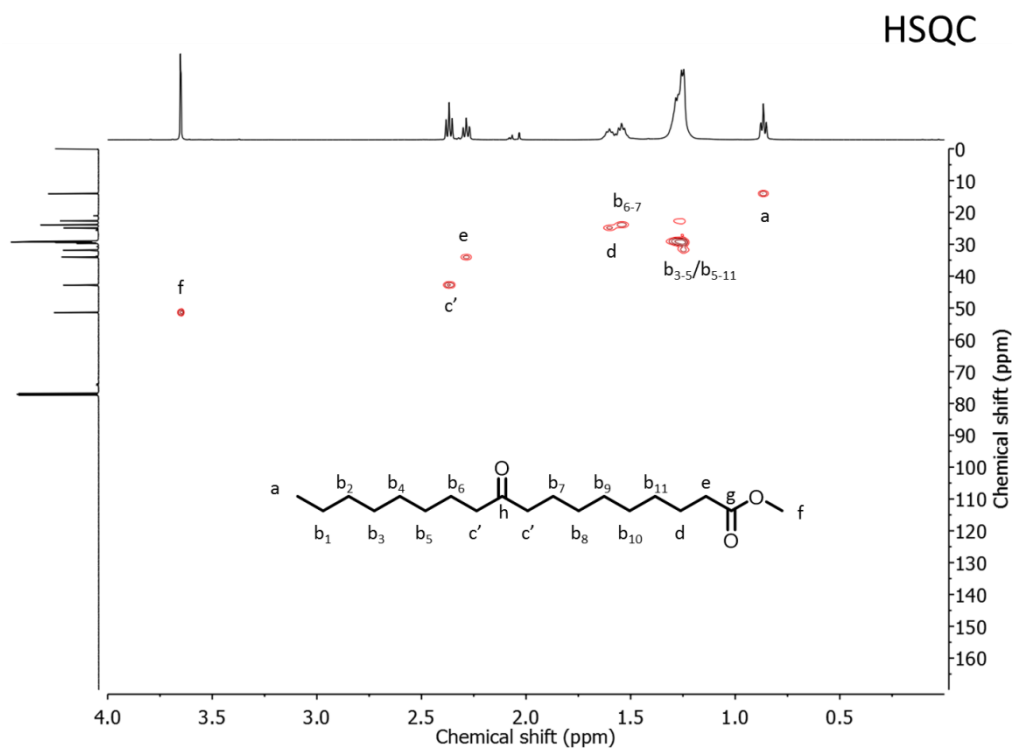


Figure S4.18 - Heteronuclear Single Quantum Correlation (HSQC) NMR spectrum of EVHOSO-Al(salen)₂.

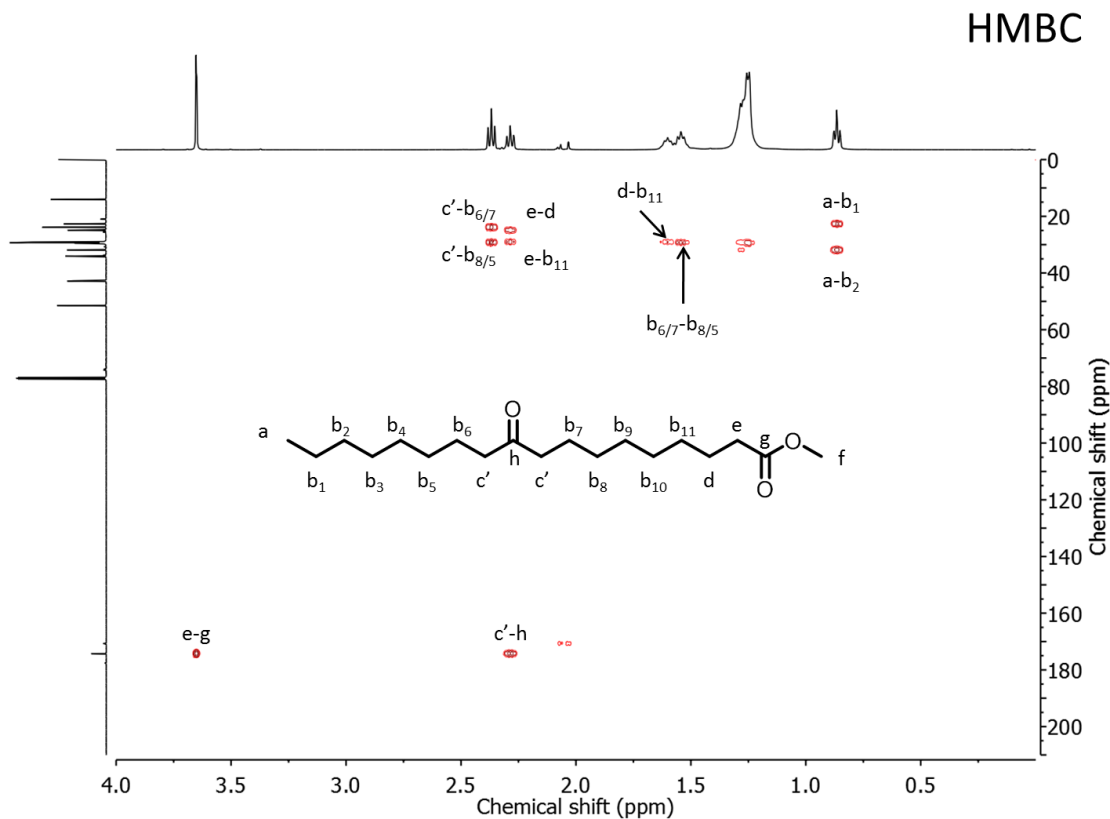


Figure S4.19 - Heteronuclear Multiple Bond Correlation (HMBC) NMR spectrum of EVHOSO-Al(salen)₂.

Conclusion chapitre 4

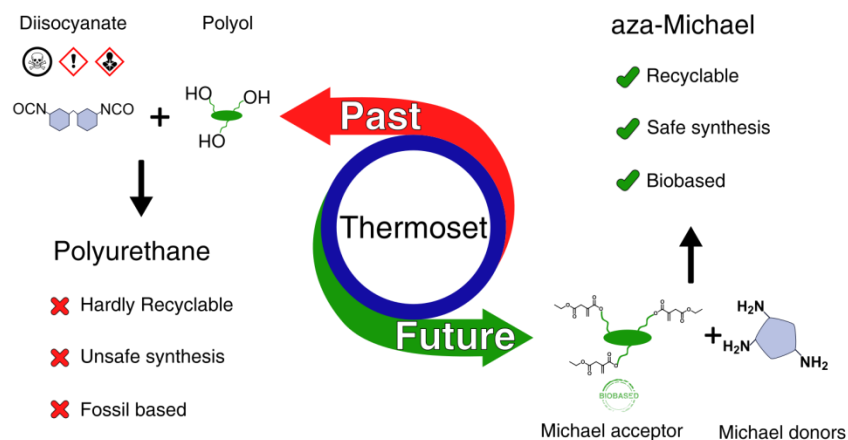
La formation des oxazolidones par réaction des huiles époxydées dans les mousses polyuréthanes a été étudiée dans ce chapitre. Les résultats montrent que le remplacement du polyol directement par l'huile époxydée (soja) impacte négativement la formation des mousses polyuréthanes. La hauteur maximale et la densité diminuent avec l'augmentation de la quantité d'huile époxydée introduite dans les mousses. Ces résultats plutôt négatif ont amené à de plus amples développements. Des mousses polyuréthanes ont donc été élaborées avec 25% du polyol substitué par de l'huile de microalgues époxydée.

Les composés non liés par liaisons covalentes au réseau de ces mousses ont été extraits et analysés. Les analyses infra-rouge et RMN démontrent la présence d'huile époxydée dans les extraits. Ces résultats montrent une réaction incomplète entre les huiles époxydées avec les isocyanates pour la fabrication de mousses polyuréthanes.

Les huiles époxydées et les isocyanates utilisés précédemment ont été modélisés par des composés monofonctionnels pour former de nouveaux modèles réactionnels. Le but était d'identifier les groupements produits par réaction entre les deux composés mis en présence. Les oxazolidones sont clairement produits lors de la réaction entre les époxydes terminaux et les isocyanates aromatiques et ceci quel que soit le catalyseur utilisé. Les conditions dans ce cas sont favorables, par rapport à celles développées précédemment. Le groupement oxazolidone est qualitativement formé avec l'huile époxydée dans les conditions du modèle réactionnel correspondant. Ces résultats montrent la difficulté de produire des fonctions oxazolidones en quantité significative à partir d'huiles époxydées dans les mousses polyuréthanes. Les conditions de formation des oxazolidones ne sont donc pas remplies dans les mousses polyuréthanes. La gêne stérique induite par la disubstitution des époxydes provenant des triglycérides limite et empêche la formation de groupements oxazolidone.

Les futures études devraient se focaliser sur la comparaison quantitative entre la formation d'oxazolidone et les réactions secondaires comme l'homopolymérisation des époxydes ou la trimérisation des isocyanates dans les mousses polyuréthanes. Les conditions idéales (catalyseurs, températures et solvants) pour obtenir quantitativement des oxazolidones à partir d'huiles époxydées et d'isocyanates devraient aussi être explorées.

CHAPITRE 5. ÉTUDE DE LA RÉACTIVITÉ DE LA RÉACTION D'AZA-MICHAEL POUR REEMPLACER LE POLYURÉTHANE DE FAÇON DURABLE



Introduction chapitre 5

Les travaux présentés dans ce chapitre sont sous la forme d'un article intitulée « Study of aza-Michael reactivity for biobased thermosets synthesis to substitute polyurethanes in a greener, safer and more sustainable way » soumis dans *ACS Sustainable Chemistry & Engineering*.

Ce chapitre est une ouverture pour de potentiels futurs travaux qui pourraient mener à l'élaboration de mousses biosourcées plus sûres et plus respectueuses de l'environnement. En effet, les polyisocyanates utilisés dans les chapitres précédents sont toxiques, (carcinogène ...) et leur synthèse nécessite des composés dangereux (phosgène). Certes l'élaboration de polyuréthanes sans isocyanates (NIPU) est une solution envisageable mais les NIPU n'offre pas actuellement, dans l'état des connaissances, toutes les réponses pour remplacer les voies classiques avec de plus une vision de changement d'échelle vers l'industrialisation. Ceci avait été mis en exergue dans le chapitre bibliographique qui avait décrit les différentes voies à développer pour l'élaboration de matériaux alvéolaires durables dans une approche de perspectives. Parmi elle, la transition vers de nouvelles réactions plus en adéquation avec les principes de la chimie verte représente un défi conséquent.

Les produits obtenus par polyaddition de Michael font partie intégrante des voies qui potentiellement permettrait de remplacer les polyuréthanes. Arthur Michael décrit pour la première fois en 1887, l'addition entre un nucléophile (donneur de Michael) et une double liaison activée par un groupement électroattracteur (accepteur de Michael). La réaction d'aza-Michael explorée avec une optique d'une chimie verte. Celle-ci permet la synthèse de groupement amino-ester par addition d'une amine sur une double liaison activée comme un acrylate.

L'addition d'aza-Michael est réalisée sans chauffage avec une économie d'atome de 100%. comme dans le cas de la polyaddition pour former des polyuréthanes. Les groupements amino-esters produits sont cependant sensibles à l'hydrolyse. Ceci peut être un gros avantage en permettant d'envisager une fin de vie du matériau par recyclage enzymatique ou chimique. Les donneurs et accepteurs de Michael sont en outre biosourcables. Plusieurs amines sont industriellement produites à partir de diols biosourcés. Une voie de synthèse des accepteurs de Michael a été développée par époxydation d'huiles biosourcées. Les époxydes sont ensuite ouverts par l'acide acrylique pour former des groupements acrylates et hydroxyles. Dans une étude récente, les accepteurs de Michael comportant des groupements hydroxyles ont été plus réactifs que leurs équivalents sans hydroxyle.

Le remplacement du polyuréthane par la chimie d'Aza-Michael est évalué en terme cinétique. Sur un système réactionnel modèle, la réactivité de différents monomères est étudiée afin de classer les différents groupements réactifs. La formation du gel (temps de gel ...) lors de l'élaboration du réseau polymère est ensuite mesuré par une méthode rhéologique multi-ondes. La variation des structures des donneurs et accepteurs de Michael, les catalyseurs utilisés ainsi que de la stoechiométrie devraient permettre de définir l'impact de ces différents facteurs sur le temps de gel des polyadditions.

Study of aza-Michael reactivity for biobased thermosets synthesis to substitute polyurethanes in a greener, safer and more sustainable way

Julien Peyrton and Luc Avérous

Article submitted in *ACS Sustainable Chemistry & Engineering*

1. ABSTRACT

Polyurethanes (PUs) such as foams or coatings are generally obtained by polyaddition between polyols and toxic polyisocyanates. In the frame of green chemistry principles, which claims, e.g., the reduction of hazardous derivatives and the design of safer chemicals, aza-Michael addition has been recently explored to substitute, for instance, usual PUs in a safer way. Aza-Michael reaction is based on the addition between a primary or secondary amine (Michael donor) and an activated double bond (Michael acceptor). In this study, polymer network formations from biobased soybean and olive oil derivatives were largely investigated via aza-Michael addition. Firstly, on a reactional model, the impact of the Michael donor structure on the aza-Michael reaction was demonstrated by deep NMR kinetics. Secondly, the model results were confirmed by monitoring of the aza-Michael polyaddition by multi-waves rheology experiments. The effect of several factors, i.e., Michael donors, Michael acceptors, catalysts and stoichiometry, on the gelation has been largely investigated. Controlling these parameters, the aza-Michael polyaddition was evaluated as a substitute for green and safer thermosets.

2. INTRODUCTION

Nowadays, the planet is facing severe and urgent challenges. Among them, there is climate change, the depletion of some fossil resources and environmental degradations. In this global context, the development of new and/or greener polymer materials with high performances and low environmental impacts is a huge priority (Manzardo et al. 2019). This recent trend is driven by the development of new molecular architectures starting from various macromers extracted from biomass, without food competition.

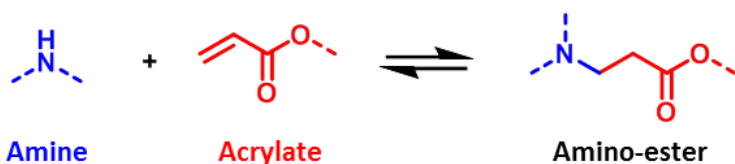
PUs rank 6th among all polymers with a production of around 22 million tons (Hicks and Austin 2017) and a global market of \$50 billion (2016). Although PUs present a broad range of structures and applications, the PU market is primarily dominated by rigid or flexible foams (65% of the market). The complex macromolecular architectures based on PU are actually mainly obtained by polyaddition between fossil-based polyisocyanates and polyols, although safer PUs can be obtained without isocyanates (Non-Isocyanate Polyurethanes) but till now mainly at lab scale (Blattmann et al. 2016; Carré et al. 2019; Cornille et al. 2016). The research trend in renewable PUs focuses on alternatives to replace fossil-based polyols (Agrawal et al. 2017; Furtwengler and Avérous 2018; Hayati et al. 2018). However, it is very challenging to substitute a fossil-based polyisocyanate whose fabrication process uses toxic chemicals, by biobased compounds with equivalent properties at the end. Furthermore, the acute toxicity for the human health of isocyanate group (Brugsch and Elkins 1963; Peters 1970) is a major drawback in the green chemistry frame, which promotes the implementation of less hazardous chemical synthesis and the design of safer chemicals (Anastas and Eghbali 2010).

Arthur Michael, in 1887, was the first to describe the addition of an enolate to an α,β -unsaturated carbonyl compound (Michael 1887). Over the years, the Michael addition scope was extended to the base-catalyzed addition between a nucleophile (Michael donor) and a double bond activated by an electron-withdrawing group (EWG) (Michael acceptor) represented in Scheme 5.1 (Bergmann et al. 2004; Mather et al. 2006). The Michael addition is one useful method for the C-C bond formation in mild conditions. One of the derived reactions named aza-Michael involves a secondary or primary amine (Michael donor) and an activated double bond (Michael acceptor), often an acrylate producing amino-ester groups (Scheme 5.1).

Michael Addition scope



Aza-Michael Addition



Scheme 5.1 - Michael addition general scope and the particular case of the aza-Michael addition.

Similarly to PUs synthesis, the aza-Michael reaction can be conducted at ambient temperature with a 100% atom economy, which fulfills at least two principles for a green chemistry (Anastas and Eghbali 2010). Aza-Michael addition is considered greener than isocyanate/hydroxyl addition. Contrary to the urethane group, the polyamino-ester group obtained by aza-Michael addition is sensible to the hydrolysis. Consequently, it can be sustainably and efficiently managed at the end of

life, biodegraded by enzymes (biological recycling) or degraded (chemical recycling) to form new monomers. Furthermore, both the amines (Froidevaux et al. 2016) and the activated double bonds can be extracted or bioproduced from biomass. Generally, the biobased Michael acceptors are obtained by ring-opening of epoxidized oils with acrylic acid (Ecochard et al. 2020; Paramarta and Webster 2017). Although acrylic acid can be potentially synthesized from different biobased resources (e.g., glycerol or lactic acid) (Bozell and Petersen 2010), it is conventionally obtained by oxidation of propylene or propane derived from fossil resources (Chu et al. 2015; Lee et al. 2019). Recently, the fossil-based acrylic acid was substitute by fully biobased itaconic acid and derivatives (Pérocheau Arnaud et al. 2020) which is industrially produced from various biomasses by different companies such as Itaconix (UK).

PUs elaboration is based on a fast and exothermic polyaddition. The high reactivity of the components is crucial in the formation of the thermosetting structures. Aza-Michael reaction has several advantages (e.g., atom economy, mild condition reaction, biobased and safe reagents) over PU synthesis to bring high perspectives to tailor sustainable system for e.g., foams or coatings. Recently, Michael acceptors synthesized by ring-opening of epoxidized linseed oil by acrylic acid were demonstrated to be highly reactive (Ecochard et al. 2020). However, the polymer formation kinetic was not investigated in this previous paper.

This study aims to wholly investigate aza-Michael reaction and kinetic from biobased Michael acceptors obtained by ring-opening of epoxidized oils with acrylic acid or ethyl itaconate (Iet). This synthesis of Michael acceptors forms reactive double bonds in aza-Michael addition and hydroxyl (OH) groups. In order to deeply investigate the role of OH groups on the aza-Michael addition, the epoxidized oil ring-opened by acrylic acid or Iet were modeled. The kinetics, intermediate compounds formation and chemical pathways of modeled aza-Michael reactions were identified and compared through coupled ¹H and ¹³C NMR monitoring. To understand better the results obtained on the reactional model, the reactivity of aza-Michael polyadditions was investigated through the gelation phenomenon and gel times were determined by multi-waves rheology experiments. In order to obtain aza-Michael system with gel time comparable to conventional PUs, different factors were investigated such as (i) the poly-Michael acceptors with EOSa, EOOa or ESO_Iet, (ii) the catalysts, (iii) the chemical structure of the Michael donor and finally, (iv) the stoichiometry. The thermal properties of the synthesized biobased polymers were studied and compared to select the best systems.

3. MATERIALS AND METHODS

3.1. Materials

Glacial acetic acid, H₂O₂ (30%), 1,2-Dimethylethylenediamine (DMEDA), Tetraethylenepentamine (TEPA), Diethylenetriamine (DETA), furfurylamine (99%), Methyleneethylenediamine (MEDA) (95%), N-(n-butyl)ethylenediamine (BEDA), acid itaconic (99%), anhydride itaconic (97%), anhydrous ethylene glycol (99.8%), dicyclohexylcarbodiimide (99%) (DCC), 2-hydroxyethyl acrylate (2-OHa) (97%), 1,1,3,3-tetramethylguanidine (TMG) (99%), 1,8-Diazabicyclo(5.4.0)undec-7-ene (DBU) (98%), Aluminium trichloride (AlCl₃) (98.5%), p-toluenesulfonic acid (PTSa) (99%), 1,5-Diazabicyclo(4.3.0)non-5-ene (DBN) (98%), acid hydrochloric (37% in water) (HCl), sulfuric acid (H₂SO₄) (95%), ethyl acetate (99%), anhydrous magnesium sulfate,

cyclohexane (99.8%), toluene (99%) and diethyl ether (99.5%) were obtained from Fisher Scientific (France). Amberlyst® 15H (strongly acidic cation exchanger dry), Amberlite® IR120H (strongly acidic ion exchange resin), CDCl_3 , m-Xylylenediamine (mXDA), Diaminopropane (DAP), acrylic acid (99%), sodium bicarbonate, 4-Dimethylaminopyridine (DMAP) and hydroquinone (99%) were provided by Sigma-Aldrich (France). Ethanol absolute, deuterated dimethyl sulfoxide (d-DMSO) (99.8%) and acetone were purchased from VWR (France). Octylamine (OA) (99%) was provided by TCI chemicals (France). Weepox01 is commercial ESO provided by Brenntag (Germany). Olive oil from EU (OO) was purchased at Auchan (France). All chemicals were used without any purification.

3.2. Synthesis of ethyl itaconate (Iet)

According to a previously described protocol (Pérocheau Arnaud et al. 2020), 10 g of anhydride itaconic (0.09 mol, 1 eq.) were introduced in a round bottom flask equipped with a magnetic stirrer. 2 mL of toluene and 6 mL of ethanol (0.1 mol, 1.15 eq.) were added to the mixture. After 16h at 50 °C, the solvent was removed under reduced pressure. Ethyl itaconate is obtained with 94 wt% yield. ^1H NMR (ppm): 12.6 (1H, COOH), 6.16 (1H, s), 5.8 (1H, s), 4.1 (2H, q), 3.3 (2H, s), 1.2 (3H, t).

3.3. Synthesis of 4-ethyl 1-(2-hydroxyethyl) 2-methylenesuccinate (Ietgl)

This synthesis was adapted from a previously described protocol (Tremblay- Parrado and Avérous 2020). 2 g of Iet (12.6 mmol, 1 eq.) were introduced in a round bottom flask equipped with a magnetic stirrer. 0.15 g of DMAP (1.2 mmol, 0.1 eq.) and 15 mL of anhydrous ethylene glycol (268 mmol, 21 eq.) were added to the mixture. The flask was cooled down to 0 °C. 3 g of DCC (14.5 mmol, 1.15 eq.) dissolved in 15 mL of dichloromethane were introduced drop by drop. When the addition is complete, the mixture was stirred 30 min at 0 °C. Then, the reaction mixture was left stirring 15 hours at room temperature. The mixture was filtered to remove most of the N,N'-dicyclohexylurea (DCU) byproduct formed during the reaction. The product was then purified by chromatography column with a 8/2 diethyl ether/cyclohexane eluent. The solvent was evaporated under reduced pressure. The crude mixture was dissolved in a minimum of dichloromethane and put at 0 °C to crystallize the DCU and then filtered to remove the residual DCU. The dissolution, crystallization and filtration process was repeated twice. The final yield of the pure product is 62 wt%. ^1H NMR (ppm): 6.3 (1H, s), 5.7 (1H, s), 4.2 (2H, q), 4.1 (2H, q), 3.3 (2H, s), 1.3 (3H, t), 1.2 (3H, t). ^{13}C NMR (ppm): 171 (C=O), 166 (C=O), 134 (C=C), 128 (C=C), 67, 61, 59, 38, 14.

3.4. Synthesis of diethyl itaconate (Deti)

1 g of itaconic acid (7.7 mmol, 1 eq.) were introduced in a round bottom flask equipped with a magnetic stirrer. A large excess of absolute ethanol was introduced with few drops of sulfuric acid. The mixture was stirred under reflux for 20 hours. After cooling down to room temperature, the mixture was neutralized with a saturated solution of NaHCO_3 . The organic solution was dried over anhydrous magnesium sulfate and concentrated under vacuum to obtain a brown liquid. The final yield

of the product is 80 wt%. ^1H NMR (ppm): 6.3 (1H, s), 5.8 (1H, s), 4.8 (1H, OH), 4.1 (2H, q), 3.6 (2H, s), 3.4 (2H, t) 1.2 (3H, t). ^{13}C NMR (ppm): 171 (C=O), 166 (C=O), 134 (C=C), 129 (C=C), 61, 38, 14.

3.5. Synthesis of epoxidized olive oil (EOO)

According to a previously described protocol (Arbenz et al. 2017; Petrović et al. 2002), 100 g of OO (0.29 mol, 1 eq.), 25 g of Amberlite® IR 120H were introduced in a 1 L three-neck flask equipped with a reflux condenser, a magnetic stirrer and a dropping funnel. 8.3 mL of acetic acid (0.15 mol, 0.5 eq.) and 100 mL of toluene were added. The mixture was heated to 70 °C under vigorous magnetic stirring. Then 44.8 mL of H_2O_2 30% (0.45 mmol, 1.5 eq.) were added dropwise by the dropping funnel for 30 min to prevent overheating and epoxide ring-opening. The mixture was heated at 70 °C for 7h additional hours. In the end, the mixture was recovered in 500 mL of ethyl acetate. The catalyst was filtered off. The organic phase was washed with saturated NaHCO_3 solution until neutral pH. Then it was washed with brine solution, dried with anhydrous magnesium sulfate and then filtered. The solvent was evaporated under reduced pressure. The EOO was dried overnight in a vacuum oven at 40 °C. The yield was 90 mol%.

3.6. Ring-opening of epoxidized oils with acrylic acid

The protocol was adapted from a previously published work (Peyrton et al. 2019). In a typical procedure, the reaction was carried out in a round bottom flask equipped with a reflux condenser and a magnetic stirrer. The flask was filled with epoxidized oil (1 eq. of epoxide), hydroquinone (0.02 eq.) and acrylic acid (1.7 eq.). The mixture was stirred at 90 °C for 15 hours. In the end, the exceeding acrylic acid was distilled under vacuum. The mixture was recovered with ethyl acetate. The organic phase was washed with saturated NaHCO_3 solution until neutral pH. Then it was washed with brine solution, dried with anhydrous sodium sulfate and then filtered. The solvent was evaporated under reduced pressure. The ESO and EOO ring-opened with acrylic acid named ESOa and EOOa, respectively, were dried overnight in a vacuum oven at 40 °C. The yield was 90 wt%.

3.7. Ring-opening of ESO with Iet (ESO_Iet)

The protocol was adapted from a previously published work (Peyrton et al. 2019). The reaction was carried out in a round bottom flask equipped with a reflux condenser and a magnetic stirrer. The flask was filled with 20 g of ESO 2.2 mmol epoxide/g, (44 mmol, 1 eq.), 0.1 g of hydroquinone (0.9 mmol, 0.02 eq.) and 12 g of Iet (75 mmol, 1.7 eq.). The mixture was stirred at 120 °C for 2 days. The mixture was recovered with ethyl acetate. The organic phase was washed with saturated NaHCO_3 solution until neutral pH. Then it was washed with brine solution, dried with anhydrous sodium sulfate and then filtered. The solvent was evaporated under reduced pressure. The ring-opened ESO with Iet (ESO_Iet) was dried overnight in a vacuum oven at 40 °C. The yield was 94 wt%.

3.8. Synthesis of Difurfurylamine (DIFFA)

According to a previously described protocol (Holfinger et al. 1995; Janvier et al. 2017), 25 mL of Furfurylamine (0.28 mol, 2.1 eq.) were introduced in a round bottom flask equipped with a magnetic stirrer and a reflux condenser. The flask was cooled down to 0 °C with an ice bath. An aqueous solution of HCl (18 wt%) (0.68 mol, 5 eq.) was then added dropwise to furfurylamine over 1 hour. After complete addition, the mixture was stirred for 30 min at 25 °C. 10 mL of acetone (0.13 mol, 1 eq.) is then added, and the mixture is stirred at 40 °C. After 3 days, 4 mL of acetone (0.4 eq.) is added to the mixture. The reaction was completed after an additional day of reaction. The mixture is then cooled down to 0 °C, and 75 ml of water were added. An aqueous solution of NaOH (15 w%) is added until pH 10 is exceeded. The mixture is extracted with ethyl acetate (3x100 mL), washed with brine, dried over anhydrous magnesium sulfate and concentrated under vacuum to obtain DIFFA (19.3 g, 80% crude yield). ^1H NMR (ppm): 6.0 (2H, d), 5.9 (2H, d), 3.76 (4H, s), 1.6 (6H, s), 1.5 (4H, NH_2).

3.9. Characterizations

Epoxide index (EI) is expressed in wt% of oxygen in the form of epoxides in the fatty compound. In an Erlenmeyer flask, between 150 and 200 mg of sample was precisely weighed and dissolved in 5 mL of MEK. Exactly 10 mL of 0.4 mol/L HCl solution in MEK was added. The flask was closed and left to react at ambient temperature under magnetic stirring for 30 min. Then, 3 mL of water were added. The excess of HCl is titrated with 0.1 mol/L KOH solution. Phenolphthalein was used as the equivalence indicator. The epoxide index is determined according to Equation 5.1.

$$EI = \frac{(V_{Bl} - V_{eq} + V_{Ac}) * C_{KOH}}{W_s * 10} * 16 \quad (5.1)$$

NMR analyses were realized on a 400 MHz Bruker spectrometer. The Michael donor was diluted with CDCl_3 in an NMR tube. An equimolar quantity of Michael acceptor was added and launched the kinetic experiment. The ^1H spectra were obtained in quantitative conditions (i.e., the number of scans was set to 16 with a relaxation delay of 15 seconds). Straight after each proton acquisition, a ^{13}C spectrum was recorded using a ^{13}C attached proton test (APT) program with 128 scans. The APT program was chosen for better resolution. Furthermore, the methyl (CH_3) and methine (CH) carbons are differentiated from the methylene (CH_2) and quaternary (C) carbons. The reaction was followed by alternated ^1H and ^{13}C NMR for 6 hours. Each spectrum was calibrated with the CDCl_3 signals, set at 7.26 ppm for ^1H and 77.2 ppm for ^{13}C .

Rheological measurements were realized on a discovery HR-3 (TA instruments, France). The oscillatory shear experiments were performed with a 25 mm aluminum plate for the upper and lower plate.

Gel times were determined from rheological measurements by the crossover of the $\tan \Delta$ (delta) curves at different frequencies. Several experiments conducted at unique frequency are required to apply this procedure. A multi-wave oscillation program was used to improve the precision. This program tests the samples at different frequencies in one experiment. Figure 5.1 described the construction of the multi-wave oscillation. The fundamental, 2nd, 6th and 10th harmonic are uniques sinusoidal waves. The 2nd, 6th, and 10th harmonics correspond to a frequency of solicitation of 2, 6 and 10 times the fundamental frequency, respectively. The stress fixed the amplitude of each harmonic.

Figure 1 shows that the fundamental, 2nd, 6th and 10th harmonic stresses are fixed at 1, 0.9, 0.8 and 0.7%, respectively. The resulting multi-wave oscillation is formed by the sum of all the unique oscillations. The sample stressed by this multi-wave oscillation react with a similar wave. After Fourier transformation of the material response to the multi-wave stress, the different parameters (e.g., G', G'', tan Δ) are obtained for the different solicitation frequencies.

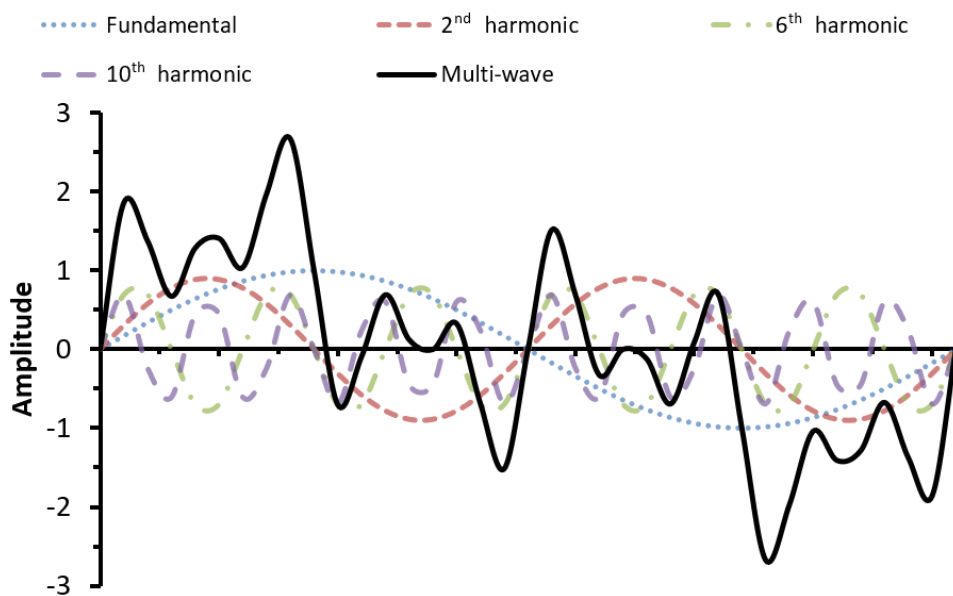


Figure 5.1 – Mutli-wave program presentation.

In a typical procedure, one gram of activated double bond oil is weighed in a Teflon becker. The convection oven temperature was set to 0 °C to cool down. The equivalent amount of amine was added and launched the experiment. The mixture was stirred between 10 and 45 sec to homogenized. Then it was put in-between the rheometer plate. The multi-wave oscillatory experiment was launched with a 1% strain and a 0.5 Hz frequency for the fundamental. The additional harmonics used were the 2nd, 6th and 10th with an amplitude of 0.9, 0.8 and 0.7, respectively. The maximum stress for the multi-wave method was 3.4%, corresponding to the sum of all individual stresses.

The gel time determinations were realized within the linear viscoelastic region of each material. The determination of the linear viscoelastic domain was realized before the gel determination in the most critical conditions: most crosslinked material, lower temperature and higher solicitation frequency. Therefore, an amplitude oscillation was realized at a frequency of 5 Hz, with a percentage of strain from 0.02 to 100%.

TGA was performed using a TA Instrument Hi-Res TGA Q5000 under N₂ (flow rate 25 mL/min). Samples of 1–3 mg were heated from room temperature to 700 °C at 10 °C/min. The main characteristic degradation temperatures were determined at the maximum of the derivative thermogravimetric (DTG) curve.

DSC was performed using a TA Instrument Q200 calorimeter under a nitrogen flow (50 mL·min⁻¹). Samples of 1–3 mg were sealed in standard aluminum pans. The thermal properties (crystallization, fusion and glass transition temperature (T_g)) were recorded using a cyclic procedure. Samples were heated from room temperature to 150 °C to erase the thermal history of samples,

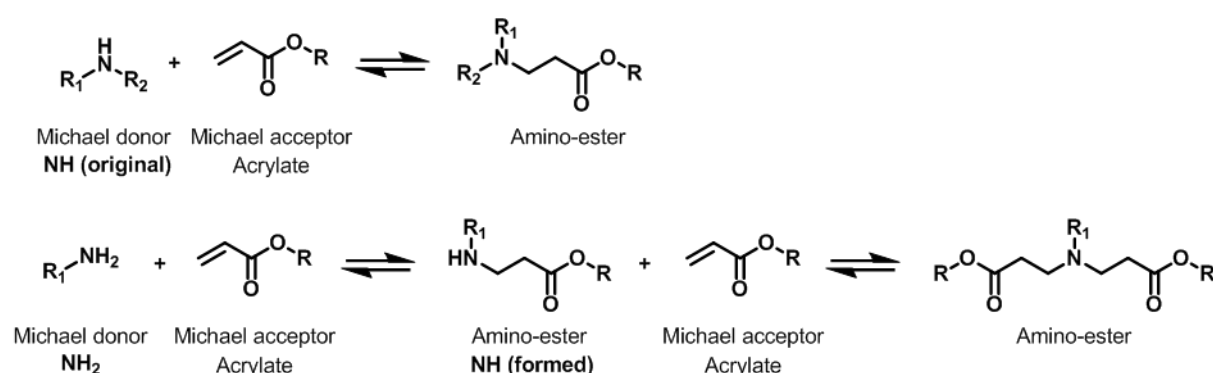
followed by a cooling ramp at 10 °C/min to -80 °C and finally a second heating to 150 °C at the same rate. The temperature was kept constant for 5 min at the end of each temperature ramp.

4. RESULTS AND DISCUSSION

4.1. Study of reactional models

On the contrary to the original Michael addition, aza-Michael addition proceeds without strong base catalysis. The Michael donor (amine) has sufficient nucleophilic and basic properties to react at ambient temperature. The secondary amines are more nucleophile and, therefore, more reactive than primary amines. The primary amine reacts with a Michael acceptor to form a secondary amine, which can further react with another equivalent of the acceptor (Scheme 5.2). The secondary amines and the primary amines are considered monofunctional and difunctional, respectively.

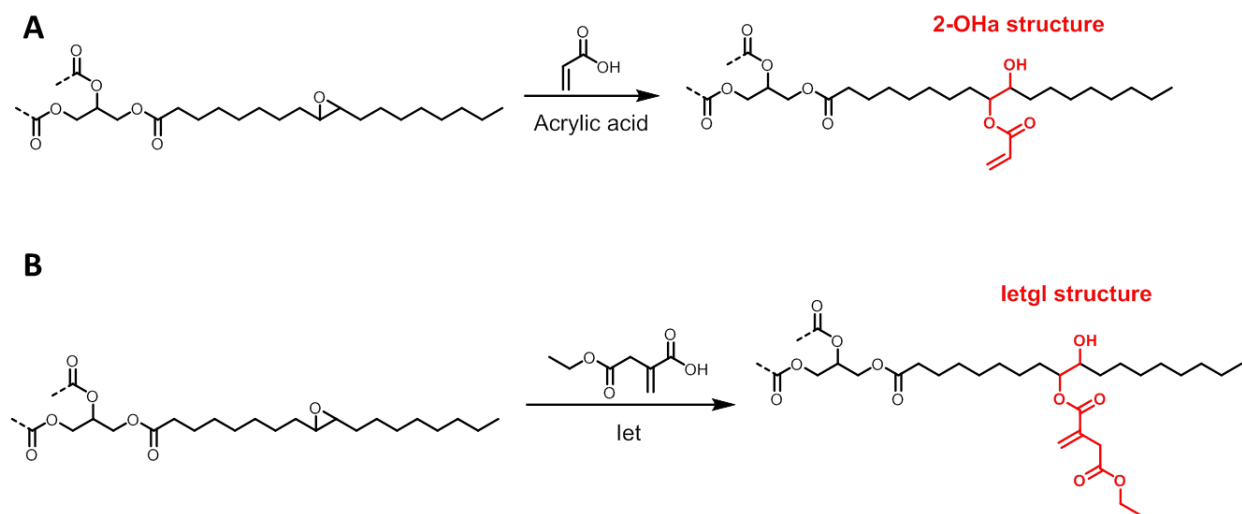
The evaluation of the reactivity and the functionality are key parameters for the control of the polymerization. In aza-Michael reaction, there are three types of Michael donors, represented in Scheme 5.2 (i) the secondary amine substituted by an alkyl chain (NH original), (ii) the primary amine (NH₂), and (iii) the secondary amine obtained from the addition of a first acrylate equivalent on NH₂ (NH formed). The gap of reactivities between these three types of Michael donors was studied with 1,4 butanediol diacrylate and MEDA or BEDA (Wu et al. 2004). The ¹³C NMR analysis performed on the polymerization determined the following reactional order: NH (original) > NH₂ >> NH (formed) (Wu et al. 2004). This order can be reversed between NH (original) and NH₂ when the secondary amine is sterically hindered. A reduction of the nucleophilic character and the steric hindrance explains the reduced reactivity of NH (formed) with Michael acceptors. Recently, Caillol and coworkers demonstrated the fast addition in bulk of two equivalents of 2-OHa with OA, compared to butyl acrylate (Ecochard et al. 2020). The authors hypothesized a catalyst activity of the hydroxyl (OH) group on the aza-Michael reaction.



Scheme 5.2 - Aza-Michael reaction with secondary and primary amines.

In order to understand the impact of the OH group on the aza-Michael pathways with primary and secondary amines, the studied system is composed of 2-OHa as Michael acceptor and MEDA or BEDA as Michael donor. 2-OHa was used to model the ring-opening of epoxidized oil with acrylic acid, as described in Scheme 5.3A. As in the case of published works (Wu et al. 2004), the reaction conversion was followed by ¹H NMR, and the chemical pathway was investigated by ¹³C APT NMR.

To follow the full reaction, kinetics studies were realized directly in NMR tube with CDCl_3 as a solvent, at 25 °C.



Scheme 5.3 - Ring-opening of epoxidized oil with acrylic acid (A) or Iet (B).

Figure 5.2 presented the conversion over time of stoichiometric amounts of 2-OHa and BEDA or MEDA. The reaction was followed by the integration of the double bond signals in ^1H NMR. After six hours, the conversion evolution seems to plateau at 66% of conversion for both Michaelis donors, which indicated that only two double bonds equivalents have reacted. It can be hypothesized that one reactive site among NH (original), NH_2 and NH (formed) did not react after six hours. The slower consumption of 2-OHa with BEDA compared to MEDA could be explained by the higher steric hindrance of the NH (original). These results are consistent with the results obtained in previous works (Wu et al. 2004).

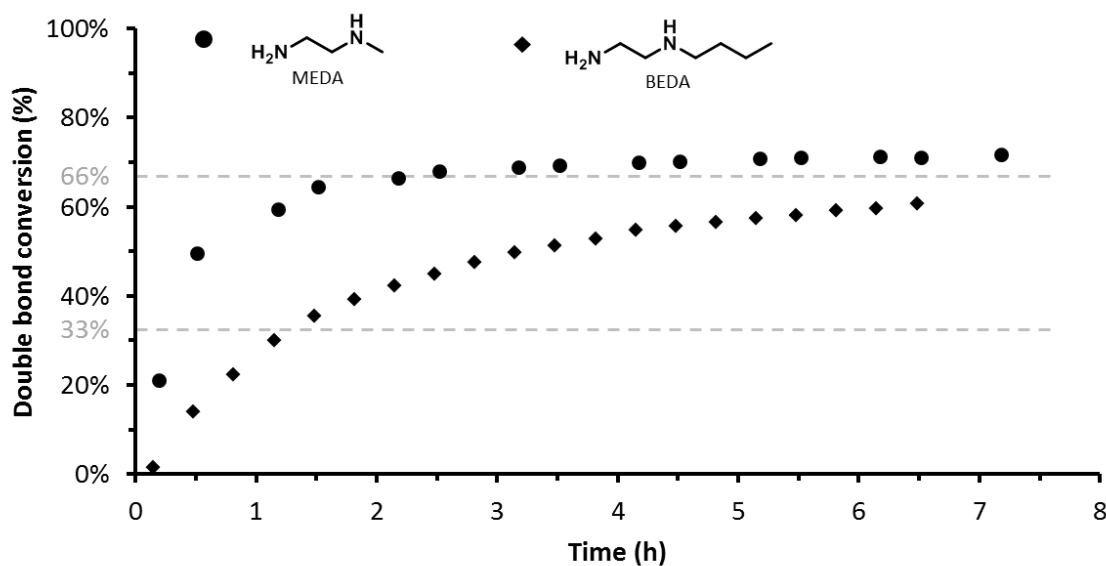


Figure 5.2 - MEDA and BEDA conversions by reaction with 2-OHa at 25 °C and followed by ^1H NMR.

The different pathways for the reaction between MEDA and 2-OHa were shown in Figure 5.3A. As previously stated, the corresponding chemicals are introduced in stoichiometric portions of reactive groups. Therefore, 2-OHa and MEDA or BEDA are mixed in a 3:1 molar ratio. The products are named according to the addition sequence. They are called “A”, “B” or “C” with NH (original), NH₂, or NH (formed), respectively. For example, if the first equivalent of 2-OHa is added on the NH₂ and the second on the NH (formed), the product is named “BC”. The final product obtained after three additions is independent of the sequence and named “3”. Figure 5.3B is zoomed between 32 and 68 ppm of stacked ¹³C at different times. The full ¹³C spectrum is presented in Figure S5.11, in SI. The CH and CH₃ are negatives, whereas the C and CH₂ are positives. Figure 5.3B assigned the carbons produced by the reaction between three equivalents of 2-OHa with MEDA. The environment of the ¹³C affects their chemical shifts. Therefore, each addition pathway has unique ¹³C signals. For example, the carbon in alpha position of the NH (original) (7 in Figure 5.3B), located at δ =54.0 ppm for the MEDA, shifts at δ =59.0 or δ =50.5 ppm for 7^A or 7^B, respectively. Furthermore, after two additions, the 7^{AB} carbon is located at δ =56.0 ppm and shifts upfield at δ =55.0 ppm for the final product (7³).

The signals associated with the A addition disappeared faster than the signals of the B additions. This result indicates the NH (original) faster reactivity compared to the NH₂, which is consistent with previous observations (Wu et al. 2004).

After 200 min of reaction, two equivalents of double bonds were consumed (Figure 5.2), and the chemical shifts associated with the first addition products (A or B) had entirely disappeared (Figure 5.3B). The only remaining signals corresponded to the AB or BA addition. Furthermore, no signal corresponding to the BC structure was identified. A first hypothesis is that the intermediate BC could be unstable and react fast to form the final product. However, the fast reaction of the BC intermediate is not consistent with results previously obtained (Wu et al. 2004). A more accurate hypothesis would be that the intermediate BC was never synthesized due to the slower reaction of NH (formed) compared to NH (original) and NH₂.

The reaction between 2-OHa and MEDA proceeds according to the following order of reaction: NH (original) < NH₂ << NH (formed). This confirmed previously published results with acrylate without OH groups (Wu et al. 2004). This result reinforced the hypothesis exposed by Caillol et al. of the inducted catalysis on the Michael reaction by OH groups (Ecochard et al. 2020).

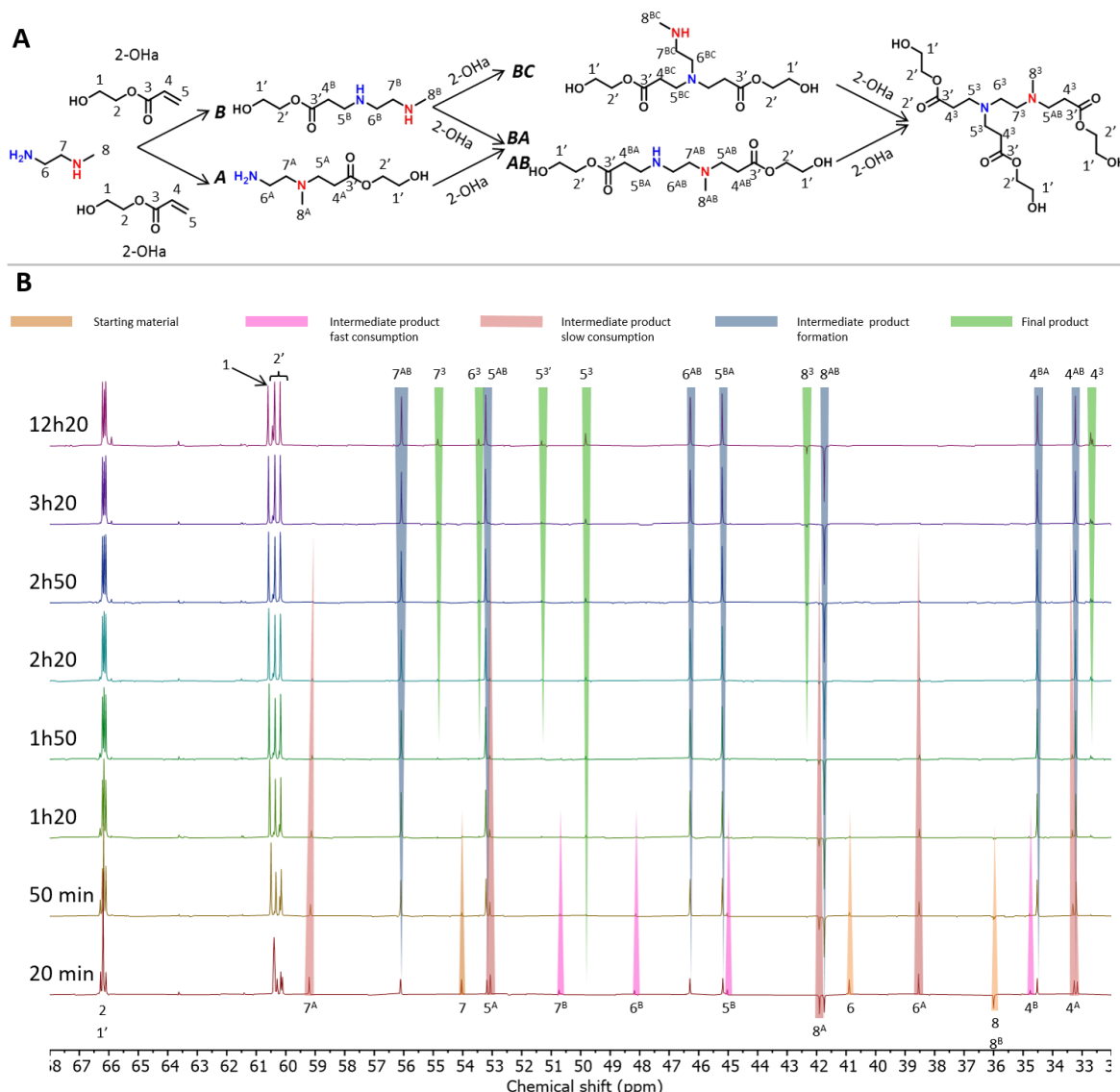
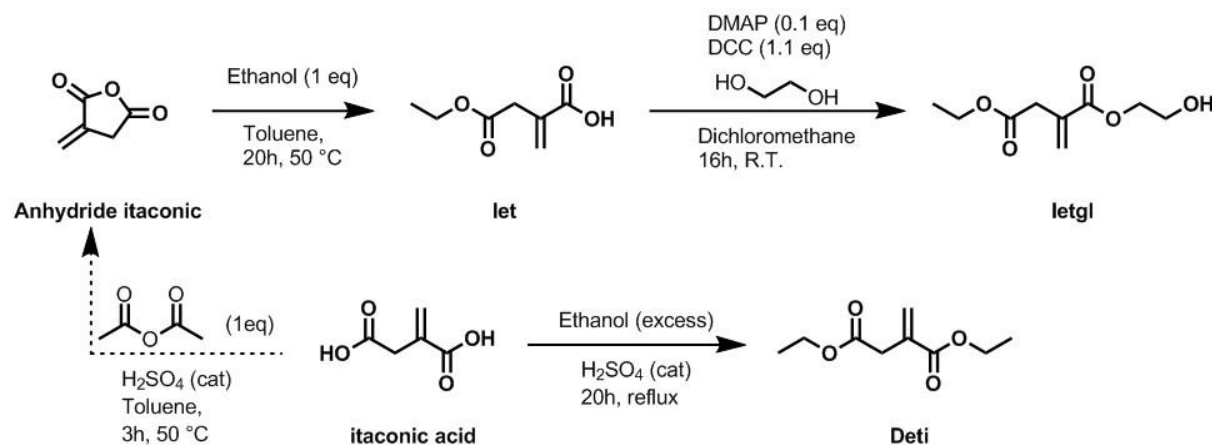


Figure 5.3 - (A) Reaktional mechanisms: potential pathways for the chemical reaction between 2-OHa and MEDA (B) Assigned stacked ^{13}C NMR spectra of the reaction at different times in the 32-68 ppm region.

The ^{13}C monitoring of the reaction between 2-OHa and BEDA was presented in Figure S5.12 in SI. On the contrary to the results presented in Figure 5.3, the numerous concomitant signals did not permit a full analysis of the spectra. However, a similar growth rate of 4^{A} and 4^{B} in Figure S5.12 in SI indicates a similar reactivity of NH (original) and NH₂ formed. This result differs from the 2-OHa-MEDA reaction, where 4^{B} signals disappeared faster than 4^{A} (Figure 5.3B) and could explain the slower reactivity of BEDA observed in Figure 5.2. As already observed in the literature, the steric hindrance of NH (original) decreases their reactivity (Wu et al. 2004). Therefore, in the BEDA addition, NH (original) is less reactive than in MEDA. The evolution of 2-OHa-BEDA reaction monitored by ^{13}C NMR (Figure S5.12 in SI) also confirmed that the BC intermediate was never formed.

The previous results corroborate the hypothesized catalytic activity of the OH-containing groups through the conservation of the reactivity order between NH (original), NH₂ and NH (formed). To develop a greener and biobased alternative to the acrylic acid, Ietgl and Deti derived from itaconic

acid were synthesized (Scheme 5.4) and tested as Michael acceptor. Their reactivities were investigated with OA by ^1H NMR and compared with 2-OHa.



Scheme 5.4 - Synthetic pathways from itaconic acid to Deti and Ietgl.

Iet was quantitatively obtained by esterification of anhydride itaconic with ethanol, in toluene. Although longer reaction times are required to obtain full conversions, toluene could be potentially substituted by a greener solvent, ethyl acetate (Pérocheau Arnaud et al. 2020). Nevertheless, Iet could also be obtained less efficiently in a greener way by mono-esterification of itaconic acid, catalyzed by enzyme (Ferraboschi et al. 1994). Iet was identified in ^1H NMR (Figure 5.4) by the apparition of the methylene (f) and the terminal methyl (g) protons of the ethyl ester at $\delta=4.05$ and 1.17 ppm, respectively. Furthermore, the methylene protons between the double bond and the carbonyl were shifted upfield from $\delta=3.66$ to 3.31 ppm compared to the anhydride itaconic. The methylene protons of the ethyl ester appeared in two distinct peaks at $\delta=4.05$ and 4.14 ppm. They are corresponding to the β -ethyl ester and the α -ethyl ester (Pérocheau Arnaud et al. 2020). The full spectrum presented in Figure S5.13 in SI, shows a ratio 9/1 between the two signals. Only the β -ethyl ester of Iet was represented in Figure 5.4 for clarity reasons.

Ietgl was synthesized by Steglich esterification of Iet with ethylene glycol catalyzed by DMAP and DCC (Scheme 5.4). This esterification process was used because the classical esterification conditions with acid and heat were slow and not selective, probably due to the double bond vicinal to the carboxylic acid group. Furthermore, Steglich esterification was carried out at room temperature using a minimum amount of energy according to the green chemistry principles (Anastas and Eghbali 2010; Tremblay- Parrado and Avérous 2020). The dichloromethane could be substituted by a greener acetonitrile (Lutjen et al. 2018; Prat et al. 2016). It was also demonstrated that supported base-catalyst, which could be recovered and reused, and solvent-free conditions are suitable for green Steglich reaction (Sakakura et al. 2007). The formation of Ietgl was confirmed by the appearance in the ^1H NMR (Figure 5.4) of the methylene proton of the glycol ester (i) and the OH group (j) at $\delta=3.35$ and 4.82 ppm, respectively. The methylene protons between the double bond and the carbonyl groups (c) were shifted downfield from $\delta=3.31$ to 3.60 ppm compared to Iet. Ietgl was synthesized to model the structure obtained by the ring-opening of epoxidized oil with Iet (Scheme 5.3B). The molecular structure of Ietgl was confirmed by full NMR analysis, presented in Figure S5.14 to Figure S5.19, in SI.

The Deti molecule was synthesized by esterification of the itaconic acid in refluxing ethanol and acidic conditions (Scheme 5.4) to investigate the difference of reactivities between close molecules, with and without OH groups. The successful synthesis of Deti was confirmed by ^1H NMR spectra presented in Figure 5.4. The methylene (h, f) and methyl end group (i, g) of the ethyl ester appeared at $\delta=4.23\text{-}4.08$ and $1.30\text{-}1.20$ ppm, respectively. As previously explained, the two signals slightly shifted were identified as the α -ester (h, i) and the β -ester (f, g). The molecular structure of Deti was confirmed by full NMR analysis presented in Figure S5.20 to Figure S5.25, in SI.

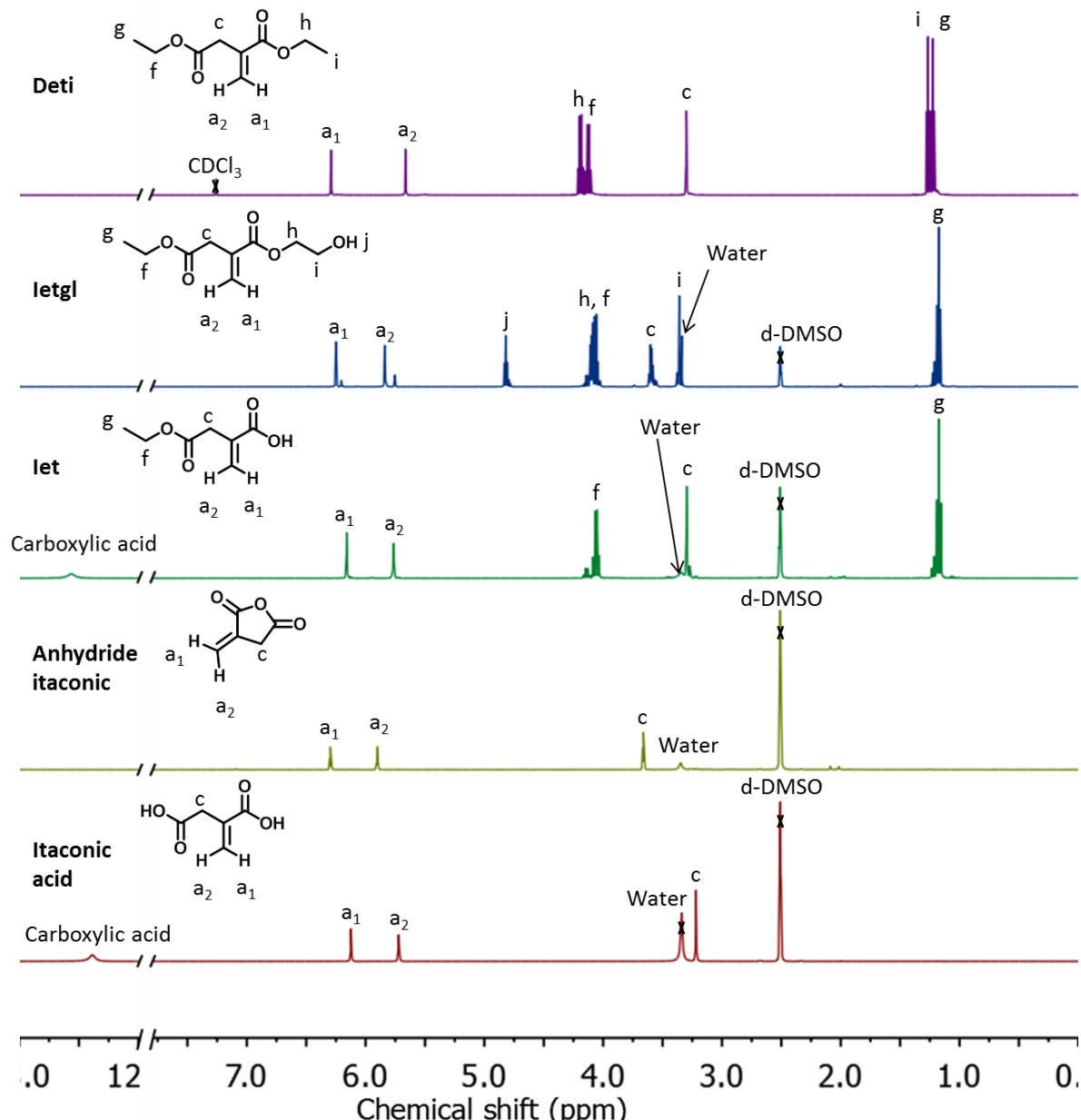


Figure 5.4 - ^1H NMR spectra of itaconic acid, anhydride itaconic, Iet, Ietgl and Deti. For clarity's sake, the x-axis was broken once (from 7.75 to 12 ppm) to show a potential carboxylic acid signal at around 12.5 ppm.

The reactivity of 2-OHa, Ietgl and Deti in Michael addition was measured by reaction with OA. The integrations of the double bonds in quantitative ^1H NMR spectra determined the conversions

shown in Figure 5.5. The reactivity of the 2-OHa was higher than the others, with 61% of conversion after 6.3 hours compared to 43 and 16% for Ietgl and Deti, respectively. The steric hindrance around the Ietgl and Deti double bond could explain their lower reactivities compared to 2-OHa. In this case, the activated double bond of 2-OHa is terminal and readily accessible. On the contrary, the double bonds of Ietgl and Deti are disubstituted and, consequently, less reactive than a terminal one.

After two hours, the conversion of 2-OHa by reaction with OA in diluted condition was 50%. In a previous study, the conversion after two hours of 2-OHa reaction with OA at ambient temperature in bulk was higher than 90% (Ecochard et al. 2020). The absence of agitation and addition of the solvent could explain the lower reaction yield obtained in this study compared to previous results obtained in better conditions. In similar conditions as the literature (Ecochard et al. 2020) (i.e., bulk reaction under stirring), the reaction between 2-OHa and OA has reached 82% of conversion after 2.5 hours, confirming the impact of the synthesis conditions on the conversion yield.

The structure of the Michael acceptor explains the higher reactivity of Ietgl than Deti, as shown in Figure 5.5. A previous study showed that hydrogen bonding solvents (i.e., water and alcohols) increase the reaction rate (De et al. 2009). Similarly, the OH group present in Ietgl induces catalysis of the aza-Michael addition due to the hydrogen-donation ability and the activation of the Michael acceptor by the OH.

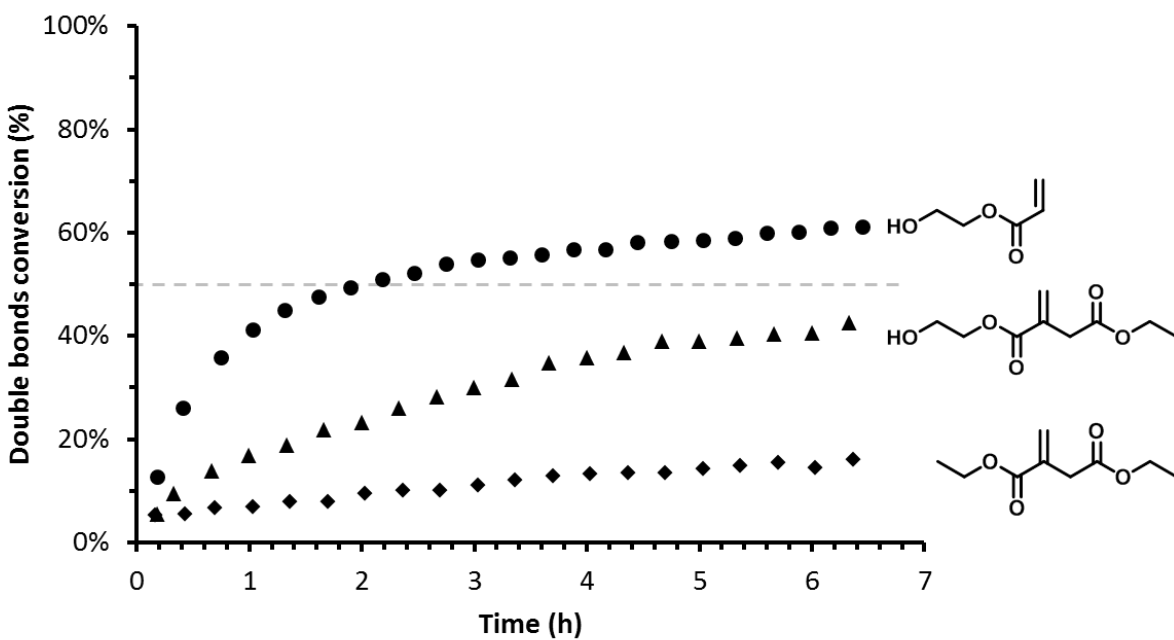


Figure 5.5 - Conversion of the double bond via the aza-Michael reaction between OA and 2OHa, Ietgl or Deti.

It was previously reported that the aza-Michael reaction between itaconic acid and primary amine was followed by an intra-molecular ring-closing reaction to form N-alkyl-pyrrolidone (Malferrari et al. 2015; Noordzij et al. 2019; Okada et al. 2009). The ring-closing reaction was previously conducted in bulk with methyl itaconate and was quantitative in 30 min at room temperature (Malferrari et al. 2015). In our case, the reactions were realized in diluted conditions, which should favor the intramolecular ring-closing reaction. Therefore, the reactions were also monitored by ¹³C to confirm the formation of aza-Michael reaction products with Ietgl and Deti. The

results presented in Figure S5.26 to Figure S5.28 in SI presented typical chemical shifts of aza-Michael addition. Furthermore, the typical signal of the pyrrolidone group identified by the CH group at $\delta=34$ ppm (Okada et al. 2009) was not observed in Figure S5.27 or Figure S5.28 in SI. The esterification of Deti and Ietgl with ethanol could prevent the cyclization reaction.

4.2. Gel formations with Michael acceptors from epoxidized oils

To confirm the results observed on the reactional models, various biobased Michael acceptors were synthesized and tested. ESO and EOO were ring-opened by acrylic acid to obtain ESOa and EOOa, respectively, to study the impact of the glyceride source and chemical structure on the polymerization reactivity. Furthermore, a fully biobased Michael acceptor was produced by ring-opening of ESO by Iet to obtain ESO_Iet to confirm the lower reactivity observed with this reactional model. The application of several green chemistry principles was achieved, most notably (i) atom economy, (ii) renewable feedstock use, and (iii) minimized use of solvents (Anastas and Eghbali 2010). The synthesized Michael acceptors were characterized by the epoxide conversion, the selectivity, the quantity of activated double-bonds, the functionality, the viscosity, and the thermal resistance. These different results are summarized in Table 5.1.

The epoxide conversion shown in Table 5.1 was higher than 90%, and the selectivity was between 70 and 76% for the three systems. The difference in fatty acids compositions between ESO and EOO can explain the gap of conversion. EOO is primarily composed of epoxidized oleic acid, which contains a single epoxide group. On the contrary, the ESO has a higher density of epoxide with epoxidized linoleic and linolenic acid bearing 2 and 3 epoxide groups, respectively. The reaction of one or two epoxides on the same fatty acid decreases the accessibility of the last epoxide group. Therefore, fewer epoxide groups are ring-opened on ESO due to the steric hindrance.

The selectivity, presented in Table 5.1, was around 75%. It was lower than the conversion due to the side reactions inherent to the ring-opening reaction, such as epoxide homopolymerization, observed in acidic conditions (Lligadas et al. 2006a; Miao et al. 2008; Peyrton et al. 2020). SEC results are shown in Figure S5.29 and Figure S5.30 in SI. Contrary to ESO and EOO where a single peak is observed, ESO_Iet, ESOa and EOOa present a distribution of molar masses. The high molar masses confirmed the epoxide polymerization during the synthesis of the three Michael acceptors.

The activated double bond quantities were determined by quantitative ^1H NMR using pentafluorobenzoic acid as an internal standard. They ranged from 1.4 to 2.3 mmol of activated double bonds/g. Despite similar conversion, ESO_Iet presented a lower quantity of activated double bonds than ESOa. This is explained by the molar mass difference between ESO_Iet and ESOa. Iet has a higher molar mass than the acrylic acid and the ring-opening yields were similar. Therefore, the ring-opening reaction of ESO led to a higher molar mass of ESO_Iet than ESOa, as also indicated by SEC results, presented in Figure S5.29. Consequently, the quantity of activated double bonds per gram of Michael acceptor decreased.

Table 5.1 - Properties of Michael acceptors synthesized from epoxidized oils.

	Units	ESOa	EOOa	ESO_Iet
Plant oil		Soybean	Olive	Soybean
Ring-opening nucleophile		Acrylic acid	Acrylic acid	Iet
Conversion	%	90 ± 2	97 ± 2	90 ± 2
Selectivity	%	74 ± 2	70 ± 2	76 ± 2
Activated double bond quantity	mmol/g	2.3 ± 0.1	1.4 ± 0.1	1.9 ± 0.1
Functionality	Double-bond	4.8 ± 0.2	3.3 ± 0.3	5.0 ± 0.3
Viscosity 25 °C (Pa.s)		103 ± 1	3.3 ± 0.1	98 ± 1
T _{deg max}	°C	395	384	388

The functionality determination method was adapted from previously published works on PUs (Peyrton et al. 2020) to aza-Michael addition. The rheometer results (Figure S5.31 to Figure S5.33 in SI) and the corresponding method were detailed in SI. ESOa, EOOa and ESO_Iet has an average number of activated double bond per molecules of 4.8, 3.3 and 5.0, respectively (Table 5.1). Although starting from the same oil, ESO_Iet had a slightly higher functionality than the ESOa. This modest difference could be explained by the higher selectivity of the ring-opening of ESO with Iet.

The viscosity of ESOa was 40 times higher than EOOa (Table 5.1). It can be explained by the difference in crystallization and melting point linked to the fatty acid distribution and the H-bonding differences (Gunstone et al. 2007). The results of the DSC experiments realized on the modified oils, shown in Figure S5.34 in SI, confirmed the difference in fusion behavior. Although the crystallization temperatures were similar (around -25 °C), the fusion temperature of OOEa (-34 °C) was lower than ESOa (-25 °C). Surprisingly, ESOa and ESO_Iet had similar crystallization and fusion temperatures. Therefore, the ring-opening nucleophiles (i.e., acrylic acid or Iet) did not affect the viscosity and the crystallization behavior.

The thermal stability of the biobased Michael acceptors was investigated through TGA experiments at 10 °C/min under inert atmosphere (N₂). The TGA and DTG profiles were presented in Figure S5.35 in SI. Michael acceptors presented a unique degradation peak in DTG, expressed in Table 5.1 as T_{deg max}. The T_{deg max} similar for the three triglycerides derivatives was around 390 °C. It indicates a similar degradation of the three Michael donors, confirmed by the similar weight loss profiles presented in Figure S5.35 in SI. Two consecutive phenomena could explain the thermal degradation behavior. At the beginning of the degradation, the ester bond scissions fragment the Michael donor in lighter molecules. The resulting fatty acids were then evaporated or decomposed by the temperature increase.

4.3. Gelation behavior of thermosets via Michael addition

The reactional model study demonstrated the higher reactivity of the acrylic acid derivatives compared to the itaconic acid ones, in diluted conditions. The monitoring of gel formation provides new insights into the polyaddition reactivity in bulk of the three Michael acceptors derived from epoxidized oil. The gel time was determined by the crossover between the storage modulus (G') and the loss modulus (G'') or expressed otherwise tan Δ = 1, in DMA (ASTM D4473-03 2003; Paramarta and Webster 2017; Tung and Dynes 1982). However, G' and G'' depends upon the frequency of

solicitation. Therefore, the most accurate interpretation of the gel point was described as the instant where $\tan \Delta$ is independent of solicitation frequency (Chambon and Winter 1987; Pascault et al. 2002; Winter and Chambon 1986). It can be expressed as the crossover of $\tan \Delta$ measured at different frequencies.

In this study, the determination of the gel time was conducted by a multi-wave oscillation. The results obtained with the polyaddition of EOOa and DMEDA (EOOa_DMEDA) at 0 °C are presented in Figure 5.6 with the representation of $\tan \Delta$, G' and G'' at different frequencies. The intersection of G' and G'' varied from 30 000 to 35 000 seconds with the frequency variation from 0.5 to 5 Hz. These results illustrate the strong limitation of this method for gel time determination. In contrast, the measurement by the $\tan \Delta$ crossover at different frequencies reaches a single value (22 500 seconds).

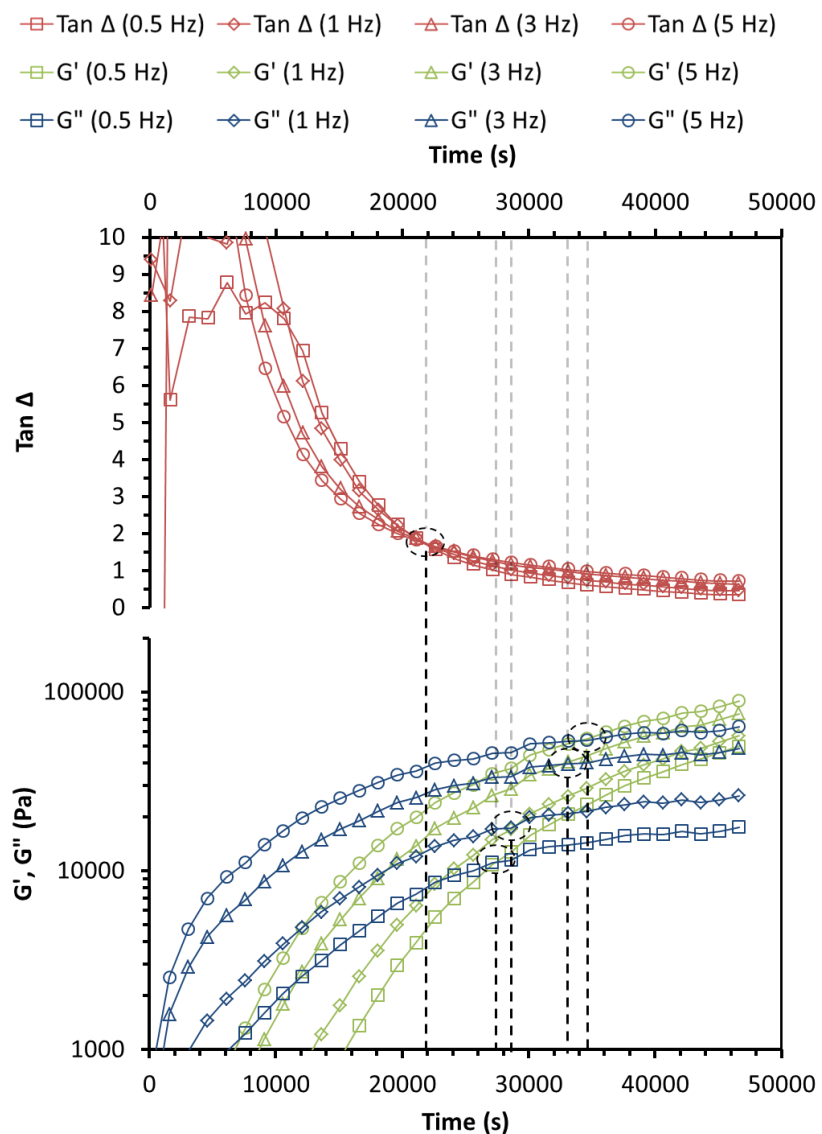


Figure 5.6 - $\tan \Delta$, G' and G'' at 0.5, 1, 3 and 5 Hz resulting from the multi-waves method applied on EOOa and DMEDA polyaddition. Presentation of the different gel points.

Gel time is a key parameter on the gelation of a polymer network. In PU formulation with catalysts, the gel time is between 5 to 165 seconds at ambient temperature with oil-based polyols

(Fridrihsone-Girone et al. 2016). Without a catalyst, the ESOa_DMEDA gelled under 300 seconds at 25 °C. This result is close to the values obtained on PU networks. However, the crossover of $\tan \Delta$ was not clear, and the standard deviation was considerable. The slow data acquisition combined with the sample preparation (15-45 seconds) prevents accurate gel time measurements under 500 seconds by the method previously described. Therefore, the gel times of aza-Michael polyadditions were measured at 0 °C to increase the time analysis and accumulate comprehensive data.

Figure 5.7 presents the average values of the gel times at 0 °C for the polymerization of ESOa, EOOa and ESO_Iet with DMEDA. Examples of gel time measurements are presented in Figure S5.37 in SI. The average gel time of ESOa_DMEDA, EOOa_DMEDA and ESO_Iet_DMEDA were 1938, 22 425 and 165 000 seconds, respectively. According to the Flory-Stockmayer theory (Flory 1941; Stockmayer 1944), the higher the functionality of the monomers, the lower the conversion at the gel point, and consequently, the lower the gel time will be. This theory could explain the higher gel time of ESOa_DMEDA ($f=4.8$) compared to EOOa_DMEDA ($f=3.3$). Although similar functionality, the gel time of ESO_Iet_DMEDA was two orders of magnitude longer than ESOa_DMEDA. As already explained for the reactional model, the steric hindrance of the itaconic acid derivative decreases the accessibility and the global reactivity.

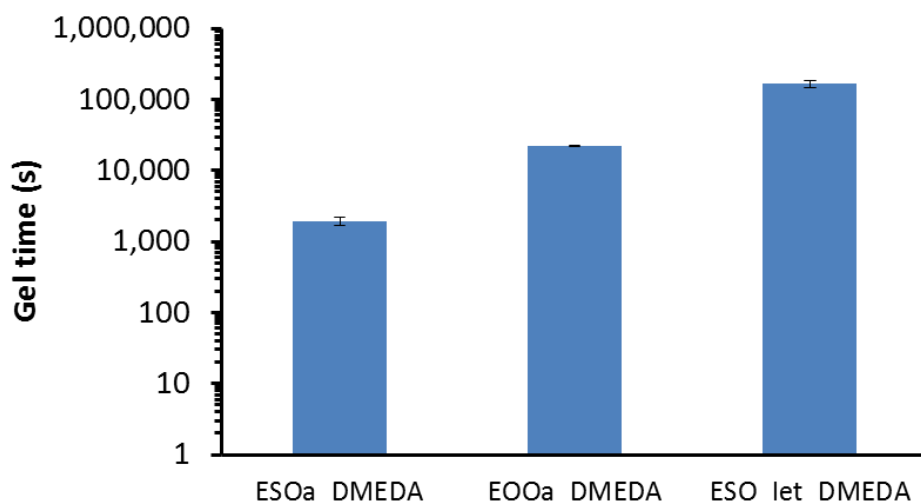


Figure 5.7 - Gel times of aza-Michael thermosets. From left to right: ESOa_DMEDA, EOOa_DMEDA and ESO_Iet_DMEDA.

The ESOa demonstrated the fastest reactivity with DMEDA compared to EOOa and ESO_Iet. Several catalysts were tested with ESOa_DMEDA system to decrease the gel time and match with e.g., PU performances. The catalyst activity of the OH group on the aza-Michael addition was proved in the study of the reactional model. However, the aza-Michael addition is known to be catalyzed by organic bases (Clemens and Del Rector 1989) (i.e. TMG, DBU, DBN), protic solvents (i.e. water, ethanol) (Ranu and Banerjee 2007), Lewis (Pérez and Pleixats 1995; Wabnitz and Spencer 2003) (i.e. AlCl_3) or Brønsted (Vedejs and Gingras 1994; Wabnitz and Spencer 2003) (i.e. PTSa) acids. The catalyst loading was set at 10 mol%. The gel time, an indicator of the reaction rate, was determined according to the previously described method.

The gel times presented in Figure 5.8A were 2760, 2570 and 2140 seconds with TMG, DBU and DBN as a catalyst, respectively. These results were higher than without catalyst (1940 seconds).

Therefore, the organic bases did not catalyze the reaction. In our case, the DMEDA is exceptionally reactive due to its nucleophile and base character. The activation of DMEDA by complexation with TMG, DBU or DBN could increase the steric hindrance around the amine and decrease the reactivity.

The gel times with ethanol (1260 seconds) and water (1730 seconds) as catalyst were lower than without catalyst (Figure 5.8A). In organic synthesis, the Michael addition is well known to be catalyzed by water. The water increases the Michael donor nucleophilicity by hydrogen bonding with the electron-withdrawing group of the Michael acceptor. The capacity of the water molecule to bond with the amine group via the oxygen atom was also hypothesized as a cause of the acceleration of the reaction (Rulev 2011). Furthermore, catalytic activities were also observed with a solvent containing OH groups such as polyethylene glycol or glycerol. These two phenomena explained the lower gel time measured with ethanol or water as a catalyst. A similar mechanism occurs with OH-containing compounds. The lower gel time of the ESOa_DMEDA with AlCl_3 (1520 seconds) and PTSa (1680 seconds) confirmed the catalytic activity of Lewis and Brønsted acids, respectively (Figure 5.8A). They activate Michael acceptor by coordination with the electron-withdrawing group (i.e., the ester). The most efficient catalyst to accelerate the polyaddition of ESOa_DMEDA was the ethanol, with almost half the gelation time.

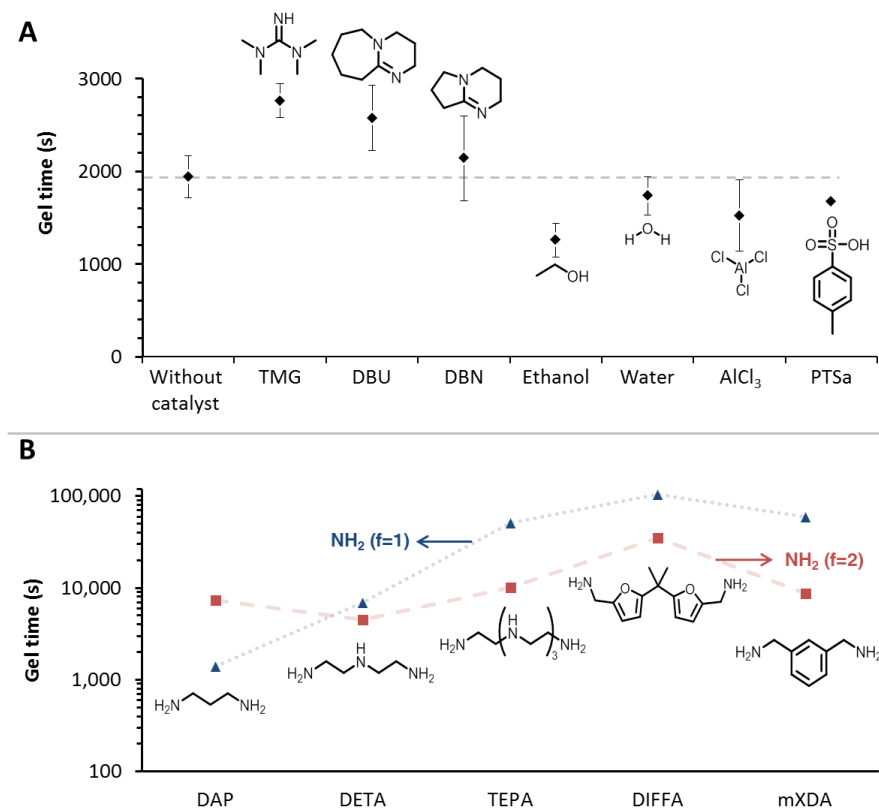


Figure 5.8 - (A) Gel times of ESOa with DMEDA with 0.1 mol% of different catalysts. (B) Gel times linked to the reaction between ESOa and DAP, DETA, TEPA, DIFFA and mXDA, with the NH_2 considered as monofunctional and difunctional.

The reactional model study confirmed the slow reactivity of the NH (formed) compared to NH (original) and NH_2 . In order to further understand the role of the amine structure on the reactivity of the system, different amines were tested in various quantities. For each tested amine which contained NH_2 groups, two materials were synthesized to investigate the stoichiometry effect. In the first series,

the NH_2 group was considered monofunctional ($f=1$), whereas it was difunctional ($f=2$) in the second series. The equimolar ratio of Michael donors and acceptors was always set. For example, the DAP contains two NH_2 that are counted as monofunctional (DAP2) or difunctional (DAP4) for the quantity calculation. The gel times of the polymerizations of ESOa and DAP, DETA, TEPA, DIFFA or mXDA were determined using the previously described procedure.

The different amine used could potentially be biobased or have a biobased equivalent. The DAP could be replaced by the diaminobutane produced from glucose by an engineered strain of *E. coli* (Froidevaux et al. 2016). The DETA and TEPA are synthesized from the addition of ammonia and an ethylene derivative. Biobased ethylene is now produced in large quantities, e.g., in Brazil, by catalytic dehydration of bioethanol (Morschbäcker 2009). The biobased aromatic DIFFA could substitute the fossil-based mXDA, also studied. The DIFFA was synthesized from the dimerization of biobased furfurylamine with acetone. The full analysis of the ^1H NMR spectra is presented in Figure S5.36 in SI.

The gel times of the two different series with the five amines were presented in Figure 5.8B. The gel times were lower when the NH_2 was considered difunctional, except for DAP. Therefore, the polyadditions were faster to gel at the exact stoichiometry. The correlation between the functionality and the gel time, explained previously, is conditioned by equivalent reactivities of all the reactive groups. However, it was demonstrated in the model study that the gap in reactivity between NH (formed) and NH_2 is substantial. The gel times of ESO_DAP were 1 400 and 7 400 seconds for the NH_2 considered mono- and difunctional, respectively. This exemplifies the slower reactivity of NH (formed) compared to NH_2 . This phenomenon is only shown with DAP due to the higher mobility of the DAP molecule compared to the other tested amines.

Surprisingly, the gel times of TEPA were higher than DETA despite a higher functionality and higher content of highly reactive NH (original). As demonstrated in the reactional study with MEDA and BEDA, the reactivity of the amine group depends on their electronic and steric environment (Mather et al. 2006). The first acrylate addition could enhance the steric hindrance around the other amines of the Michael donor. The gel time of the aromatic DIFFA and mXDA were similar. Despite identical functionality, the gel times of DIFFA and mXDA were two orders of magnitude higher than the aliphatic DAP. The proximity of the aromatic ring decreases the availability of the doublet and the basicity (Froidevaux et al. 2016). Therefore, the reactivity of the amine decreases. The polyaddition between DAP with NH_2 considered as monofunctional, and ESOa has the lowest gel time.

All the materials tested were fully cured at 50 °C and analyzed by DSC and TGA to determine their thermal properties and then compared to PU systems in an approach of substitution. The T_g of the aza-Michael thermosets was measured on the second heating ramp at 10°C/min in DSC experiments and presented in Figure 5.9. The materials realized by considering NH_2 monofunctional have higher or similar T_g than the related materials with NH_2 difunctional. Previous results demonstrated that 1.5:1 ratio of NH_2 :acrylate was the optimal ratio (Paramarta and Webster 2017). In another study, the T_g was constant, with ratios ranging from 1:1 to 2:1 NH_2 :acrylate (Ecochard et al. 2020).

The T_g of ESOa_DAP, ESOa_DETA, ESOa_TEPA in the NH_2 monofunctional series was 3, 7.5 and 19 °C, respectively. In these materials, the T_g evolution is correlated with the amine functionality and, consequently, the crosslink density. Despite similar functionality, the T_g of ESOa_DIFFA and ESOa_mXDA was higher than ESOa_DAP. It is well-known that the aromaticity increases the stiffness of the network and the T_g .

The T_g of ESOa_DMEDA, EOOa_DMEDA and ESO_Iet_DMEDA were -12.9, -25.5 and -13.3 °C, respectively. The two materials derived from ESO had higher T_g (- 13 °C) compared to OOEa_DMEDA (-25 °C). This difference can be explained by the functionality variation between Michael acceptors synthesized from ESO and EOO. As previously explained, functionality, crosslink density and T_g are correlated. Furthermore, the OOEa had more flexible dangling ends that increased chain mobility when integrated into a polymer network. Otherwise, the functionalization of ESO by the biobased Iet or acrylic acid did not affect the T_g .

The higher T_g was obtained with the aromatic amines (i.e., DIFFA and mXDA) or the highest functionality (i.e., TEPA). Similarly to PUs, the T_g of aza-Michael materials could be tuned by variation of the monomer type and ratio. However, the particular macromolecular architecture of PUs induced phase separation between hard and soft domains. Generally, the soft segments have a T_g below room temperature and the hard segments above room temperature (Szycer 2013). The T_g of PUs made with oil-based polyols and aromatic isocyanates were reported between -20 and 20 °C (Gaikwad et al. 2015; Hablot et al. 2008; Stirna et al. 2012), which is relatively close to the results presented in Figure 5.9. Although different in macromolecular architecture, the thermal properties of aza-Michael network are comparable to PUs.

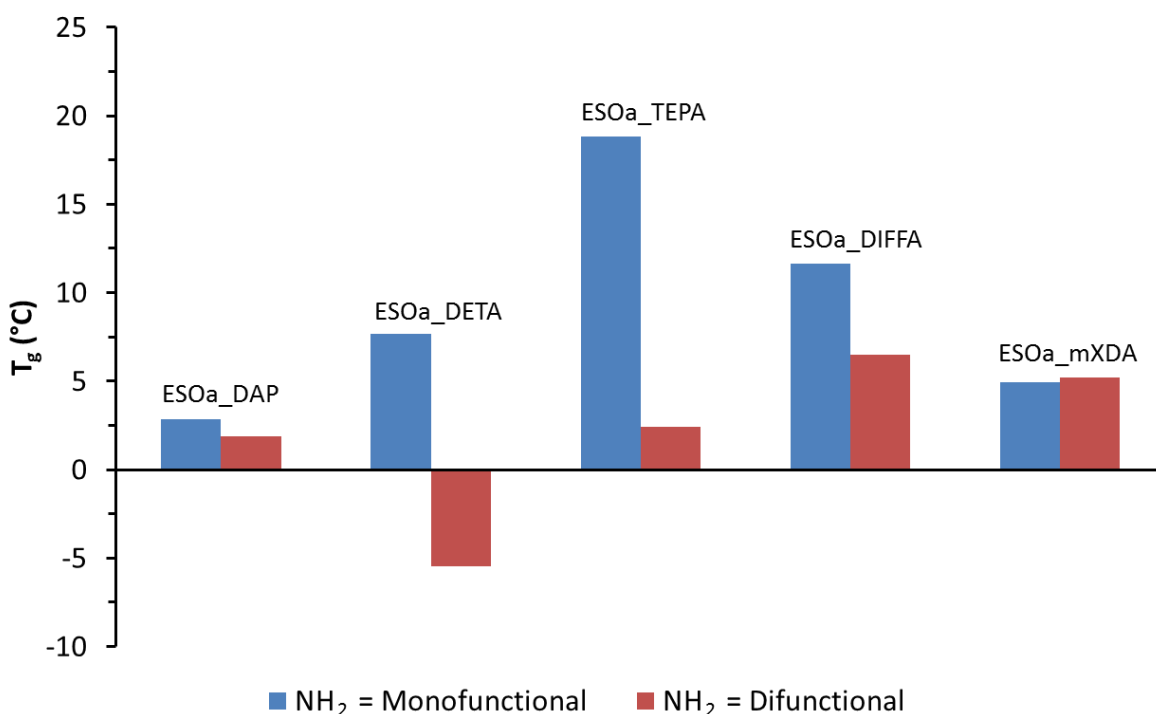


Figure 5.9 - T_g determined by DSC of the thermosets obtained by Michael addition of ESOa with different amines structures and stoichiometries.

The thermal stability determined by TGA under inert atmosphere (N_2) of the aza-Michael thermosets was measured on fully cured samples. The TGA and DTG profiles of ESOa_DMEDA, EOOa_DMEDA and ESO_Iet_DMEDA are shown in Figure 5.10A. The main degradation temperatures determined at the highest peak of DTG are presented in Table S5.2 and Table S5.3 in SI. ESOa_DMEDA, EOOa_DMEDA and ESO_Iet_DMEDA demonstrate two main degradations steps (Table S5.2). The first step, around 210 °C, was identified as the dissociation of the amine-carbon

bond (Pellis et al. 2019). Around 390 °C, a second degradation step, similar to the degradation of Michael acceptors presented in Figure S5.35, was associated with the ester scission (Ecochard et al. 2020).

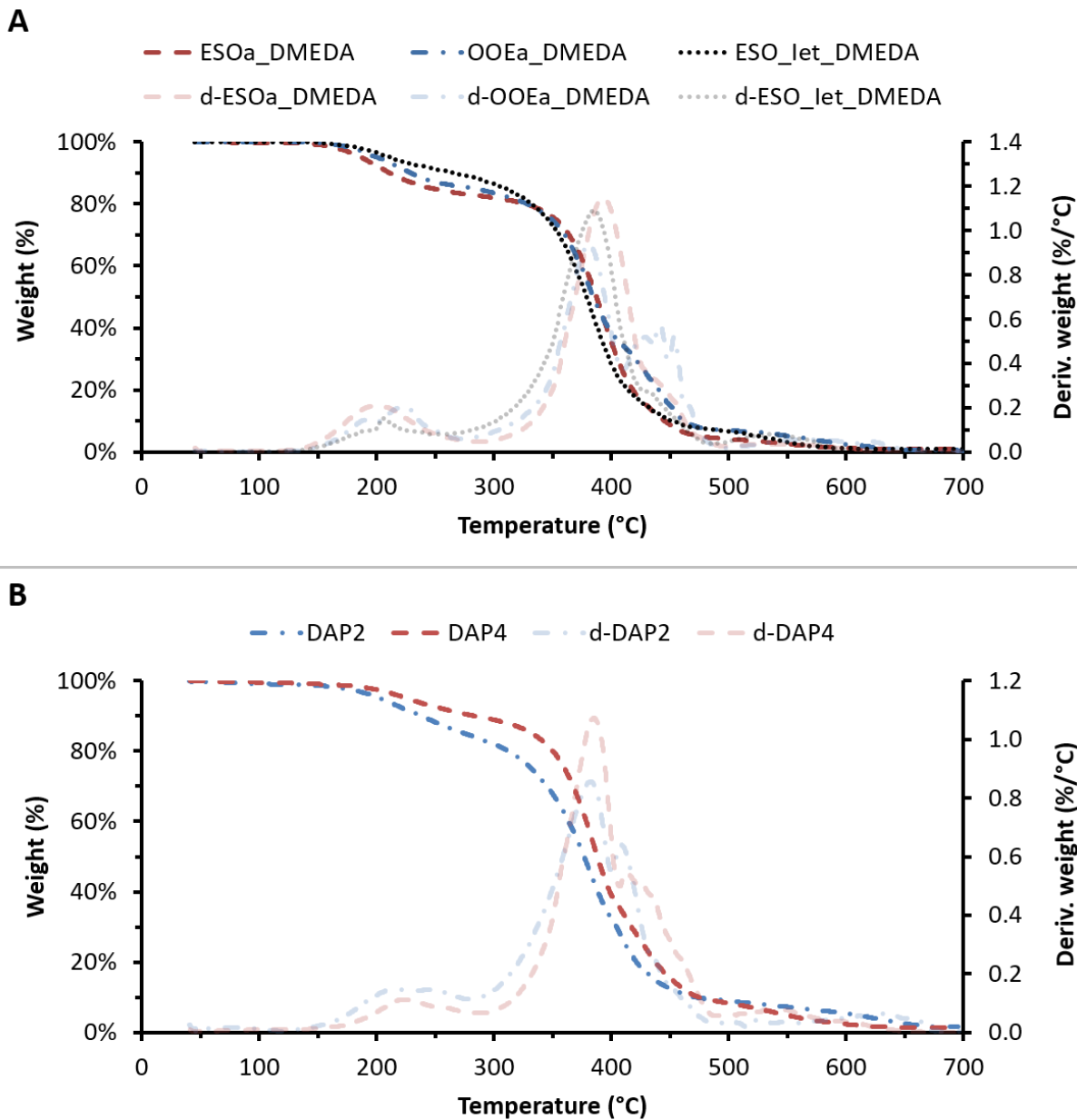


Figure 5.10 - TGA and DTG results of (A) ESOa_DMEDA, EOOa_DMEDA and ESO_Iet_DMEDA and (B) DAP2 and DAP4.

The thermal stability of the materials realized with NH₂ difunctional was higher compared to the series NH₂ monofunctional (Table S5.3). As an example, the thermal degradation of ESOa_DAP2 and ESOa_DAP4 are presented in Figure 5.10B. The first thermal degradation around 200 °C was more prominent in ESOa_DAP2 than ESOa_DAP4. As the NH₂ was considered monofunctional in ESOa_DAP2, the DAP quantity to attained the stoichiometry was double compared to ESOa_DAP4. This increased quantity of DAP for ESOa_DAP2 explained the higher degradation around 200 °C. The ESOa_DAP4 was more thermally stable than ESOa_DAP2 above 400 °C. The higher crosslink density of ESOa_DAP4 than ESOa_DAP2 can explain the higher thermal stability. Furthermore, secondary

amines could be more thermally sensible than the tertiary amine. This would also explain the higher thermal stability of ESOa_DAP4.

Similarly to the oil-based Michael acceptors, the primary degradation of the aza-Michael thermosets was around 380 °C (Figure S5.35). Despite different macromolecular architecture, the degradation mechanism in two steps of the aza-Michael materials is similar to PUs. The thermal degradation of PU thermosets starts between 150 and 250 °C with the urethane bond decomposition (Furtwengler et al. 2018b; Laurichesse et al. 2014; Yang et al. 2012). The second step attributed to the soft segment degradation occurs around 400 °C (Laurichesse et al. 2014; Omrani et al. 2016; Yang et al. 2012). The biobased aza-Michael materials demonstrate thermal stability equal to the Pus and suitable for thermoset applications such as coating or foams.

5. CONCLUSION

Combining different issues, PUs thermosets do not fit the major expectations for a greener and more sustainable future, following the main principles for a green chemistry. However, their specific molecular architectures and efficient processing make the PUs essential to daily life with a large range of applications. In the frame of green and safer chemistry, the aza-Michael reaction was investigated as a potential substitute to PU in thermosets applications. In this frame, the reactivity of the aza-Michael reaction was studied with a particular emphasis on Michael acceptors derived from biobased lipid resources.

The in-depth NMR investigation on the reactional model systems demonstrates the catalysis activity of OH-based compounds on the aza-Michael reaction. Furthermore, the order of reactivity is preserved compared to equivalent systems without OH groups. NH (formed) remains less reactive than NH (original) and NH₂. The steric hindrance of the biobased molecules synthesized from itaconic acid was proved to decrease the reactivity of the Michael acceptor compared to the acrylic acid derivative.

The gel times of the studied aza-Michael polyadditions were accurately measured by a multi-waves experiment method. The reactions between ESOa and aliphatic amines were proved to be extremely fast to reach the gel point, which is suitable for formulation such as reactive foams, as in the case of PU. However, the amino-ester bonds composing the macromolecular architecture of the aza-Michael materials should form less hydrogen bonding. Therefore, the mechanical properties should be affected. This point needs to be further investigated.

The thermal properties measurement of the aza-Michael materials prepared with amine variation presented unique T_g ranging from -5 to 20 °C. No phase separation was observed in the aza-Michael materials due to their lack of hydrogen bonding compared to PUs. Despite differences in macromolecular architecture, aza-Michael-based and PUs material presented similar thermal properties and stabilities.

To further increase the reactivity, the preparation of biobased Michael acceptors could be applied to systems with higher functionality, such as e.g., polyunsaturated microalgal oils. Future experiments should also focus on the exothermic character of the aza-Michael addition to evaluate its potential as e.g., a substitute for the PU foams and the corresponding uses. Foams elaboration process with aza-Michael polyaddition could then be investigated with a surfactant and a blowing agent.

6. REFERENCES

Agrawal, A., Kaur, R., Walia, R.S., 2017. PU foam derived from renewable sources: Perspective on properties enhancement: An overview. *Eur. Polym. J.* **95**, 255–274. <https://doi.org/10.1016/j.eurpolymj.2017.08.022>

Anastas, P., Eghbali, N., 2010. Green Chemistry: Principles and Practice. *Chem Soc Rev* **39**, 301–312. <https://doi.org/10.1039/B918763B>

Arbennz, A., Perrin, R., Avérous, L., 2017. Elaboration and Properties of Innovative Biobased PUFR Foams from Microalgae. *J. Polym. Environ.* **26**, 254–262. <https://doi.org/10.1007/s10924-017-0948-y>

ASTM D4473-03, 2003. Standard Test Method for Plastics: Dynamic Mechanical Properties: Cure Behavior. ASTM International, West Conshohocken, PA. <https://doi.org/10.1520/D4473-03>

Bergmann, E.D., Ginsburg, D., Pappo, R., 2004. The Michael Reaction. *Org. React.* **10**, 179–556.

Blattmann, H., Lauth, M., Mülhaupt, R., 2016. Flexible and Bio-Based Nonisocyanate Polyurethane (NIPU) Foams. *Macromol. Mater. Eng.* **301**, 944–952. <https://doi.org/10.1002/mame.201600141>

Bozell, J.J., Petersen, G.R., 2010. Technology development for the production of biobased products from biorefinery carbohydrates—the US Department of Energy’s “Top 10” revisited. *Green Chem.* **12**, 539. <https://doi.org/10.1039/b922014c>

Brugsch, H.G., Elkins, H.B., 1963. Toluene Di-Isocyanate (TDI) Toxicity. *N. Engl. J. Med.* **268**, 353–357. <https://doi.org/10.1056/NEJM196302142680705>

Carré, C., Ecochard, Y., Caillol, S., Avérous, L., 2019. From the Synthesis of Biobased Cyclic Carbonate to Polyhydroxyurethanes: A Promising Route towards Renewable Non-Isocyanate Polyurethanes. *ChemSusChem* **12**, 3410–3430. <https://doi.org/10.1002/cssc.201900737>

Chambon, F., Winter, H.H., 1987. Linear Viscoelasticity at the Gel Point of a Crosslinking PDMS with Imbalanced Stoichiometry. *J. Rheol.* **31**, 683–697. <https://doi.org/10.1122/1.549955>

Chu, H.S., Ahn, J.-H., Yun, J., Choi, I.S., Nam, T.-W., Cho, K.M., 2015. Direct fermentation route for the production of acrylic acid. *Metab. Eng.* **32**, 23–29. <https://doi.org/10.1016/j.ymben.2015.08.005>

Clemens, R.J., Del Rector, F., 1989. A comparison of catalysts for crosslinking acetoacetylated resins via the Michael reaction. *J. Coat. Technol.* **61**, 83–91.

Cornille, A., Guillet, C., Benyahya, S., Negrell, C., Boutevin, B., Caillol, S., 2016. Room temperature flexible isocyanate-free polyurethane foams. *Eur. Polym. J.* **84**, 873–888. <https://doi.org/10.1016/j.eurpolymj.2016.05.032>

De, K., Legros, J., Crousse, B., Bonnet-Delpon, D., 2009. Solvent-Promoted and -Controlled Aza-Michael Reaction with Aromatic Amines. *J. Org. Chem.* **74**, 6260–6265. <https://doi.org/10.1021/jo9012699>

Ecochard, Y., Auvergne, R., Boutevin, B., Caillol, S., 2020. Linseed Oil-Based Thermosets by Aza-Michael Polymerization. *Eur. J. Lipid Sci. Technol.* **122**, 1900145. <https://doi.org/10.1002/ejlt.201900145>

Ferraboschi, P., Casati, S., Grisenti, P., Santaniello, E., 1994. Selective enzymatic transformations of itaconic acid derivatives: An access to potentially useful building blocks. *Tetrahedron* **50**, 3251–3258. [https://doi.org/10.1016/S0040-4020\(01\)81120-0](https://doi.org/10.1016/S0040-4020(01)81120-0)

Flory, P.J., 1941. Molecular Size Distribution in Three Dimensional Polymers. I. Gelation. *J. Am. Chem. Soc.* **63**, 3083–3090. <https://doi.org/10.1021/ja01856a061>

Fridrihsone-Girone, A., Stirna, U., Misāne, M., Lazdiņa, B., Deme, L., 2016. Spray-applied 100% volatile organic compounds free two component polyurethane coatings based on rapeseed oil polyols. *Prog. Org. Coat.* **94**, 90–97. <https://doi.org/10.1016/j.porgcoat.2015.11.022>

Froidevaux, V., Negrell, C., Caillol, S., Pascault, J.-P., Boutevin, B., 2016. Biobased Amines: From Synthesis to Polymers; Present and Future. *Chem. Rev.* **116**, 14181–14224. <https://doi.org/10.1021/acs.chemrev.6b00486>

Furtwengler, P., Avérous, L., 2018. Renewable polyols for advanced polyurethane foams from diverse biomass resources. *Polym. Chem.* **9**, 4258–4287. <https://doi.org/10.1039/C8PY00827B>

Furtwengler, P., Matadi Boumbimba, R., Sarbu, A., Avérous, L., 2018b. Novel Rigid Polyisocyanurate Foams from Synthesized Biobased Polyester Polyol with Enhanced Properties. *ACS Sustain. Chem. Eng.* **6**, 6577–6589. <https://doi.org/10.1021/acssuschemeng.8b00380>

Gaikwad, M.S., Gite, V.V., Mahulikar, P.P., Hundiwale, D.G., Yemul, O.S., 2015. Eco-friendly polyurethane coatings from cottonseed and karanja oil. *Prog. Org. Coat.* **86**, 164–172. <https://doi.org/10.1016/j.porgcoat.2015.05.014>

Gunstone, F.D., Harwood, J.L., Harwood, J.L., 2007. The Lipid Handbook with CD-ROM, 3rd ed. CRC Press. <https://doi.org/10.1201/9781420009675>

Hablot, E., Zheng, D., Bouquey, M., Avérous, L., 2008. Polyurethanes Based on Castor Oil: Kinetics, Chemical, Mechanical and Thermal Properties. *Macromol. Mater. Eng.* **293**, 922–929. <https://doi.org/10.1002/mame.200800185>

Hayati, A.N., Evans, D.A.C., Laycock, B., Martin, D.J., Annamalai, P.K., 2018. A simple methodology for improving the performance and sustainability of rigid polyurethane foam by incorporating industrial lignin. *Ind. Crops Prod.* **117**, 149–158. <https://doi.org/10.1016/j.indcrop.2018.03.006>

Hicks, D., Austin, A., 2017. A review of the global PU industry 2016 and outlook for 2017. *PU Mag.* **14**, 4–16.

Holfinger, M.S., Conner, A.H., Holm, D.R., Hill, C.G., 1995. Synthesis of Difurfuryl Diamines by the Acidic Condensation of Furfurylamine with Aldehydes and Their Mechanism of Formation. *J. Org. Chem.* **60**, 1595–1598. <https://doi.org/10.1021/jo00111a017>

Janvier, M., Hollande, L., Jaufurally, A.S., Pernes, M., Ménard, R., Grimaldi, M., Beaugrand, J., Balaguer, P., Ducrot, P.-H., Allais, F., 2017. Syringaresinol: A Renewable and Safer Alternative to Bisphenol A for Epoxy-Amine Resins. *ChemSusChem* **10**, 738–746. <https://doi.org/10.1002/cssc.201601595>

Laurichesse, S., Huillet, C., Avérous, L., 2014. Original polyols based on organosolv lignin and fatty acids: new bio-based building blocks for segmented polyurethane synthesis. *Green Chem.* **16**, 3958–3970. <https://doi.org/10.1039/C4GC00596A>

Lee, S.Y., Kim, H.U., Chae, T.U., Cho, J.S., Kim, J.W., Shin, J.H., Kim, D.I., Ko, Y.-S., Jang, W.D., Jang, Y.-S., 2019. A comprehensive metabolic map for production of bio-based chemicals. *Nat. Catal.* **2**, 18–33. <https://doi.org/10.1038/s41929-018-0212-4>

Lligadas, G., Ronda, J.C., Galià, M., Biermann, U., Metzger, J.O., 2006a. Synthesis and characterization of polyurethanes from epoxidized methyl oleate based polyether polyols as renewable resources. *J. Polym. Sci. Part Polym. Chem.* **44**, 634–645. <https://doi.org/10.1002/pola.21201>

Lutjen, A.B., Quirk, M.A., Barbera, A.M., Kolonko, E.M., 2018. Synthesis of (E)-cinnamyl ester derivatives via a greener Steglich esterification. *Bioorg. Med. Chem.* **26**, 5291–5298. <https://doi.org/10.1016/j.bmc.2018.04.007>

Malferrari, D., Armenise, N., De Cesari, S., Galletti, P., Tagliavini, E., 2015. Surfactants from Itaconic Acid: Physicochemical Properties and Assessment of the Synthetic Strategies. *ACS Sustain. Chem. Eng.* **3**, 1579–1588. <https://doi.org/10.1021/acssuschemeng.5b00264>

Manzardo, A., Marson, A., Roso, M., Boaretti, C., Modesti, M., Scipioni, A., Lorenzetti, A., 2019. Life Cycle Assessment Framework To Support the Design of Biobased Rigid Polyurethane Foams. *ACS Omega* **4**, 14114–14123. <https://doi.org/10.1021/acsomega.9b02025>

Mather, B.D., Viswanathan, K., Miller, K.M., Long, T.E., 2006. Michael addition reactions in macromolecular design for emerging technologies. *Prog. Polym. Sci.* **31**, 487–531. <https://doi.org/10.1016/j.progpolymsci.2006.03.001>

Miao, S., Zhang, S., Su, Z., Wang, P., 2008. Chemoenzymatic synthesis of oleic acid-based polyesters for use as highly stable biomaterials. *J. Polym. Sci. Part Polym. Chem.* **46**, 4243–4248. <https://doi.org/10.1002/pola.22721>

Michael, A., 1887. Ueber die Addition von Natriumacetessig- und Natriummalonsäureäthern zu den Aethern ungesättigter Säuren. *J. Für Prakt. Chem.* **35**, 349–356. <https://doi.org/10.1002/prac.18870350136>

Morschbäcker, A., 2009. Bio-Ethanol Based Ethylene. *Polym. Rev.* **49**, 79–84. <https://doi.org/10.1080/15583720902834791>

Noordzij, G.J., van den Boomen, Y.J.G., Gilbert, C., van Elk, D.J.P., Roy, M., Wilsens, C.H.R.M., Rastogi, S., 2019. The aza-Michael reaction: towards semi-crystalline polymers from renewable itaconic acid and diamines. *Polym. Chem.* **10**, 4049–4058. <https://doi.org/10.1039/C9PY00463G>

Okada, Y., Banno, T., Toshima, K., Matsumura, S., 2009. Synthesis and Properties of Polycarboxylate-type Green Surfactants with S- or N-Linkages. *J. Oleo Sci.* **58**, 519–528. <https://doi.org/10.5650/jos.58.519>

Omraní, I., Farhadian, A., Babanejad, N., Shendi, H.K., Ahmadi, A., Nabid, M.R., 2016. Synthesis of novel high primary hydroxyl functionality polyol from sunflower oil using thiol-yne reaction and their application in polyurethane coating. *Eur. Polym. J.* **82**, 220–231. <https://doi.org/10.1016/j.eurpolymj.2016.07.021>

Paramarta, A., Webster, D.C., 2017. The exploration of Michael-addition reaction chemistry to create high performance, ambient cure thermoset coatings based on soybean oil. *Prog. Org. Coat.* **108**, 59–67. <https://doi.org/10.1016/j.porgcoat.2017.04.004>

Pascault, J.-P., Sauterau, H., Verdu, J., Williams, R.J.J., 2002. Gelation and Network Formation. In 'Thermosetting Polymers' 'Plastics Engineering'. Marcel Dekker, New York, pp. 78–129.

Pellis, A., Hanson, P.A., Comerford, J.W., Clark, J.H., Farmer, T.J., 2019. Enzymatic synthesis of unsaturated polyesters: functionalization and reversibility of the aza-Michael addition of pendants. *Polym. Chem.* **10**, 843–851. <https://doi.org/10.1039/C8PY01655K>

Pérez, M., Pleixats, R., 1995. FeCl₃-catalyzed conjugate addition of secondary amines, imidazole and pyrazole to methyl 2-acetamidoacrylate. Preparation of β -dialkylamino- α -alanine and β -(N-heteroaryl)- α -alanine derivatives. *Tetrahedron* **51**, 8355–8362. [https://doi.org/10.1016/0040-4020\(95\)00446-F](https://doi.org/10.1016/0040-4020(95)00446-F)

Pérocheau Arnaud, S., Andreou, E., Pereira Köster, L.V.G., Robert, T., 2020. Selective Synthesis of Monoesters of Itaconic Acid with Broad Substrate Scope: Biobased Alternatives to Acrylic Acid? *ACS Sustain. Chem. Eng.* **8**, 1583–1590. <https://doi.org/10.1021/acssuschemeng.9b06330>

Peters, J.M., 1970. Studies of isocyanate toxicity. *Proc. R. Soc. Med.* **63**, 372–375.

Petrović, Z.S., Zlatanić, A., Lava, C.C., Sinadinović-Fišer, S., 2002. Epoxidation of soybean oil in toluene with peroxyacetic and peroxyformic acids — kinetics and side reactions. *Eur. J. Lipid Sci. Technol.* **104**, 293–299. [https://doi.org/10.1002/1438-9312\(200205\)104:5<293::AID-EJLT293>3.0.CO;2-W](https://doi.org/10.1002/1438-9312(200205)104:5<293::AID-EJLT293>3.0.CO;2-W)

Peyrton, J., Chambaretaud, C., Avérous, L., 2019. New Insight on the Study of the Kinetic of Biobased Polyurethanes Synthesis Based on Oleo-Chemistry. *Molecules* **24**, 4332. <https://doi.org/10.3390/molecules24234332>

Peyrton, J., Chambaretaud, C., Sarbu, A., Avérous, L., 2020. Biobased Polyurethane Foams Based on New Polyol Architectures from Microalgae Oil. *ACS Sustain. Chem. Eng.* **8**, 12187–12196. <https://doi.org/10.1021/acssuschemeng.0c03758>

Prat, D., Wells, A., Hayler, J., Sneddon, H., McElroy, C.R., Abou-Shehada, S., Dunn, P.J., 2016. CHEM21 selection guide of classical- and less classical-solvents. *Green Chem.* **18**, 288–296. <https://doi.org/10.1039/C5GC01008J>

Ranu, B.C., Banerjee, S., 2007. Significant rate acceleration of the aza-Michael reaction in water. *Tetrahedron Lett.* **48**, 141–143. <https://doi.org/10.1016/j.tetlet.2006.10.142>

Rulev, A.Y., 2011. Aza-Michael reaction: achievements and prospects. *Russ. Chem. Rev.* **80**, 197–218. <https://doi.org/10.1070/rc2011v080n03abeh004162>

Sakakura, A., Kawajiri, K., Ohkubo, T., Kosugi, Y., Ishihara, K., 2007. Widely Useful DMAP-Catalyzed Esterification under Auxiliary Base- and Solvent-Free Conditions. *J. Am. Chem. Soc.* **129**, 14775–14779. <https://doi.org/10.1021/ja075824w>

Stirna, U., Lazdiņa, B., Vilsone, D., Lopez, M.J., Vargas-Garcia, M. del C., Suárez-Estrella, F., Moreno, J., 2012. Structure and properties of the polyurethane and polyurethane foam synthesized from castor oil polyols. *J. Cell. Plast.* **48**, 476–488. <https://doi.org/10.1177/0021955X12445178>

Stockmayer, W.H., 1944. Theory of Molecular Size Distribution and Gel Formation in Branched Polymers II. General Cross Linking. *J. Chem. Phys.* **12**, 125–131. <https://doi.org/10.1063/1.1723922>

Szycher, M., 2013. Szycher's handbook of polyurethanes, 2nd ed. Taylor & Francis, Boca Raton, FL.

Tremblay-Parrado, K., Avérous, L., 2020. Renewable Responsive Systems Based on Original Click and Polyurethane Cross-Linked Architectures with Advanced Properties. *ChemSusChem* **13**, 238–251. <https://doi.org/10.1002/cssc.201901991>

Tung, C.-Y.M., Dynes, P.J., 1982. Relationship between viscoelastic properties and gelation in thermosetting systems. *J. Appl. Polym. Sci.* **27**, 569–574. <https://doi.org/10.1002/app.1982.070270220>

Vedejs, E., Gingras, M., 1994. Aza-Claisen Rearrangements Initiated by Acid-Catalyzed Michael Addition. *J. Am. Chem. Soc.* **116**, 579–588. <https://doi.org/10.1021/ja00081a019>

Wabnitz, T.C., Spencer, J.B., 2003. A General, Brønsted Acid-Catalyzed Hetero-Michael Addition of Nitrogen, Oxygen, and Sulfur Nucleophiles. *Org. Lett.* **5**, 2141–2144. <https://doi.org/10.1021/ol034596h>

Winter, H.H., Chambon, F., 1986. Analysis of Linear Viscoelasticity of a Crosslinking Polymer at the Gel Point. *J. Rheol.* **30**, 367–382. <https://doi.org/10.1122/1.549853>

Wu, Liu, Y., He, Chung, Goh, 2004. Effects of Chemistries of Trifunctional Amines on Mechanisms of Michael Addition Polymerizations with Diacrylates. *Macromolecules* **37**, 6763–6770. <https://doi.org/10.1021/ma0493832>

Yang, L.-T., Zhao, C.-S., Dai, C.-L., Fu, L.-Y., Lin, S.-Q., 2012. Thermal and Mechanical Properties of Polyurethane Rigid Foam Based on Epoxidized Soybean Oil. *J. Polym. Environ.* **20**, 230–236. <https://doi.org/10.1007/s10924-011-0381-6>

7. SUPPORTING INFORMATION

7.1. Reactional model for kinetic studies with MEDA

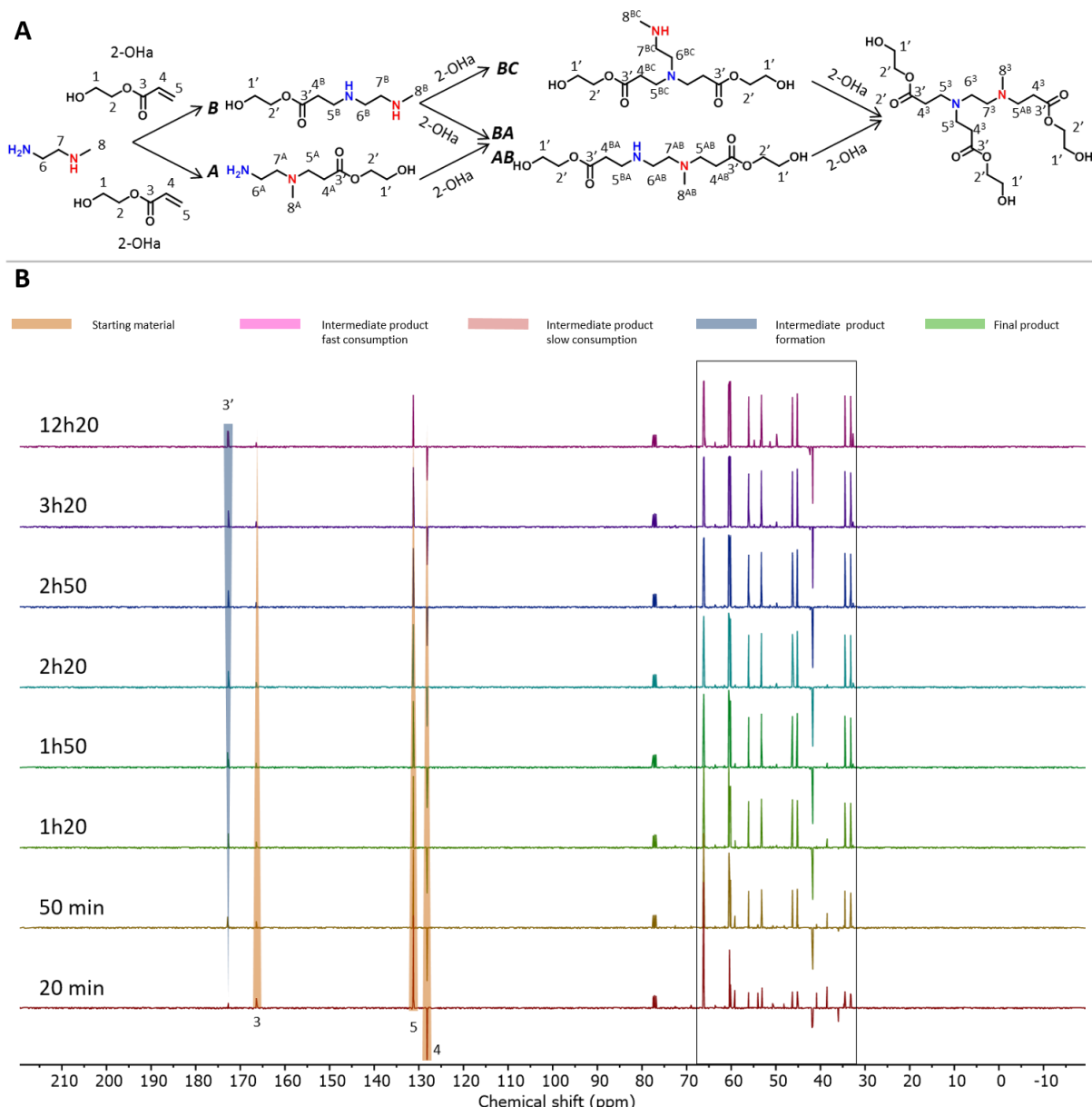


Figure S5.11 - ^{13}C NMR kinetic study of the reaction between MEDA and 2-OHa. A: The reaction path with the assignation of the different carbon. B: Full ^{13}C spectra at different reaction times.

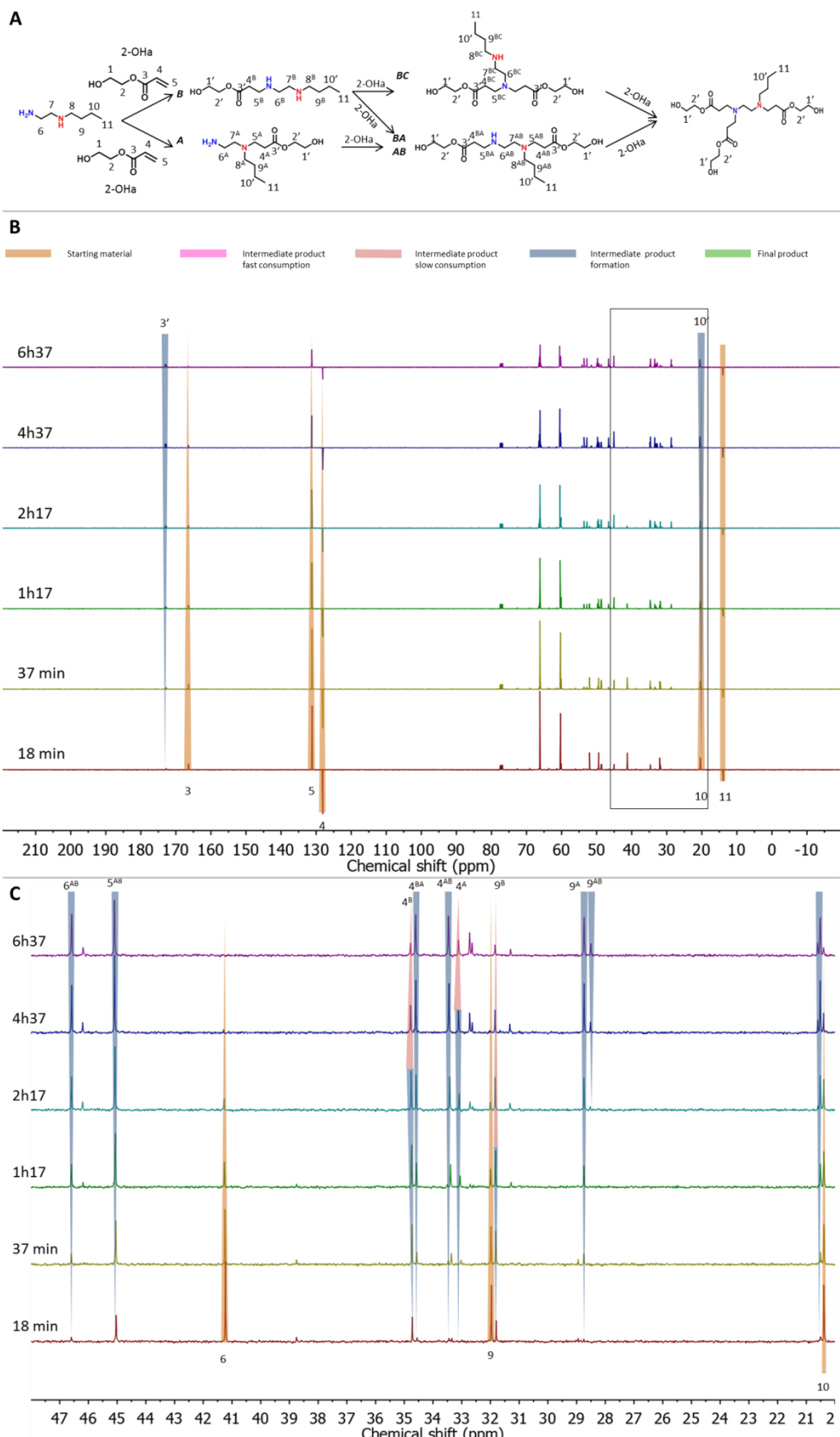


Figure S5.12 - (A) The reaction path with the assignation of the different carbon. (B) Full-scale stacked ^{13}C NMR spectra of the reaction at different times. (C) Assigned stacked ^{13}C NMR spectra of the reaction at different times in the 22-48 ppm region.

7.2. Detailed proton spectra of Iet

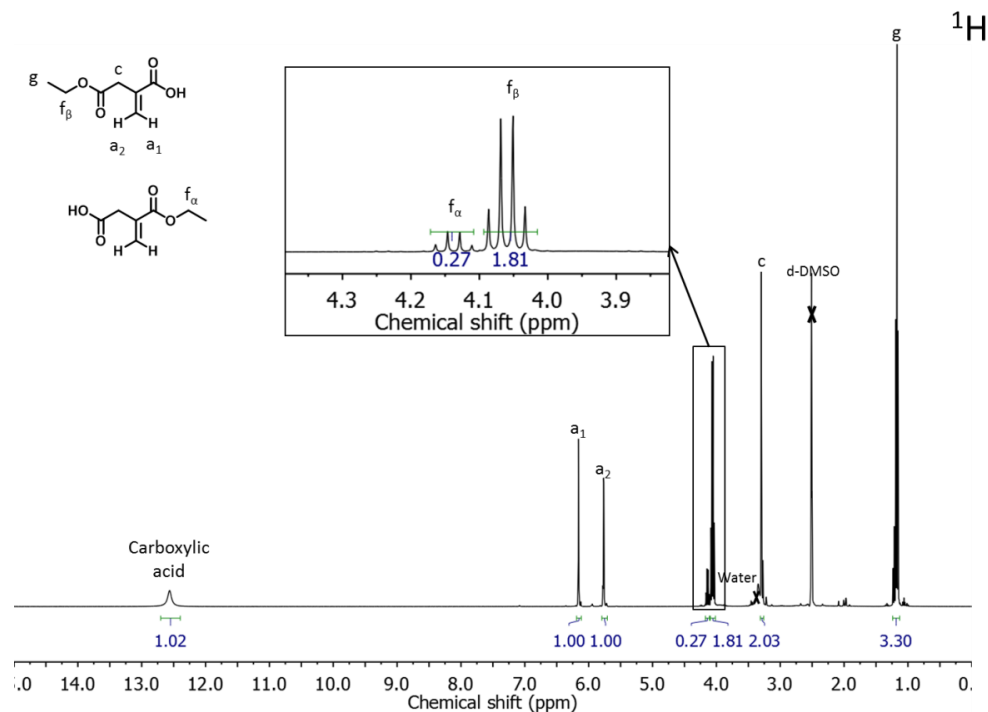


Figure S5.13 - ^1H NMR spectrum of Iet.

7.3. Full NMR analysis of Ietgl

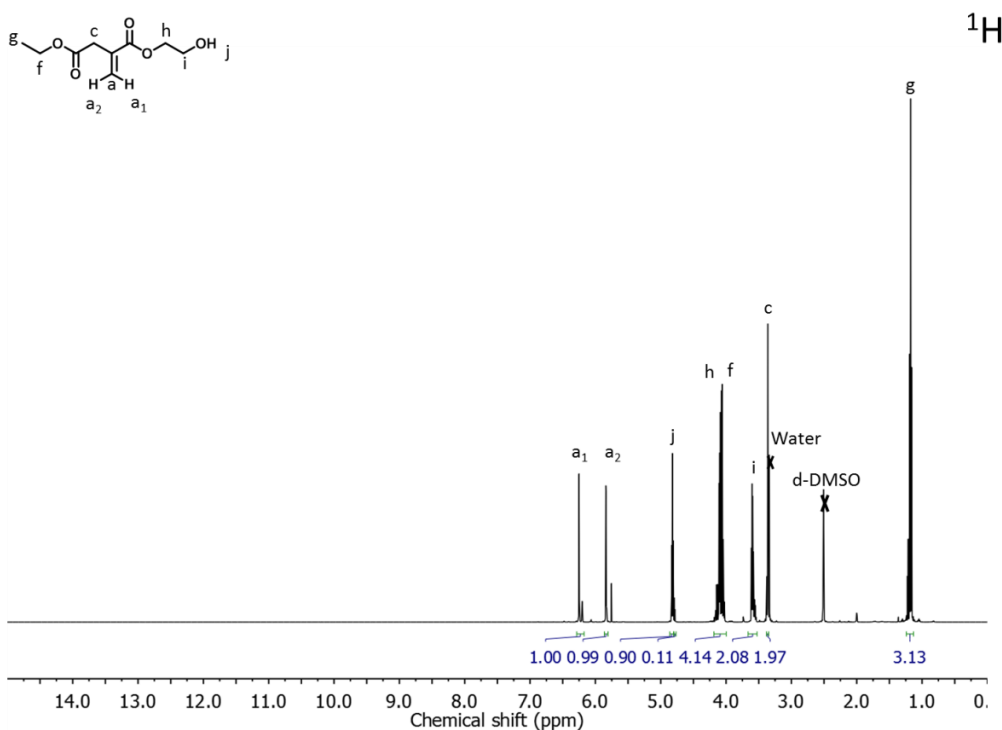


Figure S5.14 - ^1H NMR spectrum of Ietgl.

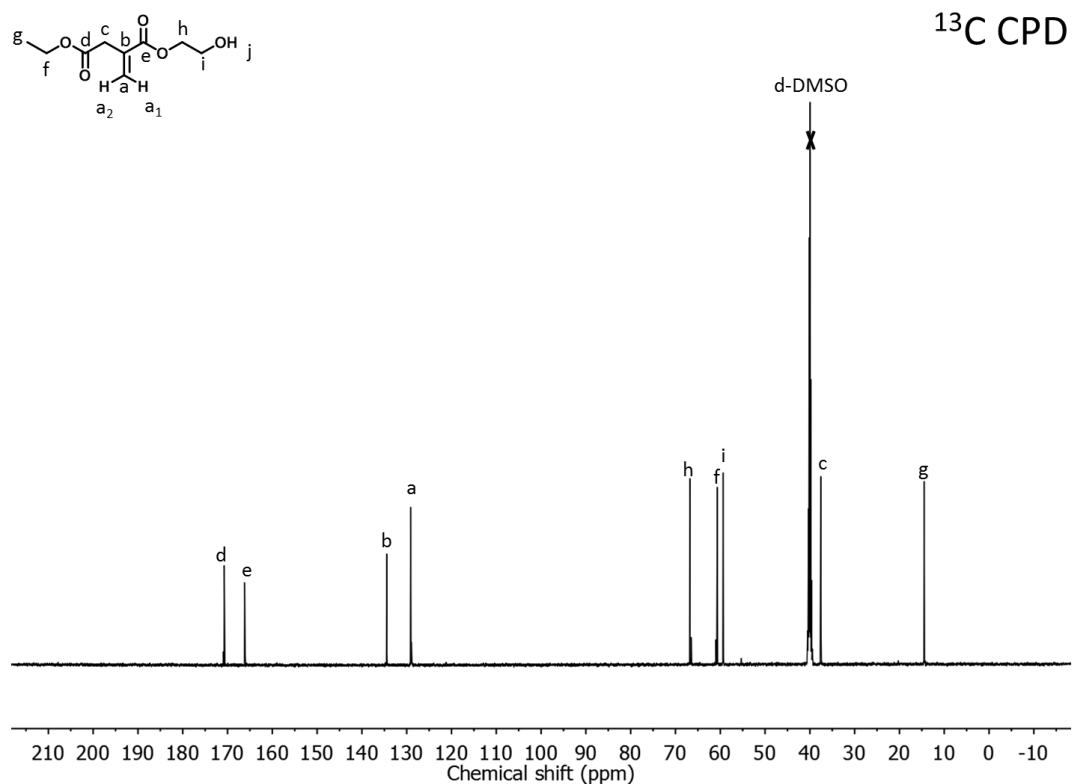


Figure S5.15 - ¹³C NMR Composite Programmed Decoupling (CPD) spectrum of Ietgl.

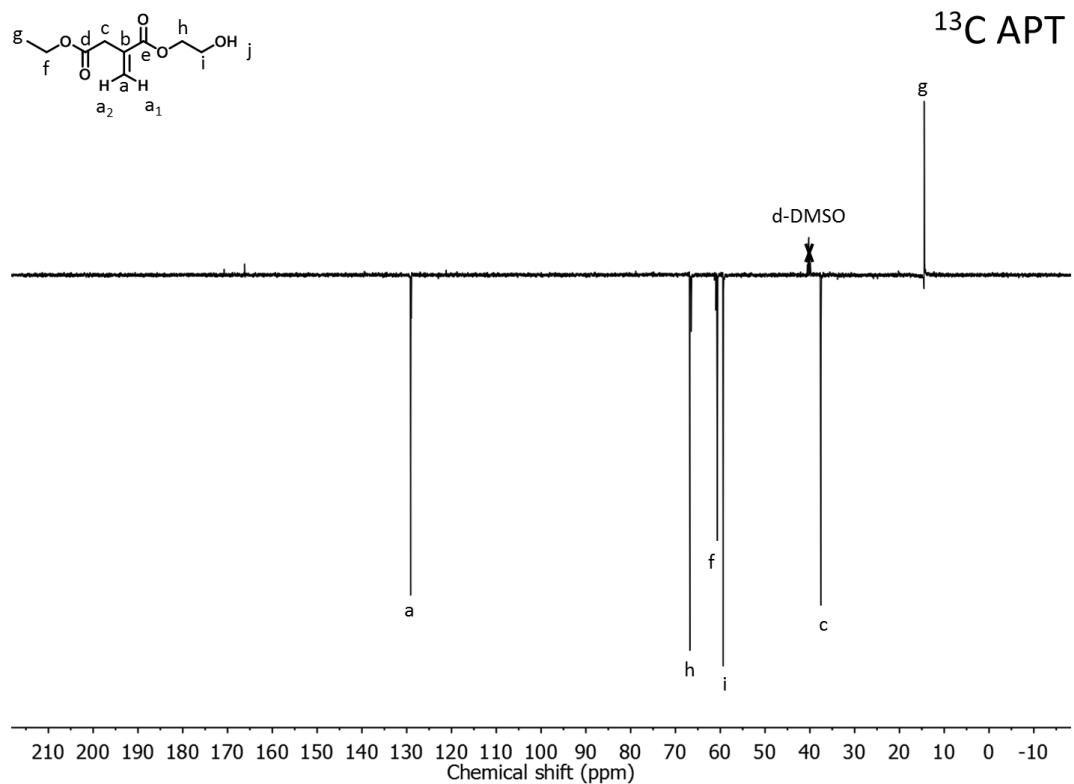


Figure S5.16 - ¹³C Attached Proton test (APT) NMR spectrum of Ietgl.

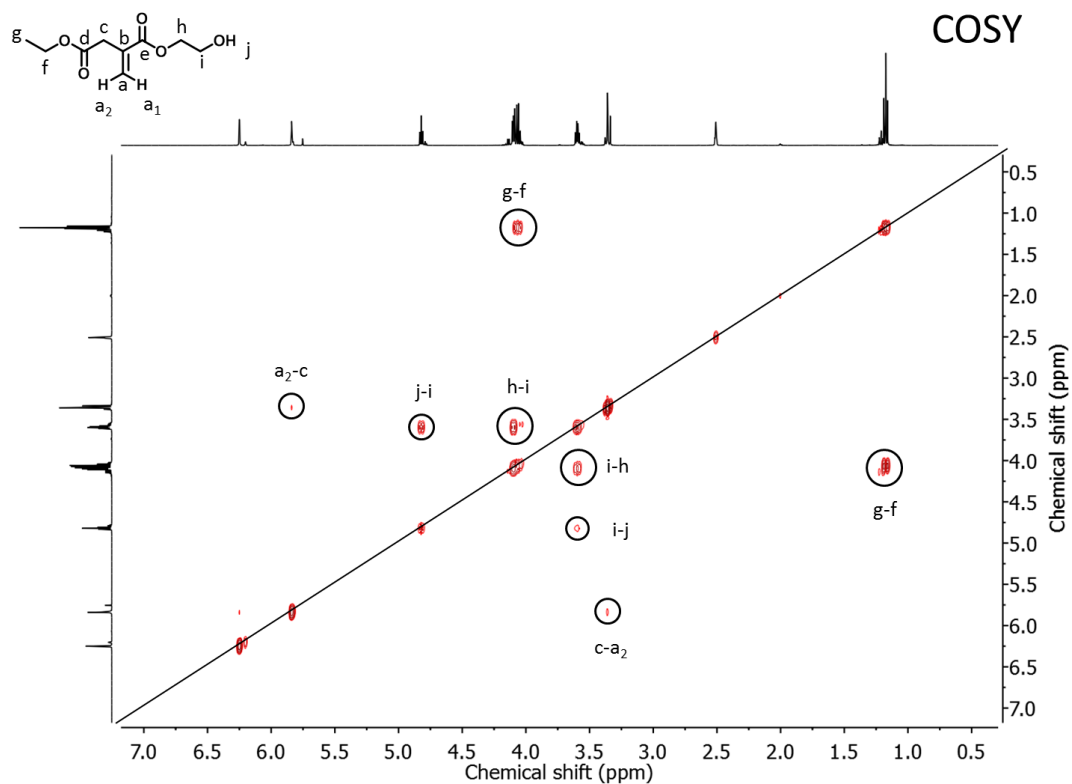


Figure S5.17 - Correlation spectroscopy (COSY) NMR spectrum of Ietgl.

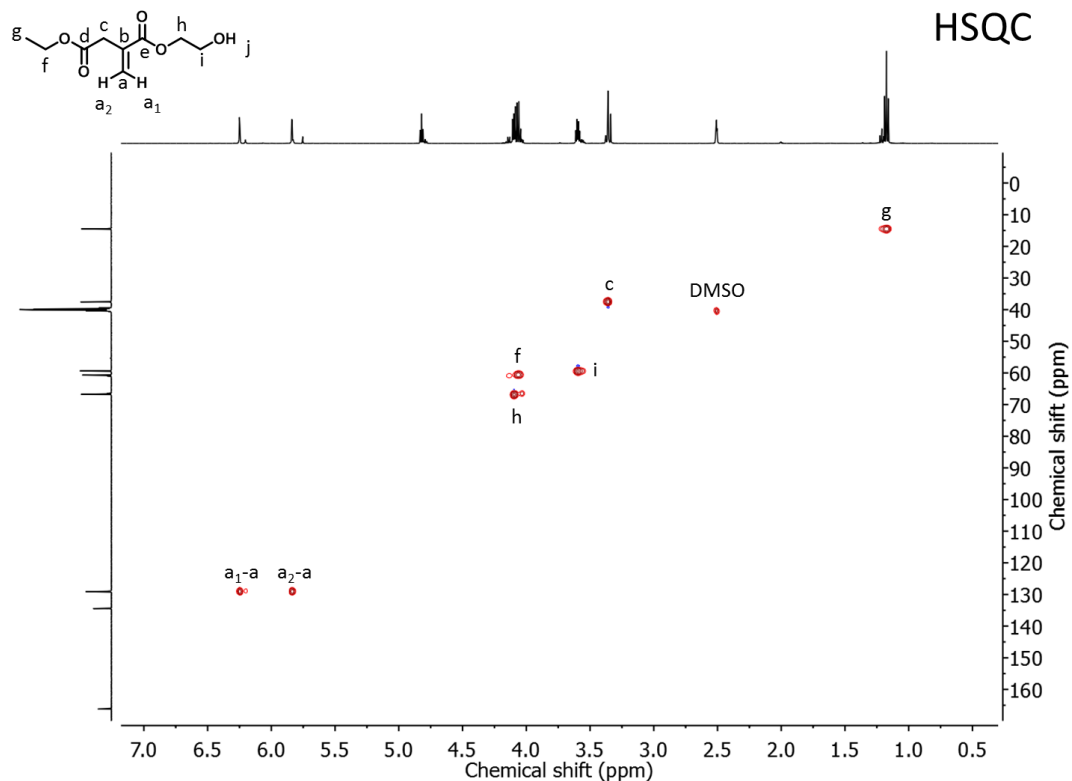


Figure S5.18 - Heteronuclear Single Quantum Correlation (HSQC) NMR spectrum of Ietgl.

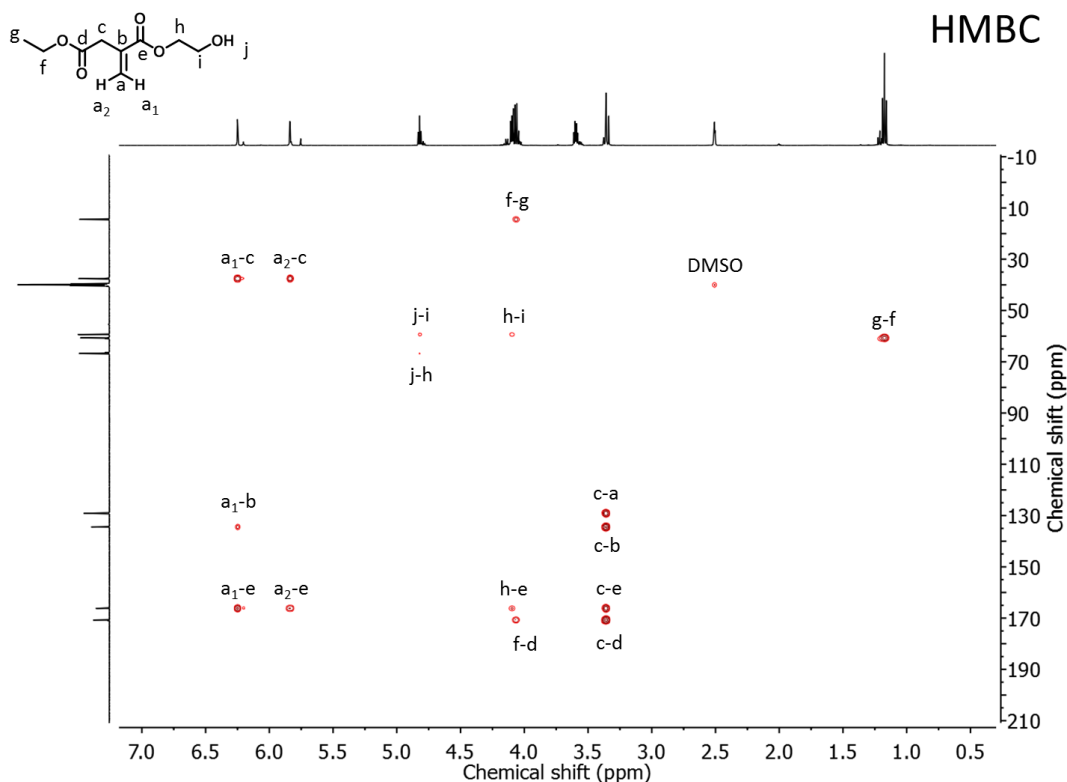


Figure S5.19 - Heteronuclear Multiple Bond Correlation (HMBC) NMR spectrum of Ietgl.

7.4. Full NMR analysis of Deti

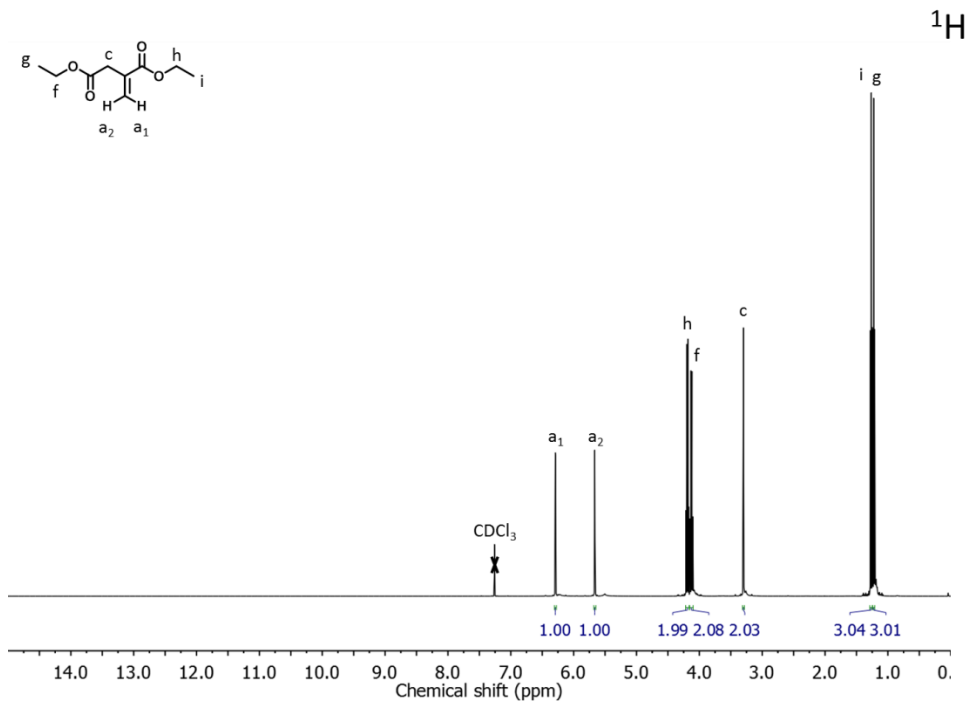


Figure S5.20 - ^1H NMR spectrum of Deti.

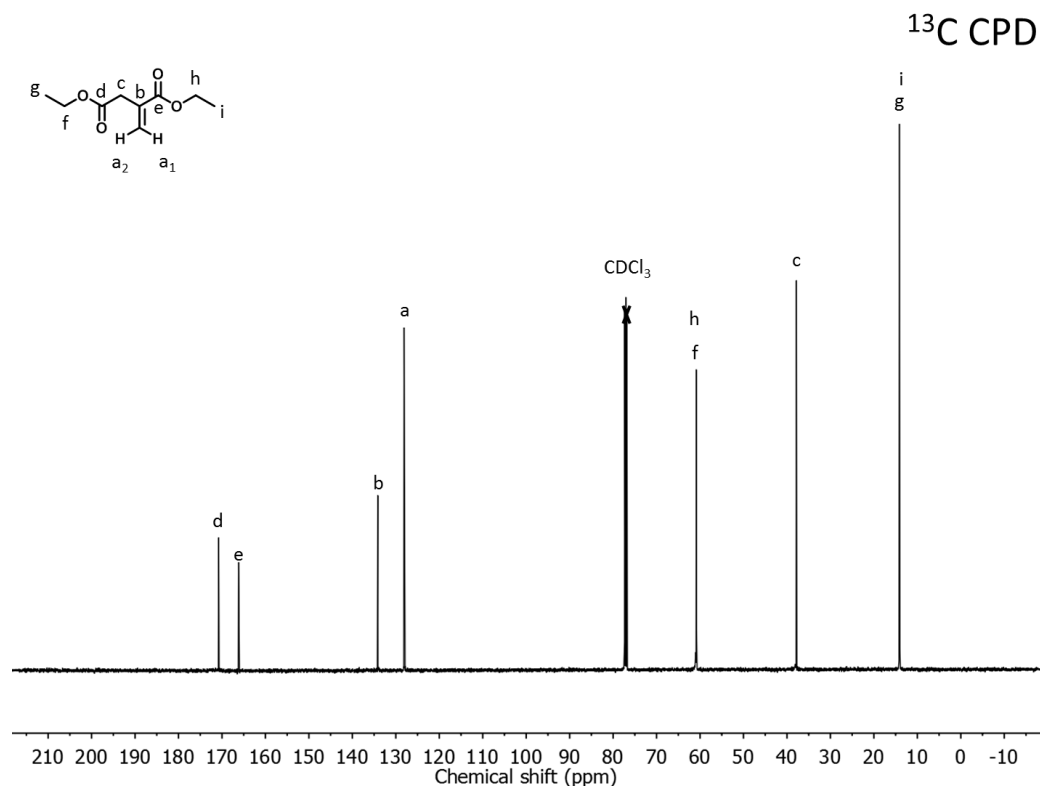


Figure S5.21 - ¹³C Composite Programmed Decoupling (CPD) NMR spectrum of Deti.

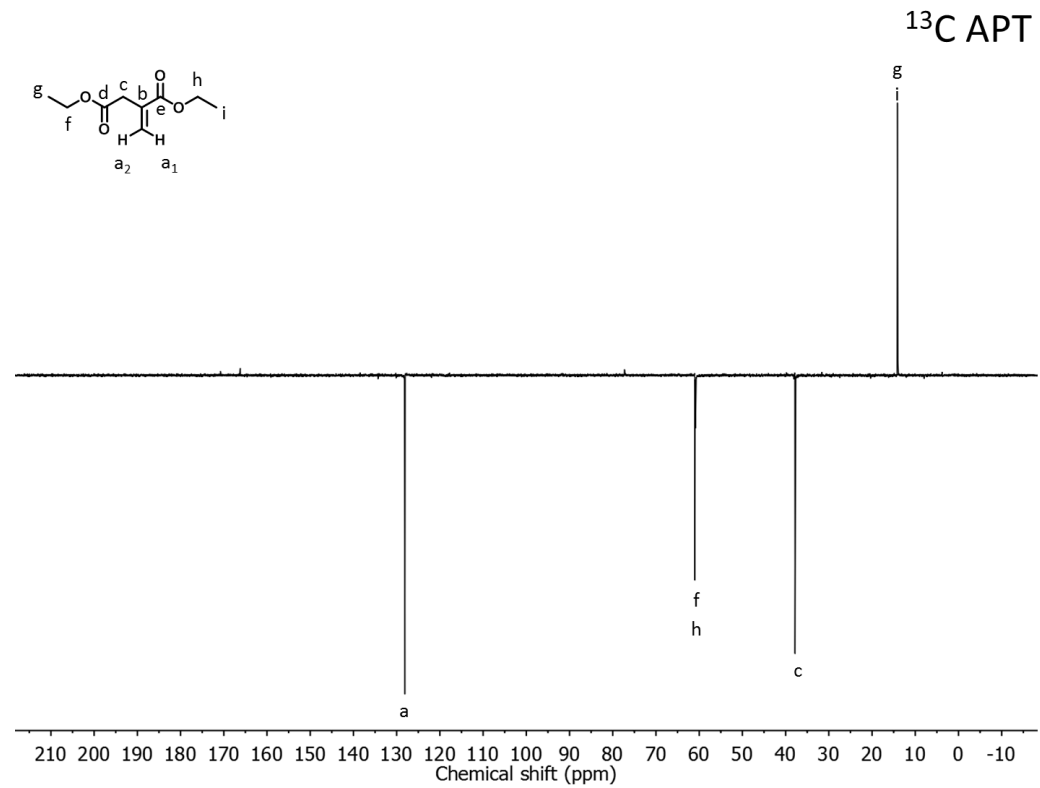


Figure S5.22 - ¹³C Attached Proton test (APT) NMR spectrum of Deti.

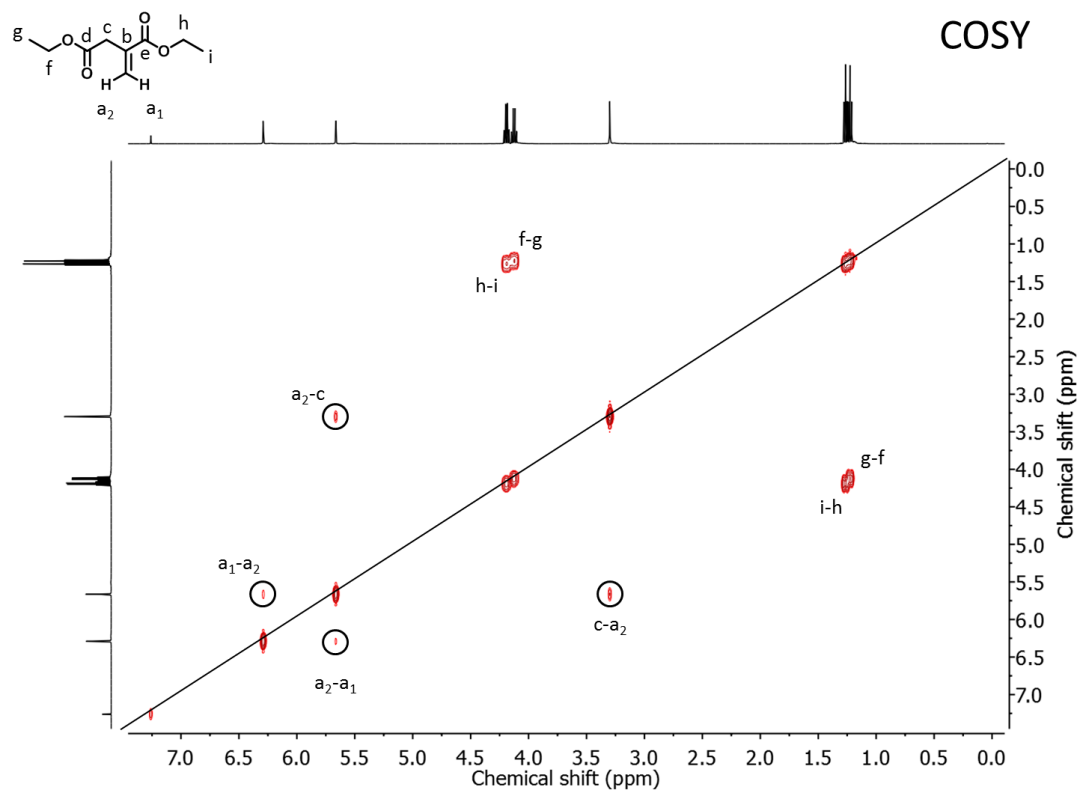


Figure S5.23 - Correlation spectroscopy (COSY) NMR spectrum of Deti.

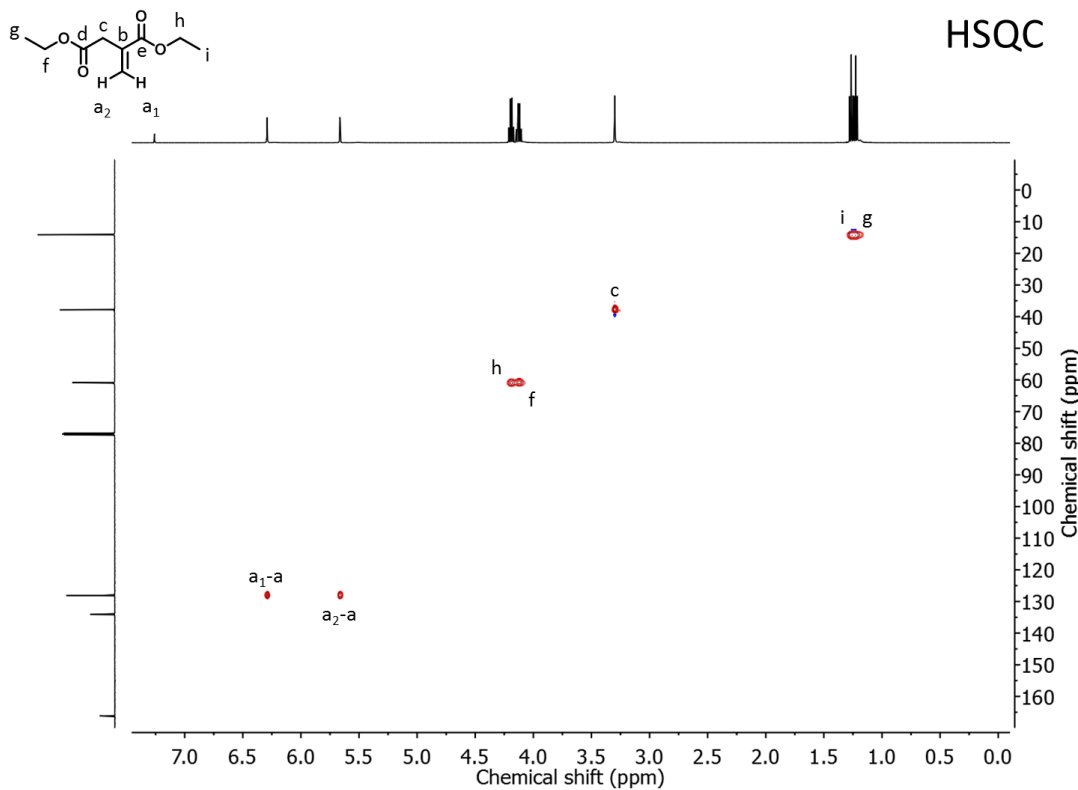


Figure S5.24 - Heteronuclear Single Quantum Correlation (HSQC) NMR spectrum of Deti.

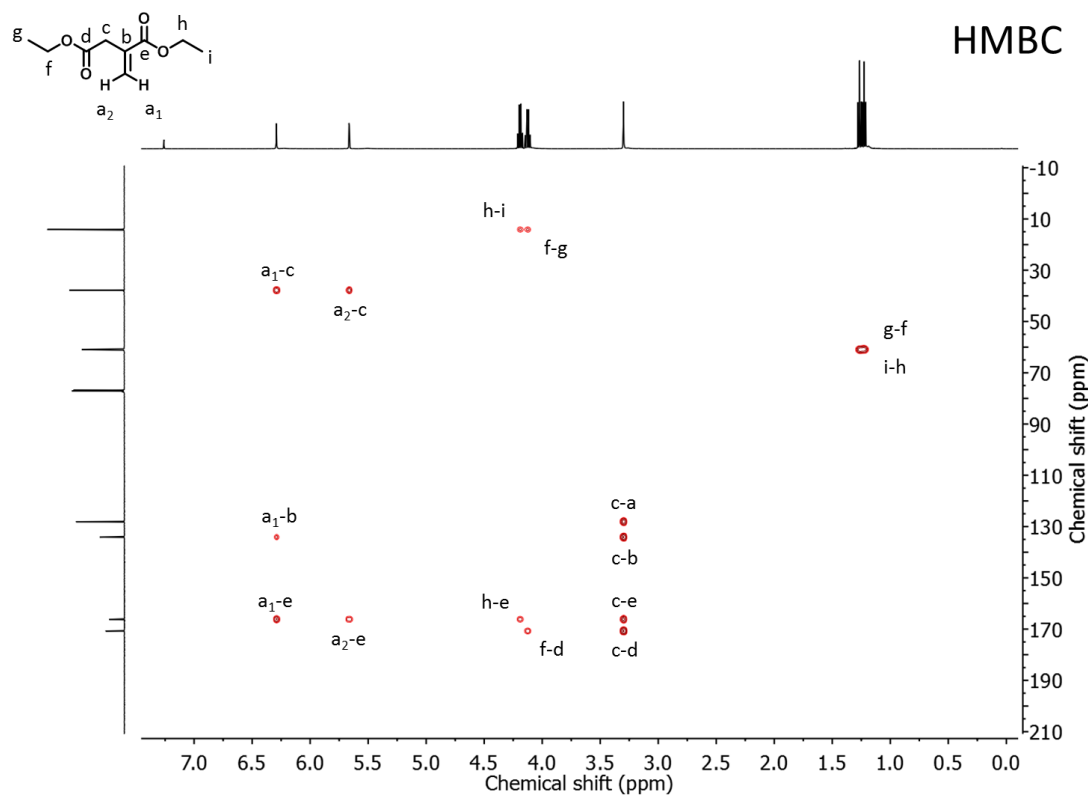


Figure S5.25 - Heteronuclear Multiple Bond Correlation (HMBC) NMR spectrum of Deti.

7.5. ^{13}C APT NMR analysis of the reaction with OA

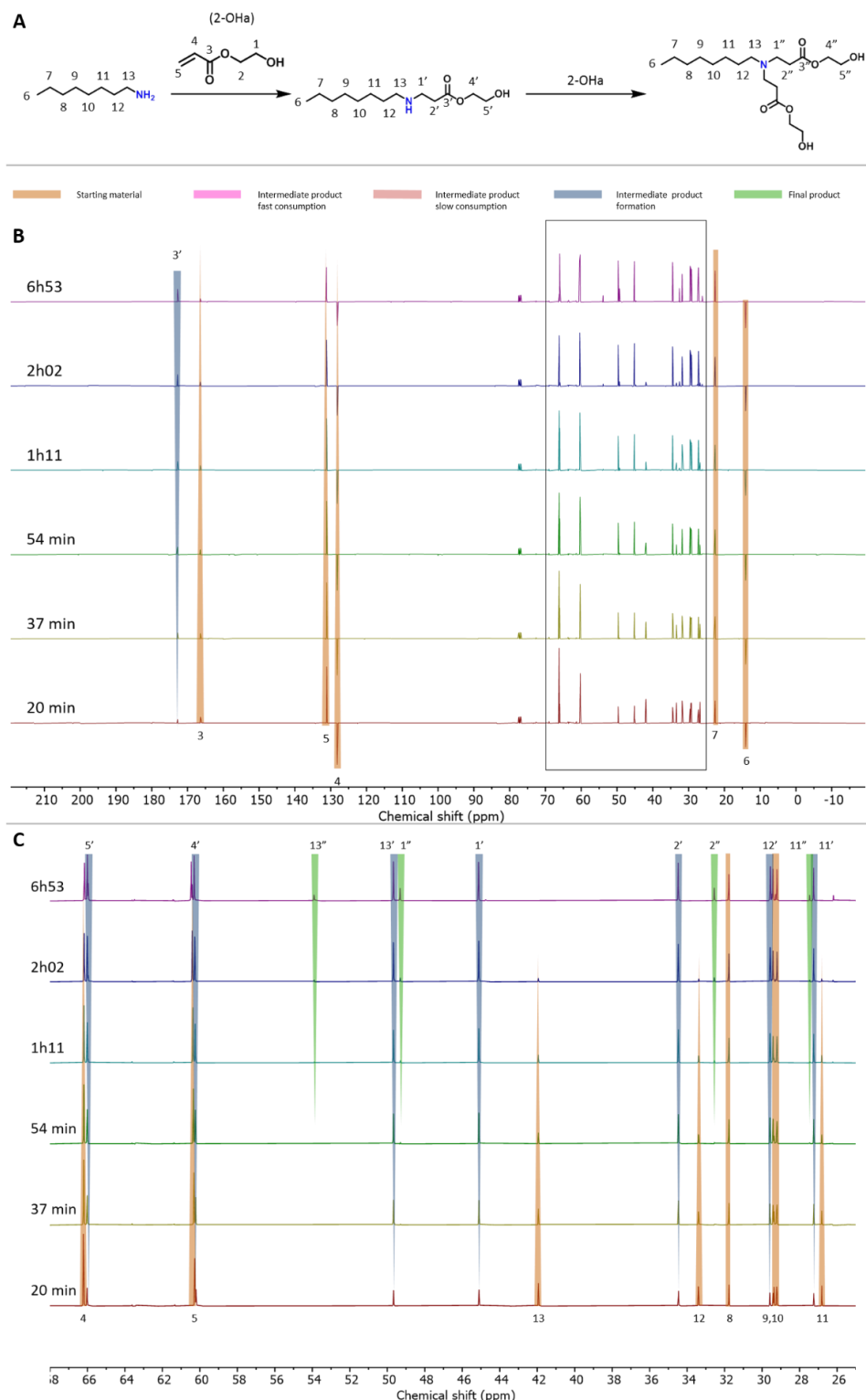


Figure S5.26 - ^{13}C NMR kinetic study of the reaction between OA and 2-OHa. (A) The reaction path with the assignation of the different carbon. (B) Full-scale stacked ^{13}C NMR spectra of the reaction at different times. (C) Assigned stacked ^{13}C NMR spectra of the reaction at different times in the 22-68 ppm region.

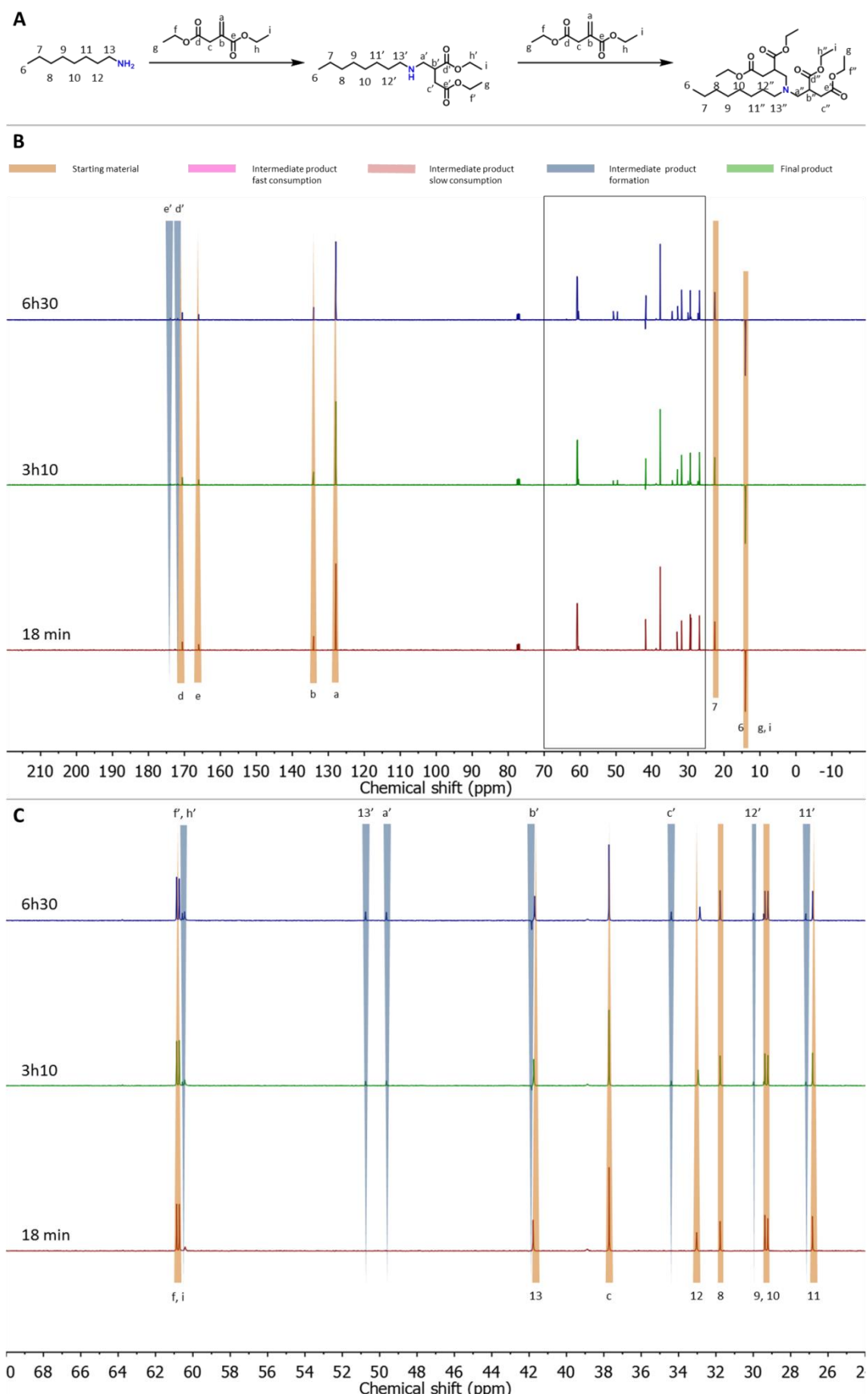


Figure S5.27 - ^{13}C NMR kinetic study of the reaction between OA and Deti. (A) The reaction path with the assignation of the different carbon. (B) Full-scale stacked ^{13}C NMR spectra of the reaction at different times. (C) Assigned stacked ^{13}C NMR spectra of the reaction at different times in the 24-70 ppm region.

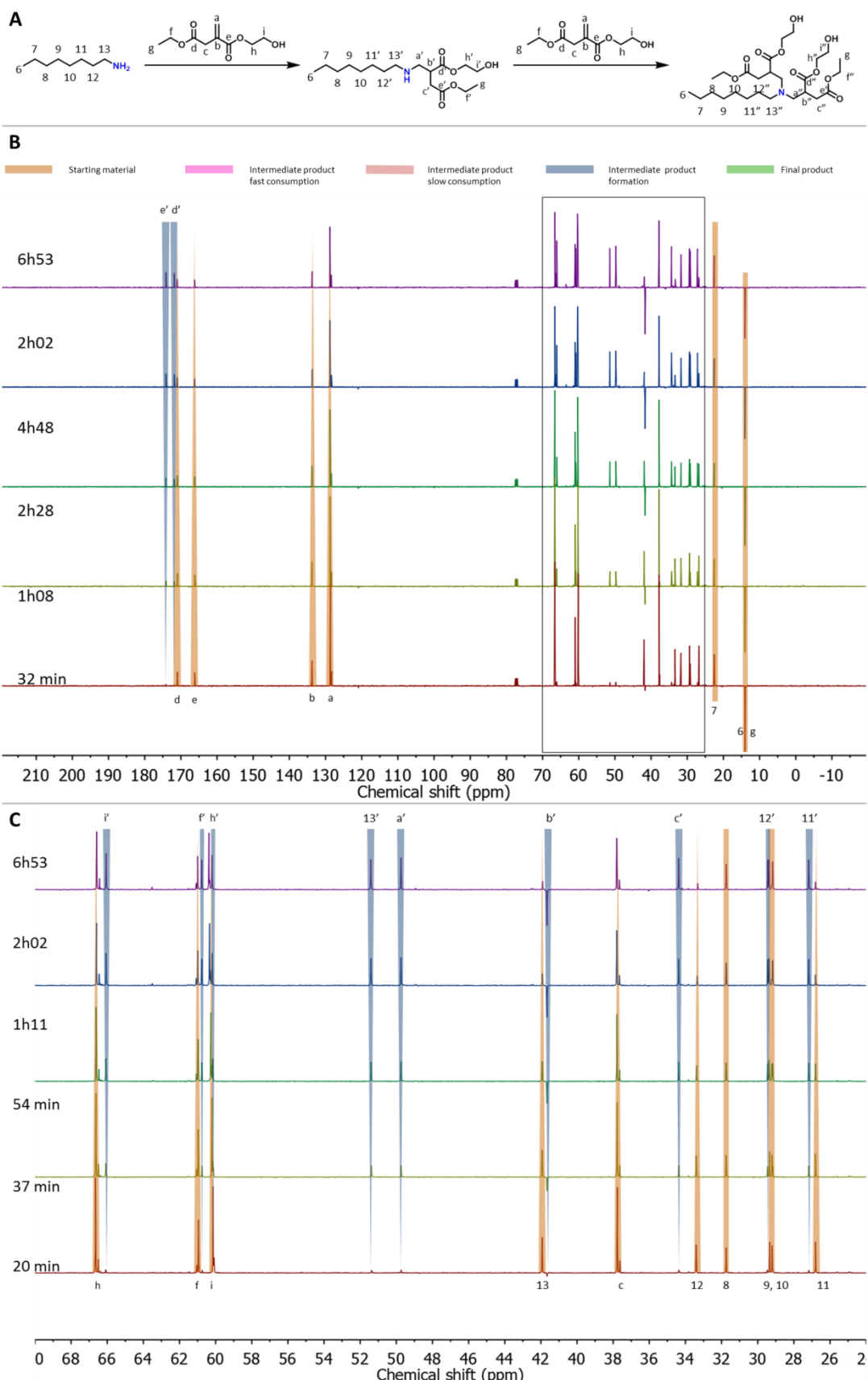


Figure S5.28 - ^{13}C NMR kinetic study of the reaction between OA and Ietgl. (A) The reaction path with the assignation of the different carbon. (B) Full-scale stacked ^{13}C NMR spectra of the reaction at different times. (C) Assigned stacked ^{13}C NMR spectra of the reaction at different times in the 24-70 ppm region.

7.6. SEC of the Michael donors derived from triglycerides

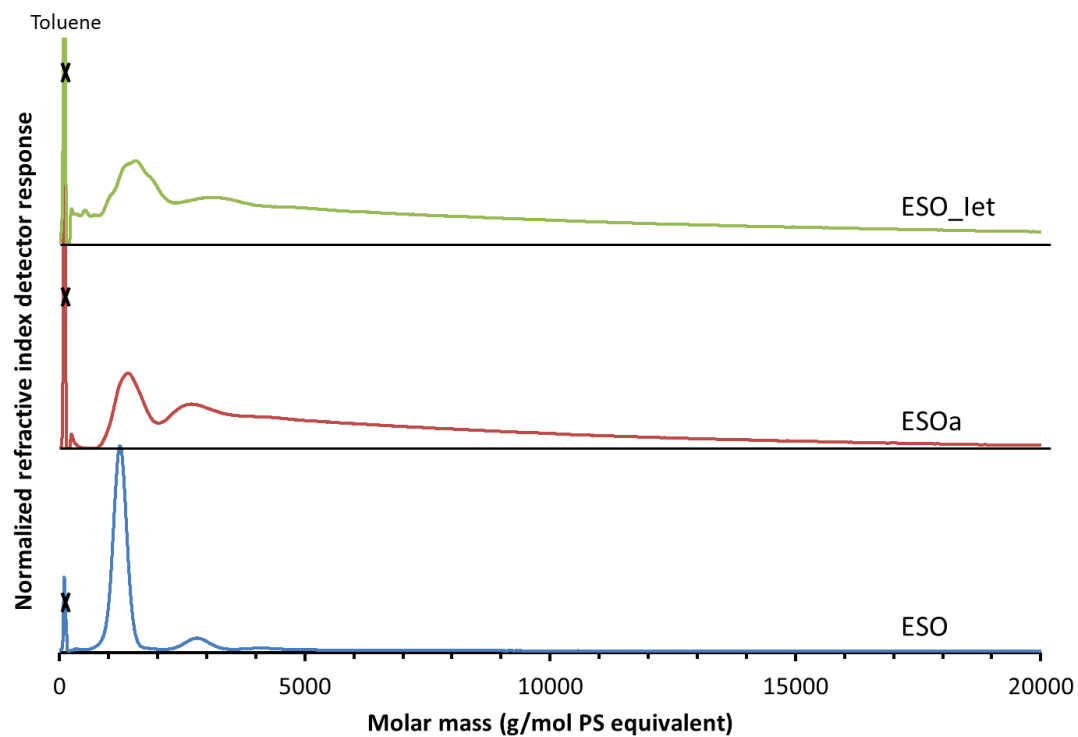


Figure S5.29 - SEC analysis based on PS equivalent molar mass of ESO, ESOa and ESO_let with toluene as flow marker.

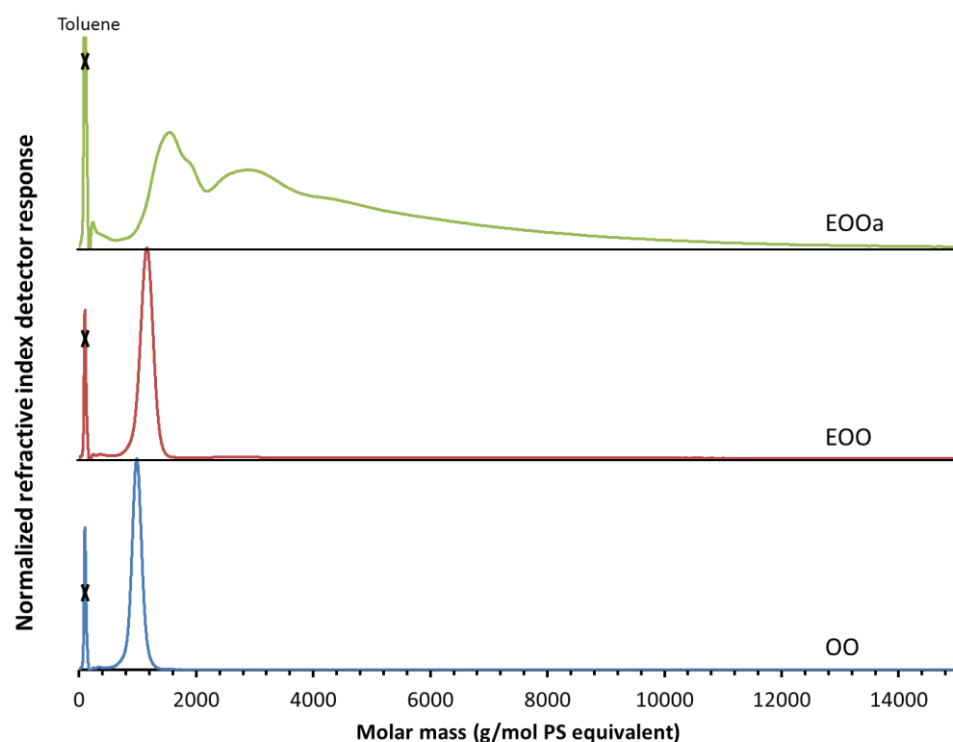


Figure S5.30 - SEC analysis based on PS equivalent molar mass of Olive oil, EOO and EOOa with toluene as flow marker.

7.7. Determination of the functionality of the Michael acceptors

Thermosets differ from thermoplastics by the branching units, which form a continuous macromolecule to the boundaries of the system: a 3D network. During a thermoset synthesis, gelation occurs when one molecule is percolating throughout the system. This moment is called the gel point. It depends on the conversion and the functionality of the monomers. The higher the functionality of monomers is, the lower the conversion at the gel point will be. The gel point characterization is critical for the functionality determination via the Flory-Stockmayer theory of gelation (Flory 1941; Stockmayer 1944). The storage modulus (G') is related to the solid part of the material and the loss modulus (G'') to the liquid viscoelastic part. The classical approach defined the gel point as the crossover between the G' and G'' modulus. Another approach was developed by Winter & Chambon, who demonstrated the linear dependency of G' and G'' with solicitation frequency at the gel point (Chambon and Winter 1987; Winter and Chambon 1986). Three hypotheses condition the Flory-Stockmayer theory described in Equation S5.1: (i) all functions are equally reactive, (ii) there is no intramolecular reaction and (iii) the network is only formed by the reaction between the A and B group.

$$\alpha_c = \frac{1}{(f_A - 1)(f_B - 1)} \quad (\text{S5.1})$$

With f_A and f_B the functionality of the two reactive units and α_c the probability that a given functional groups of a branch unit lead to another branch rather than a terminal group at the gel point. It can be expressed as a function of the conversion of monomer A or B and r the molar ratio of reactive function defined in Equation S5.2.

$$r = \frac{n_A}{n_B} \quad (\text{S5.2})$$

$$r * p_A^2 = \frac{p_B^2}{r} = \frac{1}{(f_A - 1)(f_B - 1)} \quad (\text{S5.3})$$

With n_A and n_B the quantity of A and B group respectively, p_A and p_B the conversion of A and B group, respectively. The determination of the functionality can be realized by two methods: (i) the determination of the conversion by a dosage of A or B group at the gel point for a material realized with an equimolar quantity of A and B ($r = 1$) or (ii) the preparation of material with a gradual variation of the molar ratio (r) and full conversion of the monomer introduced in defect until one material is at the gel point. The second method is more comfortable to implement and precise. In both cases, the functionality of one of the two monomers is precisely known.

This method was developed to determine the functionality of polyol via polyurethane network formation. However, the Aza-Michael polyaddition respects the conditions previously detailed for the application of the Flory-Stockmayer theory. Therefore, the method can be used to measure the functionality of the Michael acceptor (B group) derived from epoxidized oils. In this case, the DMEDA, a bifunctional molecule with very reactive secondary amine, was used as Michael acceptor (A monomer). The full conversion of amine was checked by IR spectra and the disappearance of the

N-H stretching band at 2800 cm^{-1} . Therefore, the Equation S5.3 of material at the gel point can be simplified in Equation S5.4 by considering the full conversion of amine and $f_A=2$.

$$r = \frac{1}{(f_B - 1)} \quad (\text{S4.4})$$

As stated above, the gel point is characterized by the linear G' and G'' dependency on the frequency. Therefore, the material is subjected to a frequency sweep to determine G' and G'' evolution. At the gel point, the answer (G' and G'') will be a straight line in function of the frequency sollicitation.

The results presented in Figures S22-S24 presented the frequency sweep operated on material with different stoichiometric ratios. The molar ratio values at the gel point were 0.26, 0.3 and 0.25 for ESOa, EOOa and ESO_Iet, respectively. The functionalities were determined by reversing the Equation S5.4.

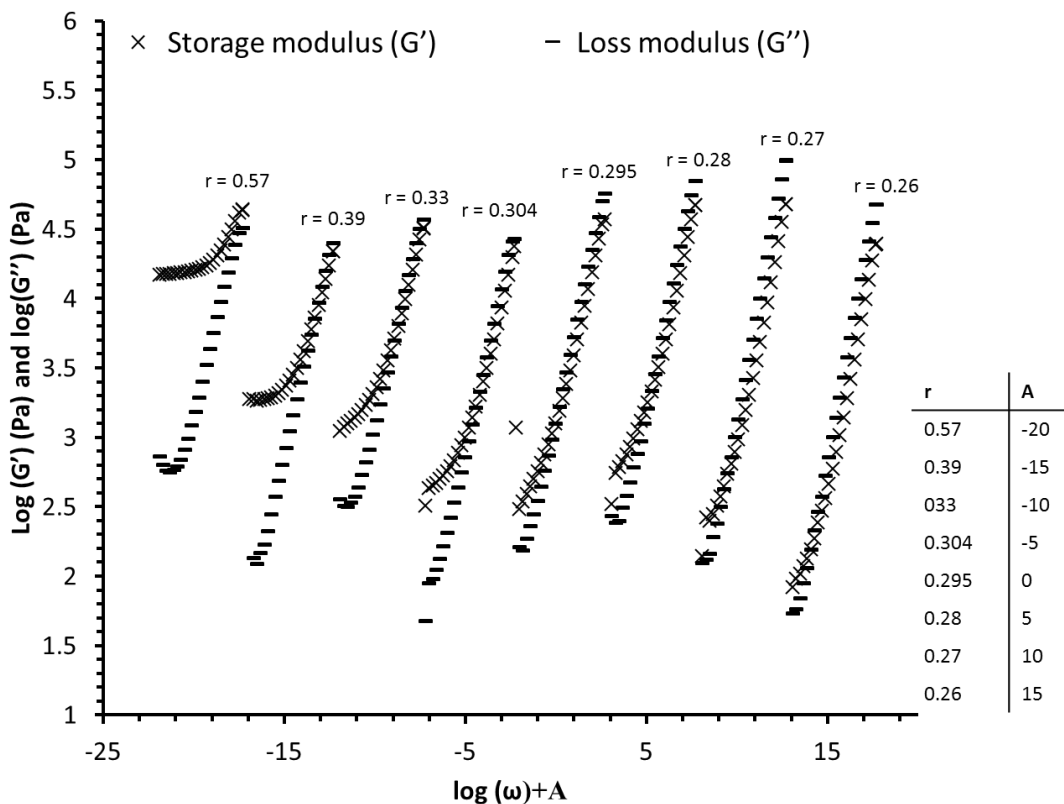


Figure S5.31 - ESOa functionality determination by measurement of the storage and loss modulus with frequency sweep experiments for different stoichiometry.

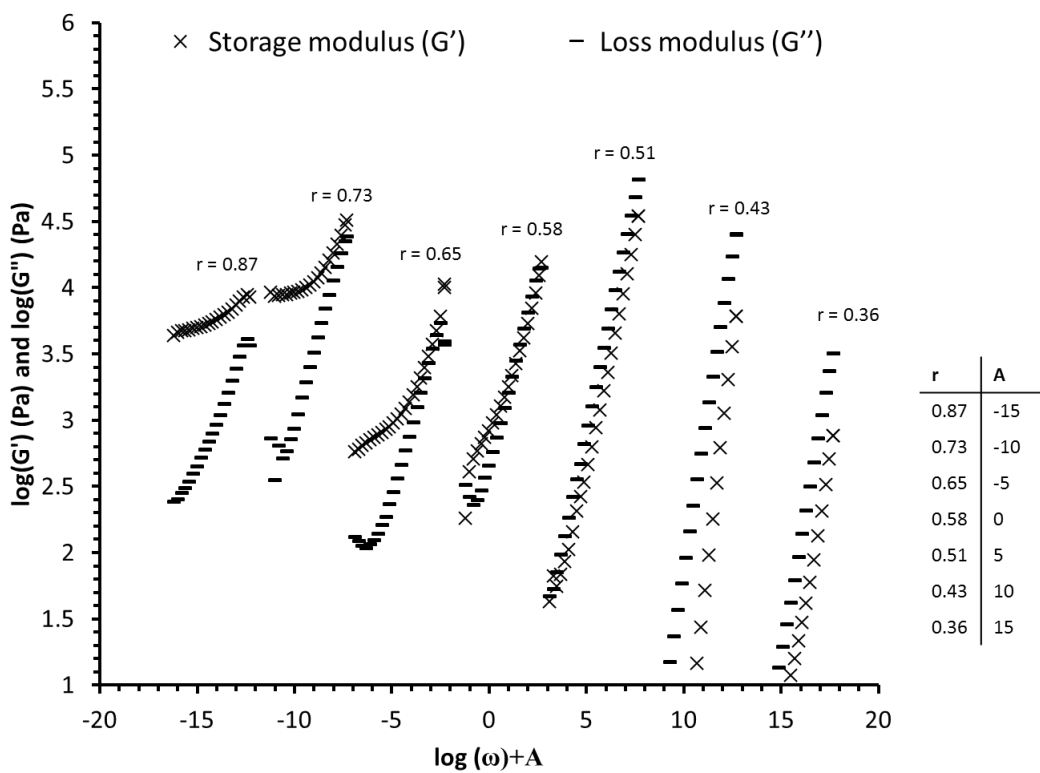


Figure S5.32 - EOOa functionality determination by measurement of the storage and loss modulus with frequency sweep experiments for different stoichiometry.

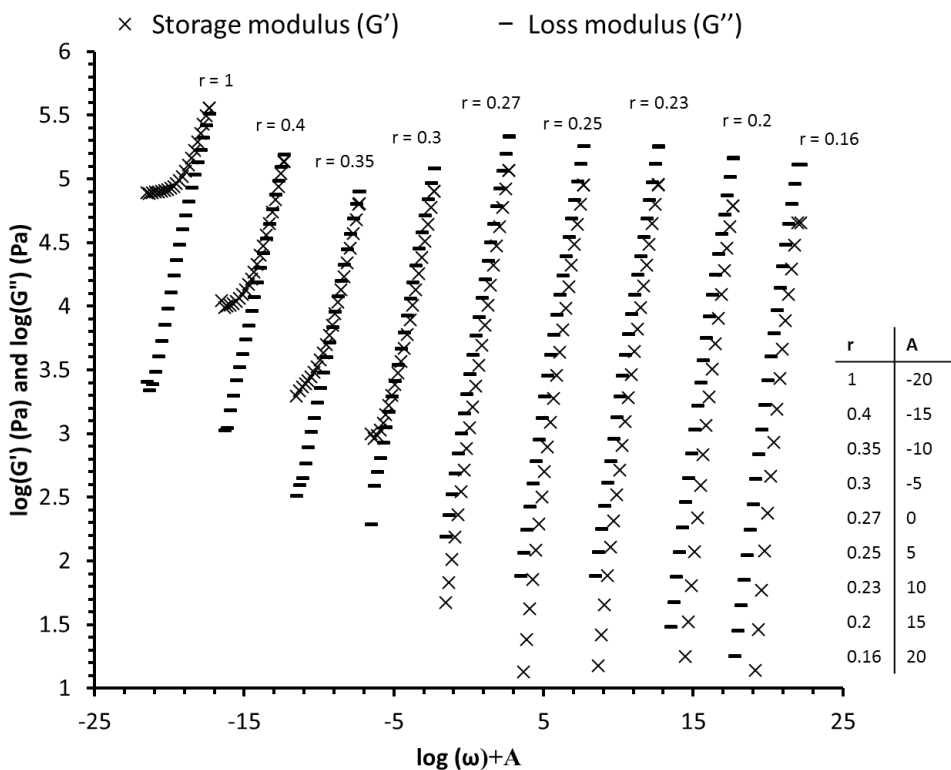


Figure S5.33 - ESO_Iet functionality determination by measurement of the storage and loss modulus with frequency sweep experiments for different stoichiometry.

7.8. DSC and TGA of the different Michael acceptors

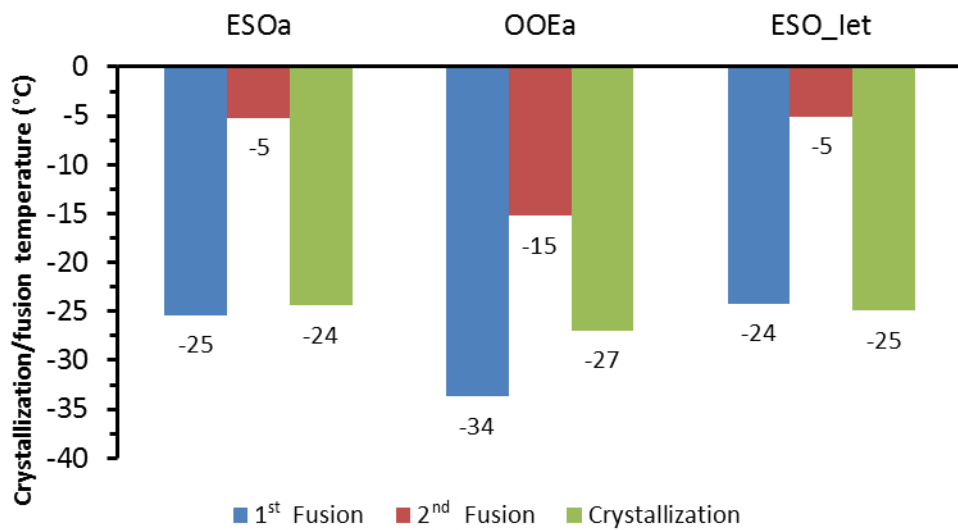


Figure S5.34 - Crystallization and fusion temperatures of the Michael donor synthesized by ring-opening of epoxidized oil.

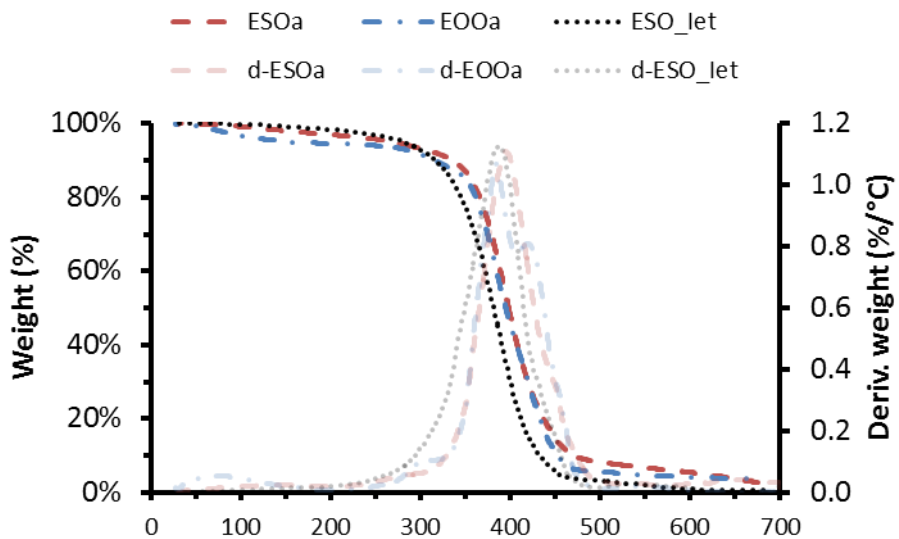


Figure S5.35 - TGA and DTG results of ESOa, EOOa and ESO_let.

7.9. Detailed ^1H spectra of DIFFA

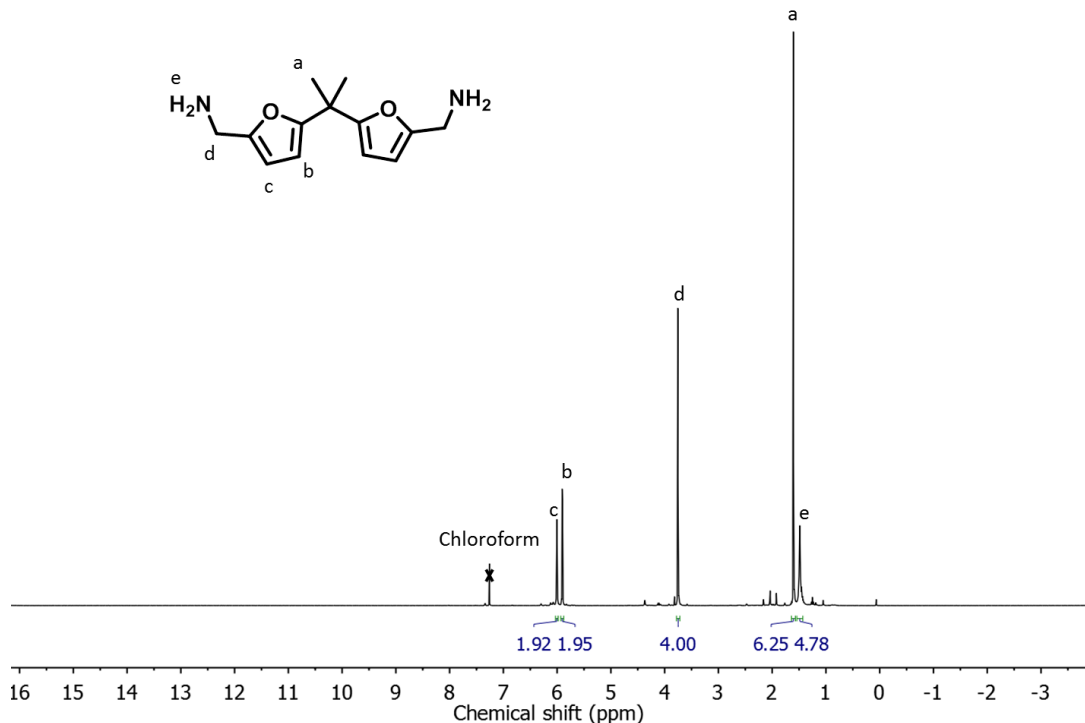


Figure S5.36 – Detailed ^1H NMR spectra of DIFFA.

7.10. Examples of gel time determination

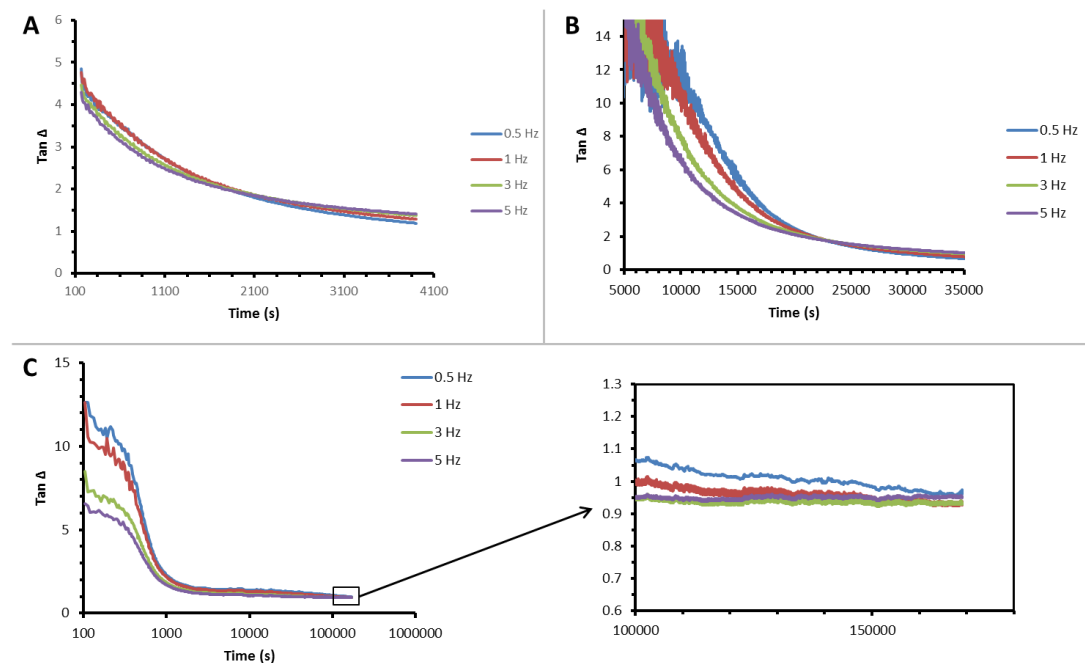


Figure S5.37 - Examples of gel time determination of (A) ESOa-DMEDA, (B) EOOa-DMEDA and (C) ESO_Iet_DMEDA.

7.11. TGA

Table S5.2 - Temperature of first and second maximum degradation for the Michael donors and the materials realized with DMEDA.

Sample	T _{degmax1} (°C)	T _{degmax2} (°C)
EOOa_DMDEDA	221	380
ESOa_DMEDA	199	393
ESO_IEt_DMEDA	206	385

Table S5.3 - Temperature of first and second maximum degradation for materials realized with ESOa and different amines and stoichiometries.

Sample	T _{degmax1} (°C)	T _{degmax2} (°C)
ESOa_DAP2	380	411
ESOa_DAP4	384	435
ESOa_DETA3	373	414
ESOa_DETA5	388	423
ESOa_TEPA5	370	400
ESOa_TEPA7	394	442
ESOa_DIFFA2	378	407
ESOa_DIFFA4	390	439
ESOa_mXDA2	390	459
ESOa_mXDA4	392	456

Conclusion chapitre 5

L'objectif de ce chapitre était donc d'explorer la chimie d'aza-Michael pour la synthèse de thermodurcissables durables qui pourraient potentiellement remplacer les polyuréthanes. Les accepteurs de Michael dérivés d'huiles époxydées ont été plus particulièrement étudiés.

Les monomères utilisés pour la synthèse de matériaux par addition d'aza-Michael ont été modélisés afin d'explorer leur réactivité. Les résultats obtenus par RMN du proton et du carbone ont démontré l'activité catalytique des groupements hydroxyles sur l'addition d'aza-Michael. Un substitut à l'acide acrylique, qui était biosourcé et synthétisé à partir d'acide itaconique a été examiné pour la synthèse d'accepteurs de Michael biosourcés. Les résultats prouvent que la réactivité est dépendante de l'encombrement stérique de la double liaison. L'acide itaconique, possédant une double liaison plus encombrée que l'acide acrylique, est donc moins réactif.

Les mesures de temps de gel par rhéologie ont permis de confronter les résultats obtenus sur le modèle aux polymérisations. Les polymérisations sont des systèmes plus complexes comparés aux modèles réactionnels. Les résultats obtenus montrent, comme le modèle réactionnel, que les accepteurs de Michael totalement biosourcés réagissent plus lentement que ceux synthétisés à partir d'acide acrylique. L'analyse thermique a permis de confirmer le potentiel des matériaux aza-Michael en tant que substitut aux polyuréthanes. Malgré des architectures macromoléculaires différentes, les résistances à la dégradation thermique des deux types de polymères sont similaires.

Ce travail ouvre des perspectives sur la substitution des polyuréthanes. L'addition d'aza-Michael a démontré au cours de cette étude une réactivité pertinente qui pourrait être mise à profit pour la synthèse, par exemple de mousses. L'étude de l'exothermie de la réaction permettrait de confirmer la possibilité de former des matériaux alvéolaires de façon analogue aux polyuréthanes. Les relations structures-propriétés, notamment mécaniques, devront être étudiées afin de confirmer le potentiel de l'addition d'aza-Michael entrevu dans cette étude.

CONCLUSION GÉNÉRALE

Cette thèse a été menée dans l'équipe BioTeam dirigée par le Pr. Luc Avérous au sein de l'Institut de Chimie et Procédés pour l'Energie, l'Environnement et la Santé (ICPEES – UMR CNRS 7515) à Strasbourg. Ce travail s'intègre également dans Mutaxio, un laboratoire commun de recherche créé en 2017 entre la BioTeam et SOPREMA, le leader mondial des solutions d'étanchéité et spécialiste de la couverture, des sous-couches phoniques et de l'isolation des bâtiments. Dans le cadre de cette thèse, la BioTeam et SOPREMA sont parties intégrantes du consortium Trans'alg financé par la Banque Publique d'Investissement France dans le cadre du programme d'investissements d'avenir. Ce groupement d'entreprises a pour but de développer la production de microalgues afin de produire des molécules d'intérêts pour la chimie de commodité. Le projet de thèse s'attache à produire de nouveaux synthons à partir d'huile de microalgues pour l'élaboration de matériaux alvéolaires.

La présente thèse s'inscrit dans la continuité des travaux de recherches menés au sein de la BioTeam : le développement de matériaux polyuréthanes innovants à partir de nouvelles ressources issue de biomasses. Les connaissances de cette équipe sur les matériaux alvéolaires se sont étendues suite à différents projets impliquant des ressources phénoliques ou des glucides. La BioTeam a d'ores et déjà synthétisé des nouveaux polyols biosourcés à partir de tannins ou de sorbitol, adaptés à l'élaboration de mousse polyuréthanes rigides. En 2017, l'équipe dirigée par le Pr. Luc Avérous devenait une des premières équipes à valoriser l'huile de microalgues comme polyol dans un matériau alvéolaire. Ces matériaux sont principalement utilisés pour l'isolation des bâtiments. Parce que la majorité des mousse polyuréthanes rigides sont actuellement produites à partir de composés d'origine fossile la conception de nouveaux matériaux durables et biosourcés pour l'isolation des bâtiments revêt donc une grande importance pour l'économie d'énergie et l'environnement. Les propriétés de ces nouveaux matériaux qui présentent de nouvelles architectures macromoléculaires doivent égaler les standards actuels dans le domaine.

Ce manuscrit, au-delà de l'introduction et la conclusion générale, a été organisé en 5 chapitres dont 4 expérimentaux. Chacun d'eux est articulé autour d'une publication. Dans un contexte de valorisation du travail de recherche, deux articles sont actuellement publiés dans *Molecules* (2019, Vol. 24, p. 4332) et dans *ACS Sustainable Chemistry & Engineering* (2020, Vol. 8, p. 12187) qui correspondent respectivement aux cœurs des chapitres 2 et 3. Deux autres articles dont une review ont été soumis et sont en phase d'expertise dans *Materials Science and Engineering : R : Report* et dans *Polymer Chemistry*. Ils correspondent aux chapitres 1 et 4. Pour finaliser, le dernier article qui correspond au dernier chapitre a été soumis dans *ACS Sustainable Chemistry & Engineering*.

L'étude bibliographique présentée dans le chapitre 1 de ce manuscrit, dresse un état de l'art des relations structures-propriétés dans les mousse polyuréthanes biosourcées. Cette analyse permet d'appréhender les problématiques liées à l'élaboration de mousse polyuréthanes biosourcées. Les multiples réactions chimiques et phénomènes physiques advenant lors de la synthèse de ces matériaux alvéolaires sont à prendre en compte pour établir les corrélations entre structures et propriétés. Cet état de l'art montre aussi la richesse de la chimie et des voies de synthèse explorées pour produire des mousse polyuréthanes à base de composés biosourcés. Les lipides, glucides, polyphénols ou les composés issus de biotechnologies blanches sont détaillés. Concernant les lipides, l'étude bibliographique présente la voie d'époxydation suivie d'une ouverture de cycle avec un nucléophile comme très prometteuse. Cette méthode permet, en variant la structure chimique du nucléophile

CONCLUSION GÉNÉRALE

utilisée, d'obtenir des polyols ou des additifs qui pourront entrer dans la composition des mousses polyuréthanes. L'étude bibliographique permet également de détailler les relations entre les structures des monomères et les propriétés des mousses polyuréthanes rigides. La mise en œuvre est un point clé pour l'obtention de matériaux alvéolaires conforme à l'application visée. L'équilibre entre la rigidification du réseau polymère et son expansion est notamment déterminant. Une discussion sur l'avenir des mousses polyuréthanes est également présentée à la fin de cette étude avec l'utilisation de composés moins nocifs pour la santé. L'addition de cyclocarbonates et d'amines représente la réaction la plus encourageante pour synthétiser des polyuréthanes sans isocyanates dans le cadre d'une chimie plus verte. Ce thème déjà abordé dans l'équipe BioTeam ne sera pas développé dans le cadre de ce travail de doctorat. L'avenir des matériaux alvéolaires a été également plus globalement abordé dans cette revue. Les additions de Michael actuellement en plein essor ont été mises en exergue pour potentiellement remplacer les mousses polyuréthanes à l'avenir. Ce dernier thème sera plus particulièrement développé dans le dernier chapitre de la thèse.

La partie expérimentale ce travail est présentée dans les chapitres 2 à 5. Dans le second chapitre, la formation de polyols à partir d'huile par époxydation et ouverture de cycle est explorée sur un système simplifié. L'étude des ouvertures de cycle par l'éthanol ou l'acide acétique permet la validation d'une nouvelle méthode de suivi par spectroscopie RMN. Les données cinétiques et thermodynamiques des réactions sont aussi déterminées. Les propriétés observées et les protocoles développés, dans cette étude, permettent d'envisager la production de polyols par cette voie de synthèse sur des huiles de microalgues. Des modèles mono-hydroxyles ont été synthétisés par réactions d'ouvertures avec différents nucléophiles. L'analyse de la réactivité de ces groupements hydroxyles modèles permet de classer les produits des réactions d'ouvertures dans différentes catégories. Les molécules obtenues par ouverture de l'huile époxydée avec l'éthanol, l'acide acétique, chlorhydrique ou bromhydrique sont des polyols. Il est à noter que les composés synthétisés avec la diéthylamine comme nucléophile sont à la fois des polyols et des catalyseurs.

Le troisième chapitre décrit la synthèse de polyols à partir de microalgues par application des protocoles précédemment développés. L'ouverture des époxydes pour la synthèse de polyols est opérée avec l'éthanol, la diéthylamine, l'acide acétique, chlorhydrique ou bromhydrique. Le polyol standard, d'origine fossile, est partiellement remplacé par 25% de chaque dérivé d'huile de microalgues dans des formulations de mousses polyuréthanes rigides. Le but est d'étudier leur impact sur la mise en œuvre des matériaux cellulaires. Les résultats démontrent que l'huile de microalgues époxydée ouverte avec l'éthanol produit le polyol le plus adapté, pour la mise en œuvre des mousses. Trois autres mousses sont aussi mises en forme avec ce polyol introduit à hauteur de 35, 50 et 75%. Les temps de mise en œuvre de ces matériaux sont malheureusement trop importants par rapport à une référence fossile. Les mousses les plus prometteuses en terme de mise en œuvre ont été très largement caractérisées. La résistance à la compression, la tenue au feu et la conductivité thermique valident la conclusion dressée lors de la mise en œuvre : le polyol obtenu par ouverture de l'huile de microalgues époxydée avec l'éthanol est le plus adapté pour remplacer un polyol standard d'origine fossile. Cette étude a permis également de valider l'activité catalytique des polyols synthétisés avec la diéthylamine, précédemment étudiés sur le modèle réactionnel. L'huile de soja étudiée est plus adaptée que l'huile de microalgues en tant que catalyseur. Une mousse a été réalisée avec pour unique catalyseur un polyol synthétisé par ouverture de l'huile de soja époxydée par la diéthylamine. Quoique la mise en

œuvre de cette mousse soit plus lente qu'une mousse standard, la densité obtenue est cependant similaire.

A la suite de ce travail, la formation d'oxazolidone est étudiée dans le chapitre 4 par réaction directe entre une huile époxydée et un polyisocyanate dans les mousse polyuréthanes. Un polyol conventionnel, issu de ressources fossiles, a graduellement été remplacé par de l'huile de soja époxydée dans des mousse polyuréthanes. La hauteur finale des matériaux mis en œuvre a été mesurée afin de déterminer l'impact de ces remplacements. Les résultats montrent que l'huile de soja affecte négativement la mise en œuvre des mousse polyuréthanes en diminuant leur expansion. Suite à ces résultats, de nouvelles mousse ont été réalisées avec 25% d'huile de microalgues époxydée. Par une poly-insaturation originelle supérieure, elle présente une teneur en groupements époxydes en moyenne largement supérieure à l'huile de soja. Le potentiel de réaction époxydes-isocyanates est par conséquent augmenté. Les mousse ainsi mise en œuvre ont une hauteur et une densité, similaire à la mousse de référence fossile. L'extraction des composés non liés par liaisons covalentes au réseau polymère a été réalisée sur les matériaux alvéolaires contenant des huiles époxydées. La séparation en composé individuel de ces extraits, suivi d'une analyse structurelle a permis d'identifier l'huile de microalgues comme non lié au réseau polymère. Ce résultat montre que la réaction est incomplète entre l'huile de microalgues époxydée et les polyisocyanates lors de la synthèse des mousse polyuréthanes. La formation d'oxazolidone n'étant pas cependant exclue, une étude modèle a été lancée. L'étude réactionnelle entre des époxydes et des isocyanates modèles avait pour but d'identifier les conditions de formation de groupement oxazolidone. Cet hétérocycle à cinq membres est synthétisé avec les époxydes terminaux. Comme les huiles époxydées sont composées d'époxydes disubstitués, plus encombrés et donc moins réactifs, la formation quantitative d'oxazolidone n'a jamais été observée sur l'huile modèle quel que soit le catalyseur employé. Les études menées dans ce chapitre indiquent la difficulté de synthétiser quantitativement des oxazolidones dans les mousse polyuréthanes par réaction directe entre les huiles époxydées et les polyisocyanates.

Le chapitre 5 est un chapitre d'ouverture qui permettra l'amorce de nouveaux axes de recherche innovants sur le thème des mousse biosourcés pour l'isolation. L'addition d'aza-Michael pour la synthèse de thermodurcissables durables et biosourcés a été donc explorée. Les accepteurs de Michael dérivés d'huiles époxydées ouvertes par l'acide acrylique ont été modélisés. La réaction entre les composés modèles a été ensuite suivie par spectroscopie RMN du proton et du carbone. Cette technique a permis d'identifier les différentes structures intermédiaires formées. Les résultats démontrent que le groupement hydroxyle formé lors de la synthèse des accepteurs de Michael catalyse la réaction d'aza-Michael. L'acide itaconique, produit industriellement par fermentation de différentes biomasses, a été modifié afin de remplacer l'acide acrylique. Les résultats sur un système réactionnel modèle a montré une réactivité moins importante de cette molécule biosourcée par rapport à l'acide acrylique moins facilement biosourçable. L'encombrement stérique autour de la double liaison réactive contrôle la réactivité des accepteurs de Michael. Les mesures du temps de gel sur les polymérisations par rhéologie, confortent les résultats obtenus sur le modèle réactionnel. Les accepteurs de Michael synthétisés par ouverture de l'huile de soja époxydée par l'éthyle itaconate forment un réseau polymère plus lentement que ceux avec l'acide acrylique. Enfin, les matériaux thermodurcissables synthétisés par les polyadditions d'aza-Michael ont été caractérisés afin d'étudier leurs propriétés thermiques et les comparer à celles du polyuréthanes. Les stabilités thermiques et les

CONCLUSION GÉNÉRALE

températures de transition vitreuses mesurées sont similaires aux polyuréthanes présentant des structures analogues. Ces résultats, dans l'ensemble, démontrent le potentiel des polymères obtenus par addition de Michael pour remplacer les polyuréthanes et leurs synthèses, notamment dans le domaine des mousses.

Au cours des différentes études, la polyvalence des huiles époxydés pour synthétiser des monomères adaptés à l'élaboration de matériaux alvéolaires a été largement démontrée. L'huile de microalgues a été modifiée avec succès pour l'obtention in fine de systèmes alvéolaires complexes. De nombreuses connaissances scientifiques ont pu être collectées sur la cinétique et la réactivité des différentes réactions étudiées et répondre aussi à certaines questions scientifiques qui étaient ouvertes.

Les résultats prometteurs obtenus dans le cadre de cette étude permettent d'ouvrir de nombreuses perspectives pour la synthèse de nouveaux synthons à base d'huile de microalgues pour l'élaboration de matériaux alvéolaires.

Avant de passer à des phases de changement d'échelle vers des voies de production industrielles de mousses biosourcés par exemple pour l'isolation thermique, un travail important d'optimisation des synthèses développées dans cette présente thèse reste à réaliser. Les nombreuses doubles liaisons de l'huile de microalgues sont un avantage par rapport aux huiles végétales. Cependant, lors de la synthèse des polyols, la faible sélectivité lors de l'ouverture des époxydes n'a pas permis d'obtenir tous les groupements hydroxyles attendus. En diminuant le nombre de réactions secondaires la densité en groupement hydroxyles pourrait augmenter. Les performances des polyols et des mousses biosourcés seraient ainsi améliorées.

De plus, l'équilibre économique de ces nouveaux polyols devra aussi être démontré lorsque les processus de production massique seront arrêtés. Actuellement, le coût de production des polyols biosourcés à partir d'huile de microalgues est bien supérieur aux polyols disponibles, d'origine fossile. La production d'huile de microalgues est en pleine essor mais ne permet pas, à présent, de subvenir aux besoins en polyols du marché des mousses polyuréthanes pour l'isolation. Quelques éléments vont dans le bon sens. L'introduction d'huile époxydée dans les mousses polyuréthanes permettrait la réduction d'une étape de synthèse par rapport aux polyols. Ceci pourrait donc se traduire en gain économique. Les propriétés des mousses polyuréthanes pourraient aussi bénéficier de la formation quantitatives d'oxazolidones. Afin de compléter nos études, la structure du catalyseur devrait être étudiée afin de faire réagir sélectivement les huiles époxydées et les polyisocyanates. Les matériaux alvéolaires potentiellement formés seraient plus résistant à la dégradation thermique. Ces mousses polyuréthanes pourraient être utilisées dans un contexte compétitif et adéquat.

La synthèse d'accepteurs de Michael par ouverture de l'huile de microalgues époxydée pourrait être envisagée suite à nos études. Les protocoles développés sur l'huile de soja pourraient être adaptés dans la synthèse de polymères. Cependant, les nombreux époxydes présents sur l'huile de microalgues nécessiteront une attention particulière. En effet, au cours de ces travaux, les protocoles précédemment développés sur les huiles végétales ont dû être adaptés pour obtenir les produits souhaités avec l'huile de microalgues. L'utilisation d'un solvant pourrait permettre d'obtenir quantitativement un accepteur de Michael à partir d'huile de microalgues.

Les mousses polyuréthanes synthétisées lors de ces travaux ont une teneur en biosourcé non majoritaire. Une étude portant sur l'optimisation des formulations contenant uniquement des polyols biosourcés est nécessaire afin de compléter nos travaux. Celle-ci pourrait permettre la synthèse de nouveaux matériaux alvéolaires aux propriétés semblables aux standards actuels du marché.

L'augmentation des composés biosourcés permettrait néanmoins d'accéder à de nouvelles architectures macromoléculaires et de nouvelles propriétés pour les matériaux alvéolaires. L'huile de microalgues pourrait donc être utilisée sur un marché de niche des mousses polyuréthanes hautes performances. Les recherches menées sur matériaux polyuréthanes biosourcés concerne la synthèse de polyols. Or au cours de cette thèse, les huiles époxydées ont été transformées en polyols présentant des propriétés catalytiques ou ignifugeantes. Il serait donc intéressant d'envisager, l'utilisation de ces dérivés d'huiles et d'un isocyanate biosourcé, comme le dimère diacide diisocyanate. Cette association permettrait l'élaboration d'une mousse polyuréthane totalement biosourcé. Ce futur matériau alvéolaire pourrait être caractérisé par des propriétés supérieures aux matériaux actuels. La viabilité économique d'une mousse totalement biosourcée dépendra des nouvelles propriétés obtenues et du prix des produits d'origine fossile correspondants.

Enfin, l'étude sur le remplacement des polyuréthanes pour la synthèse de thermodurcissables a montré le potentiel des polyadditions d'aza-Michael. Les amines sont des précurseurs des isocyanates ce qui réduit les étapes de synthèses de ce monomère par rapport aux polyuréthanes. Les accepteurs de Michael biosourcés sont obtenus par le même nombre d'étapes que leur analogues, les polyols. Economiquement, la production d'accepteurs et donneurs de Michael est donc favorable. Au niveau environnemental ces nouvelles polymérisations compensent certains défauts du polyuréthane, notamment au niveau de la synthèse et de la fin de vie. Néanmoins, une étude approfondie des propriétés mécaniques de ces nouveaux matériaux est nécessaire afin d'envisager le remplacement du polyuréthane. Au vu des résultats obtenus, il serait intéressant d'envisager des mousses élaborées par réaction d'aza-Michael. Celles-ci pourraient être totalement biosourcées comme démontré par nos études. Ces matériaux alvéolaires à l'architecture macromoléculaire nouvelle permettraient potentiellement d'améliorer les propriétés d'isolation actuelles tout en ayant un faible impact environnemental. Ces nouveaux polymères biosourcés synthétisés par polyaddition d'aza-Michael sont prometteurs. Cependant, la fin de vie des matériaux devra être explorée par recyclage chimique ou biologique qu'ils soient intégrés dans une économie circulaire. Par ailleurs, afin de compléter notre étude, une analyse complète du cycle de vie des polymères aza-Michael permettrait de confirmer leur potentiel de thermodurcissables durables et verts.

LISTE COMPLÈTE DES RÉFÉRENCES BIBLIOGRAPHIQUES

Abdel Hakim, A.A., Nassar, M., Emam, A., Sultan, M., 2011. Preparation and characterization of rigid polyurethane foam prepared from sugar-cane bagasse polyol. *Mater. Chem. Phys.* **129**, 301–307. <https://doi.org/10.1016/j.matchemphys.2011.04.008>

Abdel-Rahman, M.A., Tashiro, Y., Sonomoto, K., 2013. Recent advances in lactic acid production by microbial fermentation processes. *Biotechnol. Adv.* **31**, 877–902. <https://doi.org/10.1016/j.biotechadv.2013.04.002>

Abu-Jdayil, B., Mourad, A.-H., Hittini, W., Hassan, M., Hameedi, S., 2019. Traditional, state-of-the-art and renewable thermal building insulation materials: An overview. *Constr. Build. Mater.* **214**, 709–735. <https://doi.org/10.1016/j.conbuildmat.2019.04.102>

Acik, G., Karabulut, H.R.F., Altinkok, C., Karatavuk, A.O., 2019. Synthesis and characterization of biodegradable polyurethanes made from cholic acid and 1-lysine diisocyanate ethyl ester. *Polym. Degrad. Stab.* **165**, 43–48. <https://doi.org/10.1016/j.polymdegradstab.2019.04.015>

Aeschelmann, F., Carus, M., 2015. Biobased Building Blocks and Polymers in the World: Capacities, Production, and Applications—Status Quo and Trends Towards 2020. *Ind. Biotechnol.* **11**, 154–159. <https://doi.org/10.1089/ind.2015.28999.fae>

Agrawal, A., Kaur, R., Walia, R.S., 2017. PU foam derived from renewable sources: Perspective on properties enhancement: An overview. *Eur. Polym. J.* **95**, 255–274. <https://doi.org/10.1016/j.eurpolymj.2017.08.022>

Akindoyo, J.O., Beg, M.D.H., Ghazali, S., Islam, M.R., Jeyaratnam, N., Yuvaraj, A.R., 2016. Polyurethane types, synthesis and applications – a review. *RSC Adv.* **6**, 114453–114482. <https://doi.org/10.1039/C6RA14525F>

Al Nabulsi, A., Cozzula, D., Hagen, T., Leitner, W., Müller, T.E., 2018. Isocyanurate formation during rigid polyurethane foam assembly: a mechanistic study based on *in situ* IR and NMR spectroscopy. *Polym. Chem.* **9**, 4891–4899. <https://doi.org/10.1039/C8PY00637G>

Alagi, P., Choi, Y.J., Seog, J., Hong, S.C., 2016. Efficient and quantitative chemical transformation of vegetable oils to polyols through a thiol-ene reaction for thermoplastic polyurethanes. *Ind. Crops Prod.* **87**, 78–88. <https://doi.org/10.1016/j.indcrop.2016.04.027>

Amarnath, N., Appavoo, D., Lochab, B., 2018. Eco-Friendly Halogen-Free Flame Retardant Cardanol Polyphosphazene Polybenzoxazine Networks. *ACS Sustain. Chem. Eng.* **6**, 389–402. <https://doi.org/10.1021/acssuschemeng.7b02657>

Amran, U.A., Zakaria, S., Chia, C.H., Roslan, R., Jaafar, S.N.S., Salleh, K.M., 2019. Polyols and rigid polyurethane foams derived from liquefied lignocellulosic and cellulosic biomass. *Cellulose* **26**, 3231–3246. <https://doi.org/10.1007/s10570-019-02271-w>

Anastas, P., Eghbali, N., 2010. Green Chemistry: Principles and Practice. *Chem Soc Rev* **39**, 301–312. <https://doi.org/10.1039/B918763B>

Anastas, P.T., Warner, J.C., 2000. Green chemistry: theory and practice, 1. paperback. ed. Oxford Univ. Press, Oxford.

Andersons, J., Kirpluks, M., Stiebra, L., Cabulis, U., 2016. Anisotropy of the stiffness and strength of rigid low-density closed-cell polyisocyanurate foams. *Mater. Des.* **92**, 836–845. <https://doi.org/10.1016/j.matdes.2015.12.122>

Ansari, M.H., Ahmad, M., 1987. Reaction of methyl *trans* -2,3-epoxyoctadecanoate with phenyl isocyanate: Synthesis of fatty 3-phenyl-2-oxazolidones. *J. Am. Oil Chem. Soc.* **64**, 1544–1547. <https://doi.org/10.1007/BF02609363>

Arbenz, A., Avérous, L., 2015. Chemical modification of tannins to elaborate aromatic biobased macromolecular architectures. *Green Chem.* **17**, 2626–2646. <https://doi.org/10.1039/C5GC00282F>

Arbenz, A., Avérous, L., 2014. Synthesis and characterization of fully biobased aromatic polyols – oxybutylation of condensed tannins towards new macromolecular architectures. *RSC Adv* **4**, 61564–61572. <https://doi.org/10.1039/C4RA10691A>

Arbenz, A., Frache, A., Cuttica, F., Avérous, L., 2016. Advanced biobased and rigid foams, based on urethane-modified isocyanurate from oxypropylated gambier tannin polyol. *Polym. Degrad. Stab.* **132**, 62–68. <https://doi.org/10.1016/j.polymdegradstab.2016.03.035>

Arbenz, A., Perrin, R., Avérous, L., 2017. Elaboration and Properties of Innovative Biobased PUIR Foams from Microalgae. *J. Polym. Environ.* **26**, 254–262. <https://doi.org/10.1007/s10924-017-0948-y>

Argyropoulos, D.S., Bolker, H.I., Heitner, C., Archipov, Y., 1993. ^{31}P NMR Spectroscopy in Wood Chemistry. Part IV. Lignin Models: Spin Lattice Relaxation Times and Solvent Effects in ^{31}P NMR. *Holzforschung* **47**, 50–56. <https://doi.org/10.1515/hfsg.1993.47.1.50>

Aroua, L., Baklouti, A., 2007. Synthesis of α,ω -Bis(oxazolidinone)polyoxyethylene via a Lithium Bromide-Catalyzed Reaction of Oligoethylene Glycol Diglycidyl Ethers with Isocyanates. *Synth. Commun.* **37**, 1935–1942. <https://doi.org/10.1080/00397910701316920>

LISTE COMPLÈTE DES RÉFÉRENCES BIBLIOGRAPHIQUES

Arshanitsa, A., Paberza, A., Vevere, L., Cabulis, U., Telysheva, G., 2014. Two approaches for introduction of wheat straw lignin into rigid polyurethane foams. Presented at the Proceedings of PPS-29: The 29th International Conference of the Polymer Processing Society - Conference Papers, Nuremberg, Germany, pp. 388–391. <https://doi.org/10.1063/1.4873806>

Ashida, K., 2007. Polyurethane and related foams: chemistry and technology. CRC/Taylor & Francis, Boca Raton, FL.

Ashida, K., Frisch, K.C., Kordomenos, P., 1978. Oxazolidone catalyst. US4066628A.

ASTM D4473-03, 2003. Standard Test Method for Plastics: Dynamic Mechanical Properties: Cure Behavior. ASTM International, West Conshohocken, PA. <https://doi.org/10.1520/D4473-03>

Austin, A., Levis, W., Pizzini, L., Hartman, R., 1978a. Process for preparing a polyurethane foam from an oxyalkylated product. US4177335A.

Austin, A., Levis, W., Pizzini, L., Hartman, R., 1978b. Polyurethane foam from an oxyalkylated product. US4105597A.

Avery, H.E., 1974. Basic reaction kinetics and mechanisms. Macmillan, London.

Azechi, M., Endo, T., 2014. Synthesis and property of polyoxazolidone having fluorene moiety by polyaddition of diisocyanate and diepoxide. *J. Polym. Sci. Part Polym. Chem.* **52**, 1755–1760. <https://doi.org/10.1002/pola.27181>

Babu, R.P., O'Connor, K., Seeram, R., 2013. Current progress on bio-based polymers and their future trends. *Prog. Biomater.* **2**, 8. <https://doi.org/10.1186/2194-0517-2-8>

Bachmann, F., Reimer, J., Ruppenstein, M., Thiem, J., 2001. Synthesis of Novel Polyurethanes and Polyureas by Polyaddition Reactions of Dianhydrohexitol Configurated Diisocyanates. *Macromol. Chem. Phys.* **202**, 3410–3419. [https://doi.org/10.1002/1521-3935\(20011101\)202:17<3410::AID-MACP3410>3.0.CO;2-Q](https://doi.org/10.1002/1521-3935(20011101)202:17<3410::AID-MACP3410>3.0.CO;2-Q)

Baker, J.W., Holdsworth, J.B., 1947. 135. The mechanism of aromatic side-chain reactions with special reference to the polar effects of substituents. Part XIII. Kinetic examination of the reaction of aryl isocyanates with methyl alcohol. *J. Chem. Soc. Resumed* 713–726. <https://doi.org/10.1039/jr9470000713>

Bakry, A., Aversano, R., D'Ilario, L., Di Lisio, V., Francolini, I., Piozzi, A., Martinelli, A., 2016. Flexible aliphatic poly(isocyanurate-oxazolidone) resins based on poly(ethylene glycol) diglycidyl ether and 4,4'-methylene dicyclohexyl diisocyanate. *J. Appl. Polym. Sci.* **133**, 43404. <https://doi.org/10.1002/app.43404>

Banerjee, A., Banerjee, C., Negi, S., Chang, J.-S., Shukla, P., 2018. Improvements in algal lipid production: a systems biology and gene editing approach. *Crit. Rev. Biotechnol.* **38**, 369–385. <https://doi.org/10.1080/07388551.2017.1356803>

Banerjee, C., Singh, P.K., Shukla, P., 2016. Microalgal bioengineering for sustainable energy development: Recent transgenesis and metabolic engineering strategies. *Biotechnol. J.* **11**, 303–314. <https://doi.org/10.1002/biot.201500284>

Banik, I., Sain, M.M., 2008. Water Blown Soy Polyol-Based Polyurethane Foams of Different Rigidities. *J. Reinf. Plast. Compos.* **27**, 357–373. <https://doi.org/10.1177/0731684407083955>

Baronsky, T., Beattie, C., Harrington, R.W., Irfan, R., North, M., Osende, J.G., Young, C., 2013. Bimetallic Aluminum(salen) Catalyzed Synthesis of Oxazolidinones from Epoxides and Isocyanates. *ACS Catal.* **3**, 790–797. <https://doi.org/10.1021/cs4001046>

Barros, M.T., Phillips, A.M.F., 2010. The first enantioselective [3+2] cycloaddition of epoxides to arylisocyanates: asymmetric synthesis of chiral oxazolidinone phosphonates. *Tetrahedron Asymmetry* **21**, 2746–2752. <https://doi.org/10.1016/j.tetasy.2010.10.028>

Basso, M., Pizzi, A., Lacoste, C., Delmotte, L., Al-Marzouki, F., Abdalla, S., Celzard, A., 2014a. MALDI-TOF and ¹³C NMR Analysis of Tannin–Furanic–Polyurethane Foams Adapted for Industrial Continuous Lines Application. *Polymers* **6**, 2985–3004. <https://doi.org/10.3390/polym6122985>

Basso, M.C., Giovando, S., Pizzi, A., Pasch, H., Pretorius, N., Delmotte, L., Celzard, A., 2014b. Flexible-elastic copolymerized polyurethane-tannin foams. *J. Appl. Polym. Sci.* **131**, 40499. <https://doi.org/10.1002/app.40499>

Baumann, G.F., Dietrich, W., 1981. Isocyanurate Rigid Foam: Relationship Between Structure and Properties. *J. Cell. Plast.* **17**, 144–147. <https://doi.org/10.1177/0021955X8101700302>

Bayer, O., 1947. Das Di-Isocyanat-Polyadditionsverfahren (Polyurethane). *Angew. Chem.* **59**, 257–272. <https://doi.org/10.1002/ange.19470590901>

Becker, E.W., 2008. Microalgae: biotechnology and microbiology 'Cambridge studies in biotechnology'. Cambridge Univ. Press, Cambridge.

Belgacem, M.N., Quillerou, J., Gandini, A., 1993. Urethanes and polyurethanes bearing furan moieties—3. Synthesis, characterization and comparative kinetics of the formation of diurethanes. *Eur. Polym. J.* **29**, 1217–1224. [https://doi.org/10.1016/0014-3057\(93\)90151-5](https://doi.org/10.1016/0014-3057(93)90151-5)

Beneventi, D., Carre, B., Gandini, A., 2001. Role of surfactant structure on surface and foaming properties. *Colloids Surf. Physicochem. Eng. Asp.* **189**, 65–73. [https://doi.org/10.1016/S0927-7757\(01\)00602-1](https://doi.org/10.1016/S0927-7757(01)00602-1)

Berardi, U., Madzarevic, J., 2020. Microstructural analysis and blowing agent concentration in aged polyurethane and polyisocyanurate foams. *Appl. Therm. Eng.* **164**, 114440. <https://doi.org/10.1016/j.aplthermaleng.2019.114440>

Bergmann, E.D., Ginsburg, D., Pappo, R., 2004. The Michael Reaction. *Org. React.* **10**, 179–556.

Bhoyate, S., Ionescu, M., Kahol, P.K., Gupta, R.K., 2018. Sustainable flame-retardant polyurethanes using renewable resources. *Ind. Crops Prod.* **123**, 480–488. <https://doi.org/10.1016/j.indcrop.2018.07.025>

Bioplastic materials [WWW Document], 2019. . *Eur. Bioplastics*. URL <https://www.european-bioplastics.org/bioplastics/materials/> (accessed 8.25.20).

Biron, M., 2003. Polymères alvéolaires Monographies et transformation. *Tech. Ing. Appl. Plast.*

Biswas, A., Adhvaryu, A., Gordon, S.H., Erhan, S.Z., Willett, J.L., 2005. Synthesis of Diethylamine-Functionalized Soybean Oil. *J. Agric. Food Chem.* **53**, 9485–9490. <https://doi.org/10.1021/jf050731o>

Blattmann, H., Lauth, M., Mülhaupt, R., 2016. Flexible and Bio-Based Nonisocyanate Polyurethane (NIPU) Foams. *Macromol. Mater. Eng.* **301**, 944–952. <https://doi.org/10.1002/mame.201600141>

Bobbo, S., Nicola, G.D., Zilio, C., Brown, J.S., Fedele, L., 2018. Low GWP halocarbon refrigerants: A review of thermophysical properties. *Int. J. Refrig.* **90**, 181–201. <https://doi.org/10.1016/j.ijrefrig.2018.03.027>

Borowicz, M., Paciorek-Sadowska, J., Lubczak, J., Czupryński, B., 2019. Biodegradable, Flame-Retardant, and Bio-Based Rigid Polyurethane/Polyisocyanurate Foams for Thermal Insulation Application. *Polymers* **11**, 1816. <https://doi.org/10.3390/polym11111816>

Borowitzka, M.A., 2013. High-value products from microalgae—their development and commercialisation. *J. Appl. Phycol.* **25**, 743–756. <https://doi.org/10.1007/s10811-013-9983-9>

Boufi, S., Belgacem, M.N., Quillerou, J., Gandini, A., 1993. Urethanes and polyurethanes bearing furan moieties. 4. Synthesis, kinetics and characterization of linear polymers. *Macromolecules* **26**, 6706–6717. <https://doi.org/10.1021/ma00077a003>

Boufi, S., Gandini, A., Belgacem, M.N., 1995. Urethanes and polyurethanes bearing furan moieties: 5. Thermoplastic elastomers based on sequenced structures. *Polymer* **36**, 1689–1696. [https://doi.org/10.1016/0032-3861\(95\)99015-M](https://doi.org/10.1016/0032-3861(95)99015-M)

Bozell, J.J., Petersen, G.R., 2010. Technology development for the production of biobased products from biorefinery carbohydrates—the US Department of Energy’s “Top 10” revisited. *Green Chem.* **12**, 539. <https://doi.org/10.1039/b922014c>

Brennan, L., Owende, P., 2010. Biofuels from microalgae—A review of technologies for production, processing, and extractions of biofuels and co-products. *Renew. Sustain. Energy Rev.* **14**, 557–577. <https://doi.org/10.1016/j.rser.2009.10.009>

Bresolin, D., Valério, A., de Oliveira, D., Lenzi, M.K., Sayer, C., de Araújo, P.H.H., 2018. Polyurethane Foams Based on Biopolyols from Castor Oil and Glycerol. *J. Polym. Environ.* **26**, 2467–2475. <https://doi.org/10.1007/s10924-017-1138-7>

Briou, B., Vu, N.D., Caillol, S., Robin, J., Duguet, N., Lemaire, M., Etienne, P., Bonnet, L., Lapinte, V., 2020. Polyurethane Thermosets Using Lipidic Poly(α -Hydroxyketone). *J. Am. Oil Chem. Soc.* **97**, 81–91. <https://doi.org/10.1002/aocts.12289>

Brugsch, H.G., Elkins, H.B., 1963. Toluene Di-Isocyanate (TDI) Toxicity. *N. Engl. J. Med.* **268**, 353–357. <https://doi.org/10.1056/NEJM196302142680705>

Burkus, J., Eckert, C.F., 1958. The Kinetics of the Triethylamine-catalyzed Reaction of Diisocyanates with 1-Butanol in Toluene. *J. Am. Chem. Soc.* **80**, 5948–5950. <https://doi.org/10.1021/ja01555a015>

Caille, D., Pascault, J.P., Tighzert, L., 1990a. Reaction of a diepoxide with a diisocyanate in bulk: I. Use of a tertiary amine catalyst. *Polym. Bull.* **24**, 23–30. <https://doi.org/10.1007/BF00298317>

Caille, D., Pascault, J.-P., Tighzert, L., 1990b. Reaction of a diepoxide with a diisocyanate in bulk. II. Use of an imidazole or a blocked isocyanate catalysts. *Polym. Bull.* **24**, 30–31.

Caillol, S., Desroches, M., Boutevin, G., Loubat, C., Auvergne, R., Boutevin, B., 2012. Synthesis of new polyester polyols from epoxidized vegetable oils and biobased acids. *Eur. J. Lipid Sci. Technol.* **114**, 1447–1459. <https://doi.org/10.1002/ejlt.201200199>

Calvo-Correas, T., Martin, M.D., Retegi, A., Gabilondo, N., Corcuera, M.A., Eceiza, A., 2016. Synthesis and Characterization of Polyurethanes with High Renewable Carbon Content and Tailored Properties. *ACS Sustain. Chem. Eng.* **4**, 5684–5692. <https://doi.org/10.1021/acssuschemeng.6b01578>

Calvo-Correas, T., Santamaría-Echart, A., Saralegi, A., Martin, L., Valea, Á., Corcuera, M.A., Eceiza, A., 2015. Thermally-responsive biopolyurethanes from a biobased diisocyanate. *Eur. Polym. J.* **70**, 173–185. <https://doi.org/10.1016/j.eurpolymj.2015.07.022>

Campanella, A., Bonnallie, L.M., Wool, R.P., 2009. Polyurethane foams from soyoil-based polyols. *J. Appl. Polym. Sci.* **112**, 2567–2578. <https://doi.org/10.1002/app.29898>

LISTE COMPLÈTE DES RÉFÉRENCES BIBLIOGRAPHIQUES

Carré, C., Ecochard, Y., Caillol, S., Avérous, L., 2019. From the Synthesis of Biobased Cyclic Carbonate to Polyhydroxyurethanes: A Promising Route towards Renewable Non-Isocyanate Polyurethanes. *ChemSusChem* **12**, 3410–3430. <https://doi.org/10.1002/cssc.201900737>

Carriço, C.S., Fraga, T., Pasa, V.M.D., 2016. Production and characterization of polyurethane foams from a simple mixture of castor oil, crude glycerol and untreated lignin as bio-based polyols. *Eur. Polym. J.* **85**, 53–61. <https://doi.org/10.1016/j.eurpolymj.2016.10.012>

Cateto, C.A., Barreiro, M.F., Ottati, C., Lopretti, M., Rodrigues, A.E., Belgacem, M.N., 2014. Lignin-based rigid polyurethane foams with improved biodegradation. *J. Cell. Plast.* **50**, 81–95. <https://doi.org/10.1177/0021955X13504774>

Cateto, C.A., Barreiro, M.F., Rodrigues, A.E., Belgacem, M.N., 2009. Optimization Study of Lignin Oxypropylation in View of the Preparation of Polyurethane Rigid Foams. *Ind. Eng. Chem. Res.* **48**, 2583–2589. <https://doi.org/10.1021/ie801251r>

Cawse, J.L., Stanford, J.L., Still, R.H., 1984. Polymers from renewable sources, 1. Diamines and diisocyanates containing difurylalakne moieties. *Makromol. Chem.* **185**, 697–707. <https://doi.org/10.1002/macp.1984.021850408>

Caylı, G., Küsefoğlu, S., 2008. Biobased polyisocyanates from plant oil triglycerides: Synthesis, polymerization, and characterization. *J. Appl. Polym. Sci.* **109**, 2948–2955. <https://doi.org/10.1002/app.28401>

Chambon, F., Winter, H.H., 1987. Linear Viscoelasticity at the Gel Point of a Crosslinking PDMS with Imbalanced Stoichiometry. *J. Rheol.* **31**, 683–697. <https://doi.org/10.1122/1.549955>

Chang, B.P., Thakur, S., Mohanty, A.K., Misra, M., 2019. Novel sustainable biobased flame retardant from functionalized vegetable oil for enhanced flame retardancy of engineering plastic. *Sci. Rep.* **9**, 15971. <https://doi.org/10.1038/s41598-019-52039-2>

Charlon, M., Heinrich, B., Matter, Y., Couzigné, E., Donnio, B., Avérous, L., 2014. Synthesis, structure and properties of fully biobased thermoplastic polyurethanes, obtained from a diisocyanate based on modified dimer fatty acids, and different renewable diols. *Eur. Polym. J.* **61**, 197–205. <https://doi.org/10.1016/j.eurpolymj.2014.10.012>

Chattopadhyay, D.K., Webster, D.C., 2009. Thermal stability and flame retardancy of polyurethanes. *Prog. Polym. Sci.* **34**, 1068–1133. <https://doi.org/10.1016/j.progpolymsci.2009.06.002>

Chen, K., Tian, C., Cao, F., Liang, S., Jia, X., Wang, J., 2016. Preparation and characterization of highly thermostable polyisocyanurate foams modified with epoxy resin. *J. Appl. Polym. Sci.* **133**, 43085. <https://doi.org/10.1002/app.43085>

Chen, K., Tian, C., Liang, S., Zhao, X., Wang, X., 2018. Effect of stoichiometry on the thermal stability and flame retardation of polyisocyanurate foams modified with epoxy resin. *Polym. Degrad. Stab.* **150**, 105–113. <https://doi.org/10.1016/j.polymdegradstab.2018.02.015>

Chen, R., Zhang, C., Kessler, M.R., 2015. Polyols and polyurethanes prepared from epoxidized soybean oil ring-opened by polyhydroxy fatty acids with varying OH numbers. *J. Appl. Polym. Sci.* **132**. <https://doi.org/10.1002/app.41213>

Cherubini, F., 2010. The biorefinery concept: Using biomass instead of oil for producing energy and chemicals. *Energy Convers. Manag.* **51**, 1412–1421. <https://doi.org/10.1016/j.enconman.2010.01.015>

Chew, K.W., Yap, J.Y., Show, P.L., Suan, N.H., Juan, J.C., Ling, T.C., Lee, D.-J., Chang, J.-S., 2017. Microalgae biorefinery: High value products perspectives. *Bioresour. Technol.* **229**, 53–62. <https://doi.org/10.1016/j.biortech.2017.01.006>

Chian, K.S., Yi, S., 2001. Synthesis and characterization of an isocyanurate-oxazolidone polymer: Effect of stoichiometry. *J. Appl. Polym. Sci.* **82**, 879–888. <https://doi.org/10.1002/app.1919>

Choe, H., Choi, Y., Kim, J.H., 2019. Threshold cell diameter for high thermal insulation of water-blown rigid polyurethane foams. *J. Ind. Eng. Chem.* **73**, 344–350. <https://doi.org/10.1016/j.jiec.2019.02.003>

Chu, H.S., Ahn, J.-H., Yun, J., Choi, I.S., Nam, T.-W., Cho, K.M., 2015. Direct fermentation route for the production of acrylic acid. *Metab. Eng.* **32**, 23–29. <https://doi.org/10.1016/j.ymben.2015.08.005>

Clemens, R.J., Del Rector, F., 1989. A comparison of catalysts for crosslinking acetoacetylated resins via the Michael reaction. *J. Coat. Technol.* **61**, 83–91.

Contreras, J., Valdés, O., Mirabal-Gallardo, Y., de la Torre, A.F., Navarrete, J., Lisperguer, J., Durán-Lara, E.F., Santos, L.S., Nachtigall, F.M., Cabrera-Barjas, G., Abril, D., 2020. Development of eco-friendly polyurethane foams based on *Lesquerella fendleri* (A. Grey) oil-based polyol. *Eur. Polym. J.* **128**, 109606. <https://doi.org/10.1016/j.eurpolymj.2020.109606>

Cornille, A., Dworakowska, S., Bogdal, D., Boutevin, B., Caillol, S., 2015. A new way of creating cellular polyurethane materials: NIPU foams. *Eur. Polym. J.* **66**, 129–138. <https://doi.org/10.1016/j.eurpolymj.2015.01.034>

Cornille, A., Guillet, C., Benyahya, S., Negrell, C., Boutevin, B., Caillol, S., 2016. Room temperature flexible isocyanate-free polyurethane foams. *Eur. Polym. J.* **84**, 873–888. <https://doi.org/10.1016/j.eurpolymj.2016.05.032>

Coste, G., Negrell, C., Caillol, S., 2020. From gas release to foam synthesis, the second breath of blowing agents. *Eur. Polym. J.* **140**, 110029.

Cotarca, L., Eckert, H., 2003. Phosgenations - A Handbook, 1st ed. Wiley. <https://doi.org/10.1002/3527602623>

Cozar, A., Echevarria, F., Gonzalez-Gordillo, J.I., Irigoien, X., Ubeda, B., Hernandez-Leon, S., Palma, A.T., Navarro, S., Garcia-de-Lomas, J., Ruiz, A., Fernandez-de-Puelles, M.L., Duarte, C.M., 2014. Plastic debris in the open ocean. *Proc. Natl. Acad. Sci.* **111**, 10239–10244. <https://doi.org/10.1073/pnas.1314705111>

Czonka, S., Bertino, M.F., Kośny, J., Strąkowska, A., Maśłowski, M., Strzelec, K., 2018. Linseed oil as a natural modifier of rigid polyurethane foams. *Ind. Crops Prod.* **115**, 40–51. <https://doi.org/10.1016/j.indcrop.2018.02.019>

Dai, H., Yang, L., Lin, B., Wang, C., Shi, G., 2009. Synthesis and Characterization of the Different Soy-Based Polyols by Ring Opening of Epoxidized Soybean Oil with Methanol, 1,2-Ethanediol and 1,2-Propanediol. *J. Am. Oil Chem. Soc.* **86**, 261–267. <https://doi.org/10.1007/s11746-008-1342-7>

Dai, Z., Hatano, B., Kadokawa, J., Tagaya, H., 2002. Effect of diaminotoluene on the decomposition of polyurethane foam waste in superheated water. *Polym. Degrad. Stab.* **76**, 179–184. [https://doi.org/10.1016/S0141-3910\(02\)00010-1](https://doi.org/10.1016/S0141-3910(02)00010-1)

Dais, P., Spyros, A., 2007. ³¹P NMR spectroscopy in the quality control and authentication of extra-virgin olive oil: A review of recent progress. *Magn. Reson. Chem.* **45**, 367–377. <https://doi.org/10.1002/mrc.1985>

De, K., Legros, J., Crousse, B., Bonnet-Delpon, D., 2009. Solvent-Promoted and -Controlled Aza-Michael Reaction with Aromatic Amines. *J. Org. Chem.* **74**, 6260–6265. <https://doi.org/10.1021/jo9012699>

Debuissy, T., Pollet, E., Avérous, L., 2018. Biotic and Abiotic Synthesis of Renewable Aliphatic Polyesters from Short Building Blocks Obtained from Biotechnology. *ChemSusChem* **11**, 3836–3870. <https://doi.org/10.1002/cssc.201801700>

Del Rio, E., Galià, M., Cádiz, V., Lligadas, G., Ronda, J.C., 2010. Polymerization of epoxidized vegetable oil derivatives: Ionic-coordinative polymerization of methylepoxyoleate. *J. Polym. Sci. Part Polym. Chem.* **48**, 4995–5008. <https://doi.org/10.1002/pola.24297>

Delucis, R. de A., Magalhães, W.L.E., Petzhold, C.L., Amico, S.C., 2018. Thermal and combustion features of rigid polyurethane biofoams filled with four forest-based wastes. *Polym. Compos.* **39**, E1770–E1777. <https://doi.org/10.1002/pc.24784>

Dence, C.W., Lin, S.Y., 1992. Introduction. In 'Methods in Lignin Chemistry' 'Springer Series in Wood Science' (Eds. Lin, S.Y., Dence, C.W.). Springer Berlin Heidelberg, Berlin, Heidelberg, pp. 3–19. https://doi.org/10.1007/978-3-642-74065-7_1

Denissen, W., Rivero, G., Nicolay, R., Leibler, L., Winne, J.M., Du Prez, F.E., 2015. Vinylogous Urethane Vitrimers. *Adv. Funct. Mater.* **25**, 2451–2457. <https://doi.org/10.1002/adfm.201404553>

Desroches, M., Escouvois, M., Auvergne, R., Caillol, S., Boutevin, B., 2012. From Vegetable Oils to Polyurethanes: Synthetic Routes to Polyols and Main Industrial Products. *Polym. Rev.* **52**, 38–79. <https://doi.org/10.1080/15583724.2011.640443>

Dileone, R.R., 1970. Synthesis of poly-2-oxazolidones from diisocyanates and diepoxides. *J. Polym. Sci. [A1]* **8**, 609–615. <https://doi.org/10.1002/pol.1970.150080304>

Dong, T., Laurens, L.M.L., Pienkos, P.T., Fabian Spinelli, P., 2020. Renewable Polymers and resins and methods of making the same. US2020/0017638.

D'Souza, J., Camargo, R., Yan, N., 2017. Biomass Liquefaction and Alkoxylation: A Review of Structural Characterization Methods for Bio-based Polyols. *Polym. Rev.* **57**, 668–694. <https://doi.org/10.1080/15583724.2017.1283328>

D'Souza, J., Camargo, R., Yan, N., 2014. Polyurethane foams made from liquefied bark-based polyols. *J. Appl. Polym. Sci.* **131**, 40599. <https://doi.org/10.1002/app.40599>

Duquesne, S., Le Bras, M., Bourbigot, S., Delobel, R., Camino, G., Eling, B., Lindsay, C., Roels, T., Vezin, H., 2001. Mechanism of fire retardancy of polyurethanes using ammonium polyphosphate. *J. Appl. Polym. Sci.* **82**, 3262–3274. <https://doi.org/10.1002/app.2185>

Duquesne, S., Le Bras, M., Bourbigot, S., Delobel, R., Poutch, F., Camino, G., Eling, B., Lindsay, C., Roels, T., 2000. Analysis of Fire Gases Released from Polyurethane and Fire-Retarded Polyurethane Coatings. *J. Fire Sci.* **18**, 456–482. <https://doi.org/10.1106/6CRG-Q8VD-PV3G-ELDD>

Durán Pachón, L., Gamez, P., van Brussel, J.J.M., Reedijk, J., 2003. Zinc-catalyzed aminolysis of epoxides. *Tetrahedron Lett.* **44**, 6025–6027. [https://doi.org/10.1016/S0040-4039\(03\)01480-1](https://doi.org/10.1016/S0040-4039(03)01480-1)

Durbetaki, A.J., 1956. Direct Titration of Oxirane Oxygen with Hydrogen Bromide in Acetic Acid. *Anal. Chem.* **28**, 2000–2001. <https://doi.org/10.1021/ac60120a055>

Dussenne, C., Delaunay, T., Wiatz, V., Wyart, H., Suisse, I., Sauthier, M., 2017. Synthesis of isosorbide: an overview of challenging reactions. *Green Chem.* **19**, 5332–5344. <https://doi.org/10.1039/C7GC01912B>

LISTE COMPLÈTE DES RÉFÉRENCES BIBLIOGRAPHIQUES

Duval, A., Avérus, L., 2017. Cyclic Carbonates as Safe and Versatile Etherifying Reagents for the Functionalization of Lignins and Tannins. *ACS Sustain. Chem. Eng.* **5**, 7334–7343. <https://doi.org/10.1021/acssuschemeng.7b01502>

Duval, A., Avérus, L., 2016. Oxyalkylation of Condensed Tannin with Propylene Carbonate as an Alternative to Propylene Oxide. *ACS Sustain. Chem. Eng.* **4**, 3103–3112. <https://doi.org/10.1021/acssuschemeng.6b00081>

Dworakowska, S., Cornille, A., Bogdał, D., Boutevin, B., Caillol, S., 2015. Formulation of bio-based epoxy foams from epoxidized cardanol and vegetable oil amine: Cardanol-based epoxy foams. *Eur. J. Lipid Sci. Technol.* **117**, 1893–1902. <https://doi.org/10.1002/ejlt.201500232>

Dyen, M.E., Swern, D., 1968. Chemistry of epoxy compounds. xxii. preparation of some long-cham 2-oxazolidones. *J. Am. Oil Chem. Soc.* **45**, 325–330. <https://doi.org/10.1007/BF02667102>

Dyer, Elizabeth., Taylor, H.A., Mason, S.J., Samson, Jan., 1949. The Rates of Reaction of Isocyanates with Alcohols. I. Phenyl Isocyanate with 1- and 2-Butanol. *J. Am. Chem. Soc.* **71**, 4106–4109. <https://doi.org/10.1021/ja01180a064>

Ecochard, Y., Auvergne, R., Boutevin, B., Caillol, S., 2020. Linseed Oil-Based Thermosets by Aza-Michael Polymerization. *Eur. J. Lipid Sci. Technol.* **122**, 1900145. <https://doi.org/10.1002/ejlt.201900145>

Erjavec, M., 2011. Mechanical properties of cellular materials. *Fac. Math. Phys. Univ. Ljubl.* **15**.

Espenson, J.H., 1995. Chemical kinetics and reaction mechanisms, 2. ed. ed McGraw Hill series in advanced chemistry. McGraw Hill, New York.

Fabris, M., Abbriano, R.M., Pernice, M., Sutherland, D.L., Commault, A.S., Hall, C.C., Labeeuw, L., McCauley, J.I., Kuzhiuparambil, U., Ray, P., Kahlke, T., Ralph, P.J., 2020. Emerging Technologies in Algal Biotechnology: Toward the Establishment of a Sustainable, Algae-Based Bioeconomy. *Front. Plant Sci.* **11**, 279. <https://doi.org/10.3389/fpls.2020.00279>

Fallah-Mehrjardi, M., Kiasat, A.R., Niknam, K., 2018. Nucleophilic ring-opening of epoxides: trends in β -substituted alcohols synthesis. *J. Iran. Chem. Soc.* **15**, 2033–2081. <https://doi.org/10.1007/s13738-018-1400-5>

Fan, H., Tekeei, A., Suppes, G.J., Hsieh, F.-H., 2013. Rigid polyurethane foams made from high viscosity soy-polyols. *J. Appl. Polym. Sci.* **127**, 1623–1629. <https://doi.org/10.1002/app.37508>

Fang, Z., Qiu, C., Ji, D., Yang, Z., Zhu, N., Meng, J., Hu, X., Guo, K., 2019. Development of High-Performance Biodegradable Rigid Polyurethane Foams Using Full Modified Soy-Based Polyols. *J. Agric. Food Chem.* **67**, 2220–2226. <https://doi.org/10.1021/acs.jafc.8b05342>

Ferkl, P., Toulec, M., Laurini, E., Pricl, S., Fermeglia, M., Auffarth, S., Eling, B., Settels, V., Kosek, J., 2017. Multi-scale modelling of heat transfer in polyurethane foams. *Chem. Eng. Sci.* **172**, 323–334. <https://doi.org/10.1016/j.ces.2017.06.035>

Ferraboschi, P., Casati, S., Grisenti, P., Santaniello, E., 1994. Selective enzymatic transformations of itaconic acid derivatives: An access to potentially useful building blocks. *Tetrahedron* **50**, 3251–3258. [https://doi.org/10.1016/S0040-4020\(01\)81120-0](https://doi.org/10.1016/S0040-4020(01)81120-0)

Figovsky, O., Shapovalov, L., Potashnikov, R., Tzaid, Y., Bordado, J.C., Letnik, D., De Schijuer, A., 2004. Foamable photo-polymerized composition. US 2004/0176485 A1.

Fink, J.K., 2018. Poly(urethane)s. In 'Reactive Polymers: Fundamentals and Applications'. Elsevier, pp. 71–138. <https://doi.org/10.1016/B978-0-12-814509-8.00002-6>

Flores, M., Fernández-Francos, X., Moráncho, J.M., Serra, À., Ramis, X., 2012. Ytterbium triflate as a new catalyst on the curing of epoxy-isocyanate based thermosets. *Thermochim. Acta* **543**, 188–196. <https://doi.org/10.1016/j.tca.2012.05.012>

Flory, P.J., 1941. Molecular Size Distribution in Three Dimensional Polymers. I. Gelation. *J. Am. Chem. Soc.* **63**, 3083–3090. <https://doi.org/10.1021/ja01856a061>

Fourati, Y., Hassen, R.B., Bayramoğlu, G., Boufi, S., 2017. A one step route synthesis of polyurethane network from epoxidized rapeseed oil. *Prog. Org. Coat.* **105**, 48–55. <https://doi.org/10.1016/j.porgcoat.2016.12.021>

Frey, J.H., Grimminger, J., Stevens, R.E., 1996. New Silicone Surfactants for Rigid Polyurethane Foam. Presented at the UTECH, p. 24.

Fridrihsone-Girone, A., Stirna, U., Misāne, M., Lazdiņa, B., Deme, L., 2016. Spray-applied 100% volatile organic compounds free two component polyurethane coatings based on rapeseed oil polyols. *Prog. Org. Coat.* **94**, 90–97. <https://doi.org/10.1016/j.porgcoat.2015.11.022>

Froidevaux, V., Negrell, C., Caillol, S., Pascault, J.-P., Boutevin, B., 2016. Biobased Amines: From Synthesis to Polymers; Present and Future. *Chem. Rev.* **116**, 14181–14224. <https://doi.org/10.1021/acs.chemrev.6b00486>

Furtwengler, P., Avérus, L., 2018. Renewable polyols for advanced polyurethane foams from diverse biomass resources. *Polym. Chem.* **9**, 4258–4287. <https://doi.org/10.1039/C8PY00827B>

LISTE COMPLÈTE DES RÉFÉRENCES BIBLIOGRAPHIQUES

Furtwengler, P., Boumbimba, R.M., Avérous, L., 2018a. Elaboration and Characterization of Advanced Biobased Polyurethane Foams Presenting Anisotropic Behavior. *Macromol. Mater. Eng.* **303**, 1700501. <https://doi.org/10.1002/mame.201700501>

Furtwengler, P., Matadi Boumbimba, R., Sarbu, A., Avérous, L., 2018b. Novel Rigid Polyisocyanurate Foams from Synthesized Biobased Polyester Polyol with Enhanced Properties. *ACS Sustain. Chem. Eng.* **6**, 6577–6589. <https://doi.org/10.1021/acssuschemeng.8b00380>

Furtwengler, P., Perrin, R., Redl, A., Avérous, L., 2017. Synthesis and characterization of polyurethane foams derived of fully renewable polyester polyols from sorbitol. *Eur. Polym. J.* **97**, 319–327. <https://doi.org/10.1016/j.eurpolymj.2017.10.020>

Gaidukova, G., Ivdre, A., Fridrihsone, A., Verovkins, A., Cabulis, U., Gaidukovs, S., 2017. Polyurethane rigid foams obtained from polyols containing bio-based and recycled components and functional additives. *Ind. Crops Prod.* **102**, 133–143. <https://doi.org/10.1016/j.indcrop.2017.03.024>

Gaikwad, M.S., Gite, V.V., Mahulikar, P.P., Hundiwale, D.G., Yemul, O.S., 2015. Eco-friendly polyurethane coatings from cottonseed and karanja oil. *Prog. Org. Coat.* **86**, 164–172. <https://doi.org/10.1016/j.porgcoat.2015.05.014>

Galante, M.J., Williams, R.J.J., 1995. Polymer networks based on the diepoxide–diisocyanate reaction catalyzed by tertiary amines. *J. Appl. Polym. Sci.* **55**, 89–98. <https://doi.org/10.1002/app.1995.070550109>

Gale, C.B., Chin, B., Tambe, C., Graiver, D., Brook, M.A., 2019. Silicone Structurants for Soybean Oil: Foams, Elastomers, and Candles. *ACS Sustain. Chem. Eng.* **7**, 1347–1352. <https://doi.org/10.1021/acssuschemeng.8b05047>

Galià, M., de Espinosa, L.M., Ronda, J.C., Lligadas, G., Cádiz, V., 2010. Vegetable oil-based thermosetting polymers. *Eur. J. Lipid Sci. Technol.* **112**, 87–96. <https://doi.org/10.1002/ejlt.200900096>

Gan, L.H., Goh, S.H., Ooi, K.S., 1992. Kinetic studies of epoxidation and oxirane cleavage of palm olein methyl esters. *J. Am. Oil Chem. Soc.* **69**, 347–351. <https://doi.org/10.1007/BF02636065>

Gandhi, T.S., Patel, M.R., Dholakiya, B.Z., 2015. Mechanical, thermal and fire properties of sustainable rigid polyurethane foam derived from cashew nut shell liquid. *Int. J. Plast. Technol.* **19**, 30–46. <https://doi.org/10.1007/s12588-015-9114-3>

Gandini, A., Lacerda, T.M., 2015. From monomers to polymers from renewable resources: Recent advances. *Prog. Polym. Sci.* **48**, 1–39. <https://doi.org/10.1016/j.progpolymsci.2014.11.002>

Gandini, A., Lacerda, T.M., Carvalho, A.J.F., Trovatti, E., 2016. Progress of Polymers from Renewable Resources: Furans, Vegetable Oils, and Polysaccharides. *Chem. Rev.* **116**, 1637–1669. <https://doi.org/10.1021/acs.chemrev.5b00264>

Gao, L., Zheng, G., Zhou, Y., Hu, L., Feng, G., 2015. Improved mechanical property, thermal performance, flame retardancy and fire behavior of lignin-based rigid polyurethane foam nanocomposite. *J. Therm. Anal. Calorim.* **120**, 1311–1325. <https://doi.org/10.1007/s10973-015-4434-2>

García, D.E., Glasser, W.G., Pizzi, A., Paczkowski, S.P., Laborie, M.-P., 2016. Modification of condensed tannins: from polyphenol chemistry to materials engineering. *New J. Chem.* **40**, 36–49. <https://doi.org/10.1039/C5NJ02131F>

Garg, P., Kumar, P., Srinivasan, K., Dutta, P., 2013. Evaluation of isopentane, R-245fa and their mixtures as working fluids for organic Rankine cycles. *Appl. Therm. Eng.* **51**, 292–300. <https://doi.org/10.1016/j.applthermaleng.2012.08.056>

Garside, M., 2020. Production capacity of bioplastics worldwide from 2017 to 2024, by type [WWW Document]. *Statista*. URL <https://www.statista.com/statistics/678684/global-production-capacity-of-bioplastics-by-type/#statisticContainer> (accessed 8.25.20).

Ge, J., Shi, X., Cai, M., Wu, R., Wang, M., 2003. A novel biodegradable antimicrobial PU foam from wattle tannin. *J. Appl. Polym. Sci.* **90**, 2756–2763. <https://doi.org/10.1002/app.12928>

Ge, J., Zhong, W., Guo, Z., Li, W., Sakai, K., 2000. Biodegradable polyurethane materials from bark and starch. I. Highly resilient foams. *J. Appl. Polym. Sci.* **77**, 2575–2580. [https://doi.org/10.1002/1097-4628\(20000919\)77:12<2575::AID-APP30>3.0.CO;2-L](https://doi.org/10.1002/1097-4628(20000919)77:12<2575::AID-APP30>3.0.CO;2-L)

Ghaderian, A., Haghghi, A.H., Taromi, F.A., Abdeen, Z., Boroomand, A., Taheri, S.M.-R., 2015. Characterization of Rigid Polyurethane Foam Prepared from Recycling of PET Waste. *Period. Polytech. Chem. Eng.* **59**, 296–305. <https://doi.org/10.3311/PPch.7801>

Ghasemlou, M., Daver, F., Ivanova, E.P., Adhikari, B., 2019a. Polyurethanes from seed oil-based polyols: A review of synthesis, mechanical and thermal properties. *Ind. Crops Prod.* **142**, 111841. <https://doi.org/10.1016/j.indcrop.2019.111841>

Ghasemlou, M., Daver, F., Ivanova, E.P., Adhikari, B., 2019b. Bio-based routes to synthesize cyclic carbonates and polyamines precursors of non-isocyanate polyurethanes: A review. *Eur. Polym. J.* **118**, 668–684. <https://doi.org/10.1016/j.eurpolymj.2019.06.032>

LISTE COMPLÈTE DES RÉFÉRENCES BIBLIOGRAPHIQUES

Ghosh, T., Karak, N., 2018. Biobased Multifunctional Macroglycol Containing Smart Thermoplastic Hyperbranched Polyurethane Elastomer with Intrinsic Self-Healing Attribute. *ACS Sustain. Chem. Eng.* **6**, 4370–4381. <https://doi.org/10.1021/acssuschemeng.8b00001>

Gibb, J.N., Goodman, J.M., 2013. The formation of high-purity isocyanurate through proazaphosphatrane-catalysed isocyanate cyclo-trimerisation: computational insights. *Org. Biomol. Chem.* **11**, 90–97. <https://doi.org/10.1039/C2OB26547H>

Gibson, L.J., Ashby, M.F., 1997. The mechanics of foams: Basic results. In 'Cellular Solids: Structure and Properties'. Cambridge University Press. <https://doi.org/10.1017/CBO9781139878326>

Gil, B., Kasperski, J., 2018. Efficiency Evaluation of the Ejector Cooling Cycle using a New Generation of HFO/HCFO Refrigerant as a R134a Replacement. *Energies* **11**, 2136. <https://doi.org/10.3390/en11082136>

Gordon, J.M., Polle, J.E.W., 2007. Ultrahigh bioproduction from algae. *Appl. Microbiol. Biotechnol.* **76**, 969–975. <https://doi.org/10.1007/s00253-007-1102-x>

Greim, H., Bury, D., Klimisch, H.-J., Oeben-Negele, M., Ziegler-Skylakakis, K., 1998. Toxicity of aliphatic amines: Structure-activity relationship. *Chemosphere* **36**, 271–295. [https://doi.org/10.1016/S0045-6535\(97\)00365-2](https://doi.org/10.1016/S0045-6535(97)00365-2)

Grignard, B., Thomassin, J.-M., Gennen, S., Poussard, L., Bonnaud, L., Raquez, J.-M., Dubois, P., Tran, M.-P., Park, C.B., Jerome, C., Detrembleur, C., 2016. CO₂ -blown microcellular non-isocyanate polyurethane (NIPU) foams: from bio- and CO₂ -sourced monomers to potentially thermal insulating materials. *Green Chem.* **18**, 2206–2215. <https://doi.org/10.1039/C5GC02723C>

Grunwald, P. (Ed.), 2016. Handbook of carbohydrate-modifying biocatalysts 'Pan Stanford series on biocatalysis. Pan Stanford Publishing, Singapore.

Guan, J., Song, Y., Lin, Y., Yin, X., Zuo, M., Zhao, Y., Tao, X., Zheng, Q., 2011. Progress in Study of Non-Isocyanate Polyurethane. *Ind. Eng. Chem. Res.* **50**, 6517–6527. <https://doi.org/10.1021/ie101995j>

Gunstone, F.D., Harwood, J.L., Harwood, J.L., 2007. The Lipid Handbook with CD-ROM, 3rd ed. CRC Press. <https://doi.org/10.1201/9781420009675>

Guo, A., Cho, Y., Petrović, Z.S., 2000. Structure and properties of halogenated and nonhalogenated soy-based polyols. *J. Polym. Sci. Part Polym. Chem.* **38**, 3900–3910. [https://doi.org/10.1002/1099-0518\(20001101\)38:21<3900::AID-POLA70>3.0.CO;2-E](https://doi.org/10.1002/1099-0518(20001101)38:21<3900::AID-POLA70>3.0.CO;2-E)

Gupta, R.K., Ionescu, M., Wan, X., Radojcic, D., Petrović, Z.S., 2015. Synthesis of a Novel Limonene Based Mannich Polyol for Rigid Polyurethane Foams. *J. Polym. Environ.* **23**, 261–268. <https://doi.org/10.1007/s10924-015-0717-8>

Gustini, L., Lavilla, C., Finzel, L., Noordover, B.A.J., Hendrix, M.M.R.M., Koning, C.E., 2016. Sustainable coatings from bio-based, enzymatically synthesized polyesters with enhanced functionalities. *Polym. Chem.* **7**, 6586–6597. <https://doi.org/10.1039/C6PY01339B>

Gustini, L., Noordover, B.A.J., Gehrels, C., Dietz, C., Koning, C.E., 2015. Enzymatic synthesis and preliminary evaluation as coating of sorbitol-based, hydroxy-functional polyesters with controlled molecular weights. *Eur. Polym. J.* **67**, 459–475. <https://doi.org/10.1016/j.eurpolymj.2014.12.025>

Hablot, E., Zheng, D., Bouquey, M., Avérous, L., 2008. Polyurethanes Based on Castor Oil: Kinetics, Chemical, Mechanical and Thermal Properties. *Macromol. Mater. Eng.* **293**, 922–929. <https://doi.org/10.1002/mame.200800185>

HAGERMAN, A., 2002. Tannin handbook. <http://www.users.muohio.edu/hagermae/>.

Halley, P.J., Avérous, L., 2014. Starch polymers: from genetic engineering to green applications. Elsevier, Burlington, MA.

Harry-O'kuru, R.E., Tisserat, B., Gordon, S.H., Gravett, A., 2015. Osage Orange (*Maclura pomifera* L.) Seed Oil Poly(α-hydroxydibutylamine) Triglycerides: Synthesis and Characterization. *J. Agric. Food Chem.* **63**, 6588–6595. <https://doi.org/10.1021/acs.jafc.5b01625>

de Haseth, J.A., Andrews, J.E., McClusky, J.V., Priester, R.D., Harthcock, M.A., Davis, B.L., 1993. Characterization of Polyurethane Foams by Mid-Infrared Fiber/FT-IR Spectrometry. *Appl. Spectrosc.* **47**, 173–179. <https://doi.org/10.1366/0003702934048334>

Hatakeyama, H., Hatakeyama, T., 2005. Environmentally Compatible Hybrid-Type Polyurethane Foams Containing Saccharide and Lignin Components. *Macromol. Symp.* **224**, 219–226. <https://doi.org/10.1002/masy.200550619>

Hatakeyama, H., Hirogaki, A., Matsumura, H., Hatakeyama, T., 2013. Glass transition temperature of polyurethane foams derived from lignin by controlled reaction rate. *J. Therm. Anal. Calorim.* **114**, 1075–1082. <https://doi.org/10.1007/s10973-013-3132-1>

Hatakeyama, T., Matsumoto, Y., Asano, Y., Hatakeyama, H., 2004. Glass transition of rigid polyurethane foams derived from sodium lignosulfonate mixed with diethylene, triethylene and polyethylene glycols. *Thermochim. Acta* **416**, 29–33. <https://doi.org/10.1016/j.tca.2002.12.002>

Hawkins, M.C., O'Toole, B., Jackovich, D., 2005. Cell Morphology and Mechanical Properties of Rigid Polyurethane Foam. *J. Cell. Plast.* **41**, 267–285. <https://doi.org/10.1177/0021955X05053525>

Hayati, A.N., Evans, D.A.C., Laycock, B., Martin, D.J., Annamalai, P.K., 2018. A simple methodology for improving the performance and sustainability of rigid polyurethane foam by incorporating industrial lignin. *Ind. Crops Prod.* **117**, 149–158. <https://doi.org/10.1016/j.indcrop.2018.03.006>

Hejna, A., Kirpluks, M., Kosmela, P., Cabulis, U., Haponiuk, J., Piszczyk, Ł., 2017. The influence of crude glycerol and castor oil-based polyol on the structure and performance of rigid polyurethane-polyisocyanurate foams. *Ind. Crops Prod.* **95**, 113–125. <https://doi.org/10.1016/j.indcrop.2016.10.023>

Hejna, A., Kosmela, P., Kirpluks, M., Cabulis, U., Klein, M., Haponiuk, J., Piszczyk, Ł., 2018. Structure, Mechanical, Thermal and Fire Behavior Assessments of Environmentally Friendly Crude Glycerol-Based Rigid Polyisocyanurate Foams. *J. Polym. Environ.* **26**, 1854–1868. <https://doi.org/10.1007/s10924-017-1086-2>

Herrán, R., Amalvy, J.I., Chiacciarelli, L.M., 2019. Highly functional lactic acid ring-opened soybean polyols applied to rigid polyurethane foams. *J. Appl. Polym. Sci.* **136**, 47959. <https://doi.org/10.1002/app.47959>

Herweh, J.E., Foglia, T.A., Swern, D., 1968. Synthesis and nuclear magnetic resonance spectra of 2-oxazolidones. *J. Org. Chem.* **33**, 4029–4033. <https://doi.org/10.1021/jo01275a007>

Herweh, J.K., 1968. Bis-2-oxazolidones-preparation and characterization. *J. Heterocycl. Chem.* **5**, 687–690.

Herzberger, J., Niederer, K., Pohlitz, H., Seiwert, J., Worm, M., Wurm, F.R., Frey, H., 2016. Polymerization of Ethylene Oxide, Propylene Oxide, and Other Alkylene Oxides: Synthesis, Novel Polymer Architectures, and Bioconjugation. *Chem. Rev.* **116**, 2170–2243. <https://doi.org/10.1021/acs.chemrev.5b00441>

Hicks, D., Austin, A., 2017. A review of the global PU industry 2016 and outlook for 2017. *PU Mag.* **14**, 4–16.

Hill, R.M., 2019. Siloxane Surfactants. In 'Silicone Surfactants' (Ed. Hill, R.M.). Routledge, pp. 1–48. <https://doi.org/10.1201/9780203739754-1>

Hilyard, N.C., Cunningham, A. (Eds.), 1994. Low density cellular plastics: Physical basis of behaviour. Springer Netherlands, Dordrecht. <https://doi.org/10.1007/978-94-011-1256-7>

Hilyard, N.C., Cunningham, A., Glicksman, L.R., 2012. Heat transfer in foams. In 'Low Density Cellular Plastics: Physical Basis of Behaviour'. Springer Netherlands, Dordrecht.

Hoffman, D.K., 1984. Model System for a Urethane-Modified Isocyanurate Foam. *J. Cell. Plast.* **20**, 129–137. <https://doi.org/10.1177/0021955X8402000205>

Hojabri, L., Kong, X., Narine, S.S., 2010. Novel long chain unsaturated diisocyanate from fatty acid: Synthesis, characterization, and application in bio-based polyurethane. *J. Polym. Sci. Part Polym. Chem.* **48**, 3302–3310. <https://doi.org/10.1002/pola.24114>

Holfinger, M.S., Conner, A.H., Holm, D.R., Hill, C.G., 1995. Synthesis of Difurfuryl Diamines by the Acidic Condensation of Furfurylamine with Aldehydes and Their Mechanism of Formation. *J. Org. Chem.* **60**, 1595–1598. <https://doi.org/10.1021/jo00111a017>

Howell, B.A., Oberdorfer, K.L., Ostrander, E.A., 2018. Phosphorus Flame Retardants for Polymeric Materials from Gallic Acid and Other Naturally Occurring Multihydroxybenzoic Acids. *Int. J. Polym. Sci.* **2018**, 1–12. <https://doi.org/10.1155/2018/7237236>

Hu, M., Hwang, J.-Y., Kurth, M.J., Hsieh, Y.-L., Shoemaker, C.F., Krochta, J.M., 1997. Polyurethane Rigid Foam Derived from Reduced Sweet Whey Permeate. *J. Agric. Food Chem.* **45**, 4156–4161. <https://doi.org/10.1021/jf9701650>

Hu, S., Luo, X., Li, Y., 2014. Polyols and Polyurethanes from the Liquefaction of Lignocellulosic Biomass. *ChemSusChem* **7**, 66–72. <https://doi.org/10.1002/cssc.201300760>

Hu, S., Wan, C., Li, Y., 2012. Production and characterization of biopolymers and polyurethane foams from crude glycerol based liquefaction of soybean straw. *Bioresour. Technol.* **103**, 227–233. <https://doi.org/10.1016/j.biortech.2011.09.125>

Hu, Y., Tian, Y., Cheng, J., Zhang, J., 2020. Synthesis of Eugenol-Based Polyols via Thiol-Ene Click Reaction and High-Performance Thermosetting Polyurethane Therefrom. *ACS Sustain. Chem. Eng.* **8**, 4158–4166. <https://doi.org/10.1021/acssuschemeng.9b06867>

Huang, X., Yang, X., Liu, H., Shang, S., Cai, Z., Wu, K., 2019. Bio-based thermosetting epoxy foams from epoxidized soybean oil and rosin with enhanced properties. *Ind. Crops Prod.* **139**, 111540. <https://doi.org/10.1016/j.indcrop.2019.111540>

Huo, S., Jin, C., Liu, G., Chen, J., Wu, G., Kong, Z., 2019. Preparation and properties of biobased autocatalytic polyols and their polyurethane foams. *Polym. Degrad. Stab.* **159**, 62–69. <https://doi.org/10.1016/j.polymdegradstab.2018.11.019>

Huo, S.-P., Nie, M.-C., Kong, Z.-W., Wu, G.-M., Chen, J., 2012. Crosslinking kinetics of the formation of lignin-aminated polyol-based polyurethane foam. *J. Appl. Polym. Sci.* **125**, 152–157. <https://doi.org/10.1002/app.35401>

LISTE COMPLÈTE DES RÉFÉRENCES BIBLIOGRAPHIQUES

IEA, 2020. World Energy Balances: Overview [WWW Document]. *iea.org*. URL <https://www.iea.org/reports/world-energy-balances-overview> (accessed 8.15.20).

Ionescu, M., 2005. Chemistry and technology of polyols for polyurethanes, 1st ed. Rapra Technology, Shawbury, Shrewsbury, Shropshire, U.K.

Ionescu, M., Petrović, Z.S., 2010. High Functionality Polyether Polyols Based on Polyglycerol. *J. Cell. Plast.* **46**, 223–237. <https://doi.org/10.1177/0021955X09355887>

Ionescu, M., Radojčić, D., Wan, X., Shrestha, M.L., Petrović, Z.S., Upshaw, T.A., 2016. Highly functional polyols from castor oil for rigid polyurethanes. *Eur. Polym. J.* **84**, 736–749. <https://doi.org/10.1016/j.eurpolymj.2016.06.006>

Ionescu, M., Wan, X., Bilić, N., Petrović, Z.S., 2012. Polyols and Rigid Polyurethane Foams from Cashew Nut Shell Liquid. *J. Polym. Environ.* **20**, 647–658. <https://doi.org/10.1007/s10924-012-0467-9>

Isikgor, F.H., Becer, C.R., 2015. Lignocellulosic biomass: a sustainable platform for the production of bio-based chemicals and polymers. *Polym. Chem.* **6**, 4497–4559. <https://doi.org/10.1039/C5PY00263J>

Iwata, T., 2015. Biodegradable and Bio-Based Polymers: Future Prospects of Eco-Friendly Plastics. *Angew. Chem. Int. Ed.* **54**, 3210–3215. <https://doi.org/10.1002/anie.201410770>

J. C. Thompson, B. B. He, 2006. Characterization of crude glycerol from biodiesel production from multiple feedstocks. *Appl. Eng. Agric.* **22**, 261–265. <https://doi.org/10.13031/2013.20272>

Jacobsberg, B., Oh Chuan Ho, 1976. Studies in palm oil crystallization. *J. Am. Oil Chem. Soc.* **53**, 609–617. <https://doi.org/10.1007/BF02586272>

Janvier, M., Hollande, L., Jaufurally, A.S., Pernes, M., Ménard, R., Grimaldi, M., Beaugrand, J., Balaguer, P., Ducrot, P.-H., Allais, F., 2017. Syringaresinol: A Renewable and Safer Alternative to Bisphenol A for Epoxy-Amine Resins. *ChemSusChem* **10**, 738–746. <https://doi.org/10.1002/cssc.201601595>

Jaratrotkamjorn, R., Tanrattanakul, V., 2020. Bio-based flexible polyurethane foam synthesized from palm oil and natural rubber. *J. Appl. Polym. Sci.* **137**, 49310. <https://doi.org/10.1002/app.49310>

Jarfelt, U., Ramnäs, O., 2006. Thermal conductivity of polyurethane foam Best performance. Presented at the 10th International Symposium on district heating and cooling, Chalmers University of Technology Goteborg, Sweden, pp. 3–5.

Jasiūnas, L., McKenna, S.T., Bridžiuvienė, D., Miknius, L., 2020. Mechanical, Thermal Properties and Stability of Rigid Polyurethane Foams Produced with Crude-Glycerol Derived Biomass Biopolymers. *J. Polym. Environ.* **28**, 1378–1389. <https://doi.org/10.1007/s10924-020-01686-y>

Javaid, M.A., Zia, K.M., Iqbal, A., Ahmad, S., Akram, N., Liu, X., Nawaz, H., Khosa, M.K., Awais, M., 2020. Utilization of waxy corn starch as an efficient chain extender for the preparation of polyurethane elastomers. *Int. J. Biol. Macromol.* **148**, 415–423. <https://doi.org/10.1016/j.ijbiomac.2020.01.011>

Javni, I., Guo, A., Petrovic, Z.S., 2003. The study of oxazolidone formation from 9,10-epoxyoctadecane and phenylisocyanate. *J. Am. Oil Chem. Soc.* **80**, 595–600. <https://doi.org/10.1007/s11746-003-0744-7>

Jiang, T., Wang, W., Yu, D., Huang, D., Wei, N., Hu, Y., Huang, H., 2018. Synthesis and characterization of polyurethane rigid foams from polyether polyols with isosorbide as the bio-based starting agent. *J. Polym. Res.* **25**, 140. <https://doi.org/10.1007/s10965-018-1538-y>

Jiang, Y., Loos, K., 2016. Enzymatic Synthesis of Biobased Polyesters and Polyamides. *Polymers* **8**, 243. <https://doi.org/10.3390/polym8070243>

John, J., Bhattacharya, M., Turner, R.B., 2002. Characterization of polyurethane foams from soybean oil. *J. Appl. Polym. Sci.* **86**, 3097–3107. <https://doi.org/10.1002/app.11322>

de Jong, E., Dam, M.A., Sipos, L., Gruter, G.-J.M., 2012. Furandicarboxylic Acid (FDCA), A Versatile Building Block for a Very Interesting Class of Polyesters. In 'Biobased Monomers, Polymers, and Materials' 'ACS Symposium Series' (Eds. Smith, P.B., Gross, R.A.). American Chemical Society, Washington, DC, pp. 1–13. <https://doi.org/10.1021/bk-2012-1105.ch001>

Jongedijk, E., Cankar, K., Buchhaupt, M., Schrader, J., Bouwmeester, H., Beekwilder, J., 2016. Biotechnological production of limonene in microorganisms. *Appl. Microbiol. Biotechnol.* **100**, 2927–2938. <https://doi.org/10.1007/s00253-016-7337-7>

Kadurina, T.I., Prokopenko, V.A., Omelchenko, S.I., 1992. Curing of epoxy oligomers by isocyanates. *Polymer* **33**, 3858–3864. [https://doi.org/10.1016/0032-3861\(92\)90373-5](https://doi.org/10.1016/0032-3861(92)90373-5)

Kahlerras, Z., Irinislimane, R., Bruzaud, S., Belhaneche-Bensemra, N., 2020. Elaboration and Characterization of Polyurethane Foams Based on Renewably Sourced Polyols. *J. Polym. Environ.* **28**, 3003–3018. <https://doi.org/10.1007/s10924-020-01833-5>

Kang, M.J., Kim, Y.H., Park, G.P., Han, M.S., Kim, W.N., Park, S.D., 2010. Liquid nucleating additives for improving thermal insulating properties and mechanical strength of polyisocyanurate foams. *J. Mater. Sci.* **45**, 5412–5419. <https://doi.org/10.1007/s10853-010-4594-1>

Karunaratna, M.S., Smith, R.C., 2020. Valorization of Lignin as a Sustainable Component of Structural Materials and Composites: Advances from 2011 to 2019. *Sustainability* **12**, 734. <https://doi.org/10.3390/su12020734>

LISTE COMPLÈTE DES RÉFÉRENCES BIBLIOGRAPHIQUES

Katritzky, A.R., Lagowski, J.M., 1967. Heterocyclic Compounds with Three- and Four-Membered Rings. In 'The Principles of Heterocyclic Chemistry'. Elsevier, pp. 159–164. <https://doi.org/10.1016/B978-1-4832-3304-8.50009-9>

Kaur, R., Kumar, M., 2020. Addition of anti-flaming agents in castor oil based rigid polyurethane foams: studies on mechanical and flammable behaviour. *Mater. Res. Express* **7**, 015333. <https://doi.org/10.1088/2053-1591/ab68a2>

Kausar, A., 2018. Polyurethane Composite Foams in High-Performance Applications: A Review. *Polym.-Plast. Technol. Eng.* **57**, 346–369. <https://doi.org/10.1080/03602559.2017.1329433>

Kaushiva, B.D., 1999. Structure-Property Relationships Of Flexible Polyurethane Foams (Dissertation). Virginia Polytechnic Institute and State University, Blacksburg, Virginia.

Kenaston, C.B., Wilbur, K.M., Ottolenghi, A., Bernheim, F., 1955. Comparison of methods for determining fatty acid oxidation produced by ultraviolet irradiation. *J. Am. Oil Chem. Soc.* **32**, 33–35. <https://doi.org/10.1007/BF02636476>

Khanderay, J.C., Gite, V.V., 2019. Fully biobased polyester polyols derived from renewable resources toward preparation of polyurethane and their application for coatings. *J. Appl. Polym. Sci.* **47558**. <https://doi.org/10.1002/app.47558>

Khundamri, N., Aouf, C., Fulcrand, H., Dubreucq, E., Tanrattanakul, V., 2019. Bio-based flexible epoxy foam synthesized from epoxidized soybean oil and epoxidized mangosteen tannin. *Ind. Crops Prod.* **128**, 556–565. <https://doi.org/10.1016/j.indcrop.2018.11.062>

Kim, Y.-H., Koczo, K., Wasan, D.T., 1997. Dynamic Film and Interfacial Tensions in Emulsion and Foam Systems. *J. Colloid Interface Sci.* **187**, 29–44. <https://doi.org/10.1006/jcis.1996.4507>

Kinjo, N., Numata, S.-I., Koyama, T., Narahara, T., 1983. Synthesis and viscoelastic properties of new thermosetting resins having isocyanurate and oxazolidone rings in their molecular structures. *J. Appl. Polym. Sci.* **28**, 1729–1741. <https://doi.org/10.1002/app.1983.070280516>

Knölker, H.-J., Braxmeier, T., Schlechtingen, G., 1995. A Novel Method for the Synthesis of Isocyanates Under Mild Conditions. *Angew. Chem. Int. Ed. Engl.* **34**, 2497–2500. <https://doi.org/10.1002/anie.199524971>

Knothe, G., Steidley, K.R., 2005. Kinematic viscosity of biodiesel fuel components and related compounds. Influence of compound structure and comparison to petrodiesel fuel components. *Fuel* **84**, 1059–1065. <https://doi.org/10.1016/j.fuel.2005.01.016>

Kobilka, B., Kuczynski, J., Porter, J., Wertz, J., 2019. Pinene-Derived diisocyanates. US 2019/0106383A1.

Konieczny, J., Loos, K., 2019. Green Polyurethanes from Renewable Isocyanates and Biobased White Dextrans. *Polymers* **11**, 256. <https://doi.org/10.3390/polym11020256>

Kordomenos, P.I., Kresta, J.E., Frisch, K.C., 1987. Thermal stability of isocyanate-based polymers. 2. Kinetics of the thermal dissociation of model urethane, oxazolidone, and isocyanurate block copolymers. *Macromolecules* **20**, 2077–2083. <https://doi.org/10.1021/ma00175a006>

Korntner, P., Sumerskii, I., Bacher, M., Rosenau, T., Potthast, A., 2015. Characterization of technical lignins by NMR spectroscopy: optimization of functional group analysis by ³¹P NMR spectroscopy. *Holzforschung* **69**, 807–814. <https://doi.org/10.1515/hf-2014-0281>

Kosmela, P., Gosz, K., Kazimierski, P., Hejna, A., Haponiuk, J.T., Piszczyk, Ł., 2019. Chemical structures, rheological and physical properties of biopolyols prepared via solvothermal liquefaction of Enteromorpha and Zostera marina biomass. *Cellulose* **26**, 5893–5912. <https://doi.org/10.1007/s10570-019-02540-8>

Kosmela, P., Hejna, A., Formela, K., Haponiuk, J., Piszczyk, Ł., 2018. The Study on Application of Biopolyols Obtained by Cellulose Biomass Liquefaction Performed with Crude Glycerol for the Synthesis of Rigid Polyurethane Foams. *J. Polym. Environ.* **26**, 2546–2554. <https://doi.org/10.1007/s10924-017-1145-8>

Kövilein, A., Kubisch, C., Cai, L., Ochsenreither, K., 2020. Malic acid production from renewables: a review. *J. Chem. Technol. Biotechnol.* **95**, 513–526. <https://doi.org/10.1002/jctb.6269>

Kreye, O., Mutlu, H., Meier, M.A.R., 2013. Sustainable routes to polyurethane precursors. *Green Chem.* **15**, 1431. <https://doi.org/10.1039/c3gc40440d>

Kuhire, S.S., Nagane, S.S., Wadgaonkar, P.P., 2017. Poly(ether urethane)s from aromatic diisocyanates based on lignin-derived phenolic acids: Poly(ether urethane)s from aromatic diisocyanates. *Polym. Int.* **66**, 892–899. <https://doi.org/10.1002/pi.5333>

Kuhn, J., Ebert, H.-P., Arduini-Schuster, M.C., Büttner, D., Fricke, J., 1992. Thermal transport in polystyrene and polyurethane foam insulations. *Int. J. Heat Mass Transf.* **35**, 1795–1801. [https://doi.org/10.1016/0017-9310\(92\)90150-Q](https://doi.org/10.1016/0017-9310(92)90150-Q)

Kurańska, M., Banaś, J., Polaczek, K., Banaś, M., Prociak, A., Kuc, J., Uram, K., Lubera, T., 2019. Evaluation of application potential of used cooking oils in the synthesis of polyol compounds. *J. Environ. Chem. Eng.* **7**, 103506. <https://doi.org/10.1016/j.jece.2019.103506>

LISTE COMPLÈTE DES RÉFÉRENCES BIBLIOGRAPHIQUES

Kurańska, M., Pinto, J.A., Salach, K., Barreiro, M.F., Prociak, A., 2020a. Synthesis of thermal insulating polyurethane foams from lignin and rapeseed based polyols: A comparative study. *Ind. Crops Prod.* **143**, 111882. <https://doi.org/10.1016/j.indcrop.2019.111882>

Kurańska, M., Polaczek, K., Auguścik-Królikowska, M., Prociak, A., Ryszkowska, J., 2020b. Open-cell rigid polyurethane bio-foams based on modified used cooking oil. *Polymer* **190**, 122164. <https://doi.org/10.1016/j.polymer.2020.122164>

Lai, N.A., 2014. Thermodynamic properties of HFO-1243zf and their application in study on a refrigeration cycle. *Appl. Therm. Eng.* **70**, 1–6. <https://doi.org/10.1016/j.applthermaleng.2014.04.042>

Lang, S., Gerschitzka, M., Bauer, D., Drück, H., 2016. Thermal Conductivity of Vacuum Insulation Materials for Thermal Energy Stores in Solar Thermal Systems. *Energy Procedia* **91**, 172–181. <https://doi.org/10.1016/j.egypro.2016.06.196>

Laurichesse, S., Avérous, L., 2014. Chemical modification of lignins: Towards biobased polymers. *Prog. Polym. Sci.* **39**, 1266–1290. <https://doi.org/10.1016/j.progpolymsci.2013.11.004>

Laurichesse, S., Huillet, C., Avérous, L., 2014. Original polyols based on organosolv lignin and fatty acids: new bio-based building blocks for segmented polyurethane synthesis. *Green Chem.* **16**, 3958–3970. <https://doi.org/10.1039/C4GC00596A>

Lee, C.S., Ooi, T.L., Chuah, C.H., Ahmad, S., 2007. Rigid Polyurethane Foam Production from Palm Oil-Based Epoxidized Diethanolamides. *J. Am. Oil Chem. Soc.* **84**, 1161–1167. <https://doi.org/10.1007/s11746-007-1150-5>

Lee, S.-H., Yoshioka, M., Shiraishi, N., 2000. Liquefaction of corn bran (CB) in the presence of alcohols and preparation of polyurethane foam from its liquefied polyol. *J. Appl. Polym. Sci.* **78**, 319–325. [https://doi.org/10.1002/1097-4628\(20001010\)78:2<319::AID-APP120>3.0.CO;2-Z](https://doi.org/10.1002/1097-4628(20001010)78:2<319::AID-APP120>3.0.CO;2-Z)

Lee, S.Y., Kim, H.U., Chae, T.U., Cho, J.S., Kim, J.W., Shin, J.H., Kim, D.I., Ko, Y.-S., Jang, W.D., Jang, Y.-S., 2019. A comprehensive metabolic map for production of bio-based chemicals. *Nat. Catal.* **2**, 18–33. <https://doi.org/10.1038/s41929-018-0212-4>

Li, B., Zhou, M., Huo, W., Cai, D., Qin, P., Cao, H., Tan, T., 2020a. Fractionation and oxypropylation of corn-stover lignin for the production of biobased rigid polyurethane foam. *Ind. Crops Prod.* **143**, 111887. <https://doi.org/10.1016/j.indcrop.2019.111887>

Li, H.-Q., Shao, Q., Luo, H., Xu, J., 2016a. Polyurethane foams from alkaline lignin-based polyether polyol. *J. Appl. Polym. Sci.* **133**, 43261–43267. <https://doi.org/10.1002/app.43261>

Li, P., Xiao, Z., Chang, C., Zhao, S., Xu, G., 2020b. Efficient Synthesis of Biobased Glycerol Levulinate Ketal and Its Application for Rigid Polyurethane Foam Production. *Ind. Eng. Chem. Res.* **59**, 17520–17528. <https://doi.org/10.1021/acs.iecr.9b06038>

Li, Q.F., Feng, Y.L., Wang, J.W., Yin, N., Zhao, Y.H., Kang, M.Q., Wang, X.W., 2016b. Preparation and properties of rigid polyurethane foam based on modified castor oil. *Plast. Rubber Compos.* **45**, 16–21. <https://doi.org/10.1080/14658011.2015.1112538>

Li, Y., Noordover, B.A.J., van Benthem, R.A.T.M., Koning, C.E., 2015. Bio-based poly(urethane urea) dispersions with low internal stabilizing agent contents and tunable thermal properties. *Prog. Org. Coat.* **86**, 134–142. <https://doi.org/10.1016/j.porgcoat.2015.04.018>

Li, Y., Noordover, B.A.J., van Benthem, R.A.T.M., Koning, C.E., 2014. Property profile of poly(urethane urea) dispersions containing dimer fatty acid-, sugar- and amino acid-based building blocks. *Eur. Polym. J.* **59**, 8–18. <https://doi.org/10.1016/j.eurpolymj.2014.06.016>

Li, Y., Ragauskas, A.J., 2012a. Ethanol organosolv lignin-based rigid polyurethane foam reinforced with cellulose nanowhiskers. *RSC Adv.* **2**, 3347. <https://doi.org/10.1039/c2ra00646d>

Li, Y., Ragauskas, A.J., 2012b. Kraft Lignin-Based Rigid Polyurethane Foam. *J. Wood Chem. Technol.* **32**, 210–224. <https://doi.org/10.1080/02773813.2011.652795>

Lim, H., Kim, S.H., Kim, B.K., 2008. Effects of silicon surfactant in rigid polyurethane foams. *Express Polym. Lett.* **2**, 194–200. <https://doi.org/10.3144/expresspolymlett.2008.24>

List, G.R., Kenar, J.A., Moser, B.R., 2017. History of Fatty Acids Chemistry. In 'Fatty Acids Chemistry, Synthesis, and Applications'. Elsevier, pp. 1–22. <https://doi.org/10.1016/B978-0-12-809521-8.00001-5>

Liu, J., Dai, J., Wang, S., Peng, Y., Cao, L., Liu, X., 2020. Facile synthesis of bio-based reactive flame retardant from vanillin and guaiacol for epoxy resin. *Compos. Part B Eng.* **190**, 107926. <https://doi.org/10.1016/j.compositesb.2020.107926>

Liu, X., Gu, X., Sun, J., Zhang, S., 2017. Preparation and characterization of chitosan derivatives and their application as flame retardants in thermoplastic polyurethane. *Carbohydr. Polym.* **167**, 356–363. <https://doi.org/10.1016/j.carbpol.2017.03.011>

Liu, Z., Yu, F., Fang, G., Yang, H., 2009. Performance characterization of rigid polyurethane foam with refined alkali lignin and modified alkali lignin. *J. For. Res.* **20**, 161–164. <https://doi.org/10.1007/s11676-009-0028-9>

LISTE COMPLÈTE DES RÉFÉRENCES BIBLIOGRAPHIQUES

Lligadas, G., Ronda, J.C., Galià, M., Biermann, U., Metzger, J.O., 2006a. Synthesis and characterization of polyurethanes from epoxidized methyl oleate based polyether polyols as renewable resources. *J. Polym. Sci. Part Polym. Chem.* **44**, 634–645. <https://doi.org/10.1002/pola.21201>

Lligadas, G., Ronda, J.C., Galià, M., Cádiz, V., 2007. Polyurethane Networks from Fatty-Acid-Based Aromatic Triols: Synthesis and Characterization. *Biomacromolecules* **8**, 1858–1864. <https://doi.org/10.1021/bm070157k>

Lligadas, G., Ronda, J.C., Galià, M., Cádiz, V., 2006b. Synthesis and properties of thermosetting polymers from a phosphorous-containing fatty acid derivative. *J. Polym. Sci. Part Polym. Chem.* **44**, 5630–5644. <https://doi.org/10.1002/pola.21691>

Lovering, E.G., Laidler, K.J., 1962. KINETIC STUDIES OF SOME ALCOHOL-ISOCYANATE REACTIONS. *Can. J. Chem.* **40**, 31–36. <https://doi.org/10.1139/v62-006>

Lubczak, R., Szczęch, D., Lubczak, J., 2020. From starch to oligoetherols and polyurethane foams. *Polym. Bull.* **77**, 5725–5751. <https://doi.org/10.1007/s00289-019-03052-y>

Luo, X., Li, Y., 2014. Synthesis and Characterization of Polyols and Polyurethane Foams from PET Waste and Crude Glycerol. *J. Polym. Environ.* **22**, 318–328. <https://doi.org/10.1007/s10924-014-0649-8>

Lutjen, A.B., Quirk, M.A., Barbera, A.M., Kolonko, E.M., 2018. Synthesis of (E)-cinnamyl ester derivatives via a greener Steglich esterification. *Bioorg. Med. Chem.* **26**, 5291–5298. <https://doi.org/10.1016/j.bmc.2018.04.007>

Lutz, E.F., 1986. Shell higher olefins process. *J. Chem. Educ.* **63**, 202. <https://doi.org/10.1021/ed063p202>

Magnin, A., Pollet, E., Perrin, R., Ullmann, C., Persillon, C., Phalip, V., Avérous, L., 2019. Enzymatic recycling of thermoplastic polyurethanes: Synergistic effect of an esterase and an amidase and recovery of building blocks. *Waste Manag.* **85**, 141–150. <https://doi.org/10.1016/j.wasman.2018.12.024>

Magnin, A., Pollet, E., Phalip, V., Avérous, L., 2020. Evaluation of biological degradation of polyurethanes. *Biotechnol. Adv.* **39**, 107457. <https://doi.org/10.1016/j.biotechadv.2019.107457>

Mahmood, N., Yuan, Z., Schmidt, J., Charles Xu, C., 2013. Production of polyols via direct hydrolysis of kraft lignin: Effect of process parameters. *Bioresour. Technol.* **139**, 13–20. <https://doi.org/10.1016/j.biotech.2013.03.199>

Mahmood, N., Yuan, Z., Schmidt, J., Tymchyshyn, M., Xu, C.C., 2016. Hydrolytic liquefaction of hydrolysis lignin for the preparation of bio-based rigid polyurethane foam. *Green Chem.* **18**, 2385–2398. <https://doi.org/10.1039/C5GC02876K>

Mahmood, N., Yuan, Z., Schmidt, J., Xu, C.C., 2015. Preparation of bio-based rigid polyurethane foam using hydrolytically depolymerized Kraft lignin via direct replacement or oxypropylation. *Eur. Polym. J.* **68**, 1–9. <https://doi.org/10.1016/j.eurpolymj.2015.04.030>

Maisonneuve, L., Chollet, G., Grau, E., Cramail, H., 2016. Vegetable oils: a source of polyols for polyurethane materials. *OCCL* **23**, D508. <https://doi.org/10.1051/ocl/2016031>

Maisonneuve, L., Lamarzelle, O., Rix, E., Grau, E., Cramail, H., 2015. Isocyanate-Free Routes to Polyurethanes and Poly(hydroxy Urethane)s. *Chem. Rev.* **115**, 12407–12439. <https://doi.org/10.1021/acs.chemrev.5b00355>

Maldas, D., Shiraishi, N., 1996. Liquefaction of Wood in the Presence of Polyol Using NaOH as a Catalyst and its Application to Polyurethane Foams. *Int. J. Polym. Mater.* **33**, 61–71. <https://doi.org/10.1080/00914039608028608>

Malferrari, D., Armenise, N., De Cesari, S., Galletti, P., Tagliavini, E., 2015. Surfactants from Itaconic Acid: Physicochemical Properties and Assessment of the Synthetic Strategies. *ACS Sustain. Chem. Eng.* **3**, 1579–1588. <https://doi.org/10.1021/acssuschemeng.5b00264>

Malhotra, A.K., Wasan, D.T., 1987. Effects of surfactant adsorption-desorption kinetics and interfacial rheological properties on the rate of drainage of foam and emulsion films. *Chem. Eng. Commun.* **55**, 95–128. <https://doi.org/10.1080/00986448708911921>

Malwitz, N., 1987. Fire-retardant Polyurethane Foam and Method and Resin for Preparing the Same. US4654375A.

Mann, N., Mendon, S.K., Rawlins, J.W., Thames, S.F., 2008. Synthesis of Carbonated Vernonia Oil. *J. Am. Oil Chem. Soc.* **85**, 791–796. <https://doi.org/10.1007/s11746-008-1249-3>

Manzardo, A., Marson, A., Roso, M., Boaretti, C., Modesti, M., Scipioni, A., Lorenzetti, A., 2019. Life Cycle Assessment Framework To Support the Design of Biobased Rigid Polyurethane Foams. *ACS Omega* **4**, 14114–14123. <https://doi.org/10.1021/acsomega.9b02025>

Marín, R., Alla, A., Ilarduya, A.M., Muñoz- Guerra, S., 2011. Carbohydrate-based polyurethanes: A comparative study of polymers made from isosorbide and 1,4-butanediol. *E-Polym.* **11**. <https://doi.org/10.1515/epoly.2011.11.1.700>

Mateu-Royo, C., Navarro-Esbrí, J., Mota-Babiloni, A., Amat-Albuixech, M., Molés, F., 2019. Thermodynamic analysis of low GWP alternatives to HFC-245fa in high-temperature heat pumps: HCFO-1224yd(Z),

LISTE COMPLÈTE DES RÉFÉRENCES BIBLIOGRAPHIQUES

HCFO-1233zd(E) and HFO-1336mzz(Z). *Appl. Therm. Eng.* **152**, 762–777. <https://doi.org/10.1016/j.applthermaleng.2019.02.047>

Mather, B.D., Viswanathan, K., Miller, K.M., Long, T.E., 2006. Michael addition reactions in macromolecular design for emerging technologies. *Prog. Polym. Sci.* **31**, 487–531. <https://doi.org/10.1016/j.progpolymsci.2006.03.001>

Matsuura, H., Miyazawa, T., 1967. Infra-red spectra of polyethylene glycols and O-deuterated derivatives. *Spectrochim. Acta Part Mol. Spectrosc.* **23**, 2433–2447. [https://doi.org/10.1016/0584-8539\(67\)80135-1](https://doi.org/10.1016/0584-8539(67)80135-1)

Mcclusky, J.V., O'Neill, R.E., Priester, R.D., Ramsey, W.A., 1994. Vibrating Rod Viscometer: A Valuable Probe into Polyurethane Chemistry. *J. Cell. Plast.* **30**, 224–241. <https://doi.org/10.1177/0021955X9403000302>

Menzinger, M., Wolfgang, R., 1969. The Meaning and Use of the Arrhenius Activation Energy. *Angew. Chem. Int. Ed. Engl.* **8**, 438–444. <https://doi.org/10.1002/anie.196904381>

Merline, J.D., Reghunadhan Nair, C.P., Gouri, C., Sadhana, R., Ninan, K.N., 2007. Poly(urethane–oxazolidone): Synthesis, characterisation and shape memory properties. *Eur. Polym. J.* **43**, 3629–3637. <https://doi.org/10.1016/j.eurpolymj.2007.05.032>

Miao, S., Zhang, S., Su, Z., Wang, P., 2008. Chemoenzymatic synthesis of oleic acid-based polyesters for use as highly stable biomaterials. *J. Polym. Sci. Part Polym. Chem.* **46**, 4243–4248. <https://doi.org/10.1002/pola.22721>

Michael, A., 1887. Ueber die Addition von Natriumacetessig- und Natriummalonsäureäthern zu den Aethern ungesättigter Säuren. *J. Für Prakt. Chem.* **35**, 349–356. <https://doi.org/10.1002/prac.18870350136>

Michalska, K., Bednarek, E., Gruba, E., Lewandowska, K., Mizera, M., Cielecka-Piontek, J., 2017. Comprehensive spectral identification of key intermediates to the final product of the chiral pool synthesis of radezolid. *Chem. Cent. J.* **11**, 82. <https://doi.org/10.1186/s13065-017-0309-x>

Modesti, M., Simioni, F., 1996. Chemical recycling of reinforced polyurethane from the automotive industry. *Polym. Eng. Sci.* **36**, 2173–2178. <https://doi.org/10.1002/pen.10614>

Mohammadpour, R., Mir Mohamad Sadeghi, G., 2020. Effect of Liquefied Lignin Content on Synthesis of Bio-based Polyurethane Foam for Oil Adsorption Application. *J. Polym. Environ.* **28**, 892–905. <https://doi.org/10.1007/s10924-019-01650-5>

Molotsky, H., Gramera, R., 1976. Flame retardant polyurethane foams. US3957702Z.

Moncada, J., Tamayo, J.A., Cardona, C.A., 2014. Integrating first, second, and third generation biorefineries: Incorporating microalgae into the sugarcane biorefinery. *Chem. Eng. Sci.* **118**, 126–140. <https://doi.org/10.1016/j.ces.2014.07.035>

Monie, F., Grignard, B., Thomassin, J.-M., Mereau, R., Tassaing, T., Jerome, C., Detrembleur, C., 2020. Chemo- and Regioselective Additions of Nucleophiles to Cyclic Carbonates for the Preparation of Self-Blowing Non-Isocyanate Polyurethane Foams. *Angew. Chem. Int. Ed.* **59**, 17033–17041. <https://doi.org/10.1002/anie.202006267>

More, A.S., Lebarb  , T., Maisonneuve, L., Gadenne, B., Alfos, C., Cramail, H., 2013. Novel fatty acid based di-isocyanates towards the synthesis of thermoplastic polyurethanes. *Eur. Polym. J.* **49**, 823–833. <https://doi.org/10.1016/j.eurpolymj.2012.12.013>

Morschbacker, A., 2009. Bio-Ethanol Based Ethylene. *Polym. Rev.* **49**, 79–84. <https://doi.org/10.1080/15583720902834791>

M  lhaupt, R., 2013. Green Polymer Chemistry and Bio-based Plastics: Dreams and Reality. *Macromol. Chem. Phys.* **214**, 159–174. <https://doi.org/10.1002/macp.201200439>

Nadji, H., Bruzz  se, C., Belgacem, M.N., Benaboura, A., Gandini, A., 2005. Oxypropylation of Lignins and Preparation of Rigid Polyurethane Foams from the Ensuing Polyols. *Macromol. Mater. Eng.* **290**, 1009–1016. <https://doi.org/10.1002/mame.200500200>

Nagy, L., Nagy, T., Kuki,   ., Purgel, M., Zsuga, M., K  ki, S., 2017. Kinetics of Uncatalyzed Reactions of 2,4'- and 4,4'-Diphenylmethane-Diisocyanate with Primary and Secondary Alcohols: KINETICS OF UNCATALYZED REACTIONS OF 2,4'-MDI AND 4,4'-MDI WITH ALCOHOLS. *Int. J. Chem. Kinet.* **49**, 643–655. <https://doi.org/10.1002/kin.21104>

Narine, S.S., Kong, X., Bouzidi, L., Sporns, P., 2007. Physical Properties of Polyurethanes Produced from Polyols from Seed Oils: II. Foams. *J. Am. Oil Chem. Soc.* **84**, 65–72. <https://doi.org/10.1007/s11746-006-1008-2>

Nawata, T., Kresta, J.E., Frisch, K.C., 1975. Comparative Studies of Isocyanurate and Isocyanurate-Urethane Foams. *J. Cell. Plast.* **11**, 267–278. <https://doi.org/10.1177/0021955X7501100506>

Negrell, C., Cornille, A., de Andrade Nascimento, P., Robin, J.-J., Caillol, S., 2017. New bio-based epoxy materials and foams from microalgal oil: Agal oil epoxy materials and foams. *Eur. J. Lipid Sci. Technol.* **119**, 1600214. <https://doi.org/10.1002/ejlt.201600214>

LISTE COMPLÈTE DES RÉFÉRENCES BIBLIOGRAPHIQUES

Nemirovsky, J., 1883. Ueber die Einwirkung von Chlorkohlenoxyd auf Aethylenglycol; vorläufige Mittheilung. *J. Für Prakt. Chem.* **28**, 439–440. <https://doi.org/10.1002/prac.18830280136>

Neumann, C.N.D., Bulach, W.D., Rehahn, M., Klein, R., 2011. Water-Free Synthesis of Polyurethane Foams Using Highly Reactive Diisocyanates Derived from 5-Hydroxymethylfurfural. *Macromol. Rapid Commun.* **32**, 1373–1378. <https://doi.org/10.1002/marc.201100205>

Ng, W.S., Lee, C.S., Chuah, C.H., Cheng, S.-F., 2017. Preparation and modification of water-blown porous biodegradable polyurethane foams with palm oil-based polyester polyol. *Ind. Crops Prod.* **97**, 65–78. <https://doi.org/10.1016/j.indcrop.2016.11.066>

Nikje, M.M.A., Haghshenas, M., Garmarudi, A.B., 2006. Glycolysis of Waste Polyurethane Integral Skin Foams from Steering Wheel. *Polym.-Plast. Technol. Eng.* **45**, 569–573. <https://doi.org/10.1080/03602550600554174>

Noordzij, G.J., van den Boomen, Y.J.G., Gilbert, C., van Elk, D.J.P., Roy, M., Wilsens, C.H.R.M., Rastogi, S., 2019. The aza-Michael reaction: towards semi-crystalline polymers from renewable itaconic acid and diamines. *Polym. Chem.* **10**, 4049–4058. <https://doi.org/10.1039/C9PY00463G>

Obi, B.E., 2018a. Foaming Processes. In 'Polymeric Foams Structure-Property-Performance'. Elsevier, pp. 131–188. <https://doi.org/10.1016/B978-1-4557-7755-6.00006-9>

Obi, B.E., 2018b. Fundamentals of Polymeric Foams and Classification of Foam Types. In 'Polymeric Foams Structure-Property-Performance'. Elsevier, pp. 93–129. <https://doi.org/10.1016/B978-1-4557-7755-6.00005-7>

Obi, B.E., 2018c. Polymeric foams structure-property-performance: a design guide 'PDL handbook series. William Andrew is an imprint of Elsevier, Oxford, United Kingdom.

Okada, Y., Banno, T., Toshima, K., Matsumura, S., 2009. Synthesis and Properties of Polycarboxylate-type Green Surfactants with S- or N-Linkages. *J. Oleo Sci.* **58**, 519–528. <https://doi.org/10.5650/jos.58.519>

Okuzono, S., Tokumoto, K., Tamano, Y., Lowe, D.W., 2001. New Polyisocyanurate Catalysts Which Exhibit High Activity at Low Temperature. *J. Cell. Plast.* **37**, 72–89. <https://doi.org/10.1106/DWGD-PX79-WR0G-9GBW>

Olivieri, G., Salatino, P., Marzocchella, A., 2014. Advances in photobioreactors for intensive microalgal production: configurations, operating strategies and applications: Advances in photobioreactors for intensive microalgal production. *J. Chem. Technol. Biotechnol.* **89**, 178–195. <https://doi.org/10.1002/jctb.4218>

Omraní, I., Farhadian, A., Babanejad, N., Shendi, H.K., Ahmadi, A., Nabid, M.R., 2016. Synthesis of novel high primary hydroxyl functionality polyol from sunflower oil using thiol-yne reaction and their application in polyurethane coating. *Eur. Polym. J.* **82**, 220–231. <https://doi.org/10.1016/j.eurpolymj.2016.07.021>

Oncel, S.S., 2013. Microalgae for a macroenergy world. *Renew. Sustain. Energy Rev.* **26**, 241–264. <https://doi.org/10.1016/j.rser.2013.05.059>

Owen, M.J., Kendrick, T.C., Kingston, B.M., Lloyd, N.C., 1967. The surface chemistry of polyurethane foam formation. *J. Colloid Interface Sci.* **24**, 141–150. [https://doi.org/10.1016/0021-9797\(67\)90211-1](https://doi.org/10.1016/0021-9797(67)90211-1)

Palaskar, D.V., Boyer, A., Cloutet, E., Le Meins, J.-F., Gadenne, B., Alfos, C., Farcet, C., Cramail, H., 2012. Original diols from sunflower and ricin oils: Synthesis, characterization, and use as polyurethane building blocks. *J. Polym. Sci. Part Polym. Chem.* **50**, 1766–1782. <https://doi.org/10.1002/pola.25944>

Pan, X., Saddler, J.N., 2013. Effect of replacing polyol by organosolv and kraft lignin on the property and structure of rigid polyurethane foam. *Biotechnol. Biofuels* **6**, 12. <https://doi.org/10.1186/1754-6834-6-12>

Paramarta, A., Webster, D.C., 2017. The exploration of Michael-addition reaction chemistry to create high performance, ambient cure thermoset coatings based on soybean oil. *Prog. Org. Coat.* **108**, 59–67. <https://doi.org/10.1016/j.porgcoat.2017.04.004>

Pardo-Alonso, S., Solórzano, E., Estravís, S., Rodríguez-Perez, M.A., de Saja, J.A., 2012. In situ evidence of the nanoparticle nucleating effect in polyurethane–nanoclay foamed systems. *Soft Matter* **8**, 11262. <https://doi.org/10.1039/c2sm25983d>

Parker, R.E., Isaacs, N.S., 1959. Mechanisms Of Epoxide Reactions. *Chem. Rev.* **59**, 737–799. <https://doi.org/10.1021/cr50028a006>

Paruzel, A., Michałowski, S., Hodan, J., Horák, P., Prociak, A., Beneš, H., 2017. Rigid Polyurethane Foam Fabrication Using Medium Chain Glycerides of Coconut Oil and Plastics from End-of-Life Vehicles. *ACS Sustain. Chem. Eng.* **5**, 6237–6246. <https://doi.org/10.1021/acssuschemeng.7b01197>

Pascault, J.-P., Sautereau, H., Verdu, J., Williams, R.J.J., 2002. Gelation and Network Fomation. In 'Thermosetting Polymers' 'Plastics Engineering'. Marcel Dekker, New York, pp. 78–129.

Pavier, C., Gandini, A., 2000a. Oxypropylation of sugar beet pulp. 1. Optimisation of the reaction. *Ind. Crops Prod.* **12**, 1–8. [https://doi.org/10.1016/S0926-6690\(99\)00039-4](https://doi.org/10.1016/S0926-6690(99)00039-4)

LISTE COMPLÈTE DES RÉFÉRENCES BIBLIOGRAPHIQUES

Pavier, C., Gandini, A., 2000b. Oxypropylation of sugar beet pulp. 2. Separation of the grafted pulp from the propylene oxide homopolymer. *Carbohydr. Polym.* **42**, 13–17. [https://doi.org/10.1016/S0144-8617\(99\)00124-1](https://doi.org/10.1016/S0144-8617(99)00124-1)

Pawar, M.S., Kadam, A.S., Dawane, B.S., Yemul, O.S., 2016a. Synthesis and characterization of rigid polyurethane foams from algae oil using biobased chain extenders. *Polym. Bull.* **73**, 727–741. <https://doi.org/10.1007/s00289-015-1514-1>

Pawar, M.S., Kadam, A.S., Singh, P.C., Kusumkar, V.V., Yemul, O.S., 2016b. Rigid polyurethane foams from cottonseed oil using bio-based chain extenders: a renewable approach. *Iran. Polym. J.* **25**, 59–68. <https://doi.org/10.1007/s13726-015-0401-9>

Pelckmans, M., Renders, T., Van de Vyver, S., Sels, B.F., 2017. Bio-based amines through sustainable heterogeneous catalysis. *Green Chem.* **19**, 5303–5331. <https://doi.org/10.1039/C7GC02299A>

Pelletier, M.G., Holt, G.A., Wanjura, J.D., Greetham, L., McIntyre, G., Bayer, E., Kaplan-Bie, J., 2019. Acoustic evaluation of mycological biopolymer, an all-natural closed cell foam alternative. *Ind. Crops Prod.* **139**, 111533. <https://doi.org/10.1016/j.indcrop.2019.111533>

Pellis, A., Hanson, P.A., Comerford, J.W., Clark, J.H., Farmer, T.J., 2019. Enzymatic synthesis of unsaturated polyesters: functionalization and reversibility of the aza-Michael addition of pendants. *Polym. Chem.* **10**, 843–851. <https://doi.org/10.1039/C8PY01655K>

Pelzer, T., Eling, B., Thomas, H.-J., Luinstra, G.A., 2018. Toward polymers with oxazolidin-2-one building blocks through tetra-n-butyl-ammonium halides (Cl, Br, I) catalyzed coupling of epoxides with isocyanates. *Eur. Polym. J.* **107**, 1–8. <https://doi.org/10.1016/j.eurpolymj.2018.07.039>

Pérez, E., Tuck, C.O., 2018. Quantitative analysis of products from lignin depolymerisation in high-temperature water. *Eur. Polym. J.* **99**, 38–48. <https://doi.org/10.1016/j.eurpolymj.2017.11.053>

Pérez, M., Pleixats, R., 1995. FeCl₃-catalyzed conjugate addition of secondary amines, imidazole and pyrazole to methyl 2-acetamidoacrylate. Preparation of β -dialkylamino- α -alanine and β -(N-heteroaryl)- α -alanine derivatives. *Tetrahedron* **51**, 8355–8362. [https://doi.org/10.1016/0040-4020\(95\)00446-F](https://doi.org/10.1016/0040-4020(95)00446-F)

Pérez-Sena, W.Y., Cai, X., Kebir, N., Vernières-Hassimi, L., Serra, C., Salmi, T., Leveneur, S., 2018. Aminolysis of cyclic-carbonate vegetable oils as a non-isocyanate route for the synthesis of polyurethane: A kinetic and thermal study. *Chem. Eng. J.* **346**, 271–280. <https://doi.org/10.1016/j.cej.2018.04.028>

Pérocheau Arnaud, S., Andreou, E., Pereira Köster, L.V.G., Robert, T., 2020. Selective Synthesis of Monoesters of Itaconic Acid with Broad Substrate Scope: Biobased Alternatives to Acrylic Acid? *ACS Sustain. Chem. Eng.* **8**, 1583–1590. <https://doi.org/10.1021/acssuschemeng.9b06330>

Peters, J.M., 1970. Studies of isocyanate toxicity. *Proc. R. Soc. Med.* **63**, 372–375.

Petrovic, Z., 2008. Polyurethanes from Vegetable Oils. *Polym. Rev.* **48**, 109–155. <https://doi.org/10.1080/15583720701834224>

Petrović, Z.S., Wan, X., Bilić, O., Zlatanić, A., Hong, J., Javni, I., Ionescu, M., Milić, J., Degruson, D., 2013. Polyols and Polyurethanes from Crude Algal Oil. *J. Am. Oil Chem. Soc.* **90**, 1073–1078. <https://doi.org/10.1007/s11746-013-2245-9>

Petrović, Z.S., Zhang, W., Javni, I., 2005. Structure and Properties of Polyurethanes Prepared from Triglyceride Polyols by Ozonolysis. *Biomacromolecules* **6**, 713–719. <https://doi.org/10.1021/bm049451s>

Petrović, Z.S., Zlatanić, A., Lava, C.C., Sinadinović-Fišer, S., 2002. Epoxidation of soybean oil in toluene with peroxyacetic and peroxyformic acids — kinetics and side reactions. *Eur. J. Lipid Sci. Technol.* **104**, 293–299. [https://doi.org/10.1002/1438-9312\(200205\)104:5<293::AID-EJLT293>3.0.CO;2-W](https://doi.org/10.1002/1438-9312(200205)104:5<293::AID-EJLT293>3.0.CO;2-W)

Peyrton, J., Chambaretaud, C., Avérous, L., 2019. New Insight on the Study of the Kinetic of Biobased Polyurethanes Synthesis Based on Oleo-Chemistry. *Molecules* **24**, 4332. <https://doi.org/10.3390/molecules24234332>

Peyrton, J., Chambaretaud, C., Sarbu, A., Avérous, L., 2020. Biobased Polyurethane Foams Based on New Polyol Architectures from Microalgae Oil. *ACS Sustain. Chem. Eng.* **8**, 12187–12196. <https://doi.org/10.1021/acssuschemeng.0c03758>

Pfister, D.P., Xia, Y., Larock, R.C., 2011. Recent Advances in Vegetable Oil-Based Polyurethanes. *ChemSusChem* **4**, 703–717. <https://doi.org/10.1002/cssc.201000378>

Pilawka, R., Goracy, K., Wilpiszewska, K., 2014. High-performance isocyanate-epoxy materials. *Pigment Resin Technol.* **43**, 332–340. <https://doi.org/10.1108/PRT-11-2013-0110>

Pillai, P.K.S., Li, S., Bouzidi, L., Narine, S.S., 2018. Polyurethane foams from chlorinated and non-chlorinated metathesis modified canola oil polyols: Research Article. *J. Appl. Polym. Sci.* **135**, 46616. <https://doi.org/10.1002/app.46616>

Pillai, P.K.S., Li, S., Bouzidi, L., Narine, S.S., 2016. Solvent-free synthesis of polyols from 1-butene metathesized palm oil for use in polyurethane foams. *J. Appl. Polym. Sci.* **133**, 43509. <https://doi.org/10.1002/app.43509>

Piszczek, Ł., Strankowski, M., Danowska, M., Hejna, A., Haponiuk, J.T., 2014. Rigid polyurethane foams from a polyglycerol-based polyol. *Eur. Polym. J.* **57**, 143–150. <https://doi.org/10.1016/j.eurpolymj.2014.05.012>

Pizzi, 2019. Tannins: Prospectives and Actual Industrial Applications. *Biomolecules* **9**, 344. <https://doi.org/10.3390/biom9080344>

Plastics Europe, 2019. Plastics-the Facts 2019.

Prat, D., Wells, A., Hayler, J., Sneddon, H., McElroy, C.R., Abou-Shehada, S., Dunn, P.J., 2016. CHEM21 selection guide of classical- and less classical-solvents. *Green Chem.* **18**, 288–296. <https://doi.org/10.1039/C5GC01008J>

Pretsch, E., Bühlmann, P., Badertscher, M., 2009. Structure determination of organic compounds: tables of spectral data, 4th, rev.enl. ed ed. Springer, Berlin.

Prociak, A., Kurańska, M., Cabulis, U., Ryszkowska, J., Leszczyńska, M., Uram, K., Kirpluks, M., 2018. Effect of bio-polyols with different chemical structures on foaming of polyurethane systems and foam properties. *Ind. Crops Prod.* **120**, 262–270. <https://doi.org/10.1016/j.indcrop.2018.04.046>

Qian, C., Zhu, D., 1994. A facile synthesis of oxazolidinones via lanthanide-catalyzed cycloaddition of epoxides with isocyanates. *Synlett* 129–130.

Qin, H., Wang, K., 2019. Study on preparation and performance of PEG-based polyurethane foams modified by the chitosan with different molecular weight. *Int. J. Biol. Macromol.* **140**, 877–885. <https://doi.org/10.1016/j.ijbiomac.2019.08.189>

Quinn, E.J., 1970. Properties and Stability of Fire-Retardant Rigid Polyurethane Foams from Phosphonopropionate Polyols. *Ind. Eng. Chem. Prod. Res. Dev.* **9**, 48–53. <https://doi.org/10.1021/i360033a009>

Quirino, R.L., Garrison, T.F., Kessler, M.R., 2014. Matrices from vegetable oils, cashew nut shell liquid, and other relevant systems for biocomposite applications. *Green Chem.* **16**, 1700–1715. <https://doi.org/10.1039/C3GC41811A>

Ramanujam, S., Zequine, C., Bhoyate, S., Neria, B., Kahol, P., Gupta, R., 2019. Novel Biobased Polyol Using Corn Oil for Highly Flame-Retardant Polyurethane Foams. *C* **5**, 13. <https://doi.org/10.3390/c5010013>

Randall, D., Lee, S. (Eds.), 2002. The polyurethanes book. John Wiley & Sons, Inc., Everberg, Belgium.

Ranu, B.C., Banerjee, S., 2007. Significant rate acceleration of the aza-Michael reaction in water. *Tetrahedron Lett.* **48**, 141–143. <https://doi.org/10.1016/j.tetlet.2006.10.142>

Rapra, S., 2014. Blowing agents & foaming processes 'conference proceedings. Presented at the Blowing Agents & Foaming Processes Conference, Smithers Rapra, Imperial Riding School Renaissance.

Rashmi, B.J., Rusu, D., Prashantha, K., Lacrampe, M.F., Krawczak, P., 2013. Development of water-blown bio-based thermoplastic polyurethane foams using bio-derived chain extender. *J. Appl. Polym. Sci.* **128**, 292–303. <https://doi.org/10.1002/app.38183>

Rastegarfar, N., Behrooz, R., Barikani, M., 2018. Characterization of polyurethane foams prepared from liquefied sawdust by crude glycerol and polyethylene glycol. *J. Polym. Res.* **25**, 154. <https://doi.org/10.1007/s10965-018-1516-4>

Rawat, I., Ranjith Kumar, R., Mutanda, T., Bux, F., 2013. Biodiesel from microalgae: A critical evaluation from laboratory to large scale production. *Appl. Energy* **103**, 444–467. <https://doi.org/10.1016/j.apenergy.2012.10.004>

Reese, J., Moore, M., Wardius, D., Hager, S., 2010. Polyether polyols based on cashew nutshell liquid and flexible foams. US 7,828,991 B2.

Reignier, J., Alcouffe, P., Méchin, F., Fenouillot, F., 2019. The morphology of rigid polyurethane foam matrix and its evolution with time during foaming – New insight by cryogenic scanning electron microscopy. *J. Colloid Interface Sci.* **552**, 153–165. <https://doi.org/10.1016/j.jcis.2019.05.032>

Reymore, H.E., Carleton, P.S., Kolakowski, R.A., Sayigh, A.A.R., 1975. Isocyanurate Foams: Chemistry, Properties and Processing. *J. Cell. Plast.* **11**, 328–344. <https://doi.org/10.1177/0021955X7501100608>

Rigby, M., Park, S., Saito, T., Western, L.M., Redington, A.L., Fang, X., Henne, S., Manning, A.J., Prinn, R.G., Dutton, G.S., Fraser, P.J., Ganesan, A.L., Hall, B.D., Harth, C.M., Kim, J., Kim, K.-R., Krummel, P.B., Lee, T., Li, S., Liang, Q., Lunt, M.F., Montzka, S.A., Mühlé, J., O'Doherty, S., Park, M.-K., Reimann, S., Salameh, P.K., Simmonds, P., Tunnicliffe, R.L., Weiss, R.F., Yokouchi, Y., Young, D., 2019. Increase in CFC-11 emissions from eastern China based on atmospheric observations. *Nature* **569**, 546–550. <https://doi.org/10.1038/s41586-019-1193-4>

Rinaudo, M., 2006. Chitin and chitosan: Properties and applications. *Prog. Polym. Sci.* **31**, 603–632. <https://doi.org/10.1016/j.progpolymsci.2006.06.001>

Rios, L. alberto, 2003. Heterogeneously Catalyzed Reactions with Vegetable Oils: Epoxidation and Nucleophilic Epoxide Ring-Opening with Alcohols. RWTH Aachen University, Germany.

LISTE COMPLÈTE DES RÉFÉRENCES BIBLIOGRAPHIQUES

Riyapan, D., Saetung, A., Saetung, N., 2019. A Novel Rigid PU Foam Based on Modified Used Palm Oil as Sound Absorbing Material. *J. Polym. Environ.* **27**, 1693–1708. <https://doi.org/10.1007/s10924-019-01460-9>

Robert, T.M., Nair, S., Mathew, D., Reghunadhan Nair, C.P., 2018. Room temperature processable heat-resistant epoxy-oxazolidone-based syntactic foams. *Polym. Adv. Technol.* **29**, 121–129. <https://doi.org/10.1002/pat.4094>

Roesle, P., Stempfle, F., Hess, S.K., Zimmerer, J., Río Bártulos, C., Lepetit, B., Eckert, A., Kroth, P.G., Mecking, S., 2014. Synthetic Polyester from Algae Oil. *Angew. Chem. Int. Ed.* **53**, 6800–6804. <https://doi.org/10.1002/anie.201403991>

Rokicki, G., Parzuchowski, P.G., Mazurek, M., 2015. Non-isocyanate polyurethanes: synthesis, properties, and applications: Non-Isocyanate Polyurethanes: Synthesis, Properties, and Applications. *Polym. Adv. Technol.* **26**, 707–761. <https://doi.org/10.1002/pat.3522>

Roux, D., Paulus, E., 1962. Condensed tannins. 13. Interrelationships of flavonoid components from the heartwood of Robinia pseudacacia. *Biochem. J.* **82**, 324–330. <https://doi.org/10.1042/bj0820324>

Rowland, F.S., Molina, M.J., 1975. Chlorofluoromethanes in the environment. *Rev. Geophys.* **13**, 1. <https://doi.org/10.1029/RG013i001p00001>

Rulev, A.Y., 2011. Aza-Michael reaction: achievements and prospects. *Russ. Chem. Rev.* **80**, 197–218. <https://doi.org/10.1070/rc2011v080n03abeh004162>

Saffar, T., Bouafif, H., Braghieri, F.L., Magdouli, S., Langlois, A., Koubaa, A., 2020. Production of Bio-based Polyol from Oxypropylated Pyrolytic Lignin for Rigid Polyurethane Foam Application. *Waste Biomass Valorization* **11**, 6411–6427. <https://doi.org/10.1007/s12649-019-00876-7>

Sahoo, S., Kalita, H., Mohanty, S., Nayak, S.K., 2016. Synthesis of Vegetable Oil-Based Polyurethane: A Study on Curing Kinetics Behavior. *Int. J. Chem. Kinet.* **48**, 622–634. <https://doi.org/10.1002/kin.21020>

Saiki, K., Sasaki, K., Ashida, K., 1994. Carbodiimide-Modified Polyisocyanurate Foams: Preparation and Flame Resistance. *J. Cell. Plast.* **30**, 470–484. <https://doi.org/10.1177/0021955X9403000504>

Sakakura, A., Kawajiri, K., Ohkubo, T., Kosugi, Y., Ishihara, K., 2007. Widely Useful DMAP-Catalyzed Esterification under Auxiliary Base- and Solvent-Free Conditions. *J. Am. Chem. Soc.* **129**, 14775–14779. <https://doi.org/10.1021/ja075824w>

Salanti, A., Zoia, L., Orlandi, M., 2016. Chemical modifications of lignin for the preparation of macromers containing cyclic carbonates. *Green Chem.* **18**, 4063–4072. <https://doi.org/10.1039/C6GC01028H>

Sandler, S.R., 1967. Preparation of mono and poly-2-oxazolidones from 1,2-epoxides and isocyanates. *J. Polym. Sci. [A1]* **5**, 1481–1485. <https://doi.org/10.1002/pol.1967.150050628>

Santiago-Calvo, M., Tirado-Mediavilla, J., Ruiz-Herrero, J.L., Villaña, F., Rodríguez-Pérez, M.Á., 2019. Long-term thermal conductivity of cyclopentane–water blown rigid polyurethane foams reinforced with different types of fillers. *Polym. Int.* **68**, 1826–1835. <https://doi.org/10.1002/pi.5893>

Sato, M., 1962. The Rate of the Reaction of Isocyanates with Alcohols. II. *J. Org. Chem.* **27**, 819–825. <https://doi.org/10.1021/jo01050a031>

Sato, M., 1960. The Rates of Reaction of 1-Alkenyl Isocyanates with Methanol. *J. Am. Chem. Soc.* **82**, 3893–3897. <https://doi.org/10.1021/ja01500a027>

Schmidt, D.L., Clarke, D.H., Urchick, D., 1984. The Effect of Surfactant Properties on a Rigid Foam System. *J. Cell. Plast.* **20**, 220–226. <https://doi.org/10.1177/0021955X8402000306>

Schneiderman, D.K., Vanderlaan, M.E., Mannion, A.M., Panthani, T.R., Batiste, D.C., Wang, J.Z., Bates, F.S., Macosko, C.W., Hillmyer, M.A., 2016. Chemically Recyclable Biobased Polyurethanes. *ACS Macro Lett.* **5**, 515–518. <https://doi.org/10.1021/acsmacrolett.6b00193>

Schuster, H., Rios, L.A., Weckes, P.P., Hoelderich, W.F., 2008. Heterogeneous catalysts for the production of new lubricants with unique properties. *Appl. Catal. Gen.* **348**, 266–270. <https://doi.org/10.1016/j.apcata.2008.07.004>

Sendijarević, A., Sendijarević, V., Frisch, K.C., 1987. Studies in the formation of poly(oxazolidones) I. Kinetics and mechanism of the model oxazolidone formation from phenyl isocyanate and phenylglycidyl ether. Selectivity of catalysts. *J. Polym. Sci. Part Polym. Chem.* **25**, 151–170. <https://doi.org/10.1002/pola.1987.080250113>

Sendijarevic, I., Pietrzik, K.W., Schiffman, C.M., Sendijarevic, V., Kiziltas, A., Mielewski, D., 2020. Polyol from spent coffee grounds: Performance in a model pour-in-place rigid polyurethane foam system. *J. Cell. Plast.* **0021955X2091220**. <https://doi.org/10.1177/0021955X2091220>

Sendijarevic, V., 2007. Chemical Recycling of Mixed Polyurethane Foam Stream Recovered from Shredder Residue into Polyurethane Polyols. *J. Cell. Plast.* **43**, 31–46. <https://doi.org/10.1177/0021955X07066107>

Shao, H., Zhao, H., Xie, J., Qi, J., Shupe, T.F., 2019. Agricultural and Forest Residues towards Renewable Chemicals and Materials Using Microwave Liquefaction. *Int. J. Polym. Sci.* **2019**, 1–16. <https://doi.org/10.1155/2019/7231263>

Sharma, B.K., Adhvaryu, A., Erhan, S.Z., 2006a. Synthesis of Hydroxy Thio-ether Derivatives of Vegetable Oil. *J. Agric. Food Chem.* **54**, 9866–9872. <https://doi.org/10.1021/jf061896f>

Sharma, B.K., Adhvaryu, A., Liu, Z., Erhan, S.Z., 2006b. Chemical modification of vegetable oils for lubricant applications. *J. Am. Oil Chem. Soc.* **83**, 129–136. <https://doi.org/10.1007/s11746-006-1185-z>

Shin, S., Kim, H., Liang, J., Lee, S., Lee, D., 2019a. Sustainable rigid polyurethane foams based on recycled polyols from chemical recycling of waste polyurethane foams. *J. Appl. Polym. Sci.* **136**, 47916. <https://doi.org/10.1002/app.47916>

Shin, S.-R., Liang, J.-Y., Ryu, H., Song, G.-S., Lee, D.-S., 2019b. Effects of Isosorbide Incorporation into Flexible Polyurethane Foams: Reversible Urethane Linkages and Antioxidant Activity. *Molecules* **24**, 1347. <https://doi.org/10.3390/molecules24071347>

Shine, K.P., 2009. The global warming potential—the need for an interdisciplinary retrial: An editorial comment. *Clim. Change* **96**, 467–472. <https://doi.org/10.1007/s10584-009-9647-6>

Shrestha, M.L., Ionescu, M., 2018. Aliphatic–Aromatic Polyols by Thiol–Ene Reactions. *J. Polym. Environ.* **26**, 2257–2267. <https://doi.org/10.1007/s10924-017-1123-1>

Shuo, X., Ligong, C., Lan, X., Liang, L., Xin, Y., Liye, Z., 2015. Diester Derivatives from Chemically Modified Waste Cooking Oil as Substitute for Petroleum Based Lubricating Oils 8.

Siegel, H., Wittmann, H., 1982. Substitutions-und Additionsreaktionen an Spiro-oxiranen. *Monatshefte Für Chemie/Chemical Mon.* **113**, 1005–1017.

Silva, A.L., Bordado, J.C., 2004. Recent Developments in Polyurethane Catalysis: Catalytic Mechanisms Review. *Catal. Rev.* **46**, 31–51. <https://doi.org/10.1081/CR-120027049>

da Silva, J.A.P., Cardozo, N.S.M., Petzhold, C.L., 2018. Enzymatic synthesis of andiroba oil based polyol for the production of flexible polyurethane foams. *Ind. Crops Prod.* **113**, 55–63. <https://doi.org/10.1016/j.indcrop.2018.01.020>

Singh, A.P., Kumar, S., 2020. Applications of Tannins in Industry. In 'Tannins- Structural Properties, Biological Properties and Current Knowledge' (Ed. Aires, A.). IntechOpen, Rijeka. <https://doi.org/10.5772/intechopen.85984>

Singh, I., Samal, S.K., Mohanty, S., Nayak, S.K., 2020. Recent Advancement in Plant Oil Derived Polyol-Based Polyurethane Foam for Future Perspective: A Review. *Eur. J. Lipid Sci. Technol.* **122**, 1900225. <https://doi.org/10.1002/ejlt.201900225>

Singh, S.N., 2002. Blowing agents for polyurethane foams. ISMithers Rapra Publishing, Shawbury, U.K.

Sonnenschein, M.F., Werness, J.B., Patankar, K.A., Jin, X., Larive, M.Z., 2016. From rigid and flexible foams to elastomers via Michael addition chemistry. *Polymer* **106**, 128–139. <https://doi.org/10.1016/j.polymer.2016.10.054>

Speranza, G.P., Peppel, W.J., 1958. Preparation of Substituted 2-Oxazolidones from 1,2-Epoxides and Isocyanates. *J. Org. Chem.* **23**, 1922–1924. <https://doi.org/10.1021/jo01106a027>

Stick, R.V., 2001. Grandfather Glucose. In 'Carbohydrates'. Elsevier, pp. 9–18. <https://doi.org/10.1016/B978-012670960-5/50004-2>

Stirna, U., Lazdiņa, B., Vilsone, D., Lopez, M.J., Vargas-Garcia, M. del C., Suárez-Estrella, F., Moreno, J., 2012. Structure and properties of the polyurethane and polyurethane foam synthesized from castor oil polyols. *J. Cell. Plast.* **48**, 476–488. <https://doi.org/10.1177/0021955X12445178>

Stock, L.M., 1972. The origin of the inductive effect. *J. Chem. Educ.* **49**, 400. <https://doi.org/10.1021/ed049p400>

Stockmayer, W.H., 1944. Theory of Molecular Size Distribution and Gel Formation in Branched Polymers II. General Cross Linking. *J. Chem. Phys.* **12**, 125–131. <https://doi.org/10.1063/1.1723922>

Suryawanshi, Y., Sanap, P., Wani, V., 2019. Advances in the synthesis of non-isocyanate polyurethanes. *Polym. Bull.* **76**, 3233–3246. <https://doi.org/10.1007/s00289-018-2531-7>

Syrpas, M., Venskutonis, P.R., 2020. Algae for the production of bio-based products. In 'Biobased Products and Industries'. Elsevier, pp. 203–243. <https://doi.org/10.1016/B978-0-12-818493-6.00006-3>

Szycher, M., 2013. Szycher's handbook of polyurethanes, 2nd ed. Taylor & Francis, Boca Raton, FL.

Taft, R.W., Ehrenson, S., Lewis, I.C., Glick, R.E., 1959. Evaluation of Resonance Effects on Reactivity by Application of the Linear Inductive Energy Relationship. ^{1,2} VI. Concerning the Effects of Polarization and Conjugation on the Mesomeric Order. *J. Am. Chem. Soc.* **81**, 5352–5361. <https://doi.org/10.1021/ja01529a026>

Takeuchi, M., Kishino, S., Tanabe, K., Hirata, A., Park, S.-B., Shimizu, S., Ogawa, J., 2013. Hydroxy fatty acid production by *Pediococcus* sp. *Eur. J. Lipid Sci. Technol.* **115**, 386–393. <https://doi.org/10.1002/ejlt.201200414>

Tenorio-Alfonso, A., Sánchez, M.C., Franco, J.M., 2020. A Review of the Sustainable Approaches in the Production of Bio-based Polyurethanes and Their Applications in the Adhesive Field. *J. Polym. Environ.* **28**, 749–774. <https://doi.org/10.1007/s10924-020-01659-1>

Testud, B., Pintori, D., Grau, E., Taton, D., Cramail, H., 2017. Hyperbranched polyesters by polycondensation of fatty acid-based AB_n-type monomers. *Green Chem.* **19**, 259–269. <https://doi.org/10.1039/C6GC02294D>

LISTE COMPLÈTE DES RÉFÉRENCES BIBLIOGRAPHIQUES

Thakur, V.K., Thakur, M.K., Raghavan, P., Kessler, M.R., 2014. Progress in Green Polymer Composites from Lignin for Multifunctional Applications: A Review. *ACS Sustain. Chem. Eng.* **2**, 1072–1092. <https://doi.org/10.1021/sc500087z>

Thirumal, M., Khastgir, D., Singha, N.K., Manjunath, B.S., Naik, Y.P., 2008. Effect of foam density on the properties of water blown rigid polyurethane foam. *J. Appl. Polym. Sci.* **108**, 1810–1817. <https://doi.org/10.1002/app.27712>

Tremblay-Parrado, K., Avérous, L., 2020. Renewable Responsive Systems Based on Original Click and Polyurethane Cross-Linked Architectures with Advanced Properties. *ChemSusChem* **13**, 238–251. <https://doi.org/10.1002/cssc.201901991>

Troev, K., 2000. A novel approach to recycling of polyurethanes: chemical degradation of flexible polyurethane foams by triethyl phosphate. *Polymer* **41**, 7017–7022. [https://doi.org/10.1016/S0032-3861\(00\)00054-9](https://doi.org/10.1016/S0032-3861(00)00054-9)

Tung, C.-Y.M., Dynes, P.J., 1982. Relationship between viscoelastic properties and gelation in thermosetting systems. *J. Appl. Polym. Sci.* **27**, 569–574. <https://doi.org/10.1002/app.1982.070270220>

Turco, R., Tesser, R., Vitiello, R., Russo, V., Andini, S., Serio, M.D., 2017. Synthesis of Biolubricant Basestocks from Epoxidized Soybean Oil. *Catalysts* **7**, 309. <https://doi.org/10.3390/catal7100309>

Ugarte, L., Fernández-d'Arlas, B., Valea, A., González, M.L., Corcuera, M.A., Eceiza, A., 2014. Morphology-properties relationship in high-renewable content polyurethanes. *Polym. Eng. Sci.* **54**, 2282–2291. <https://doi.org/10.1002/pen.23777>

Ugarte, L., Gómez-Fernández, S., Peña-Rodríguez, C., Prociak, A., Corcuera, M.A., Eceiza, A., 2015. Tailoring Mechanical Properties of Rigid Polyurethane Foams by Sorbitol and Corn Derived Biopolyol Mixtures. *ACS Sustain. Chem. Eng.* **3**, 3382–3387. <https://doi.org/10.1021/acssuschemeng.5b01094>

Ugwu, C.U., Aoyagi, H., Uchiyama, H., 2008. Photobioreactors for mass cultivation of algae. *Bioresour. Technol.* **99**, 4021–4028. <https://doi.org/10.1016/j.biortech.2007.01.046>

Ulrich, H., Odinak, A., Tucker, B., Sayigh, A.A.R., 1978. Recycling of polyurethane and polyisocyanurate foam. *Polym. Eng. Sci.* **18**, 844–848. <https://doi.org/10.1002/pen.760181103>

UN, 2015. Transforming our world: the 2030 Agenda for Sustainable Development. United Nation.

Uribe, M., Hodd, K.A., 1984. The catalysed reaction of isocyanate and epoxide groups: A study using differential scanning calorimetry. *Thermochim. Acta* **77**, 367–373. [https://doi.org/10.1016/0040-6031\(84\)87075-6](https://doi.org/10.1016/0040-6031(84)87075-6)

Van Der Wal, H.R., 1994. New Chemical Recycling Process for Polyurethanes. *J. Reinf. Plast. Compos.* **13**, 87–96. <https://doi.org/10.1177/073168449401300106>

Van Maris, R., Tamano, Y., Yoshimura, H., Gay, K.M., 2005. Polyurethane Catalysis by Tertiary Amines. *J. Cell. Plast.* **41**, 305–322. <https://doi.org/10.1177/0021955X05055113>

Vedejs, E., Gingras, M., 1994. Aza-Claisen Rearrangements Initiated by Acid-Catalyzed Michael Addition. *J. Am. Chem. Soc.* **116**, 579–588. <https://doi.org/10.1021/ja00081a019>

Vējelis, S., Gailius, A., Vējelienė, J., Vaitkus, S., 2010. Research on thermal conductivity of vacuum insulating materials. *10th Int. Conf. Mod. Build. Mater. Struct. Tech.*

Veronese, V.B., Menger, R.K., Forte, M.M. de C., Petzhold, C.L., 2011. Rigid polyurethane foam based on modified vegetable oil. *J. Appl. Polym. Sci.* **120**, 530–537. <https://doi.org/10.1002/app.33185>

Voorhees, P.W., 1985. The theory of Ostwald ripening. *J. Stat. Phys.* **38**, 231–252. <https://doi.org/10.1007/BF01017860>

Wabnitz, T.C., Spencer, J.B., 2003. A General, Brønsted Acid-Catalyzed Hetero-Michael Addition of Nitrogen, Oxygen, and Sulfur Nucleophiles. *Org. Lett.* **5**, 2141–2144. <https://doi.org/10.1021/ol034596h>

Wan, C., Zhang, G., Zhang, F., 2020. A novel guanidine ammonium phosphate for preparation of a reactive durable flame retardant for cotton fabric. *Cellulose* **27**, 3469–3483. <https://doi.org/10.1007/s10570-020-03003-1>

Weil, E.D., Levchik, S.V., 2004. Commercial Flame Retardancy of Polyurethanes. *J. Fire Sci.* **22**, 183–210. <https://doi.org/10.1177/0734904104040259>

Weissberger, A. (Ed.), 1964. Chemistry of Heterocyclic Compounds: Heterocyclic Compounds with Three- and Four-Membered Rings 'Chemistry of Heterocyclic Compounds: A Series Of Monographs. John Wiley & Sons, Inc., Hoboken, NJ, USA. <https://doi.org/10.1002/9780470239704>

Weißenborn, O., Ebert, C., Gude, M., 2016. Modelling of the strain rate dependent deformation behaviour of rigid polyurethane foams. *Polym. Test.* **54**, 145–149. <https://doi.org/10.1016/j.polymertesting.2016.07.007>

Wendels, S., Avérous, L., 2021. Biobased polyurethanes for biomedical applications. *Bioact. Mater.* **6**, 1083–1106. <https://doi.org/10.1016/j.bioactmat.2020.10.002>

Wertz, J.H., Tang, P.L., Quye, A., France, D.J., 2018. Characterisation of oil and aluminium complex on replica and historical 19th c. Turkey red textiles by non-destructive diffuse reflectance FTIR spectroscopy. *Spectrochim. Acta. A. Mol. Biomol. Spectrosc.* **204**, 267–275. <https://doi.org/10.1016/j.saa.2018.05.109>

Wijffels, R.H., Barbosa, M.J., Eppink, M.H.M., 2010. Microalgae for the production of bulk chemicals and biofuels. *Biofuels Bioprod. Biorefining* **4**, 287–295. <https://doi.org/10.1002/bbb.215>

Wilkie, C.A., Morgan, A.B. (Eds.), 2010. Fire retardancy of polymeric materials, 2nd ed. CRC Press, Boca Raton.

Williams, R.J.J., Vázquez, A., Pascault, J.P., 1992. Gelation in the cyclotrimerization of dicyanates considering substitution effects. *Polym. Bull.* **28**, 219–225. <https://doi.org/10.1007/BF00299659>

Wilson, M.E., Hu, M., Kurth, M.J., Hsieh, Y.-L., Kroccta, J.M., 1996. Preparation and characterization of lactitol-based poly(ether polyol)s for rigid polyurethane foam. *J. Appl. Polym. Sci.* **59**, 1759–1768. [https://doi.org/10.1002/\(SICI\)1097-4628\(19960314\)59:11<1759::AID-APP12>3.0.CO;2-P](https://doi.org/10.1002/(SICI)1097-4628(19960314)59:11<1759::AID-APP12>3.0.CO;2-P)

Winnacker, M., Rieger, B., 2016. Biobased Polyamides: Recent Advances in Basic and Applied Research. *Macromol. Rapid Commun.* **37**, 1391–1413. <https://doi.org/10.1002/marc.201600181>

Winter, H.H., Chambon, F., 1986. Analysis of Linear Viscoelasticity of a Crosslinking Polymer at the Gel Point. *J. Rheol.* **30**, 367–382. <https://doi.org/10.1122/1.549853>

Wu, H., Ding, J., Liu, Y., 2003. Samarium Triiodide Catalyzed Cycloaddition of Epoxides with Isocyanates: A Facile Synthesis of Oxazolidinones. *ChemInform* **34**, no-no.

Wu, L., Gemert, J.V., Camargo, R.E., 2008. Rheology Study in Polyurethane Rigid Foams 12.

Wu, L.C.-F., Glasser, W.G., 1984. Engineering plastics from lignin. I. Synthesis of hydroxypropyl lignin. *J. Appl. Polym. Sci.* **29**, 1111–1123. <https://doi.org/10.1002/app.1984.070290408>

Wu, Liu, Y., He, Chung, Goh, 2004. Effects of Chemistries of Trifunctional Amines on Mechanisms of Michael Addition Polymerizations with Diacrylates. *Macromolecules* **37**, 6763–6770. <https://doi.org/10.1021/ma0493832>

Wurtz, A., 1846. Note sur la Formation de l'Urethane par l'Action du Chlorure de Cyanogène. *Compte Rendus Séances Académie Sci.* **22**, 503–505.

Xi, X., Pizzi, A., Gerardin, C., Lei, H., Chen, X., Amirou, S., 2019. Preparation and Evaluation of Glucose Based Non-Isocyanate Polyurethane Self-Blowing Rigid Foams. *Polymers* **11**, 1802. <https://doi.org/10.3390/polym11111802>

Xing, W., Yuan, H., Zhang, P., Yang, H., Song, L., Hu, Y., 2013. Functionalized lignin for halogen-free flame retardant rigid polyurethane foam: preparation, thermal stability, fire performance and mechanical properties. *J. Polym. Res.* **20**, 234. <https://doi.org/10.1007/s10965-013-0234-1>

Xiong, M., Schneiderman, D.K., Bates, F.S., Hillmyer, M.A., Zhang, K., 2014. Scalable production of mechanically tunable block polymers from sugar. *Proc. Natl. Acad. Sci.* **111**, 8357–8362. <https://doi.org/10.1073/pnas.1404596111>

Xu, C., Ferdosian, F., 2017. Conversion of lignin into bio-based chemicals and materials 'Green chemistry and sustainable technology. Springer Berlin Heidelberg, Berlin, Heidelberg. <https://doi.org/10.1007/978-3-662-54959-9>

Xu, J., Jiang, J., Hse, C.-Y., Shupe, T.F., 2014. Preparation of polyurethane foams using fractionated products in liquefied wood. *J. Appl. Polym. Sci.* **131**, 40096. <https://doi.org/10.1002/app.40096>

Xue, B.-L., Huang, P.-L., Sun, Y.-C., Li, X.-P., Sun, R.-C., 2017. Hydrolytic depolymerization of corncob lignin in the view of a bio-based rigid polyurethane foam synthesis. *RSC Adv.* **7**, 6123–6130. <https://doi.org/10.1039/C6RA26318F>

Xue, B.-L., Wen, J.-L., Sun, R.-C., 2015. Producing Lignin-Based Polyols through Microwave-Assisted Liquefaction for Rigid Polyurethane Foam Production. *Materials* **8**, 586–599. <https://doi.org/10.3390/ma8020586>

Xue, S., Omoto, M., Hidai, T., Imai, Y., 1995. Preparation of epoxy hardeners from waste rigid polyurethane foam and their application. *J. Appl. Polym. Sci.* **56**, 127–134. <https://doi.org/10.1002/app.1995.070560202>

Yang, L., Wang, X., Cui, Y., Tian, Y., Chen, H., Wang, Z., 2014. Modification of renewable resources-lignin-by three chemical methods and its applications to polyurethane foams. *Polym. Adv. Technol.* **25**, 1089–1098. <https://doi.org/10.1002/pat.3356>

Yang, L.-T., Zhao, C.-S., Dai, C.-L., Fu, L.-Y., Lin, S.-Q., 2012. Thermal and Mechanical Properties of Polyurethane Rigid Foam Based on Epoxidized Soybean Oil. *J. Polym. Environ.* **20**, 230–236. <https://doi.org/10.1007/s10924-011-0381-6>

Yang, R., Wang, B., Li, M., Zhang, X., Li, J., 2019. Preparation, characterization and thermal degradation behavior of rigid polyurethane foam using a malic acid based polyols. *Ind. Crops Prod.* **136**, 121–128. <https://doi.org/10.1016/j.indcrop.2019.04.073>

Yarema, K.J. (Ed.), 2005. Handbook of Carbohydrate Engineering, 1st ed. CRC Press. <https://doi.org/10.1201/9781420027631>

Yaws, C.L., 2009. Thermophysical properties of chemicals and hydrocarbons. William Andrew, Norwich, NY.

Yaws, C.L., 1995. Handbook of Thermal Conductivity: Organic Compounds C1 to C4. Elsevier, Burlington.

LISTE COMPLÈTE DES RÉFÉRENCES BIBLIOGRAPHIQUES

Yeganeh, H., Jamshidi, S., Talemi, P.H., 2006. Synthesis, characterization and properties of novel thermally stable poly(urethane-oxazolidone) elastomers. *Eur. Polym. J.* **42**, 1743–1754. <https://doi.org/10.1016/j.eurpolymj.2006.02.011>

Yelchuri, V., Srikanth, K., Prasad, R.B.N., Karuna, M.S.L., 2019. Olefin metathesis of fatty acids and vegetable oils. *J. Chem. Sci.* **131**, 39. <https://doi.org/10.1007/s12039-019-1615-8>

Yim, H., Haselbeck, R., Niu, W., Pujol-Baxley, C., Burgard, A., Boldt, J., Khandurina, J., Trawick, J.D., Osterhout, R.E., Stephen, R., Estadilla, J., Teisan, S., Schreyer, H.B., Andrae, S., Yang, T.H., Lee, S.Y., Burk, M.J., Van Dien, S., 2011. Metabolic engineering of *Escherichia coli* for direct production of 1,4-butanediol. *Nat. Chem. Biol.* **7**, 445–452. <https://doi.org/10.1038/nchembio.580>

Yue, D., Oribayo, O., Rempel, G.L., Pan, Q., 2017. Liquefaction of waste pine wood and its application in the synthesis of a flame retardant polyurethane foam. *RSC Adv.* **7**, 30334–30344. <https://doi.org/10.1039/C7RA03546B>

Zaher, F.A., El-Mallah, M.H., El-Hefnawy, M.M., 1989. Kinetics of oxirane cleavage in epoxidized soybean oil. *J. Am. Oil Chem. Soc.* **66**, 698–700. <https://doi.org/10.1007/BF02669955>

Zappi, M.E., Bajpai, R., Hernandez, R., Mikolajczyk, A., Lord Fortela, D., Sharp, W., Chirdon, W., Zappi, K., Gang, D., Nigam, K.D.P., Revellame, E.D., 2019. Microalgae Culturing To Produce Biobased Diesel Fuels: An Overview of the Basics, Challenges, and a Look toward a True Biorefinery Future. *Ind. Eng. Chem. Res.* **58**, 15724–15746. <https://doi.org/10.1021/acs.iecr.9b01555>

Zenner, M.D., Xia, Y., Chen, J.S., Kessler, M.R., 2013. Polyurethanes from Isosorbide-Based Diisocyanates. *ChemSusChem* **6**, 1182–1185. <https://doi.org/10.1002/cssc.201300126>

Zhan, H.-J., Wu, K.-J., Hu, Y.-L., Liu, J.-W., Li, H., Guo, X., Xu, J., Yang, Y., Yu, Z.-L., Gao, H.-L., Luo, X.-S., Chen, J.-F., Ni, Y., Yu, S.-H., 2019. Biomimetic Carbon Tube Aerogel Enables Super-Elasticity and Thermal Insulation. *Chem* **5**, 1871–1882. <https://doi.org/10.1016/j.chempr.2019.04.025>

Zhang, C., Bhoyate, S., Ionescu, M., Kahol, P.K., Gupta, R.K., 2018a. Highly flame retardant and bio-based rigid polyurethane foams derived from orange peel oil. *Polym. Eng. Sci.* **58**, 2078–2087. <https://doi.org/10.1002/pen.24819>

Zhang, C., Garrison, T.F., Madbouly, S.A., Kessler, M.R., 2017a. Recent advances in vegetable oil-based polymers and their composites. *Prog. Polym. Sci.* **71**, 91–143. <https://doi.org/10.1016/j.progpolymsci.2016.12.009>

Zhang, C., Li, J., Hu, Z., Zhu, F., Huang, Y., 2012. Correlation between the acoustic and porous cell morphology of polyurethane foam: Effect of interconnected porosity. *Mater. Des.* **41**, 319–325. <https://doi.org/10.1016/j.matdes.2012.04.031>

Zhang, C., Wang, H., Zeng, W., Zhou, Q., 2019a. High Biobased Carbon Content Polyurethane Dispersions Synthesized from Fatty Acid-Based Isocyanate. *Ind. Eng. Chem. Res.* **58**, 5195–5201. <https://doi.org/10.1021/acs.iecr.8b05936>

Zhang, G., Wu, Y., Chen, W., Han, D., Lin, X., Xu, G., Zhang, Q., 2019b. Open-Cell Rigid Polyurethane Foams from Peanut Shell-Derived Polyols Prepared under Different Post-Processing Conditions. *Polymers* **11**, 1392. <https://doi.org/10.3390/polym11091392>

Zhang, H., Fang, W.-Z., Li, Y.-M., Tao, W.-Q., 2017b. Experimental study of the thermal conductivity of polyurethane foams. *Appl. Therm. Eng.* **115**, 528–538. <https://doi.org/10.1016/j.applthermaleng.2016.12.057>

Zhang, J., Hori, N., Takemura, A., 2020. Influence of NCO/OH ratio on preparation of four agricultural wastes liquefied polyols based polyurethane foams. *Polym. Degrad. Stab.* **179**, 109256. <https://doi.org/10.1016/j.polymdegradstab.2020.109256>

Zhang, J., Hori, N., Takemura, A., 2019c. Optimization of preparation process to produce polyurethane foam made by oilseed rape straw based polyol. *Polym. Degrad. Stab.* **166**, 31–39. <https://doi.org/10.1016/j.polymdegradstab.2019.05.022>

Zhang, M., Zhang, J., Chen, S., Zhou, Y., 2014. Synthesis and fire properties of rigid polyurethane foams made from a polyol derived from melamine and cardanol. *Polym. Degrad. Stab.* **110**, 27–34. <https://doi.org/10.1016/j.polymdegradstab.2014.08.009>

Zhang, P., Liao, X., Ma, C., Li, Q., Li, A., He, Y., 2019d. Chemoenzymatic Conversion of Corncob to Furfurylamine via Tandem Catalysis with Tin-Based Solid Acid and Transaminase Biocatalyst. *ACS Sustain. Chem. Eng.* **7**, 17636–17642. <https://doi.org/10.1021/acssuschemeng.9b03510>

Zhang, S., Liu, X., Jin, X., Li, H., Sun, J., Gu, X., 2018b. The novel application of chitosan: Effects of cross-linked chitosan on the fire performance of thermoplastic polyurethane. *Carbohydr. Polym.* **189**, 313–321. <https://doi.org/10.1016/j.carbpol.2018.02.034>

Zhang, X., Jeremic, D., Kim, Y., Street, J., Shmulsky, R., 2018c. Effects of Surface Functionalization of Lignin on Synthesis and Properties of Rigid Bio-Based Polyurethanes Foams. *Polymers* **10**, 706. <https://doi.org/10.3390/polym10070706>

LISTE COMPLÈTE DES RÉFÉRENCES BIBLIOGRAPHIQUES

Zhang, X., Kim, Y., Eberhardt, T.L., Shmulsky, R., 2019e. Lab-scale structural insulated panels with lignin-incorporated rigid polyurethane foams as core. *Ind. Crops Prod.* **132**, 292–300. <https://doi.org/10.1016/j.indcrop.2019.02.035>

Zhang, X., Kim, Y., Elsayed, I., Taylor, M., Eberhardt, T.L., Hassan, E.B., Shmulsky, R., 2019f. Rigid polyurethane foams containing lignin oxyalkylated with ethylene carbonate and polyethylene glycol. *Ind. Crops Prod.* **141**, 111797. <https://doi.org/10.1016/j.indcrop.2019.111797>

Zhang, X.D., Macosko, C.W., Davis, H.T., Nikolov, A.D., Wasan, D.T., 1999. Role of Silicone Surfactant in Flexible Polyurethane Foam. *J. Colloid Interface Sci.* **215**, 270–279. <https://doi.org/10.1006/jcis.1999.6233>

Zhu, Y., Romain, C., Williams, C.K., 2016. Sustainable polymers from renewable resources. *Nature* **540**, 354–362. <https://doi.org/10.1038/nature21001>

Zieleniewska, M., Leszczyński, M.K., Kurańska, M., Prociak, A., Szczepkowski, L., Krzyżowska, M., Ryszkowska, J., 2015. Preparation and characterisation of rigid polyurethane foams using a rapeseed oil-based polyol. *Ind. Crops Prod.* **74**, 887–897. <https://doi.org/10.1016/j.indcrop.2015.05.081>

**Développement de nouveaux matériaux
polymères biosourcés alvéolaires, à
partir de synthons extraits de
microalgues**

Résumé

Dans un contexte de développement durable et de chimie verte, de nouveaux synthons issues d'huile de microalgues ont été développés pour l'élaboration de nouvelles mousse polyuréthanes biosourcées. La synthèse de polyols par époxydation de ressources lipidiques est tout d'abord analysée en terme cinétique au travers d'un modèle reactionnel. Les protocoles développés ont été ensuite appliqués à des triglycérides issus microalgues. L'impact des polyols synthétisés sur les propriétés de mousse rigides à cellules fermées est étudié. L'analyse de la réaction directe entre les huiles époxydées et des polyisocyanates montre la difficulté de former des groupements oxazolidones, lequels sont plus stable thermiquement que les uréthanes. Afin de trouver un substitut aux thermosécables polyuréthanes dans un contexte de chimie plus verte, durable et moins toxique, la chimie d'aza-Michael a été explorée avec des synthons biosourcés synthétisés à partir d'huiles époxydées.

Mots clés : Oléochimie, Biosourcé, Microalgues, Polyuréthane, Matériaux alvéolaires

Résumé en anglais

In a context of sustainable development and green chemistry, new building blocks derived from microalgae oil have been developed for the elaboration of new biobased polyurethane foams. The synthesis of polyols by epoxidation of lipidic resources is first analyzed in kinetic terms through a reaction model. The developed protocols were then applied to triglycerides from microalgae. The impact of the synthesized polyols on the properties of rigid with closed-cell foams is analyzed. The analysis of the direct reaction between epoxidized oils and polyisocyanates shows the difficulty of forming oxazolidone groups, which are more thermally stable than urethanes. In order to find a substitute for thermosetting polyurethanes in a context of greener, sustainable and less toxic chemistry, the chemistry of aza-Michael has been explored from biobased compounds synthesized from epoxidized oils.

Keywords: Oleo-chemistry, Biobased, Microalgae, Polyurethane, Cellular materials